CT Teaching Manual

A Systematic Approach to CT Reading

Matthias Hofer

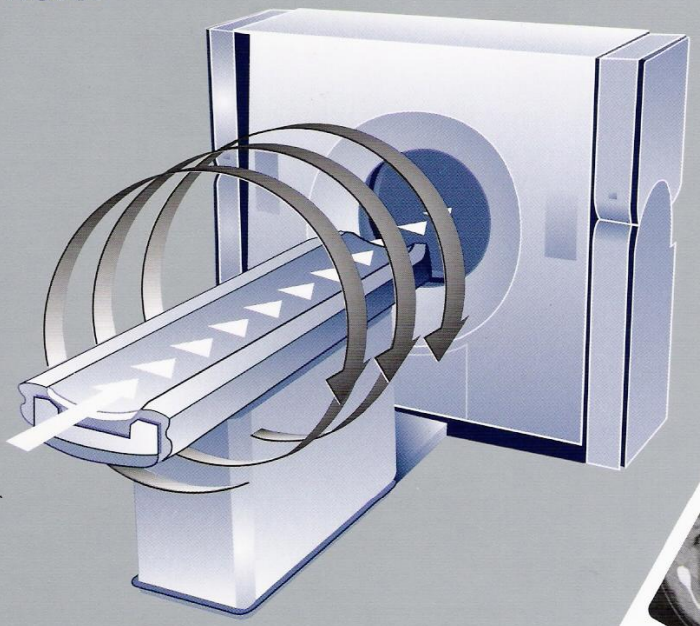

Second edition

- Technical Aspects, including MDCT, Pitch and Detector-Design
- Basic Rules of CT Reading
- Atlas of Sectional Anatomy
- Common Pathologies
- Protocols for Users
- Dose Reduction
- CT-Angiography

Thieme

Table of Contents

Table of Contents

General Principles of CT

Computed tomography is a special type of x-ray procedure that involves the indirect measurement of the weakening, or attenuation, of x-rays at numerous positions located around the patient being investigated. Basically speaking, all we know is

- what leaves the x-ray tube,
- what arrives at the detector and
- the position of the x-ray tube and detector for each position.

Simply stated, everything else is deduced from this information. Most CT slices are oriented vertical to the body's axis. They are usually called axial or transverse sections. For each section the x-ray tube rotates around the patient to obtain a preselected section thickness **(Fig. 6.1)**. Most CT systems employ the continuous rotation and fan beam design: with this design, the x-ray tube and detector are rigidly coupled and rotate continuously around the scan field while x-rays are emitted and detected. Thus, the x-rays, which have passed through the patient, reach the detectors on the opposite side of the tube. The fan beam opening ranges from 40° to 60°, depending on the particular system design, and is defined by the angle originating at the focus of the x-ray tube and extending to the outer limits of the detector array. Typically, images are produced for each 360° rotation, permitting a high number of measurement data to be acquired and sufficient dose to be applied. While the scan is being performed, attenuation profiles, also referred to as samples or projections, are obtained. Attenuation profiles are really nothing other than a collection of the signals obtained from all the detector channels at a given angular position of the tube-detector unit. Modern CT systems **(Fig. 6.4)** acquire approximately 1400 projections over 360°, or about four projections per degree. Each attenuation profile comprises the data obtained from about 1500 detector channels, about 30 channels per degree in case of a 50° fan beam. While the patient table is moving continuously through the gantry, a digital radiograph ("scanogramm" or "localizer", **Fig. 6.2**) is produced on which the desired sections can be planned. For a CT examination of the spine or the head, the gantry is angled to the optimal orientation **(Fig. 6.3)**.

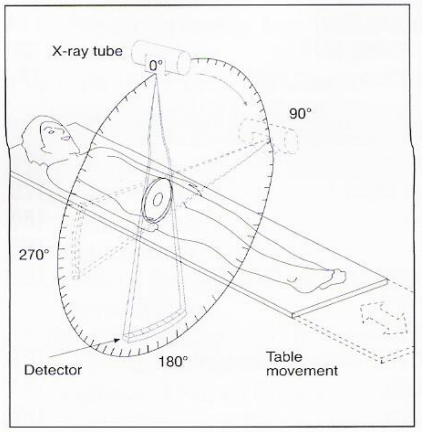

Fig. 6.1

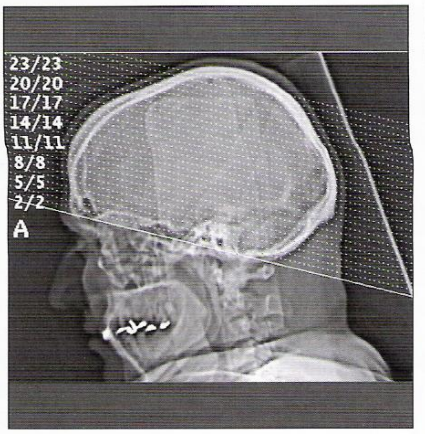

Fig. 6.2

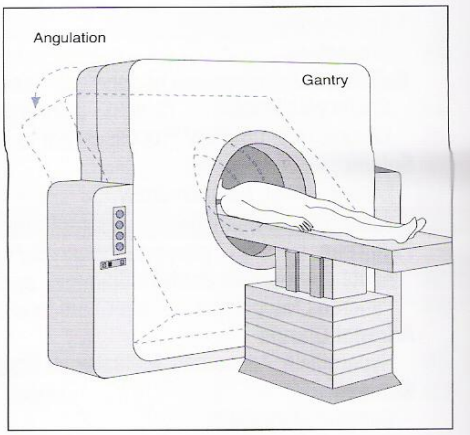

Fig. 6.3

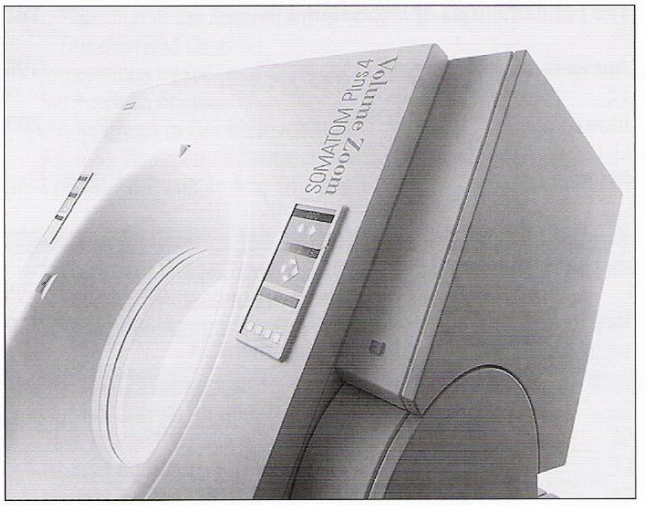

Fig. 6.4

Multiple-Row Detector Spiral CT

Multiple-row detector CT (MDCT) is the latest scanner development. Rather than one detector row, multiple detector rows are placed opposite the x-ray tube. This shortens the examination time and improves the temporal resolution, allowing, for instance, the determination of the rate of vascular enhancement.

The detector rows along the z-axis opposite the x-ray tube are unequal in width, with the outer rows wider than the inner rows to provide better conditions for image reconstruction after data acquisition (see pages 9-11).

Comparison of Conventional CT with Spiral CT

In conventional CT, a series of equally spaced images is acquired sequentially through a specific region, e.g. the abdomen or the head **(Fig. 7.1)**. There is a short pause after each section in order to advance the patient table to the next preset position. The section thickness and overlap/intersection gap are selected at the outset. The raw data for each image level is stored separately. The short pause between sections allows the conscious patient to breathe without causing major respiratory artifacts.

However, the examination may take several minutes, depending on the body region and the size of the patient. Proper timing of image acquisition after i.v. contrast media is particularly important for assessing perfusion effects. CT is the technique of choice for acquiring complete 2D axial images of the body without the disadvantages of superimposed bone and / or air as seen in conventional x-ray images.

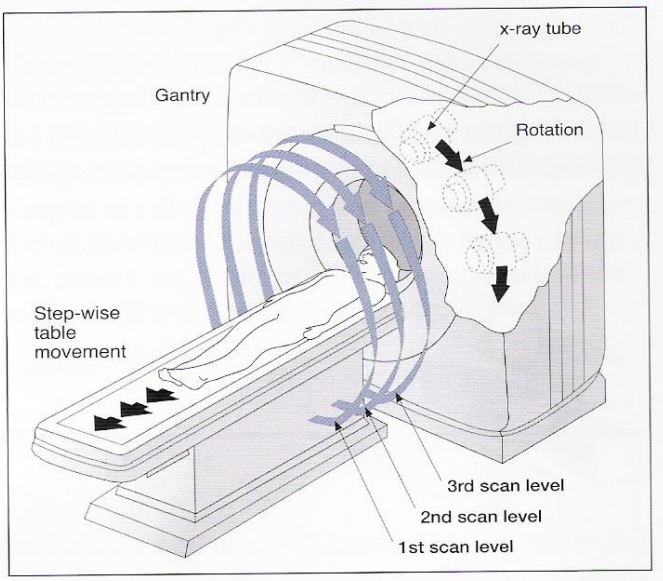

Fig. 7.1

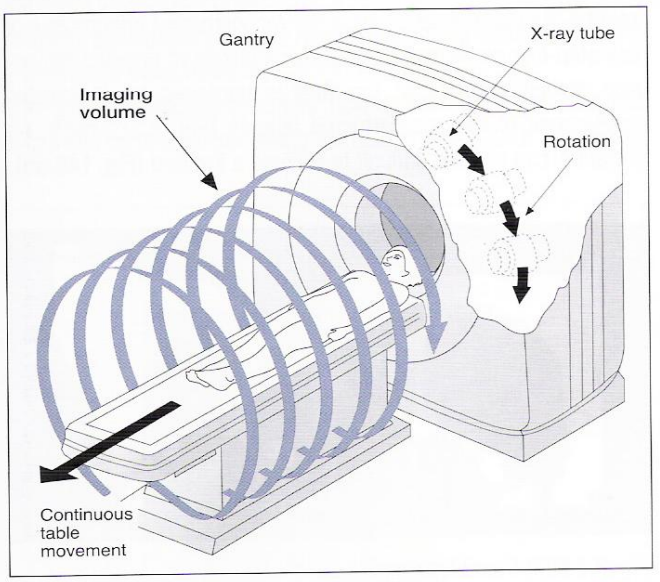

Fig. 7.2

Both single-row detector CT (SDCT) and multiple-row detector CT (MDCT) continuously acquire data of the patient while the examination table moves through the gantry. The x-ray tube describes an apparent helical path around the patient **(Fig. 7.2)**. If table advance is coordinated with the time required for a 360° rotation (pitch factor), data acquisition is complete and uninterrupted. This modern technique has greatly improved CT because respiratory artifacts and inconsistencies do not affect the single dataset as markedly as in conventional CT. The single dataset can be used to reconstruct slices of differing thickness or at differing intervals. Even overlapping slices can be reconstructed.

Data acquisition for the abdomen takes only 1–2 minutes: two or three helices, each about 10 to 20 seconds, are obtained. The time limit is determined by the duration a patient can hold his breath and the necessary cooling of the x-ray tubes. Image reconstruction takes longer. An assessment of renal function following CM will require a short break to allow for CM excretion to occur.

One of the advantages of the helical technique is that lesions smaller than the conventional thickness of a slice can be detected. Small liver metastases **(7)** will be missed if inconsistent depth of respiration results in them not being included in the section **(Fig. 7.3a)**. The metastases would appear in overlapping reconstructions from the dataset of the helical technique **(Fig. 7.3b)**.

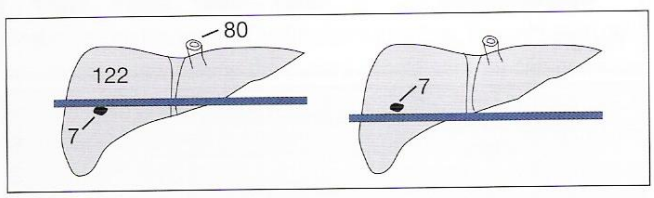

Fig. 7.3a Conventional CT

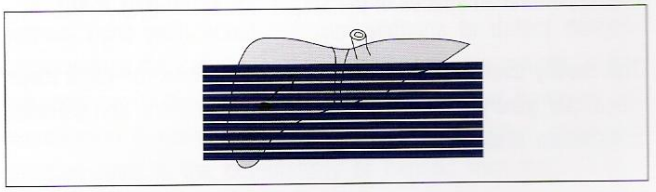

Fig. 7.3b Spiral CT

Spatial Resolution

The reconstructed images should have a high temporal resolution to separate even small structures from each other. This generally creates no problem along the x- or y-axis of the image since the selected field of view (FOV) typically encompasses 512 x 512 or more picture elements (pixel). These pixels appear on the monitor as grey values proportionate to their attenuation **(Fig. 8.1b)**. In reality, however, they are not squares but cubes (voxel = volume element) with their length along the body axis defined by the section thickness **(Fig. 8.1a)**.

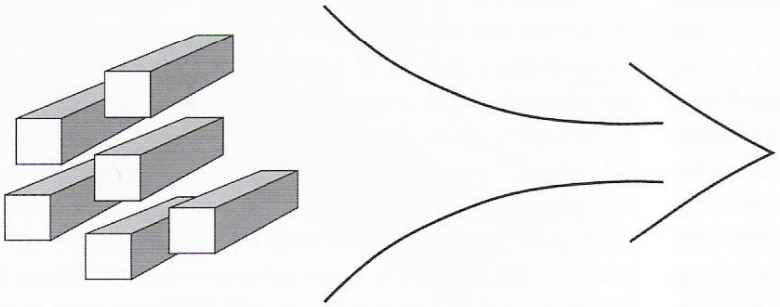

Fig. 8.1a

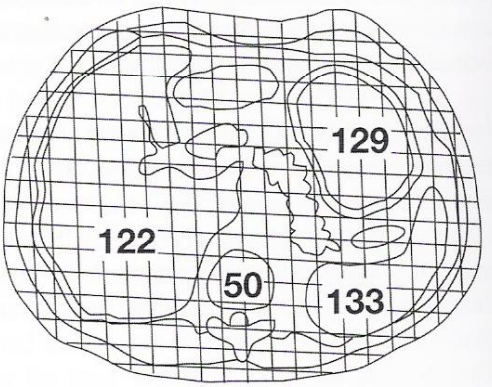

Fig. 8.1b

The image quality should improve with smaller voxels, but this only applies to the spatial resolution since a thinner section lowers the signal-to-noise ratio. Another disadvantage of thinner sections is the inevitable increase in the radiation dose to the patient (see page 175). Nonetheless, smaller voxels with identical measurements in all three dimensions (isotropic voxels) offer a crucial advantage: The multiplanar reconstruction (MPR) in coronal, sagittal or other planes displays the reconstructed images free of any step-like contour **(Fig. 8.2)**. Using voxels of unequal dimension (anisotropic voxels) for MPR is burdened by a serrated appearance of the reconstructed images **(Fig. 8.3)**, which, for instance, can make it difficult to exclude a fracture **(Fig. 148.5b)**.

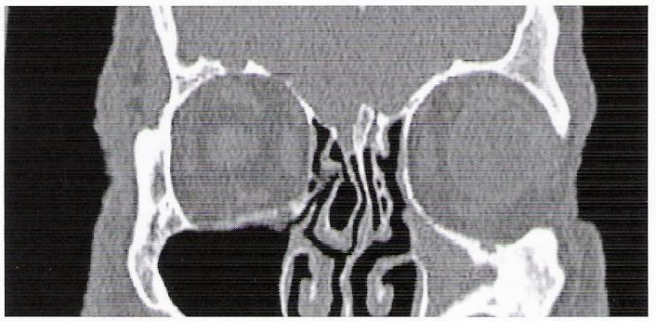

Fig. 8.2 MPR from isotropic voxels

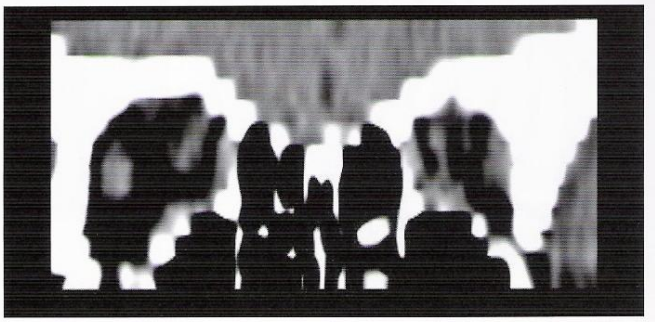

Fig. 8.3 MPR from anisotropic voxels

Pitch

By now, several definitions exist for the pitch, which describes the rate of table increment per rotation in millimeter and section thickness. A slowly moving table per rotation generates a tight acquisition spiral **(Fig. 8.4a)**. Increasing the table increment per rotation without changing section thickness or rotation speed creates interscan spaces of the acquisition spiral **(Fig. 8.4b)**.

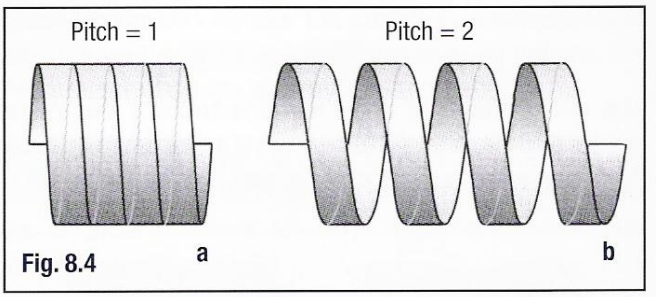

Fig. 8.4

The mostly used definition of the pitch describes the table travel (feed) per gantry rotation, expressed in millimeters, and selected collimation, also expressed in millimeters.

$$\text{Pitch} = \frac{\text{Table travel / rotation}}{\text{Collimation}}$$

$$\text{Pitch} = \frac{\text{Feed / rotation}}{\text{Collimation}} \quad \text{e.g.:} \quad \frac{24 \text{ mm / rotation}}{16 \times 1.5 \text{ mm}} = \frac{24 \text{ mm}}{24 \text{ mm}} = 1$$

Since the units (mm) in the numerator and denominator cancel out, the pitch is a dimensionless number. For a while, a so-called volume pitch was stated for multiple-row detector CT scanners, which relates the table feed to a single section rather than to the entire array of sections along the z-axis. For the example given above, this means a volume pitch of 24 mm / 1.5 mm = 16. However, there seems to be a trend to returning to the original definition of the pitch.

The new scanners give the examiner the option to select the craniocaudal extension (z-axis) of the region to be examined on the topogram as well as the rotation time, section collimation (thin or thick sections?) and examination time (breath-holding intervals?). The software, e.g., "SureView®," calculates the suitable pitch, usually providing values between 0.5 and 2.0.

Section Collimation: Resolution Along the Z-Axis

The resolution (along the body axis or z-axis) of the images can also be adapted to the particular clinical question by the choice of the collimation. Sections between 5 and 8 mm generally are totally adequate for standard examinations of the abdomen. However, the exact localization of small fracture fragments or the evaluation of subtle pulmonary changes require thin slices between 0.5 and 2 mm. What determines the section thickness?

The term collimation describes how thin or thick the acquired slices can be preselected along the longitudinal axis of the patient (= z-axis). The examiner can limit the fan-like x-ray beam emitted from the x-ray tube by a collimator, whereby the collimator's aperture determines whether the fan passing through the collimator and collected by the detector units behind the patient is either wide **(Fig. 9.1)** or narrow **(Fig. 9.2)**, with the narrow beam allowing a better spatial resolution along the z-axis of the patient. The collimator cannot only be placed next to the x-ray tube, but also in front of the detectors, i.e., "behind" the patient as seen from the x-ray source.

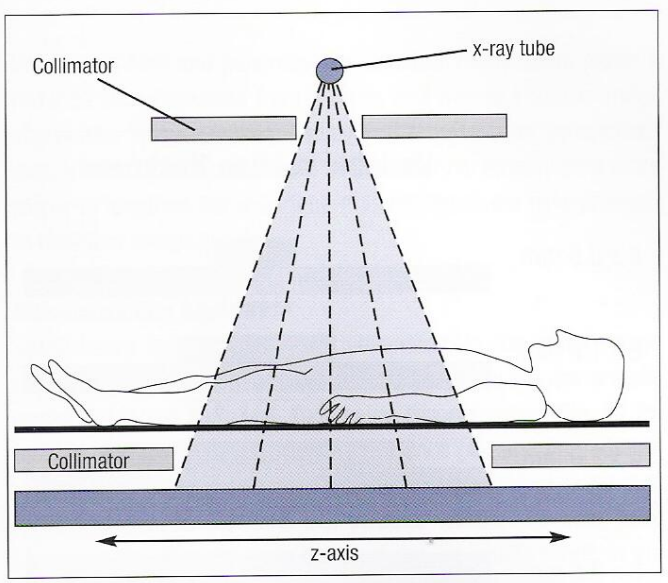

Fig. 9.1 Wide section collimation

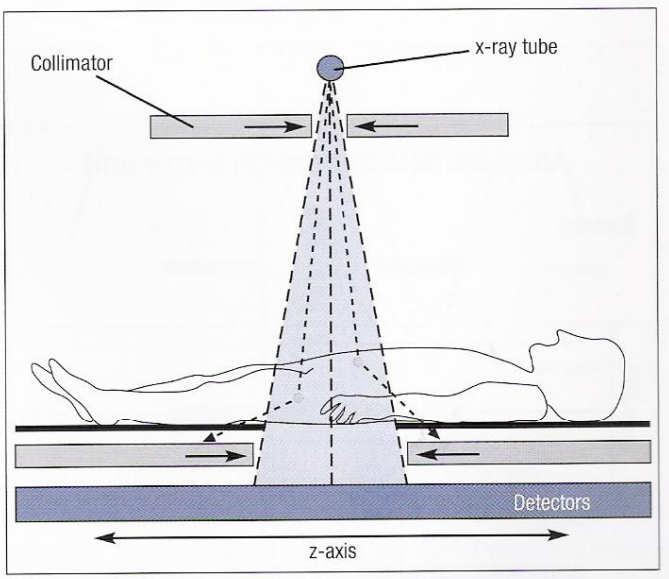

Fig. 9.2 Narrow section collimation

Depending on the width of collimator's aperture, the units with only one detector row behind the patient (single section) can generate sections with a width of 10 mm, 8 mm, 5 mm or even 1 mm. A CT examination obtained with very thin sections is also called a high resolution CT (HRCT) and, if the sections are at the sub-millimeter level, ultra high resolution CT (UHRCT). The UHRCT is used for the petrous bone with about 0.5 mm sections to detect delicate fracture lines through the cranial base or auditory ossicles in the tympanic cavity (see pages 46 – 49). For the liver, however, the examination is dominated by the contrast resolution since the question here is the detectability of hepatic metastases (here somewhat thicker sections).

Adaptive Array Design

A further development of the single-slice spiral technology is the introduction of the multislice technique, which has not one detector rows but several detector rows stacked perpendicular to the z-axis opposite the x-ray source. This enables the simultaneous acquisition of several sections.

The detector rows are not inevitably equal in width. The adaptive array design consists of detectors that increase in width from the center to the edge of the detector ring and consequently allows various combinations of thickness and numbers of acquired sections.

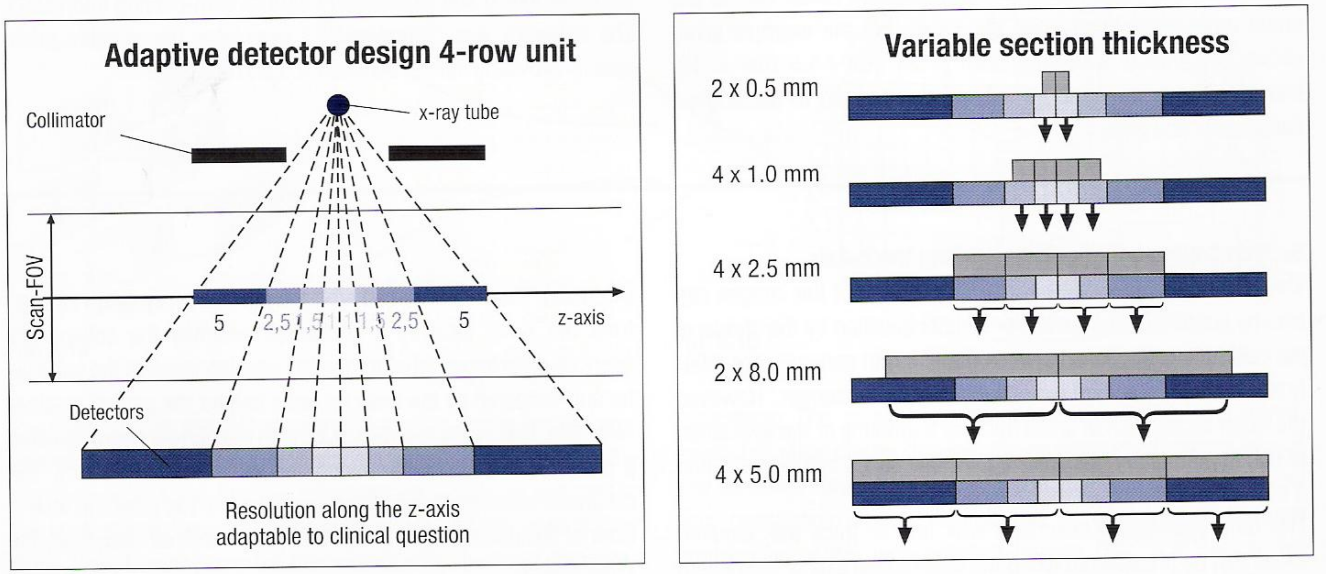

Fig. 10.1 Detector design of a 4-row unit, as found in the Siemens Sensation 4

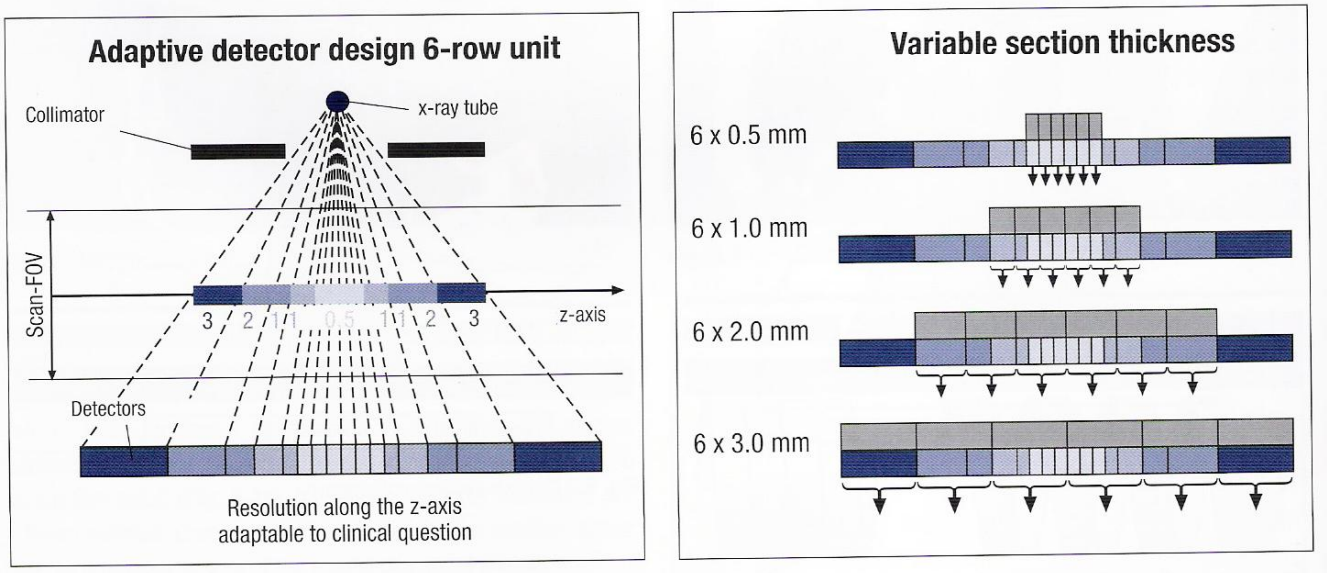

Fig. 10.2 Detector design of a 6-row unit, as found in the Siemens Emotion 6

For instance, a 16-slice examination can be performed with 16 thin sections of a higher resolution (for the Siemens Sensation 16, this means 16 x 0.75 mm) or with 16 sections of twice the thickness. For an iliofemoral CTA (see page 188), it is preferable to acquire a long volume along the z-axis in a single run, of course with a selected wide collimation of 16 x 1.5 mm.

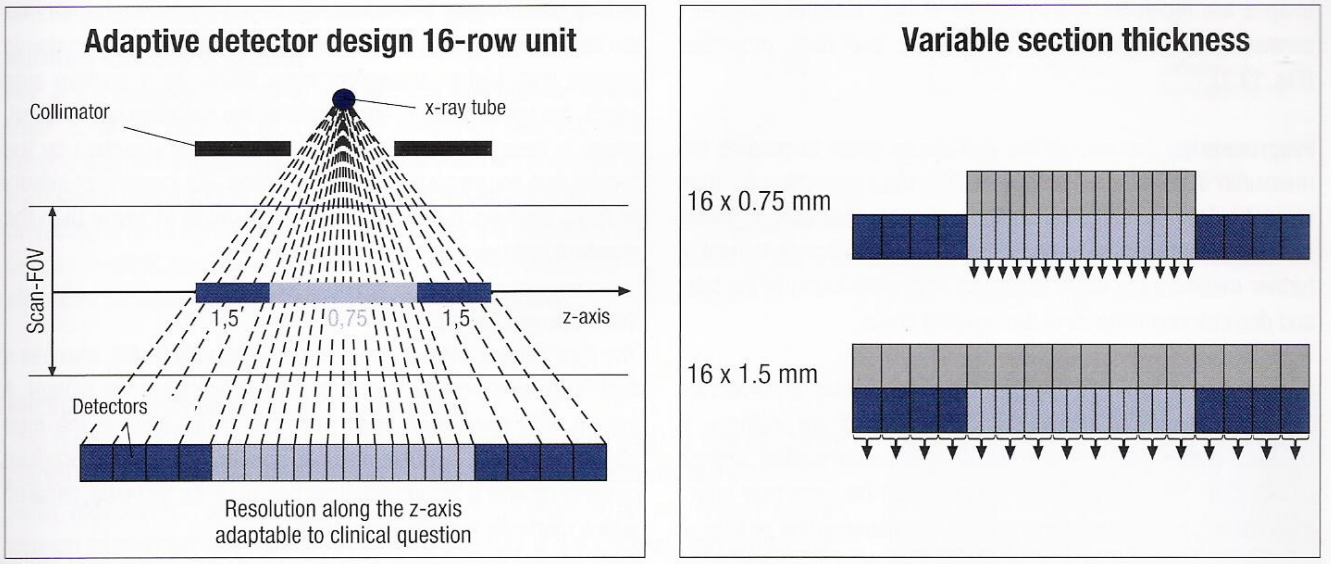

Fig. 11.1 Detector design of a 16-row unit, as found in the Siemens Sensation 16

The development of the CT hardware did not end with 16 slices and faster data acquisition can already be achieved with 32- and 64-row scanners. The trend to thinner slices is associated with higher patient exposure to radiation, requiring additional and already introduced measures for exposure reduction (see pages 174-177).

When both liver and pancreas are included, many users prefer a reduced slice thickness from 10 mm to 3 mm to improve image sharpness. This increases, however, the noise level by approximately 80%. Therefore it would be necessary to employ 80% more mA or to lengthen the scan time (this increases the mAs product) to maintain image quality.

Reconstruction Algorithm

Spiral users have an additional advantage: In the spiral image reconstruction process, most of the data points were not actually measured in the particular slice being reconstructed **(Fig. 11.2)**. Instead, data are acquired outside this slice (●) and interpolated with more importance, or "contibution", being attached to the data located closest to the slice (X). In other words: The data point closest to the slice receives more weight, or counts more, in the reconstruction of an image at the desired table position.

This results in an interesting phenomenon. The patient dose (actually given in mGy) is determined by the mAs per rotation divided by the pitch, and the image dose is equal to the mAs per rotation without considering the pitch. If for instance 150 mAs per rotation with a pitch of 1.5 are employed, the patient dose in mGy is linear related to 100 mAs, and the image dose is related to 150 mAs. Therefore spiral users can improve contrast detectability by

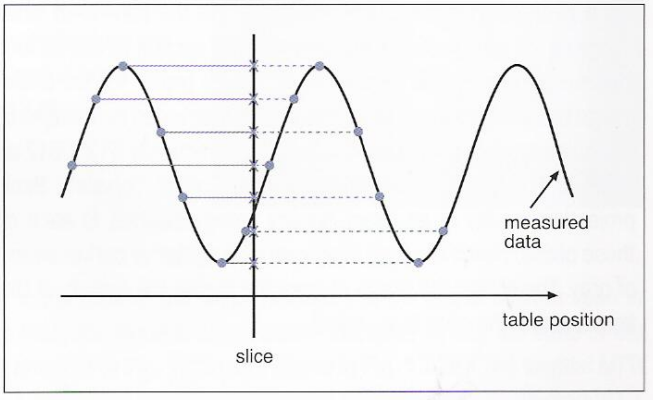

Fig. 11.2 Wide (360°) spiral reconstruction algorithm

selecting high mA values, increase the spatial resolution (image sharpness) by reducing slice thickness, and employ pitch to adjust the length of the spiral range as desired, all while reducing the patient's dose! More slices can be acquired without increasing the dose or stressing the x-ray tube.

This technique is especially helpful when data are reformatted to create other 2D views, like sagittal, oblique, coronal, or 3D views (MIP, surface shaded imaging, see pp. 8 and 13).

The data obtained at the detector channel are passed on, profile for profile, to the detector electronics as electric signals corresponding to the actual x-ray attenuation. These electric signals are digitized and then transmitted to the image processor. At this stage, the images are reconstructed by means of the "pipeline principle", consisting of preprocessing, convolution, and back projection **(Fig. 12.1)**.

Preprocessing includes all the corrections taken to prepare the measured scan data for reconstruction, e.g., correction for dark current, dose output, calibration, channel correction, beam hardening, and spacing errors. These corrections are performed to further minimize the slight variations inherently found in the tube and detector components of the imaging chain.

Convolution is basically the use of negative values to correct for smearing inherent to simple back projection. If, for instance, a cylindric water phantom is scanned and reconstructed without convolution, the edges of this phantom will be extremely blurry **(Fig. 12.2a)**: What happens when just eight attenuation profiles of a small, highly absorbent cylindrical object are superimposed to create an image? Since the same part of the cylinder is measured by two overlapping projections, a star-shaped image is produced instead of what is in reality a cylinder. By introducing negative values just beyond the positive portion of the attenuation profiles, the edges of this cylinder can be sharply depicted **(Fig. 12.2b)**.

Back projection involves the reassigning of the convolved scan data to a 2D image matrix representing the section of the patient that is scanned. This is performed profile for profile for the entire image reconstruction process. The image matrix can be thought of as analogous to a chessboard, consisting of typically 512 x 512 or 1024 x 1024 picture elements, usually called "pixels". Back projection results in an exact density being assigned to each of these pixels, which are then displayed as a lighter or darker shade of gray. The lighter the shade of gray, the higher the density of the tissue within the pixel (e.g., bone).

The Influence of kV

When examining anatomic regions with higher absorption (e.g., CT of the head, shoulders, thoracic or lumbar spine, pelvis, and larger patients), it is often advisable to use higher kV levels in addition to, or instead of, higher mA values: when you choose higher kV, you are hardening the x-ray beam. Thus x-rays can penetrate anatomic regions with higher absorption more easily. As a positive side effect, the lower energy components of the radiation are reduced, which is desirable since low energy x-rays are absorbed by the patient and do not contribute to the image. For imaging of infants or bolus tracking, it may be advisable to utilize kV lower than the standard setting.

Tube Current [mAs]

The tube current, stated in milliampere-seconds [mAs], also has a significant effect on the radiation dose delivered to the patient. A patient with more body width requires an increase in the tube current to achieve an adequate image quality. Thus, more corpulent patients receive a larger radiation dose than, for instance, children with a markedly smaller body width.

Body regions with skeletal structures that absorb or scatter radiation, such as shoulder and pelvis, require a higher tube current than, for instance, the neck, a slender abdominal torso or the legs. This relationship has been actively applied to radiation protection for some time now (compare with page 177).

Scan Time

It is advantageous to select a scan time as short as possible, particularly in abdominal or chest studies where heart movement and peristalsis may degrade image quality. Other CT investigations can also benefit from fast scan times due to decreased probability of involuntary patient motion. On the other hand, it may be necessary to select a longer scan time to provide sufficient dose or to enable more samples for maximal spatial resolution. Some users may also consciously choose longer scan times to lower the mA setting and thus increase the likelihood of longer x-ray tube life.

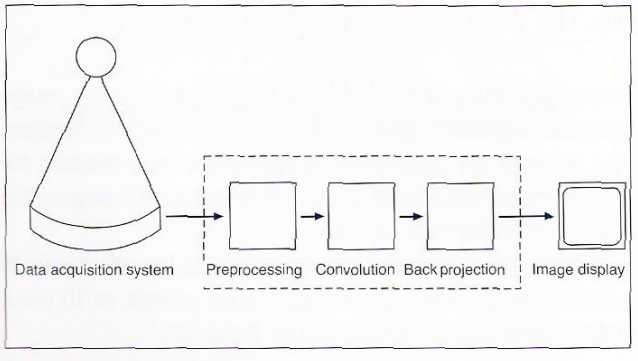

Fig. 12.1 *The pipeline principle of image reconstruction*

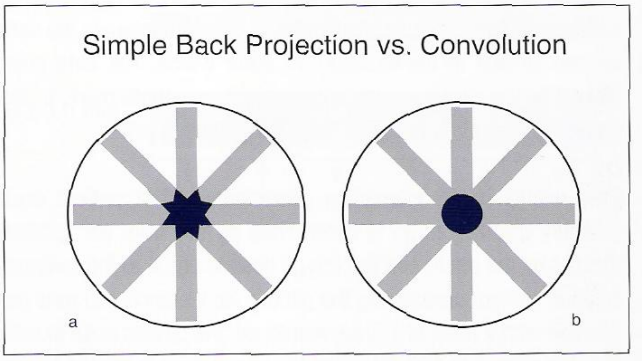

Fig. 12.2a Back projection without convolution

Fig. 12.2b Back projection with convolution

3D Reconstructions

Because the helical or spiral technique acquires a continuous, single volume dataset for an entire body region, imaging of fractures and blood vessels has improved markedly. Several different methods of 3D reconstruction have become established:

Maximal Intensity Projection

MIP is a mathematical method that extracts hyperintense voxels from 2D or 3D datasets [6, 7]. These voxels are selected from several different angles through the dataset and then projected as a 2D image **(Fig. 13.1)**. A 3D impression is acquired by altering the projection angle in small steps and then viewing the reconstructed images in quick succession (i.e., in cine mode). This procedure is also used for examining contrast-enhanced blood vessels.

Fig. 13.1

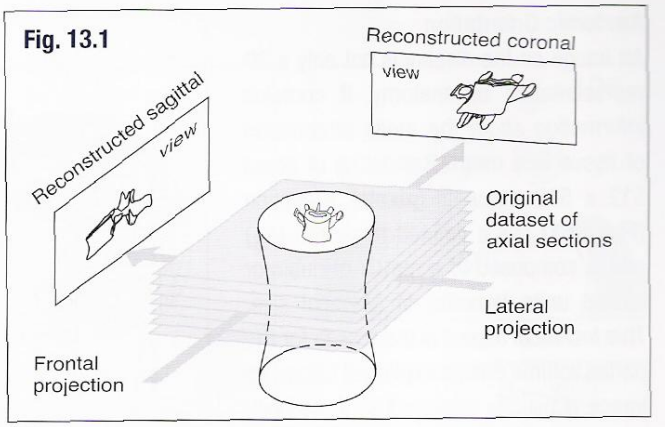

Multiplanar Reconstruction

This technique makes it possible to reconstruct coronal and sagittal as well as oblique planes. MPR has become a valuable tool in the diagnosis of fractures and other orthopedic indications. For example, conventional axial sections do not always provide enough information about fractures. A good example is the undisplaced hairline fracture (*) without cortical discontinuity that can be more effectively demonstrated by MPR **(Fig. 13.2a)**.

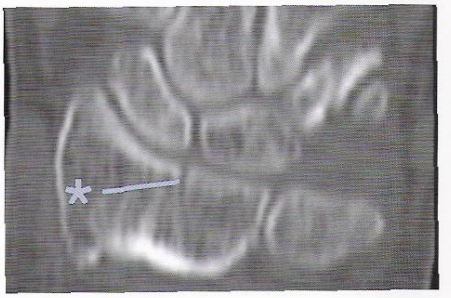

Fig. 13.2a

3D Surface Shaded Display

This method shows the surface of an organ or a bone that has been defined in Hounsfield units above a particular threshold value. The angle of view, as well as the location of a hypothetical source of light (from which the computer calculates shadowing) are crucial for obtaining optimal reconstructions. The fracture of the distal radius shown in the MPR in **Figure 13.2a** is seen clearly in the bone surface in **Figure 13.2b**.

(**Figs. 13.2a** and **13.2b** supplied with the kind permission of J. Brackins Romero, M. D., Recklinghausen, Germany)

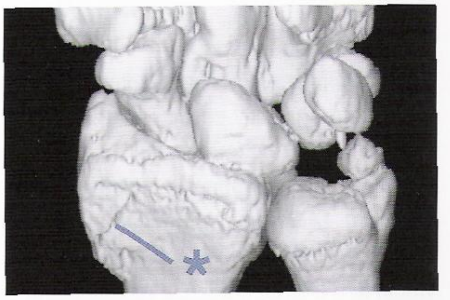

Fig. 13.2b

3D surface shaded displays are also valuable in planning surgery as in the case of the traumatic injury to the spinal column seen in **Figures 13.3 a, b,** and **c**. Since the angle of view can be freely determined, the thoracic compression fracture (*) and the state of the intervertebral foramina can be examined from several different angles (anterior in **Fig. 13.3a** and lateral in **Fig. 13.3b**). The sagittal MPR in **Figure 13.3c** determines whether any bone fragments have become dislocated into the spinal canal (compare with myelography CT on page 147).

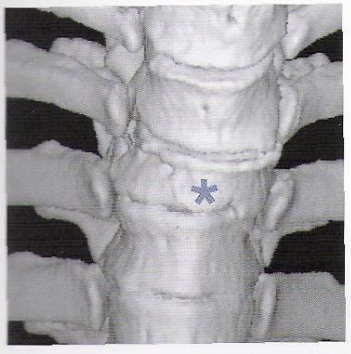

Fig. 13.3a

Fig. 13.3b

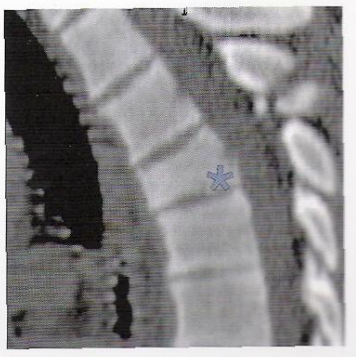

Fig. 13.3c

Anatomic Orientation

An image on the display is not only a 2D representation of anatomy, it contains information about the mean attenuation of tissue in a matrix consisting of about 512 x 512 elements **(pixels)**. A section **(Fig. 14.1)** has a defined thickness **(d_S)** and is composed of a matrix of cubic or cuboid units **(voxels)** of identical size. This technical aspect is the reason for the partial volume effects explained below. An image is usually displayed as if the body were viewed from caudal. Thus the right side of the patient is on the left side of the image and vice versa **(Fig. 14.1)**. For example, the liver **(122)** is located in the right half of the body, but appears in the left half of the image. Organs of the left side such as the stomach **(129)** and the spleen **(133)** appear on the right half of an image. Anterior aspects of the body, for example the abdominal wall, are represented in the upper parts of an image, posterior aspects such as the spine **(50)** are lower. With this system CT images are more easily compared with conventional x-ray-images.

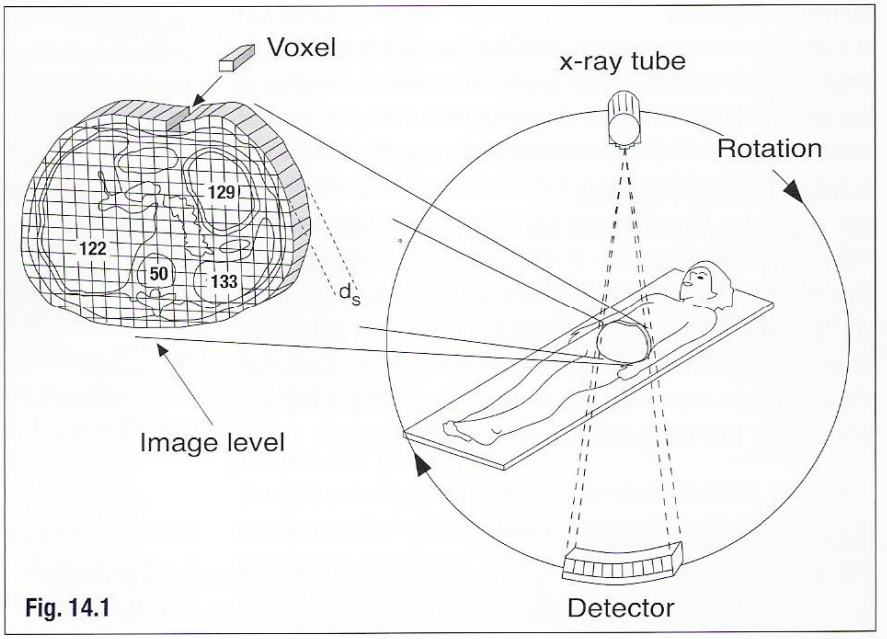

Fig. 14.1

Partial Volume Effects

The radiologist determines the thickness of the image **(d_S)**. 8–10 mm is usually chosen for thoracic or abdominal examinations, and 2–5 mm for the skull, spine, orbits, or petrosal bones. A structure may therefore be included in the entire thickness of a slice **(Fig. 14.2a)** or in only a part of it **(Fig. 14.3a)**. The gray scale value of a voxel depends on the mean attenuation of all structures within it. If a structure has a regular shape within a section, it will appear well defined. This is the case for the abdominal aorta **(89)** and the inferior vena cava **(80)** shown in **Figures 14.2a, b**.

Partial volume effects occur when structures do not occupy the entire thickness of a slice, for example when a section includes part of a vertebral body **(50)** and part of a disk **(50e)** the anatomy will be poorly defined **(Figs. 14.3a, b)**. This is also true if an organ tapers within a section as seen in **Figures 14.4a, b**. This is the reason for the poor definition of the renal poles or the borders of the gallbladder **(126)** or urinary bladder.

Artifacts caused by breathing during image acquisition are discussed on page 19.

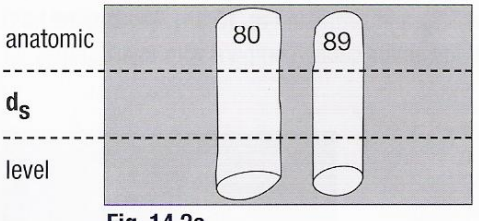

Fig. 14.2a

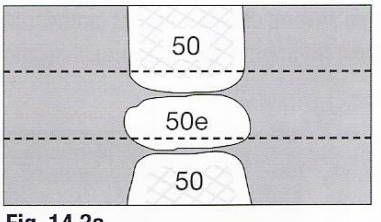

Fig. 14.3a

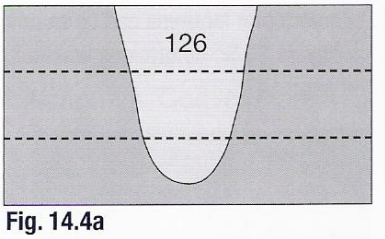

Fig. 14.4a

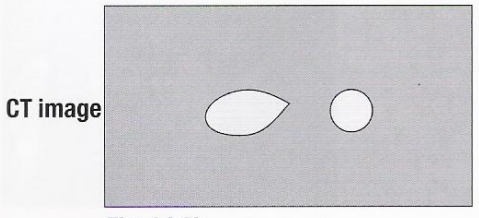

Fig. 14.2b

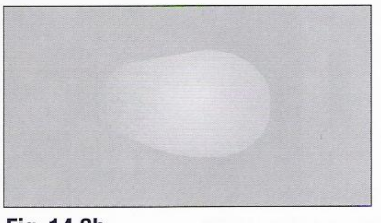
Fig. 14.3b

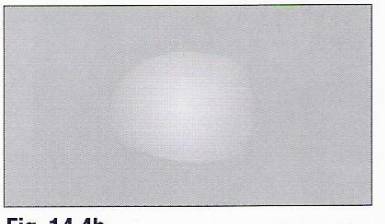
Fig. 14.4b

Distinguishing Between Nodular and Tubular Structures

It is essential to differentiate between possibly enlarged or affected LNs and vessels or muscles which have been cut in transverse section. This may be extremely difficult in a single image because these structures have similar density values (gray tones). One should therefore always analyze adjacent cranial and caudal images and compare the structures in question to determine whether they are nodular swellings or continue as more or less tubular structures **(Fig. 15.1)**: A lymph node **(6)** will appear in only one or two slices and cannot be traced in adjacent images (compare **Figs. 15.1a, b,** and **c**). The aorta **(89)** or the inferior cava **(80)**, or a muscle, for example the iliopsoas **(31)**, can be traced through a cranio-caudal series of images.

If there is a suspicious nodular swelling in one image, it should become an automatic reaction to compare adjacent levels to clarify whether it is simply a vessel or muscle in cross-section. This procedure will also enable quick identification of the partial volume effects described on the previous page.

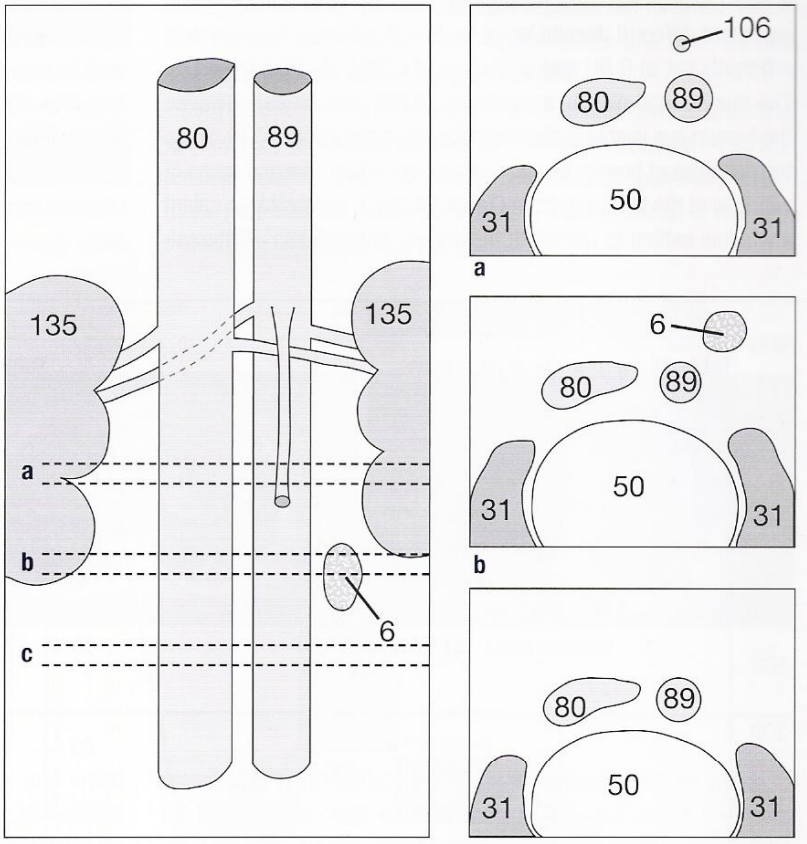

Fig. 15.1

Densitometry (Measurement of Density)

If it is uncertain, for example, whether fluid found in the pleural cavity is a pleural effusion or a hemothorax, a measurement of the liquid's density will clarify the differential diagnosis. The same applies to focal lesions in the parenchyma of the liver or the kidney. However, it is not advisable to carry out measurements of single voxels (= volume element, see **Fig. 14.1**) since such data are liable to statistical fluctuations which can make the attenuation unreliable. It is more accurate to position a larger "region of interest" (ROI) consisting of several voxels in a focal lesion, a structure, or an amount of fluid. The computer calculates the mean density levels of all voxels and also provides the standard deviation (SD).

One must be particularly careful not to overlook beam-hardening artifacts **(Fig. 19.2)** or partial volume effects. If a mass does not extend through the entire thickness of a slice, measurements of density will include the tissue next to it **(Figs. 121.2** and **133.1–133.3)**. The density of a mass will be measured correctly only if it fills the entire thickness of the slice **(d_S) (Fig. 15.2)**. It is then more likely that measurements will include only the mass (hatched area in **Fig. 15.2a**). If d_S is greater than the mass's diameter, for example a small lesion in an unfavorable position, it can only appear in partial volume at any scan level **(Fig. 15.2b)**.

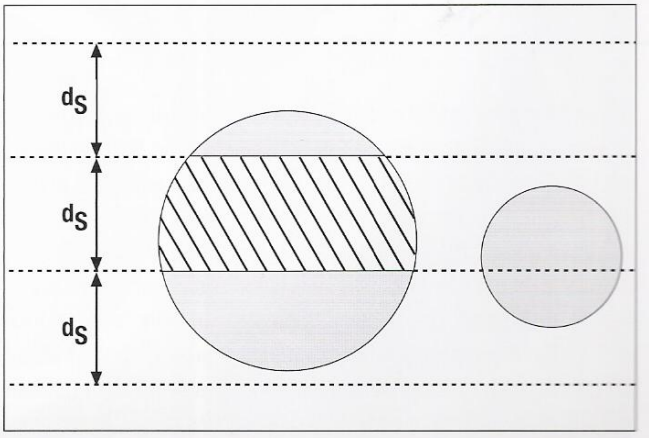

Fig. 15.2 a b

Density Levels of Different Types of Tissues

Modern equipment has a capacity of 4096 gray tones, which represent different density levels in HUs. The density of water was arbitrarily set at 0 HU and that of air at −1000 HU **(Table 16.1a)**. The monitor can display a maximum of 256 gray tones. However, the human eye is able to discriminate only approximately 20. Since the densities of human tissues extend over a fairly narrow range (a window) of the total spectrum **(Table 16.1b)**, it is possible to select a window setting to represent the density of the tissue of interest.

The mean density level of the window should be set as close as possible to the density level of the tissue to be examined. The lung, with its high air content, is best examined at a low HU window setting **(Fig. 17.1c)**, whereas bones require an adjustment to high levels **(Fig. 17.2c)**. The width of the window influences the contrast of the images: the narrower the window, the greater the contrast since the 20 gray tones cover only a small scale of densities.

Table 16.1a Density of all tissues

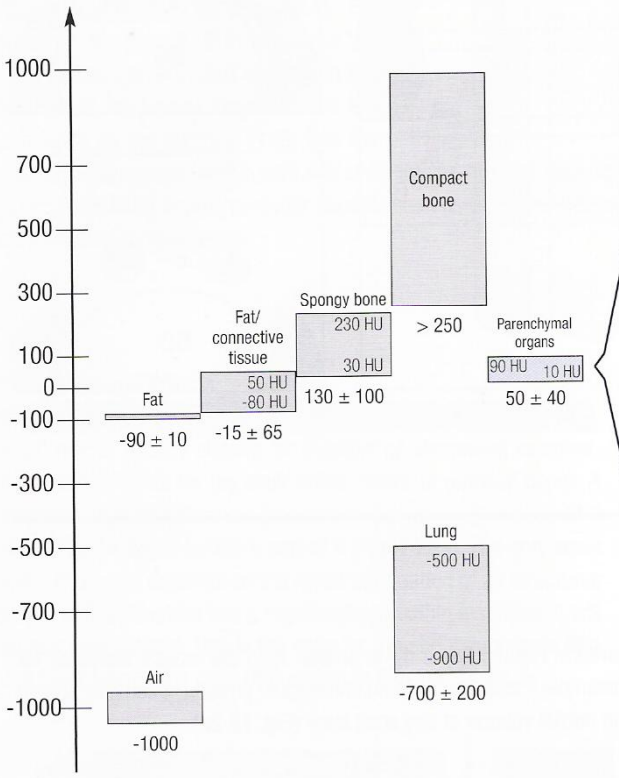

Table 16.1b Density of parenchymal organs and fluids

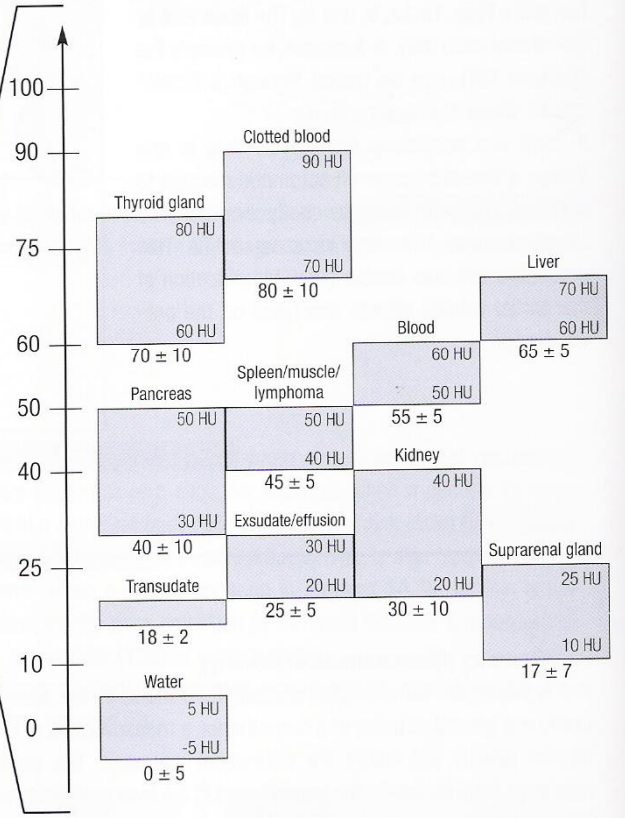

It is noteworthy that the density levels of almost all soft-tissue organs lie within a narrow range between 10 and 90 HUs **(Table 16.1b)**. The only exception is the lung and, as mentioned above, this requires a special window setting **(Figs. 17.1a–c)**. With respect to hemorrhages, it should be taken into account that the density level of recently coagulated blood lies about 30 HU above that of fresh blood. This density drops again in older hemorrhages or liquefied thromboses. An exudate with a protein content above 30 g/l cannot be readily distinguished from a transudate (protein content below 30 g/l) at conventional window settings. In addition, the high degree of overlap between the densities of, for example, lymphomas, spleen, muscles, and pancreas makes it clear that it is not possible to deduce, from density levels alone, what substance or tissue is present.

Finally, standard density values also fluctuate between individuals, depending as well on the amount of CM in the circulating blood and in the organs. The latter aspect is of particular importance for the examination of the urogenital system, since i.v. CM is rapidly excreted by the kidney, resulting in rising density levels in the parenchyma during the scanning procedure. This effect can be put to use when judging kidney function (see **Fig. 135.1**).

Documentation of Different Windows

When the images have been acquired, a hard copy is printed for documentation. For example: in order to examine the mediastinum and the soft tissues of the thoracic wall, the window is set such that muscles **(13, 14, 20–26)**, vessels **(89, 90, 92…)**, and fat are clearly represented in shades of gray. The soft-tissue window **(Fig. 17.1a)** is centered at 50 HU with a width of about 350 HU. The result is a representation of density values from –125 HU (50–350/2) up to +225 HU (50 + 350/2). All tissues with a density lower than –125 HU, such as the lung, are represented in black. Those with density levels above +225 appear white and their internal structural features cannot be differentiated.

If lung parenchyma is to be examined, for example when scanning for nodules, the window center will be lower at about –200 HU, and the window wider (2000 HU). Low-density pulmonary structures **(96)** can be much more clearly differentiated in this so-called lung window **(Fig. 17.1c)**.

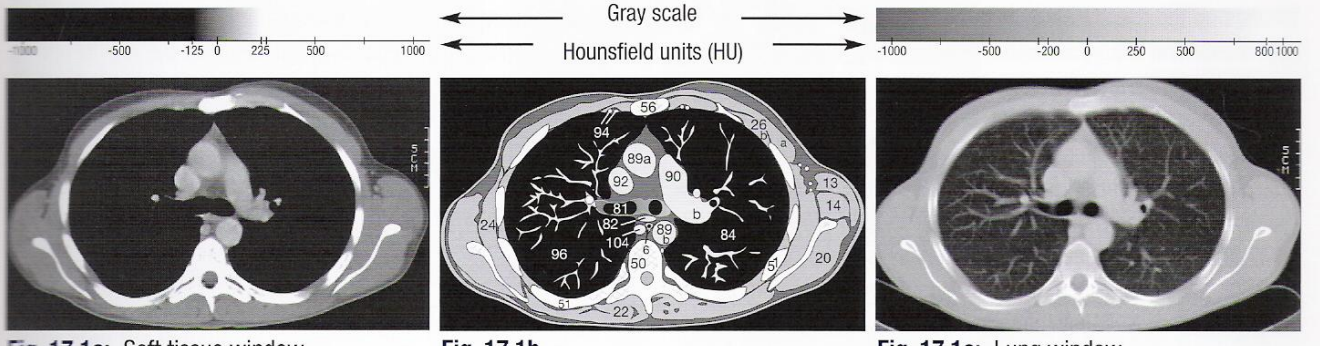

Fig. 17.1a: Soft tissue window

Fig. 17.1b

Fig. 17.1c: Lung window

In order to achieve maximal contrast between gray and white matter in the brain, it is necessary to select a special brain window because the density values of gray and white matter differ only slightly. The brain window must be very narrow (80 to 100 HU => high contrast) and the center must lie close to the mean density of cerebral tissue (35 HU) to demonstrate these slight differences **(Fig. 17.2a)**. At this setting it is of course impossible to examine the skull since all structures hyperdense to 75–85 HU appear white. The bone window should therefore have a much higher center, at about +300 HU, and a sufficient width of about 1500 HU. The metastases **(7)** in the occipital bone **(55d)** would only be visible in the appropriate bone window **(Fig. 17.2c)**, but not in the brain window **(Fig. 17.2a)**. On the other hand, the brain is practically invisible in the bone window; small cerebral metastases would not be detected. One must always be aware of these technical aspects, especially since hard copies are not usually printed at each window setting. The examiner should review thoroughly the images on the screen in additional windows to avoid missing important pathologic features. Examination of the liver poses special problems and is dealt with separately on page 120.

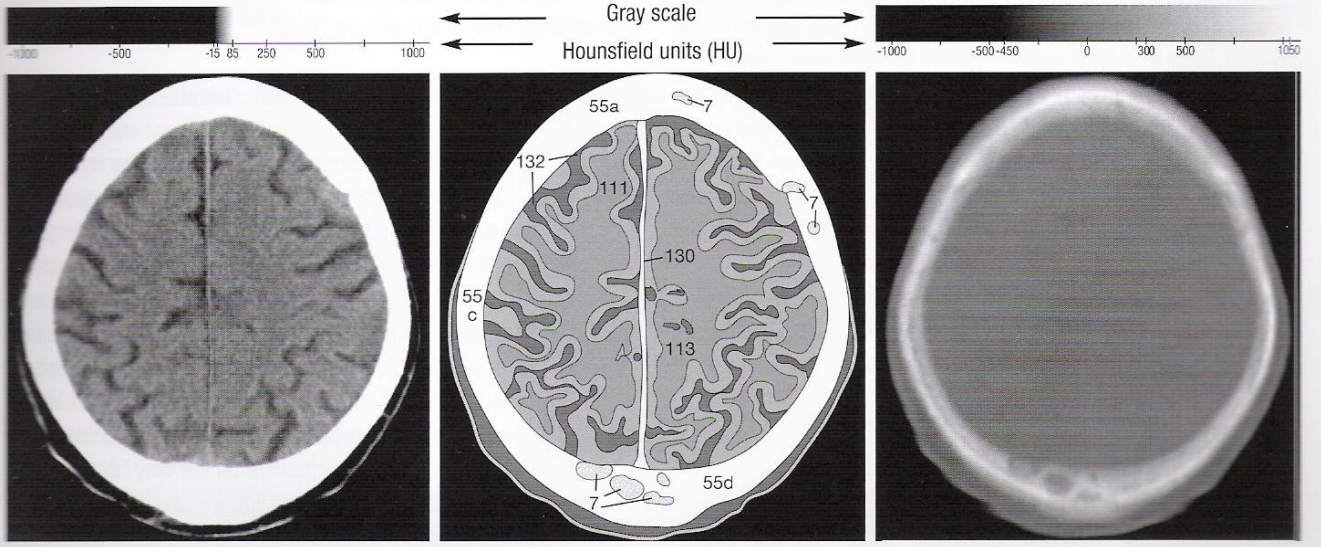

Fig. 17.2a: Brain window

Fig. 17.2b

Fig. 17.2c: Bone window

Medical History

Prior to any CT examination, a thorough medical history needs to be obtained which focuses on factors that may represent a contraindication to contrast media use or indicate an increased likelihood of a reaction. In patients with suspected renal dysfunction baseline blood urea nitrogen and creatinine levels should be obtained (see below). It is important to note whether prior CT images are available for comparison. Information about prior surgery and radiation therapy in the anatomic region to be examined by CT is also important. Careful consideration of the pertinent radiologic findings on the current study in context with prior results and the patients clinical history allow the radiologist to render a meaningful differential diagnosis.

Renal Function

With the exception of few (such as stone protocol, fracture assessment) most CT exams require the i.v. administration of iodinated contrast agents for adequate assessment of the clinical question at hand. Since contrast agents are excreted by the kidneys and may cause changes in renal hemodynamics and tubular toxicity [8], the physician should evaluate the patient's renal function by measuring the plasma creatinine prior to CT. If results suggest renal dysfunction, contrast agents should only be given in a very narrow range of indications [9, 10]. Furthermore, the use of low osmolality iodinated contrast is associated with a lower risk of renal toxicity and should be considered under this circumstance. Adequate patient hydration is also an important adjunct measure. Lastly, administration of acetylcysteine in form of tablets (Mucomyst ®) has shown a renoprotective effect in some studies. Diabetic patients on metformin therapy, an oral antihyperglycemic medication, must be given special attention [8, 9]. In these patients, contrast agents may cause lactic acidosis especially when there is coexisting renal dysfunction. Therefore it is recommended to withhold metformin on the day of the exam and the following 48 hours and to reinstate therapy after repeat serum creatinine measurement has confirmed stable renal function. Until recently, in cases where contrast agents was absolutely necessary for a dialysis patient, the CT examination was scheduled so that dialysis followed immediately. Recent reports, however, show that there is no need for urgent dialysis [11]. However, residual renal function in a dialysis patient can suffer from circulating contrast. Otherwise there seem to be no other complications if the contrast agent circulates for a day or two until the next dialysis.

Creatinine levels can be checked quickly and are inexpensive; In order to save time you may want to have the result available on the requisition for the exam for immediate review by the radiologist when prescribing the exam protocol.

Hyperthyroidism

Examining for hyperthyroidism is costly and time-consuming. Nevertheless, the referring physician must exclude hyperthyroidism if there is such a clinical suspicion before a CT examination involving CONTRAST AGENTS is carried out. Laboratory parameters and possibly scintigraphy may be necessary. In other cases, the information "no clinical evidence of hyperthyroidism" or even better, the documentation of thyroid function on the requisition is helpful. Thus, the radiologist can be sure that testing has been done. Note that reference values **(Table 18.1)** may vary from one laboratory to another. Check with your laboratory about commonly used units and normal ranges if these are not included on the report. The risk of thyrotoxicosis caused by the iodinated contrast agents can thus be avoided. If radioiodine therapy for hyperthyroidism or thyroid cancer is planned, the i.v. application of contrast agents could lead to a saturation of the iodine uptake system in the thyroid gland for several weeks. Radioiodine therapy may have to be delayed for some time as a result.

Table 18.1 Normal thyroid hormone levels

TSH:	0.23 – 4.0 pg / ml		
TT_3:	0.8 – 1.8 ng / ml	TT_4:	45 –115 ng / ml
FT_3:	3.5 – 6.0 pg / ml	FT_4:	8.0 – 20.0 pg / ml

Adverse Reactions to Contrast Media

Ever since nonionic contrast agents were introduced at the end of the 1970s, adverse reactions have only rarely been encountered [12–14]. Nevertheless, previous reactions are a pointer to an increased risk and should be elicited by taking a careful medical history. The severity of any reaction to contrast agents in the past is of great importance. If the patients give a history of itching or hives following prior contrast administration, premedication is advisable. With a history of hypotension or cardiovascular collapse, contrast agents should not be given at all or only after thorough assessment of the clinical indication and appropriate premedication. As a general rule, patients who require premedication because of a previous reaction should be kept NPO 6 hours prior to the examination. This reduces risk of aspiration in case of severe anaphylactic reaction requiring intubation and ventilation (for detailed information see pp. 24-25).

Premedication (history of previous adverse reactions to contrast agents) In cases of mild adverse reactions, premedication is accomplished with three oral doses of Prednisone, 50 mg each, taken 13, 8 and 1 hour before the examination. In addition, 50 mg of intramuscular antihistamine drug (e.g. Benadryl) is given 1 hour before the exam. Side effects such as raised intraocular pressure or urinary retention may occur. In addition, drowsiness may occur for about 8 hours following administration of these drugs so driving must be avoided for this period. If an outpatient CT examination is scheduled, the patient must be informed about potential drowsiness and the possibility of temporarily impaired vision; he or she should be accompanied on the way home.

You will find checklists of all key words concerning medical histories and suggestions for premedication on a practical card in the rear foldout.

Oral Administration of Contrast Agents

After a period of fasting, liquid contrast agents should be drunk in small portions over a period of 30–60 minutes before the CT examination starts so that the entire GIT is completely opacified. The patient should therefore arrive at least 1 hour before an abdominal CT examination. In order to facilitate the correct choice of contrast agent, the radiologist must be informed on the request card whether surgery is planned shortly after CT or whether there is any suspicion of perforation or fistula (see also p. 20). In such cases water-soluble gastrografin would be used instead of a contrast agent containing barium sulfate. And finally, where possible, CT of the abdomen should be delayed for 3 days after a conventional barium examination has been carried out (for example: barium swallow, barium meal, small bowl enema, barium enema). Usually, the digital projection radiograph (scanogram **Fig. 19.1a**, scout view) would show that residual barium in the GIT would result in major artifacts **(Fig. 19.1b)**, rendering CT valueless. The sequence of diagnostic procedures for patients with abdominal diseases should therefore be carefully planned.

Fig. 19.1a

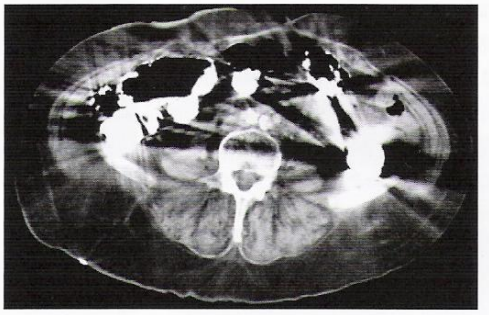

Fig. 19.1b

Informing the Patient

Understandably, patients have doubts about the harmful effects of the x-ray burden involved in CT. Worries can usually be reduced if you relate diagnostic x-ray exposure to natural background radiation. Naturally, the patient must have the feeling that he or she is being taken seriously and his or her worries are understood, otherwise confidence and trust in the radiologist are threatened. Many patients are relieved to know that they can communicate with the radiographers in the control room via an intercom and that the examination can be interrupted or terminated at any time if there are unexpected problems. Patients with claustrophobia may feel more comfortable if they close their eyes during the examination; the close proximity of the gantry is then less of a problem. In very rare cases, a mild sedative may be helpful.

Respiration

Before starting the examination, the patient should be told of the need for controlled breathing. For conventional CT, the patient is instructed to breathe before each new image acquisition and then to hold his or her breath for a few seconds. In the helical technique it is necessary to stop breathing for about 20–30 seconds. If the patient cannot comply, diaphragmatic movement will lead to image blur with a marked deterioration in image quality **(Fig. 19.2)**. In the case of neck examinations, swallowing influences the quality of the images more than breathing.

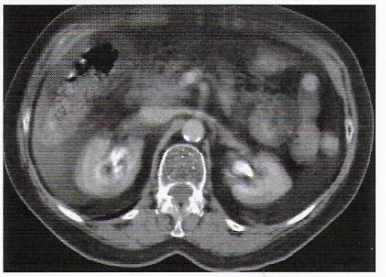

Fig. 19.2

Removal of all Metallic Objects

Naturally, jewelry of any kind and removable dental prostheses must be removed before the head or neck are examined in order to avoid artifacts. In **Figures 19.3a** and **b**, the effects of such artifacts **(3)** are obvious. Only the cervical vertebral body **(50)** and the adjacent vessels **(86)** are defined; the other structures are unrecognizable. For the same reason all clothing with metallic hooks, buttons, or zippers should be removed before thoracic or abdominal CTs are performed.

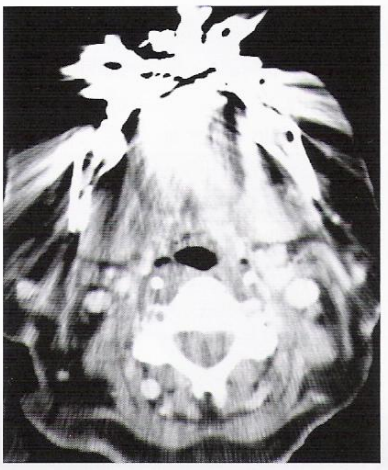

Fig. 19.3a

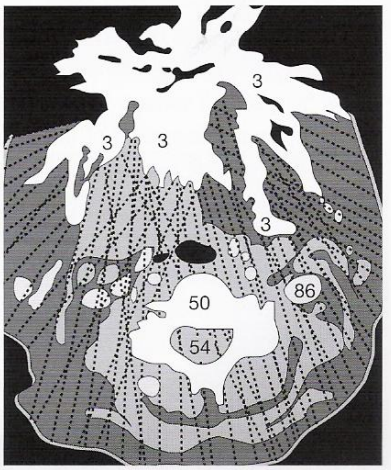

Fig. 19.3b

Oral Administration of Contrast Agents

For CT examination of the abdomen and pelvis, it is of major advantage to be able to readily differentiate the GIT from adjacent muscles or other organs. This can be accomplished by opacifying the intestinal lumen with an orally administered contrast agent. For example, without of contrast agent it is difficult to distinguish between the duodenum **(130)** and the head of the pancreas (**131** in **Fig. 20.1**).

Equally, other parts of the intestinal tract **(140)** would also be very similar to neighboring structures. After an oral contrast agent, both the duodenum and the pancreas can be well delineated **(Fig. 20.2a, b)**. In order to acquire images of optimal quality, the patient should fast (be NBM) before drinking contrast agents.

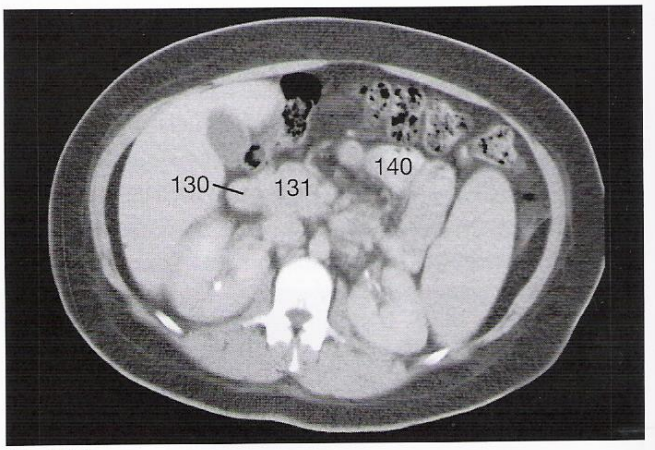

Fig. 20.1

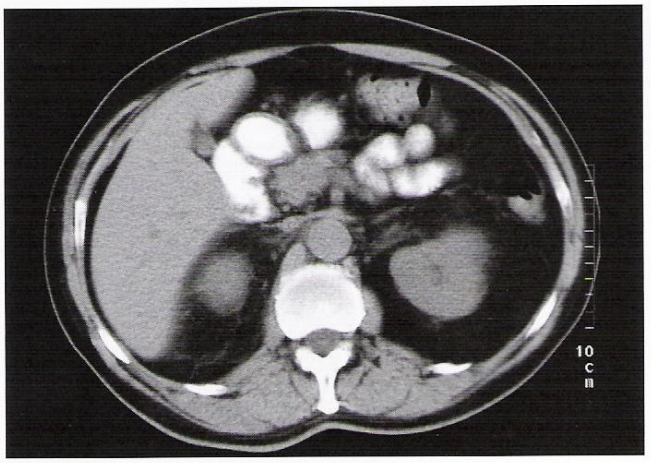

Fig. 20.2a

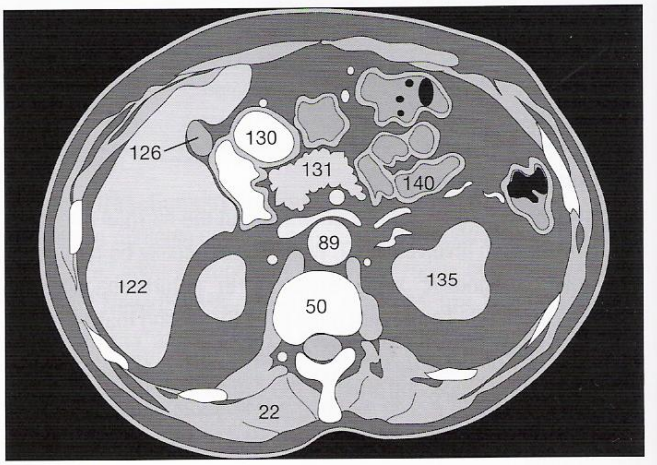

Fig. 20.2b

Choice of the Appropriate Contrast Agents

The best coating of the mucous membranes is achieved with barium sulfate; however, this is not water soluble. This oral contrast agent should therefore not be used if abdominal surgery involving opening of the bowel lumen is scheduled, such as in partial resections or anastomotic sutures, or if there is any risk of injury to the bowel. Neither should barium sulfate be used in cases of a suspected fistula or a GIT perforation. A watersoluble contrast agent, such as gastrografin, is then employed; it can be resorbed by the body after it spreads into the abdominal cavity.

For an optimal assessment of the stomach walls, plain water is increasingly used as a hypodense contrast agent in combination with intravenous buscopan, which relaxes the muscularis [15, 16]. If the urinary bladder has been removed and an ilial conduit constructed, the abdomen is examined first with an intravenous contrast agent which is excreted into the urine in the conduit but not within the native intestines. If necessary, the intestines can be examined in a second scan after oral contrast agents.

The Time Factor

To opacify the proximal parts of the GIT, a period of about 20–30 min is sufficient; the patient swallows the contrast agent in several small portions. However, if the entire colon and especially the rectum need to be opacified with barium sulfate, a period of at least 45–60 min is necessary in a fasting patient. The water-soluble contrast agent gastrografin spreads somewhat more rapidly. For the pelvic organs (bladder, cervix, or ovary), 100–200 ml of contrast agent may be given rectally to insure that tumors are clearly differentiated from the lower intestinal tract.

Dosage

To achieve complete opacification of the entire GIT, 250–300 ml of a barium sulfate suspension are dissolved and thoroughly mixed with water (1000 ml). For adequate contrast of the entire GIT, 10–20 ml of water-soluble gastrografin (in 1000 ml of water) are enough.

If only the upper part of the GIT needs to be opacified, 500 ml of either medium are sufficient.

Intravenous Contrast Agents

An increase in the density of blood vessels not only demarcates them better from muscles and organs but also provides information on the rate of blood perfusion (contrast agent uptake) in pathologically altered tissues: disturbances of the blood-brain barrier, the borders of abscesses, or the inhomogeneous uptake of contrast agents in tumorlike lesions are only a few examples. This phenomenon is called contrast enhancement, i.e. the density is increased by the contrast agent and thus the signal intensified.

Depending upon the question being asked, an unenhanced (plain) scan should be obtained before injecting the contrast agents intravenously. Vascular grafts, inflammatory processes in bone, as well as abscess walls are more easily diagnosed if unenhanced images can be compared with contrast-enhanced images. The same holds true for focal liver lesions examined using conventional CT techniques. If helical CT is available, a series of liver images in the early phase of arterial contrast agent perfusion followed by a series in the phase of venous drainage [17] would be obtained instead of unenhanced images. This procedure makes it possible to detect even small focal lesions (see p. 120).

Preparing the i.v. Line

The contrast agents are injected intravenously, and the bolus becomes longer and diluted as it passes through the pulmonary circulation. The injection should therefore ideally have a rapid flow rate of 2–6 ml / sec for achieving sufficient density enhancement of the vessels [18]. A Venflon canula with a diameter of at least 1.0 mm (20G), or preferably 1.2–1.4 mm (18G–17G), is used. Checking that the canula is correctly sited in the vessel is very important. A trial injection of sterile saline at a high flow rate into the vein should be carried out before injecting contrast agents. The absence of subcutaneous swelling confirms proper positioning; the fact that the vein can accommodate the intended flow can also be confirmed.

Dosage

Dosage is calculated on the basis of b.w. and according to the diagnostic question at hand: examinations of the neck or of an aortic aneurysm (for example in order to exclude the presence of a dissection flap), require higher concentrations than cranial CTs. When tolerance to contrast agents and optimal vessel contrast are balanced, a dosage of, for example, 1.2 ml/kg b.w. at a concentration of 0.623 g Iopromid/ml in general provides good results.

Inflow Phenomena

The streaming artifact of enhanced and unenhanced blood results from a short interval between the start of injection and the onset of data acquisition. Since inflow is usually from one side via the axillary, subclavian, and brachiocephalic veins **(91)** into the superior vena cava **(92)**, there is an apparent filling defect within the vena cava **(Figs. 21.1a–21.3b)**. Knowing about such inflow phenomena avoids a false positive diagnosis of venous thrombosis. Using too high concentrations of contrast agents in this area could result in disturbing artifacts, especially with the helical technique **(Fig. 23.3a)**. More inflow phenomena will be described on the next pages.

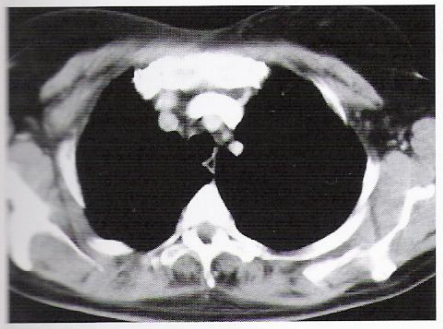

Fig. 21.1a

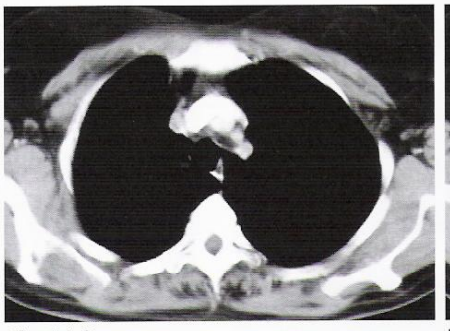

Fig. 21.2a

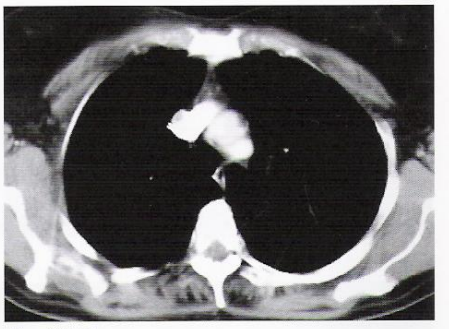

Fig. 21.3a

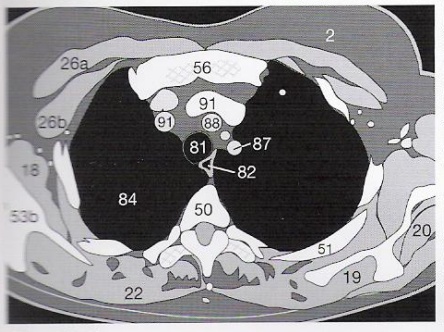

Fig. 21.1b

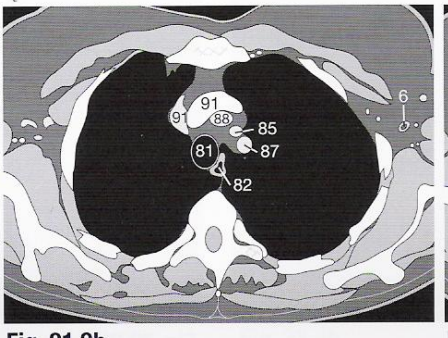

Fig. 21.2b

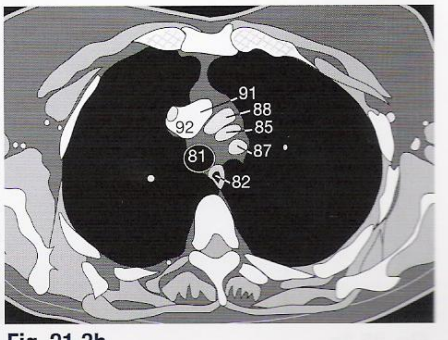

Fig. 21.3b

Application of Contrast Agents

Flow phenomena can also be seen in the inferior vena cava **(80)** at the level of the renal veins **(111)**. These veins may contain blood which has a fairly high concentration of contrast agents and this blood mixes with unenhanced blood returning from the lower extremities and pelvic organs. In the early post-contrast phase the vena cava **(80)** caudal to the level of the renal veins is hypodense relative to the adjacent aorta **(89)** as in **Figures 22.1a, b**.

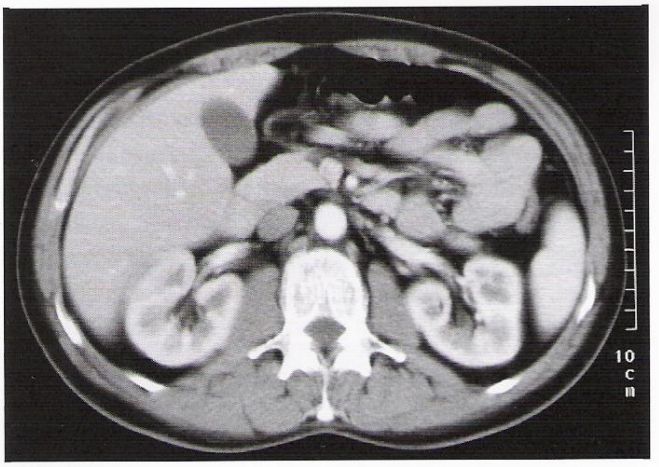

Fig. 22.1a

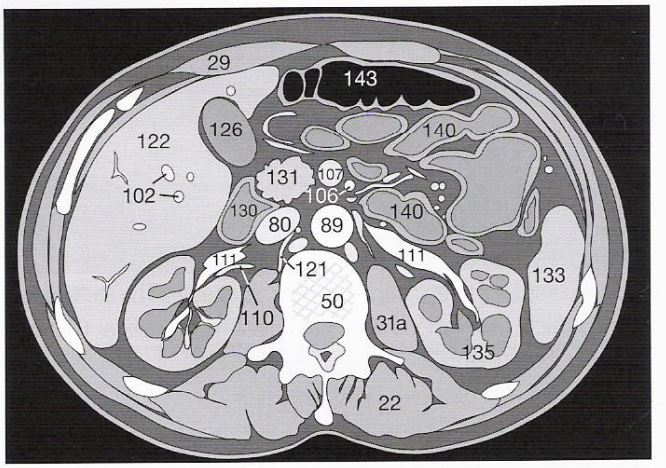

Fig. 22.1b

Immediately above the renal veins, the contents of the inferior vena cava may appear bilaterally enhanced by the blood from the kidneys whereas the central part is still unenhanced **(Fig. 22.2a, b)**. If the renal veins do not empty into the cava at the same level or if a kidney has been removed, a unilateral enhancement may occur **(Fig. 22.3a, b)**. Such differences in density should not be mistaken for thrombosis of the inferior cava (cf. **Figs. 23.1** and **144.1**).

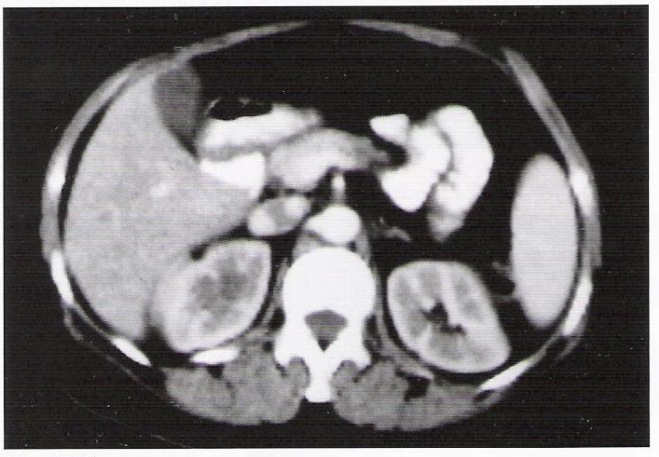

Fig. 22.2a

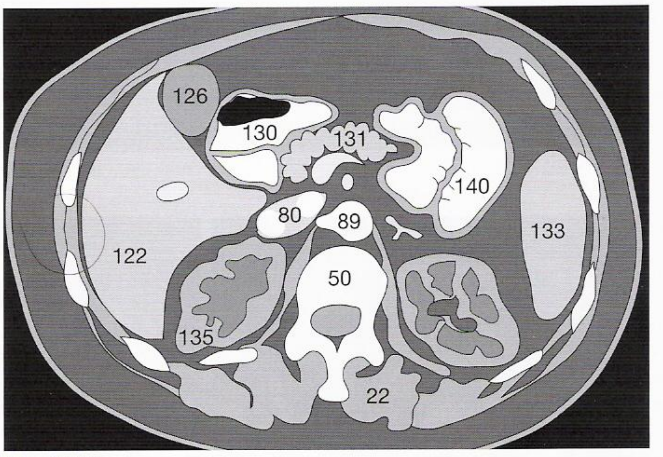

Fig. 22.2b

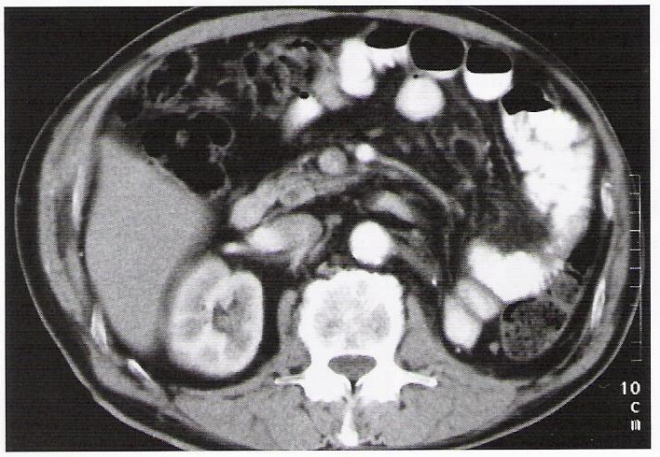

Fig. 22.3a

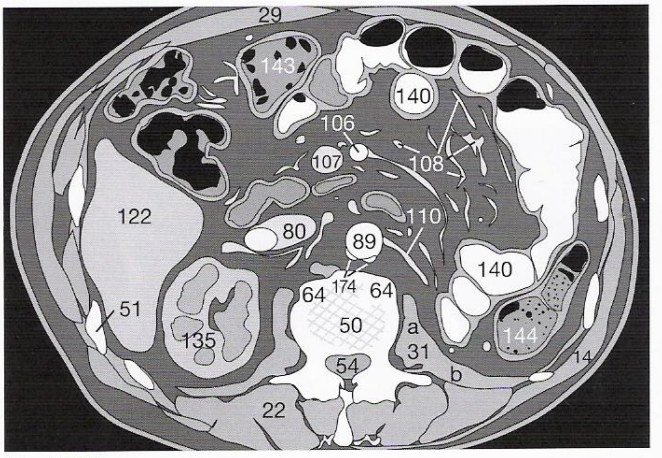

Fig. 22.3b

Flow Phenomena

If we trace the inferior vena cava cranially toward the right atrium, additional flow phenomena become apparent as more veins empty into it. The cava has spiraling eddies of inhomogeneous density (➡ in **Fig. 23.1**) caused by mixing of the blood as described on the previous page. Moments later such inhomogeneities are no longer evident in the lumen **(80)** and density levels are identical to those in the aorta **(89) (Fig. 23.2a, b)**.

By the way, did you notice the artherosclerotic plaque in the dorsal wall of the aorta (**174** in **89** in **Fig. 22.3a**)? This plaque appears also in **Figure 23.2a**. The patient had well-developed osteophytes **(64)** on the vertebral bodies **(50)**.

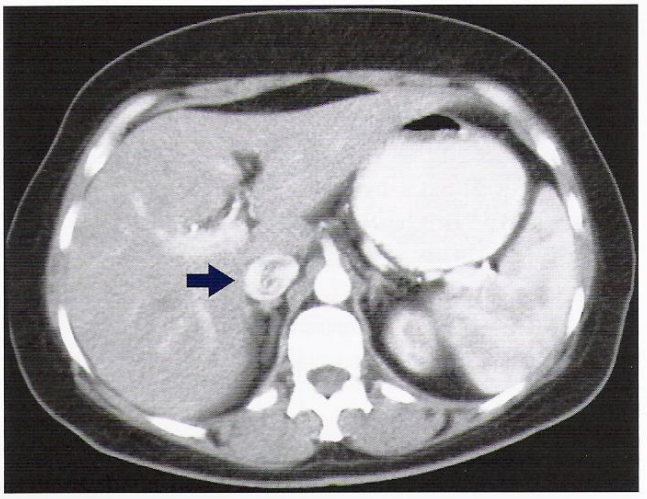

Fig. 23.1

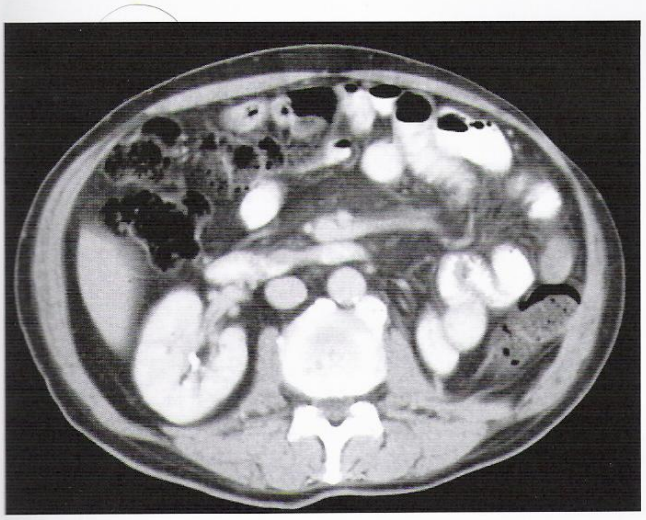

Fig. 23.2a

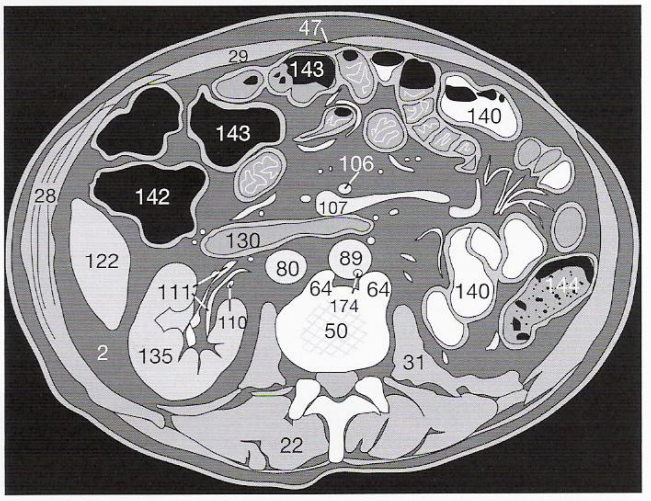

Fig. 23.2b

Details Specific for Spiral CT

If data acquisition begins immediately after contrast agents have been administered, the concentration of contrast agents in the axillary, subclavian, and brachiocephalic **(91)** veins might be high enough to cause major artifacts **(3)** in the thoracic inlet. In images such as in **Figure 23.3**, it is not possible to assess the lung or neighboring axillary tissues. An SCT of the thorax should therefore be obtained from caudal to cranial. In that way structures near the diaphragm are imaged first, and when cranial parts are scanned the contrast agents will have been spread after having passed the pulmonary circulation. This trick helps avoid the artifacts **(3)** shown in **Figure 23.3**.

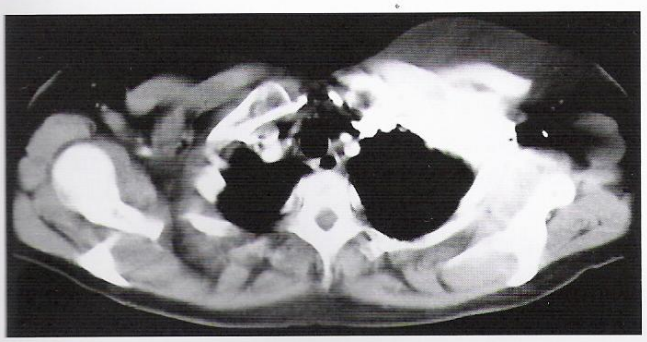

Fig. 23.3a

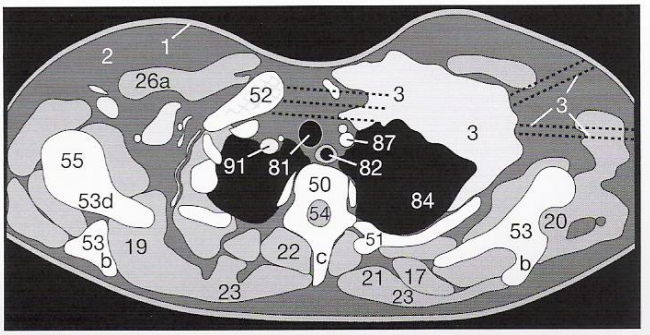

Fig. 23.3b

Administration of Contrast Agents

Adverse Reactions to Contrast Agents

Adverse reactions are rare; most appear during the first 30 minutes, 70% of cases occur within the first 5 minutes after contrast injection [13]. Only high-risk patients need to be supervised for more than 30 minutes. Since such patients can usually be recognized by taking a thorough medical history, they can be premedicated accordingly (see p. 14).

If, despite precautions, erythema develops after an i.v. injection of contrast agents, perhaps also hives, itching, nausea or vomiting, or in extreme cases even hypotension or circulatory shock or shortness of breath, the countermeasures listed below must be initiated immediately. Remember that i.v. injection of H_1- and H_2-receptor antagonists does not alleviate symptoms immediately. There is a period of latency, and these antagonists are therefore primarily effective in preventing the symptoms from worsening. Serious incidents (pulmonary edema, circulatory shock, convulsions) occur very rarely with the new contrast media; they require immediate intensive care.

Be sure to document any incident in your report. Radiologists performing future examinations will be forewarned about the patient's sensitivity to contrast agents.

Management of Acute Reactions in Adults

Urticaria

1 Discontinue injection if not completed
2 No treatment needed in most cases
3 Give H_1-receptor blocker: Diphenhydramine (Benadryl®)
PO / IM / IV 25-50 mg
If severe or widely disseminated:
Alpha agonist (arteriolar and venous constriction)
Epinephrine SC (1:1,000) 0.1-0.3 ml = 0.1-0.3 mg
(if no cardiac contraindications)

Facial or Laryngeal Edema

1 Give alpha agonist (arteriolar and venous constriction):
Ephinephrine SC or IM (1:1,000) 0.1-0.3 ml (= 0.1-0.3 mg)
or, if hypotension evident,
Epinephrine (1:10,000) slowly IV 1 ml (= 0.1 mg)
Repeat as needed up to a maximum of 1mg
2 Give O_2 6-10 liters / min (via mask)
If not responsive to therapy or if there is obvious acute laryngeal edema, seek appropriate assistance (e.g., cardiopulmonary arrest response team)

Bronchospasm

1 Give O_2 6-10 liters / min (via mask)
Monitor: electrocardiogram, O_2 saturation (pulse oximeter), and blood pressure.
2 Give beta-agonist inhalers: bronchiolar dilators, such as metaproterenol (Alupent®), terbutaline (Brethaire®), or albuterol (Proventil®, Ventolin®) 2-3 puffs; repeat prn.
If unresponsive to inhalers, us SC, IM or IV epinephrine
3 Give epinephrine SC or IM (1:1,000) 0.1-0.3 ml
(= 0.1-0.3 mg) or, if hypotension evident,
Epinephrine (1:10,000) slowly IV 1 ml (= 0.1 mg)
Repeat as needed up to a maximum of 1 mg

Alternatively:
Give aminophylline: 6 mg / kg IV in D5W over 10-20 minutes (loading dose), then 0.4-1 mg / kg / hr, as needed (caution: hypotension)

Call for assistance (e.g., cardiopulmonary arrest response team) for severe bronchospasm or if O_2 saturation < 88% persists.

Hypotension with Tachycardia

1 Legs elevated 60° or more (preferred)
or Trendelenburg position
2 Monitor: electrocardiogram, pulse oximeter, blood pressure
3 Give O_2 6-10 liters / min (via mask)
4 Rapid intravenous administration of large volumes of isotonic Ringer's lactate or normal saline.

If poorly responsive:
Epinephrine (1:10,000) slowly IV 1 ml (= 0.1 mg)
(if no cardiac contraindications)
Repeat as needed up to a maximum of 1 mg

If still poorly responsive seek appropriate assistance (e.g., cardiopulmonary arrest response team)

Management of Acute Reactions in Adults

Hypotension with Bradycardia
(Vagal Reaction)

1. Monitor vital signs
2. Legs elevated 60° or more (preferred) or Trendelenburg position
3. Secure airway: give O_2 6-10 liters / min (via mask)
4. Secure IV access: rapid fluid replacement with Ringer's lactate or normal saline
5. Give atropine 0.6 mg IV slowly if patient does not respond quickly to steps 2-4
6. Repeat atropine up to a total dose of 0.04 mg / kg (2-3 mg) in adult
7. Ensure complete resolution of hypotension and bradycardia prior to dischange

Hypertension, Severe

1. Give O_2 6-10 liters / min (via mask)
2. Monitor electrocardiogram, pulse oximeter, blood pressure
3. Give nitroglycerine 0.4-mg tablet, sublingual (may repeat x3) *or* topical 2% ointment, apply 1 in. strip
4. Transfer to intensive care unit or emergency department
5. For pheochromocytoma – phentolamine 5 mg IV

Seizures or Convulsions

1. Give O_2 6-10 liters / min (via mask)
2. Consider diazepam (Valium®) 5 mg (or more, as appropriate) or midazolam (Versed®) 0.5-1 mg IV
3. If longer effect needed, obtain consultation; consider phenytoin (Dilantin®) infusion – 15-18 mg / kg at 50 mg / min
4. Careful monitoring of vital signs required, particularly of pO_2 because of risk to respiratory depression with benzodiazepine administration
5. Consider using cardiopulmonary arrest response team for intubation if needed

Pulmonary Edema

1. Elevate torso; rotating tourniquets (venous compression)
2. Give O_2 6-10 liters / min (via mask)
3. Give diuretics – furosemide (Lasix®) 20-40 mg IV, slow push
4. Consider giving morphine (1-3 mg IV)
5. Transfer to intensive care unit or emergency department
6. Corticosteroids optional

Iodine-provoked Hyperthyroidism

Fortunately, this complication is very rare with modern non-ionic iodinated contrast agents. In patients with a medical history of hyperthyroidism consider blocking the thyroid gland before i.v. application of contrast agents by administering a thyrostatic drug such as sodium perchlorate. Alternatively, carbimazole can be used to block hormone synthesis. Both treatments take approximately 1 week to become fully effective. Effectiveness must be determined by repeating the thyroid function tests.

In patients with unrecognized subclinical hyperthyroidism, the use of iodine containing contrast agents can unmask the disease or even induce thyrotoxicosis. The symptoms may include diarrhea, muscle weakness as well as fever, sweating, dehydration, anxiety and restlessness, or even tachyarrhythmia. The main problem is the long period of latency before the thyrotoxicosis crisis becomes manifest.

"Some patients with hyperthyroidism or other thyroid disease (especially those who live in iodine-deficient areas) may develop iodine-provoked delayed hyperthyroidism. This effect may appear 4 to 6 weeks after the intravascular contrast administration in some of these patients. It can occur after the administration of either ionic, high- osmolality or nonionic, low-osmolality contrast. It is usually self-limited.

Patients with carcinoma of the thyroid deserve special consideration before the intravascular or oral administration of iodinated contrast media (ionic or nonionic). Uptake of I-131 in the thyroid becomes moderately decreased to about 50% at one week after iodinated contrast injection but seems to become normal within a few weeks. Therefore, if systemic radioactive iodine therapy is part of planned treatment, a pretherapy diagnostic study of the patient using iodinated radiographic contrast medium (intravascular or oral) may be contraindicated; consultation with the ordering clinician prior to contrast administration in these patients is recommended."

Many cranial CT (CCT) examinations can be performed without injection of contrast medium: For instance, the differential diagnosis (DD) of cerebral bleeding versus infarction in patient with sudden onset of neurologic deficits does not require the administration of contrast medium. However, intravenous injection of contrast medium is necessary to detect an impaired blood-brain barrier (BBB) as found in tumors, metastases or inflammations.

Selection of the Image Plane

The desired image planes parallel to the orbitomeatal line are selected on the sagittal localizer image (topogram) **(Fig. 26.1)**. This is a readily reproducible line drawn from the supraorbital ridge to the external auditory meatus, allowing reliable comparison with follow-up CT examinations. The posterior fossa is scanned in thin sections (2-3 mm) to minimize beam hardening artifacts, and the supratentorial brain above the pyramids in thicker sections (5 mm).

The images are displayed as seen from below (caudal view) and consequently are laterally reversed, i.e., the left lateral ventricle is on the right and vice versa. Only CTs obtained for neurosurgical planning are often displayed as seen from above (right = right) since this cranial view corresponds to the neurosurgical approach for cranial trepanation.

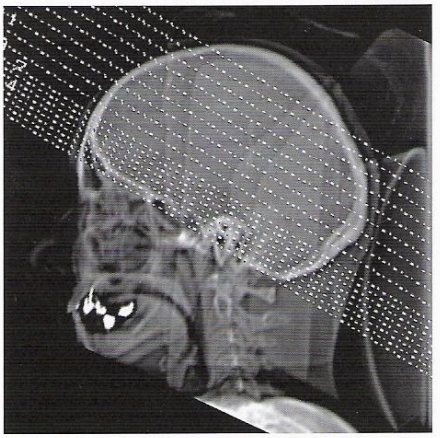

Fig. 26.1

Systematic Interpretation

Each examiner is free to find a preferred sequence for reviewing the images. This means that the examiner can choose between several acceptable approaches and is not restricted to a "one and only" strategy. However, staying with a consistent arrangement of the images to be interpreted has the advantage that fewer findings are overlooked, especially by the novice. The checklist below just contains recommendations that can serve as good guideline for the novice.

First, the size of the ventricles and extracerebral CSF spaces has to be evaluated to exclude a life threatening space-occupying process right away. Hereby, the patient's age has to be considered because of age-related widening of the CSF spaces. Any blurring of the grey-white matter junction as manifestation of cerebral edema should be looked for (see below). If a pathologic change is suspected, the adjacent sections should be inspected to avoid any misinterpretation due to a partial volume effect (see **Fig. 29.1** and **Fig. 52.2**).

Always use the legends on the front cover flap for this chapter. The listed numbers apply to all head and neck images. The subsequent pages provide you with a survey of the normal anatomy, followed by normal variants and the most frequent pathologic findings.

Checklist for Reading Cranial CT

Age? (because of the age-related width of the CSF spaces / cerebral atrophy; see page 50)		
Medical History:	• Risk factors?	(Trauma → Chance of intracranial bleeding)
		(Hypertension, diabetes, nicotine → Vascular stenoses, infarcts)
Signs of space-occupying lesion:		
	• Normal configuration of the 4th ventricle? (posterior to the pons, see pages 28 / 29)	
	• Normal configuration of the 3rd ventricle? (interthalamic, narrow / slit-like, see page 30)	
	• Normal symmetry of the lateral ventricles? (concave lateral border of the anterior horn and central ventricular region?)	
	• Midline shift? (sign of large space-occupying process)	
	• Preserved basal cistern? (e.g., quadrigeminal cistern: smilie face / bat man figure, see Fig. 30.1)	
	• Cortex ↔ white matter demarcation OK? (blurred interface = sign of edema)	
	• Width of the extracerebral CSF OK for patient's age? (Sylvian fissure, refer to p.50)	
Focal lesions:	• Unenhanced: DD physiologic calcification (choroid plexus, pineal gland / partial volume; refer to Figures 29.3 and 30.2)	
	versus genuine hyperdense bleeding (DD types of bleeding, see pages 54-57)	
	• Contrast enhanced: Sign of impaired BBB? (caused by tumors, metastases, inflammations, ...)	
Osseous lesions:	• Check cranial vault and base in bone window for osteolytic lesions / osseous infiltration	
	• In trauma patient: Rule out fractures (especially cranial base, midfacial bones – DD sutures)	

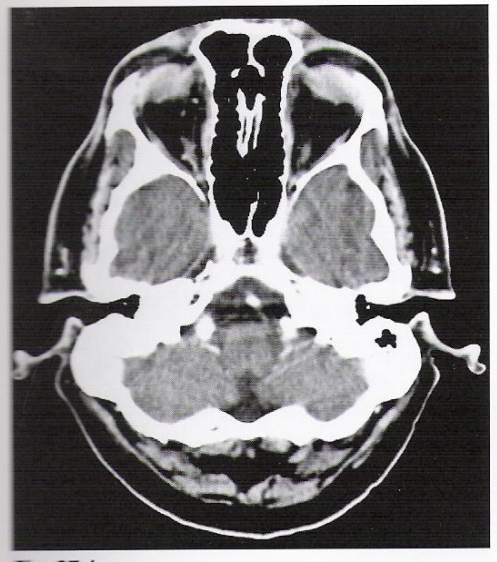

Fig. 27.1a

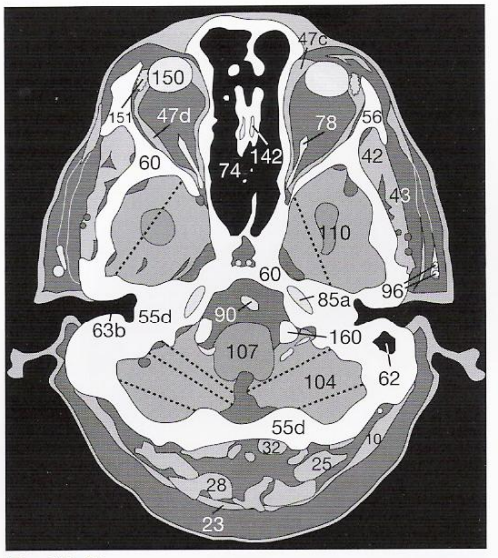

Fig. 27.1b

The scan usually begins at the base of the skull and continues upward. Since the hard copies are oriented such that the sections are viewed from caudal, all structures appear as if they were left/right reversed (see p. 14). The small topogram shows you the corresponding position of each image.

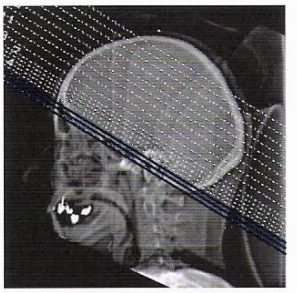

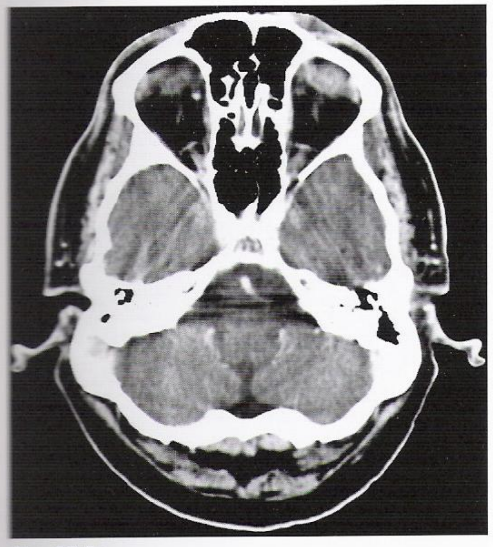

Fig. 27.2a

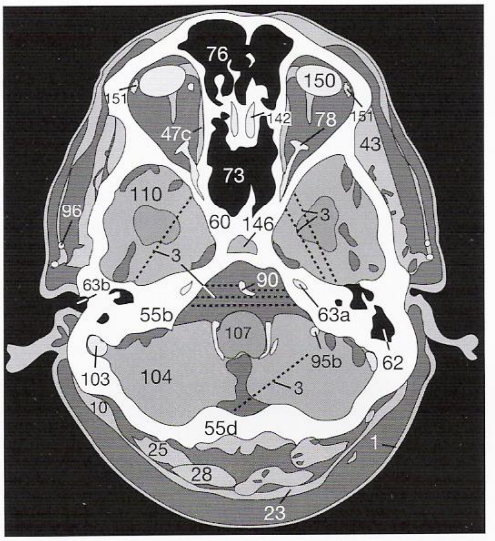

Fig. 27.2b

You should first check for any swellings in the soft tissues which may indicate trauma to the head. Always examine the condition of the basilar artery **(90)** in scans close to the base of the skull and the brainstem **(107)**. The view is often limited by streaks of artifacts **(3)** radiating from the temporal bones **(55b)**.

When examining trauma patients, remember to use the bone window to inspect the sphenoid bone **(60)**, the zygomatic bone **(56)**, and the calvaria **(55)** for fractures. In the caudal slices you can recognize basal parts of the temporal lobe **(110)** and the cerebellum **(104)**.

Orbital structures are usually viewed in another scanning plane (see pp. 33-40). In **Figure 27.1-3** we see only a partial slice of the upper parts of the globe **(150)**, the extraocular muscles **(47)**, and the olfactory bulb **(142)**.

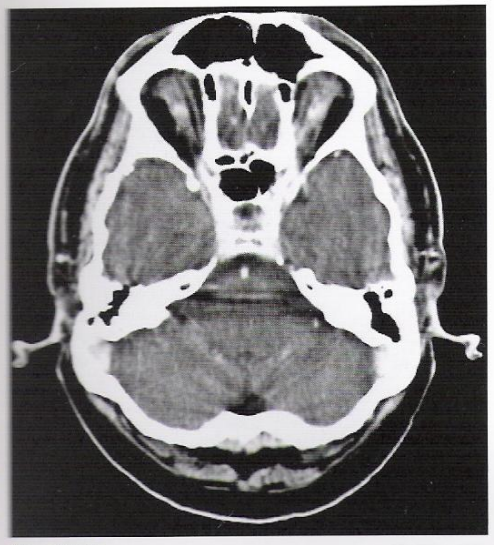

Fig. 27.3a

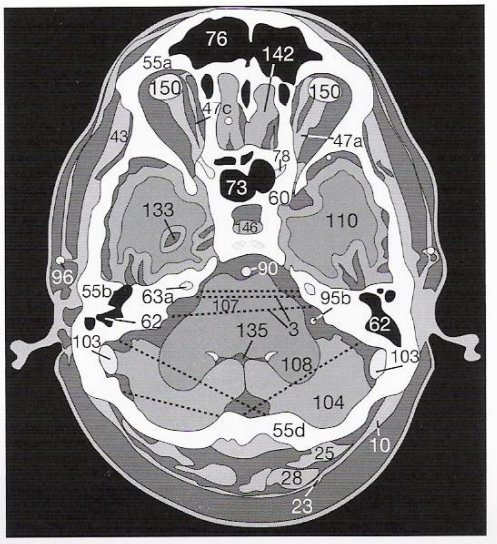

Fig. 27.3b

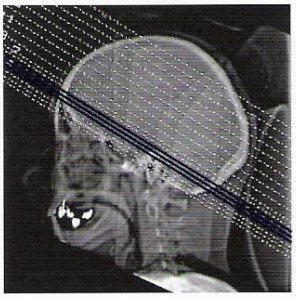

As the series of slices continues dorsally, the crista galli **(162)** and the basal parts of the frontal lobe **(111)** appear. The pons/medulla **(107)** are often obscured by artifacts **(3)**. The pituitary gland **(146)** and stalk **(147)** are seen between the upper border of the sphenoid sinus **(73)** and the clinoid process **(163)**. Of the dural sinuses, the sigmoid sinus **(103)** can be readily identified. The basilar artery **(90)** and the superior cerebellar artery **(95a)** lie anterior to the pons **(107)**. The cerebellar tentorium **(131)**, which lies dorsal to the middle cerebral artery **(91b)**, shouldn't be mistaken for the posterior cerebral artery **(91c)** at the level depicted in **Figure 29.1a** on the next page. The inferior (temporal) horns of the lateral ventricles **(133)** as well as the 4th ventricle **(135)** can be identified in **Figure 28.3**. Fluid occurring in the normally air-filled mastoid cells **(62)** or in the frontal sinus **(76)** may indicate a fracture (blood) or an infection (effusion).

A small portion of the roof of the orbit (*) can still be seen in **Figure 28.3**.

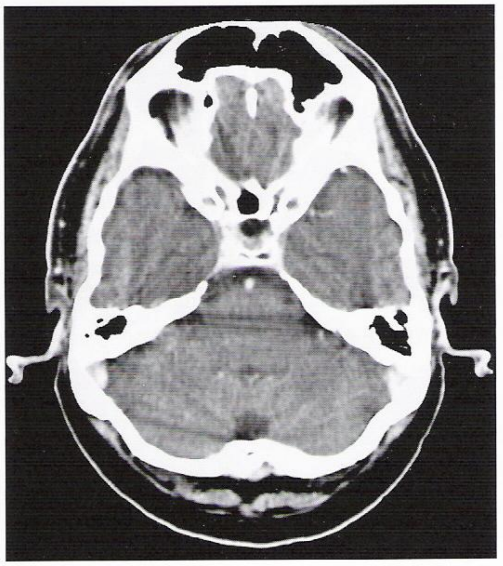

Fig. 28.1a

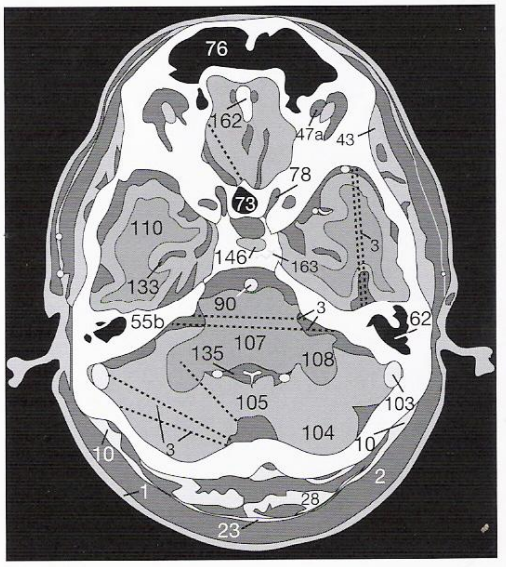

Fig. 28.1b

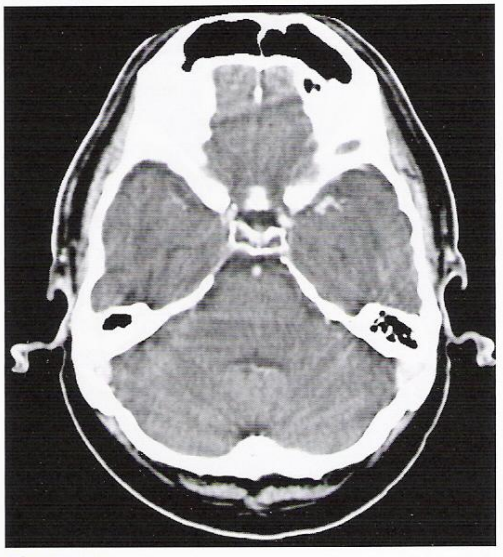

Fig. 28.2a

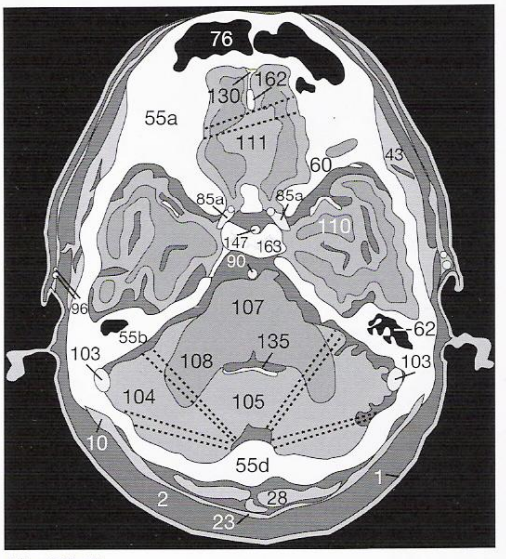

Fig. 28.2b

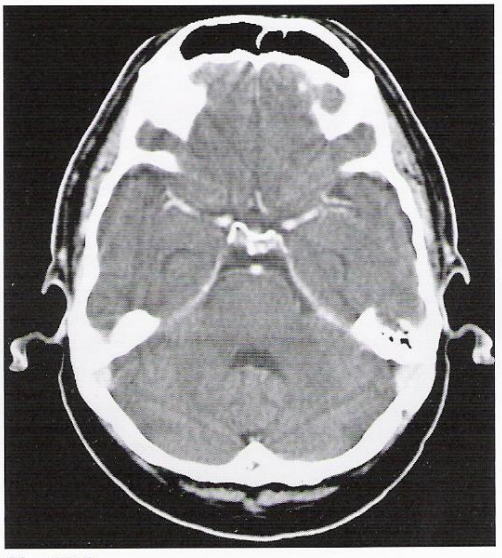

Fig. 28.3a

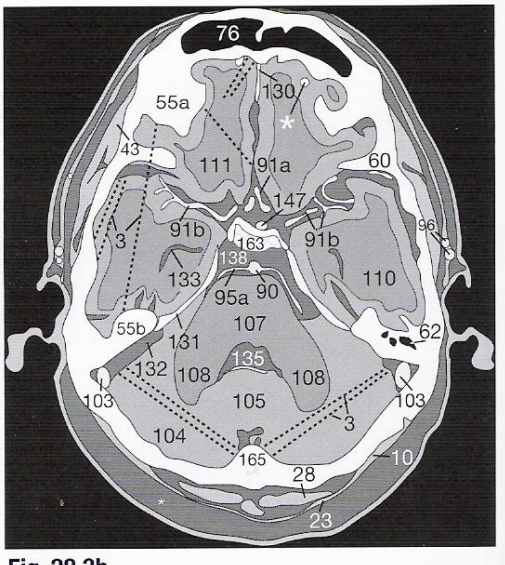

Fig. 28.3b

Fig. 29.1a

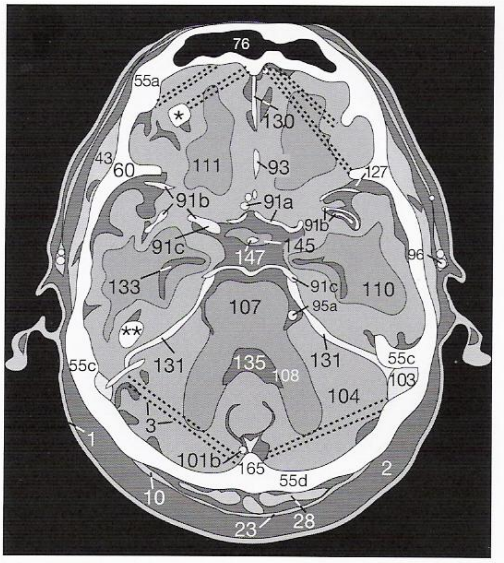

Fig. 29.1b

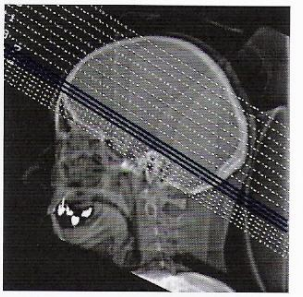

In **Figures 28.3a** and **29.1a** partial volume effects of the orbit (*) or the petrosal bone (**) might also be misinterpreted as fresh hemorrhages in the frontal **(111)** or the temporal lobe **(110)**.

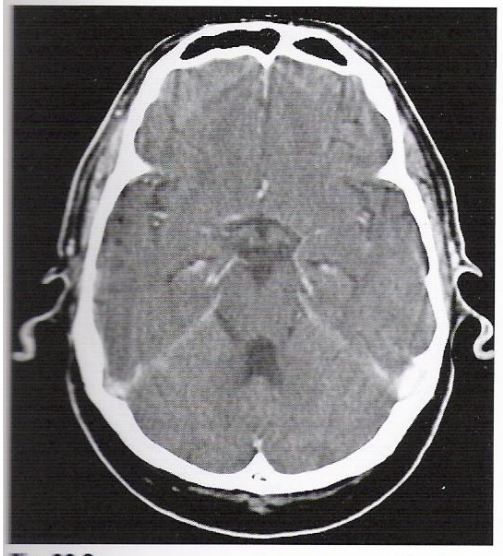

Fig. 29.2a

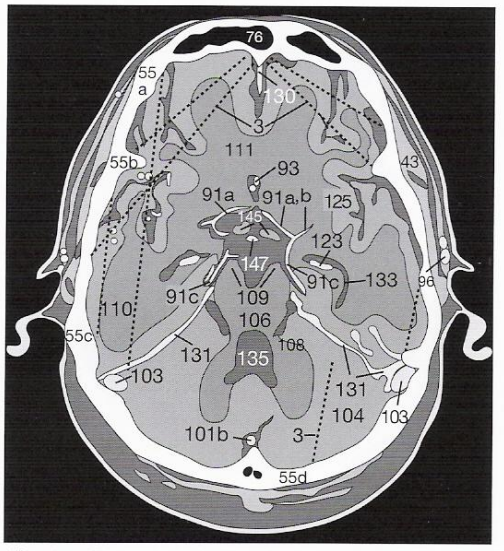

Fig. 29.2b

The cortex next to the frontal bone **(55a)** often appears hyperdense compared to adjacent brain parenchyma, but this is an artifact due to beam-hardening effects of bone. Note that the choroid plexus **(123)** in the lateral ventricle **(133)** is enhanced after i.v. infusion of CM. Even in plain scans it may appear hyperdense because of calcifications.

Fig. 29.3a

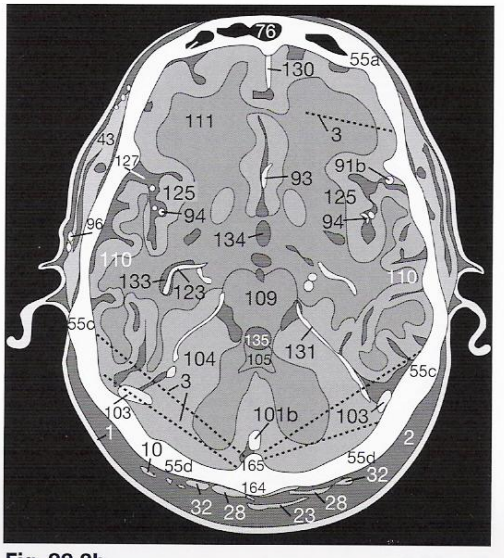

Fig. 29.3b

You will soon have recognized that the CCT images on these pages were taken after i.v. administration of CM: the vessels of the circle of Willis are markedly enhanced. The branches **(94)** of the middle cerebral artery **(91b)** are visible in the Sylvian fissure **(127)**. Even the pericallosal artery **(93)**, a continuation of the anterior cerebral artery **(91a)**, can be clearly identified. Nevertheless, it is often difficult to distinguish between the optic chiasm **(145)** and the pituitary stalk **(147)** because these structures have similar densities.

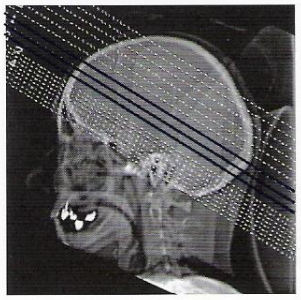

In addition to the above-mentioned cerebral arteries **(93, 94)**, the falx cerebri **(130)** is a hyperdense structure. In **Figure 30.2a** you can see the extension of the hyperdense choroid plexus **(123)** through the foramen of Monro, which connects the lateral ventricles **(133)** with the 3rd ventricle **(134)**. Check whether the contours of the lateral ventricles are symmetric.

A midline shift could be an indirect sign of edema. Calcifications in the pineal **(148)** gland and the choroid plexus **(123)** are a common finding in adults, and are generally without any pathologic significance. Due to partial volume effects, the upper parts of the tentorium **(131)** often appear without clear margins so that it becomes difficult to demarcate the cerebellar vermis **(105)** and hemispheres **(104)** from the occipital lobe **(112)**.

It is particularly important to carefully inspect the internal capsule **(121)** and the basal ganglia: caudate nucleus **(117)**, putamen **(118)**, and globus pallidus **(119)** as well as the thalamus **(120)**. Consult the number codes in the front foldout for the other structures not specifically mentioned on these pages.

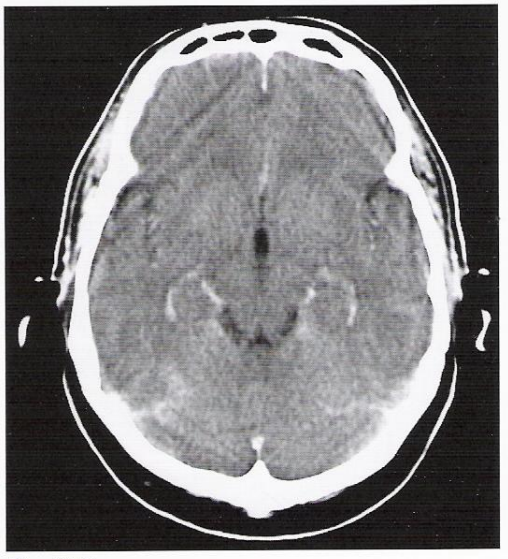

Fig. 30.1a

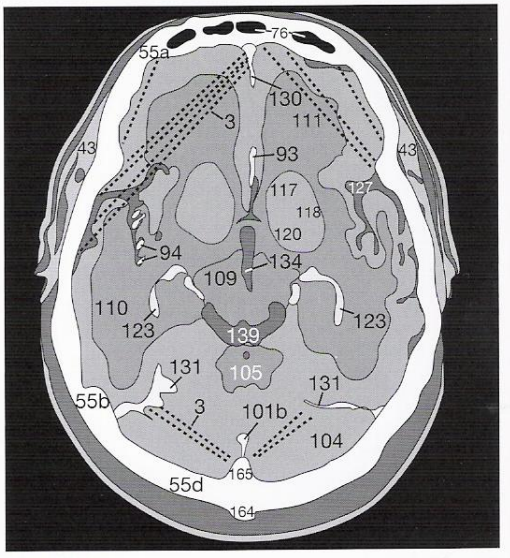

Fig. 30.1b

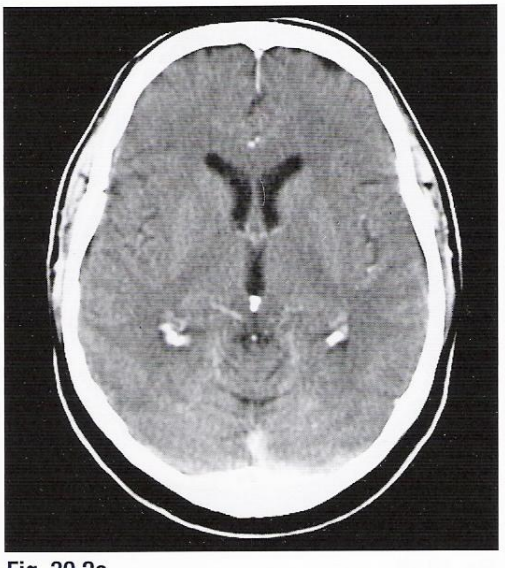

Fig. 30.2a

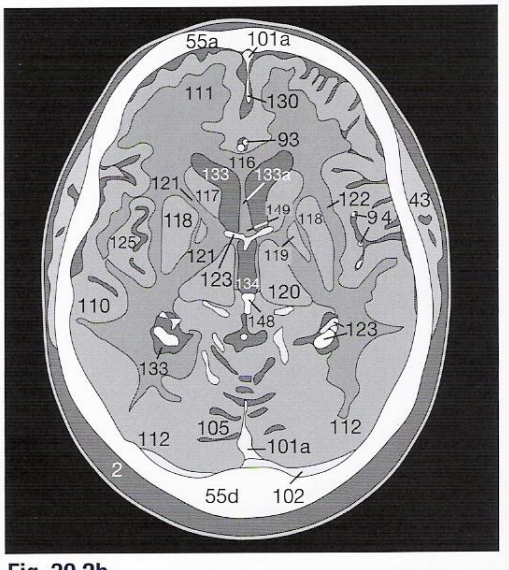

Fig. 30.2b

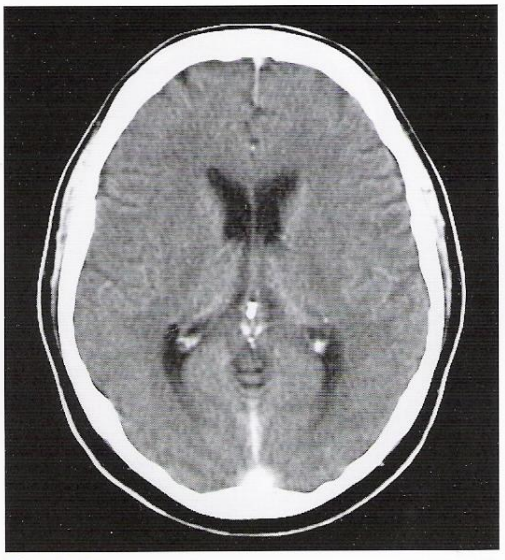

Fig. 30.3a

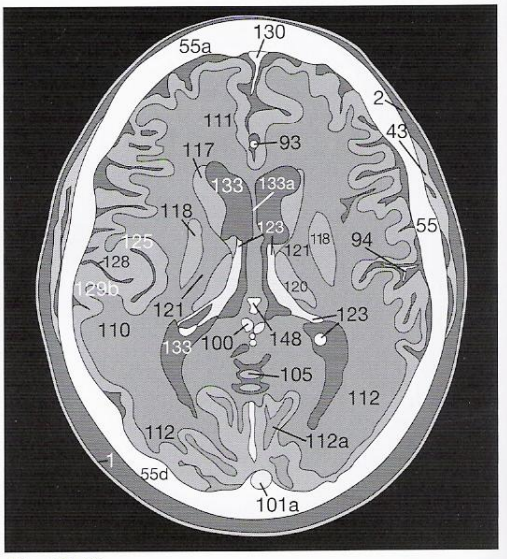

Fig. 30.3b

Fig. 31.1a

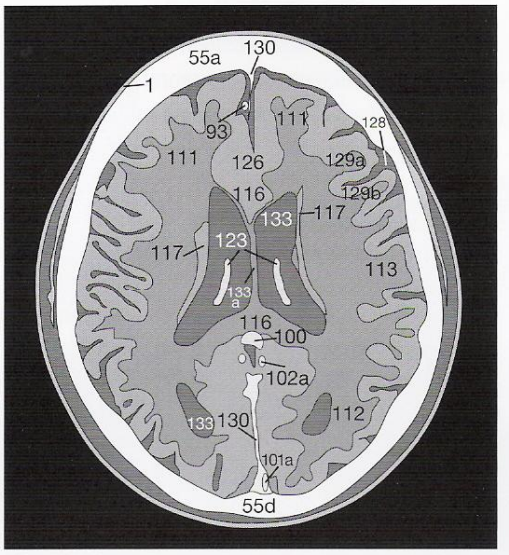

Fig. 31.1b

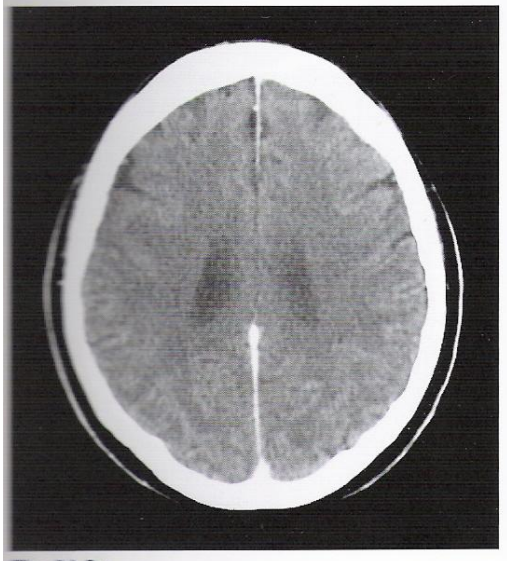

Fig. 31.2a

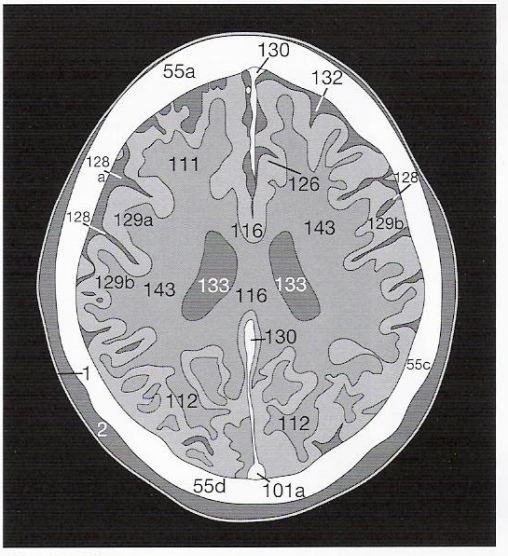

Fig. 31.2b

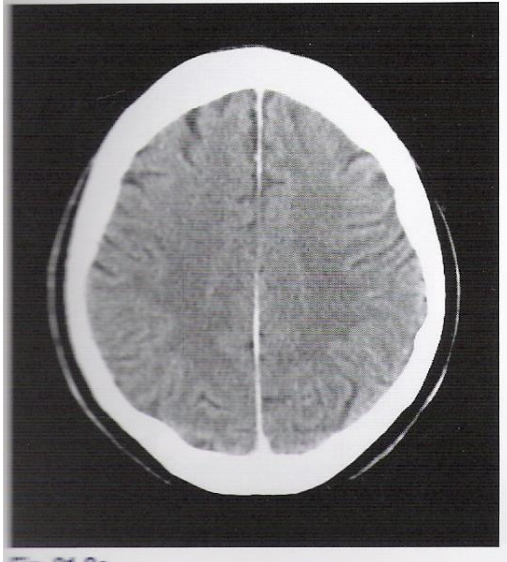

Fig. 31.3a

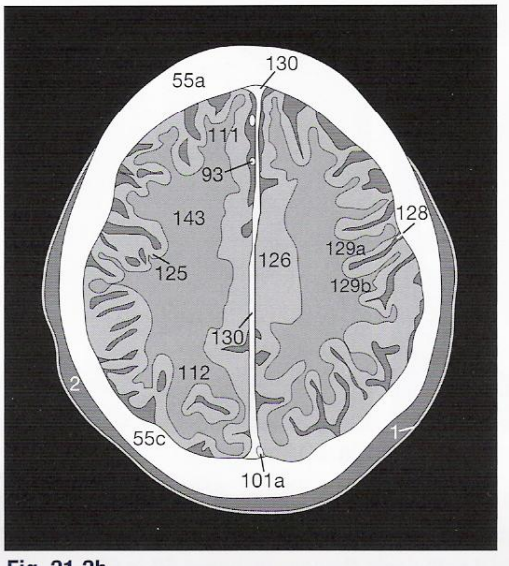

Fig. 31.3b

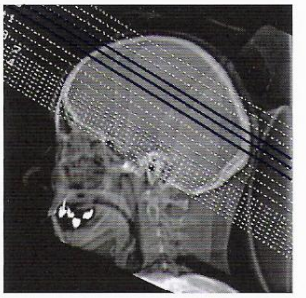

The position of the patient's head is not always as straight as in our example. Even small inclinations may lead to remarkably asymmetric pictures of the ventricular system, though in reality it is perfectly normal. You may see only a partial slice of the convex contours of the lateral ventricles **(133)**. This could give you the impression that they are not well defined **(Fig. 31.1a)**.

The phenomenon must not be confused with brain edema: as long as the sulci (external SAS) are not effaced, but configured regularly, the presence of edema is rather improbable.

For evaluating the width of the SAS, the patient's age is an important factor. Compare the images on pages 50 and 52 in this context. The paraventricular and supraventricular white matter **(143)** must be checked for poorly circumscribed hypodense regions of edema due to cerebral infarction.

As residues of older infarctions, cystic lesions may develop. In late stages they are well defined and show the same density as CSF (see p. 58).

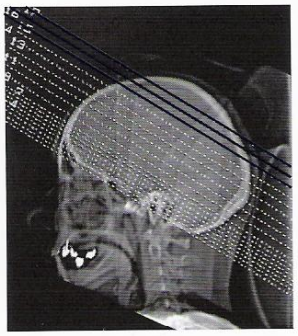

In the upper sections **(Figs. 32.1–32.3)** calcifications in the cerebral falx **(130)** often appear. You should differentiate this kind of lesion, which has no clinical significance, from calcified meningioma. The presence of CSF-filled sulci **(132)** in adults is an important finding with which to exclude brain edema. After a thorough evaluation of the cerebral soft-tissue window, a careful inspection of the bone window should follow. Continue to check for bone metastases or fracture lines. Only now is your evaluation of a cranial CT really complete.

Test yourself! Exercise 1:

Note from memory a systematic order for the evaluation of cranial CTs. If you have difficulties, return to the checklist on page 26.

Note:

-
-
-
-
-

-
-
-
-
-

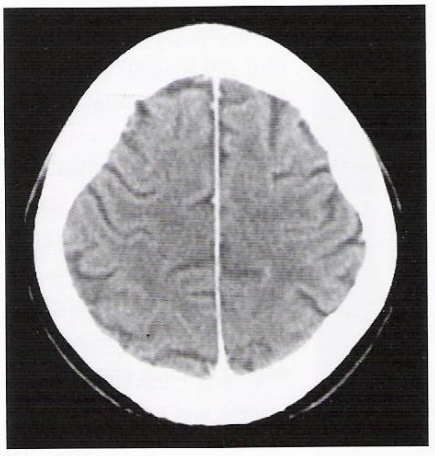

Fig. 32.1a

Fig. 32.2a

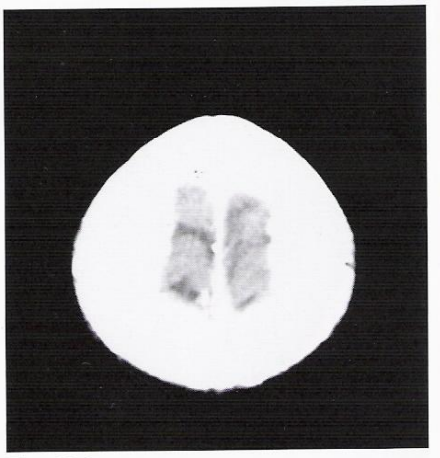

Fig. 32.3a

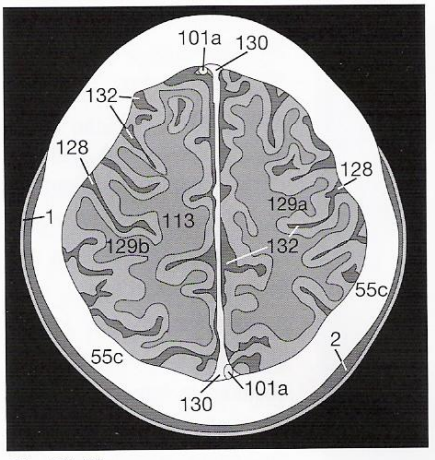

Fig. 32.1b

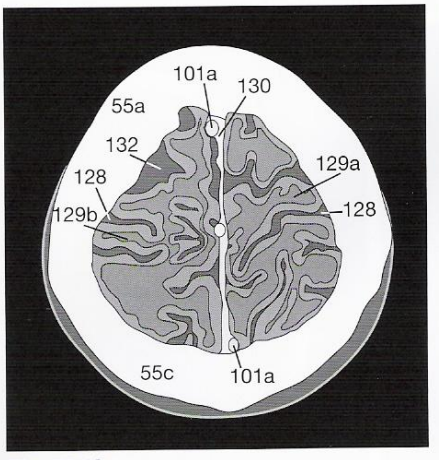

Fig. 32.2b

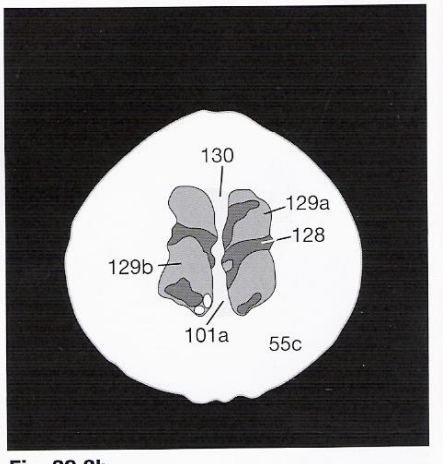

Fig. 32.3b

On the following pages the atlas of normal anatomy continues with scans of the orbits (axial), the face (coronal), and the petrosal bones (axial and coronal). After these you will find the most common anatomic variations, typical phenomena caused by partial volume effects and the most important intracranial pathologic changes on pages 50 to 60.

Fig. 33.1a

Fig. 33.1b

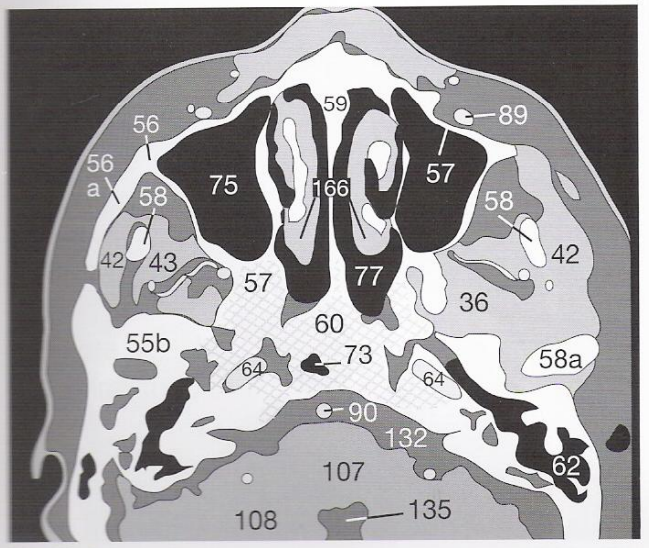

Fig. 33.1c

The face and the orbits are usually studied in thin slices (2 mm) using 2-mm collimation steps. The orientation of the scanning plane is comparable to that for CCTs (see p. 26). In the sagittal topogram the line of reference lies parallel to the floor of the orbit at an angle of about 15° to horizontal **(Fig. 33.2)**.

The printouts are usually presented in the view from caudal: all structures on the right side of the body appear on the left, and vice versa.

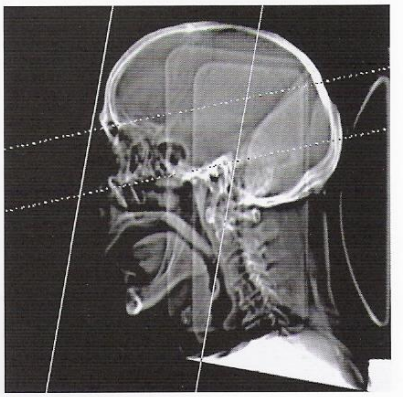

Fig. 33.2

Alterations in the soft structures of the orbits and the paranasal sinuses can be readily evaluated in the soft-tissue window **(Fig. 33.1b)**. For the detection of a tumor-related arrosion of bone or a fracture, the bone window should also be checked **(Fig. 33.1a)**. The following pages therefore present each scan level in both windows. The accompanying drawing **(Fig. 33.1c)** refers to both. The number codes for all drawings are found in the legend in the front foldout.

On the lower slices of the orbits you will see parts of the maxillary sinus **(75)**, the nasal cavity **(77)** with the conchae **(166)**, the sphenoid sinus **(73)**, and the mastoid cells **(62)** as air-filled spaces. If there is fluid or a soft-tissue mass, this may indicate a fracture, an infection, or a tumor of the paranasal sinuses. For examples of such diseases, see pages 58 to 61.
Two parts of the mandible appear on the left side: in addition to the coronoid process **(58)**, the temporomandibular joint with the head of the mandible **(58a)** is seen on the left. The carotid artery, however, is often difficult to discern in the carotid canal **(64)**, whether in the soft-tissue or bone window.

In the petrous part of the temporal bone **(55b)**, the tympanic cavity **(66)** and the vestibular system are visible. For a more detailed evaluation of the semicircular canals and the cochlea, images obtained with the petrous bone technique are more appropriate (pp. 44–47). CM was infused intravenously before the examination of the orbits. The branches of both the facial and angular vessels **(89)** as well as the basilar artery **(90)** therefore appear markedly hyperdense in the soft-tissue window **(Fig. 33.1b)**.

It is not always possible to achieve a precise sagittal position of the head. Even a slight tilt **(Fig. 34.1)** will make the temporal lobe **(110)** appear on one side, whereas on the other side the mastoid cells **(62)** can be seen.

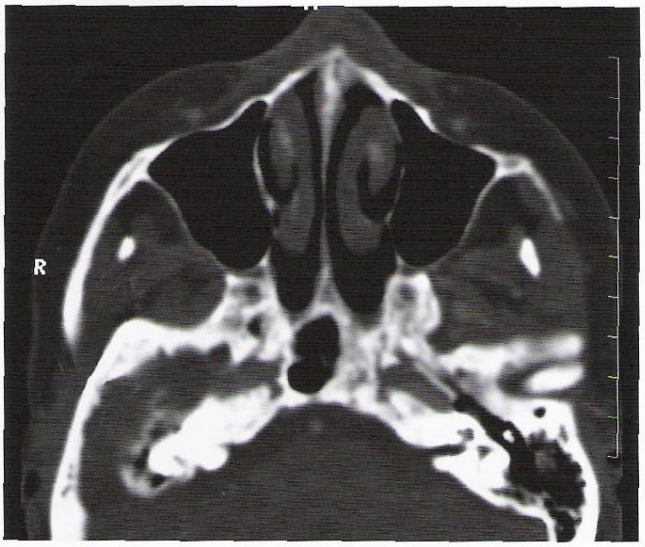

Fig. 34.1a

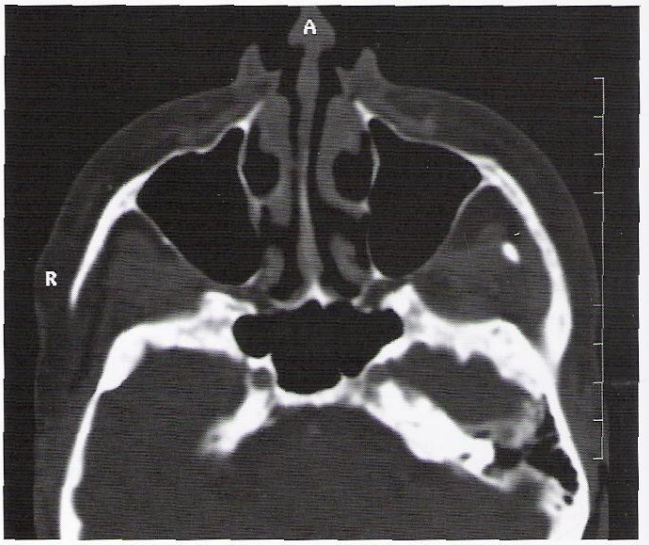

Fig. 34.2a

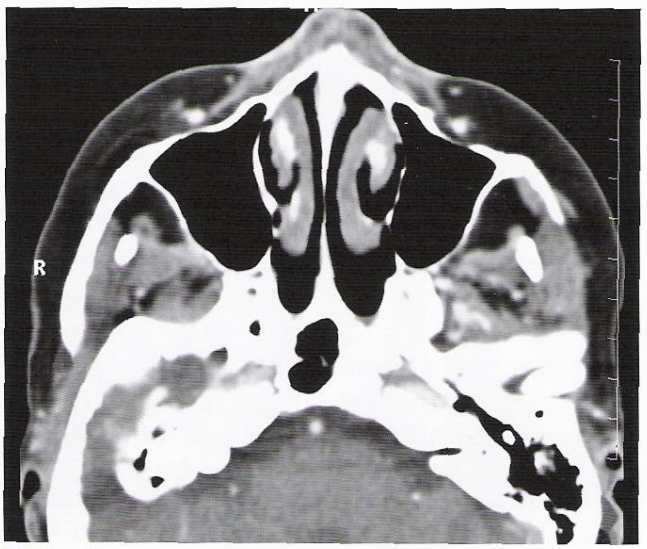

Fig. 34.1b

Fig. 34.2b

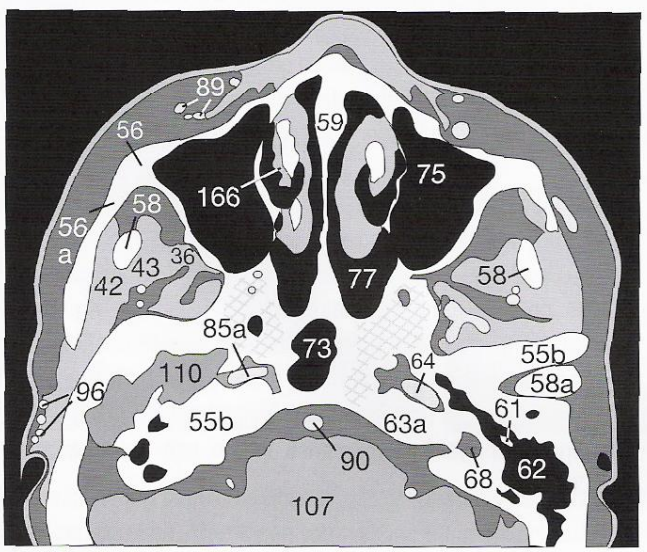

Fig. 34.1c

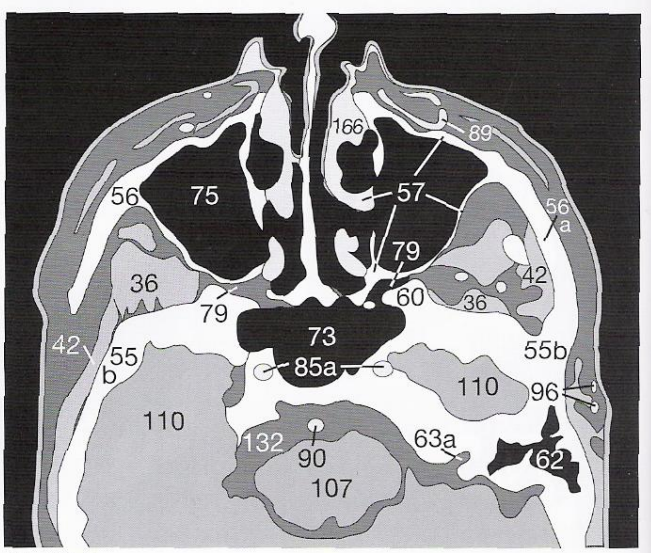

Fig. 34.2c

As experience shows, it is difficult to determine the course of the internal carotid artery **(85a)** through the base of the skull and to demarcate the pterygopalatine fossa **(79)**, through which, among other structures, the greater palatine nerve and the nasal branches of the pterygopalatine ganglion (from CN V and CN VII) pass.

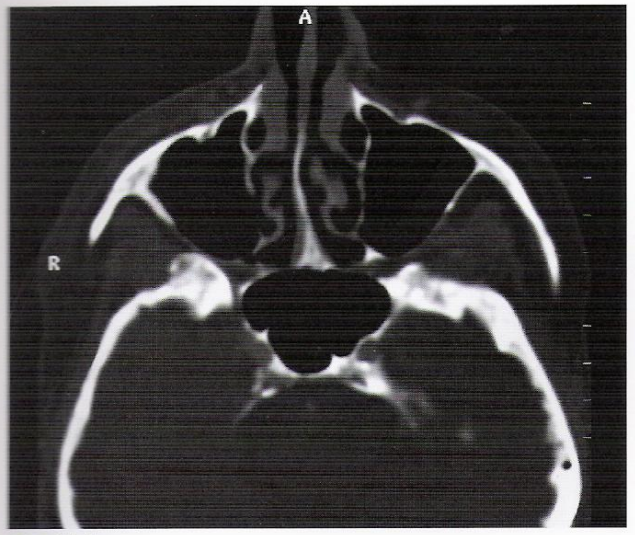

Fig. 35.1a

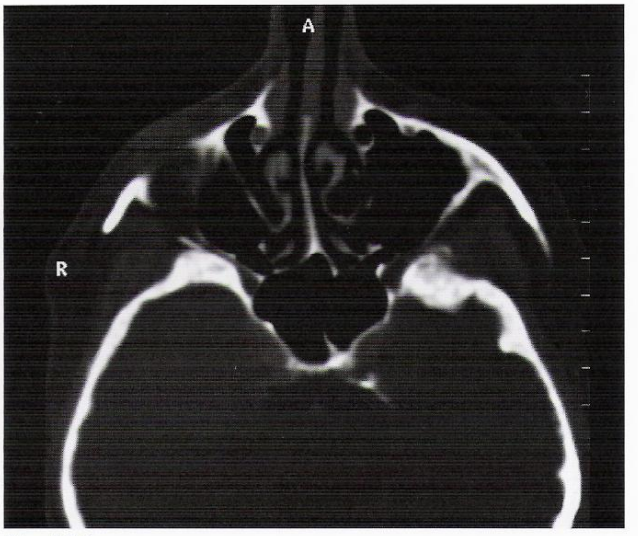

Fig. 35.2a

Fig. 35.1b

Fig. 35.2b

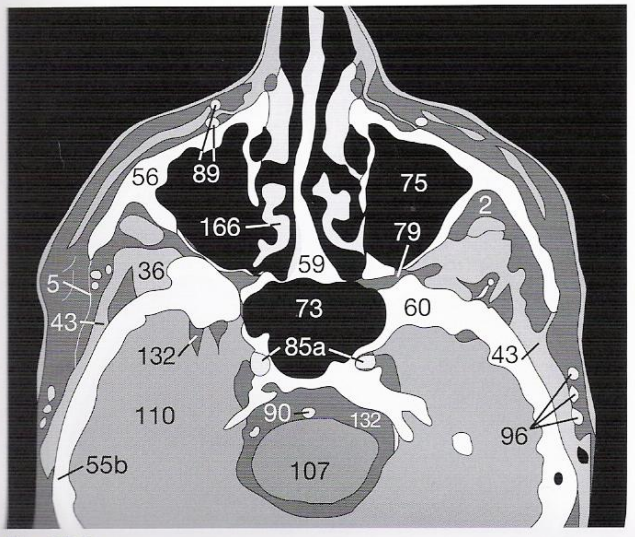

Fig. 35.1c

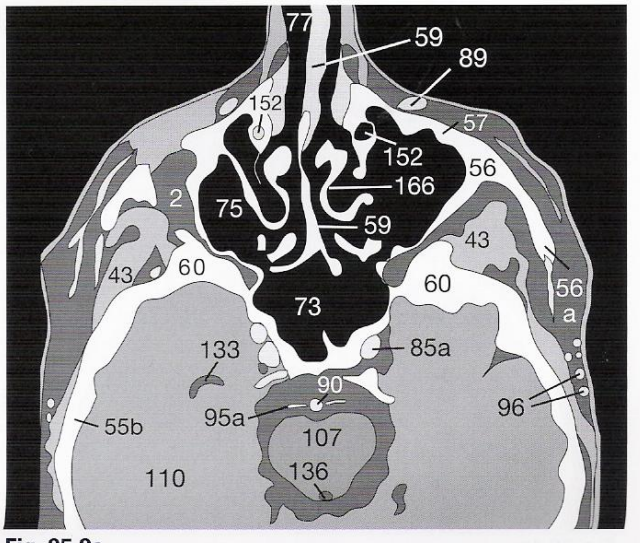

Fig. 35.2c

On the floor of the orbit, the short inferior oblique muscle **(47f)** often seems poorly delineated from the lower lid. This is due to the similar densities of these structures. Directly in front of the clinoid process/dorsum sellae **(163)** lies the pituitary gland **(146)** in its fossa, which is laterally bordered by the carotid siphon **(85a)**.

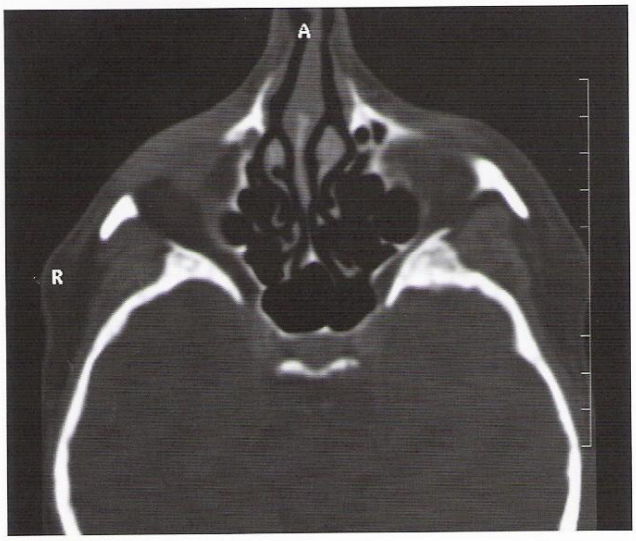

Fig. 36.1a

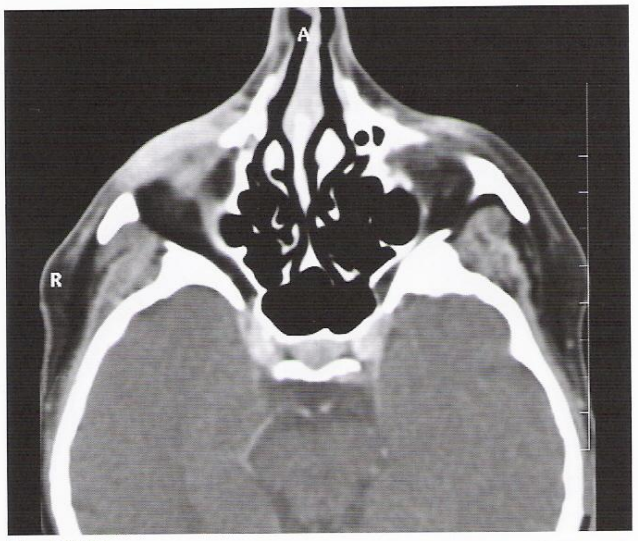

Fig. 36.1b

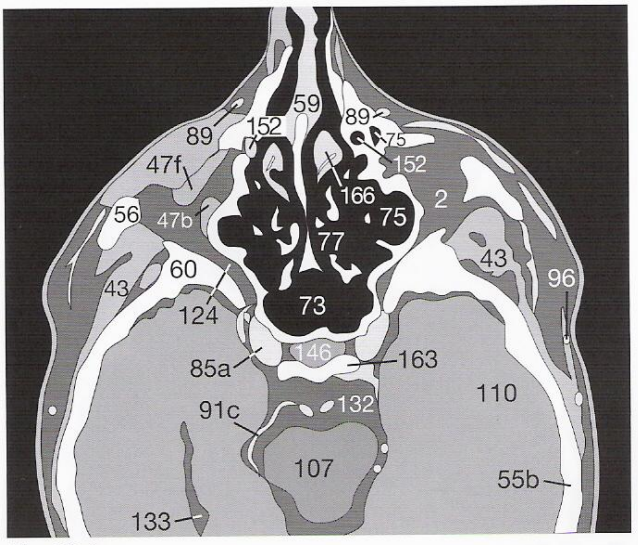

Fig. 36.1c

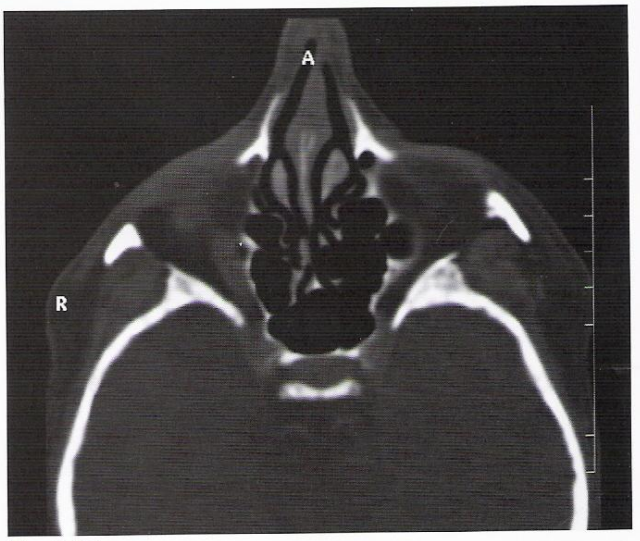

Fig. 36.2a

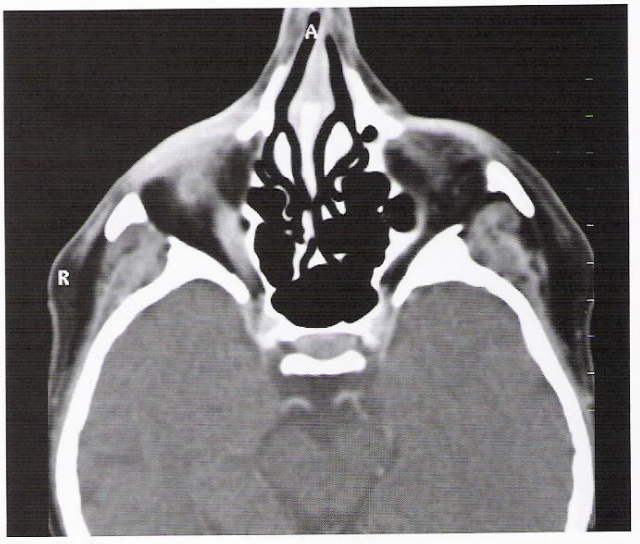

Fig. 36.2b

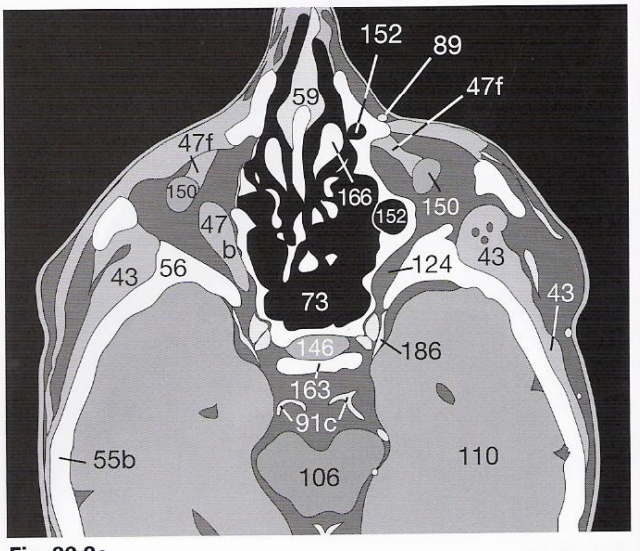

Fig. 36.2c

Small inclinations of the head cause slightly asymmetric views of the globe **(150)** and the extraocular muscles **(47)**. The medial wall of the nasolacrimal duct **(152)** is often so thin that it cannot be differentiated. At first sight the appearance of the clinoid process **(163)**, between the pituitary stalk **(147)** and the carotid siphon **(85a)** on the left side only, may be confusing in **Figure 37.2b**.

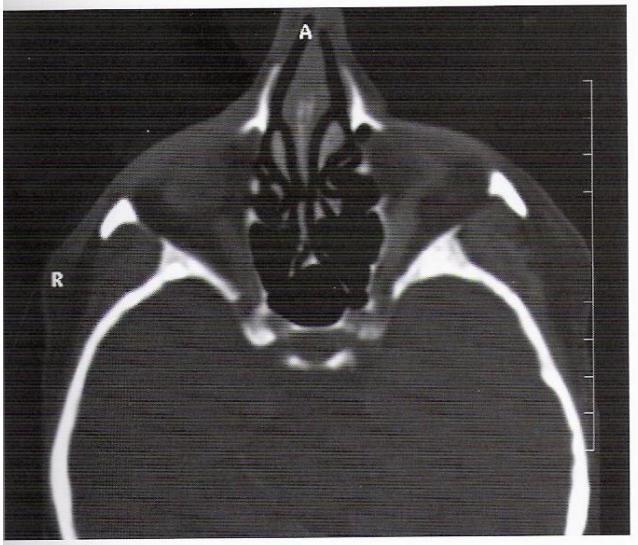

Fig. 37.1a

Fig. 37.1b

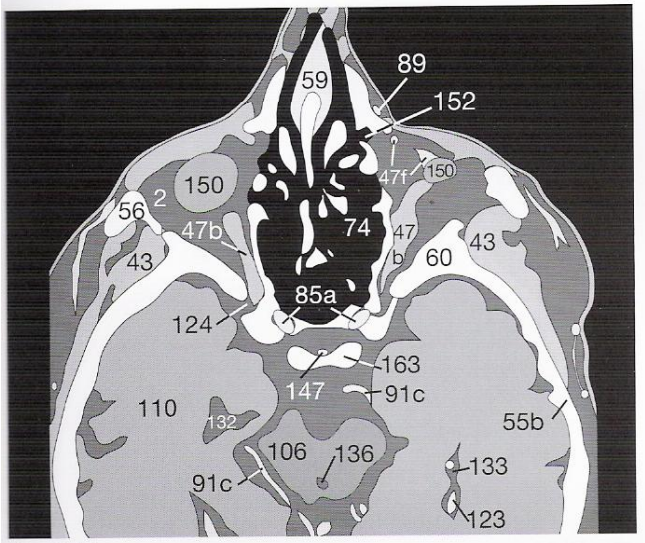

Fig. 37.1c

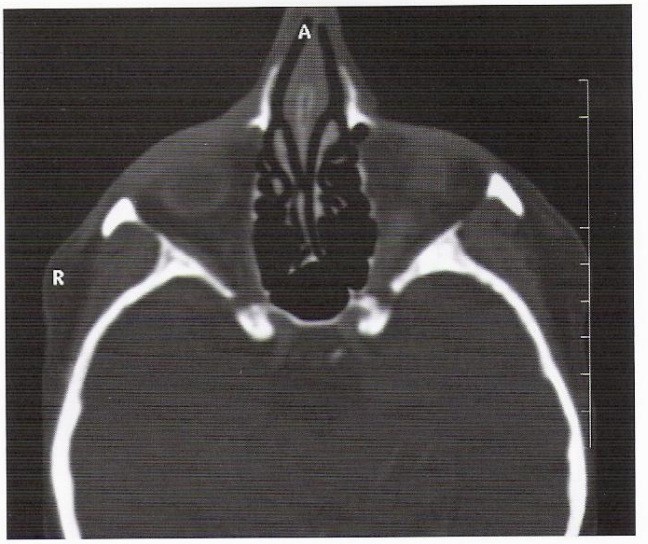

Fig. 37.2a

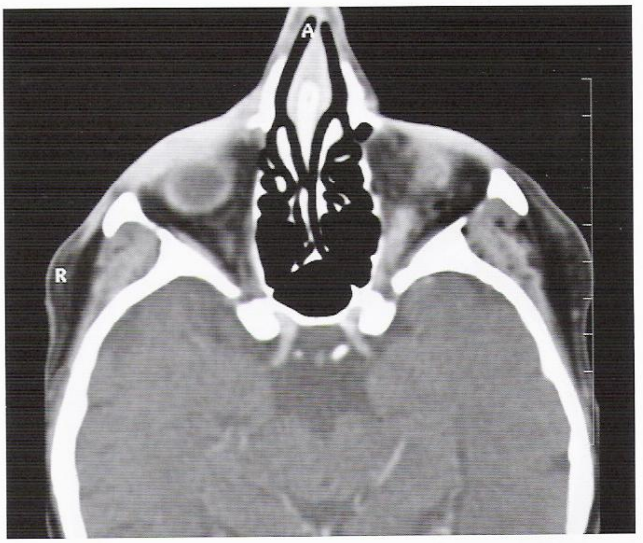

Fig. 37.2b

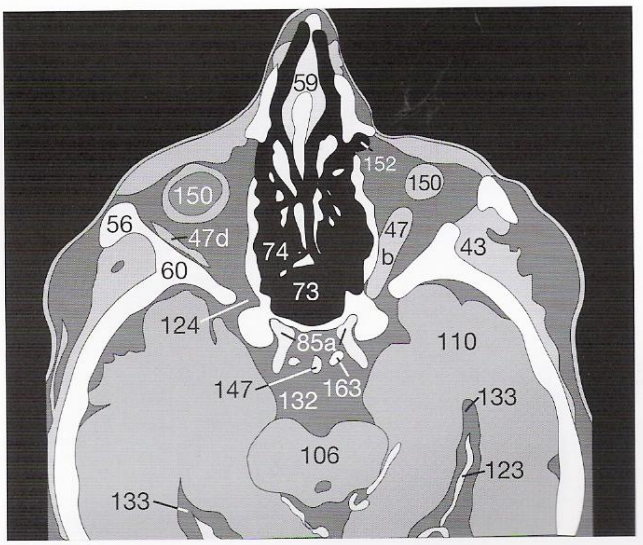

Fig. 37.2c

After intravenous injection of CM, the branches of the middle cerebral artery **(91b)** originating from the internal carotid artery **(85a)** are readily distinguished. The gray shade of the optic nerves **(78)** as they pass through the chiasm **(145)** to the optic tracts **(144)**, however, is very similar to that of the surrounding CSF **(132)**. You should always check on the symmetry of the extraocular muscles **(47)** in the retrobulbar fatty tissue **(2)**.

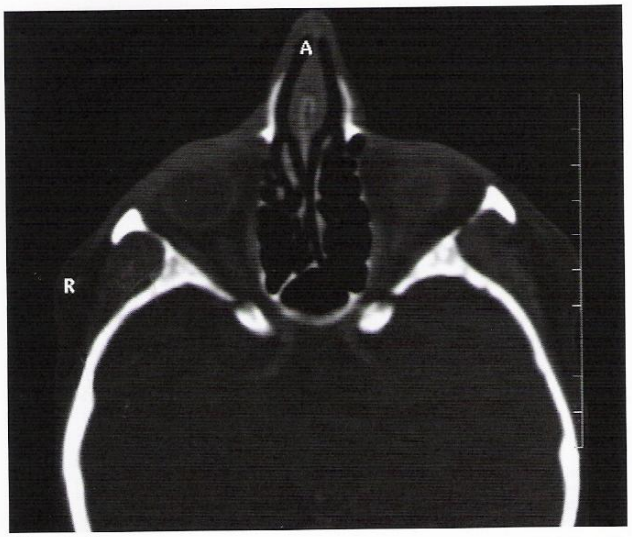

Fig. 38.1a

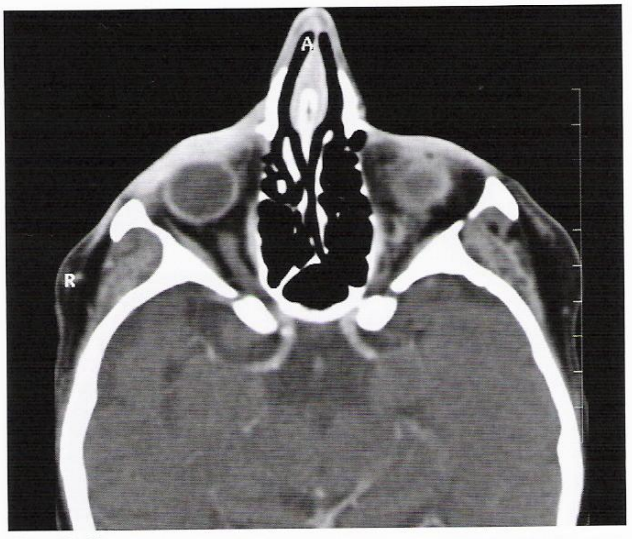

Fig. 38.1b

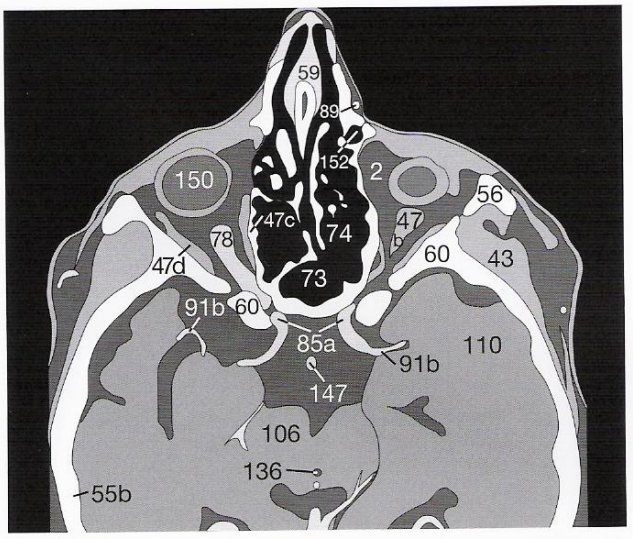

Fig. 38.1c

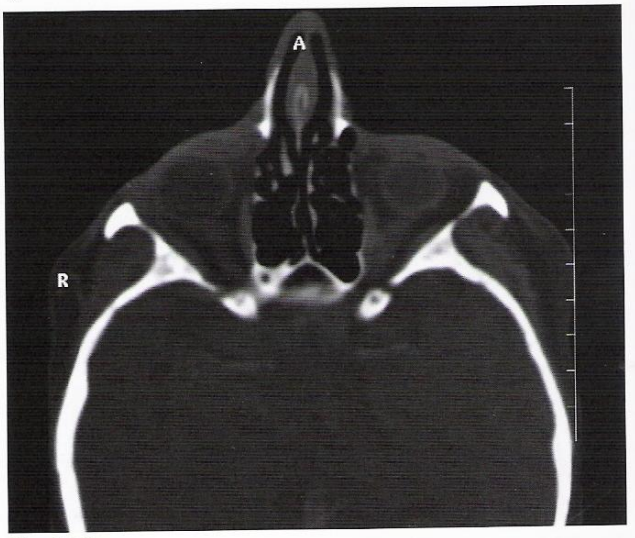

Fig. 38.2a

Fig. 38.2b

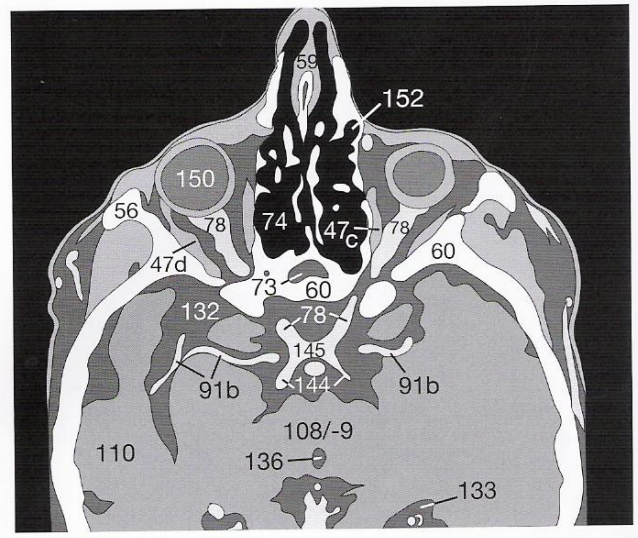

Fig. 38.2c

In the globe **(150)** you can now see the hyperdense lens **(150a)**. Notice the oblique course of the ophthalmic artery (*) crossing the optic nerve **(78)** in the retrobulbar fatty tissue **(2)**. **Figure 39.2b** shows a slight swelling **(7)** of the right lacrimal gland **(151)** compared to the left one (see **Fig. 40.1b**).

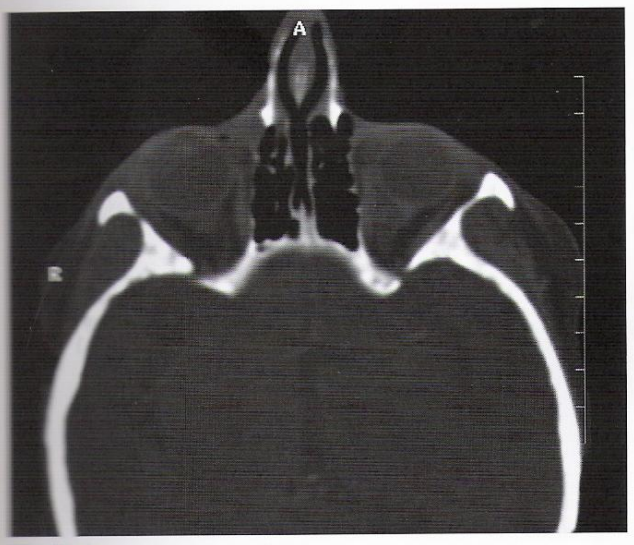

Fig. 39.1a

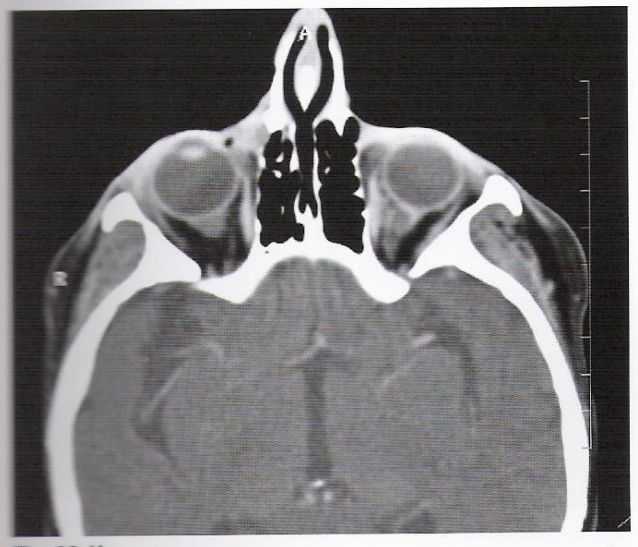

Fig. 39.1b

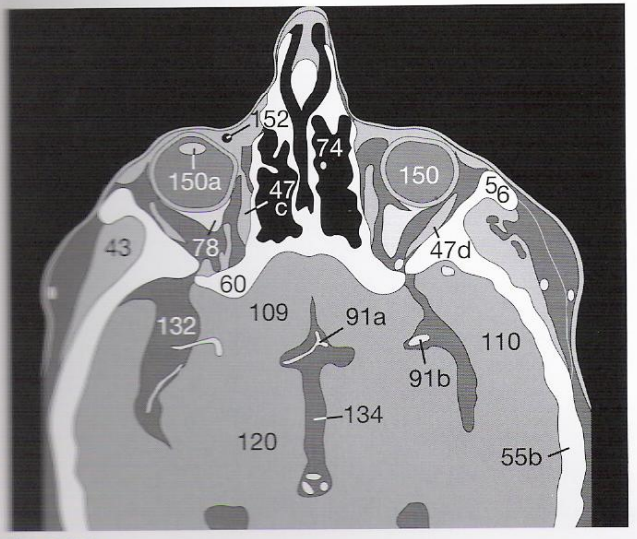

Fig. 39.1c

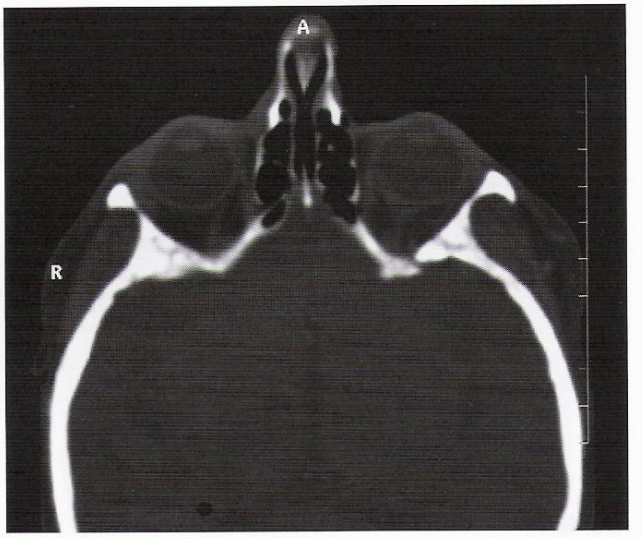

Fig. 39.2a

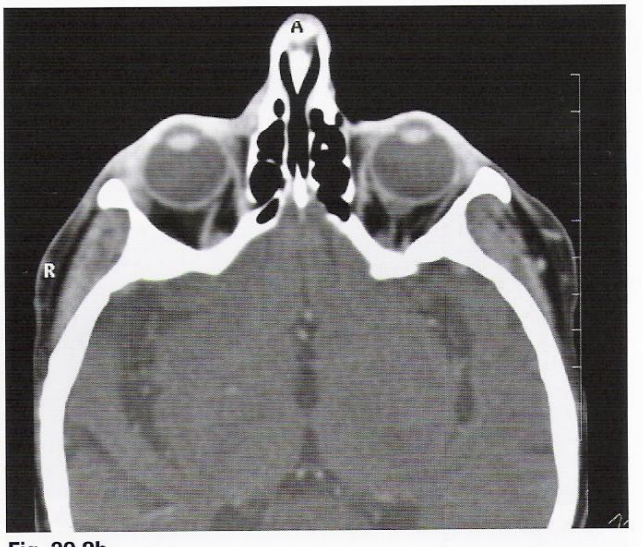

Fig. 39.2b

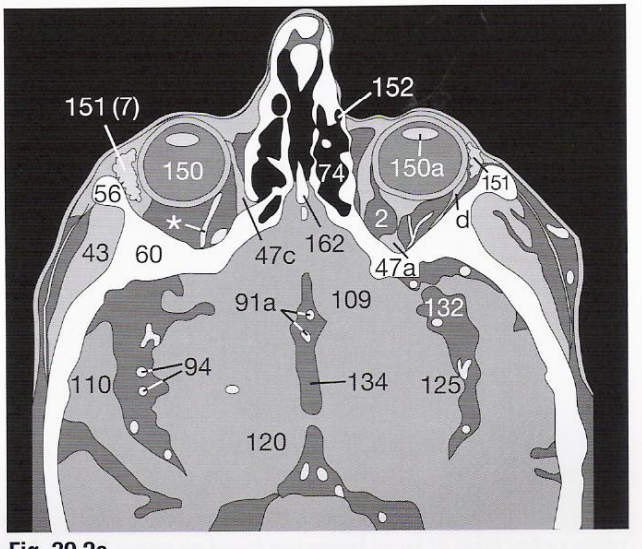

Fig. 39.2c

Figure 40.1b clarifies that in this case there is indeed an inflammation or tumor-like thickening **(7)** in the right lacrimal gland **(151)**. The *superior rectus muscle* **(47a)** *appears at the roof of the orbit and immediately next to it lies the levator palpebrae muscle* **(46)**. *Due to* similar densities, these muscles are not easily differentiated.

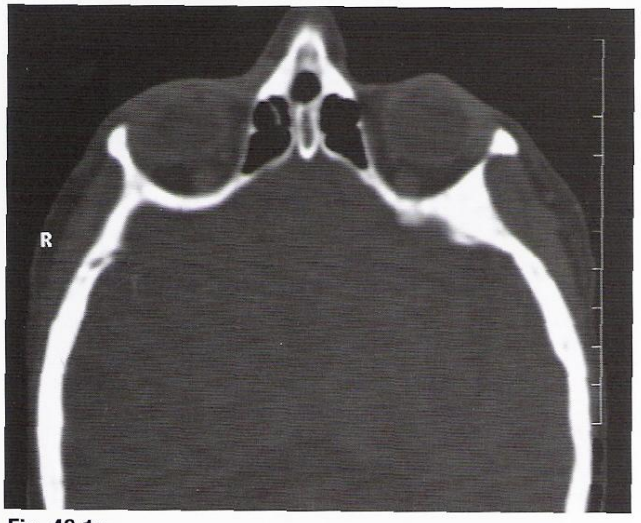

Fig. 40.1a

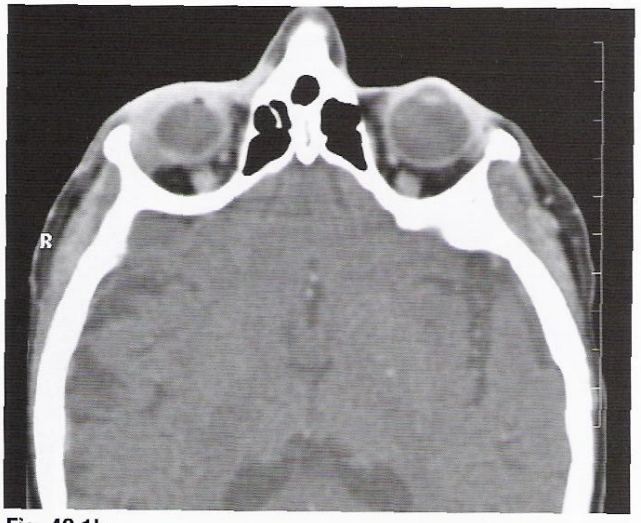

Fig. 40.1b

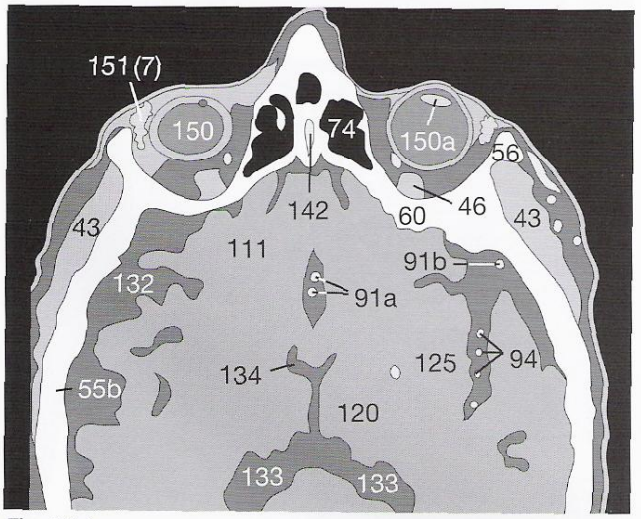

Fig. 40.1c

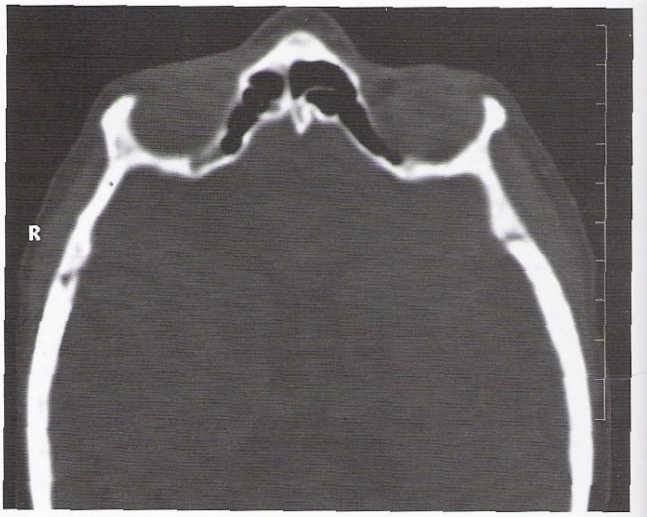

Fig. 40.2a

Fig. 40.2b

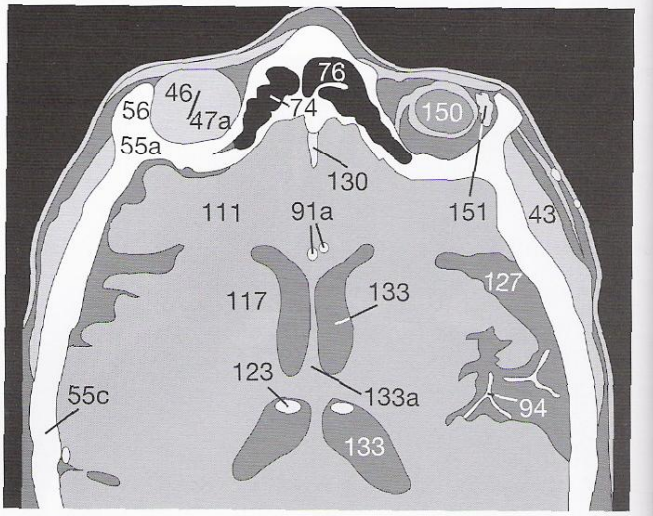

Fig. 40.2c

The axial views of the orbits and the face end here with the appearance of the frontal sinus **(76)**. Examples of pathologic changes of the orbits or fractures of facial bones are found on pages 61 to 63.

The possibilities of angling the CT gantry are limited. In order to acquire scans in the coronal plane, the patient must therefore be positioned as shown in the planning topogram to the right (**Fig. 41.1**). The patient should be in a prone position, with the head completely extended. When examining trauma patients, any lesions of the bones or ligaments of the cervical spine must always be excluded by conventional radiography prior to CCT.
Images viewed from anterior: the anatomic structures on the patient's right side appear on the left in the images and conversely, as if the examiner were facing the patient.

When looking for fractures, images are usually acquired in the thin-slice mode (slice and collimation, each 2 mm) and viewed on bone windows. Even fine fracture lines can then be detected. A suspected fracture of the zygomatic arch may require additional scans in the axial plane (see p. 34). In **Figure 41.2a** the inferior alveolar canal (*) in the mandible **(58)** and the foramen rotundum (**) in the sphenoid bone **(60)** are clearly visible. As for the previous chapter, the code numbers for the drawings are explained in the legend in the front foldout.

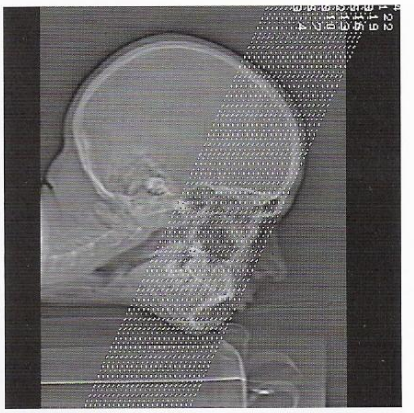

Abb. 41.1

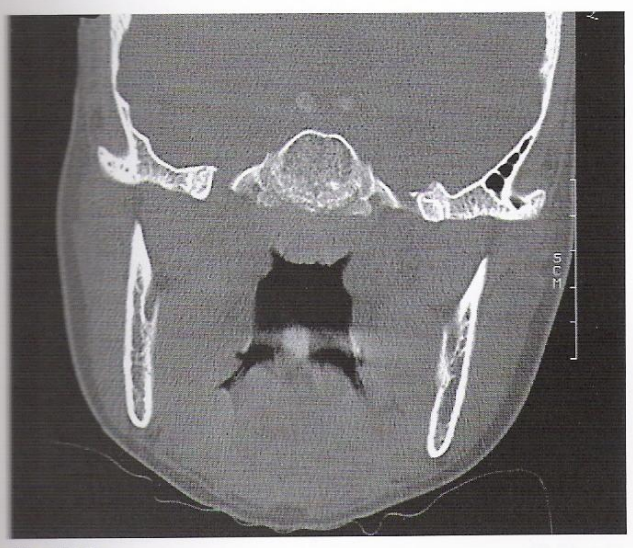

Fig. 41.2a

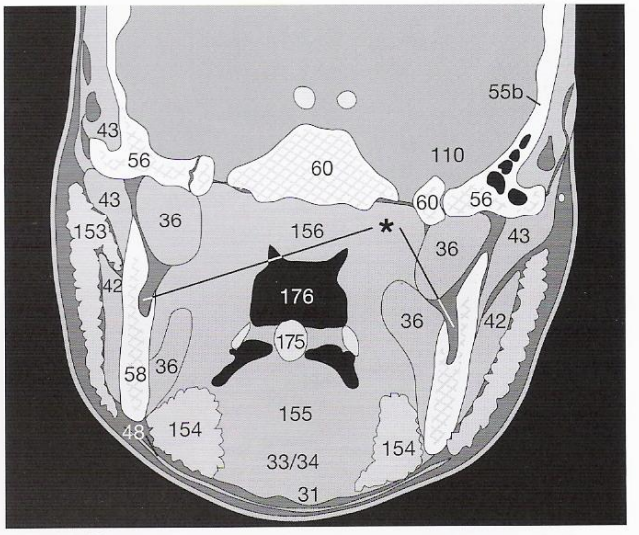

Fig. 41.2b

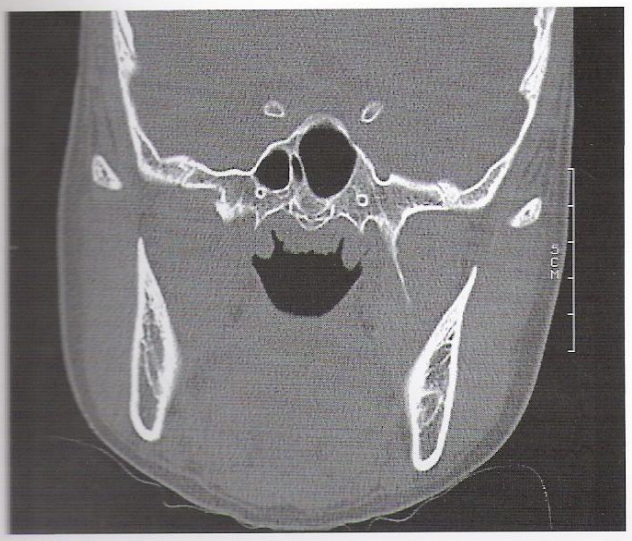

Fig. 41.3a

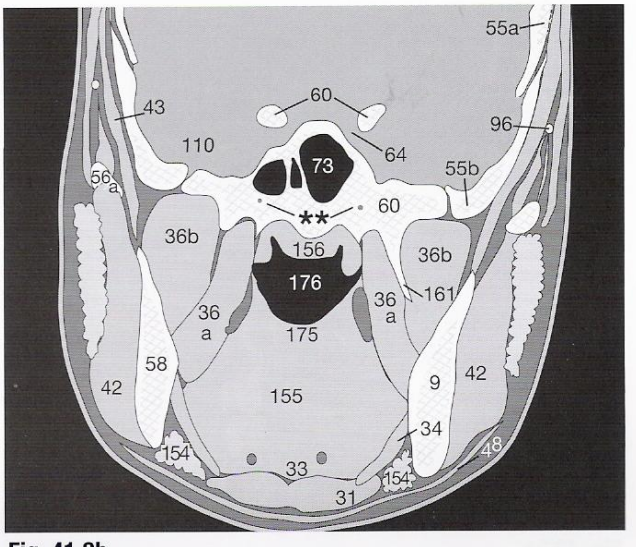

Fig. 41.3b

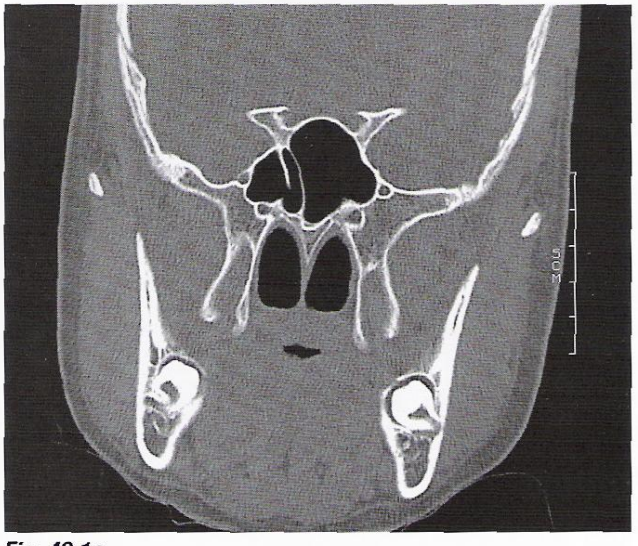

Fig. 42.1a

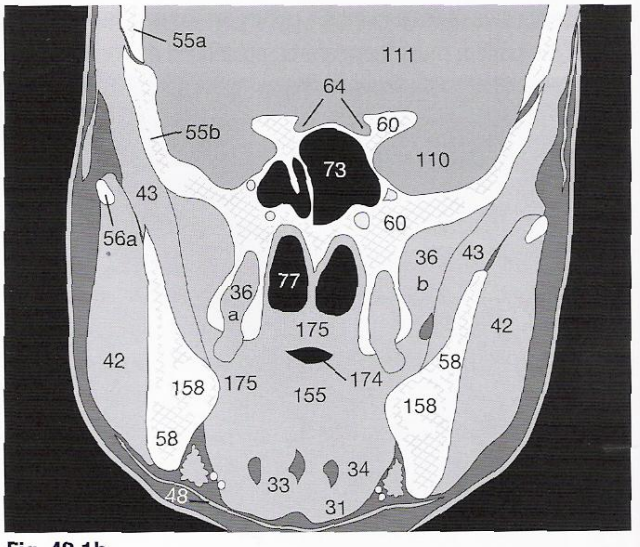

Fig. 42.1b

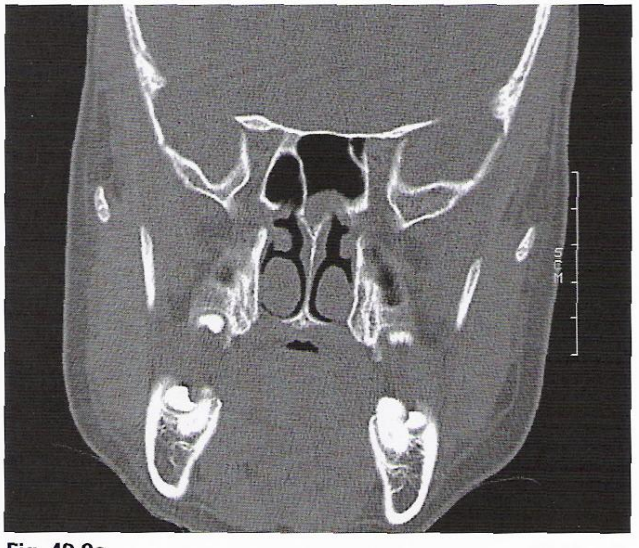

Fig. 42.2a

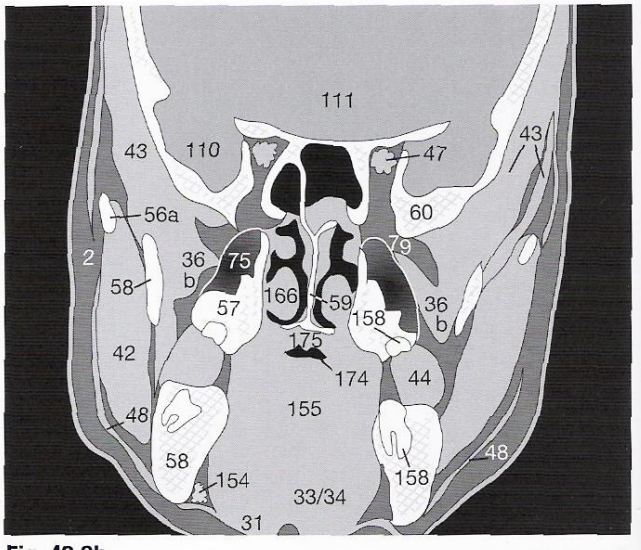

Fig. 42.2b

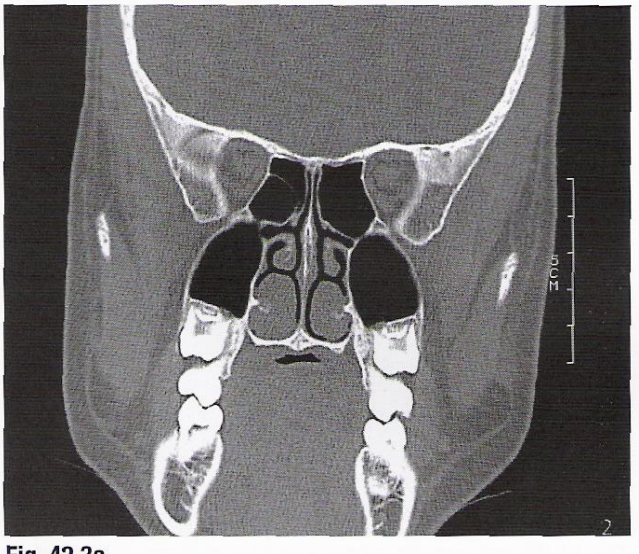

Fig. 42.3a

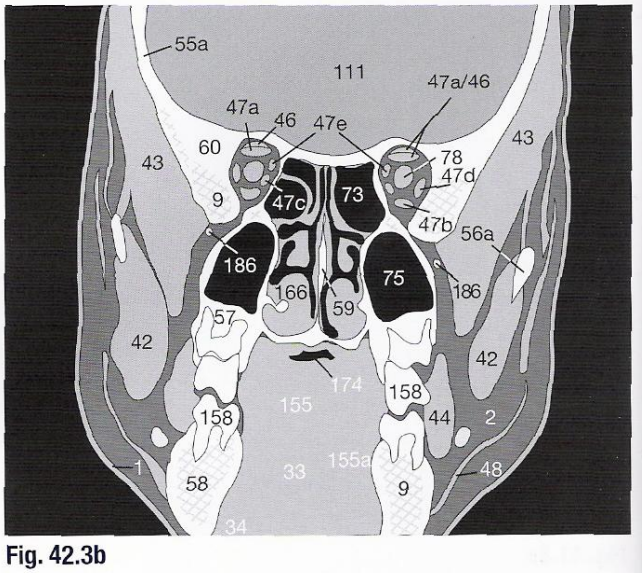

Fig. 42.3b

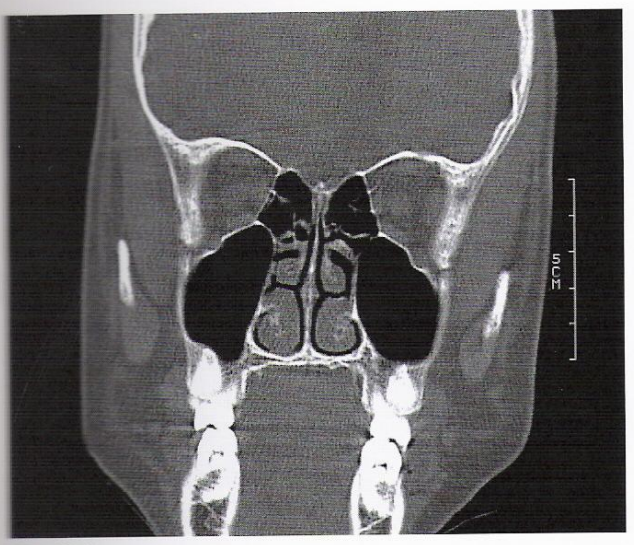

Fig. 43.1a

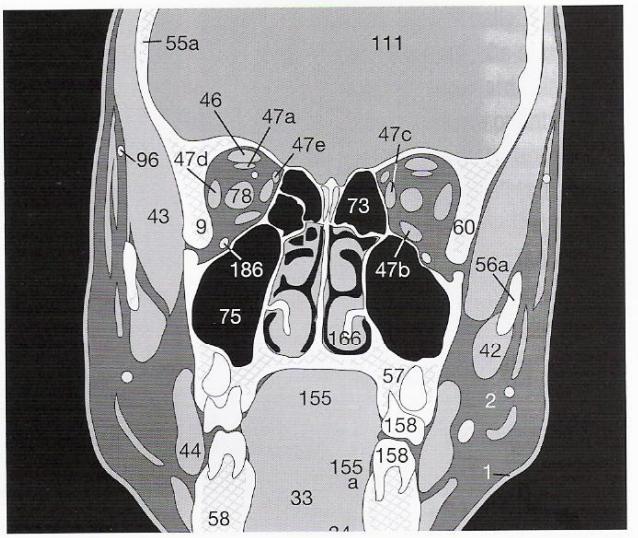

Fig. 43.1b

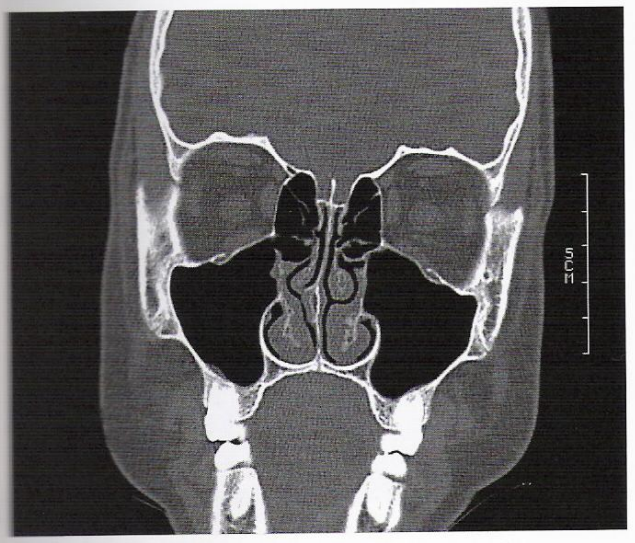

Fig. 43.2a

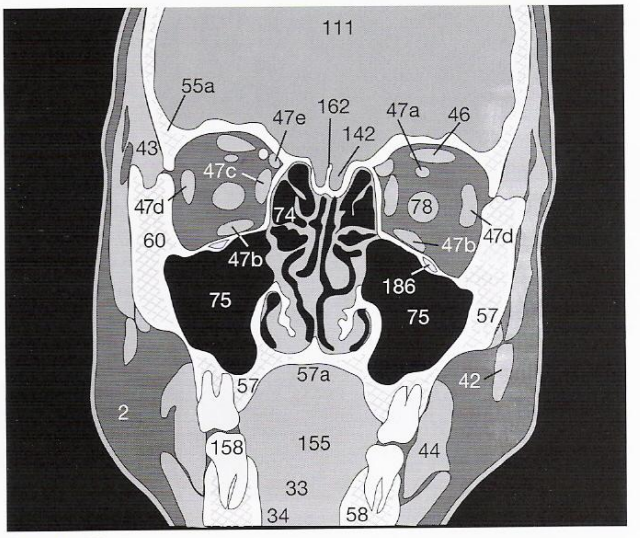

Fig. 43.2b

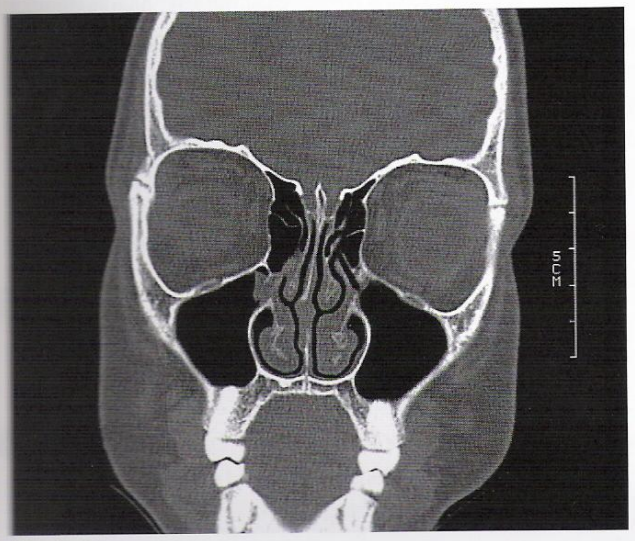

Fig. 43.3a

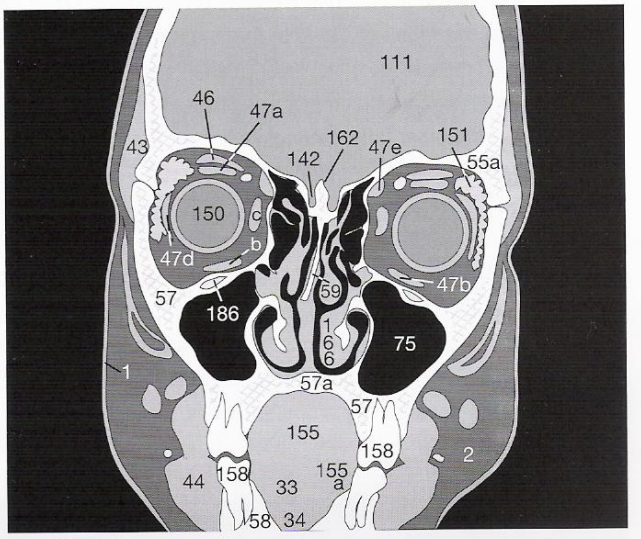

Fig. 43.3b

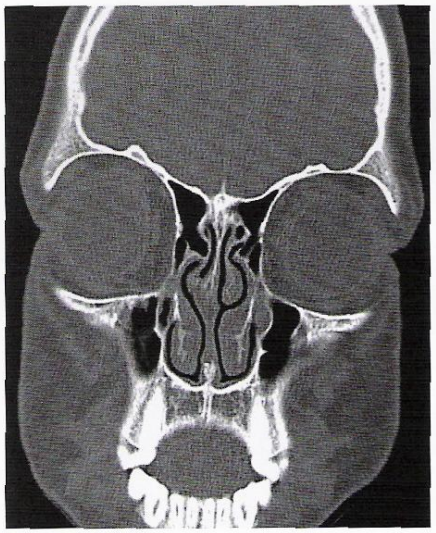

Fig. 44.1a

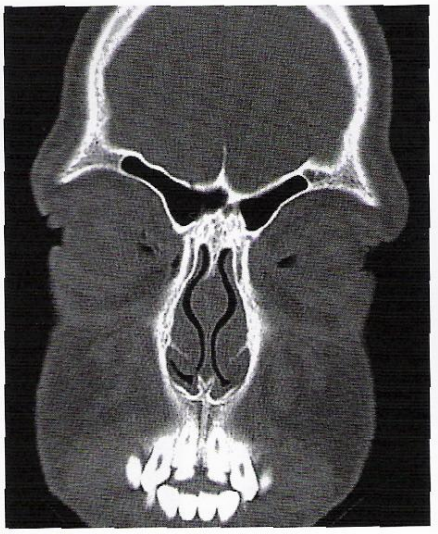

Fig. 44.2a

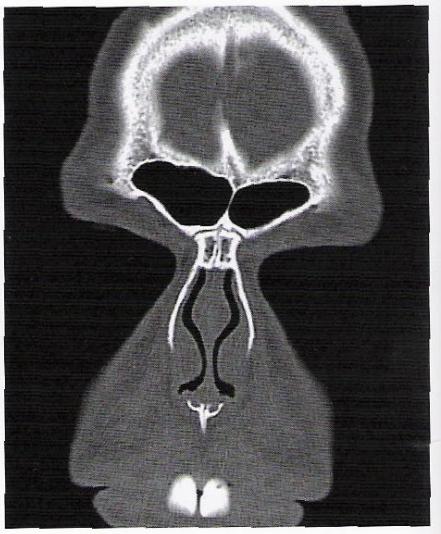

Fig. 44.3a

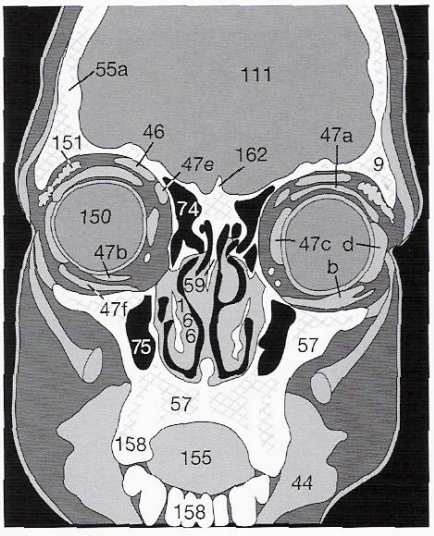

Fig. 44.1b

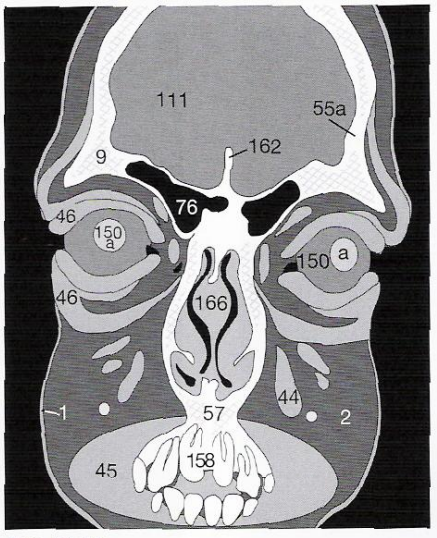

Fig. 44.2b

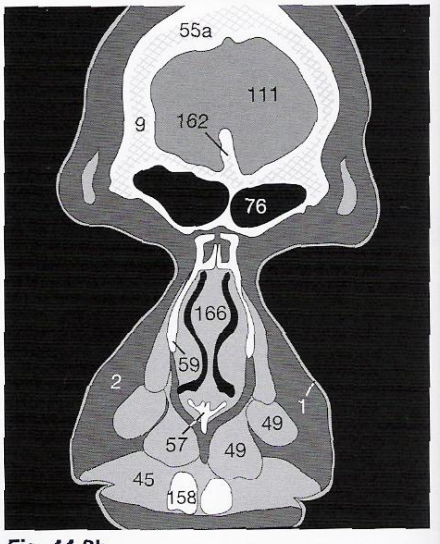

Fig. 44.3b

The insertions of the extraocular muscles on the globe **(150)** *can* also be clearly identified **(47 a–f)** in the anterior slices. The short inferior oblique muscle **(47f)**, however, is often seen only in coronal *scanning planes, because it does not pass with the others muscles* through the retrobulbar fatty connective tissue. The same problem occurs in axial scans of the face (compare with **Fig. 36.2b** and **Fig. 36.2c**).

If a case of chronic sinusitis is suspected, it is very important to check whether the semilunar hiatus is open. It represents the main channel for discharging secretions of the paranasal sinuses. In **Figure 60.3** you will find examples of anatomic variations which narrow this channel and may promote chronic sinusitis.

Sometimes one discovers a congenitally reduced pneumatization of a frontal sinus **(76)** or an asymmetric arrangement of other paranasal sinuses without any pathologic consequences. You should always make sure that all paranasal sinuses are filled exclusively with air, that they are well defined and present no air-fluid levels. Hemorrhage into the paranasal sinuses or the detection of intracranial bubbles of air must be interpreted as an indirect sign of a fracture – you will find examples of such fractures on page 63.

On the previous pages you have learned about the normal anatomy of the brain, the orbits, and the face. It may be some time ago that you studied the technical basics of CT and about adequate preparation of the patient. Before going on with the anatomy of the temporal bone, it would be good to check on and refresh your knowledge of the last chapters. All exercises are numbered consecutively, beginning with the first one on page 32.

Without doubt, you will improve your understanding of the subject if you tackle the gaps in your knowledge instead of skipping problems or looking at the answers at the end of the book. Refer to the relevant pages only if you get stuck.

Exercise 2: Write down from memory the typical window parameters for images of the lungs, bones, and soft tissues. Note precisely the width and center of each window in HU and give reasons for the differences. If you have difficulties answering this question, go back to pages 16/17 to refresh your memory.

	Center	Width	Gray scale range
Lung / pleura window:			_____ HU to _____ HU
Bone window:			_____ HU to _____ HU
Soft-tissue window:			_____ HU to _____ HU

Exercise 3: Which two types of oral CM do you know? What specific aspects must you consider when administering this kind of CM depending on the clinical problem? Are there any consequences for your list?

Oral CM (name)	Indication	Special schedule
•		
•		

Exercise 4: What aspects should you always clarify before referring your patients to a CT examination which probably requires the i.v. infusion of CM? The same applies if you consider referring someone to a venogram/angiogram or an IVU (both procedures are carried out with nonionic CM containing iodine). MRI examinations, however, are carried out with gadolinium as the CM. (The answers to questions 3 and 4 can be found on pp. 18 and 19.)

a)

b)

c)

Exercise 5: How would you differentiate between long structures such as vessels, nerves, or certain muscles and nodular structures such as lymph nodes or tumors? (You will find the answer on p. 15.)

Exercise 6: In which vessels might you find turbulence phenomena, caused by the CM injection, that must not be mistaken for a thrombus? (If you don't remember, check back to pp. 21-23.)

In order to evaluate the organ of hearing and balance, the petrosal bone is usually examined in thin slices without overlap (2/2). To ensure optimal resolution, the whole skull is not imaged, just the required part of the petrosal bone. The two petrosal bones **(55b)** are therefore enlarged and imaged separately. Only then is it possible to differentiate small structures like the ossicles **(61a–c)**, cochlea **(68)**, and the semicircular canals **(70a–c)**.

The topogram **(Fig. 46.1)** indicates the coronal imaging plane. The patient must be placed in a prone position with his or her head hyperextended. Note the pneumatization of the mastoid cells **(62)** and the usually thin walls of the outer auditory canal **(63b)**. Inflammation of these air-filled sinuses leads to characteristic effusion and swelling of the mucous membranes (see **Fig. 60.2a**).

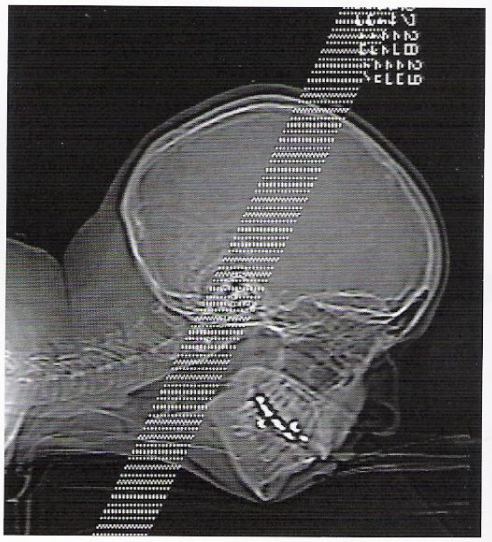

Fig. 46.1

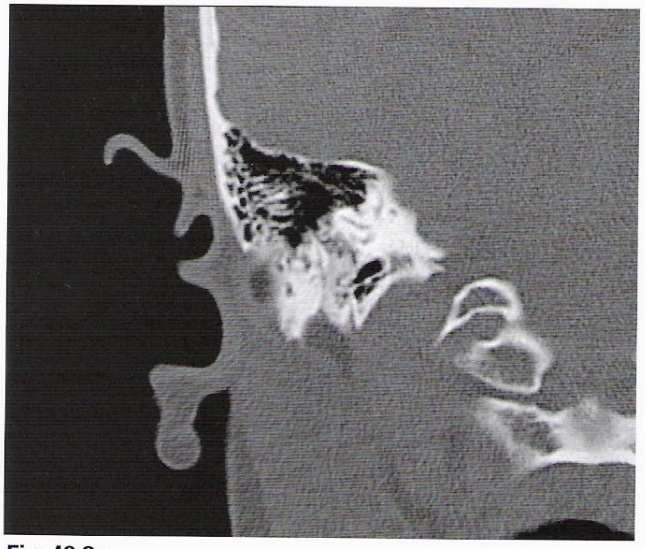

Fig. 46.2a

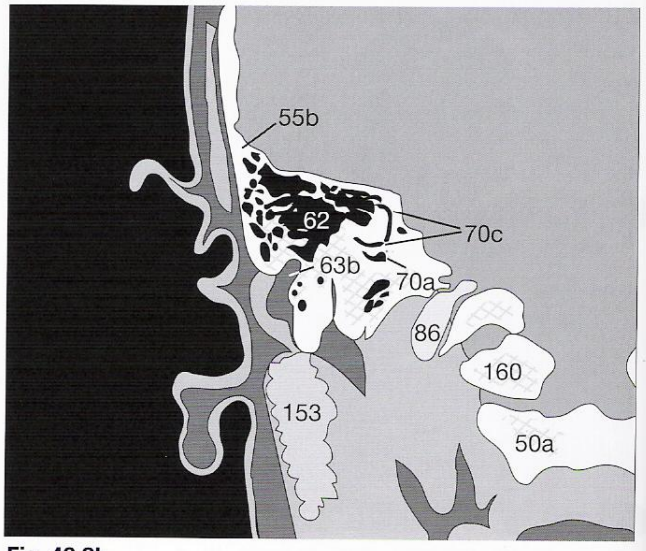

Fig. 46.2b

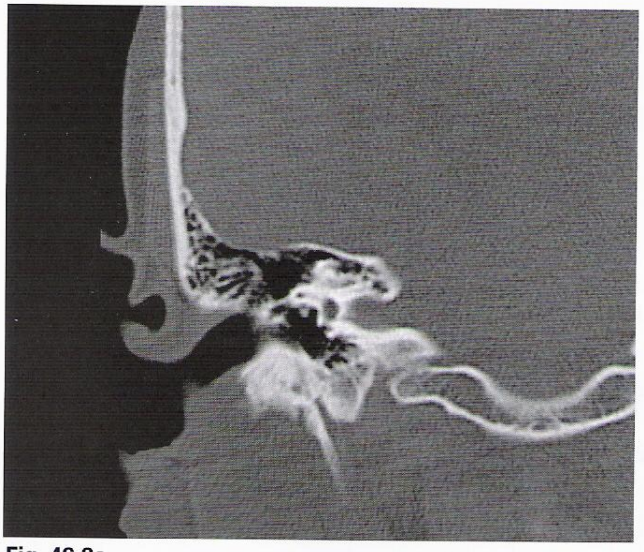

Fig. 46.3a

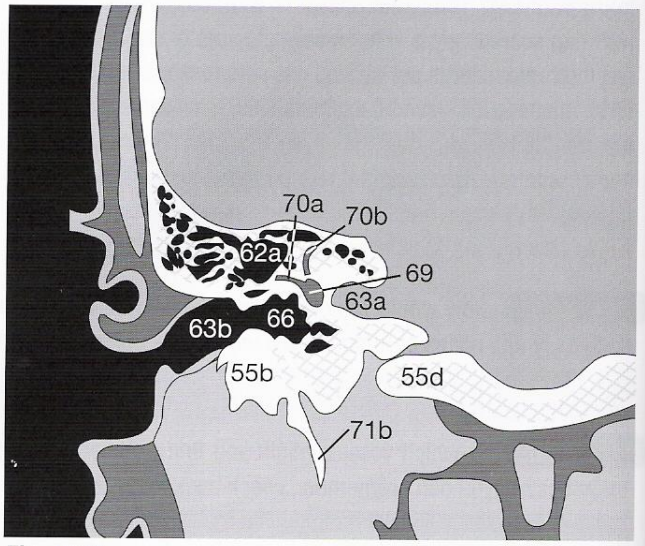

Fig. 46.3b

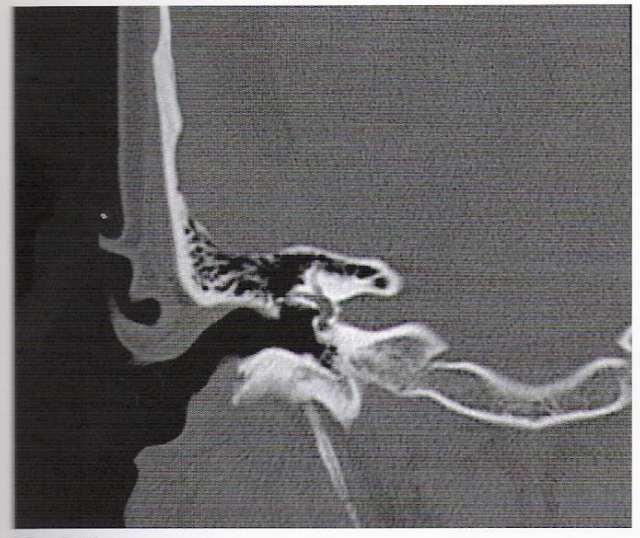

Fig. 47.1a

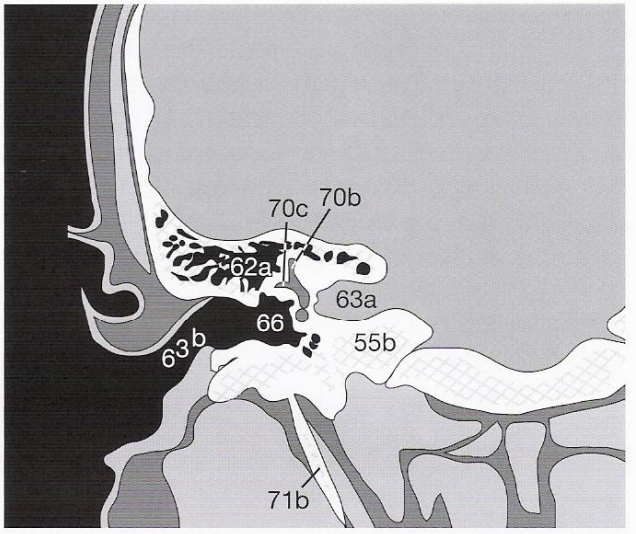

Fig. 47.1b

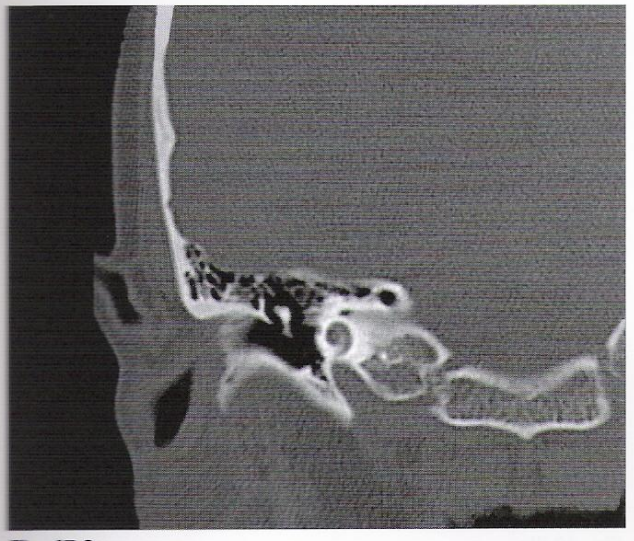

Fig. 47.2a

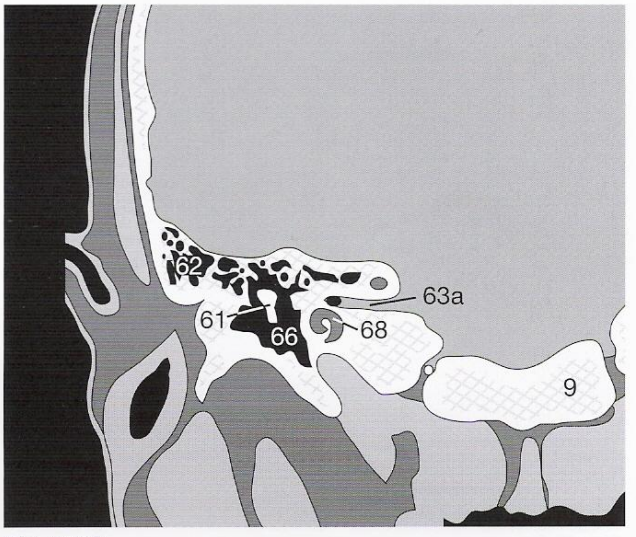

Fig. 47.2b

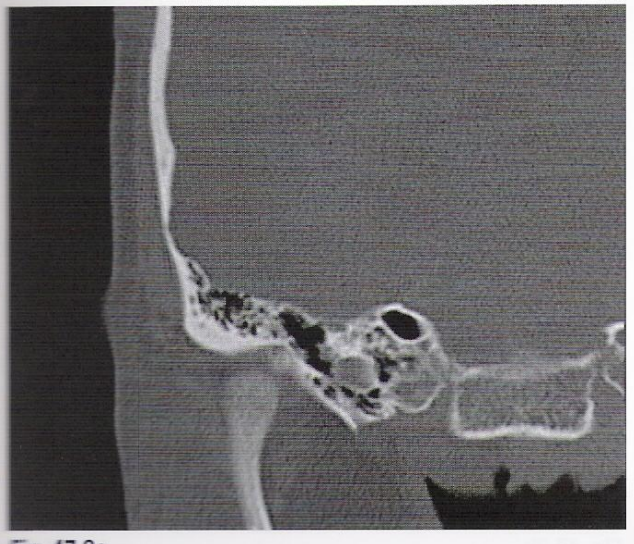

Fig. 47.3a

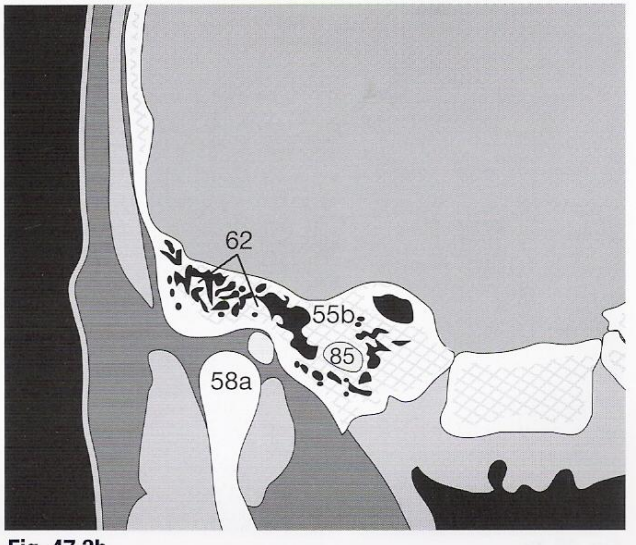

Fig. 47.3b

Analogous to coronal images, axial images are obtained with thin slices without overlap, i.e., 2 mm thickness and 2 mm increment and viewed on bone windows. The cerebellar hemispheres **(104)**, the temporal lobe **(110)**, and the soft tissues of the galea are therefore barely identifiable. Apart from the ossicles **(61a–c)** and the semicircular canals **(70a–c)**, the internal carotid artery **(64)**, the cochlea **(68)**, and the internal **(63a)** and external auditory canals **(63b)** are visualized. The funnel-shaped depression in the posterior rim of the petrosal bone **(Fig. 48.2a)** represents the opening of the perilymphatic duct (** = aqueduct of the cochlea) into the subarachnoid space. In **Figure 49.1a** note the localization of the geniculate ganglion of the facial nerve (*) ventral to the facial canal. The topogram **(Fig. 48.1)** shows an axial plane of section, obtained with the patient lying supine.

Test Yourself! Exercise No. 7: Think about differential diagnoses involving effusion in the middle ear **(66)**, the outer auditory canal, or the mastoid cells **(62)** and compare your results with the cases shown on pages 60 and 62 to 63.

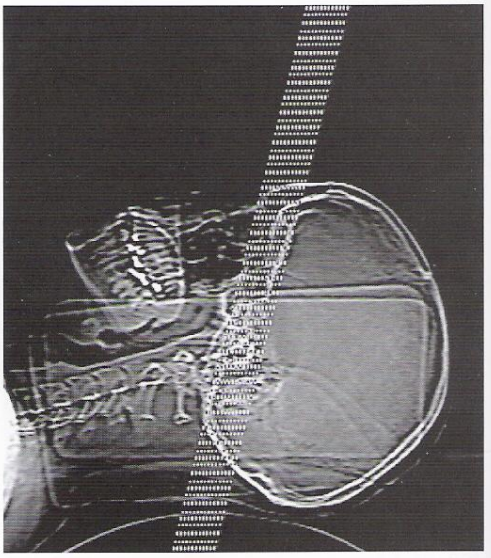

Fig. 48.1

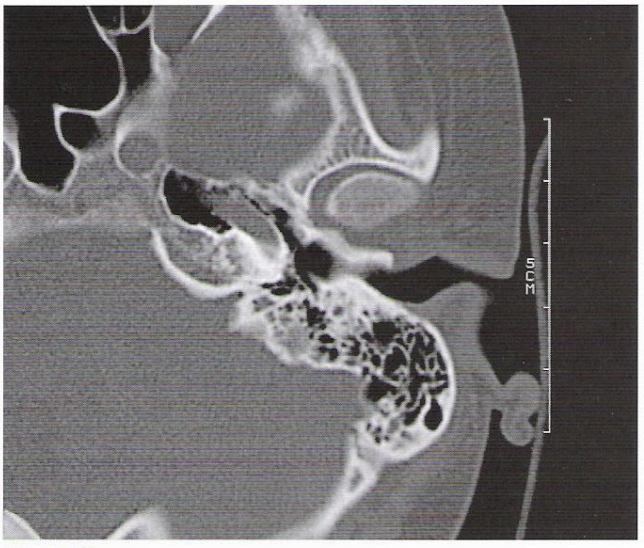

Fig. 48.2a

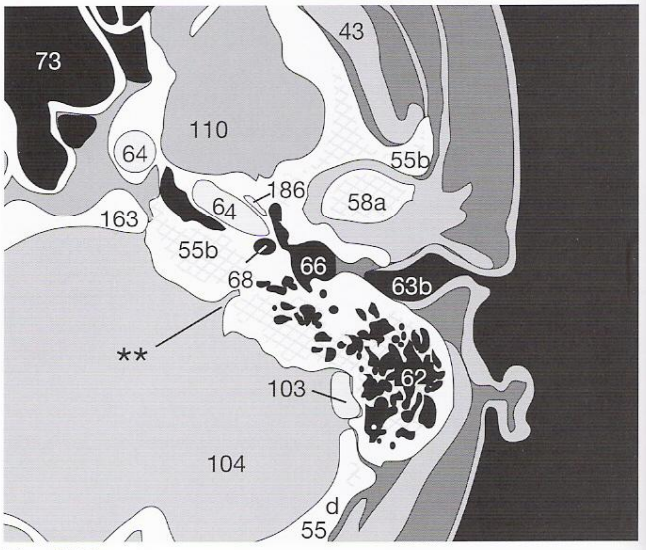

Fig. 48.2b

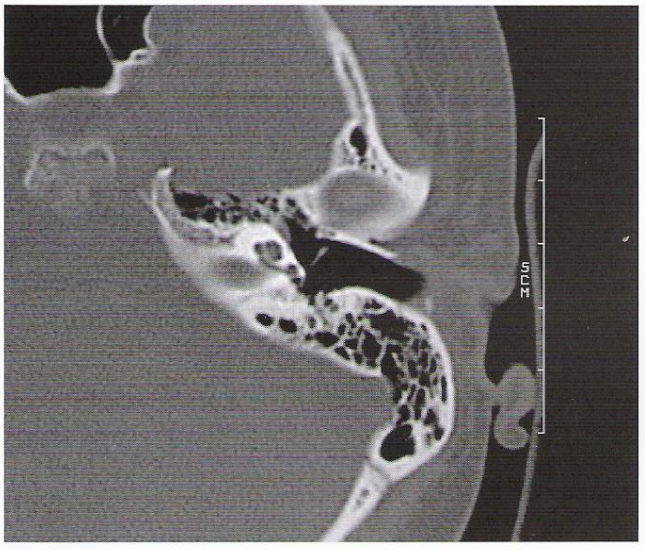

Fig. 48.3a

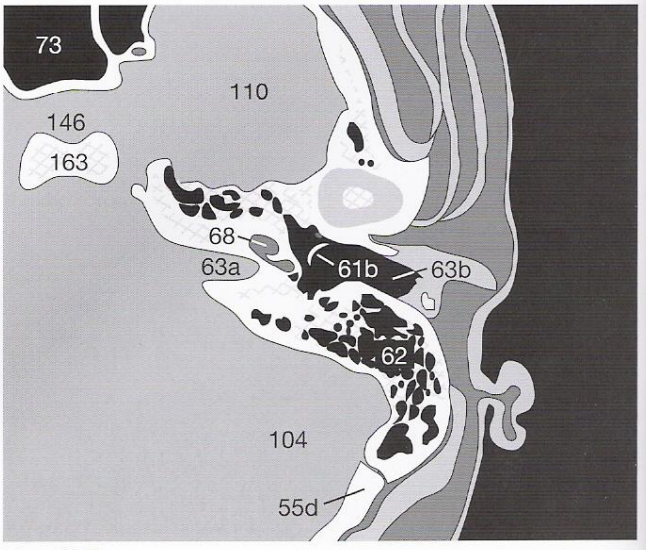

Fig. 48.3b

Fig. 49.1a

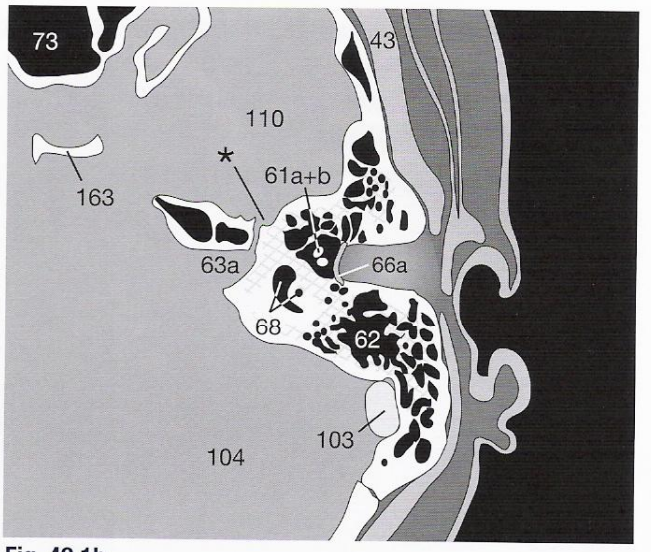

Fig. 49.1b

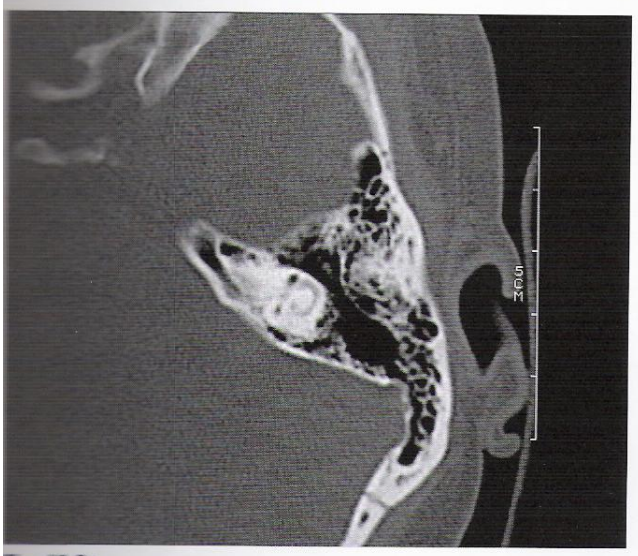

Fig. 49.2a

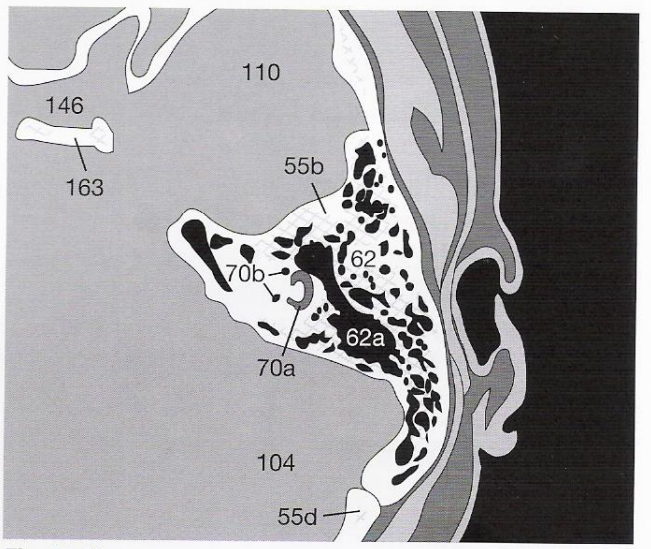

Fig. 49.2b

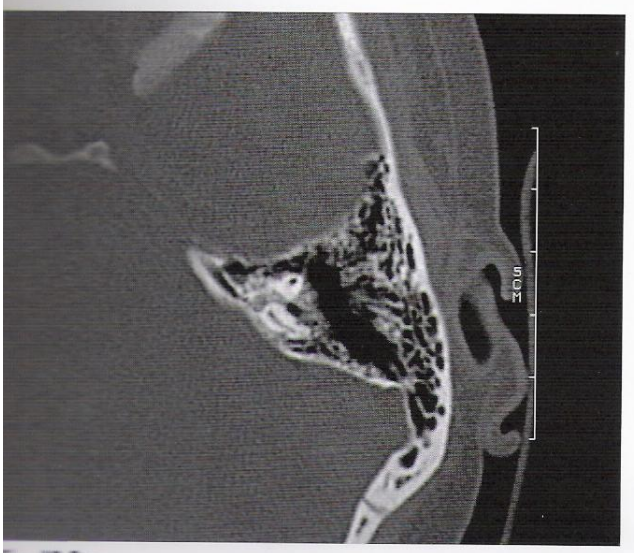

Fig. 49.3a

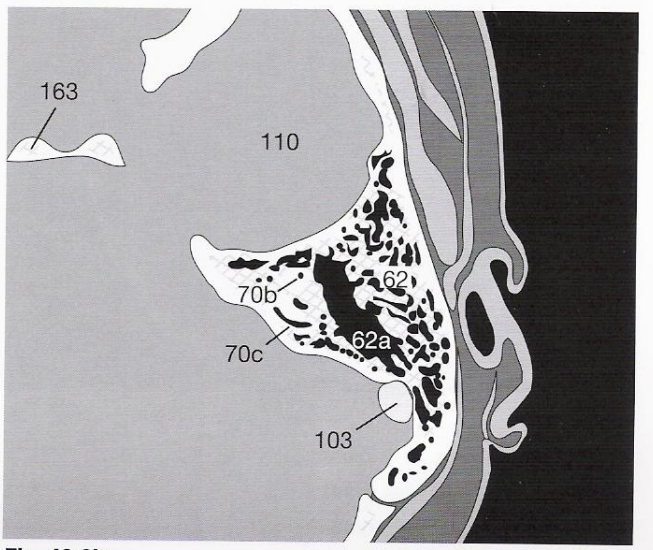

Fig. 49.3b

Do you remember the systematic sequence for evaluating CCT scans? If not, please go back to the checklist on page 26 or to your own notes on page 32.

After evaluating the soft tissues it is essential to examine the inner and outer CSF spaces. The width of the ventricles and the surface SAS increases continuously with age.

Fig. 50.1a

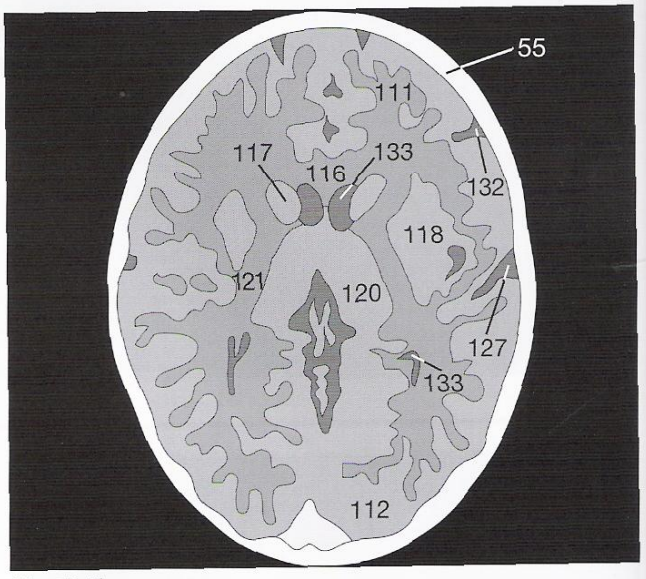

Fig. 50.1b

Since the brain of a child **(Fig. 50.1a)** fills the cranium **(55)**, the outer subarachnoid space is scarcely visible, but with increasing age the sulci enlarge **(Fig. 50.2a)** and CSF **(132)** becomes visible between cortex and calvaria. In some patients this physiologic decrease in cortex volume is especially obvious in the frontal lobe **(111)**. The space between it and the frontal bone **(55a)** becomes quite large. This so-called frontally emphasized brain involution should not be mistaken for pathologic atrophy of the brain or congenital microcephalus. If the CT scan in **Figure 50.1a** had been taken of an elderly patient, one would have to consider diffuse cerebral edema with pathologically effaced gyri. Before making a diagnosis of cerebral edema or brain atrophy you should therefore always check on the age of the patient.

Fig. 50.2a

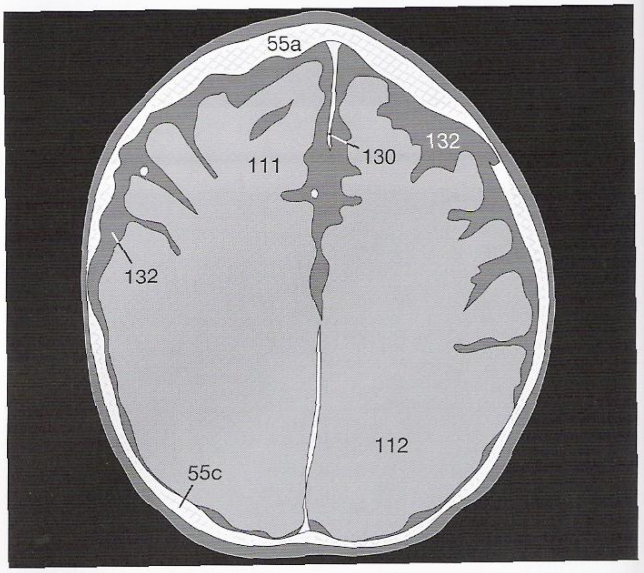

Fig. 50.2b

Figure 50.2a shows an additional variation from the norm. Especially in middle-aged female patients you will sometimes find hyperostosis of the frontal bone **(55a)** (Steward-Morel-Syndrome) without any pathologic significance. The frontal bone **(55a)** is internally thickened on both sides, sometimes with an undulating contour. In cases of doubt, the bone window can help to differentiate between normal spongiosa and malignant infiltration.

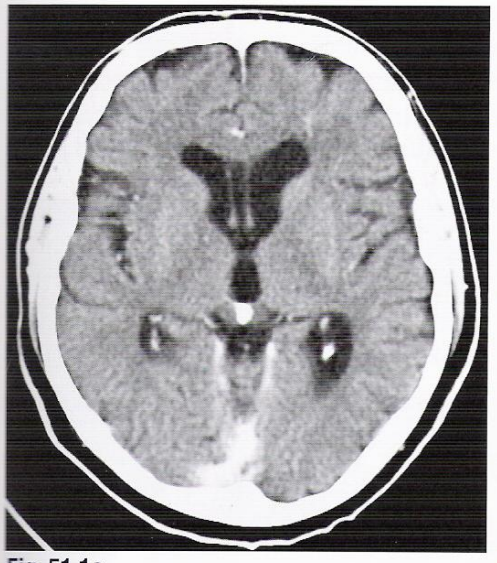

Fig. 51.1a

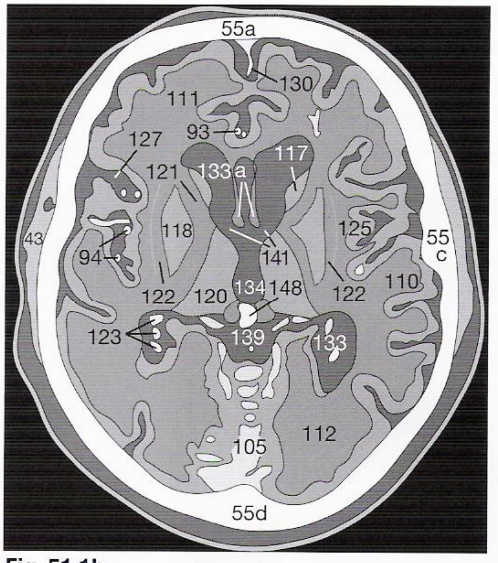

Fig. 51.1b

An incomplete fusion of the septum pellucidum **(133a)** can, as another variation, lead to the development of a so-called cavum of the septum pellucidum. Please review the normal scans in **Figures 30.2a**, **30.3a**, and **31.1a** for comparison. Usually only the part of the septum located between the two anterior horns of the lateral ventricles **(Fig. 51.1a)** is involved, less frequently the cavum extends all the way to the posterior horns **(Fig. 51.2a)**.

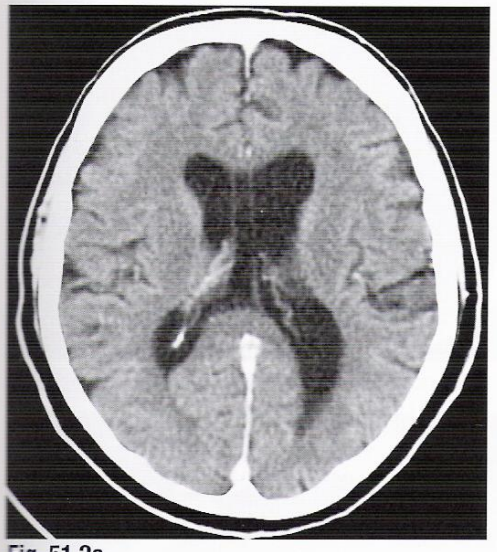

Fig. 51.2a

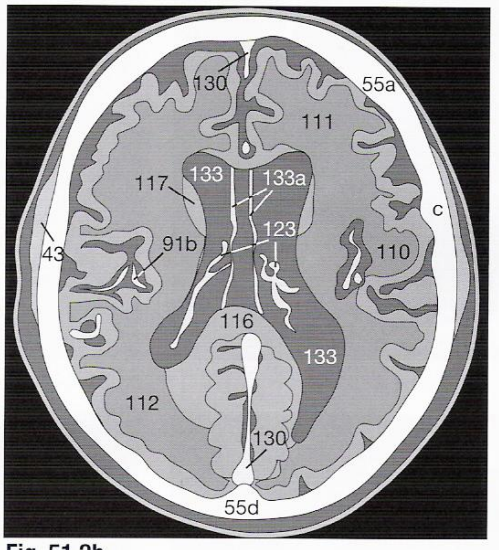

Fig. 51.2b

In the plane of **Figure 51.1**, just medial of the head of the caudate nucleus **(117)**, you can evaluate both foramina of Monro **(141)** which function as a route for the choroid plexus **(123)** and the CSF from the lateral ventricles **(133)** to the 3rd ventricle **(134)**.

Refresh your anatomic skills by naming all other structures in **Figure 51.1** and checking your results in the legend.

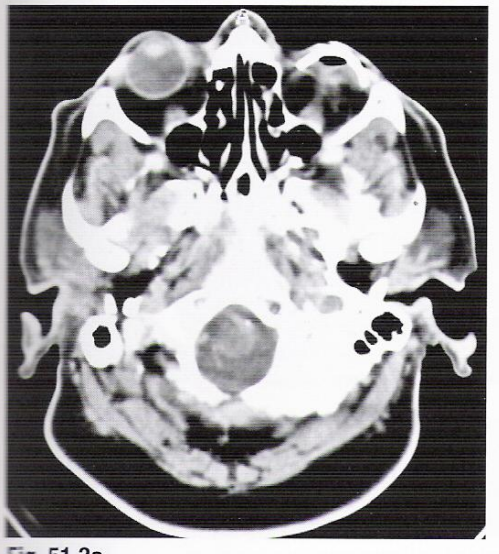

Fig. 51.3a

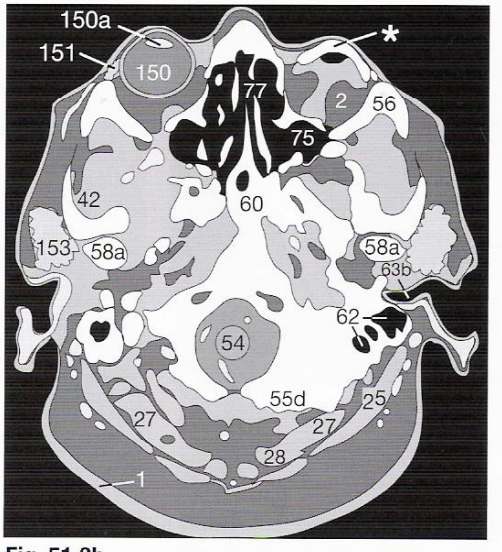

Fig. 51.3b

The radiologist will rarely be confronted with an eye prosthesis (*) after enucleation of a globe **(150)**. In patients with a history of orbital tumor, a local relapse, i.e. in the retrobulbar space **(2)** has to be ruled out in check-up CT scans.

The CT scan of the orbit in **Figure 51.3a** showed minor postoperative change without any evidence of recurrent tumor.

One of the most important rules of CT scan interpretation is to always compare several adjacent planes (see pp. 14–15). If the head is tilted even slightly during the scan procedure, one lateral ventricle **(133)** for example, can appear in the image plane **(d_S),** whereas the contralateral ventricle is still outside the plane **(Fig. 52.1)**. Only its roof will appear.

The computer therefore calculates a blurred, hypodense area which could be mistaken for a cerebral infarction **(Fig. 52.2a)**. By comparing this plane with the adjacent one below it **(Fig. 52.3a)**, the situation becomes clear, since the asymmetric contours of the imaged ventricles are now obvious.

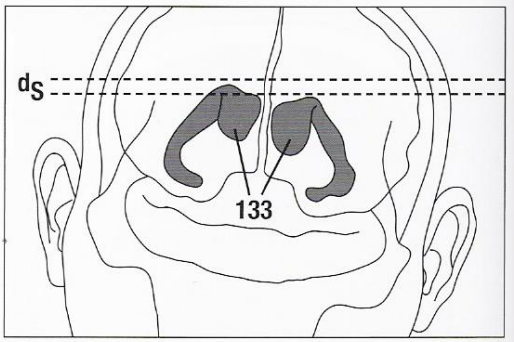

Fig. 52.1

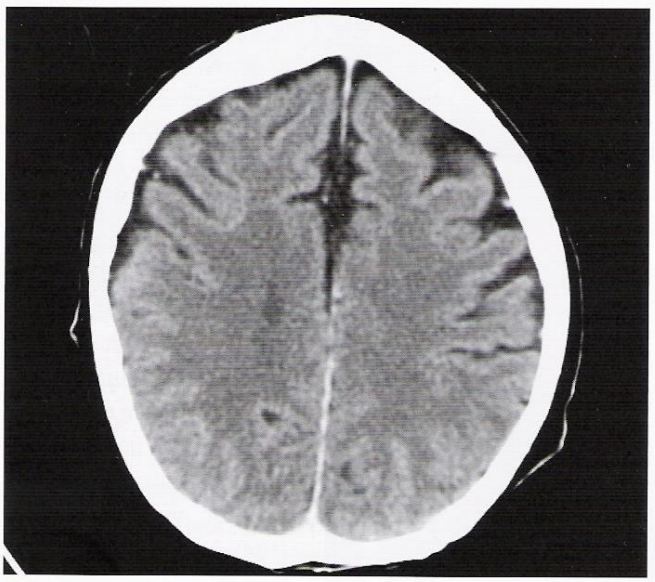

Fig. 52.2a

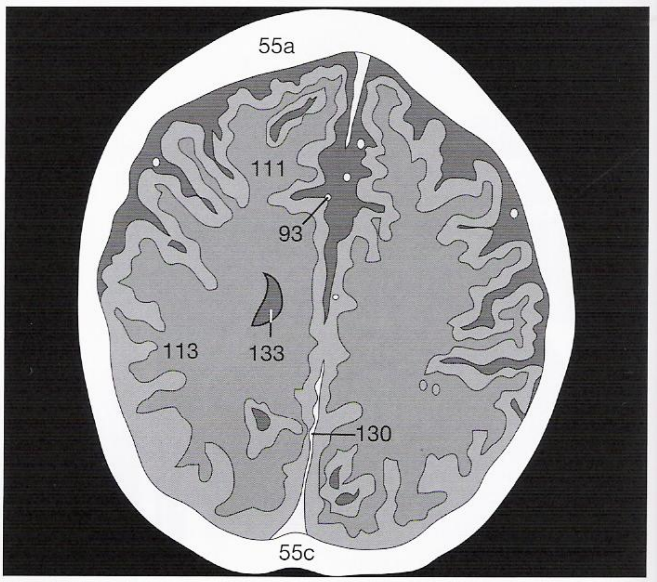

Fig. 52.2b

Fig. 52.3a

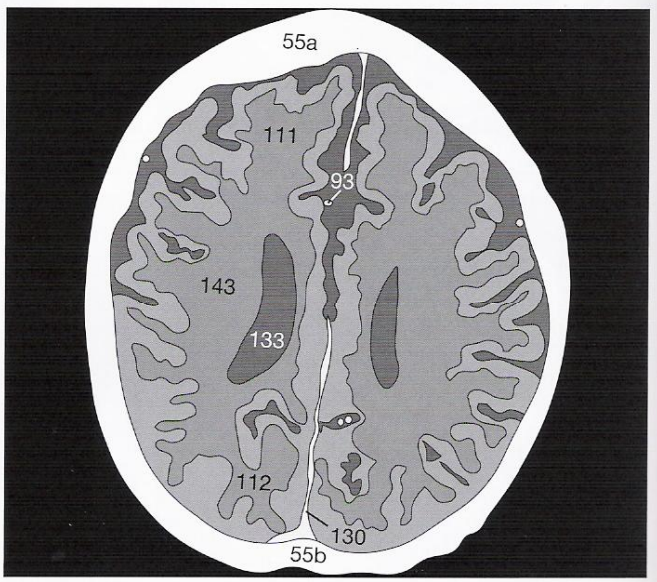

Fig. 52.3b

This example illustrates the importance of the correct placement of the patient's head. The exact position of the nose in an a.p. projection is obtained by using the gantry positioning lights. Involuntary movements of the head can be kept at a minimum by soft padding. In ventilated or unconscious patients an additional immobilization of the head with suitable bandings may be necessary.

One of the first steps in interpreting CCTs is the inspection of the soft tissues. Contusions with subcutaneous hematomas **(8)** may indicate skull trauma **(Fig. 53.1a)** and call for a careful search for an intracranial hematoma. Many injured patients cannot be expected to have their heads fixed for the duration of the CT scan, and this leads to considerable rotation. Asymmetric contours (* in **Fig. 53.1a**) of the roof of the orbit **(55a)**, the sphenoid bone **(60)**, or the petrosal bone (not asymmetric in the illustrated examples!) are therefore frequent occurrences and may lead to misinterpretations of the hyperdense bone as a fresh intracranial hematoma.

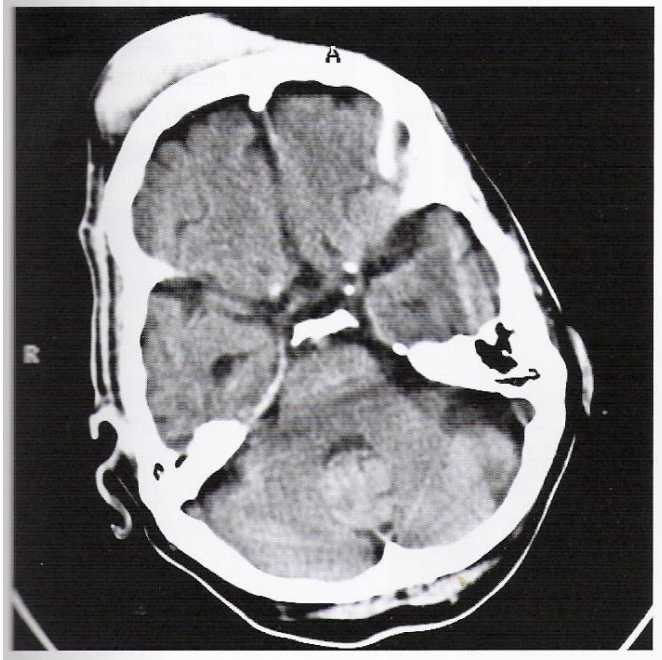

Fig. 53.1a

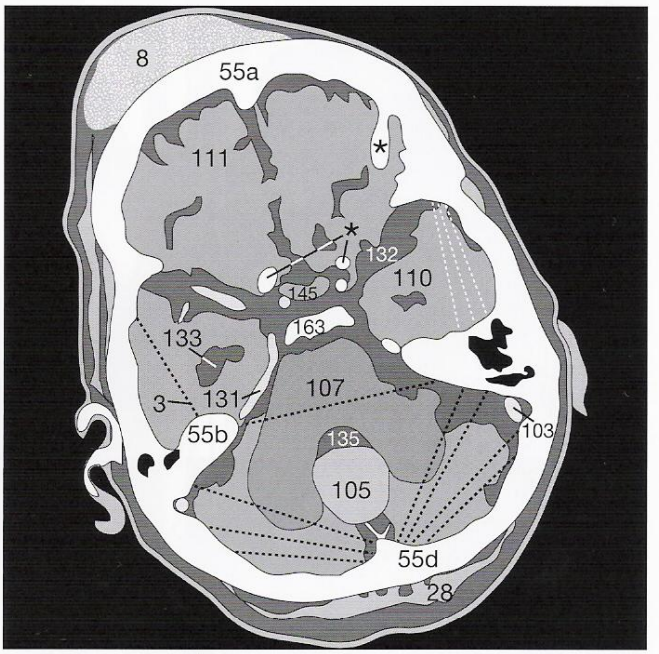

Fig. 53.1b

The question of whether it is just an asymmetric projection of the skull base or a real hematoma can be answered by comparing adjacent sections **(Fig. 53.2a)**. In this example the bones of the skull base caused the hyperdense partial volume effect. Despite the obvious right frontal extracranial contusion, intracranial bleeding could not be confirmed. Please note the considerable beam hardening (bone) artifacts **(3)** overlapping the brain stem **(107)**. Such artifacts would not appear in MR images of these levels.

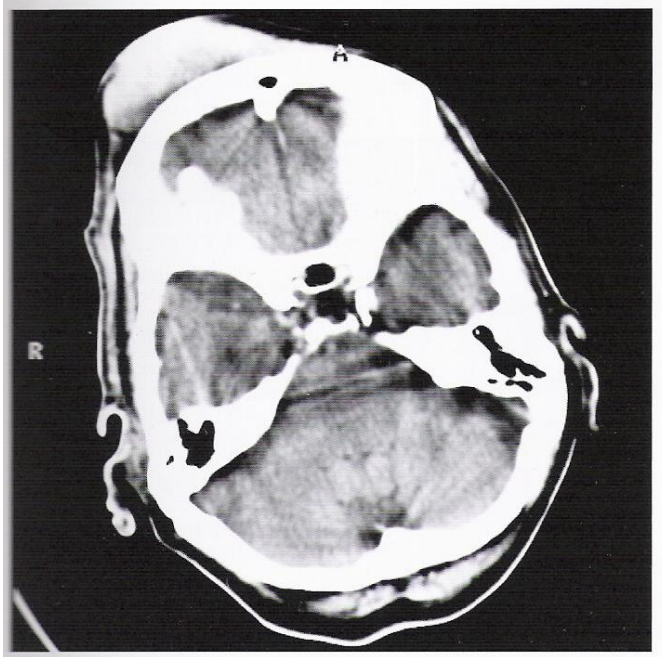

Fig. 53.2a

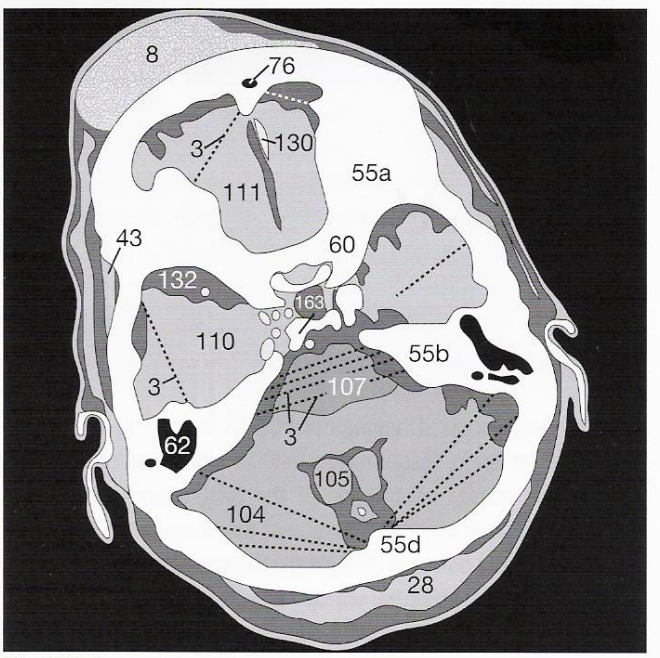

Fig. 53.2b

After having discussed that partial volume effects due to asymmetric projections (i.e., **55b** in **Fig. 54.2b**) may be misinterpreted as acute hematomas, this chapter will point out the characteristics of the different types of intracranial hemorrhage.

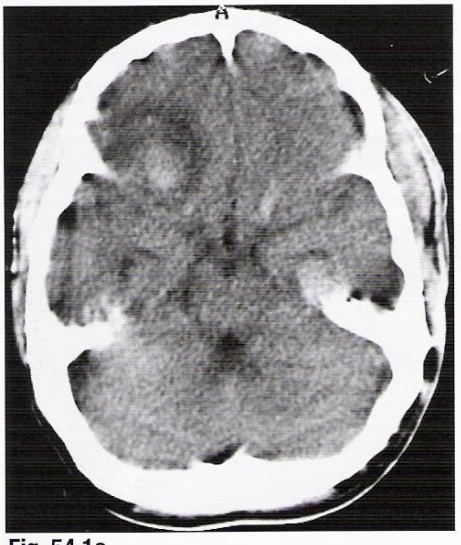

Fig. 54.1a

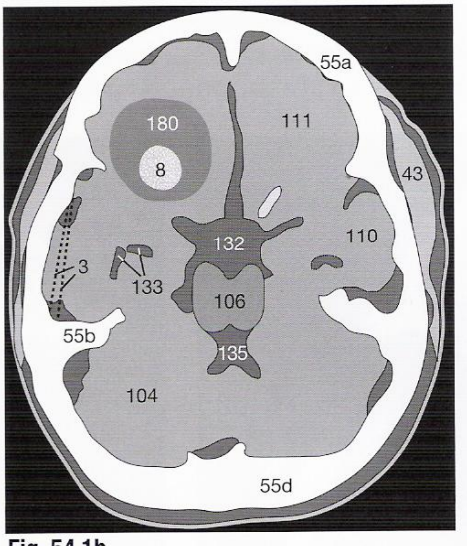

Fig. 54.1b

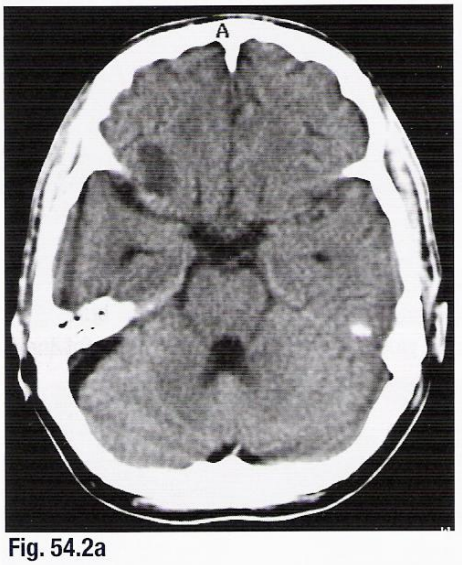

Fig. 54.2a

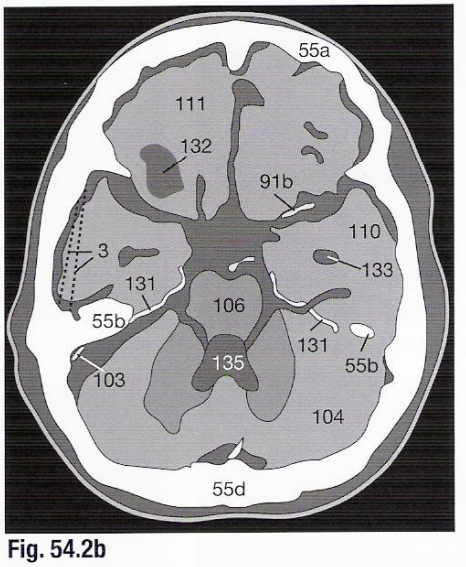

Fig. 54.2b

Bleeding Caused by a Contusion

As a direct consequence of skull trauma, cerebral contusion bleeding may occur **(Fig. 54.1a)**. An acute hemorrhage **(8)** appears as a hyperdense mass which may be accompanied by surrounding edema **(180)** and displacement of adjacent brain tissue. In anemic patients the hematoma is less dense and may therefore appear isodense to normal brain.

If the vascular wall is damaged only secondarily by hypoperfusion mediated by edema, hemorrhage may not occur until hours or, more rarely, days after skull trauma. A CCT obtained immediately after skull trauma which does not show any pathologic changes is therefore not a good predictor since delayed cerebral bleeding cannot be ruled out. A follow-up scan should be obtained if the patient's condition deteriorates. After complete resorption of a hematoma **(Fig. 54.2a)**, a well-defined defect isodense with CSF remains **(132)**.

Contusion frequently leads to an epidural, subdural, or subarachnoid hemorrhage and may leak into the ventricles **(Fig. 55.1a)**. Possible complications of such leakage or of a subarachnoid hemorrhage are disturbed CSF circulation caused by obstruction of the pacchionian granulations, the foramen of Monro, or of the 4th ventricle. An hydrocephalus with increased intracranial pressure and transtentorial herniation of the brain may result.

Epidural and subdural hematomas can also lead to major displacement of brain tissue and to midline shifts. Quite frequently this in turn causes obstruction of the contralateral foramen of Monro resulting in unilateral dilation of the lateral ventricle on the side opposite the bleeding **(Fig. 56.3)**. The characteristics useful in differential diagnosis of the various types of intracranial bleeding are listed in **Table 54.1**.

Type of bleeding	Characteristics
Subarachnoid bleeding	Hyperdense blood in the subarachnoid space or the basal cisterna instead of hypodense CSF
Subdural bleeding	Fresh hematoma: crescent-shaped, hyperdense bleeding close to the calvaria with ipsilateral edema; hematoma is concave toward hemisphere; may extend beyond cranial sutures
Epidural bleeding	Biconvex, smooth ellipsoidal in shape; close to calvaria; does not exceed cranial sutures; usually hyperdense, rarely sedimented

Table 54.1

If there is intraventricular extension of intracranial hemorrhage (Fig. 55.1a), physiologic calcification of the choroid plexus **(123)**, in the lateral **(133)** and 3rd ventricles **(134)**, as well as those of the habenulae and the pineal **(148)**, must be distinguished from fresh, hyperdense blood clots **(8)**. Please note the edema **(180)** surrounding the hemorrhage **(Fig. 55.1a)**.

If the patient has been lying supine, a horizontal fluid–fluid level caused by blood sedimenting in the posterior horns of the lateral ventricles may be seen **(Fig. 55.2a)**. The patient is in danger of transtentorial herniation if the ambient cistern is effaced **(Fig. 55.2b)**. In this case the 3rd ventricle is completely filled with clotted blood (in **Fig. 55.2a, b**), and both lateral ventricles are markedly dilated. CSF has leaked into the paraventricular white mater ( ). In addition, a lower section of this patient shows subarachnoid hemorrhage into the SAS (, in **Fig. 55.2b**).

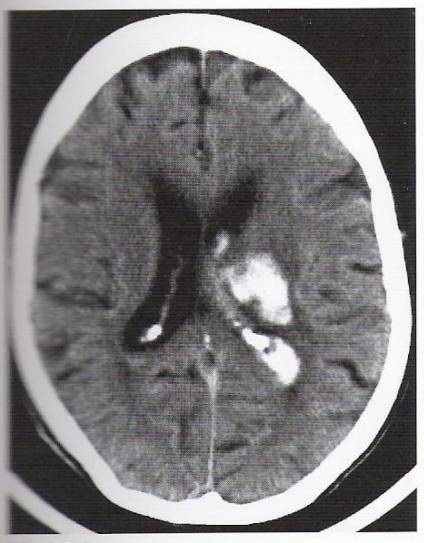

Fig. 55.1a

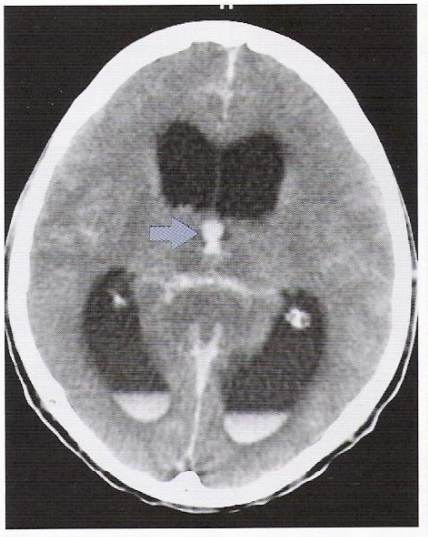

Fig. 55.2a

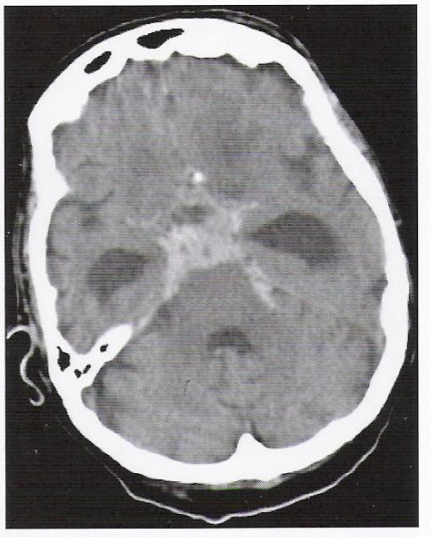

Fig. 55.3a

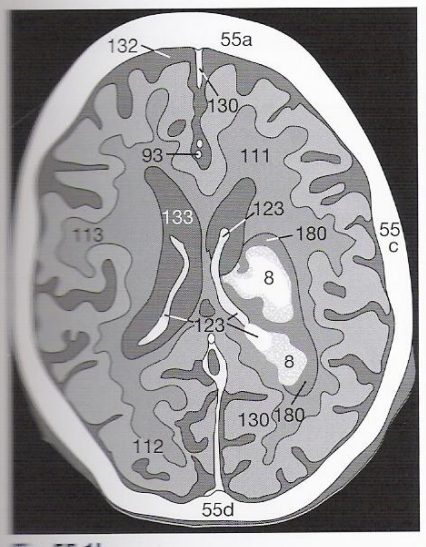

Fig. 55.1b

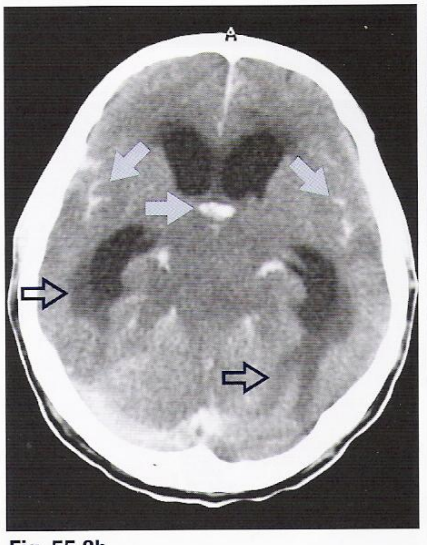

Fig. 55.2b

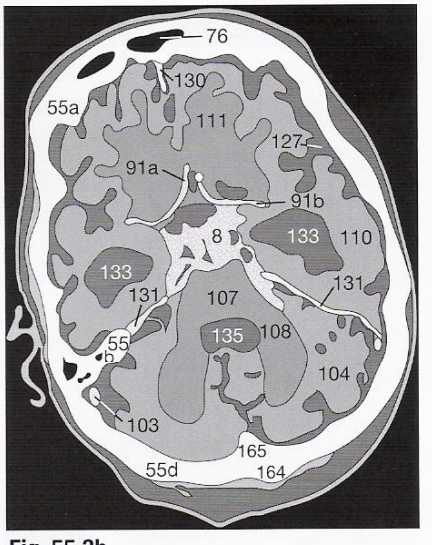

Fig. 55.3b

Subarachnoid Hemorrhage

An obstructive hydrocephalus, as caused by subarachnoid hemorrhage (**8** in **Fig. 55.3a, b**), may easily be identified because the temporal horns **(133)** of the lateral ventricles appear distended. In such cases it is important to have a closer look at the width of the SAS over the cerebral surface: blunted cerebral gyri usually indicate a diffuse cerebral edema. In the present case though, the width of the Sylvian fissure **(127)** and the surface SAS are normal. Acute edema is therefore not present (yet).

Since the surface SASs are very narrow in younger patients, it is possible to miss a subarachnoid hemorrhage in children. The only identifiable sign may be a small hyperdense area adjacent to the falx **(130)**. In adults a small subarachnoid hemorrhage also causes only a minor, circumscribed area of hyperdensity (**8** in **Fig. 56.1a**). At the time of this CT scan the bleeding was so slight that it had not yet caused any displacement of brain tissue.

Subdural Hematoma

Bleeding into the subdural space results from cerebral contusions, damaged vessels in the pia mater, or from torn emissary veins. The hematoma initially appears as a long, hyperdense margin close to the skull (**8** in **Fig. 56.2a**). In contrast to an epidural hematoma, it is usually somewhat irregular in shape and slightly concave toward the adjacent hemisphere. This kind of bleeding is not confined by cranial sutures and may spread along the entire convexity of the hemisphere.

Subdural hematomas can also cause marked displacement of brain tissue **(Fig. 56.3a)** and lead to disturbances in CSF circulation and to incarceration of the brain stem in the tentorial notch. It is therefore not as important, for treatment purposes, to distinguish between a subhematoma or an epidural hematoma as it is to ascertain the extent of the hemorrhage. Hematomas with the propensity to expand, especially if edema is a threat, should therefore be drained or treated surgically.

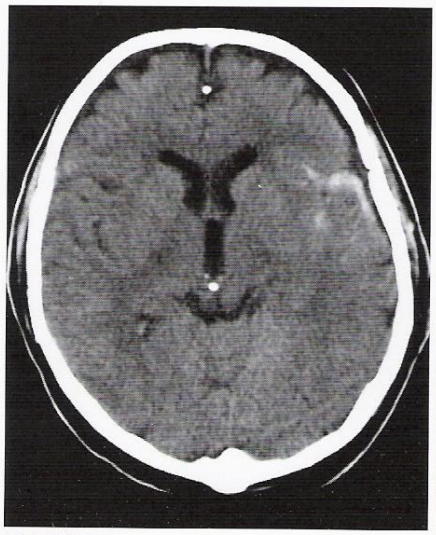

Fig. 56.1a

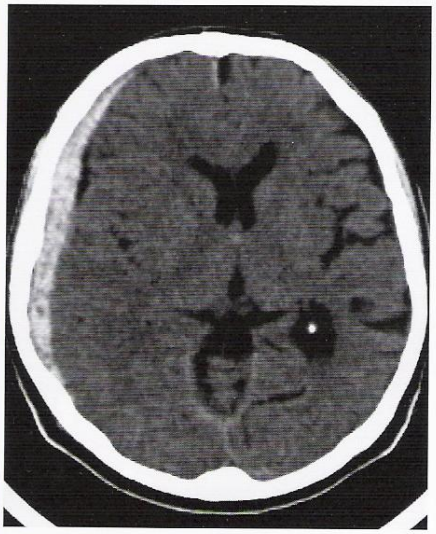

Fig. 56.2a

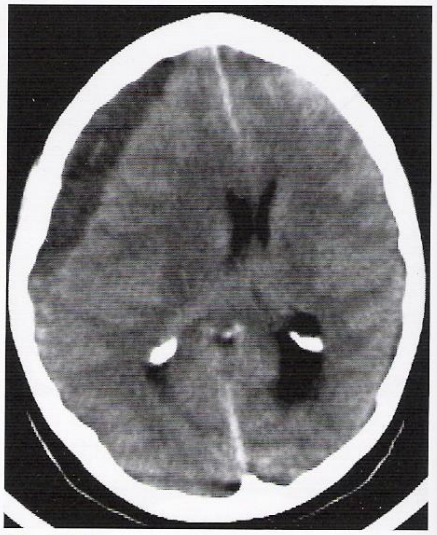

Fig. 56.3a

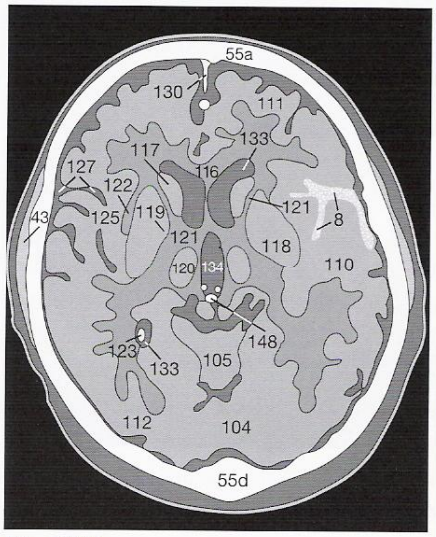

Fig. 56.1b

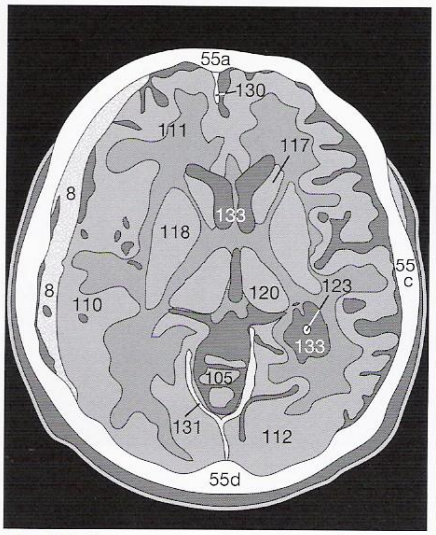

Fig. 56.2b

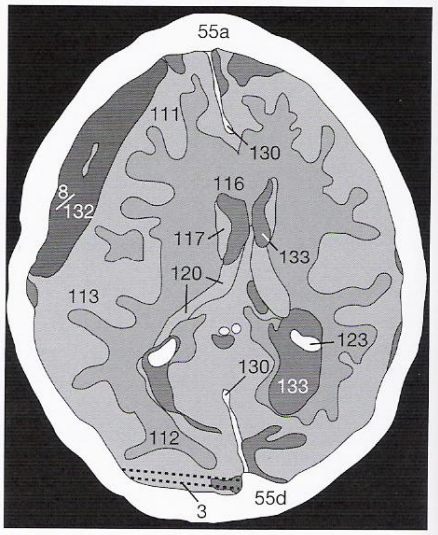

Fig. 56.3b

Chronic subdural hematomas (**8** in **Fig. 56.3a**) may appear homogeneously hypodense or show inhomogeneous density with sedimentation of blood. The danger involved in a small, venous bleed is the symptom-free interval and the slow onset of somnolence up to the development of a coma. Therefore, a patient with suspected bleeding after cranial trauma should always be kept under observation in order to detect any clinical deterioration.

Extradural Hematomas

Bleedings into the extradural spaces are usually caused by damage to the middle meningeal artery, and rarely by venous bleeding from the sinuses or the pacchionian bodies. Predisposed areas are temporoparietal regions or sometimes the posterior cranial fossa, in which case there is severe danger of tonsillar herniation. Arterial hemorrhage lifts the dura from the inner surface of the cranium **(55)** and then appears as a biconvex, hyperdense area with a smooth border to the adjacent hemisphere. The hematoma does not extend beyond the sutures between the frontal **(55a)**, temporal **(55b)**, parietal **(55c)**, or occipital **(55d)** bones. In small extradural hematomas **(8)** the biconvex shape is not distinct **(Fig. 57.1a)**, making it difficult to differentiate the finding from a subdural hematoma.

It is important to distinguish between a closed skull fracture with an intact dura, and a compound skull fracture with the danger of secondary infection. An unequivocal sign of a compound skull fracture **(Fig. 57.2a)** is the evidence of intracranial air bubbles **(4)**, which prove that there is a connection between intracranial spaces and the paranasal sinuses or the outside. It is difficult to determine whether the bilateral, hyperdense hematomas **(8)** in **Figure 57.2** are extradural or subdural. In this case the distortion of the midline was caused by the right-sided, perilesional edema (left side of **Fig. 57.2a**) since it was shifted toward the left (the side of the hematoma).

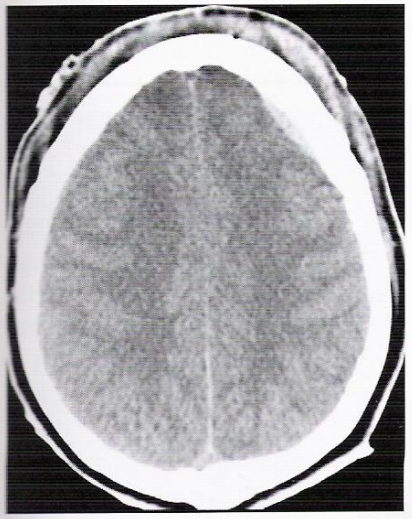

Fig. 57.1a

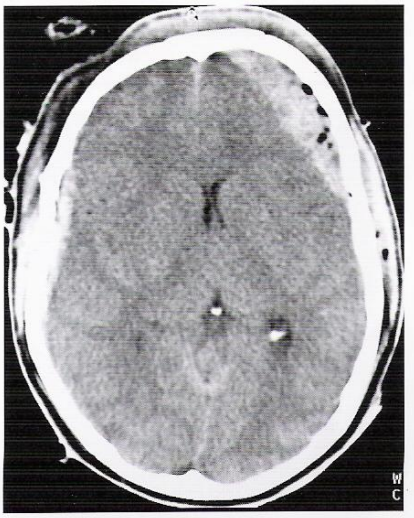

Fig. 57.2a

Test Yourself! Exercise **8:**

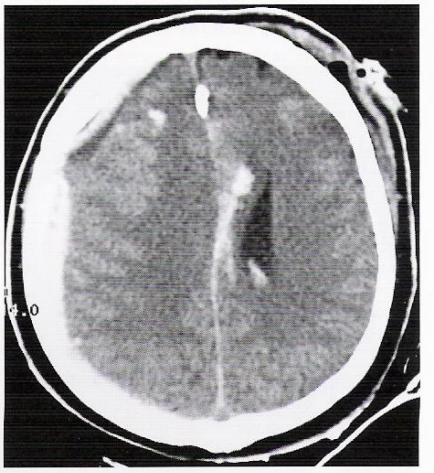

Fig. 57.3

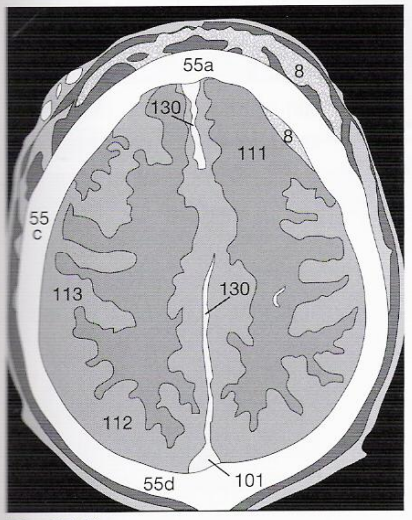

Fig. 57.1b

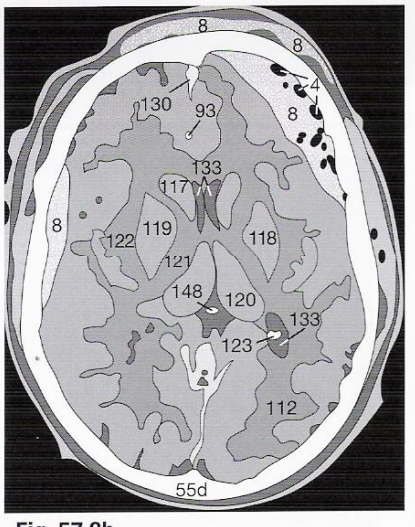

Fig. 57.2b

Space for your suggested answer:

Test Yourself! Exercise **8:**

When looking at the image of another patient **(Fig. 57.3),** you will note several pathologic changes. Use the free space below the picture to note how many different types of bleeding (if any) you can distinguish and what other pathology/complications you suspect. You will find the answers at the end of the book, but remember: be a good sport and don't cheat, think first!

Apart from cardiovascular and malignant diseases, cerebral infarctions are among the most frequent causes of death. A thrombus occludes a cerebral artery, which leads to irreversible necrosis in the area of blood supply. Vascular occlusion develops in association with atherosclerotic changes of cerebral arteries or, less frequently, as a result of arteritis. A further cause are blood clots from the left heart or thrombotic plaques from the carotid bifurcation which embolize into a cerebral vessel.

In case of embolization, diffusely situated, small, hypodense zones of infarction in both basal ganglia and hemispheres are typical. Old emboli result in small, well-defined areas **(180)** which eventually appear isodense to the CSF **(132)**. Such areas are called lacunal infarcts **(Fig. 58.1a)**. A diffuse pattern of defects calls for color flow Doppler imaging or carotid angiography and an echocardiogram to exclude atrial thrombus.

Please remember that in a suspected stroke it might take up to 30 hours to distinguish clearly the accompanying edema as a hypodense lesion from unaffected brain tissue. A CT scan should be repeated if the initial scan does not show any pathologic changes even though the patient is symptomatic and if symptoms do not resolve (resolution of symptoms points to a **t**ransient **i**schemic **a**ttack, TIA). In case of a TIA: no abnormalities are visible in the CT scan.

In contrast to the TIA, the **p**rolonged **r**eversible **i**schemic **n**eurologic **d**eficit (**PRIND**) is often associated with hypodense zones of edema in the CT scan.

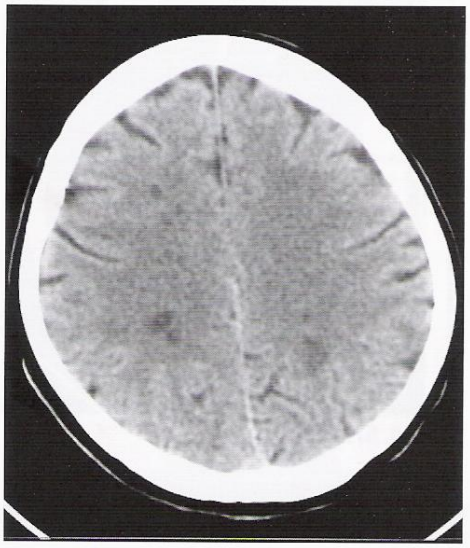

Fig. 58.1a

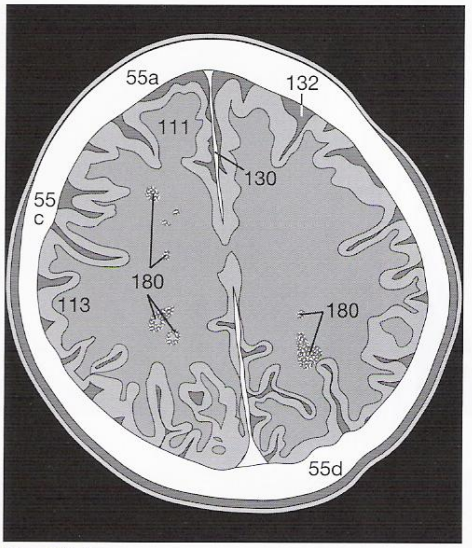

Fig. 58.1b

If the area of infarction corresponds to the distribution of a cerebral artery, one should consider an occlusion of the corresponding blood vessel. In classical infarctions of branches of the middle cerebral artery, ischemia will cause a hypodense area of edema (⬅, ↙ in **Fig. 58.2a**).

Depending on the size, the infarction may have severe mass effect and cause midline shift. Smaller areas of infarction do not usually show any significant midline shift. If the arterial walls are damaged, bleeding may occur and appear as hyperdense areas coating the neighboring gyri.

The unenhanced follow-up CT scan in **Figure 58.2b** shows an additional bleed into the head of the right caudate nucleus (⇦) and right putamen (↖). In this case the infarction is 2 weeks old and necrotic tissue has been mostly resorbed and replaced by CSF.

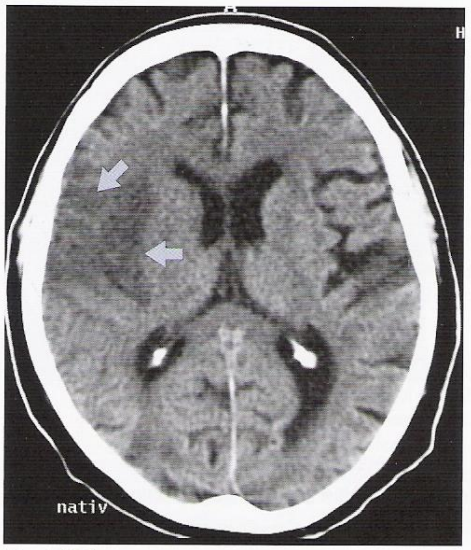

Fig. 58.2a

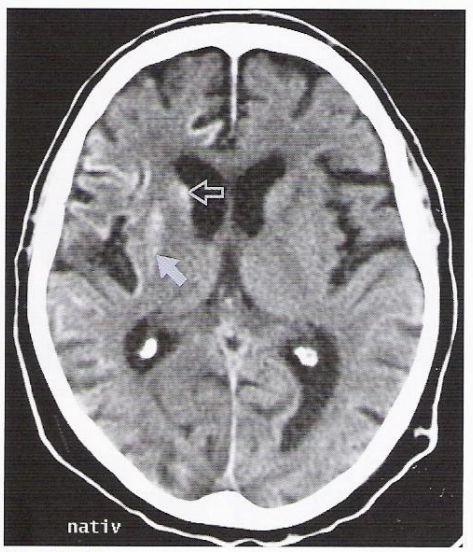

Fig. 58.2b

Fig. 59.1a

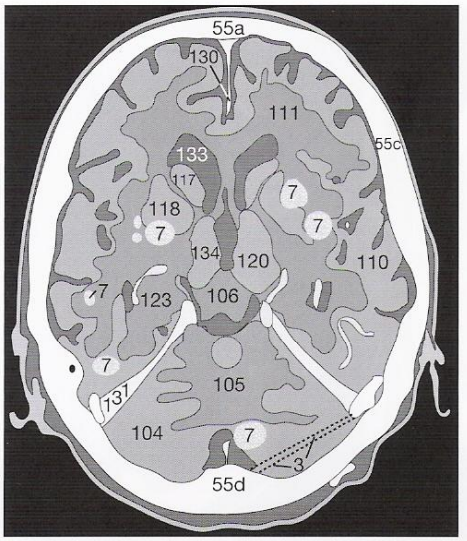

Fig. 59.1b

Whereas differential diagnosis (DD) of intracranial hemorrhage and infarction may be obtained without the use of CM, detection of cranial metastases **(7)** is definitely improved by the administration of i.v. CM. Even small areas in which the blood-brain barrier is disturbed become visible **(Fig. 59.1a)**. Large metastases sometimes cause surrounding edema **(180)** which could be misinterpreted as infarct-related edema on unenhanced images if the metastasis appears isodense to the adjacent tissue. After i.v. CM the lesion in the left hemisphere **(7)** is clearly demarcated **(Fig. 59.2a)**. Did you also spot the second, smaller metastasis within the right frontal lobe, which also shows some surrounding edema **(180)**?

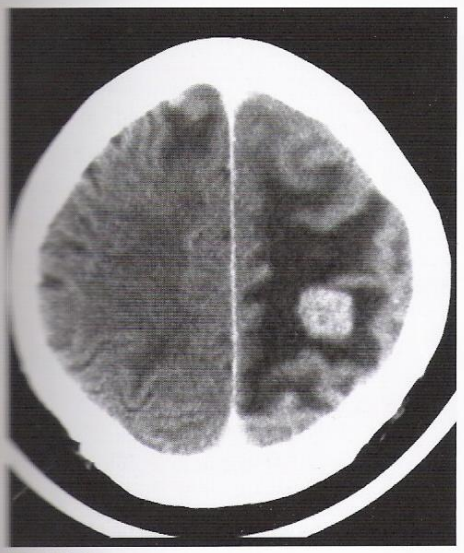

Fig. 59.2a

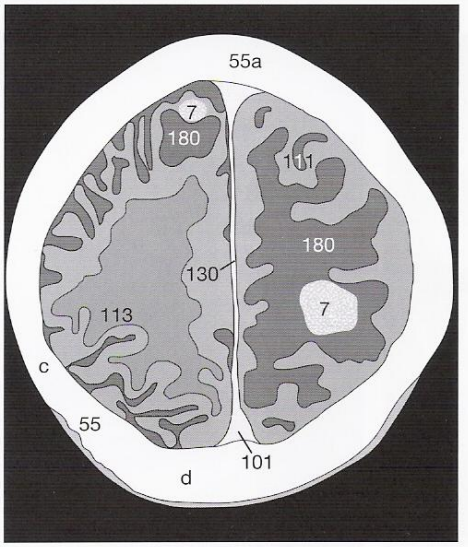

Fig. 59.2b

The differential diagnosis of brain tumors is made much easier by the injection of i.v. CM. In the unenhanced image **(Fig. 59.3a)**, the temporoparietal glioblastoma on the left **(7)** which has a central necrosis **(181)** could have been mistaken for cerebral infarction. The post-CM image, however, reveals the typical appearance of a glioblastoma with an irregular rim enhancement of its margin **(Fig. 59.3c)**.

Fig. 59.3a

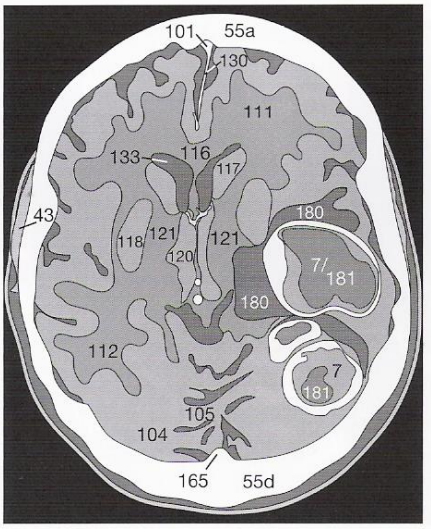

Fig. 59.3b

Abb. 59.3c

Fig. 60.1a

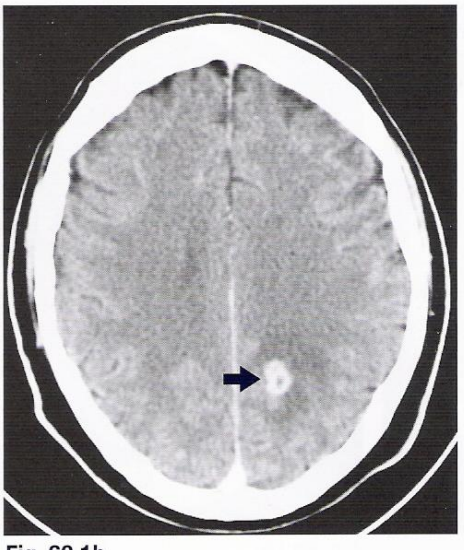

Fig. 60.1b

Another example of the advantages of i.v. CM is the demonstration of inflammatory processes, since the accompanying defect in the blood-brain barrier will not show on an unenhanced image. **Figure 60.1a** shows hypodense edema ( ) in an unenhanced section of a patient suffering from aortic valve endocarditis. Contrast medium **(Fig. 60.1b)** confirmed the finding by enhancing the inflammatory process ( ). Bacteria from the aortic valve caused this septic embolism in the left occipital lobe.

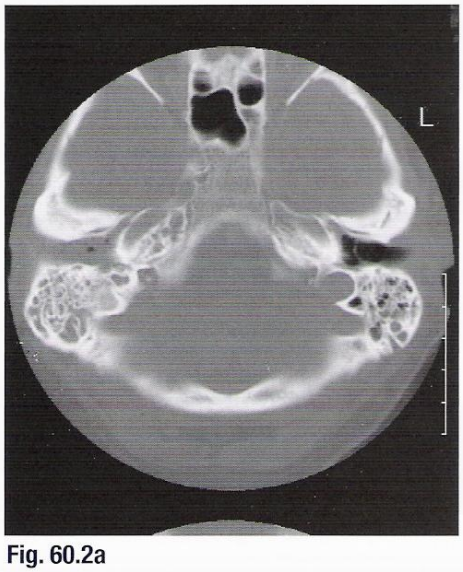

Fig. 60.2a

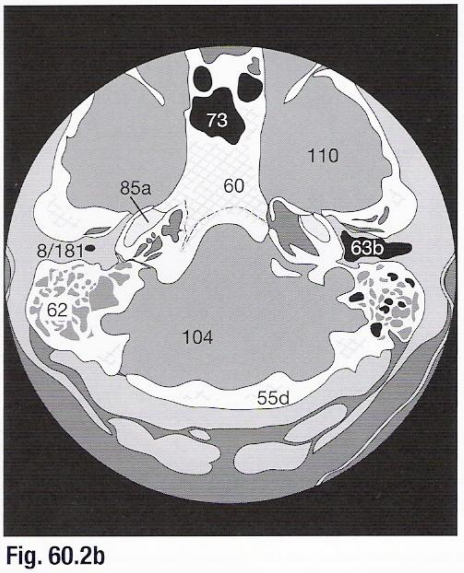

Fig. 60.2b

Inflammation of the paranasal sinuses and of the middle ear can already be diagnosed in native images as effusions **(8)**, for example in the normally air-filled mastoid cells **(62)**. Swelling of the mucous membranes of the external auditory canal **(63b)** is visible without the need for CM. **Figure 60.2a** shows bilateral otitis externa and media, which is more severe on the right side where it involves the antrum and the mastoid cells. With progressing abscess formation, an image on bone windows should be obtained in order to detect possible bone erosion.

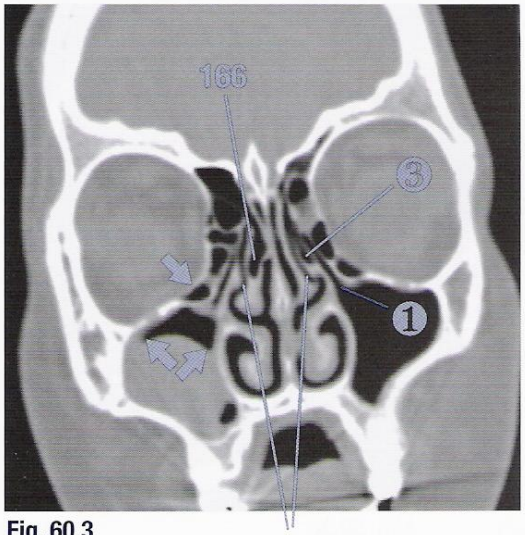

Fig. 60.3

A retention cyst, which often appears in one of the paranasal sinuses, should be considered in the differential diagnosis of advanced inflammations. They typically have a broad base on the wall of a paranasal sinus, extend into its lumen, and have a roundish convex shape (, in **Fig. 60.3**).

Such cysts are only of significance if they obstruct the infundibulum (1) of the maxillary sinus or the semilunar canal (2), causing an accumulation of secretions. In patients with chronic sinusitis, it is therefore important to check for an unobstructed lumen of the semilunar canal (2) or for variations which may restrict mucociliary transport of secretory products.

Haller's cells ( ), a pneumatized middle concha (166), and a pneumatized uncinate process (3) are among the most frequent variations. All of these variations can obstruct the semilunar canal and cause chronic, relapsing sinusitis.

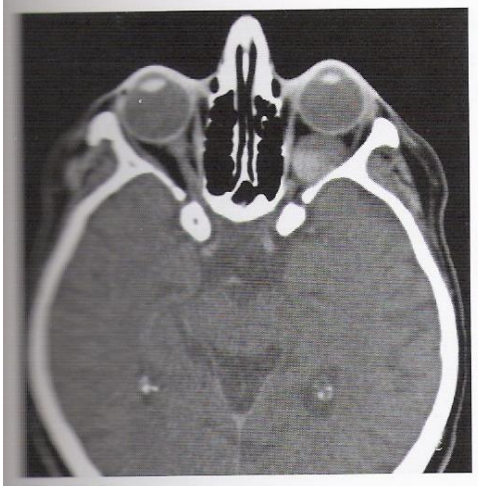

Fig. 61.1a

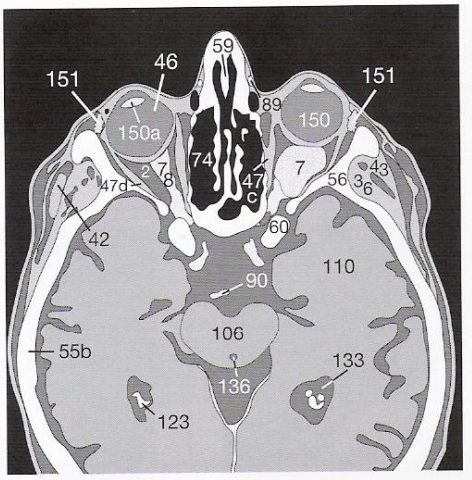

Fig. 61.1b

You have already seen pathologic changes in the lacrimal gland (pp. 39/40) and the CT morphology of an eye prosthesis (p.51). Every mass within the orbit should, of course, be diagnosed early and treated effectively because of the possibly severe consequences to vision. In order not to miss tumor invasion into the walls of the orbit, bone windows should also be obtained. In **Figure 61.1a** there is a hemangioma **(7)** within the retrobulbar fat **(2)**, which is not necessarily an indication for operation because of its benign character. In this case it causes a minor proptosis.

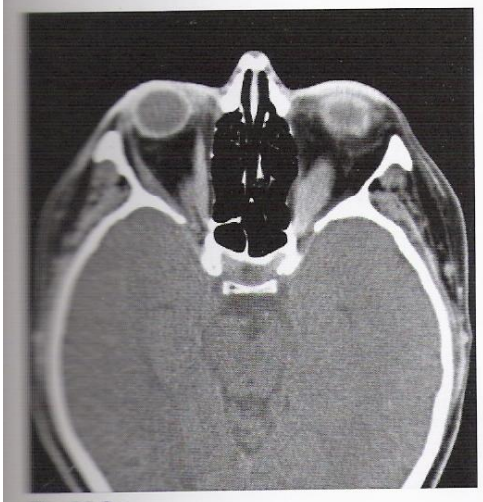

Fig. 61.2a

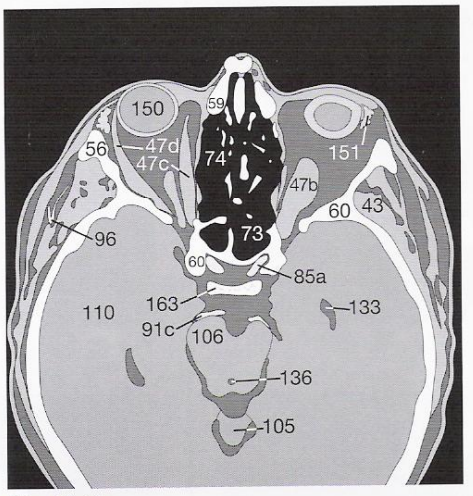

Fig. 61.2b

Endocrine Ophthalmopathy

Minimal discrete changes can be missed during the reporting of a CT scan: endocrine ophthalmopathy often appears as part of Graves' disease and can, in its early stage, only be diagnosed on the basis of a thickening of the external ocular muscles, e.g. the inferior rectus muscle (**47b** in **Figs. 61.2a**, **61.3a**).

Myositis should be considered in the differential diagnosis. If this early sign is not detected, the disease of the orbital tissue, which is most probably an autoimmune disease, may progress in the absence of therapeutic intervention. Therefore, you should always examine the symmetry of the external ocular muscles **(47)** when looking at an orbital CT scan.

There will often be a typical temporal pattern of involvement. The first finding is an increase in the volume of the inferior rectus muscle **(47b)**. The disease will continue and affect the medial rectus muscle **(47c)**, the superior rectus muscle **(47a)**, and finally all the other external ocular muscles.

Fig. 61.3a

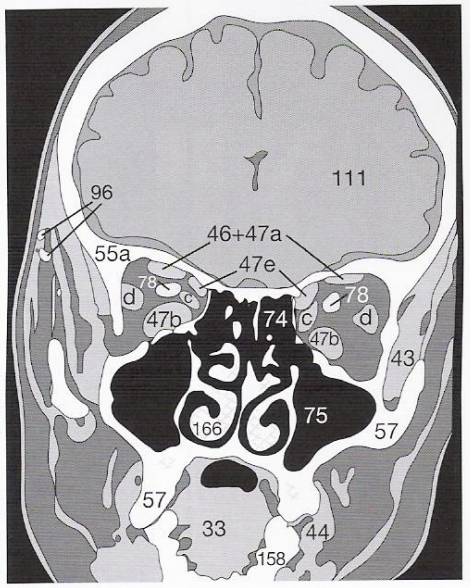

Fig. 61.3b

In contrast to benign retention cysts (p. 60), malignant tumors of the paranasal sinuses often lead to destruction of the facial bones and may invade the orbit, the nasal cavity **(77)**, or even the cranial fossa. It is therefore useful to examine both the soft tissue and bone windows. For planning a resection, different CT planes might be necessary. The following example shows a tumor of the paranasal sinuses **(7)** in an axial **(Fig. 62.1a)** and a coronal view **(Fig. 62.2a)**. Originating from the mucous membranes of the right maxillary sinus **(75)**, the tumor has infiltrated the nasal cavity **(77)** and the ethmoid cells.

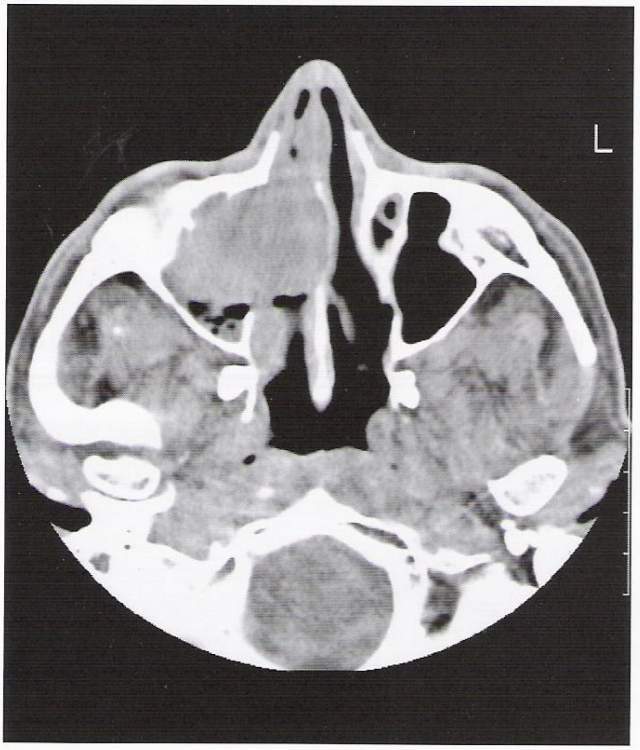

Fig. 62.1a

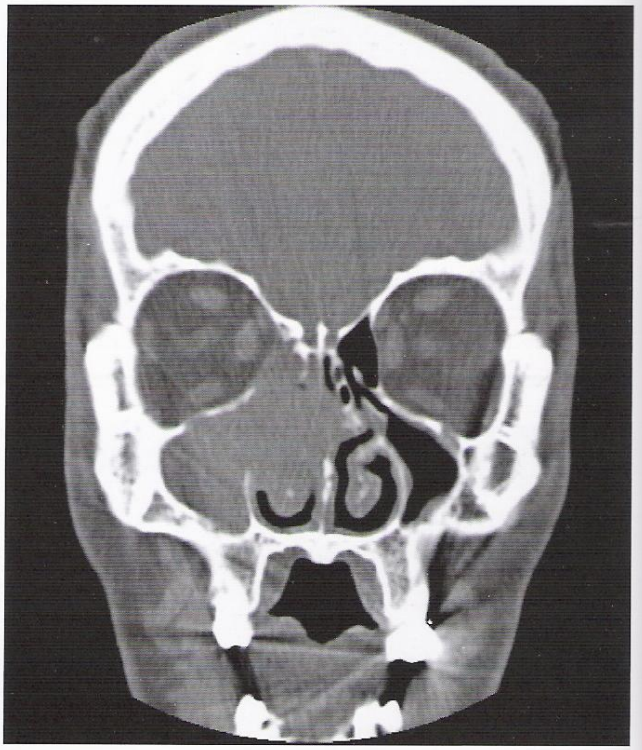

Fig. 62.2a

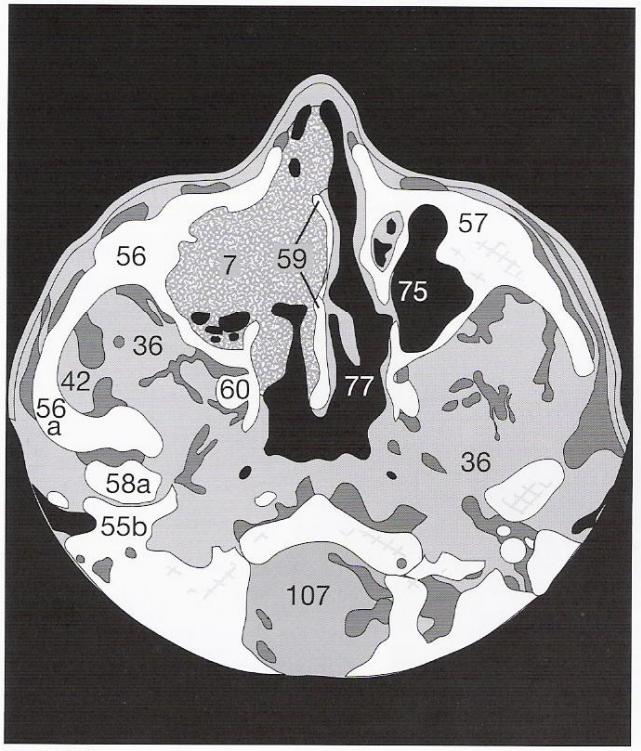

Fig. 62.1b

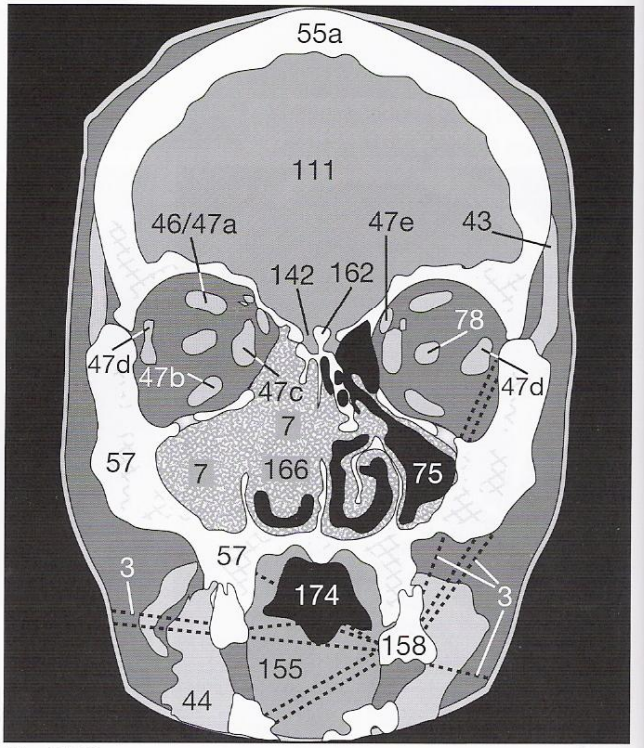

Fig. 62.2b

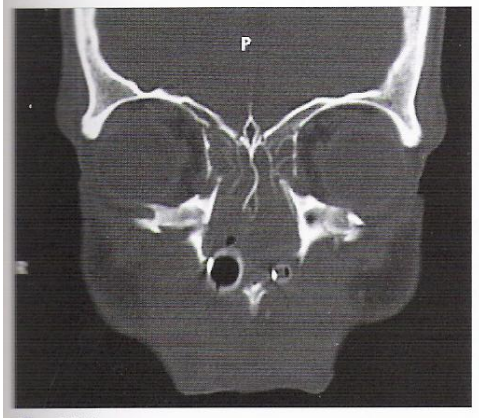

Fig. 63.1a

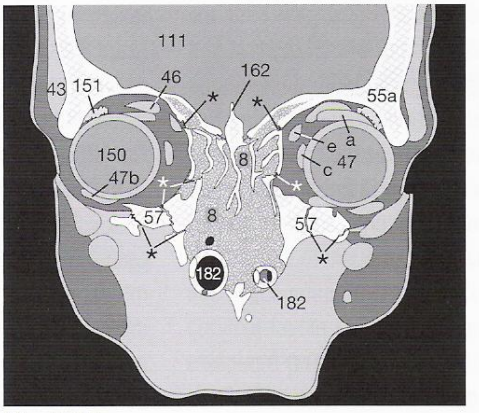

Fig. 63.1b

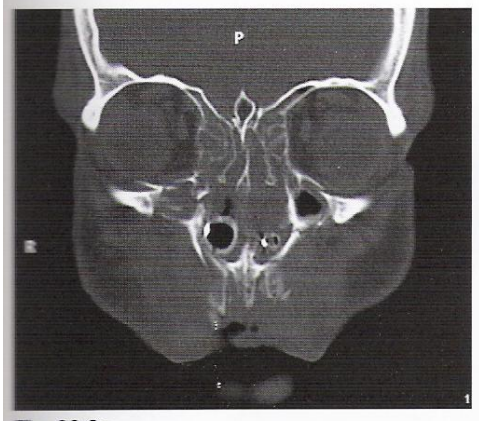

Fig. 63.2a

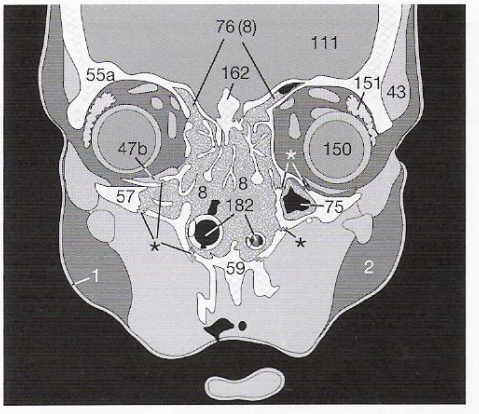

Fig. 63.2b

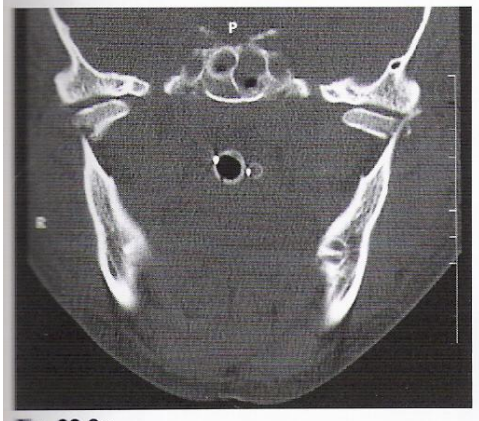

Fig. 63.3a

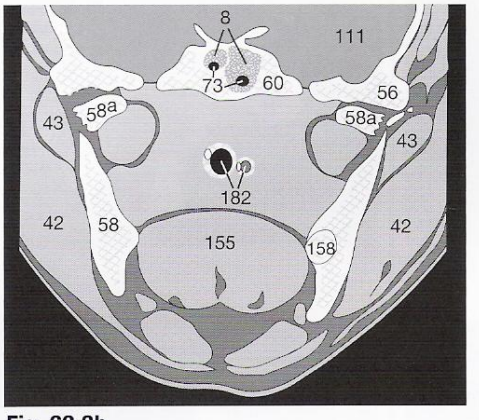

Fig. 63.3b

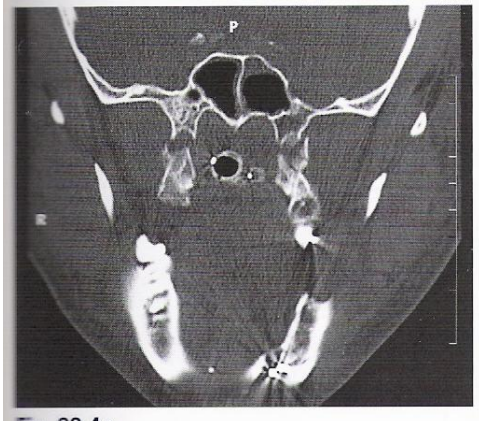

Fig. 63.4a

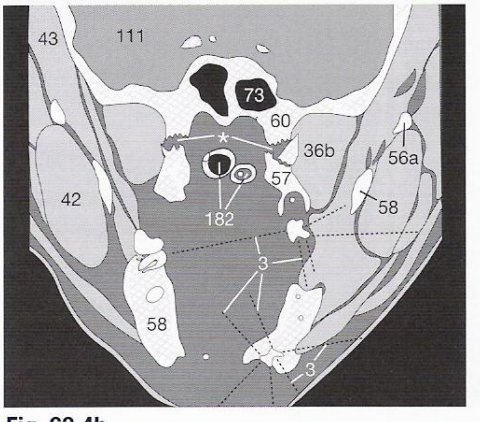

Fig. 63.4b

The most common reason for doing a coronal CT scan is, apart from determining the extent of chronic sinusitis, the diagnosis of fractures: in fractures of the orbital floor **(Figs. 63.1a, 63.2a)** any accompanying herniation of retrobulbar fat **(2)** or the inferior rectus muscle **(47b)** into the fracture site (*) or even into the subjacent maxillary sinus **(75)** should be determined preoperatively. Diagnosis of the fracture in **Figure 63.2a** is easier because there are dislocated bone fragments. In addition, it is important to detect indirect signs of fracture, such as very fine, step-like contours of the bones and secondary bleeding **(8)** into the nasal cavity **(77)** or the frontal **(76)** and maxillary sinuses **(75)**.

Another important question is whether or not the head of the mandible (**58a** in **Fig. 63.3a**) is fractured or the maxillary bone **(57)** has been fractured and displaced (*) from the sphenoid **(60)** bone **(Fig. 63.4a)**. In this case, severe bleeding **(8)** required intubation **(182)** and a nasogastric tube **(182)**.

Fractures of the facial skull (Le Fort [33])

Type I Straight across the maxillary bones and the maxillary sinuses (Guérin's fracture)

Type II Across the zygomatic process of the maxilla, into the orbit, and through the frontal process of the maxilla to the contralateral side; maxillary sinus not involved

Type III Involving the lateral wall of the orbit and the frontal process of the maxilla to the contralateral side; ethmoid cells and zygomatic arch usually involved, sometimes also affecting the base of the skull.

Cervical CT

Whenever there is no contraindication, CT examinations of the neck are carried out after i.v. administration of CM. Malignant and inflammatory processes can be depicted more accurately with the aid of CM. Adequate enhancement of cervical vessels requires higher doses of CM than, for example, in CTs of the head. In spiral CT, the injection of CM must be precisely timed to the acquisition of data. There are specific recommendations and suggested schemes for CM injection at the end of the manual.

Selection of the Image Plane

In an analogous manner to head CT, a sagittal planning topogram (scanogram) at lower resolution is obtained first. The transverse (axial) levels and gantry angulation are determined from this topogram **(Fig. 64.1)**. Usually sections of the neck are obtained using a 4–5 mm thickness. The axial images are obtained and printed as viewed from caudally so the right lobe of the thyroid is imaged to the left of the trachea, the left lobe to the right.

Images should be obtained with a small-scan field-of-view to optimize detail in smaller structures in the neck. As the thoracic inlet is approached during the scanning, the scan field-of-view is increased to include possible abnormalities in the clavicular fossa and the axilla.

Artifacts caused by dental prostheses **(3)** usually obscure surrounding structures (*) in only one or two levels **(Fig. 64.2a)**. It may be necessary to carry out a second acquisition at another angle **(Fig. 64.2b)** to reveal areas hidden by artifact (*).

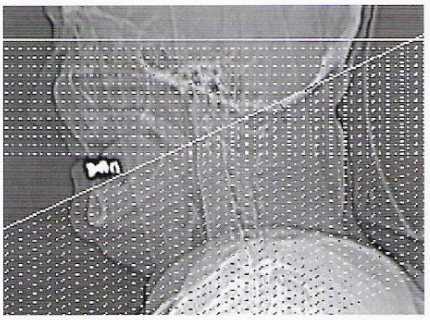

Fig. 64.1

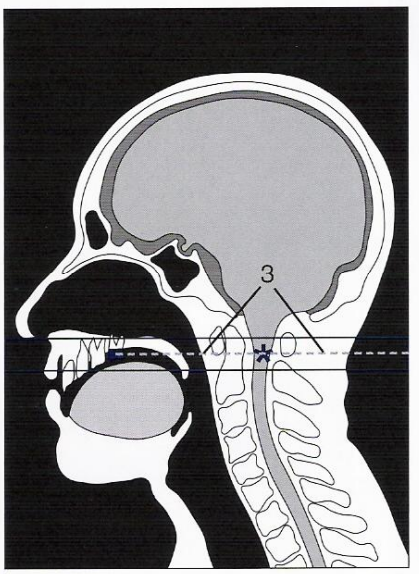

Fig. 64.2a

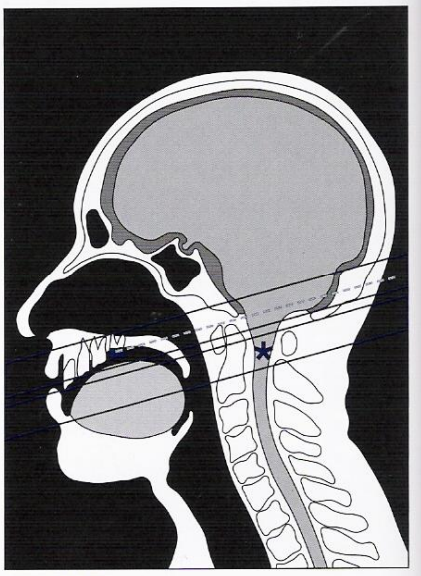

Fig. 64.2b

Systematic Sequence for Readings

We have already recommended a systematic approach with which to read CT scans of the head (see p. 26). For cervical CTs there is also no 'one and only' approach. The checklist presented here was developed through experience and is just one of many options for the beginner. Each examiner is free to set up his or her own checklist and strategy.

During neck imaging, separate hard copies at bone windows are rarely printed owing to cost. The radiologist must remember to check images at bone windows on the screen for fractures or lytic lesions.

Checklist for Reading Cervical CT Images

- → Symmetry of neck musculature?
- → Condition and clarity of fat?
- → Normal perfusion of vessels?
- → Thromboses or atherosclerotic stenoses?
- → Symmetry and definition of salivary glands?
- → Thyroid parenchyma homogeneous and without nodules?
- → Any focal pathologic enhancement with CM?
- → Narrowing of the tracheal lumen?
- → Assessment of lymph nodes? Number and size?
- → Cervical vertebrae examined in bone window?
- → Vertebral canal patent or narrowed?

The radiologist quickly reaches the limits of CT resolution (perhaps also of his/her anatomic knowledge) when trying to identify all of the different neck muscles. We have therefore reduced the amount of detail in the accompanying drawings so that smaller muscles are grouped. Single muscles have little clinical relevance and thus the legends to these images refer to combined muscle groups, e.g. the scalene muscles, the erector spinae muscles. Readers who want more anatomic detail should consult the relevant literature [5, 31].

Cervical images usually begin at the base of the skull and continue caudally to the thoracic inlet. The cranial sections **(Figs. 65.1- 65.3)** therefore include the maxillary sinus **(75)**, the nasal cavity **(77)**, and the pharynx **(176)**. Dorsal to the pharynx lie the longus capitis and longus cervicis muscles **(26)**, which extend caudally. Lateral to the mandible **(58)**, beginning in **Figure 65.2a**, the parotid gland **(153)** is situated next to the large cervical vessels and vagus nerve (also p. 64). In front of the pons/medulla oblongata **(107)**, the vertebral arteries **(88)** join to form the basilar artery **(90)**.

The spread of inflammatory processes within the cervical connective tissue spaces is restricted within compartments defined by the cervical fascia [30]. The different layers of the cervical fascia are explained on the following page **(Fig. 66.4)**.

Fig. 65.1a

Fig. 65.2a

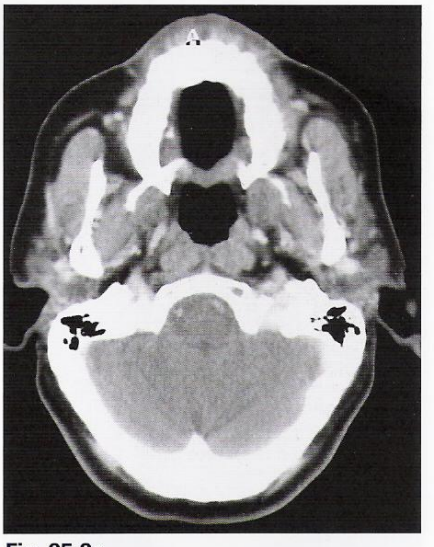

Fig. 65.3a

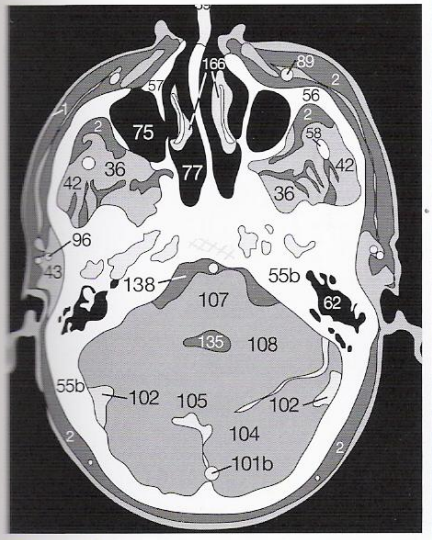

Fig. 65.1b

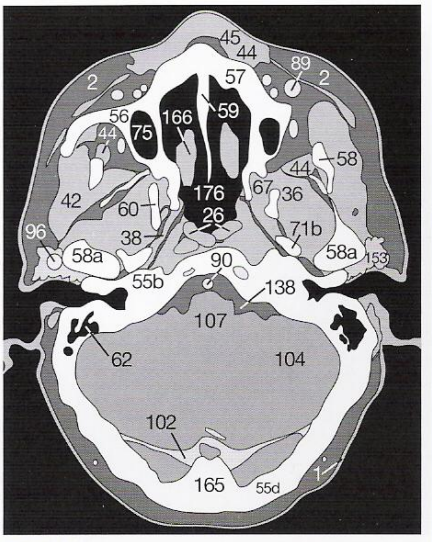

Fig. 65.2b

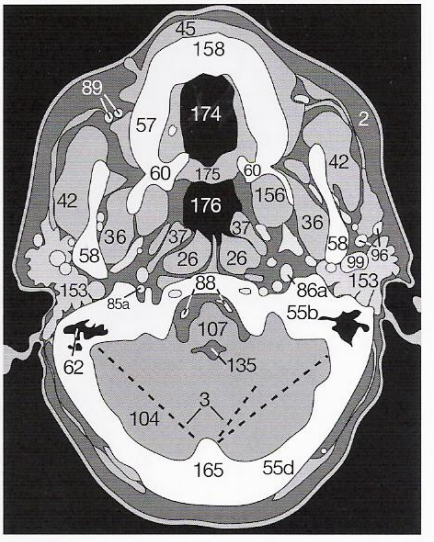

Fig. 65.3b

Further caudally the following cervical muscles become visible beneath the trapezius muscle **(23)**: medial lie the semispinalis capitis **(28)** and longissimus capitis muscles **(27)**, and more laterally the splenius capitis muscle **(25)**. The parotid gland **(153)** is situated cranial and posterior to the submandibular gland **(154)** next to the mandible **(58)**. The pharynx **(176)** is surrounded by Waldeyer's ring of tonsillar tissue **(157, 156)**. Note that the carotid bulb is situated between **Figures 67.4a** and **68.2a**; it is the point at which the common carotid artery **(85)** bifurcates into internal **(85a)** and external **(85b)** carotid branches. Under the tongue **(155)** the floor of the mouth is organized in layers. From cranial to caudal are: the genioglossus muscle **(33)**, further laterally the geniohyoid muscle **(34)**, and the anterior belly of the digastric muscle **(31)**. The thin superficial muscle is the platysma **(48)**.

Compartments of the Neck

If infections or inflammatory processes originate in the suprasternal (⊕) or pretracheal spaces between the superficial fascia (*) and the dorsal layer of the pretracheal fascia (**), they cannot spread into the mediastinum because both fascias insert into the sternum (**56** in **Fig. 66.4**). At the level of the parotid gland there is a similar barrier consisting of the sagittal septum which splits a retropharyngeal from a parapharyngeal space. Inflammations originating further dorsal, between the pretracheal (**) and the prevertebral (***) fascias, can spread caudally into the mediastinum.

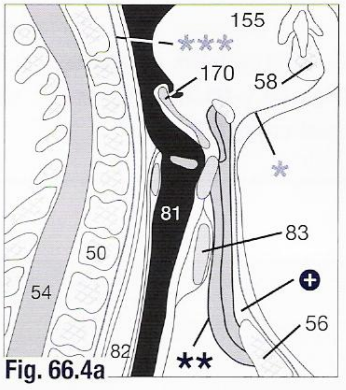

Fig. 66.4a

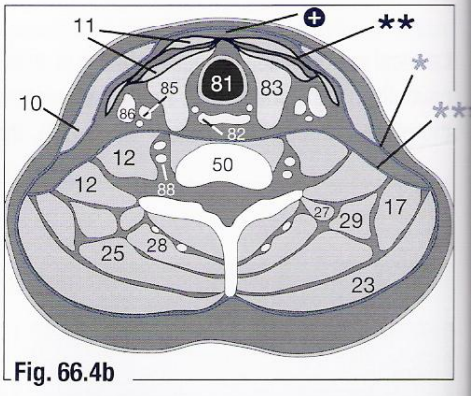

Fig. 66.4b

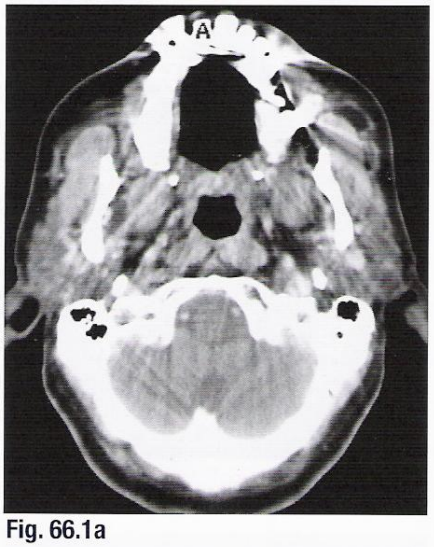

Fig. 66.1a

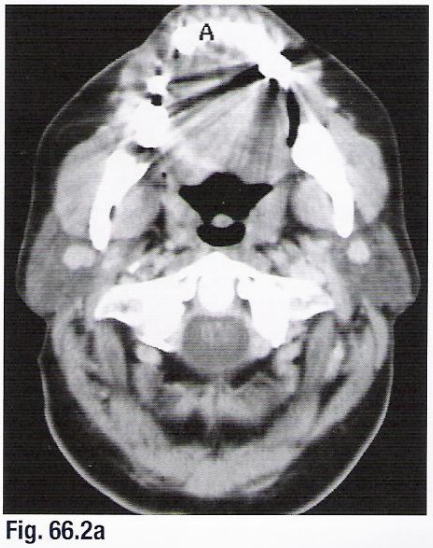

Fig. 66.2a

Fig. 66.3a

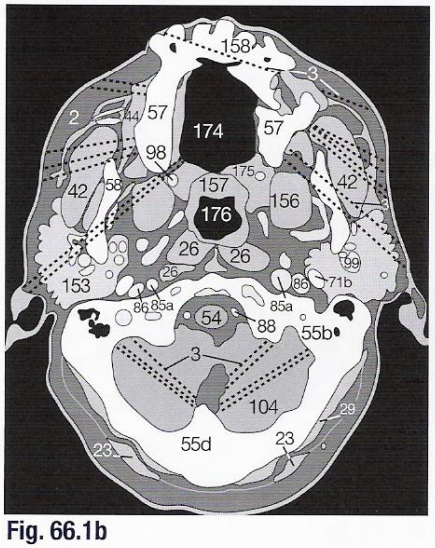

Fig. 66.1b

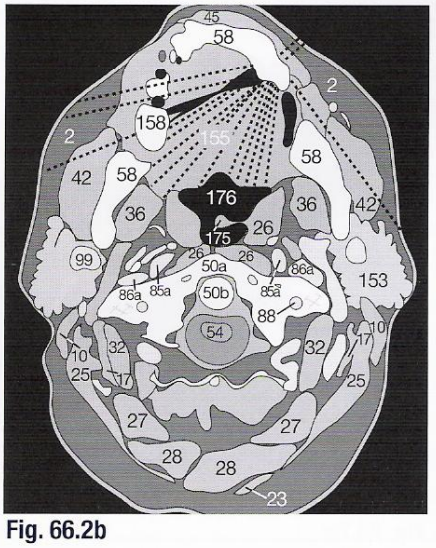

Fig. 66.2b

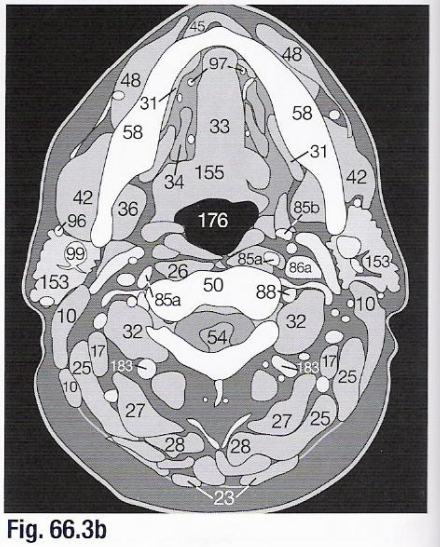

Fig. 66.3b

Fig. 67.1a

Fig. 67.2a

Fig. 67.3a

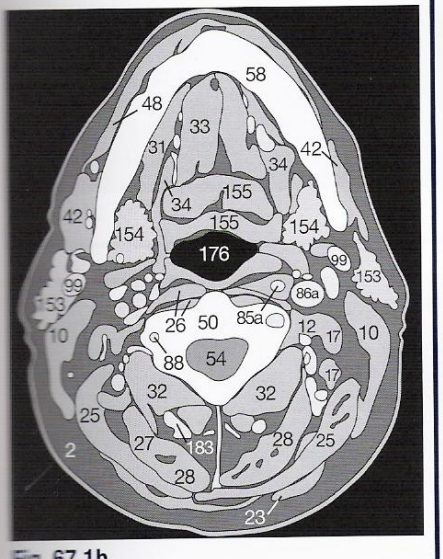

Fig. 67.1b

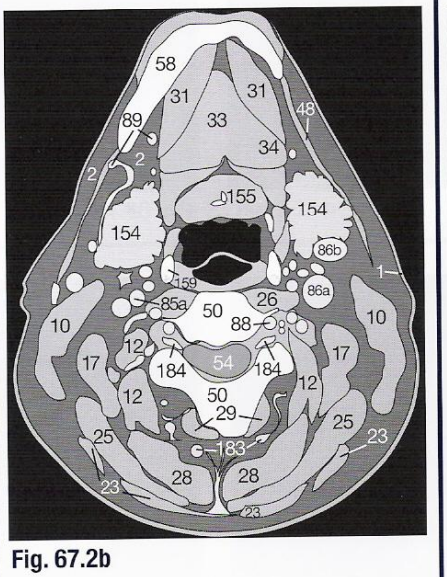

Fig. 67.2b

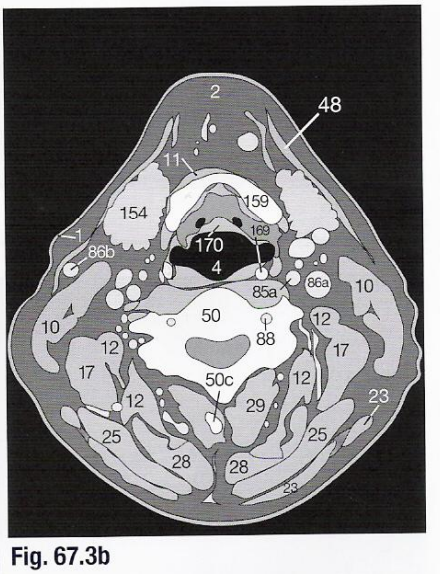

Fig. 67.3b

Fig. 67.4a

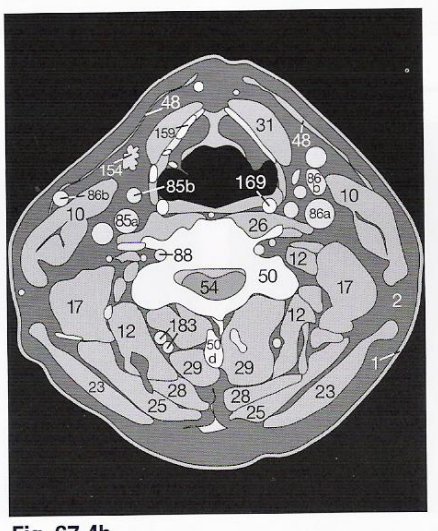

Fig. 67.4b

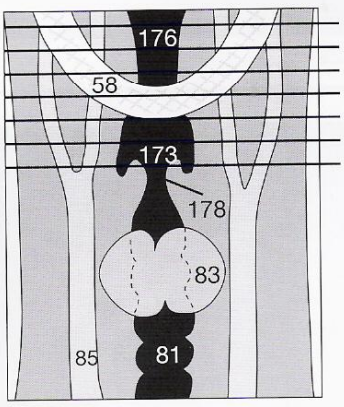

Fig. 67.5

The bifurcation of the common carotid artery **(85)** is an area of predilection for atherosclerotic plaques **(Fig. 68.1a)** which may be complicated by thrombus deposition (★). Note the positions of the cricoid **(167)** and arytenoid cartilages **(168)** at the rima glottidis **(178)**. In these normal individuals, CM enhances the density not only of the internal **(86a)**, the external **(86b)**, and the anterior jugular veins **(86c)**, but also of the vertebral artery **(88)** in the transverse foramina of the cervical vertebrae. Always check for degenerative changes at the margins of the bodies of cervical vertebrae **(50)** or for herniated discs which might narrow the spinal canal containing the cervical cord **(54)**. On either side of the trachea **(81)** lie the two lobes of the thyroid gland **(83)**, which should have a smooth outline and have homogeneous parenchyma **(Fig. 68.3a)**.

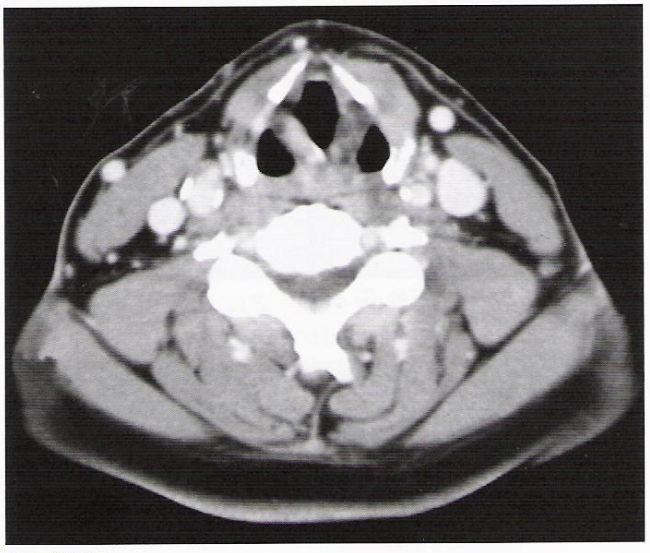

Fig. 68.1a

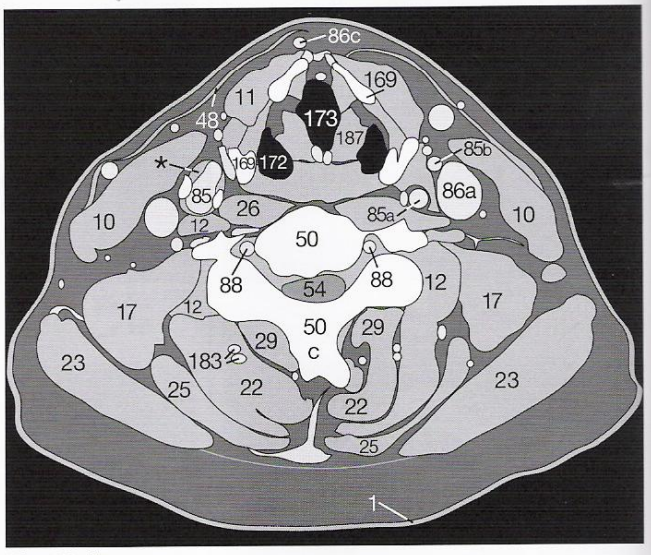

Fig. 68.1b

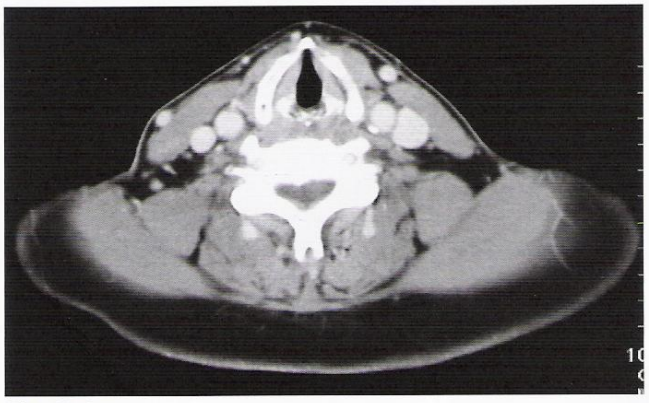

Fig. 68.2a

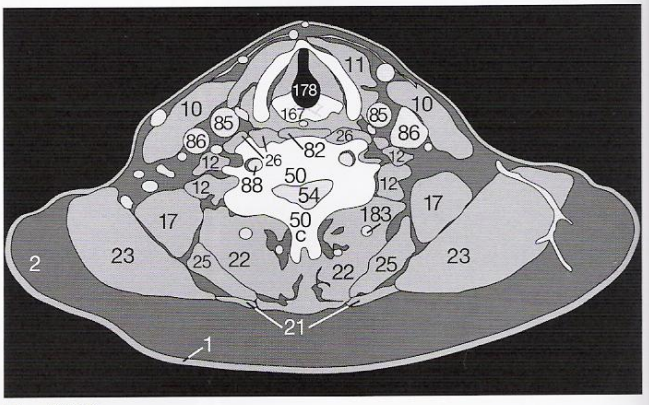

Fig. 68.2b

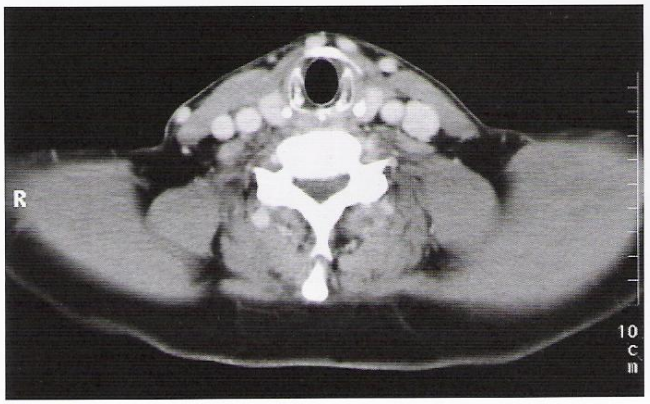

Fig. 68.3a

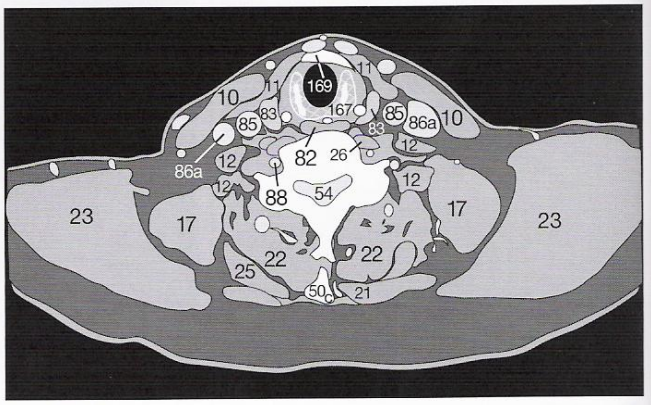

Fig. 68.3b

Because of its iodine content, the thyroid gland **(83)** appears hyperdense compared with surrounding muscles both before and, even more so, after the administration of CM **(Figs. 69.1–69.3)**. Beginners occasionally mistake the esophagus **(82)**, dorsal to the trachea **(81)**, for swollen lymph nodes or a tumor. In case of doubt, comparison with other sections is helpful: usually a small, hypodense area indicates air in the lumen of the esophagus in an adjacent section. As a rule, the cervicothoracic junction is examined with the arms elevated to minimize artifacts due to bones. The muscles of the pectoral girdle as well as the shoulder joints therefore appear in unfamiliar positions. The following chapter deals with neck pathology and includes a short "Test Yourself"; images and drawings of normal anatomy extending further caudally are continued on page 74.

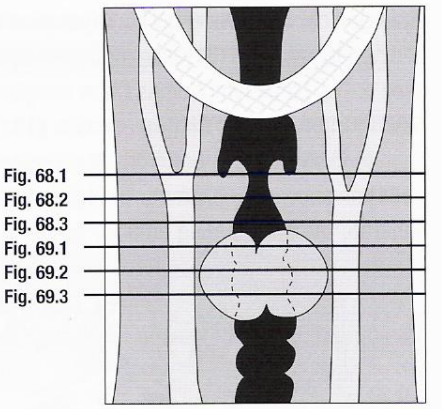

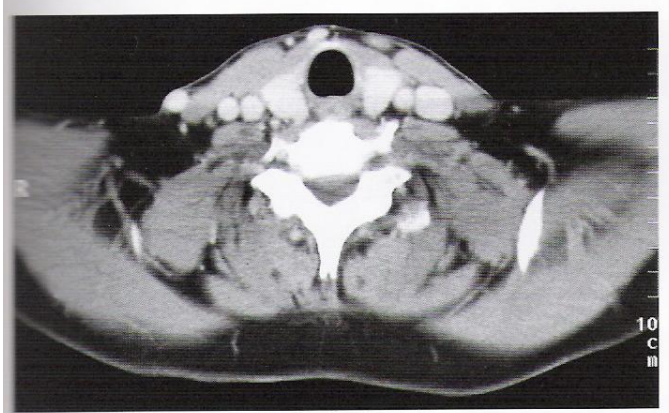

Fig. 69.1a

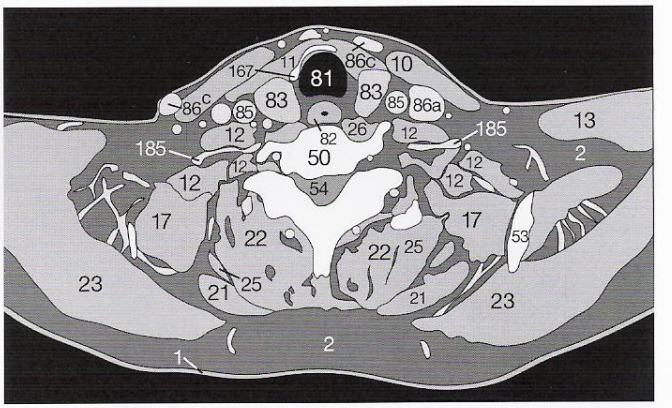

Fig. 69.1b

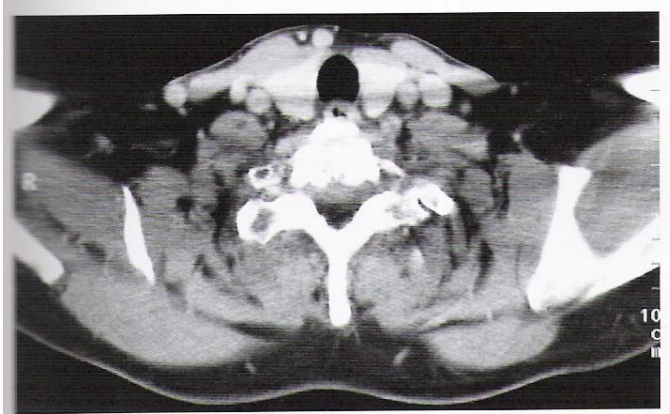

Fig. 69.2a

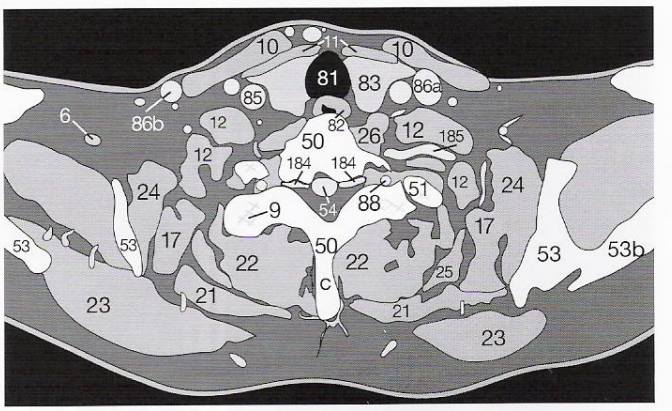

Fig. 69.2b

Fig. 69.3a

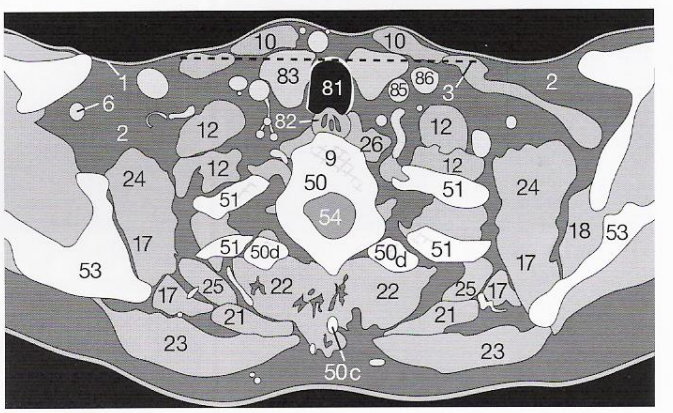

Fig. 69.3b

Enlarged cervical LNs **(Fig. 70.1a)** appear conspicuously as isolated nodular masses **(6)** that cannot be followed into adjacent levels (see p. 15). Large lymphomas **(7)** or conglomerate LN masses **(Fig. 70.1a)** often develop central necrosis **(181)**. It is sometimes difficult to distinguish them from abscesses with central necrosis **(181)** as shown, for example, in **Figure 70.2a**. Abscesses typically infiltrate the surrounding adipose tissue with a streaky pattern of edema **(180)** so that structures such as arteries, veins, or nerves (on the left side of the neck in **Fig. 70.2a**) become difficult to identify. In immune-suppressed patients, abscesses can become remarkably large. Compare the scans in **Figures 70.3a** (unenhanced) and **70.3b** (enhanced): after injection of CM, the outer wall of the abscess (*) as well as the central septa have become enhanced. These appearances are so similar to large hematomas or necrotic tumors that a differential diagnosis may be difficult without a detailed clinical history.

Note also the atherosclerotic plaques or thromboses in the lumen of the carotid artery **(85)** as in **Figure 70.1a**.

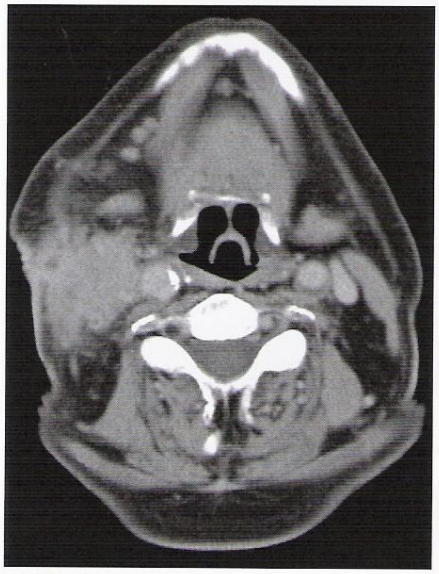

Fig. 70.1a

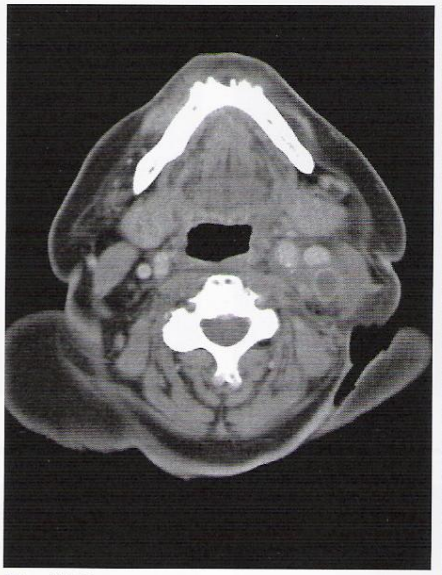

Fig. 70.2a

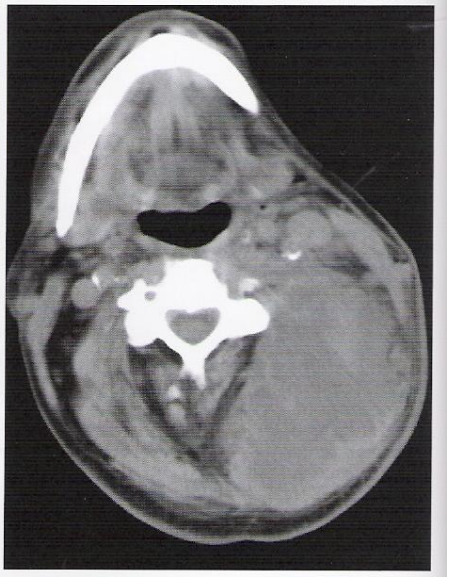

Fig. 70.3a (unenhanced)

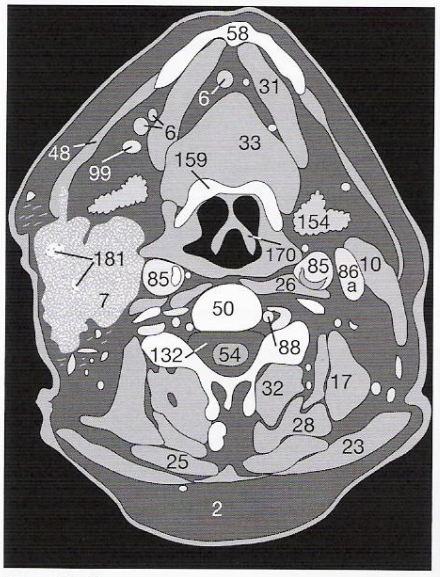

Fig. 70.1b

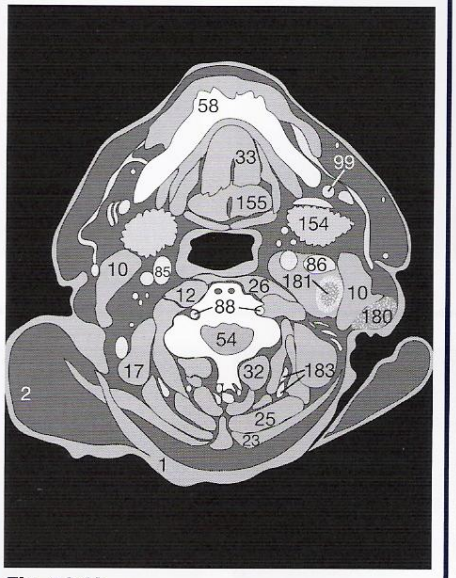

Fig. 70.2b

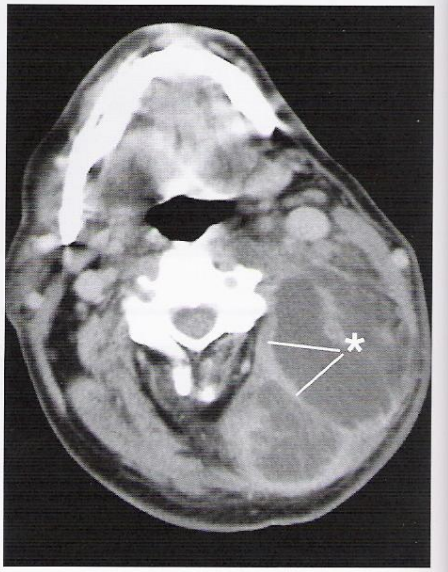

Fig. 70.3b (enhanced)

The parenchyma of the thyroid gland **(83)** should appear sharply demarcated and have an homogeneous pattern in CT scans. The average transverse diameter of each lobe is 1–3 cm, 1–2 cm sagittally and 4–7 cm in craniocaudal direction. The total volume of the thyroid gland varies between 20 and 25 ml. If the thyroid is enlarged, check for tracheal compression or stenosis **(81)** and the caudal border of the goiter should be determined.

A benign struma **(83)** may extend into retrosternal regions and laterally displace supra-aortic vessels **(85, 87, 88) (Fig. 71.2)**.

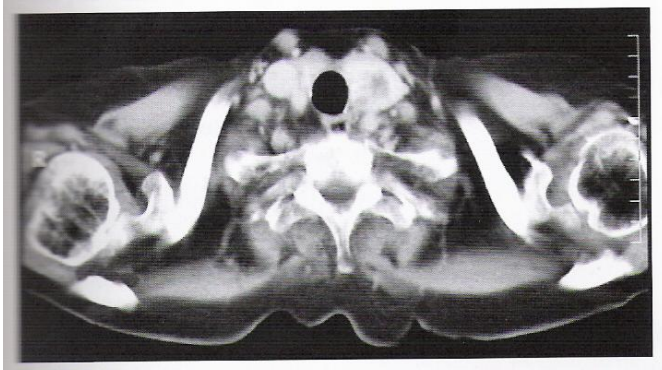

Fig. 71.1a

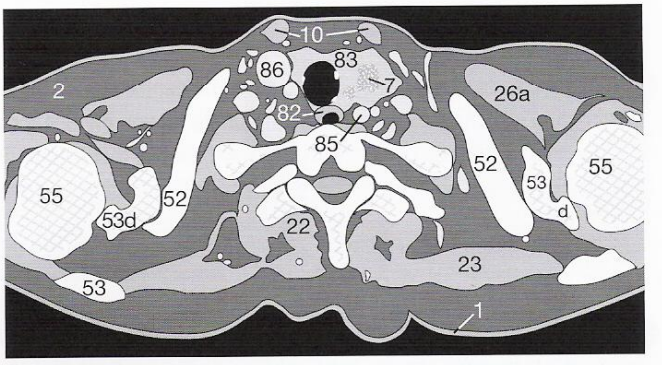

Fig. 71.1b

The parenchymal structure of a thyroid carcinoma **(7)** appears inhomogeneous, and the contours are not easily distinguished from the remaining normal parenchyma **(83) (Fig 71.1a)**.
In advanced stages of carcinoma **(Fig. 71.3)**, cervical vessels and nerves are completely surrounded by tumor, and areas of necrosis **(181)** appear. The tracheal walls **(81)** are compressed and may become infiltrated. After partial resection of a struma **(Fig. 71.4)**, some thyroid tissue **(83)** may still be seen close to the trachea. In this case the left internal jugular vein was also removed and the lumen of the right one **(86a)** is therefore larger than normal.

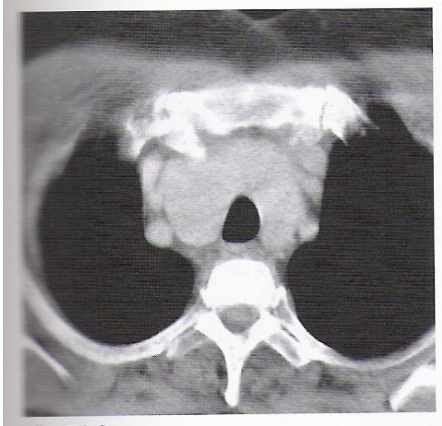

Fig. 71.2a

Fig. 71.3a

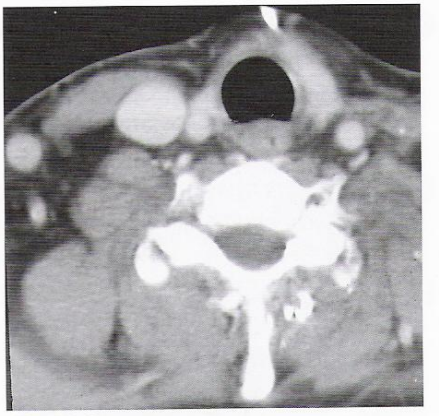

Fig. 71.4a

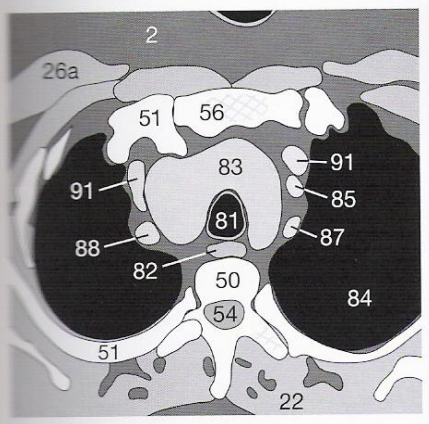

Fig. 71.2b

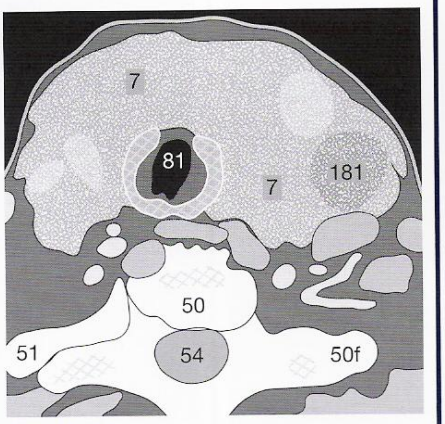

Fig. 71.3b

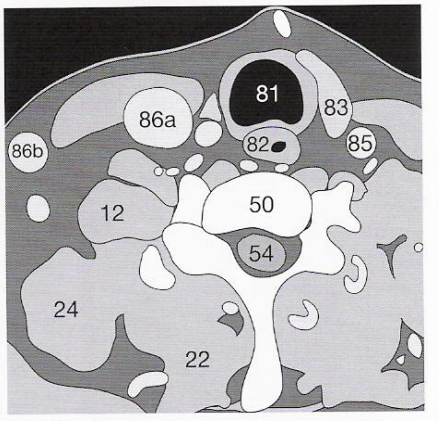

Fig. 71.4b

Test Yourself!

Before continuing to the next chapters, these exercises give you an opportunity to check your knowledge. The questions become increasingly difficult as you go along: the first question should pose no problems, whereas the last ones of each chapter will be a real challenge. Make the most of this opportunity for self-assessment and take it in good grace if you find you missed something. In our experience these little tests will help you to remember better what you have learned.

It is much more effective to look up each gap in your knowledge as it occurs than to skip a problem and turn directly to the answer. You should therefore only turn to the answers at the back of the book when you have solved each problem by yourself. That way you will not see answers to questions you haven't tackled yet. It will keep you in suspense!

Exercise 9: Which window setting (window center and window width in HU) would you select for an optimal brain CT? Why? Before beginning the examination, what gantry angle do you choose for your slices in the planning topogram and what section thickness and section increments do you use? Why did you choose these settings?

Exercise 10: What do you remember about the criteria with which to distinguish the four types of intracranial hemorrhage? With which kinds of hemorrhage are you familiar? How can you differentiate between them in CT morphology? What complications or consequences must you particularly watch out for (consult pp. 54–57 for help)?

Type of hemorrhage:

-
-
-
-

Characteristics:

Exercise 11: How can you recognize a subarachnoid hemorrhage in children?

Exercise 12: Imagine the anatomy of the cerebral basal ganglia and then draw a transverse section at the level of the internal capsule. Compare your sketch with **Figures 30.2a** and **30.2b**. Repeat this exercise occasionally until you can do it with ease.

Exercise 13: Examine **Figure 72.1** carefully. The patient was involved in a car accident. Do not settle for the most obvious feature; look for other variations or abnormalities. What do you suspect?

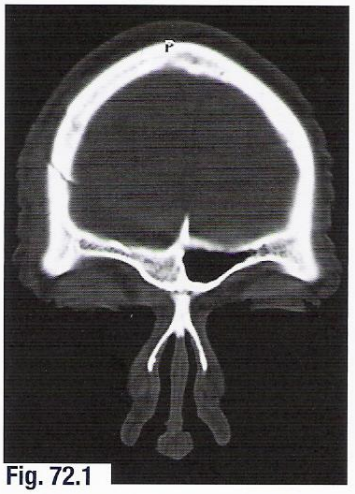

Fig. 72.1

Exercise 14: **Figure 72.2** contains an unusual variation; can you find it? After having noted it, look again to see whether you have really discovered all pathologic features.

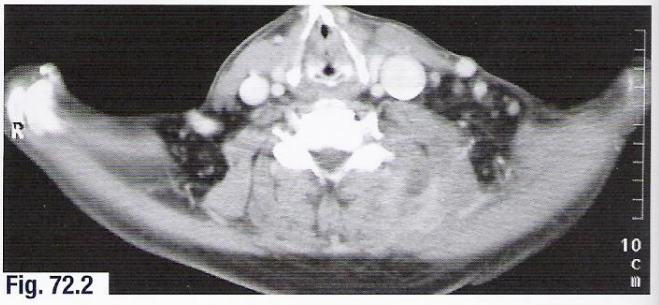

Fig. 72.2

Exercise 15:

The CCT in **Figure 73.1** is of a 43-year-old patient. Make a note of your tentative diagnosis and how you would proceed.

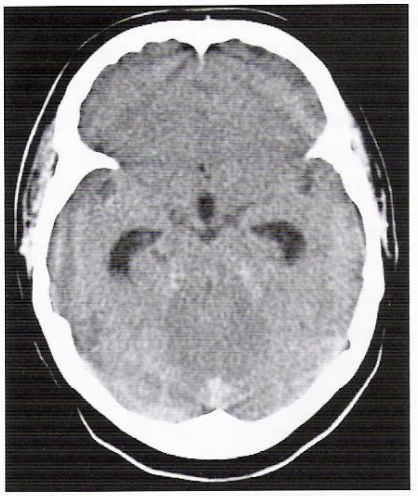

Fig. 73.1

Exercise 16:

Do you recognize anything unusual in **Figure 73.2**? Is there a pathologic abnormality? Or is it simply an artifact or even a normal finding?

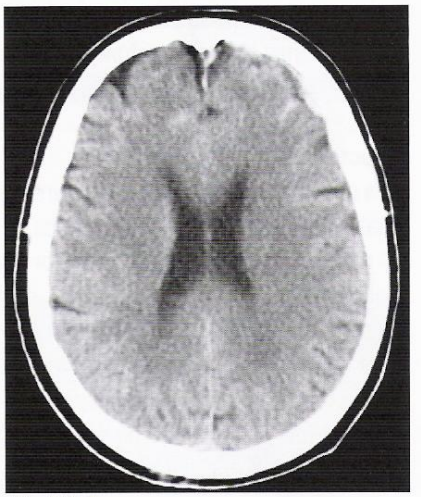

Fig. 73.2

Exercise 17:

Is there any feature in this orbital scan **(Fig. 73.3)** that would not be considered a normal finding? Note your observations below. Don't give up too quickly!

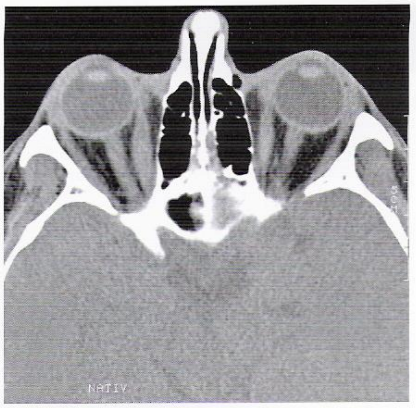

Fig. 73.3

Exercise 18:

A confused patient, from a home for the elderly, with suspected intracranial bleeding is brought in for a CCT. How many fresh hemorrhages **(Fig. 73.4)** do you see? What is your differential diagnosis? Which of them is the most probable diagnosis? Which additional information could also be helpful?

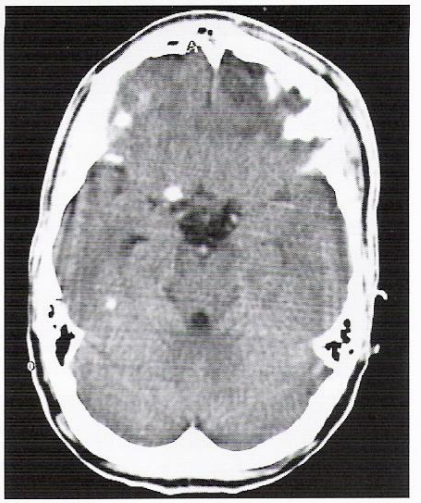

Fig. 73.4

After having discussed normal anatomy of caudal cervical sections (p. 67), normal thoracic anatomy is presented. From this page on, you will find the number codes for the drawings in the rear foldout.

Selection of Image Plane

As a rule, the sections of the thorax are chosen in the transverse or axial plane at thicknesses and steps of 8 to 10 mm. Sections 10 mm thick will overlap by 1 mm, for example, when the patient table is advanced in 8-mm steps. A small topogram **(Fig. 75.1)** accompanying each sheet of images shows the position of the sections relative to the major anatomic structures of the region. In order not to miss any pathologic changes within the lung (review p. 13), it has become accepted practice to make a hard copy of both soft-tissue and lung windows or to provide a CD with the image data. Each image can therefore be viewed at two different window settings. Again the large number of images necessitates a systematic technique for evaluation so as not to waste time looking randomly back and forth between them.

Systematic Sequence for Readings

The beginner often forgets to check the soft tissues of the thoracic wall because the examination of the mediastinum and the lungs is automatically considered more important. These tissues should therefore be evaluated first. Common sites of abnormality are the breasts and fat in the axilla **(2)**. After this–also using soft-tissue windows–the mediastinum is checked for pathologic masses. The easiest approach is to orient yourself relative to the arch of the aorta **(89b)**, which can be recognized even by the inexperienced **(Fig. 77.3)**. From this point cranially, the major branches are identified to exclude pathologic masses in the upper mediastinum next to the brachiocephalic trunk **(88)**, the left common carotid artery **(85)**, the subclavian artery **(87)**, as well as the brachiocephalic veins **(91)**, superior vena cava **(92)**, trachea **(81)**, or more dorsally, the esophagus **(82)**. Caudally, the most common sites for enlarged LNs are: at the aortopulmonary window, directly below the bifurcation of the trachea **(81a)**, in the perihilar tissue, posterior to the crura of the diaphragm (= retrocrural) next to the descending aorta **(89c)**. The presence of a few LNs smaller than 1.5 cm in diameter in the aortopulmonary window may be considered normal [19, 41]. Anterior to the aortic arch **(89b)** LNs of normal size are rarely seen in the CT. The evaluation of the soft-tissue window is complete when the heart (any coronary sclerosis, dilations?) and the lung hila (vessels well defined and not lobulated or enlarged) have been checked. Only now should the radiologist turn to the lung or pleural window.

Since the pleural window is very wide, the marrow of the spinal column as well as the parenchyma of the lung can be examined. It is therefore possible to evaluate bone structure in addition to the pulmonary vasculature. When examining the lung vessels, look for a gradual reduction in their diameter as you proceed from the hilum to the periphery. Pulmonary oligemia is normal only along the margins of the lobes and in the periphery.

It is essential to differentiate between cross-sectioned vessels and solid masses by comparing adjacent levels (cf. p. 15). More or less spherical solid masses may indicate intrapulmonary metastases. The checklist will help you read thoracic CTs systematically.

The simultaneous presentation of two window settings in one hard copy (both the lung and the soft-tissue window) has not proved practical because pathologic abnormalities which have density levels between the two would be overlooked. Consult the lung chapter on pages 84ff. for scans in the lung window.

Checklist for Thorax Readings

1. On the soft-tissue window:

- soft tissues, especially:
  - axillary LNs
  - breast (malignant lesions?)
- mediastinum in four regions:
  - from the aortic arch cranially (LNs?, thymoma / struma?)
  - hilar region (configuration and size of vessels, lobulated and enlarged?)
  - heart and coronary arteries (sclerosis?)
  - four typical sites of predilection for LNs:
    - anterior to aortic arch (normal: almost none or < 6 mm)
    - in the aortopulmonary window (normal: < 4 LNs < 15 mm)
    - subcarinal (normal: < 10 mm; DD: esophagus)
    - next to descending aorta (normal: < 10 mm; DD: azygos)

2. On the lung window:

- Parenchyma of the lung:
  - normal branching pattern and caliber of vessels?
  - vascular oligemia only at interlobar fissures? bullae?
  - any suspicious lung foci? inflammatory infiltrates?
- Pleura:
  - plaques, calcification, pleural fluid, pneumothorax?
- Bones (vertebrae, scapula, ribs):
  - normal structure of marrow?
  - degenerative osteophytes?
  - focal lytic or sclerotic processes?
  - stenoses of the spinal canal?

Artifacts **(3)** will be observed at the level of the thoracic inlet if CM is present in the subclavian vein **(87)** at the time of data acquisition (cf. **Fig. 23.3**). The parenchyma of the thyroid gland **(83)** should appear homogeneous and clearly defined from the surrounding fat **(2)**. Asymmetry in the diameter of the jugular vein **(86)** is seen quite often and has no pathologic significance. Orthogonally sectioned branches of the axillary **(93)** and lateral thoracic **(95)** vessels must be distinguished from axillary LNs. If the arms are elevated, the supraspinatus muscle **(19)** lies medial to the spine of the scapula **(53b)** and the infraspinatus muscle **(20)**. Usually the pectoralis major **(26a)** and minor **(26b)** muscles are separated by a thin layer of fat.

Fig. 75.2
Fig. 75.3
Fig. 75.4

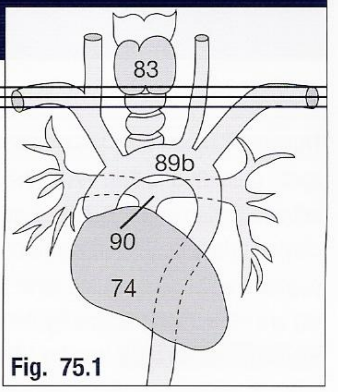

Fig. 75.1

Fig. 75.2a

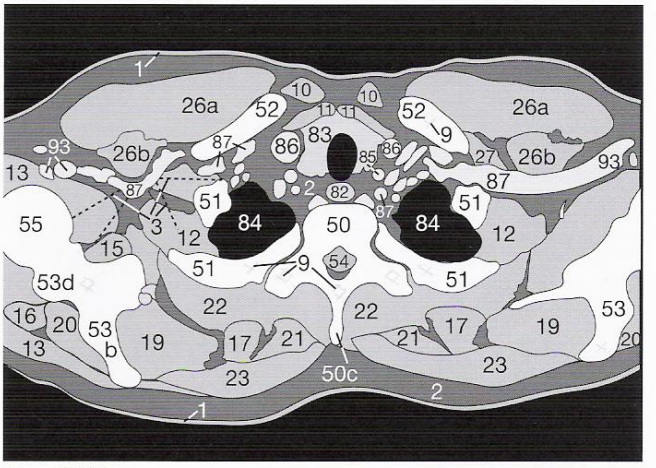

Fig. 75.2b

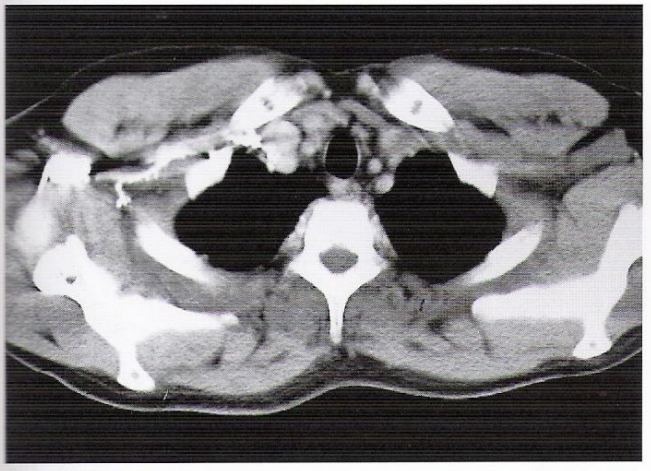

Fig. 75.3a

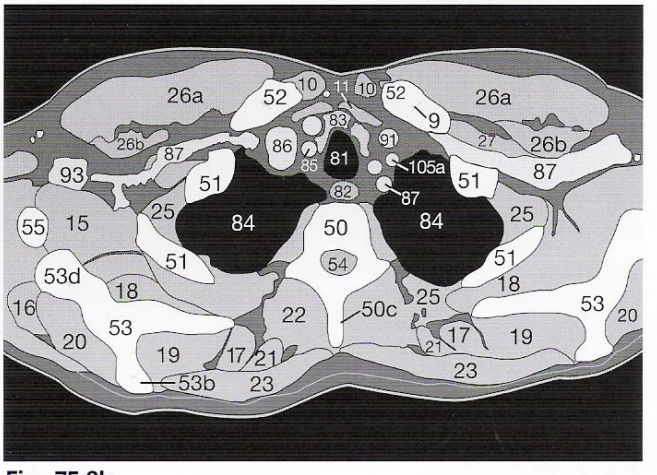

Fig. 75.3b

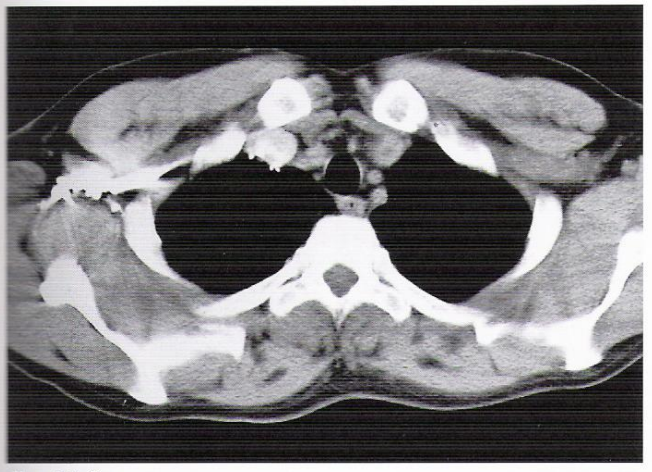

Fig. 75.4a

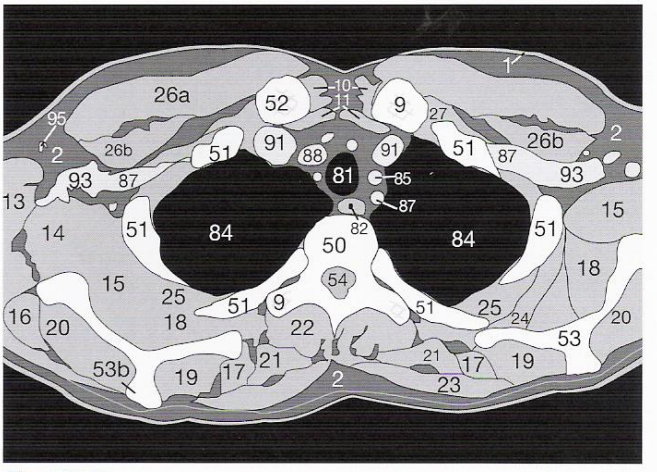

Fig. 75.4b

Thoracic CTs are also viewed from caudally. The left lung **(84)** appears on the right side of the image and vice versa. Beginning at the aortic arch (**89b** in **Fig. 77.2**), the layout of the aortic arch vessels should be thoroughly familiar to you. At the section in **Figure 76.1**, the left subclavian artery **(87)** is seen most posteriorly and can be followed in cranial direction in the images on page 75. In front of the subclavian artery lie the left common carotid artery **(85)** and the brachiocephalic trunk **(88)**. More to the right and anteriorly are the brachiocephalic veins **(91)**, which form the superior vena cava **(92)** at the levels of **Figures 76.3** to **77.1**. In the fat of the axilla **(2)**, normal LNs **(6)** are often recognizable by their typical indented shape: the hilum contains fat. At a different angle, the hypodense hilum will appear in the center of an oval. Healthy LNs are well defined and should not exceed 1 cm in diameter in this location (**Figs. 76.1** and **76.3**).

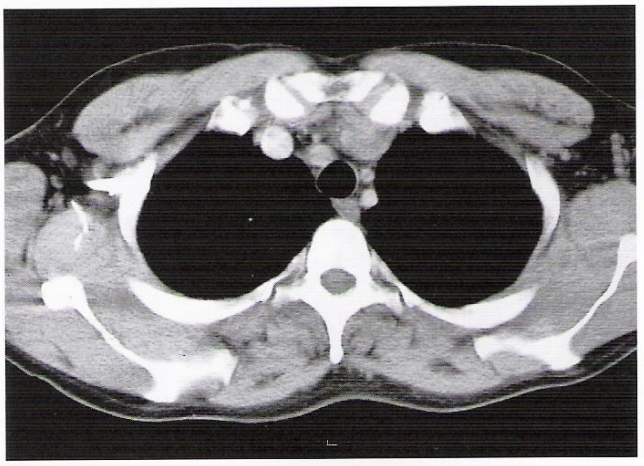

Fig. 76.1a

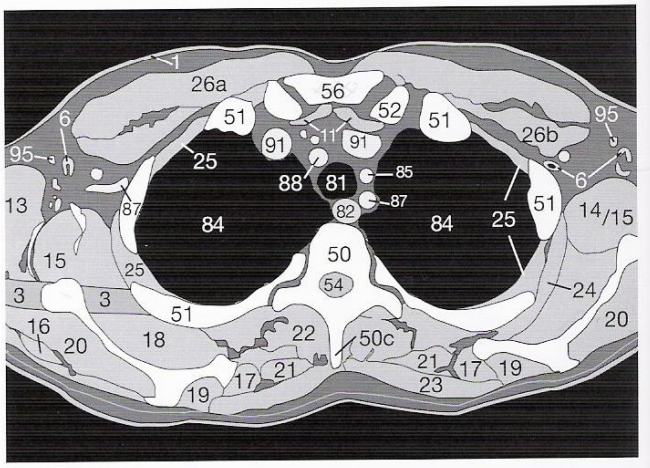

Fig. 76.1b

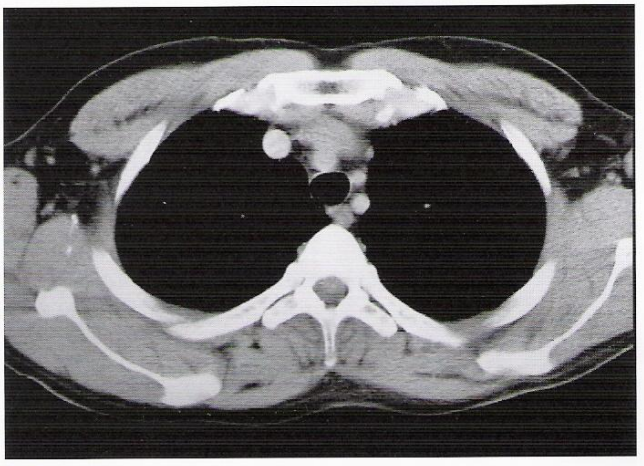

Fig. 76.2a

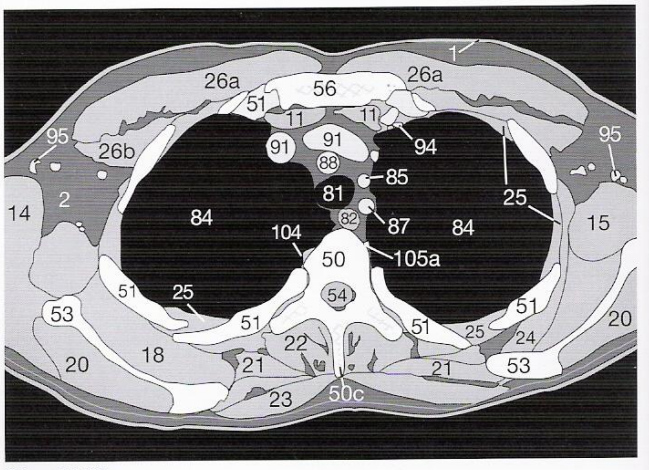

Fig. 76.2b

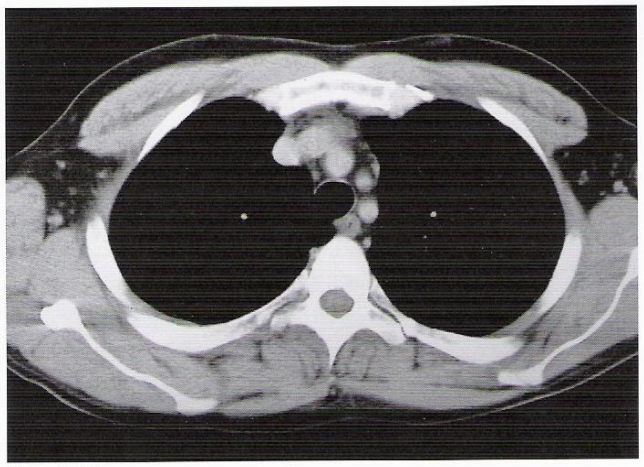

Fig. 76.3a

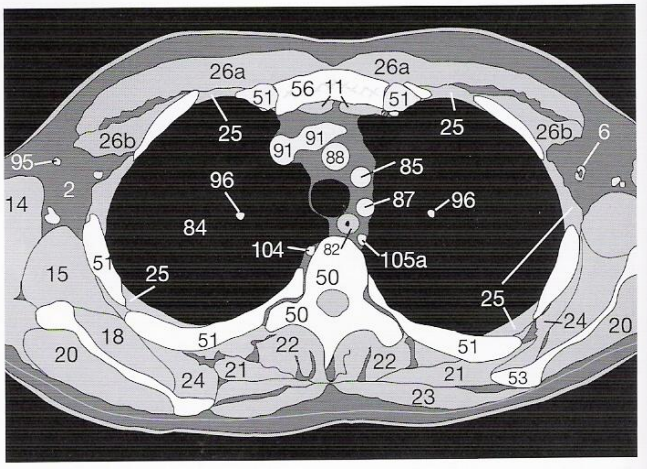

Fig. 76.3b

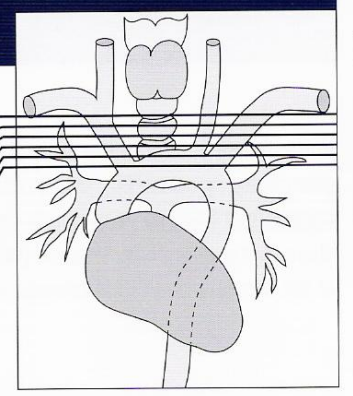

The azygos vein **(104)** lies dorsal to the trachea **(81)** next to the esophagus **(82)**. Directly above the right main bronchus, it arches anteriorly into the superior vena cava (**92** in **Fig. 77.2**). Be sure not to confuse the paravertebral azygos vein **(104)**, the hemiazygos vein **(105)** or accessory hemiazygos **(105a)** with paraaortic LNs (**Figs. 77.3** and **76.3**).

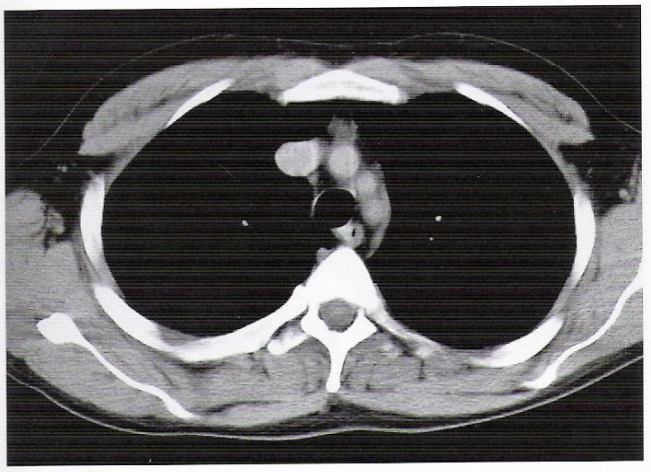

Fig. 77.1a

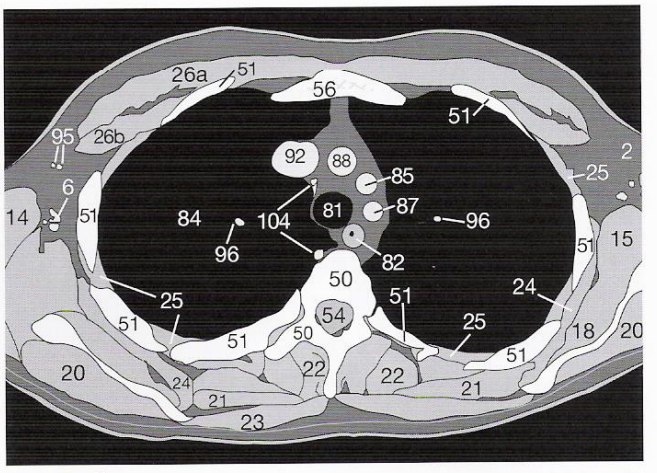

Fig. 77.1b

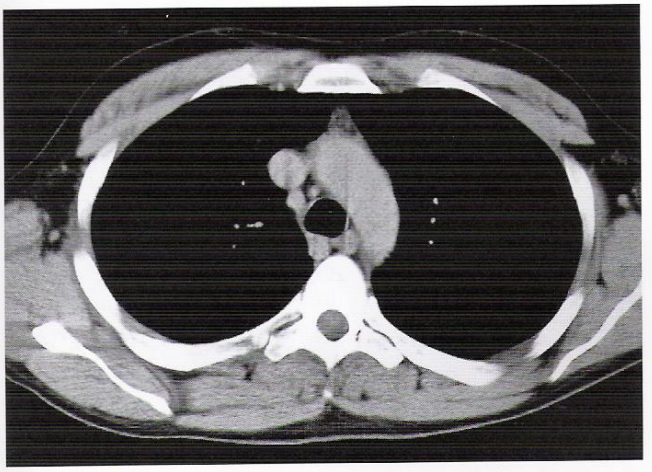

Fig. 77.2a

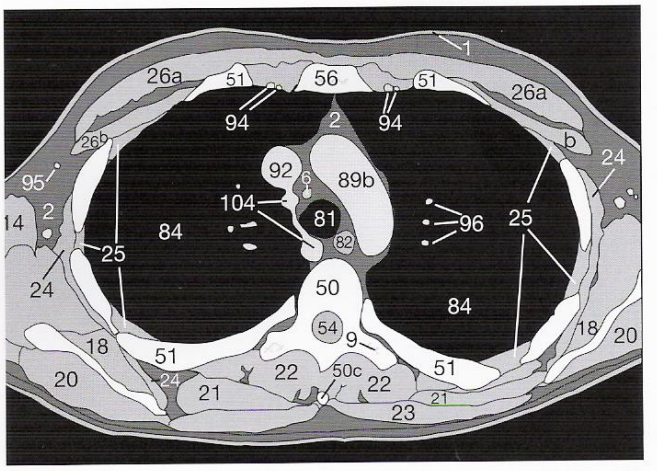

Fig. 77.2b

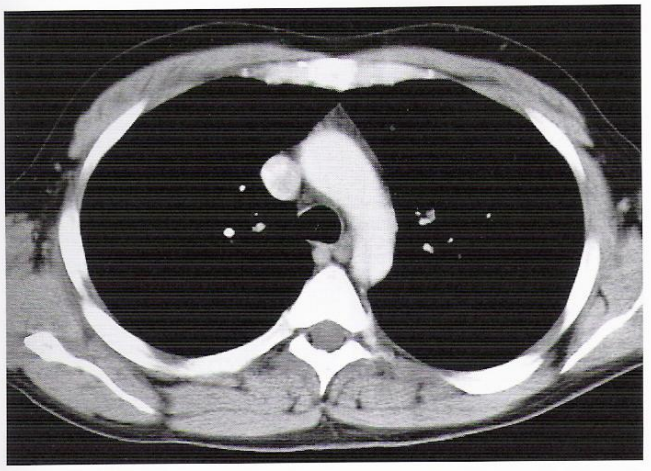

Fig. 77.3a

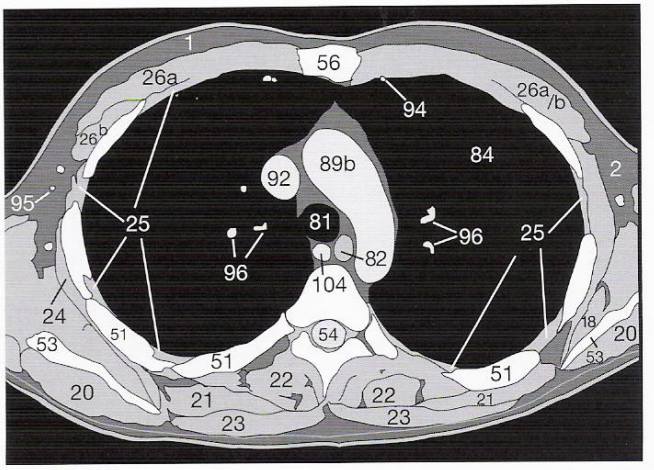

Fig. 77.3b

Immediately caudal to the arch of the aorta **(89b)** is situated the pulmonary trunk **(90)**, which divides into the right **(90a)** and left **(90b)** pulmonary arteries **(Fig. 78.2)**. At the level of **Figures 78.1** and **78.2**, there is the aortopulmonary window, a site of predilection for mediastinal LNs **(6)**. Also check for enlarged LNs or malignant masses in the subcarinal position between the two main bronchi **(81b)** close to the pulmonary vessels **(96) (Fig. 78.3)**. Near the internal thoracic (mammary) vessels **(94)** lies the regional lymphatic drainage of the medial parts of the breasts, whereas the lymphatic drainage of the lateral portions of the breasts is primarily to the axillary nodes.

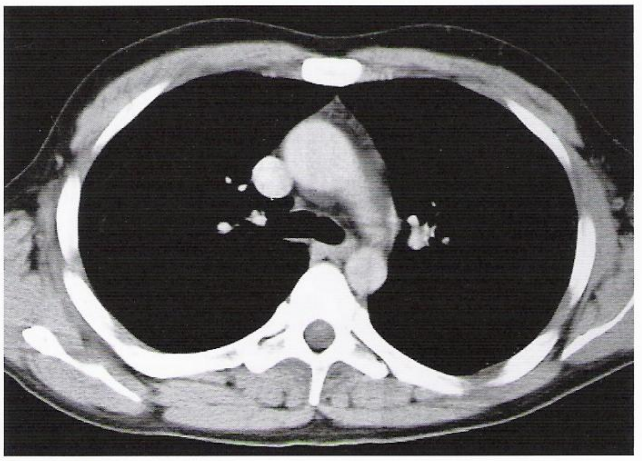

Fig. 78.1a

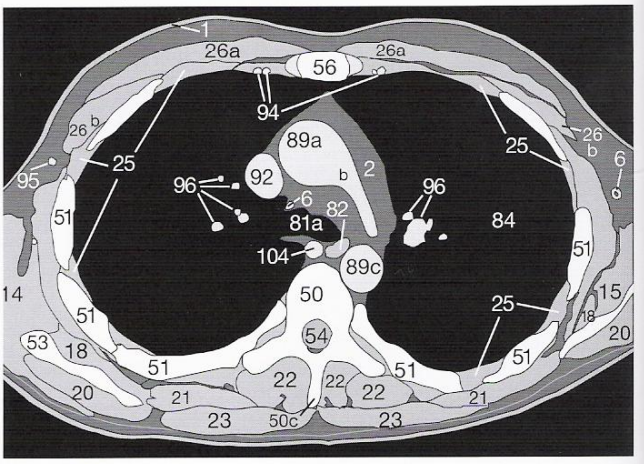

Fig. 78.1b

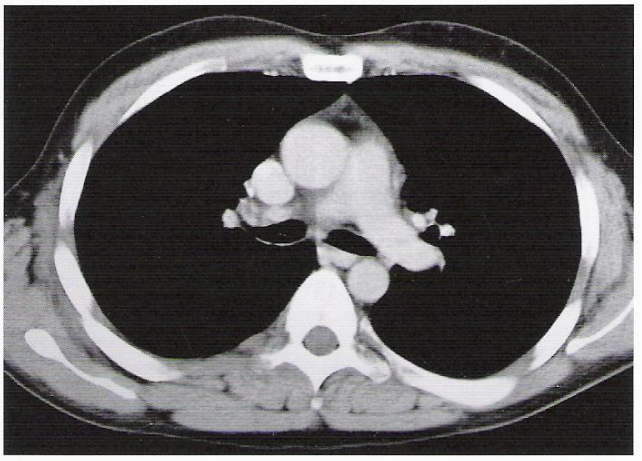

Fig. 78.2a

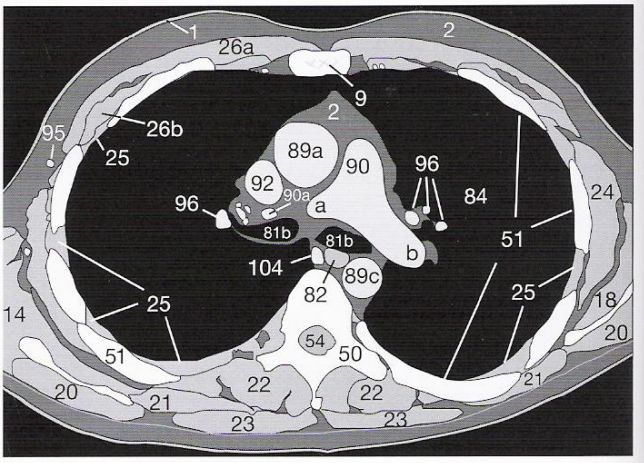

Fig. 78.2b

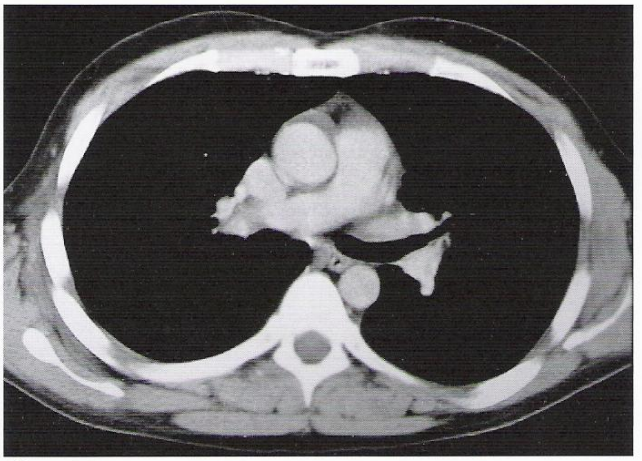

Fig. 78.3a

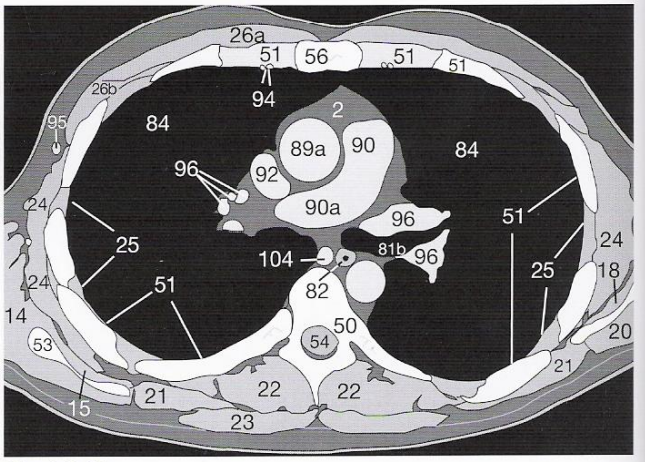

Fig. 78.3b

The glandular tissue **(73)** in the fat of the breasts of the anterior thoracic wall is easily differentiated from skin tumors because of the symmetry (**Figs. 79.1** and **79.2**). The main coronary arteries **(77)** are also distinguishable in the epicardial fat **(2)** **(Fig. 79.3)**. Develop a clear mental picture of the positions of the azygos vein **(104)** and the esophagus **(82)** next to the descending aorta **(89c)** so that you will later be able to recognize any pathologic LNs close to these structures.

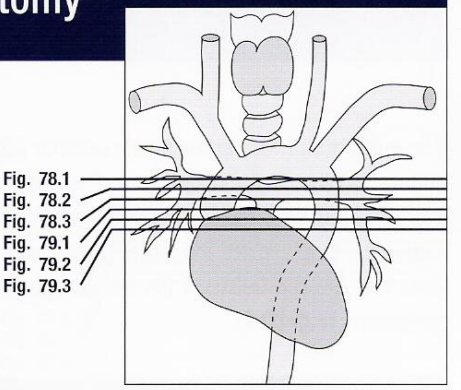

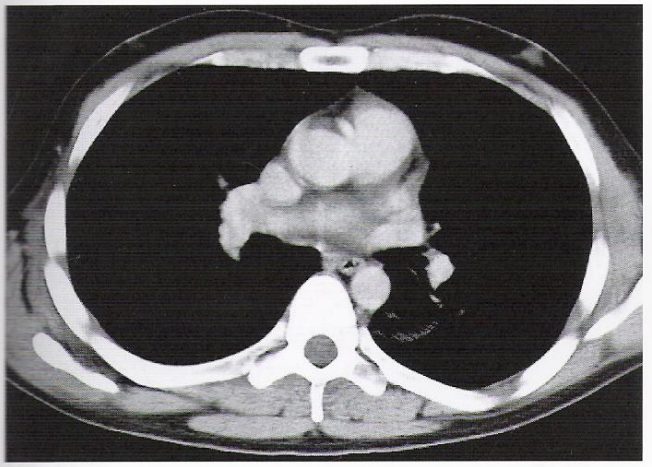

Fig. 79.1a

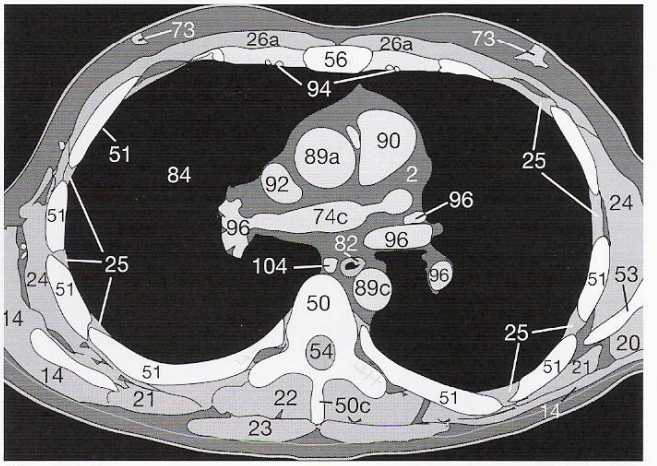

Fig. 79.1b

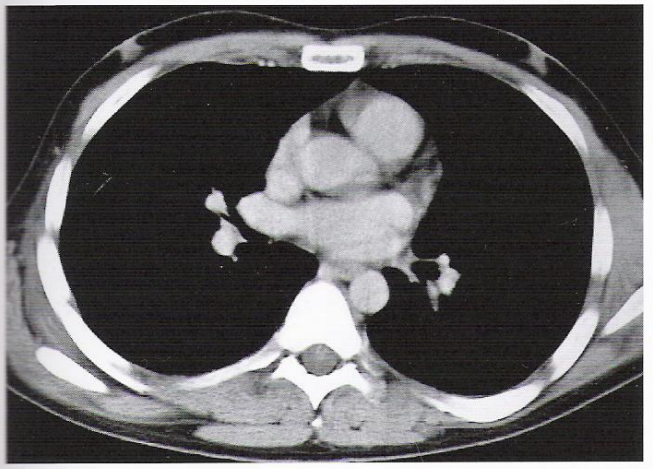

Fig. 79.2a

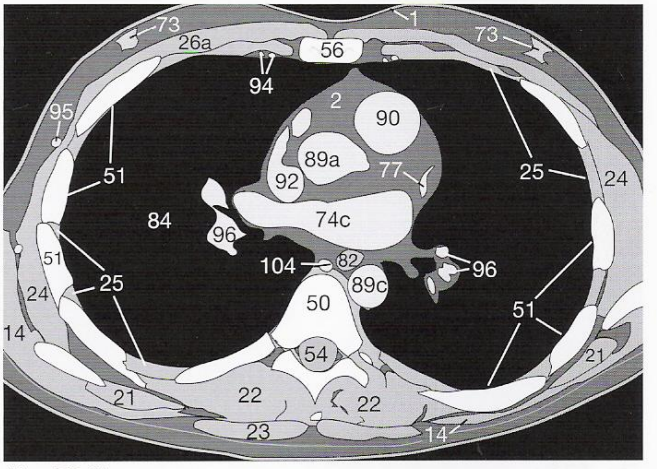

Fig. 79.2b

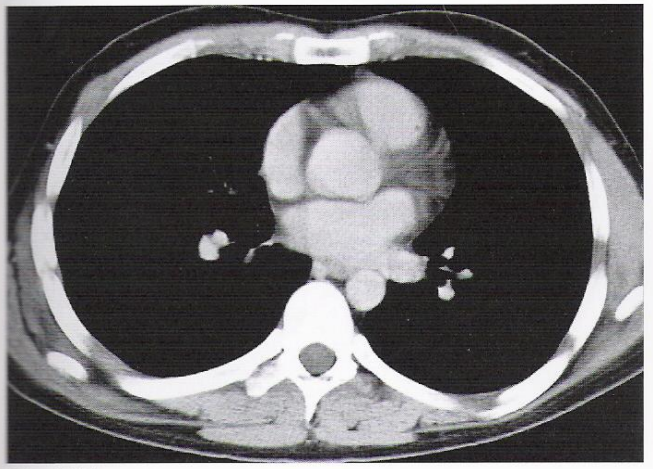

Fig. 79.3a

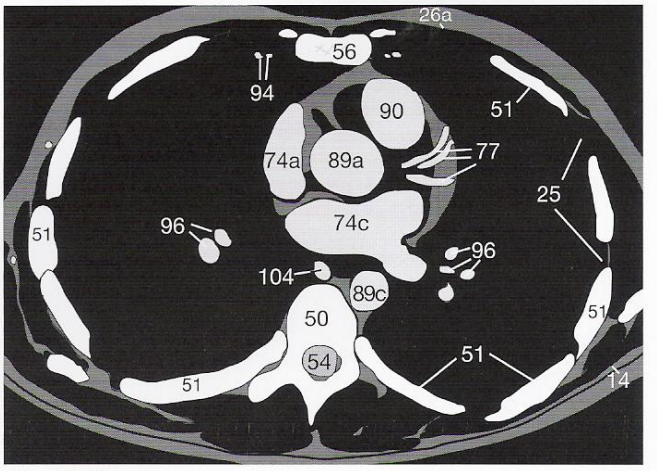

Fig. 79.3b

The left atrium **(74c)** is the most posterior chamber of the heart, whereas the outlet of the left ventricle **(74d)** and the ascending aorta **(89a)** lie in the center of the heart. The right atrium **(74a)** lies on the right lateral side and the right ventricle **(74b)** anteriorly behind the sternum **(56)**. Only the larger central branches of the pulmonary vessels **(96)** can be seen on the soft-tissue window. The smaller, more peripheral lung vessels are better judged on the lung window (not shown here).

Note the junction between the hemiazygos vein **(105)** and the azygos vein **(104)**, which must not be confused with a paravertebral lymphoma **(Fig. 80.2)**.

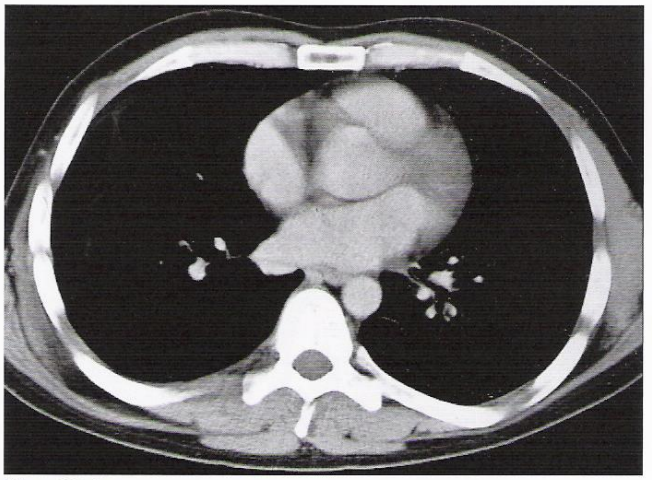

Fig. 80.1a

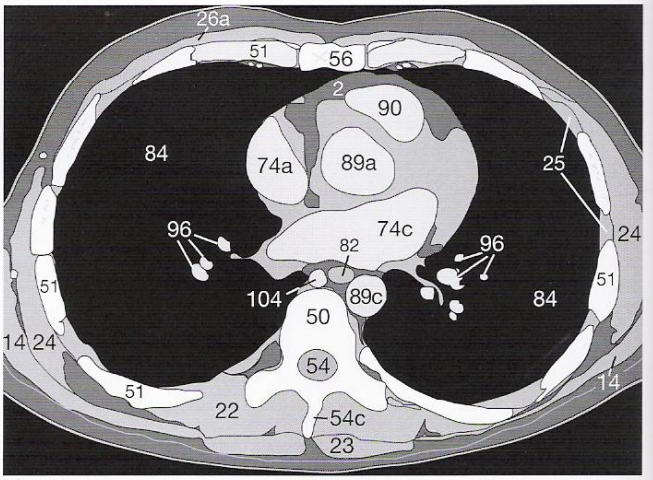

Fig. 80.1b

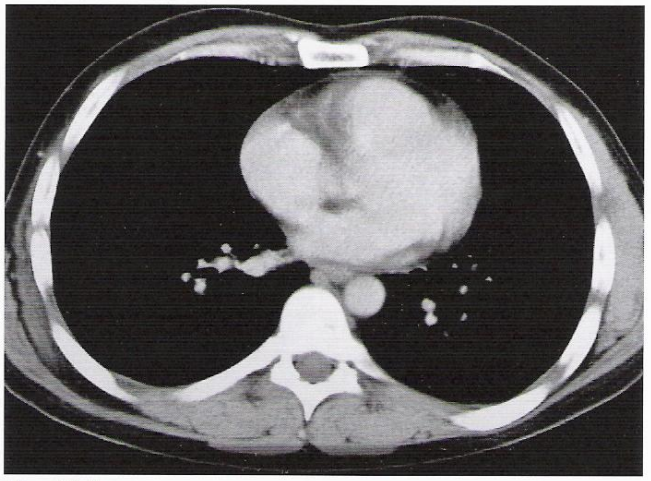

Fig. 80.2a

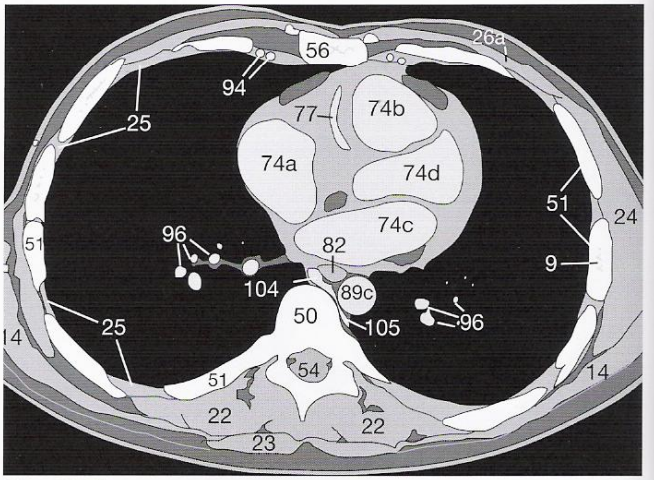

Fig. 80.2b

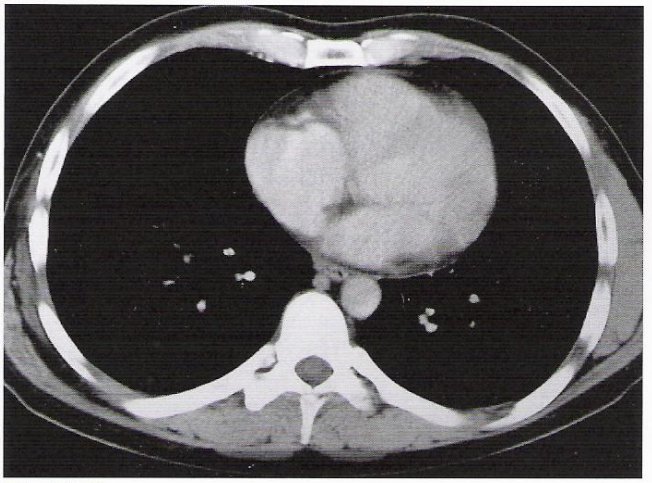

Fig. 80.3a

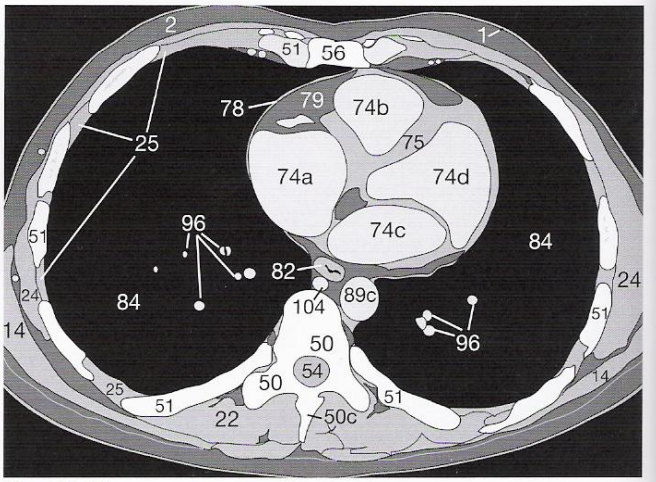

Fig. 80.3b

The sections on this page show the opening of the coronary sinus **(76)** into the right atrium **(74a)** and sequential sections of the coronary arteries **(77)**. The hypodense epicardial fat **(79)** must not be mistaken for fluid within the pericardial space. The internal thoracic artery, also known as the internal mammary artery **(94)**, is more and more frequently used in bypass operations. It is surgically anastomosed with the anterior descending branch of the left coronary artery.

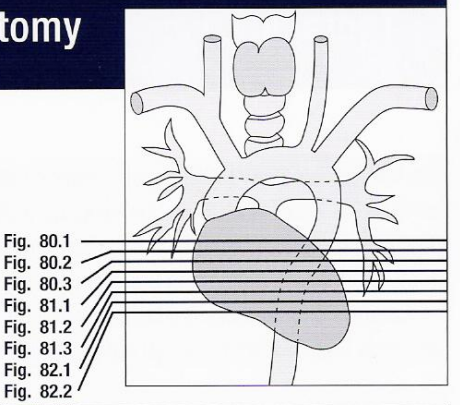

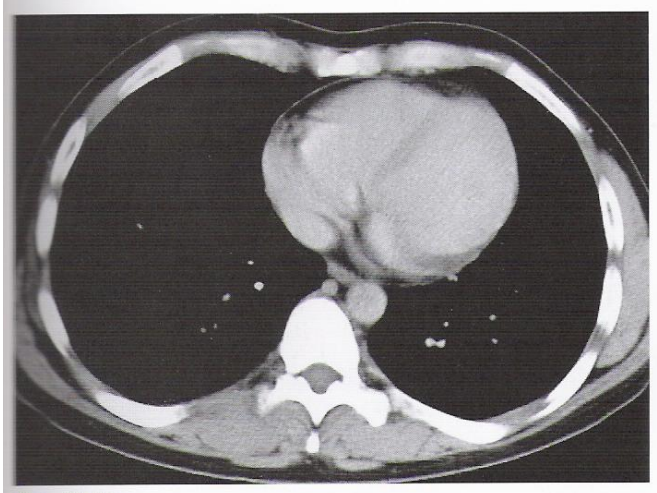

Fig. 81.1a

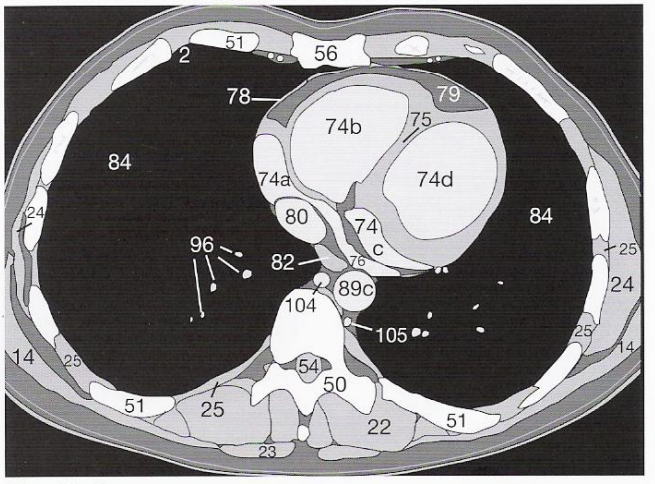

Fig. 81.1b

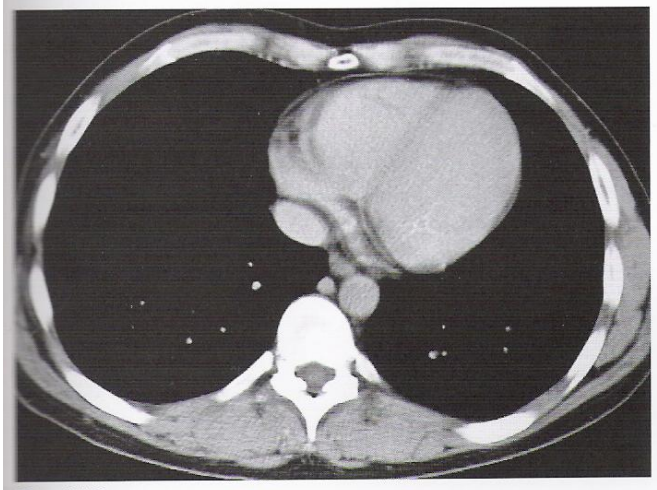

Fig. 81.2a

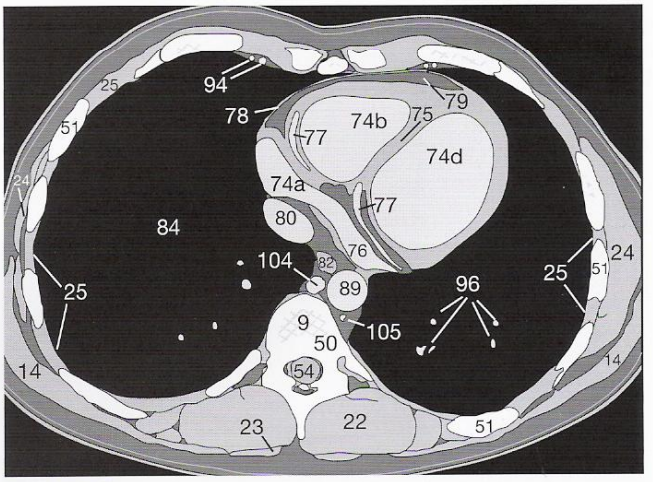

Fig. 81.2b

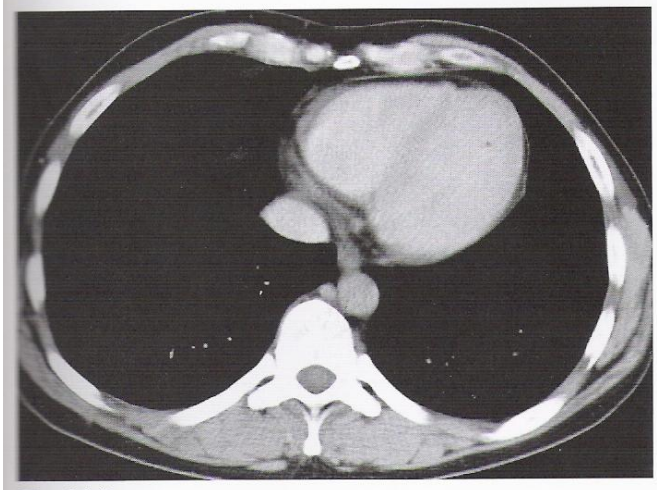

Fig. 81.3a

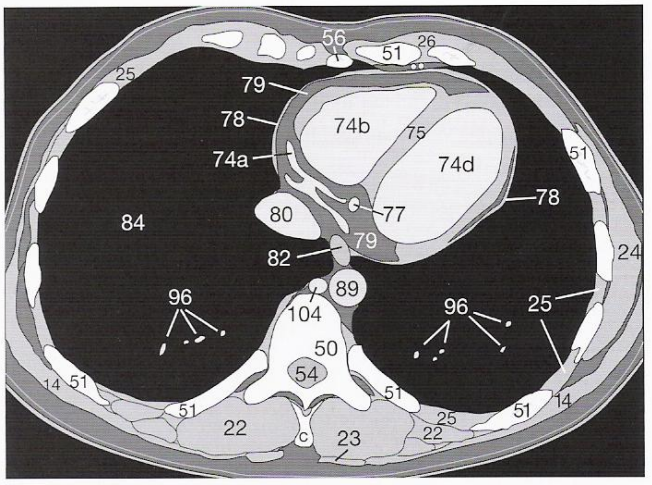

Fig. 81.3b

The inferior vena cava **(80)** is seen more caudally (**Figs. 82.1** and **82.2**), and finally the diaphragm **(30)** appears together with the upper parts of the liver **(122)**. Many radiologists who suspect the presence of a bronchial carcinoma (BC) obtain images to the caudal edge of the liver (see p. 83) because a BC often metastasizes to the liver and the adrenal glands. The caliber of lung vessels near the periphery of the diaphragm is so small that they are not visible on the soft-tissue window, as in the present images. The pattern of the pulmonary vasculature should therefore be examined on the lung windows, which include the negative density values of the Hounsfield scale. Only after this step has been carried out is the evaluation of a chest CT complete.

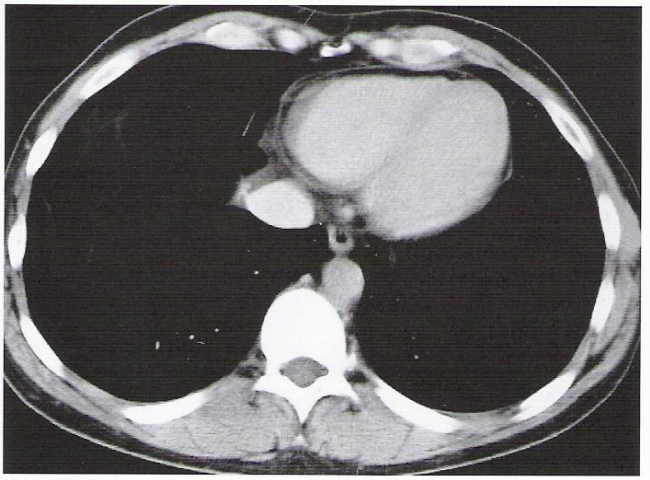

Fig. 82.1a

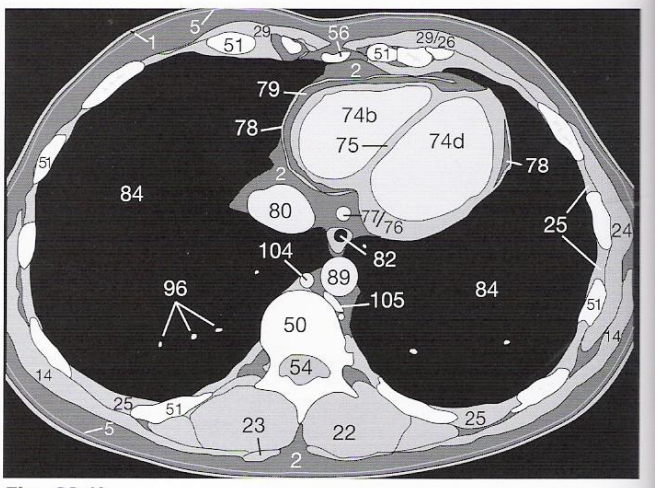

Fig. 82.1b

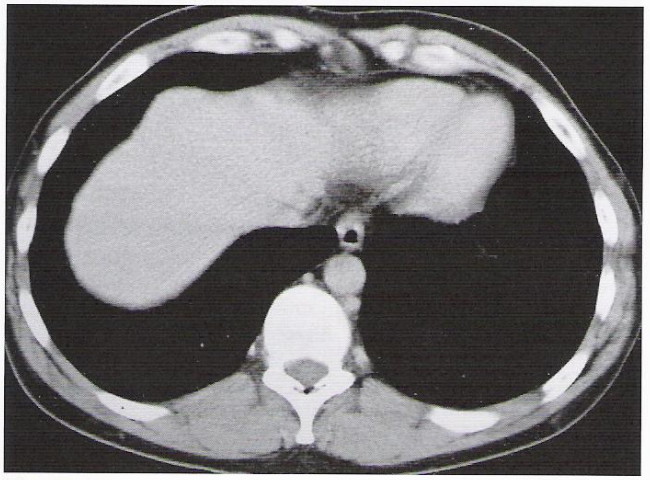

Fig. 82.2a

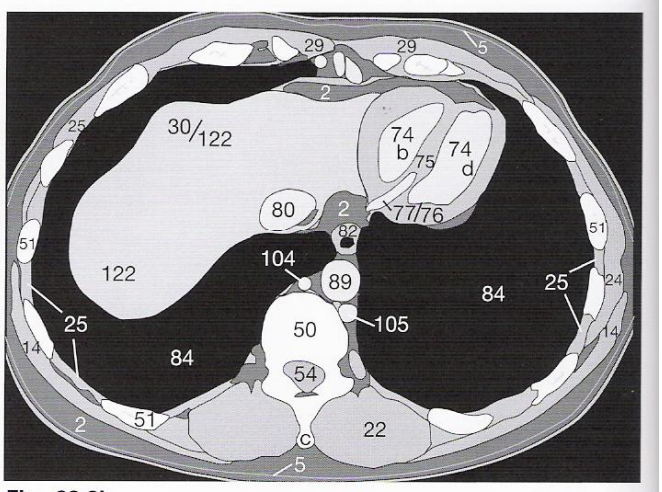

Fig. 82.2b

Test Yourself! Exercise **19:**

Write down a concise but complete sequence of all criteria for interpreting a thoracic CT. Then compare your notes with the checklist on page 74 and repeat this exercise from time to time until you remember every criterion.

1) Soft-tissue window:

soft-tissues, especially:

Segments of the Lung

It is especially important to be able to identify the segments of the lungs in CT images if bronchioscopy is planned for biopsy or to remove a foreign body. The right lung has 10 segments. In the left lung, the apical and posterior upper lobe segments have a common bronchus and there is no 7th segment (paracardiac [medial basal] segment of the lower lobe).

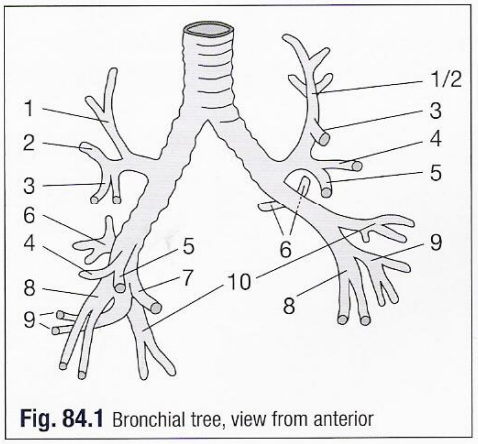

Fig. 84.1 Bronchial tree, view from anterior

Upper lobe	1 apical 2 posterior 3 anterior
Middle lobe	4 lateral (superior lingula) 5 medial (inferior lingula)
Lower lobe	6 superior/apical 7 paracardiac/medial basal 8 anterior basal 9 lateral basal 10 posterior basal

The parenchyma next to the interlobular fissures (——) appears avascular.

The borders of the segments (- - - - - -) are usually not visible in sections of normal thickness and can only be identified by the branches of the pulmonary veins **(96)** which pass along these borders.

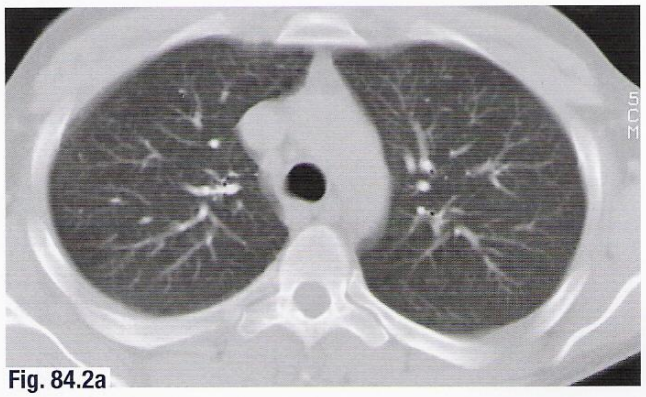

Fig. 84.2a

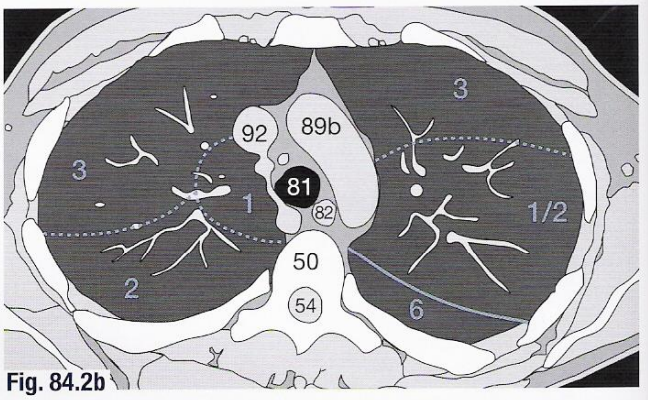

Fig. 84.2b

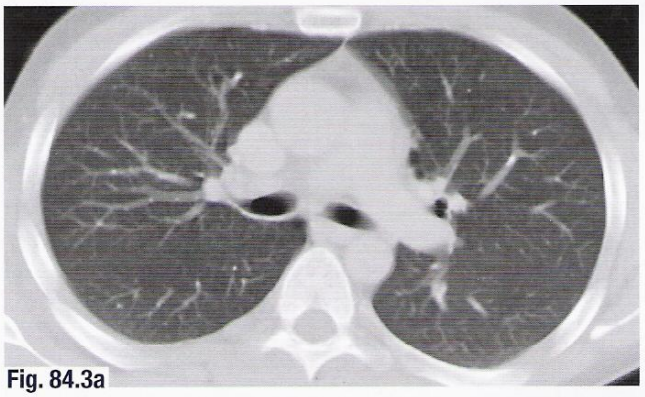

Fig. 84.3a

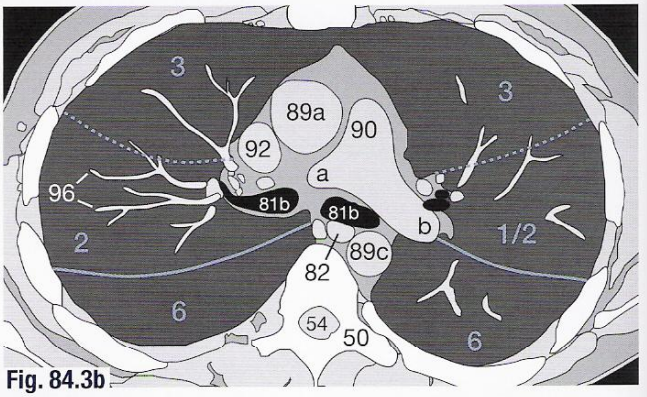

Fig. 84.3b

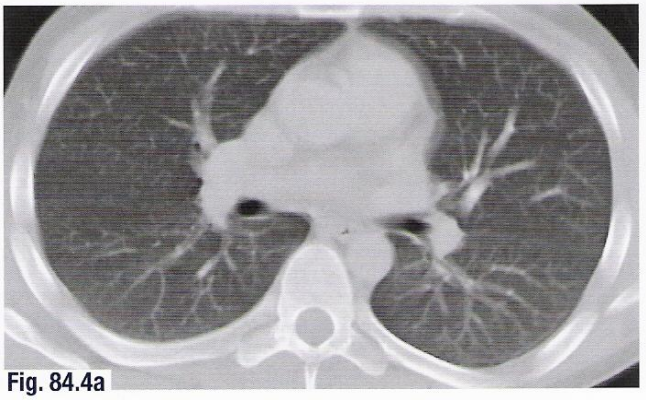

Fig. 84.4a

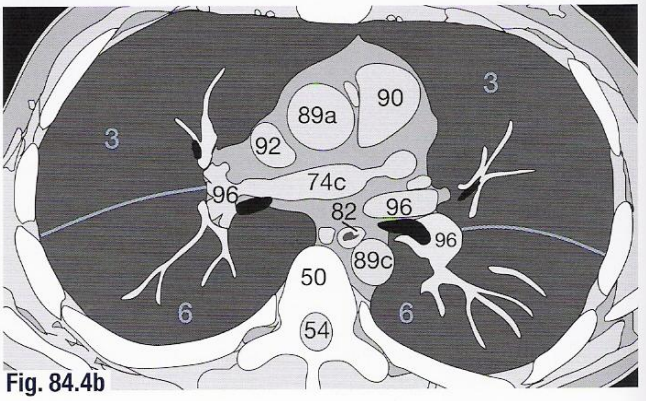

Fig. 84.4b

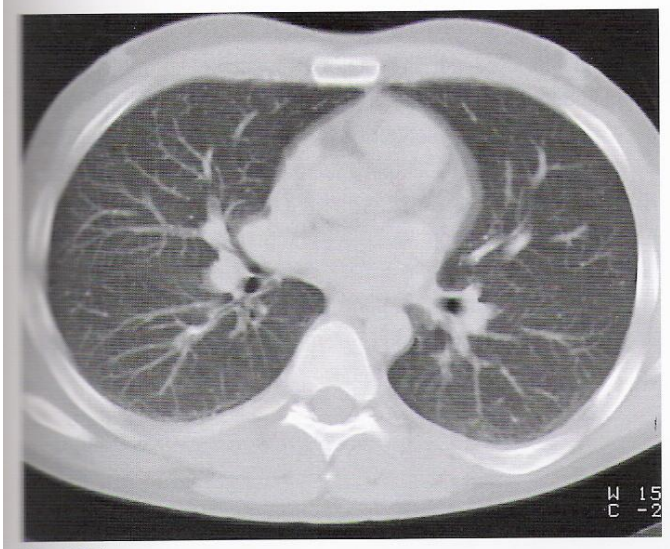

Fig. 85.1a

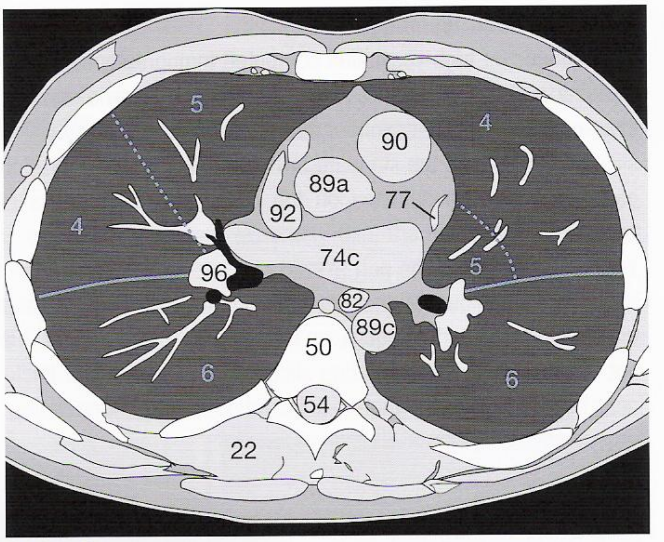

Fig. 85.1b

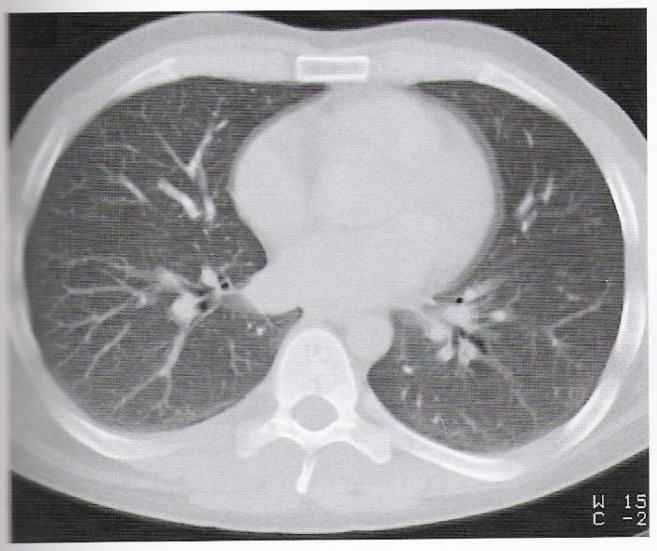

Fig. 85.2a

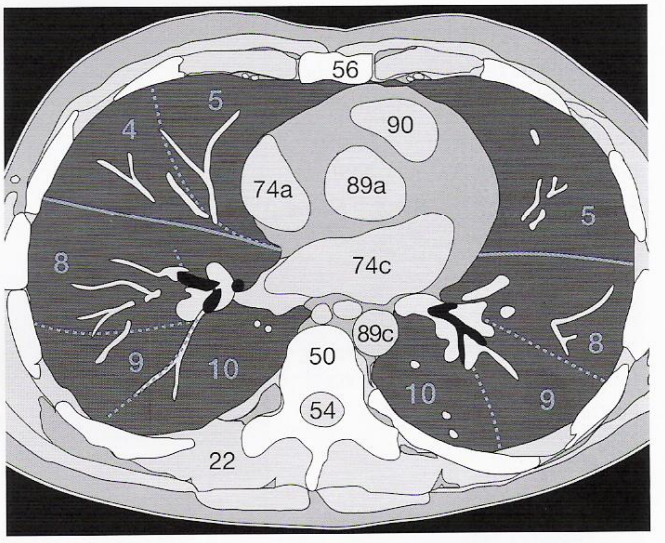

Fig. 85.2b

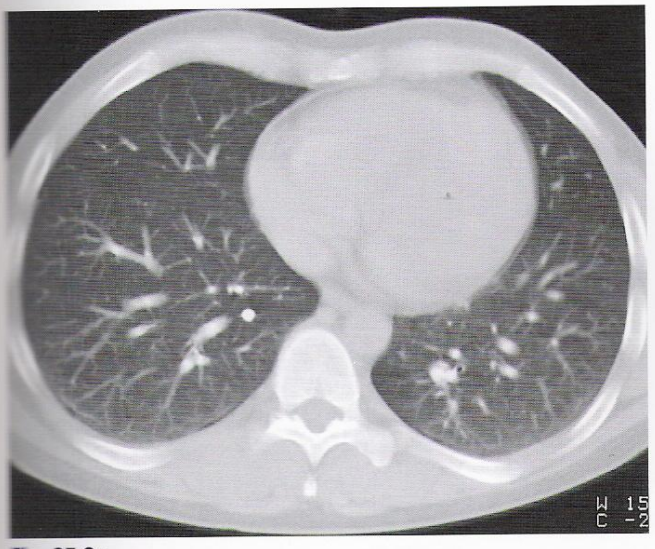

Fig. 85.3a

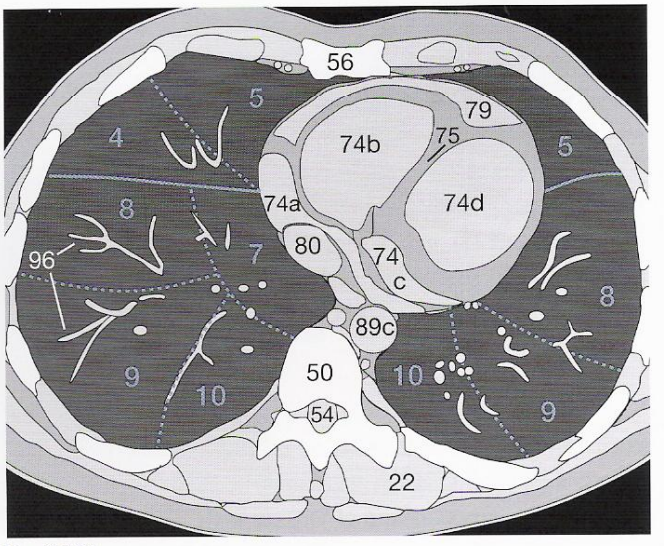

Fig. 85.3b

High-Resolution Technique

HRCT stands for **h**igh-**r**esolution **c**omputed **t**omography using thin sections and a high spatial resolution reconstruction algorithm. Even conventional CT scanners can acquire images of narrower slice thickness than the standard 5–8 mm. The image acquisition parameters can be adjusted on the console to a thickness of 1–2 mm if necessary.

In the SCT technique, thinner sections can also be computed at a pitch factor of 1:1 after acquisition (see also p. 169). However, it is not usually worth reconstructing slices of less than 1 mm thickness because the low signal-to-noise ratio reduces image quality.

HRCT is therefore not the method of choice for routine chest examination because radiation dosage is much higher if more sections are acquired. Longer examination times and higher hard-copy film cost ("slice pollution") are also arguments against using HRCT. Only structures with naturally high levels of contrast such as areas surrounding bone will be well demonstrated.

High-Resolution Effects on Image Quality

Figure 86.1 shows a conventional scan of a pulmonary lesion **(7)** surrounded by a zone of edema or an infiltrate **(185)**. At a d_S setting of 10 mm this zone closely resembles the poorly ventilated area at the back of the posterior lobe **(178)**.

HRCT distinguishes these areas of increased density more clearly **(Fig. 86.2)** because voxel averaging does not have any appreciable effect (see also p. 14).

The DD includes bronchial carcinoma, metastasis of breast cancer resulting in lymphangitis carcinomatosa, and atypical pneumonia.

These images show a rare complication after catheterization of the right heart. The catheter was positioned too peripherally and caused hemorrhage **(173)** into adjacent parts of the lung. Follow-up 3 weeks later showed complete recovery.

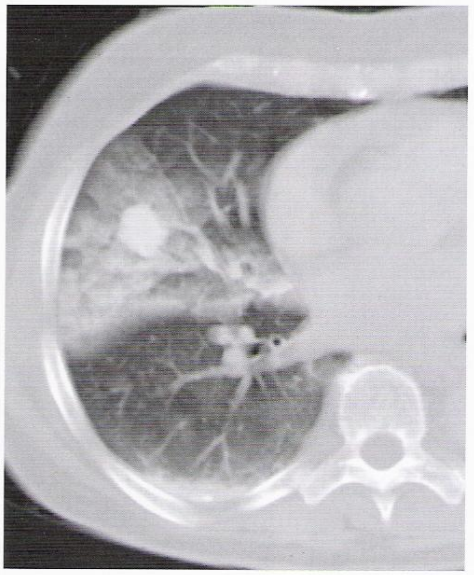

Fig. 86.1a

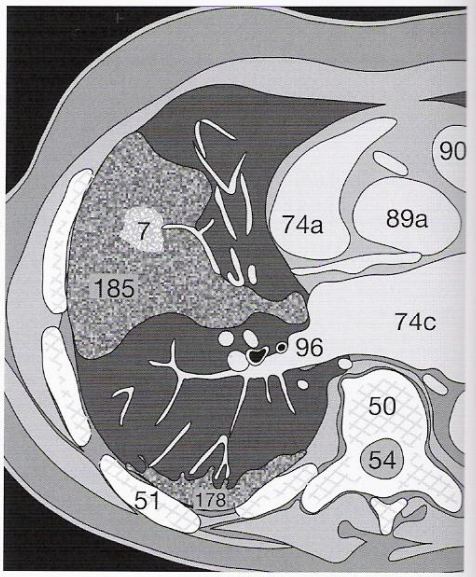

Fig. 86.1b

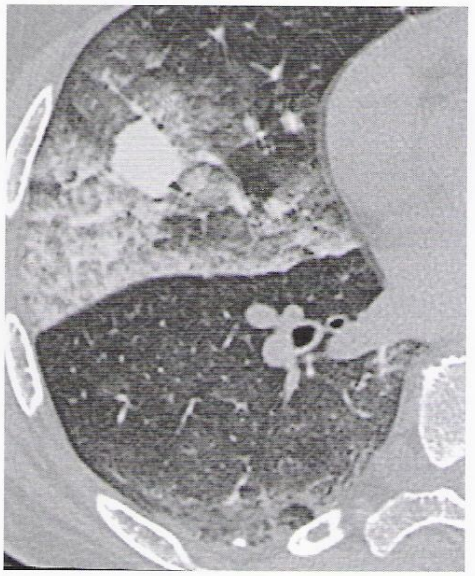

Fig. 86.2a

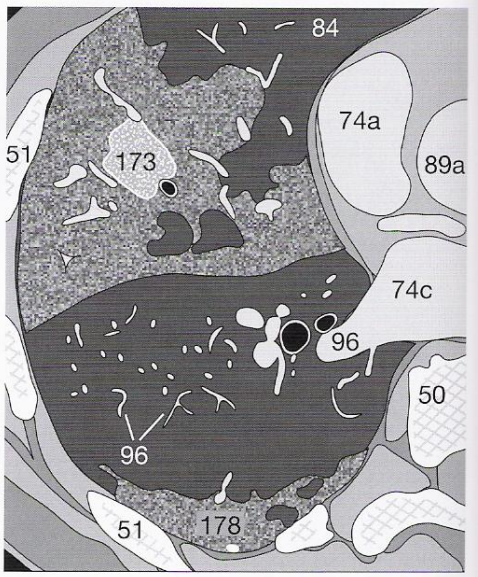

Fig. 86.2b

Indications

One of the many advantages of the HRCT technique is that older scar tissue can be distinguished from acute inflammation, for example in immune-suppressed patients or bone marrow recipients. Older scar tissue **(186)** is always well defined **(Fig. 87.1)**, whereas fresh infiltrates are surrounded by a zone of edematous tissue **(185)** as in **Figure 87.2**. HRCT is often the only method with which to determine whether chemotherapy should be continued in a lymphoma patient who is in the aplastic phase on therapy or whether chemotherapy must be discontinued because of fungal pneumonia. Fresh infiltrates **(178)** can sometimes be seen next to older scar tissue **(186) (Fig. 87.3)**.

Because the slices are extremely thin, the horizontal interlobular fissure (*) may appear as a bizarre ring or crescentic (**Figs. 87.1** and **87.2**).

Fig. 87.1a

Fig. 87.2a

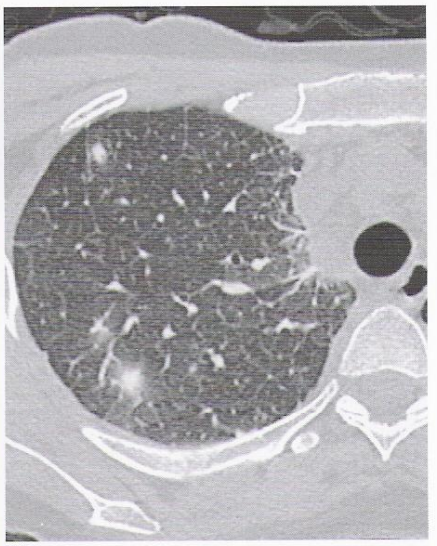

Fig. 87.3a

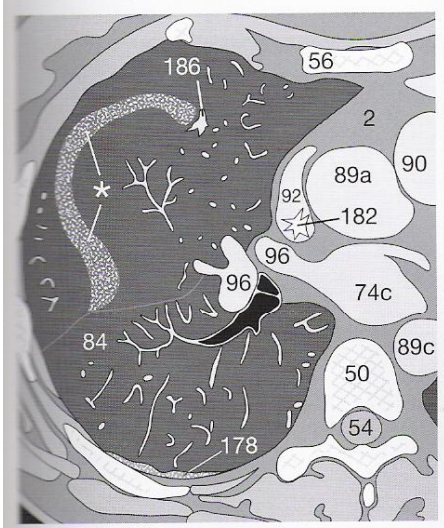

Fig. 87.1b

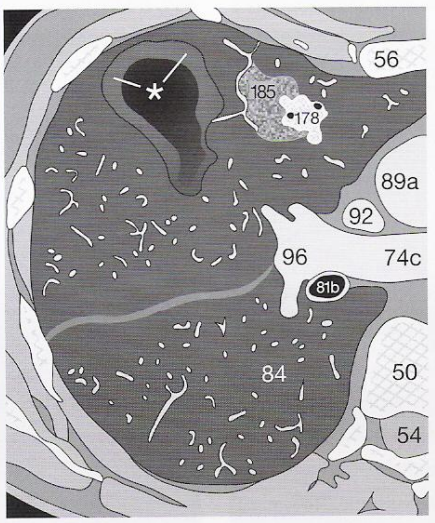

Fig. 87.2b

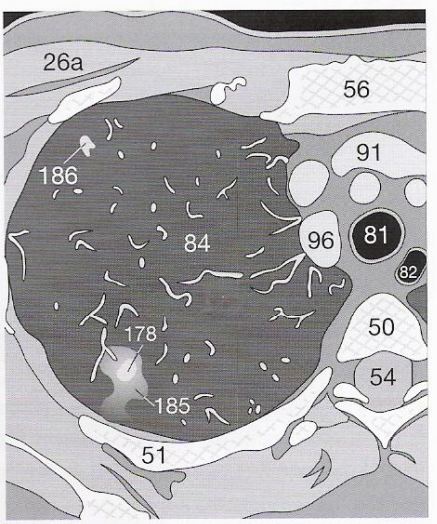

Fig. 87.3b

Minor areas of collapse, which are usually found close to the pleura posteriorly in the lung, must be differentiated from flat sections of fissures (**178** in **Fig. 87.1**). In doubtful cases, it may be helpful to repeat a scan in the prone position. Areas of collapse and poor ventilation may then disappear or be seen anteriorly. Pulmonary abnormalities due to an infiltrate or to a pneumoconiosis would be unchanged.

Among the many anatomic variations of the thorax, an atypical course of the azygos vein **(140)** is relatively common. It can pass from the posterior mediastinum through the right apical lobe to the superior vena cava **(92)**. It is located within a fold of the pleura and therefore separates the azygos lobe from the remainder of the right upper lobe. This variation is usually discovered incidentally on a conventional chest X-ray (↗ in **Fig. 88.1**) and has no clinical significance. **Figures 88.2** to **88.4** show the anomalous path of the vessel as it appears in CT images.

Atypical positions or branching of the aortic arch **(89)** vessels are rarer. An example is the right subclavian artery, known as the "Arteria lusoria," which can resemble a lesion in the upper mediastinum.

Note that normal breast tissue, surrounded by fat **(2)**, may have very irregular contours (**72** in **Fig. 88.4**). When using lung windows, you should not only look for solid round lesions and inflammatory infiltrates, but also recognize any thinning or even absence of lung vessels.

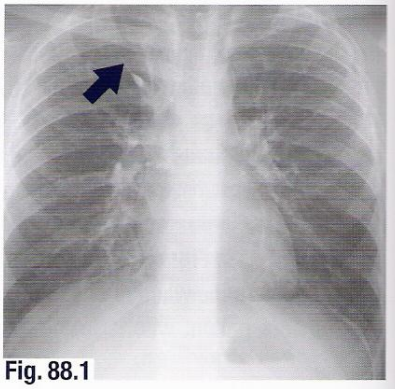

Fig. 88.1

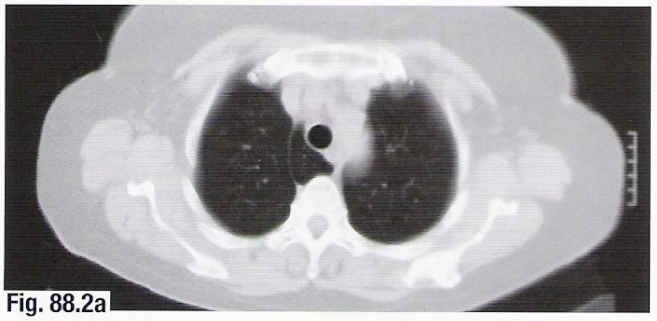

Fig. 88.2a

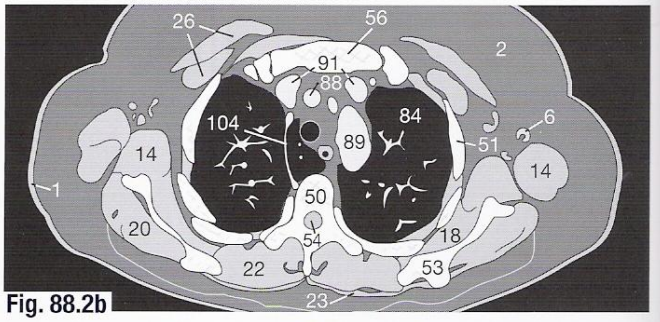

Fig. 88.2b

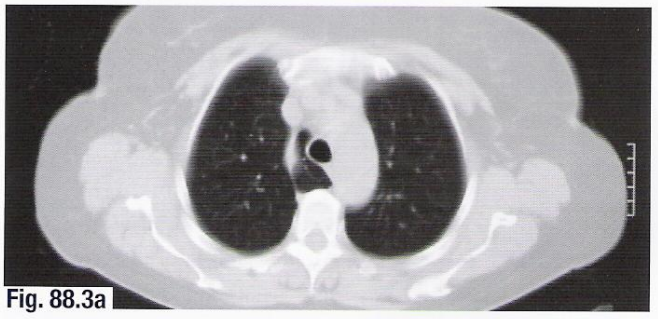

Fig. 88.3a

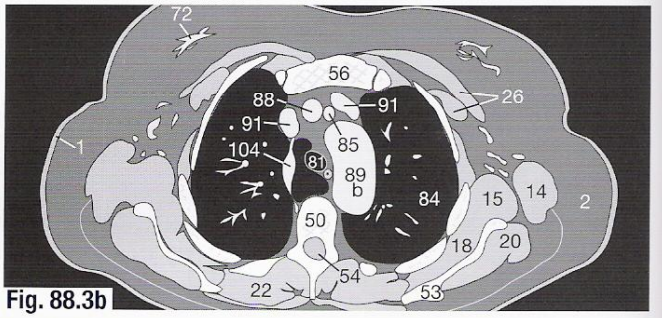

Fig. 88.3b

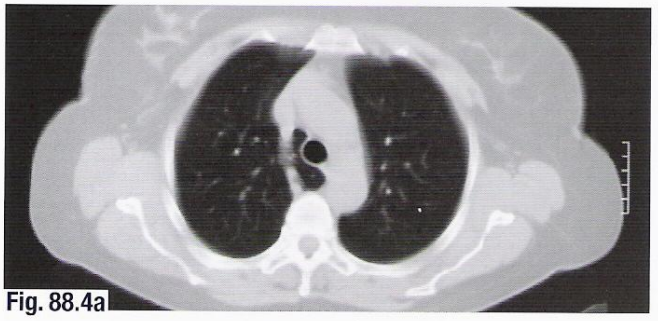

Fig. 88.4a

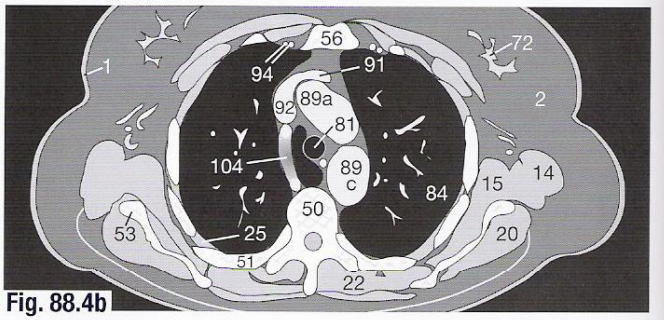

Fig. 88.4b

However, attenuation of vessels is not always a sign of emphysema. Asymmetry in the bronchovascular pattern develops after a part of the lung has been resected. In the patient imaged in **Figure 88.5**, the left upper lobe had been removed and the remaining lung tissue has compensated and filled the entire left thoracic cavity (right half of the image). There are fewer lung vessels per unit volume and an ipsilateral shift of the mediastinum. These changes are accompanied by a slight elevation of the diaphragm. At the time of this follow-up CT, the patient was healthy and had neither emphysema nor recurrent tumor.

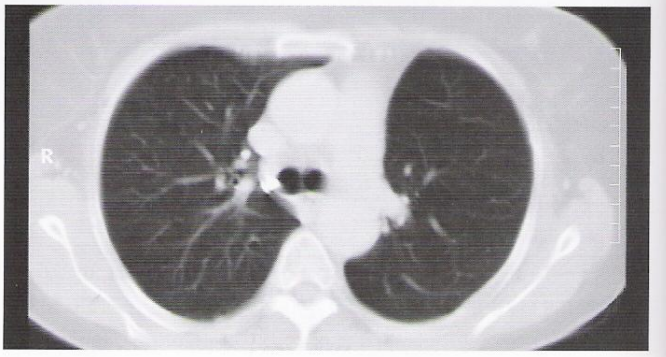

Fig. 88.5

According to the sequence in the checklist on page 74, one should now turn to soft-tissue windows in order to examine the soft tissues of the chest wall. Most abnormalities will be located in the axillae and in the female breast.

Alterations in Lymph Nodes

Normal axillary LNs **(6)** are usually oval and less than 1 cm in dimension. They often have a hypodense center or are horseshoe-shaped as in **Figure 89.1**, a feature known as the "hilum fat sign." The architecture of a normal LN is characterized by vessels entering the hilum, which contains hypodense fat. Many abnormal LNs have lost their normal contours and are rounder or irregular. Such LNs all appear solid and lack the hilum fat sign, as seen in those in the left axilla in **Figure 89.2**. For direct comparison, two lymph nodes on the other side in the same image are normal.

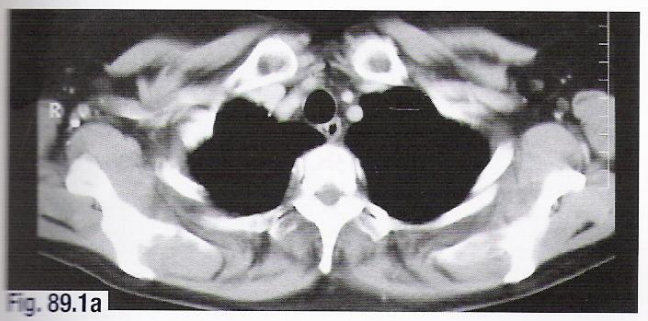
Fig. 89.1a

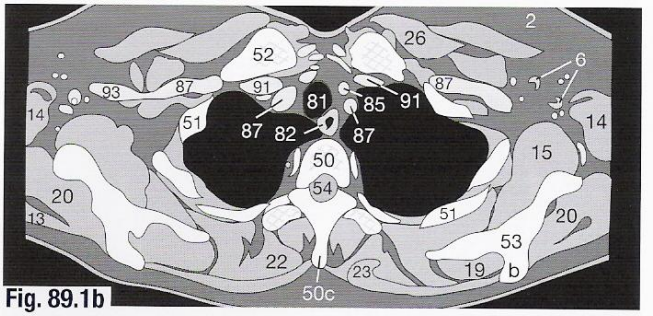

Fig. 89.1b

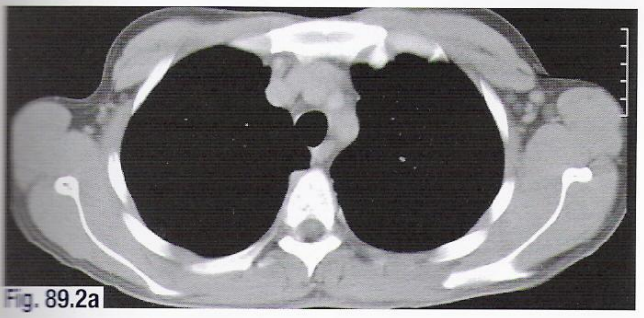
Fig. 89.2a

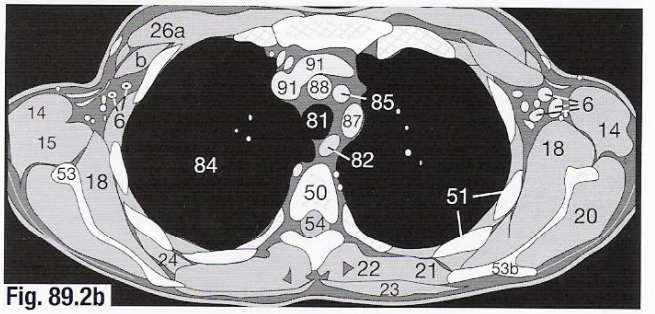

Fig. 89.2b

Larger metastatic LNs **(7)** are usually poorly defined and difficult to differentiate from surrounding fat **(2)**. They often have central areas of necrosis **(181)**, so that the differential diagnosis of an abscess with central liquefaction must be considered **(Fig. 89.3)**. If axillary lymph node metastases have been treated operatively or with radiotherapy, the date and treatment should be noted on the referral sheet for follow-up CT. Postoperative healing processes and scarring **(186)** change the morphology of LNs **(Fig. 89.4)**, so they resemble abnormal nodes (see above). Again the lack of clinical information makes diagnosis unnecessarily difficult for the radiologist.

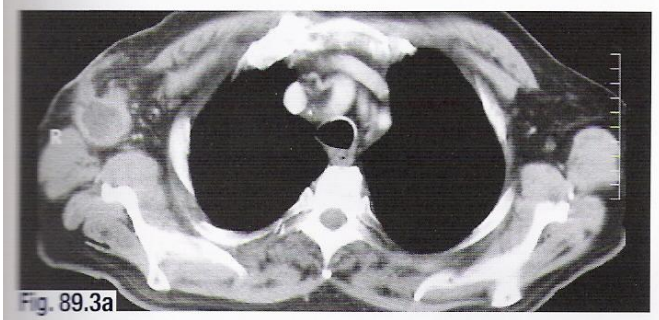
Fig. 89.3a

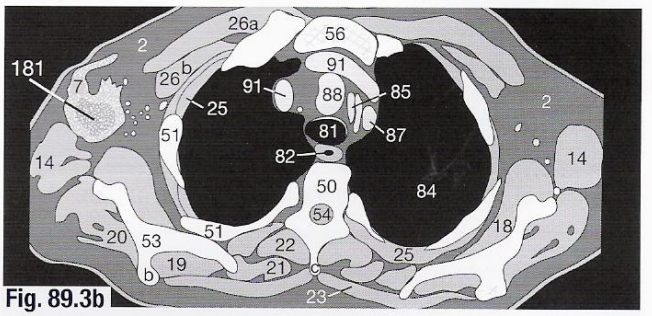

Fig. 89.3b

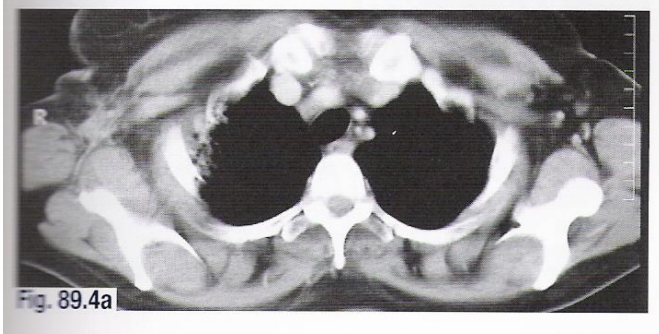
Fig. 89.4a

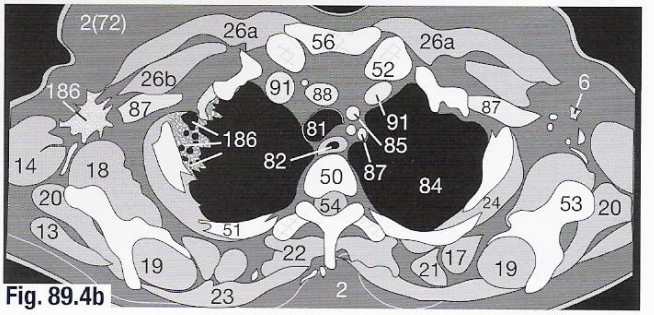

Fig. 89.4b

Breast

The normal parenchyma **(72)** of the female breast has very irregular contours and slender, finger-like extensions into the surrounding fat **(2)** (cf. **Fig. 88.4**). Bizarre shapes can often be seen **(Fig. 90.1)**. Advanced stages of breast cancer **(7)** have a solid, irregular appearance **(Fig. 90.1)**. The malignant tissue crosses the fascial planes or infiltrates the thoracic wall, depending on size. Baseline CT after mastectomy **(Fig. 90.2)** should help in the early identification of recurrent tumor. The diagnosis of recurrent tumor is made more difficult by fibrosis after radiation, postoperative scar tissue, and the absence of surrounding fat. Special attention must therefore be paid to the regional LNs (cf. pp. 74, 89) and the bones, so that metastases **(7)** in the vertebrae **(50)** **(Fig. 90.2)** are not overlooked. The bone window must be examined in such cases.

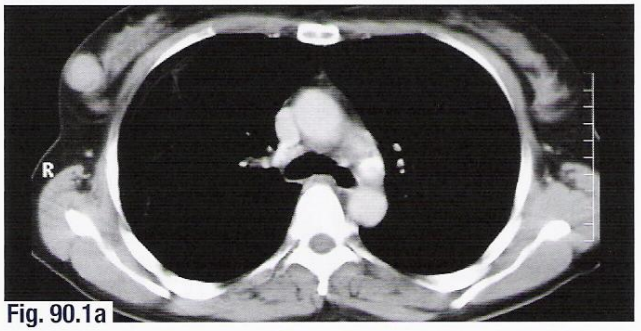

Fig. 90.1a

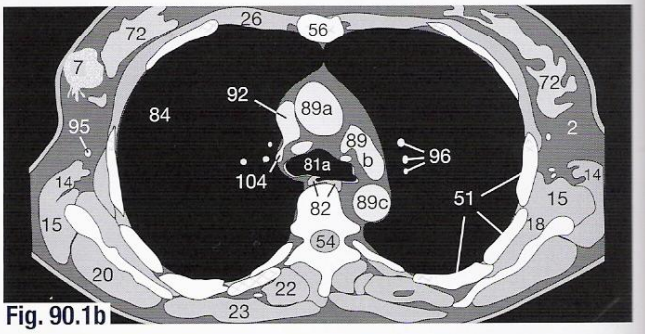

Fig. 90.1b

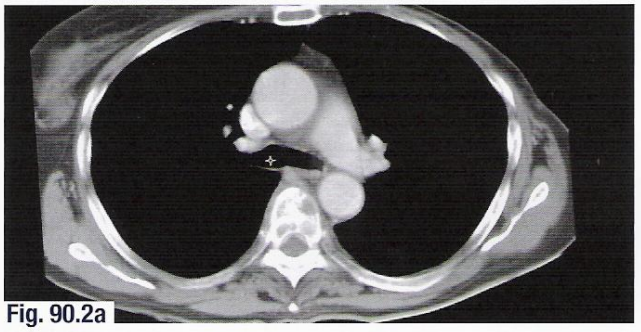
Fig. 90.2a

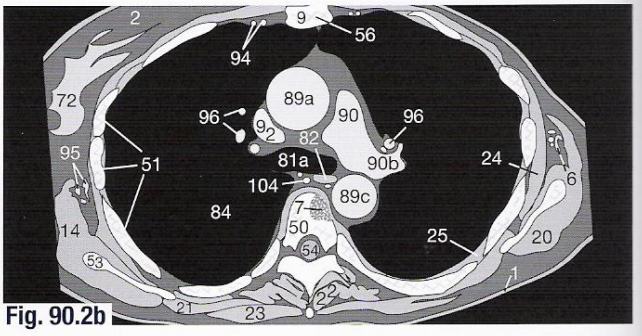

Fig. 90.2b

Thoracic Skeleton

Osteolysis within the thoracic skeleton is not uncommon and is usually due to either metastases or a plasma cell tumor. In **Figure 90.3**, a metastasis **(7)** from a thyroid carcinoma has destroyed part of the left clavicle **(52)**. Osteolysis can, however, also be caused by an enchondroma or an eosinophilic granuloma, for example of a rib. In addition to destructive processes (cf. **Fig. 22.3**), degenerative processes involving sclerosis and osteophyte formation of bone must be differentiated from osteosclerotic metastases, which are typical of, for example, prostate carcinoma (cf. p. 145).


Fig. 90.3a

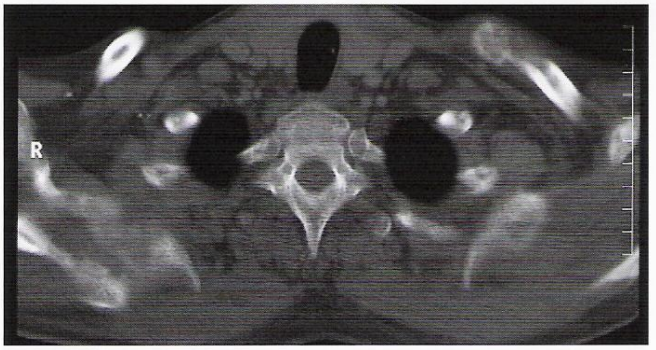

Fig. 90.3b

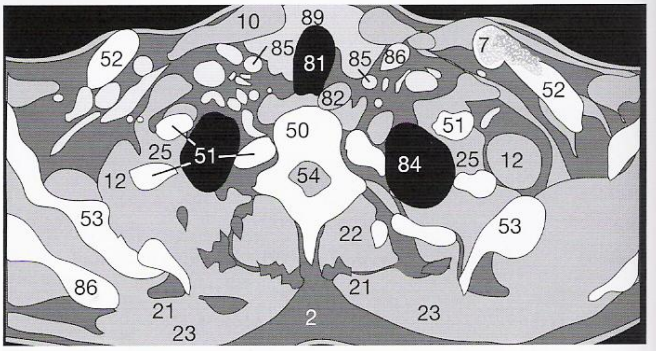

Fig. 90.3c

Before being able to detect lesions and lymphadenopathy, you must know the normal anatomy. If you are a preclinical student, you should firstly study normal sectional anatomy. It is in your own interests to work through the following pages only when you are sufficiently familiar with the previous chapters.

Tumors

A benign increase in fat **(2)** due to cortisone therapy is occasionally observed in the anterior mediastinum **(Fig. 91.1)**. In doubtful cases, densitometry is helpful in the DD (cf. p. 15). In this example, the average density within the region of interest (ROI), which is positioned in possible fatty tissue, is –89.3 HU with a standard deviation of about 20 HU (cf. **Table 16.1**). As a rule, the size of an ROI in cm^2 (AR) is also provided **(Fig. 91.1)**. The DD of such a mass would include retrosternal goiter and thymoma.

In children and young adults, the density of the thymus is about +45 HU. As a result of involution, the density of the organ decreases with age from the third decade onward until it has dropped to the density typical of fat (–90 HU). The left lobe of the thymus is often larger than the right and can reach the aortopulmonary window. A lobe should not be thicker than 1.3 cm in adults; up to the age of 20, 1.8 cm is considered normal.

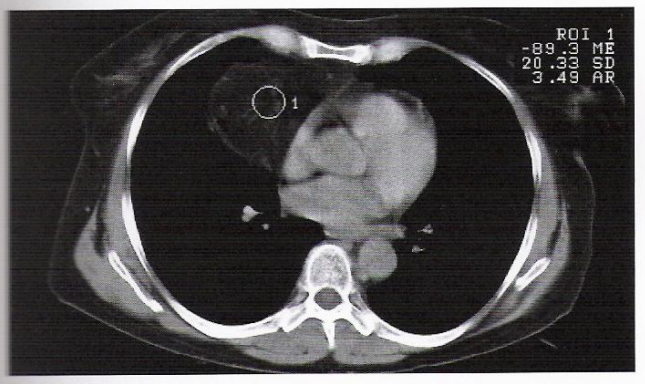

Fig. 91.1a

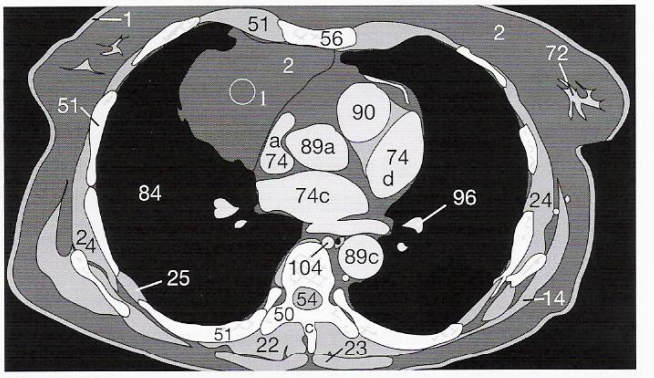

Fig. 91.1b

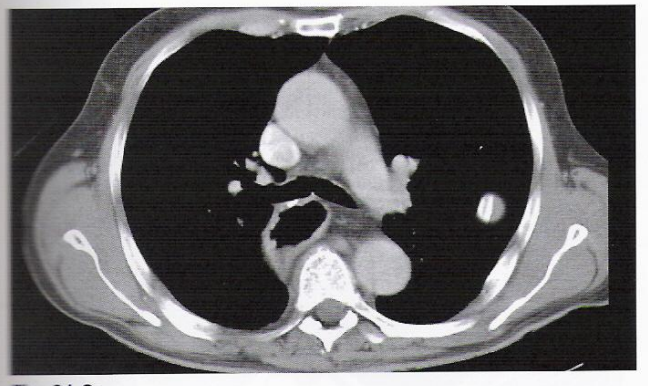

Fig. 91.2a

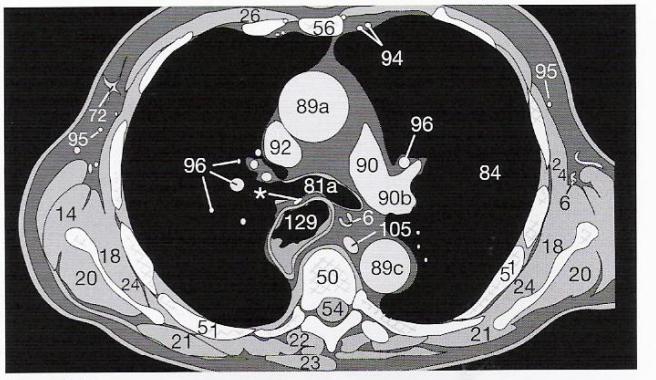

Fig. 91.2b

Malignant thickening of the walls of the esophagus must be differentiated from gastric conduits following esophageal surgery (Fig. 91.2). Possible enlargement of LNs **(6)** next to the stomach (129) must be excluded by follow-up CTs. Occasionally postoperative metal clips cause artifacts (*), which make assessment of the mediastinum more difficult. Following esophageal resection, parts of the colon (➡) may become drawn up into the anterior mediastinum **(Fig. 91.3)**. Comparison with adjacent sections quickly shows that this structure is not an emphysematous bulla, but is a tubular organ containing a lumen.

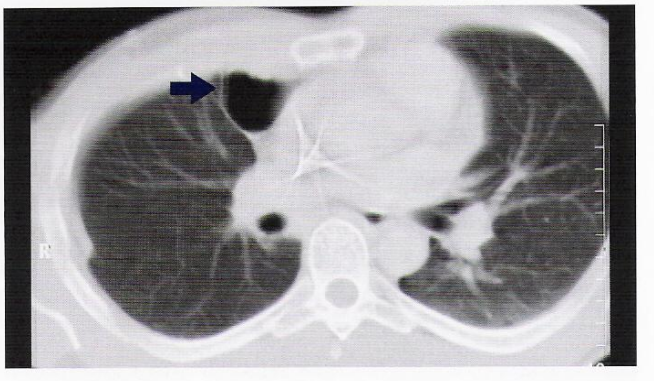

Fig. 91.3

Enlarged Lymph Nodes

Normal LNs are often found at the level of the aortopulmonary window. They are mainly oval or irregular, less than 10 mm across [19], and sharply delineated from mediastinal fat **(2)**. LNs **(6)** in this area are not usually considered suspicious until they exceed 1.5 cm in diameter. The demonstration of a "hilum fat sign" (cf. p. 89) is not obligatory, but does suggest a benign nature **(Fig. 92.1)**.

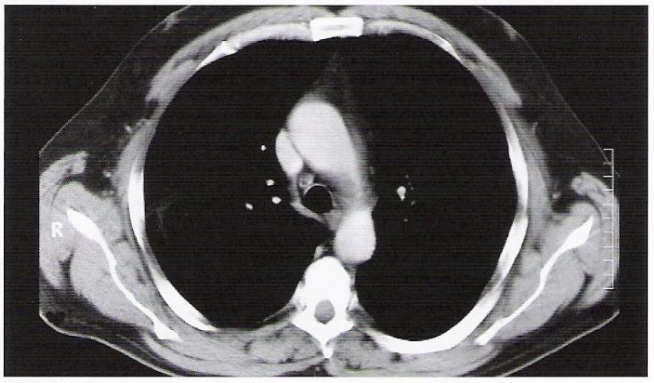

Fig. 92.1a

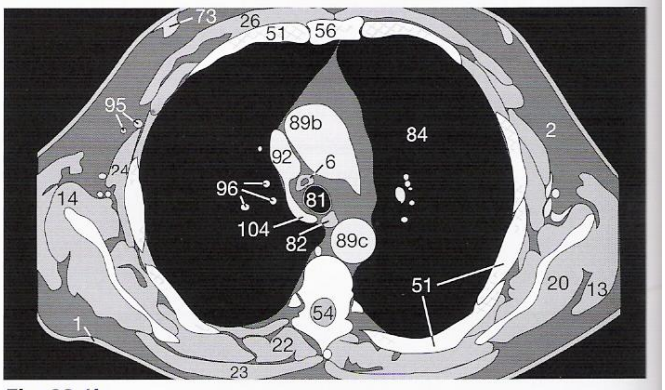

Fig. 92.1b

If more than three LNs are seen in the aortopulmonary window or if a single LN is abnormally enlarged, the DD includes not only a metastasis from a bronchial carcinoma, but also a lymphoma **(Fig. 92.2)**.

Enlarged mediastinal, and especially hilar, LNs are also characteristic of sarcoidosis (Boeck's disease) (**6** in **Fig. 92.3**). In **Figure 92.2**, there are intrapulmonary metastases **(7)** as well. Did you notice them? Other sites of predilection for abnormal LNs are anterior to the aortic arch, beneath the bifurcation of the trachea (subcarinal), and the para-aortic and retrocrural regions.

Normal size (diameter) of thoracic LNs [19, 41]:

- anterior mediastinum < 6 mm
- aortopulmonary window < 15 mm
- hilar < 10 mm
- subcarinal < 10 mm
- para-aortic < 7 mm

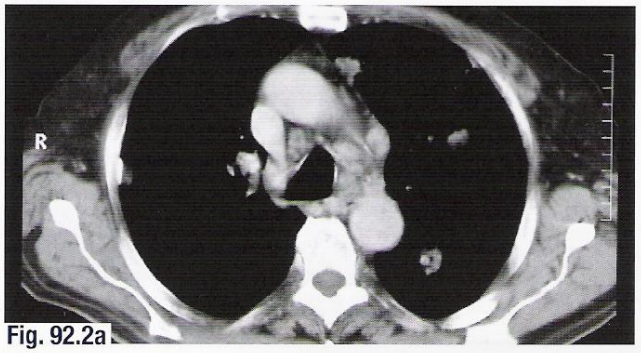

Fig. 92.2a

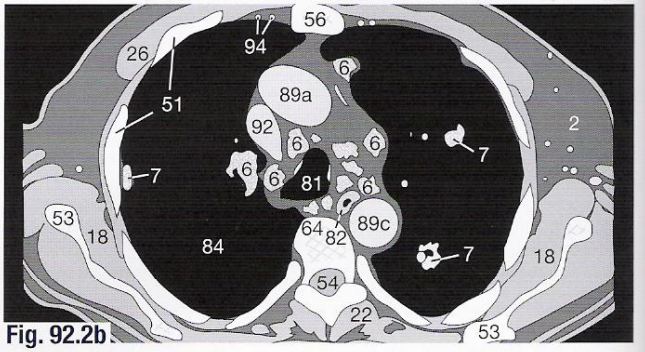

Fig. 92.2b

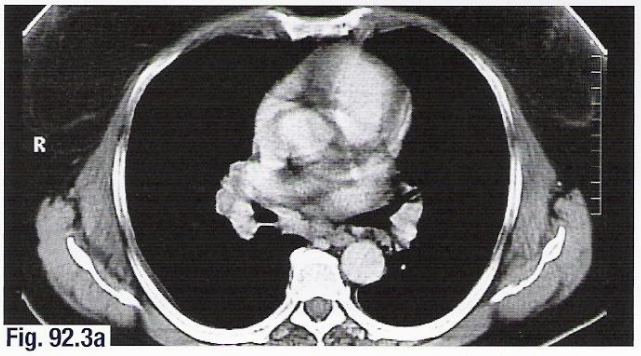

Fig. 92.3a

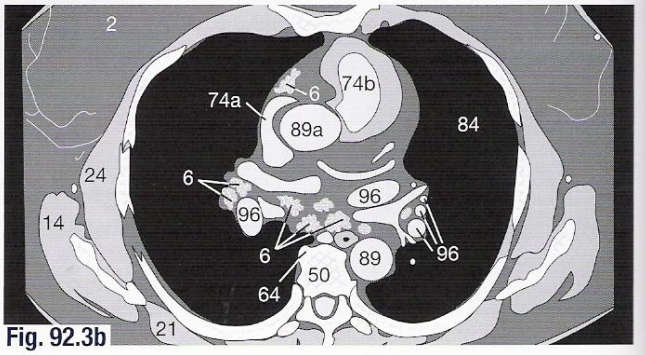

Fig. 92.3b

Vascular Pathologies

Inflow phenomena of CM injected through an arm vein (cf. p. 21) and anomalous vessels (cf. p. 88) in the mediastinum have already been discussed. Incompletely mixed CM must be distinguished from a possible thrombus **(173)** in the lumen of the brachiocephalic vein **(91)**. Such a thrombus can adhere to a central venous catheter (**182** in **Fig. 93.1**).

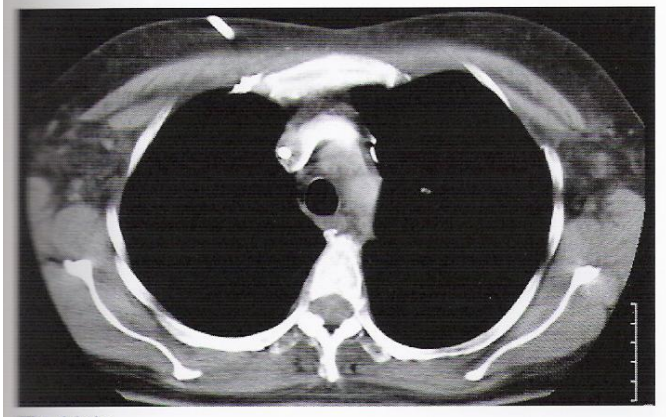

Fig. 93.1a

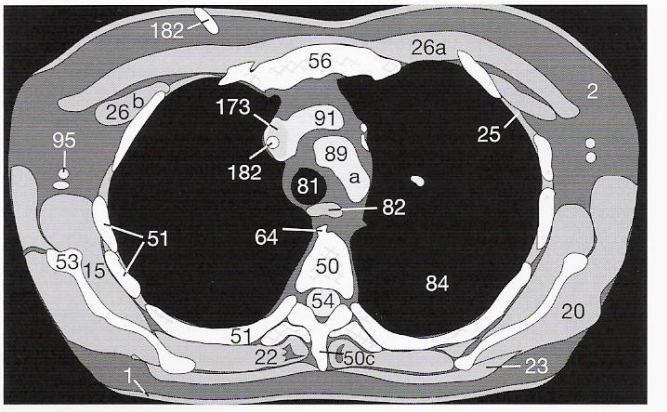

Fig. 93.1b

Atherosclerotic plaques **(174)** in the aorta **(89)** are often accompanied by thrombotic deposits (**173** in **Fig. 93.3**). They promote aortic elongation and dilation and can ultimately lead to an aneurysm **(171)**. Dilation of the thoracic aorta is considered to be an aneurysm if the lumen is wider than 4 cm. Recording the measurements of distances and sizes **(Fig. 93.2)** makes it easier to assess any progressive dilation in follow-up CTs. It is important to check for any involvement of the branches of the great vessels or for the presence of a dissection flap (**172** in **Fig. 93.4**). Three types of dissection can be diagnosed according to the extent of the dissection flap (see de Bakey [20]).

A true aneurysm with a diameter of more than 6 cm, with a more saccular than fusiform shape or with an eccentric lumen, has a higher incidence of rupture. The consequences of rupture include a mediastinal hematoma, a hemothorax, or pericardial tamponade.

Dissecting Aneurysms of the Aorta
(according to de Bakey [20])

Type I (approx. 50%)
Ascending aorta; may extend to abdominal bifurcation

Type II (approx. 15%)
Only ascending aorta, extending to brachiocephalic trunk

Type III (approx. 25%)
Torn intima distal to left subclavian artery

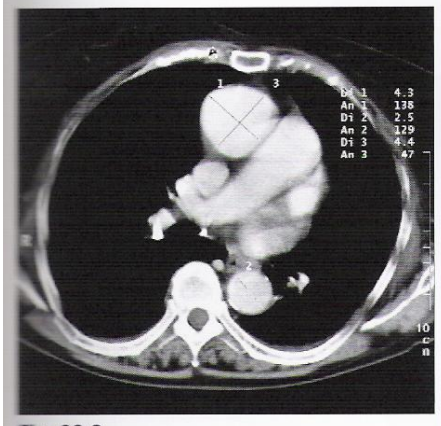

Fig. 93.2

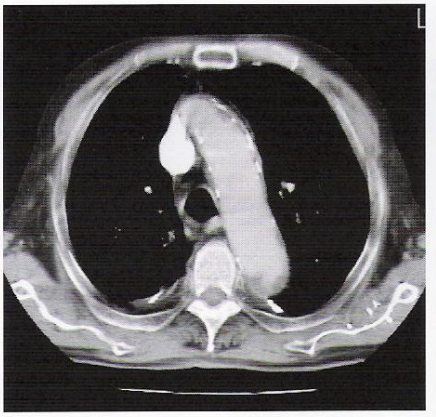

Fig. 93.3a

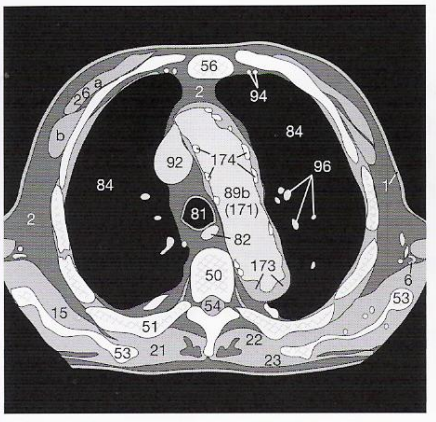

Fig. 93.3b

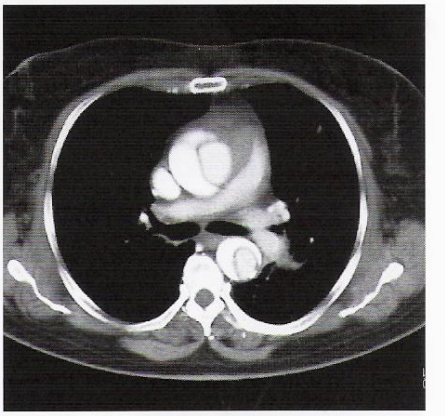

Fig. 93.4a

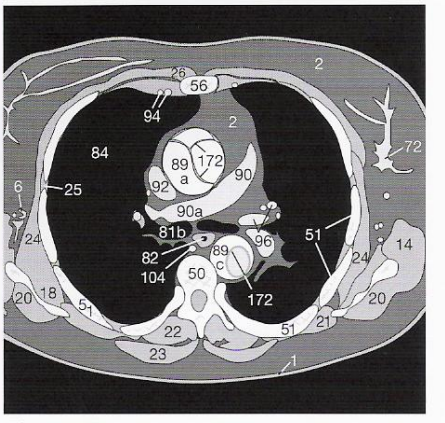

Fig. 93.4b

Pulmonary Embolism

If a large embolus has detached from a thrombus in a deep vein of the leg, it will be visible as a hypodense area (↘) within the involved pulmonary artery on contrast-enhanced images **(Fig. 94.1)**. After large pulmonary emboli, the affected segments or lobes (↖) usually become poorly ventilated and atelectasis occurs. The pulmonary vessels become attenuated, which can be demonstrated in conventional x-rays. The CT-angiographic detection of pulmonary emboli is described on page 186 in more detail.

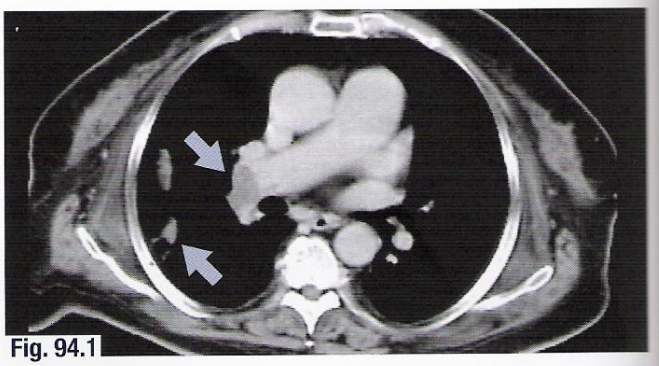

Fig. 94.1

Heart

You have already familiarized yourself with the normal anatomy of the heart on pages 79 to 81. Dilation resulting from valvular incompetence or from cardiomyopathies, as well as intracardiac filling defects can be recognized in CT images. If CM has been injected, it is possible to detect atrial thrombus or a thrombosed ventricular aneurysm. The image in **Figure 94.2** illustrates a case of global cardiac failure with markedly dilated atria (✱✱) and incidental thoracic vertebral degenerative osteophytes(➡).

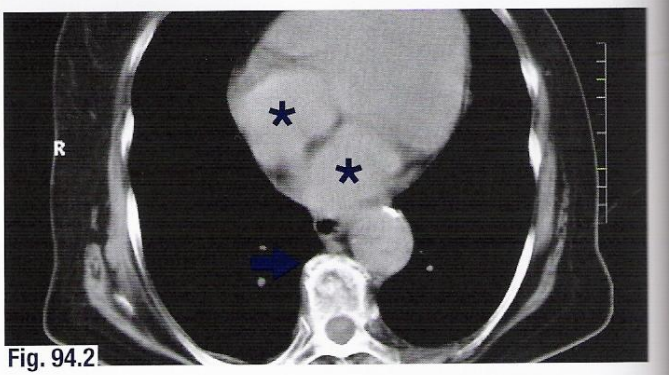

Fig. 94.2

Pericardial effusions may occur with viral infections, uremia, the collagen vascular diseases, a heart attack, or tuberculosis, among other causes. A pericardial effusion **(8)** appears as a broad rim of low-density fluid (between 10 and 40 HU) surrounding the heart **(Fig. 94.3)**. Only fresh blood would have a higher level of density. Massive effusions as seen in **Figure 94.3** not only compress the adjacent lungs **(178)**, but also compromise heart function.

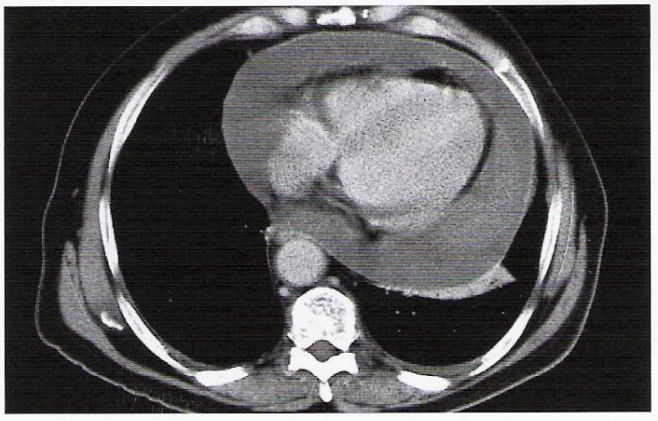

Fig. 94.3a

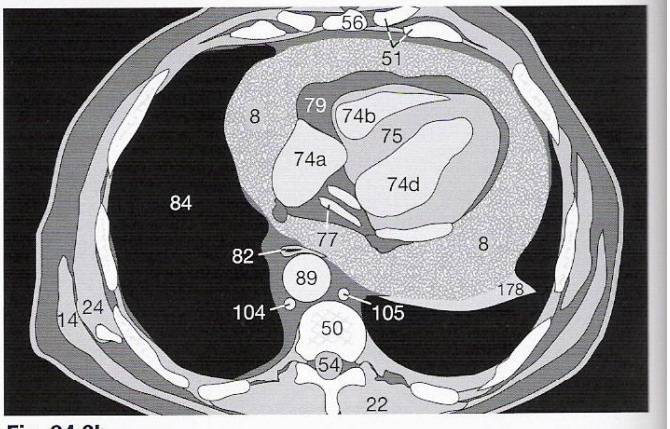

Fig. 94.3b

Effusions may lead to pericardial fibrosis or calcification (↘ ↙), which in turn causes constrictive pericarditis **(Fig. 94.4)**. Note that in such cases the vena cava, the azygos vein, or even the atria may be markedly dilated as a sign of cardiac insufficiency.

Atherosclerosis of the coronary arteries causes calcification that is well demonstrated by thin, hyperdense lines in the epicardial fat. At present, however, a complete assessment of the degree of stenosis requires angiography.

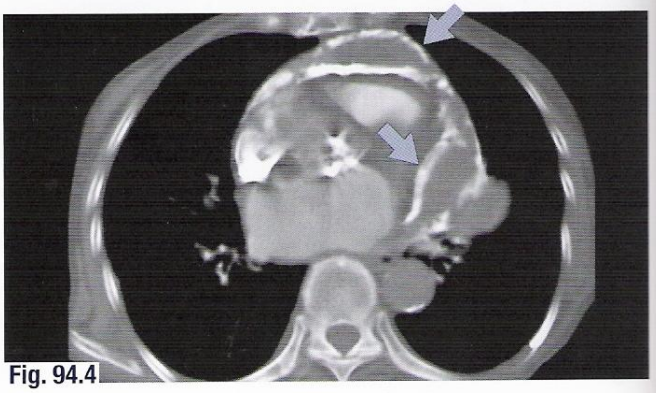

Fig. 94.4

Focal Intrapulmonary Lesions

When multiple lung metastases are far advanced, the lesions can even be recognized in the topogram **(Fig. 95.1a)**. Depending upon the age and vascularization of the metastases, they appear as spherical nodules of varying sizes **(Fig. 95.1b)**. The more irregular the contours of the lesions (for example, stellate or spiculated), the more likely they are to be malignant. If, however, they are solitary and have central calcification (like a popcorn), or peripheral calcification, the lesions are most likely to be a benign hamartoma or granuloma.

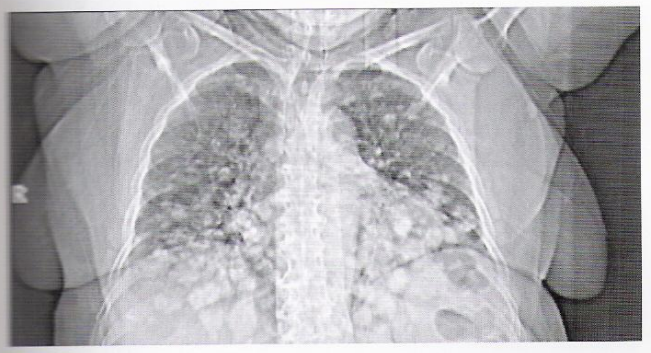

Fig. 95.1a

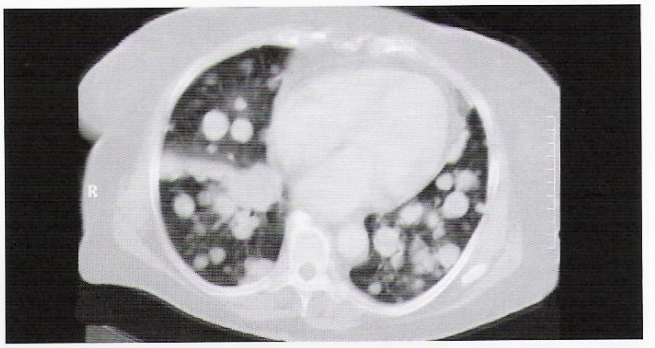

Fig. 95.1b

Pulmonary metastases are not visible in conventional x-rays unless they are larger than 5 or 6 mm in diameter. In CT images, however, they can be detected at 1 to 2 mm in diameter. If metastases are located in the periphery, it is easy to differentiate them from blood vessels cut in cross-section. Small metastases located close to the hilum are much more difficult to distinguish from vessels. In such cases, the detailed analysis of high-resolution scans (HRCT) may be the best method.

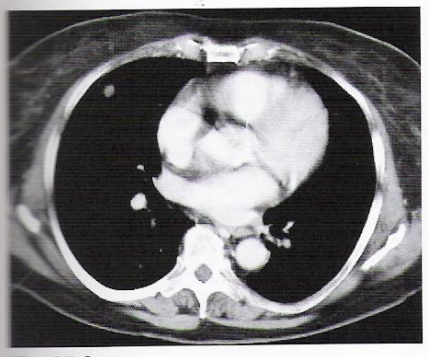

Fig. 95.2a

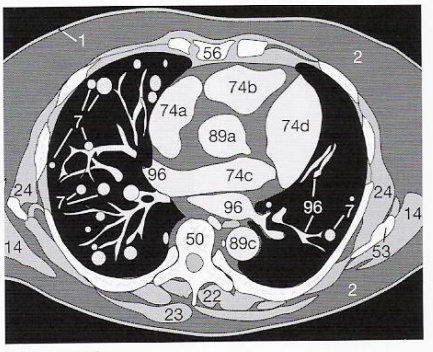

Fig. 95.2b

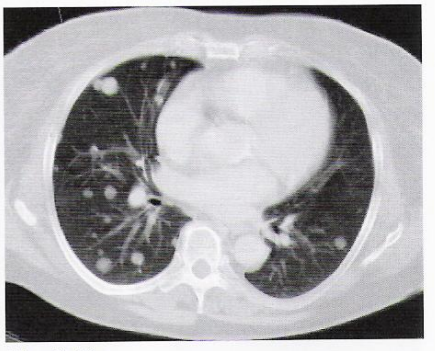

Fig. 95.2c

The correct choice of image display (window) is essential: Small focal lesions **(7)** of the lung **(84)** do not appear on soft-tissue windows **(Fig. 95.2a)** or may be mistaken for normal vessels **(96)**. Lung windows **(Fig. 95.2c)** should always be used for examining lung parenchyma. In the case below **(Fig. 95.3a)**, the multiple small metastases **(7)** close to the pleura would have been overlooked if lung windows had not been used **(Fig. 95.3c)**. These examples demonstrate the importance of viewing each image on long and soft-tissue windows.

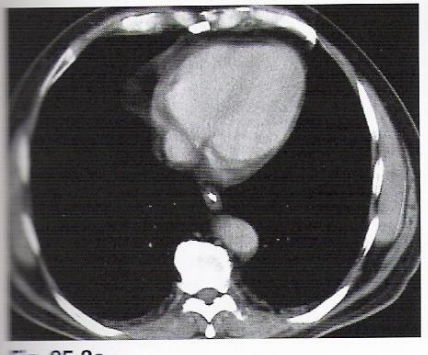

Fig. 95.3a

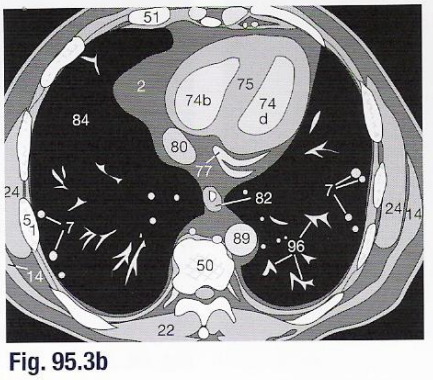

Fig. 95.3b

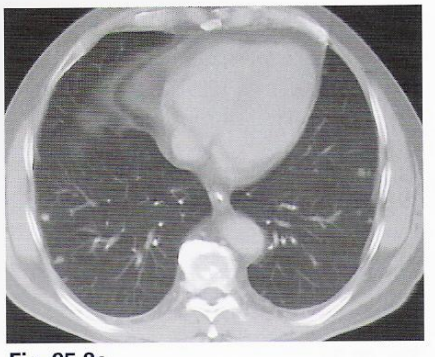

Fig. 95.3c

As a result of changes in the behavior of smokers, the incidence of bronchial carcinomas (BC), especially among women and young people, has increased. In addition to the histologic diagnosis and grading of carcinoma, the location of the lesion is an important prognostic factor: a BC of considerable size **(7)** in the periphery of the lung **(Fig. 96.1)** will almost certainly be visible on a conventional chest x-ray. More advanced BCs located centrally are usually not operable and may obstruct the bronchial lumen, resulting in distal collapse **(178)**. **Figure 96.2** illustrates an advanced case in which the tumor has areas of central necrosis **(181)** and the lung is surrounded by a pleural effusion **(8)**.

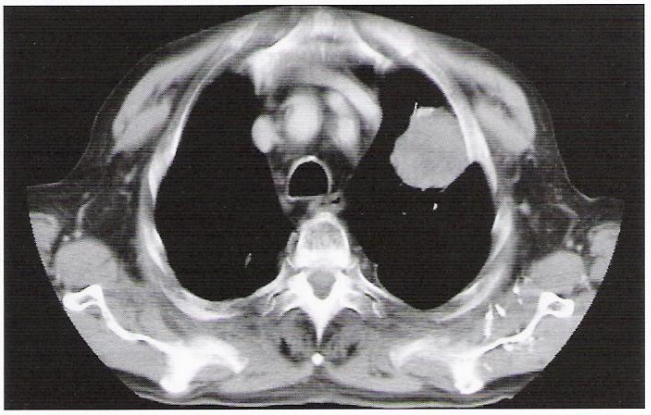

Fig. 96.1a

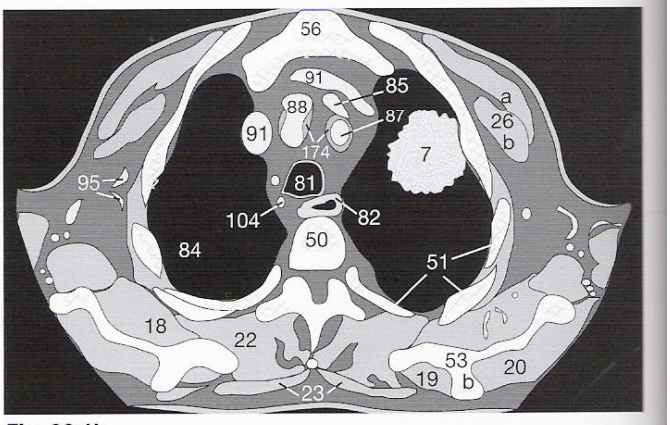

Fig. 96.1b

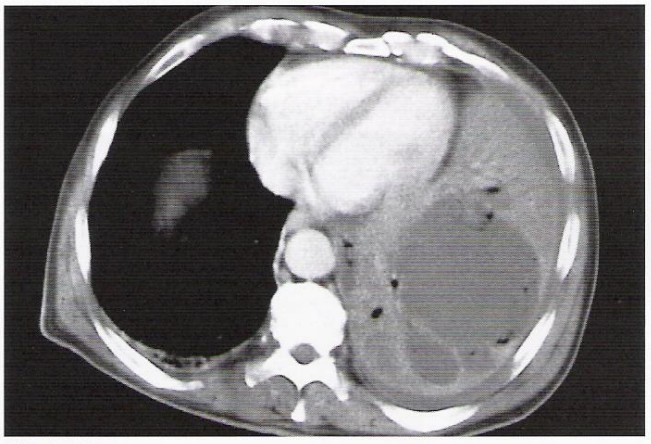

Fig. 96.2a

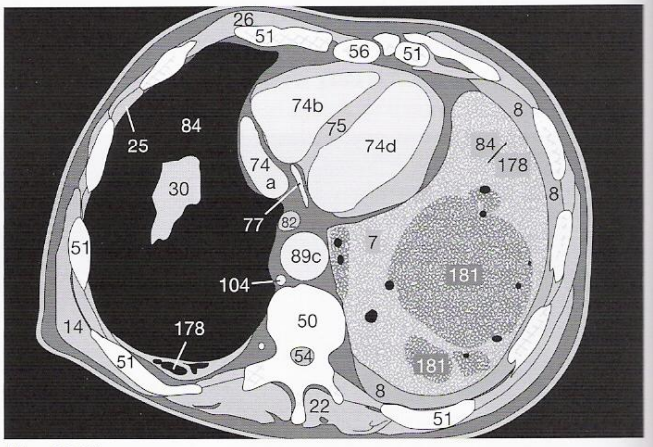

Fig. 96.2b

Lymphangitis carcinomatosa (**7** in **Fig. 96.3**) spreads from the hilum or the visceral pleura into the interstitial tissue of the lung by way of the lymphatic vessels. Obstruction of these vessels by cancer cells leads to lymphatic congestion **(185)**. At first, the upper lobes remain clear, but as the disease progresses these also become infiltrated. The larger lymphatics and LNs gradually become infiltrated by metastatic disease.

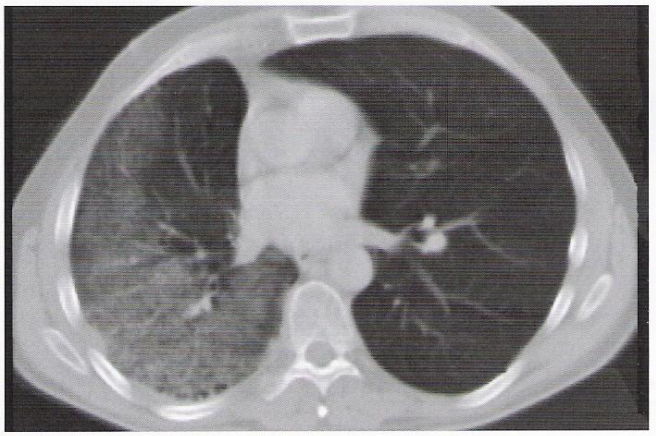

Fig. 96.3a

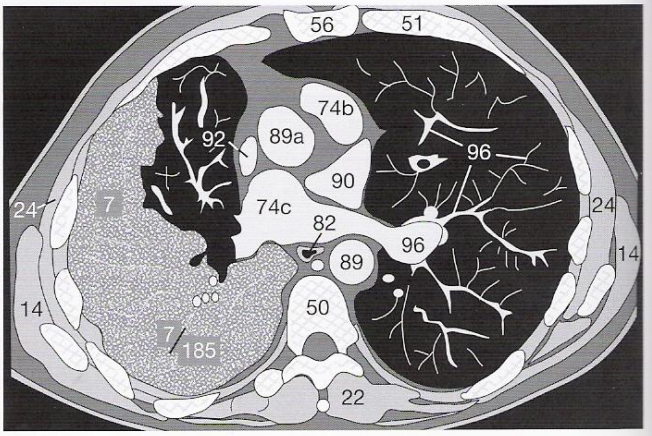

Fig. 96.3b

Sarcoidosis

The changes of sarcoidosis (Boeck's disease) must be differentiated from multiple metastases in the lung: epithelial granulomas usually infiltrate the hilar lymph nodes **(6)** bilaterally **(Fig. 97.1)** and then spread within the perivascular tissue and along the lymphatics into the periphery of the lung. Multiple small pulmonary nodules and various degrees of interstitial fibrosis may be present. Large granulomas **(7)**, as seen in **Figure 97.2**, may resemble intrapulmonary metastases.

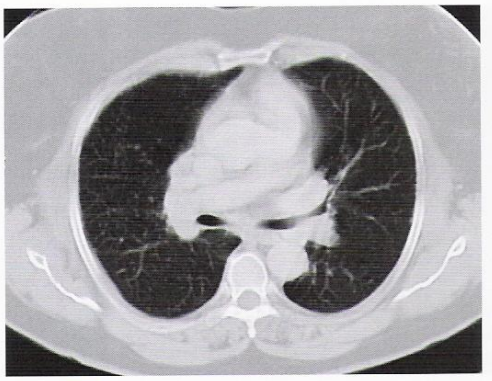

Fig. 97.1a

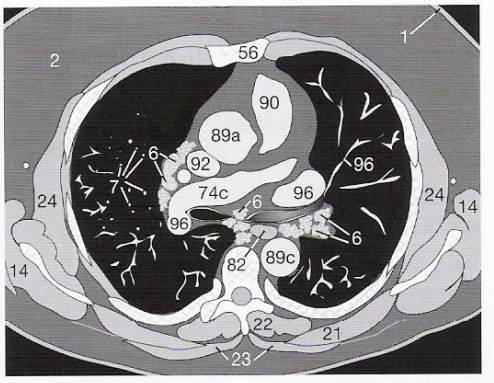

Fig. 97.1b

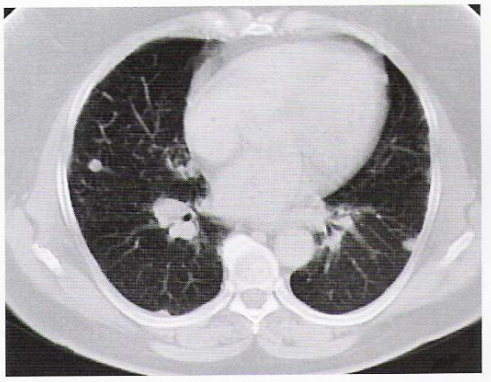

Fig. 97.2a

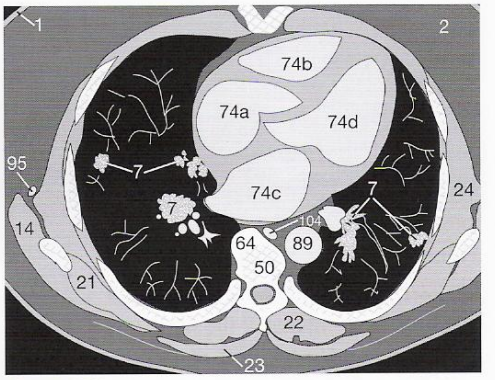

Fig. 97.2b

Tuberculosis

If a larger mass cavitates **(181)**, the DD will include, for example, a bronchial carcinoma with central necrosis or cavitary tuberculosis. **Figure 97.3** illustrates the latter in an atypical location in an HIV+, immune-compromised patient. Note also the emphysematous changes in the tissue at the periphery of the lesion **(176)**.

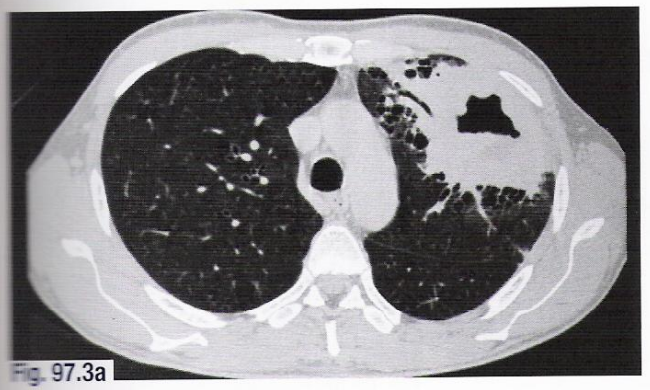

Fig. 97.3a

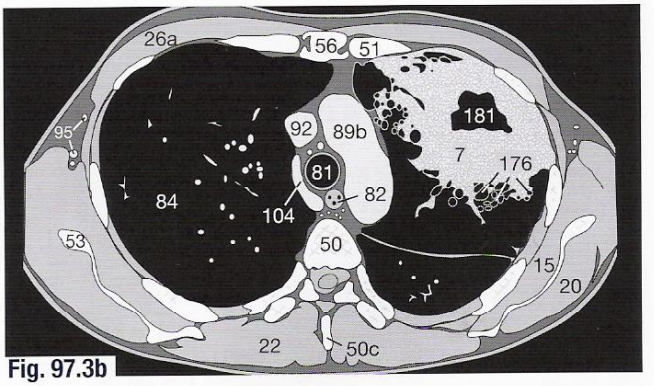

Fig. 97.3b

Aspergillus

Superinfection with Aspergillus may occur within a pre-existing cavity in immune-compromised patients. The spores of A. fumigatus are common in plant material and soil. Often the cavity is not completely filled with the aspergillus ball so that a small crescent of air can be recognized (↘ in **Fig. 97.4**). Aspergillosis may also lead to allergic bronchial asthma or provoke exogenous allergic alveolitis.

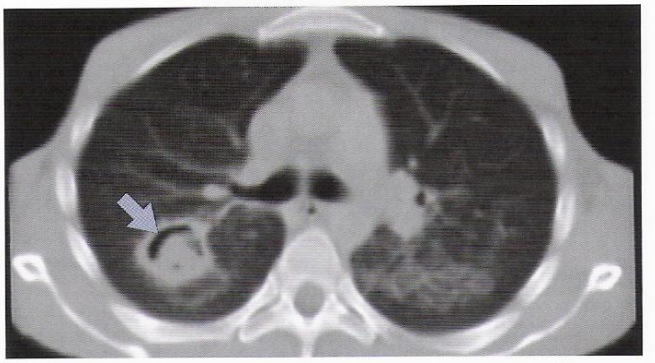

Fig. 97.4

Pleura

Massive pleural effusions **(8)**, as seen in the case illustrated in **Figure 98.1**, compress the lung **(84)** and may cause large areas of atelectasis **(178)** affecting individual segments or even an entire lobe. Effusions appear as collections of homogeneous fluid of near-water density within the pleural spaces. Effusions usually accompany infections, lung congestion due to right heart failure, as well as venous congestion due to mesothelioma and peripheral bronchial carcinoma.

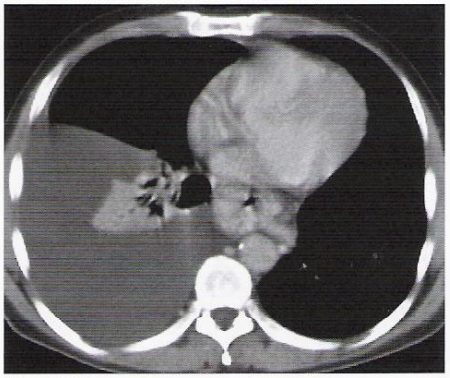

Fig. 98.1a

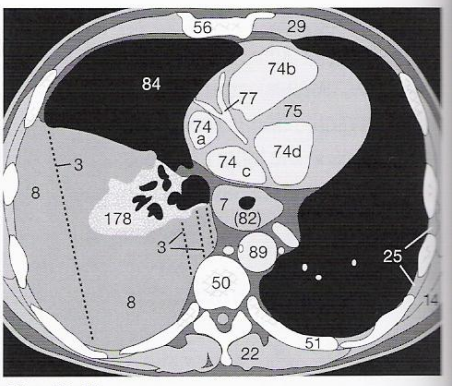

Fig. 98.1b

Pleural drainage by the insertion of a catheter **(182)** is indicated if atelectasis **(178)** affects large portions of the lung **(Fig. 98.2)**. In the case shown in **Figure 98.2**, the drainage tube was blocked by fibrin-rich fluid. The lung can only be re-inflated if the fibrin clot is cleared or the catheter is replaced.

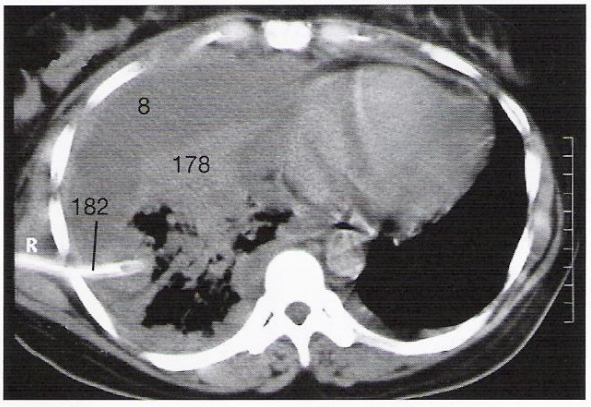

Fig. 98.2

Foreign bodies are rarely found in the pleural spaces (**166** in **Fig. 98.3**), but must be considered after thoracotomy (chest surgery). Images on lung windows **(Fig. 98.3c)** clearly show the inflammation and collapse **(178)** surrounding a lost swab.

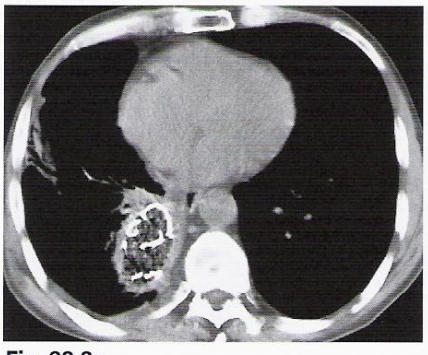

Fig. 98.3a

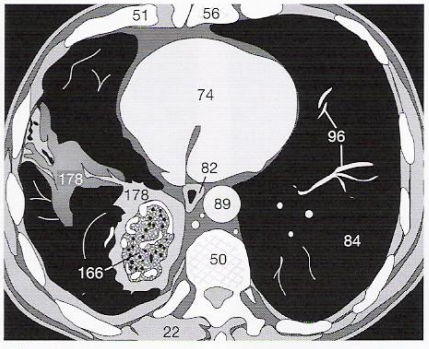

Fig. 98.3b

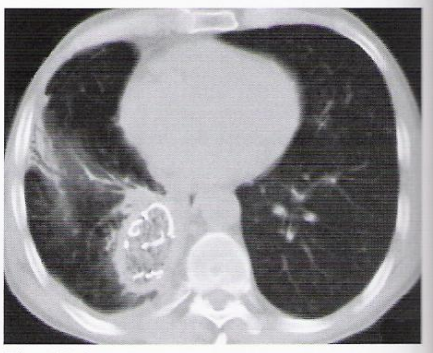

Fig. 98.3c

Asbestos-Related Lung Disease

Asbestos-related lung disease has a fine reticulonodular pattern of increased densities scattered throughout the lung tissue, especially at interlobular septa (↑ and ↗ in **Fig. 98.4**). Typical pathologic features in the pleura are thickening and plaques (**186** in **Fig. 98.4**). Fibrosis and scar emphysema appear in later stages of the disease. The spindle-shaped or more triangular areas of increased attenuation are often difficult to distinguish from those characteristic of bronchial carcinomas.

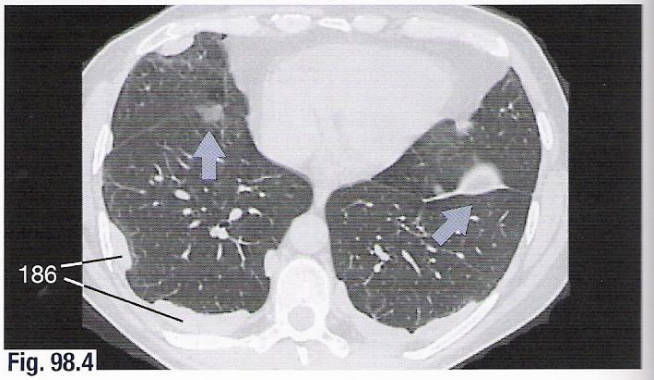

Fig. 98.4

Silicosis

Multiple, well-defined nodules appear in the interstitial connective tissue in response to phagocytosed particles of silica. The upper lobes of the lung are most commonly affected. Signs of fibrosis, which may progress to a honeycomb pattern, can best – and at earlier stages – be detected with HRCT (using 2-mm rather than 10-mm slice thickness; **Fig. 99.1**). The finer, smaller nodules can be found scattered throughout the lung; larger opacities, which may cavitate, are located within areas of denser fibrosis (in **Fig. 99.2**). Enlarged mediastinal or hilar lymph nodes **(Fig. 99.3)** often develop an eggshell pattern of calcification. As the disease progresses, fibrosis and scar emphysema increase (in **Fig. 99.1**).

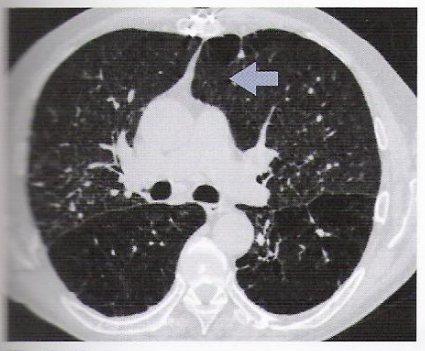

Fig. 99.1

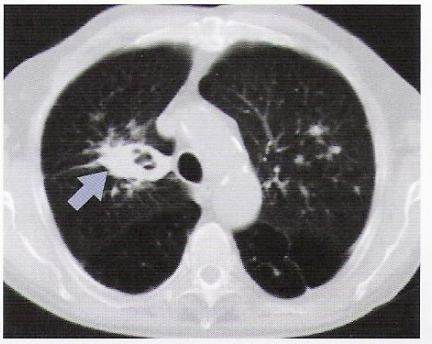

Fig. 99.2

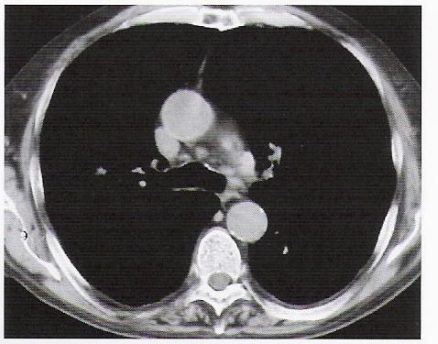

Fig. 99.3

Emphysema

Progressive emphysema with accompanying bullae (**176** in **Fig. 99.4b**) or bronchiectasis with associated inflammatory infiltrates (**178** in **Fig. 99.5**) are not visible on soft-tissue window images in the early stages. These infiltrates are more easily seen and detected sooner on thin section images using lung windows [25–27].

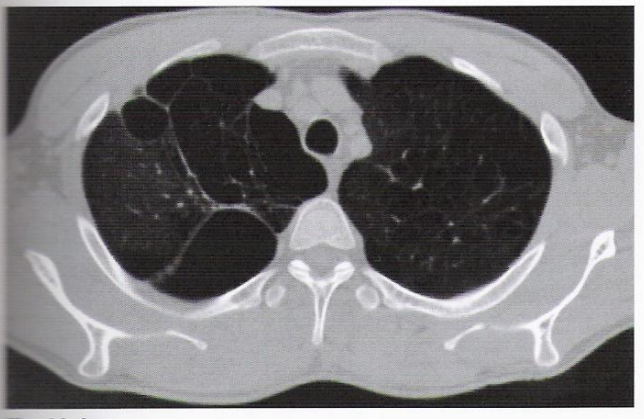

Fig. 99.4a

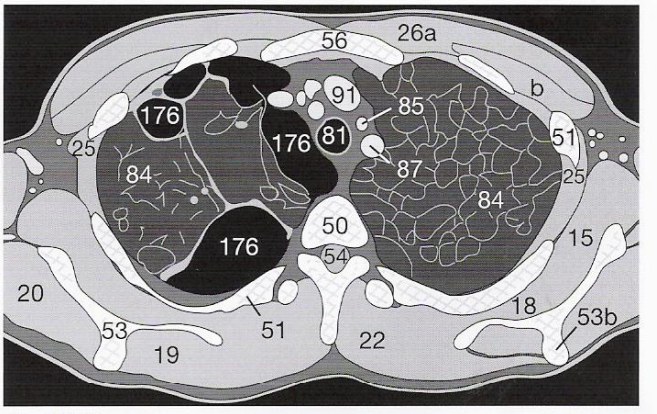

Fig. 99.4b

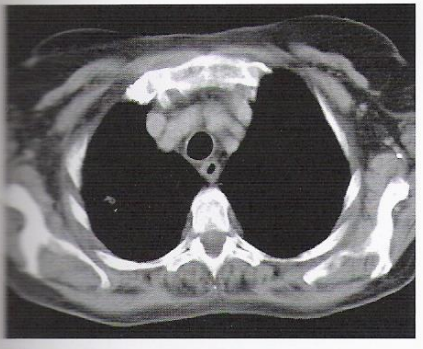

Fig. 99.5a

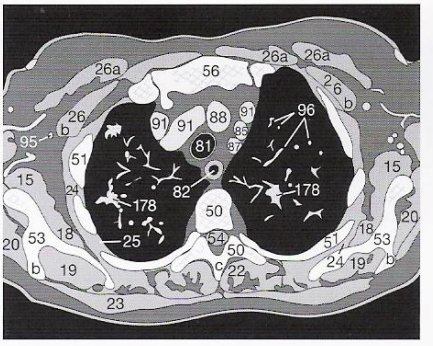

Fig. 99.5b

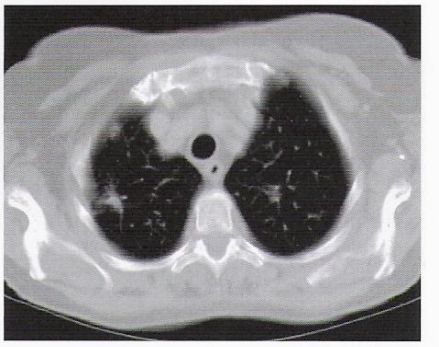

Fig. 99.5c

The pathogenesis of interstitial fibrosis of the lung **(Fig. 100.1)** cannot always be established and is referred to as idiopathic pulmonary fibrosis. This is particularly true when it affects middle-aged women. The pattern of fibrosis resembles that illustrated on the previous pages with the exception that emphysematous changes typically begin in subpleural regions. Fibrosis of the lung can accompany any of the collagen vascular diseases in the advanced stages and lead to similar morphologic changes, for example in scleroderma **(Fig. 100.2)** or polyarteritis nodosa **(Fig. 100.3)**.

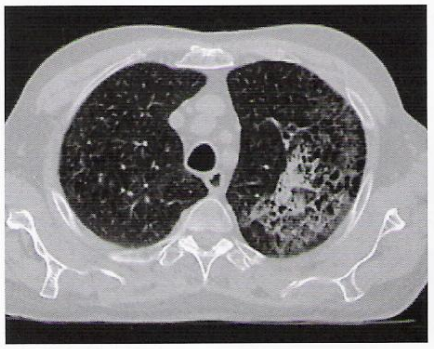

Fig. 100.1

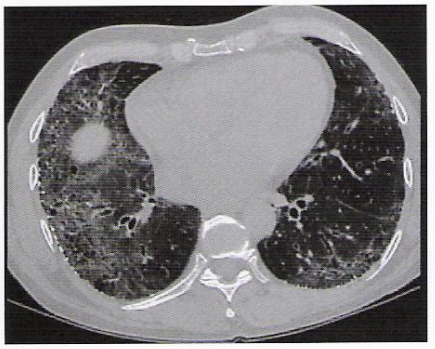

Fig. 100.2

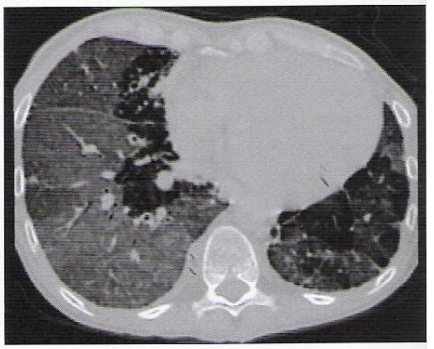

Fig. 100.3

Test Yourself!

You should try to answer all the questions on this and the following page before turning to the back of the book for the answers so as not to spoil the fun of tackling each one.

Exercise 20:
Do you recognize any abnormalities in **Figure 100.4** or is it a scan of normal anatomy? Discuss your DD.

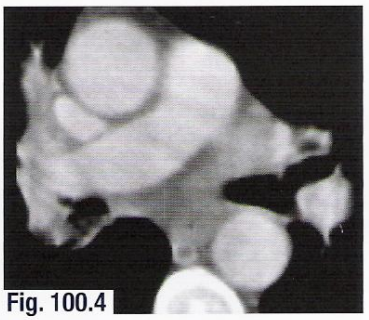

Fig. 100.4

Exercise 21:
How would you interpret the dense area in the left lung in **Figure 100.5**? Discuss your DD and make a list of additional information that you need and the steps necessary in order to be certain about the lesion.

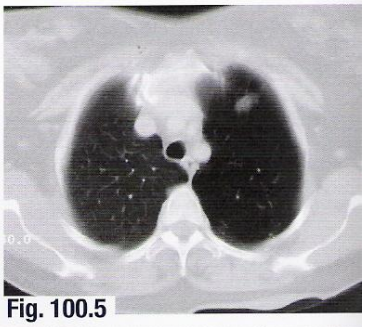

Fig. 100.5

Exercise 22:
A 62-year-old patient presented with intense back pain and was examined by CT. What is your diagnosis of the changes seen in **Figure 100.6**? Can you classify the type of change and the degree of severity?

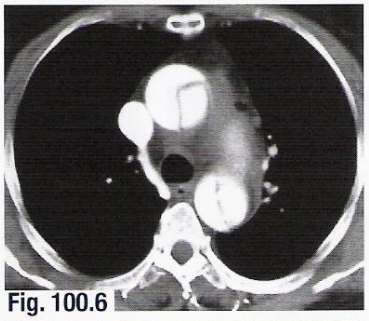

Fig. 100.6

Exercise 23: Describe in detail the pathologic changes visible in **Figure 100.7** and the steps in your DD.

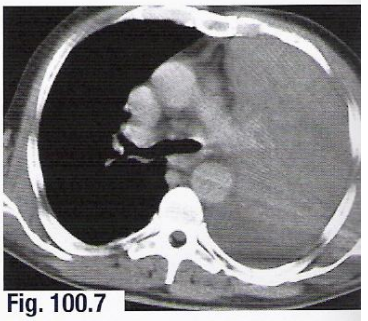

Fig. 100.7

Exercise 24:

What further diagnostic procedures would you recommend for the case illustrated in **Figure 101.1**? What do you suspect the lesion to be? What other changes do you recognize?

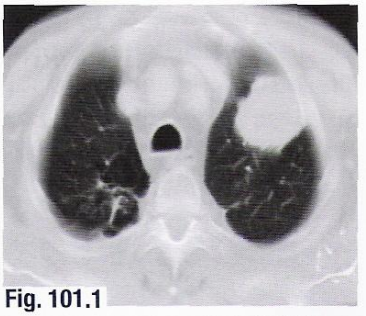

Fig. 101.1

Exercise 25:

Detecting even minute changes may be decisive in order to arrive at the correct diagnosis. What do you see in **Figure 101.2**?

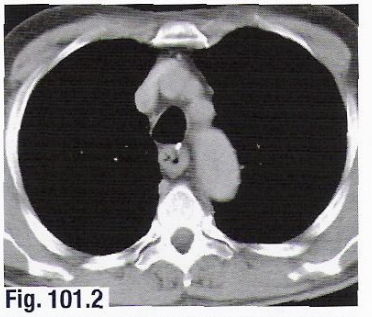

Fig. 101.2

Exercise 26:

A patient in her 26th week of pregnancy complained of shortness of breath. Her physician initially thought it was because of a high diaphragm. Two weeks later she was examined by CT. Make careful note of all abnormal changes you see in **Figure 101.3** and the steps in your DD.

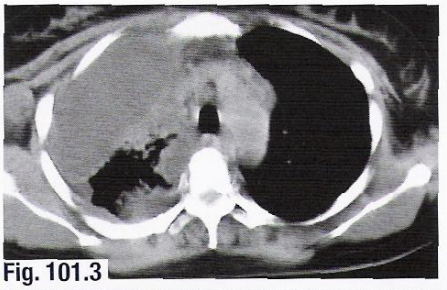

Fig. 101.3

Exercise 27:

A 56-year-old woman with a history of smoking presented with unintended weight loss and severe attacks of coughing which had already lasted for 3 months. She had no previous illnesses. Does **Figure 101.4** illustrate normal anatomy, a normal variant, or an abnormality?

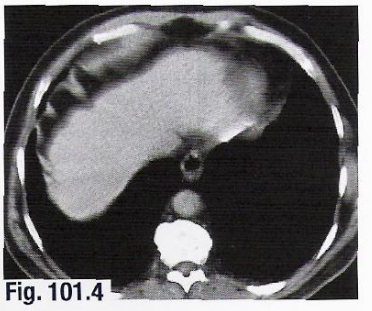

Fig. 101.4

Exercise 28: Do **Figures 101.5a** and **101.5b** illustrate normal anatomy, an anomaly, or a lymphoma? Discuss your opinion.

Fig. 101.5a

Fig. 101.5b

In general, all soft-tissue organs should appear uniform and be well defined, except when partial volume effects occur (cf. p.14) or during the early arterial phase of CM enhancement in a helical scan (cf. pp.120 and 126). Structures such as blood vessels and bowel loops should be clearly defined in intra-abdominal fat. The same applies to the fat in muscles.

Poorly defined connective-tissue spaces may indicate edema or an inflammatory or malignant infiltration. If the anatomy cannot be clearly resolved, additional information can be gained by measuring the density of specific areas or by comparing unenhanced with CM-enhanced scans (cf. pp. 15 and 121).

Again, the proposed checklist is not intended to be "prescriptive", but to give an useful tool for the novice in order to reduce the number of missed pathological findings.

Selection of Image Plane

The sections of the abdomen are also acquired transversally (=axially). If the table advance is set at 8 mm with a slice thickness of 10 mm, there will be an overlap of 1 mm on each side of the section. In recent years, there is a trend towards thinner slices with a slice thickness between 5 and 8 mm.

The small topograms on the following pages (based on **Fig. 103.1**) clearly show the slice positions as related to the anatomy of major structures for each series of images.

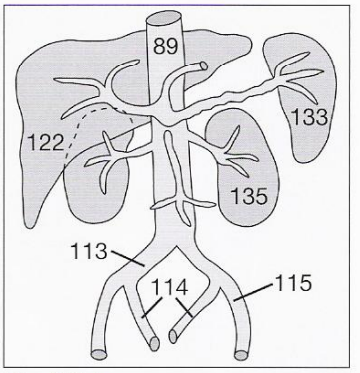

Fig. 103.1

Systematic Sequence for Readings

Analogous to interpreting chest CTs, we suggest you begin with the tissues of the abdominal wall. Considerable time is saved if you consistently look at them from cranial to caudal. For beginners a systematic inspection of each organ or system from cranial to caudal is recommended, so that you do not need to concentrate on too many structures at once. The proposed procedure encompasses two or three passages through the images. As you become experienced, you may wish to devise your own method. Experienced readers are more easily able to detect all pathologic changes in one passage from cranial to caudal.

It is sensible to evaluate internal organs that lie in the same transverse plane. The uniformity of the parenchyma, the size and the smooth surface of liver and spleen should be checked together. The same is true for the assessment of the pancreas and the adrenal glands: they also lie at the same level (cf. pp. 105/106). If the entire urinary system is to be examined, it saves time to inspect the reproductive organs and bladder in the lesser pelvis before looking at the cranial parts of the GIT, or the regional lymph nodes and the retroperitoneal vessels (see checklist on the right).

Finally, the presence of sclerotic and lytic bone lesions and the state of the spinal canal should be checked (cf. p.155).

Checklist for Abdominal Readings

Abdominal wall:	(especially periumbilical and inguinal regions) hernias, enlarged lymph nodes?
Liver and spleen:	homogeneous parenchyma without focal lesions? well-defined surfaces?
Gallbladder:	well-defined, thin wall? calculi?
Pancreas, adrenals:	well-defined, size normal?
Kidneys, ureter, and bladder	symmetric excretion of CM? obstruction, atrophy, bladder wall smooth and thin?
Reproductive organs:	uniform prostate of normal size? spermatic cord, uterus, and ovaries?
GIT:	well defined? normal thickness of walls? stenoses or dilations?
Retroperitoneum:	vessels: aneurysms? thromboses? enlarged lymph nodes? mesenteric (normally < 10 mm) retrocrural (normally < 7 mm) para-aortic (normally < 7 mm) parailiacal (normally < 12 mm) parainguinal (normally < 18 mm)
Bone window:	lumbar spine and pelvis: degenerative lesions? fractures? focal sclerotic or lytic lesions? spinal stenoses?

The images of the abdominal organs include the costodiaphragmatic recesses of the lungs **(84)**, which extend quite far caudally, laterally, and dorsally. Liver **(122)** and spleen **(133)** parenchyma usually appear homogeneous without focal lesions in the venous phase of CM enhancement: branches of the portal vein **(102)** and the falciform ligament **(124)** can be distinguished. In order to assess the gastric wall **(129a)**, the stomach **(129)** can be filled with water, which acts as a low-density CM, after an i.v. injection of Buscopan. The diaphragm **(30)** between the thoracic and abdominal cavities has an attenuation similar to the parenchyma of the liver and spleen and can therefore not be differentiated from these organs if its thin dome is sectioned obliquely.

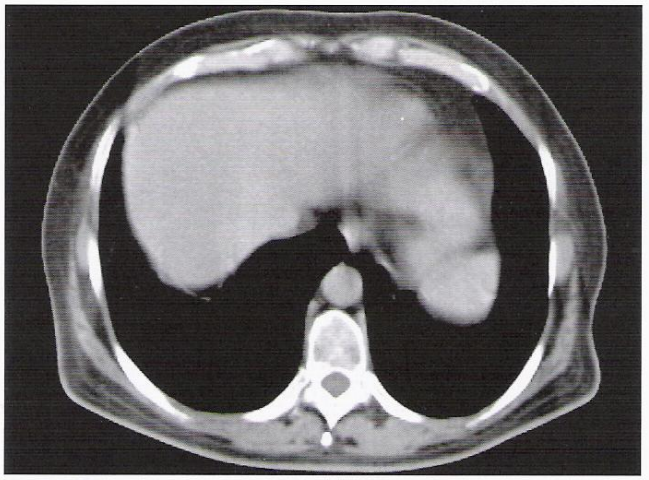

Fig. 104.1a

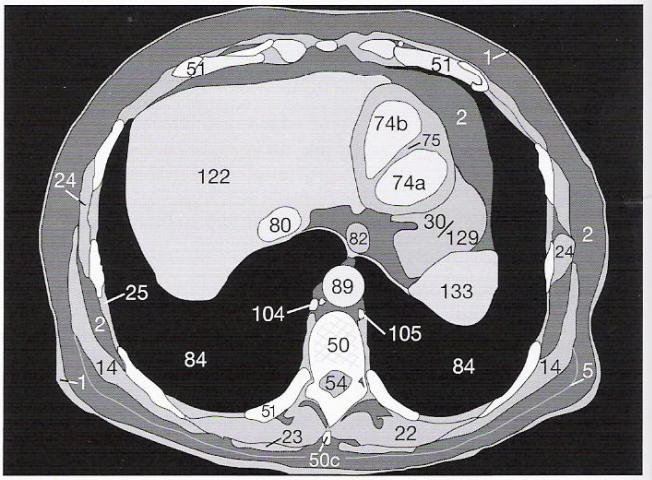

Fig. 104.1b

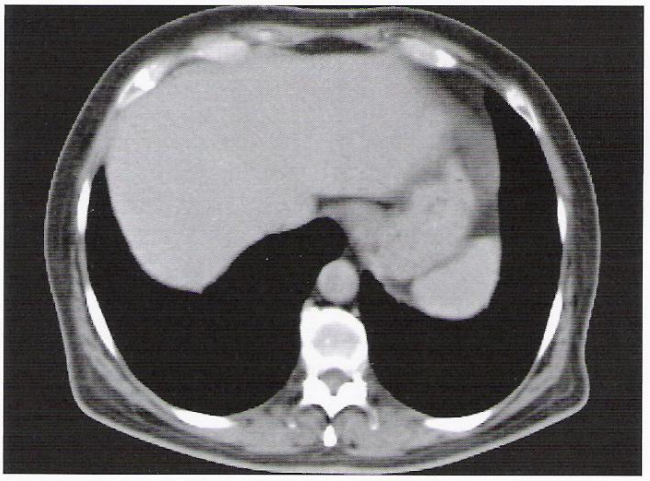

Fig. 104.2a

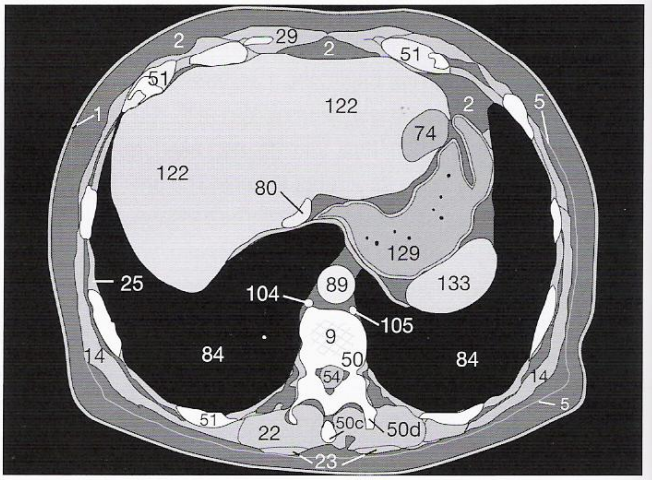

Fig. 104.2b

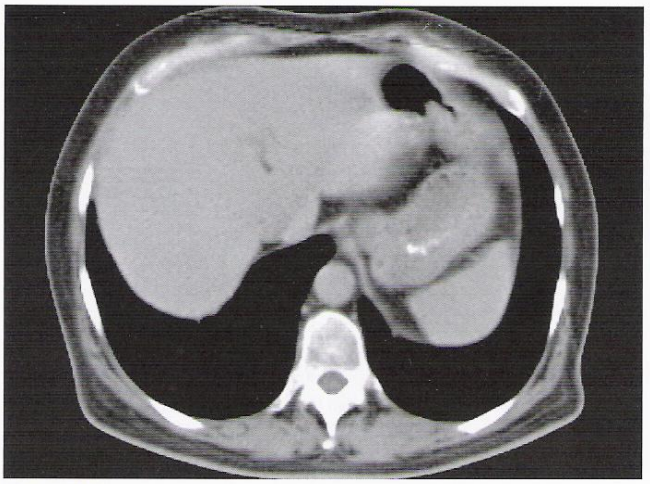

Fig. 104.3a

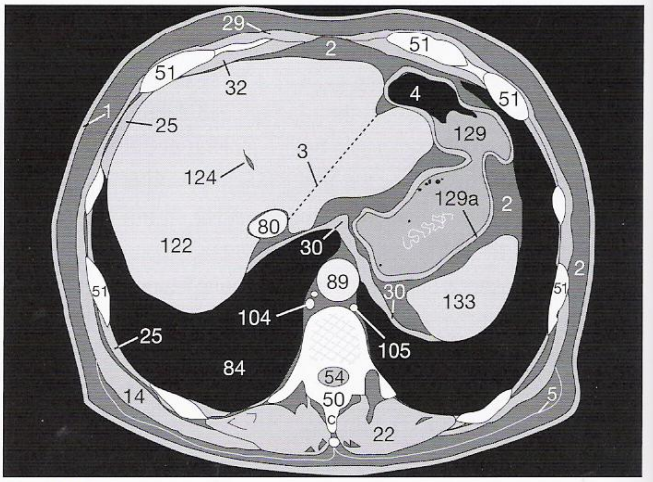

Fig. 104.3b

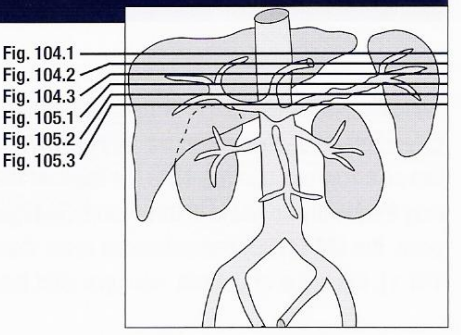

The right adrenal gland usually lies cranial to the upper pole of the kidney **(135)**, whereas the left adrenal gland lies ventral to the upper pole of the kidney. Consequently, the two adrenal glands **(134)** are seen on the same sections. Note the position of the diaphragm **(30)** between the lung **(84)** and the inferior vena cava **(80)**. The vessels on the lesser curvature of the stomach **(109)** and the gastric walls **(129a)** are usually well defined and clearly demarcated in the surrounding fat and connective tissue **(2)**.

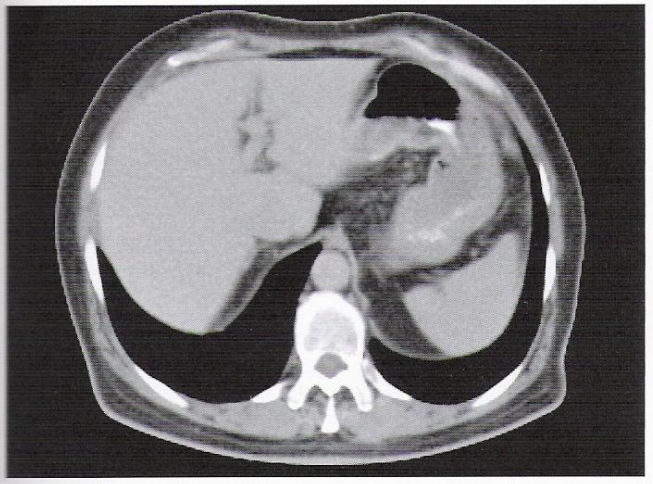

Fig. 105.1a

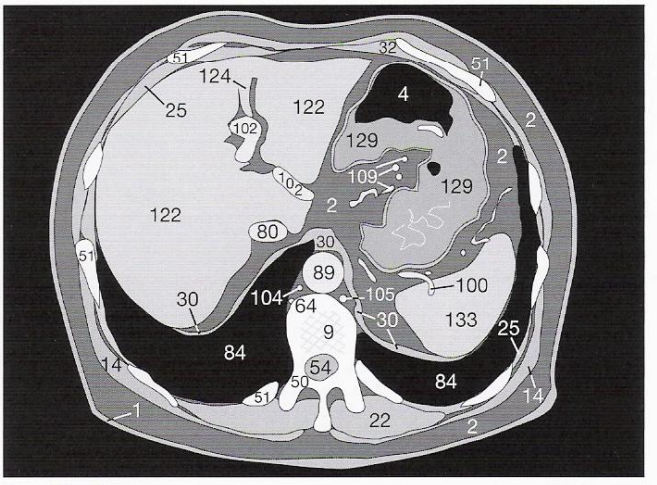

Fig. 105.1b

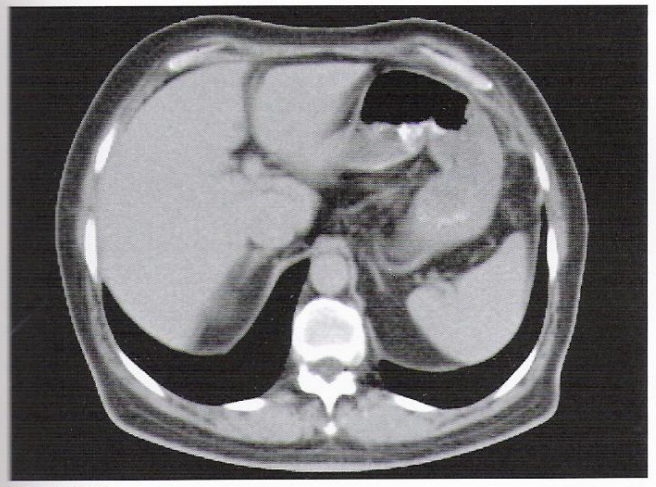

Fig. 105.2a

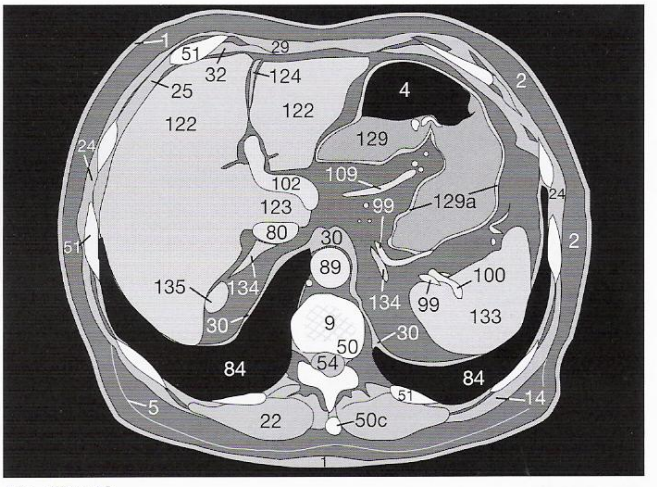

Fig. 105.2b

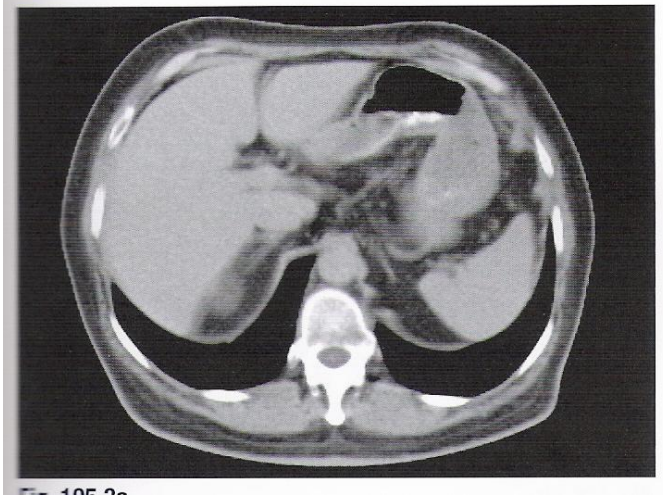

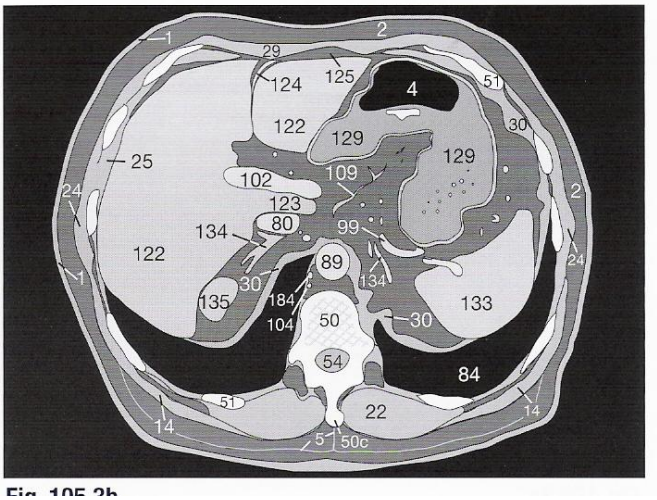

Typically the pancreas **(131)** has well-defined parenchyma with an irregular outline. The head and uncinate process of the pancreas extend quite far caudally (down to **Fig. 107.2**). The left adrenal gland **(134)** is often Y-shaped, whereas the right adrenal gland may look like an arrow or a comma. Note the origin of the celiac trunk **(97)** and the SMA **(106)** from the abdominal aorta **(89)**. Enlarged lymph nodes may frequently be found in this vicinity. In **Figure 106.3**, the contrast-enhancing effect of an arterial bolus of CM becomes evident. At this point, the SMA **(106)** has enhanced more than the accompanying vein **(107)**, which does not contain any CM yet. Within moments **(Fig. 107.1)**, the bolus of CM has also opacified the superior mesenteric vein **(107)**.

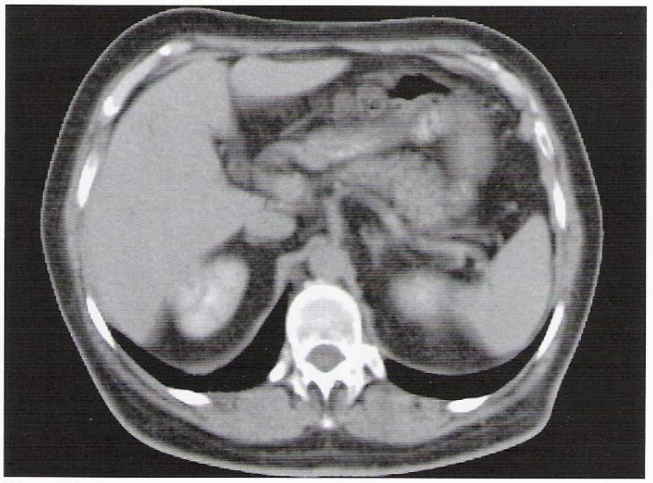

Fig. 106.1a

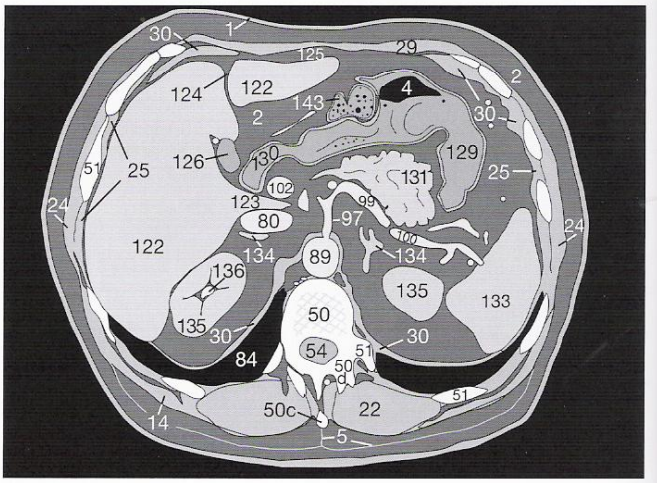

Fig. 106.1b

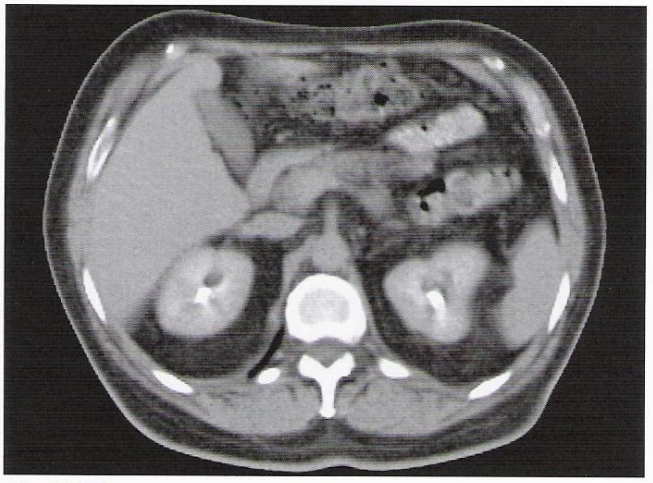

Fig. 106.2a

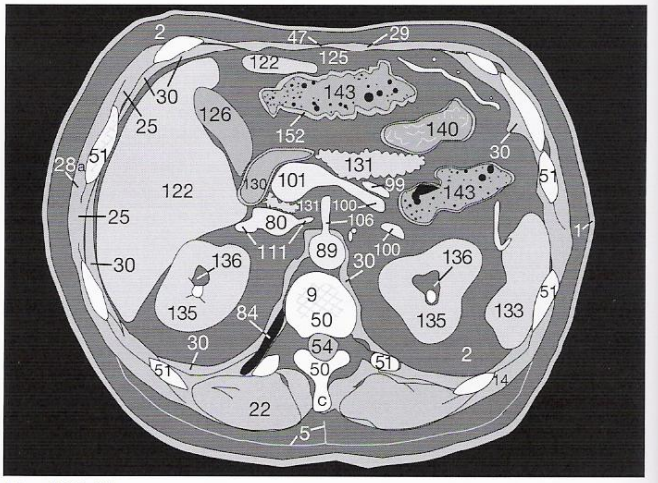

Fig. 106.2b

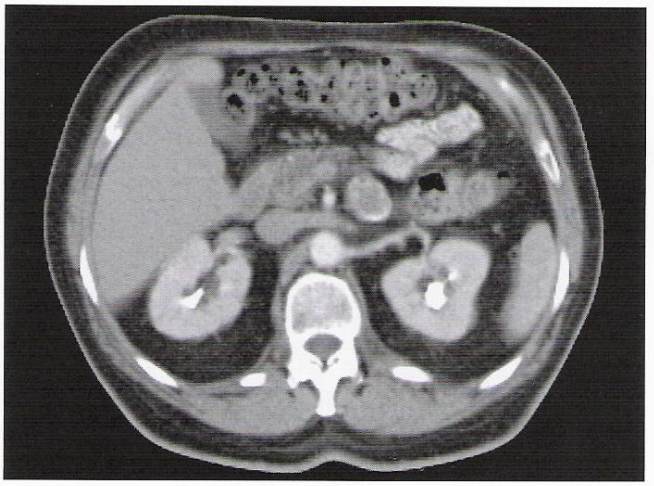

Fig. 106.3a

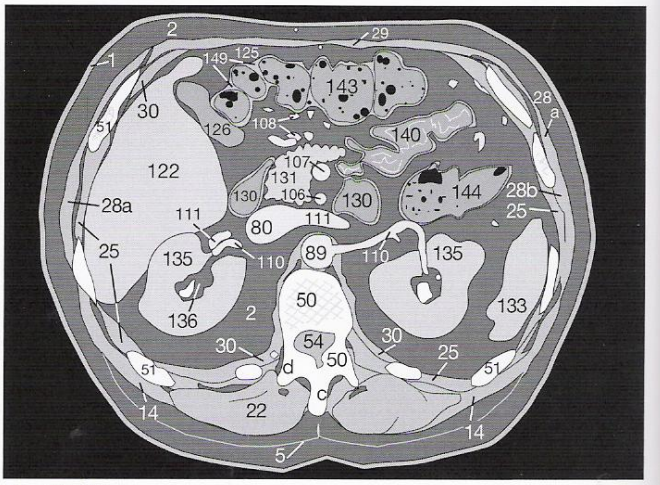

Fig. 106.3b

Look for arterial calcifications in the origins of the renal arteries **(110)** at the level of the renal veins **(111)**. The left renal vein does not always pass between the aorta **(89)** and the SMA **(106)** to the inferior vena cava **(80)**, as it does in **Figure 107.1**. Anatomic variations are not unusual (cf. p.116). Benign cysts **(169)** frequently occur in the renal pelvis **(136)** next to the ureter **(137)** or in the renal parenchyma **(135) (Figs. 107.2 and 107.3)**. Such cysts do not enhance after CM injection (cf. p.133).

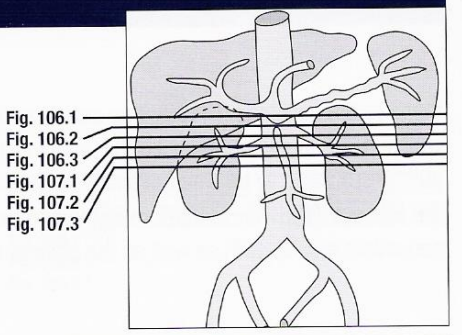

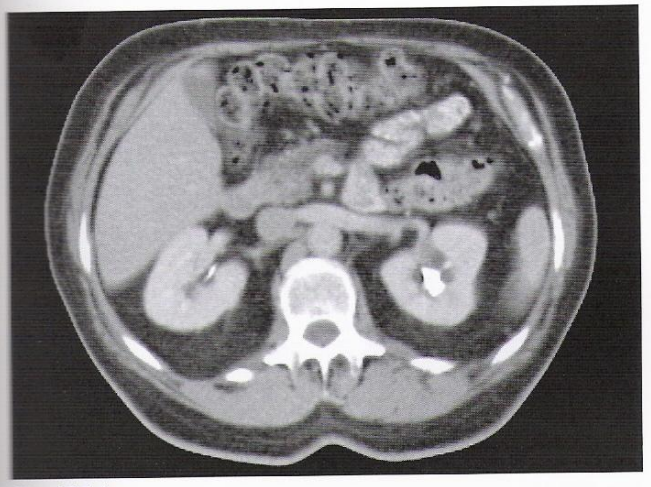

Fig. 107.1a

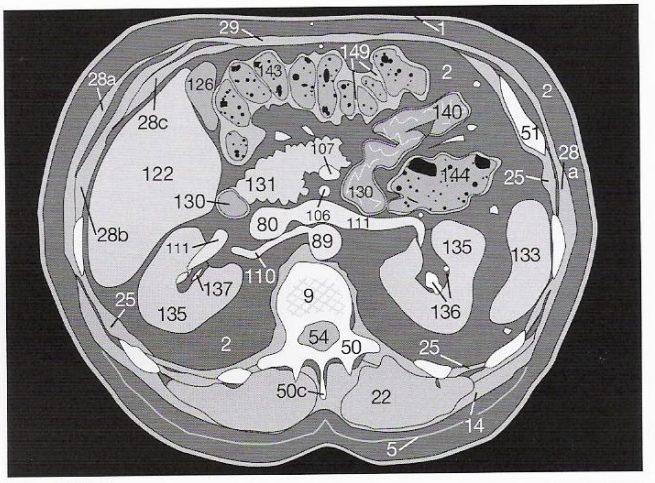

Fig. 107.1b

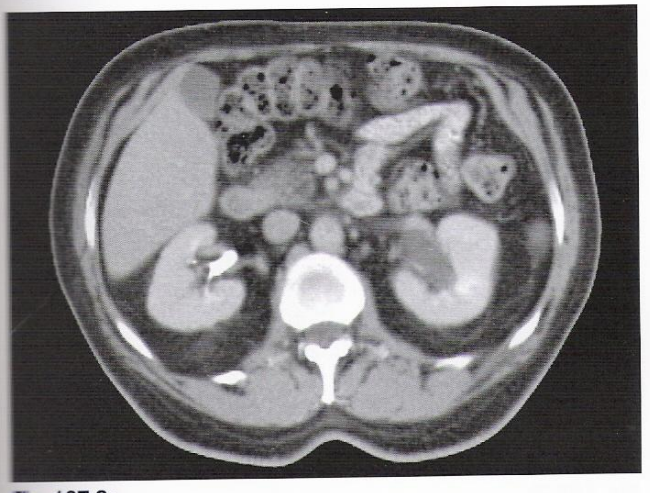

Fig. 107.2a

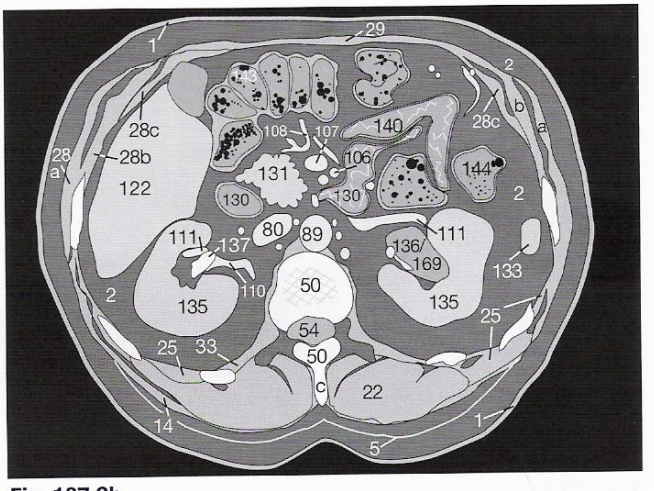

Fig. 107.2b

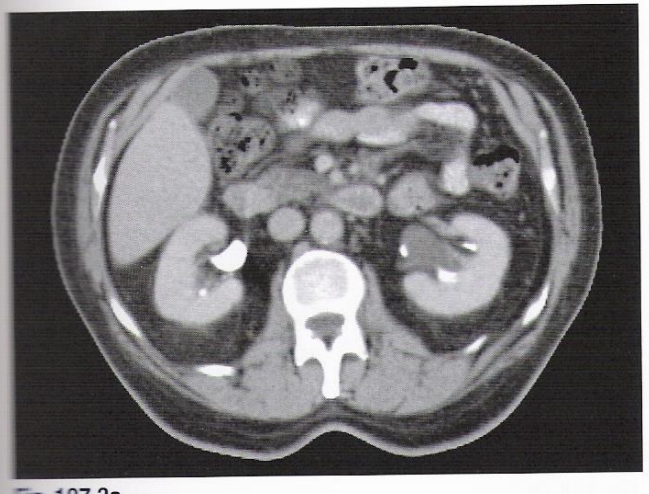

Fig. 107.3a

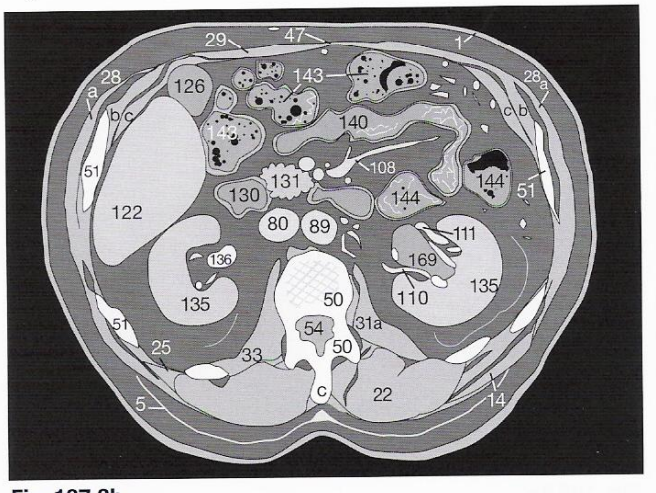

Fig. 107.3b

Close to the gallbladder **(126)**, you can sometimes see partial volume effects **(Fig. 108.1)** of the adjacent colon **(143/144)**, the walls of which **(152)** should normally be thin and well defined in contrast to the root of the small bowel mesentery (as in **Fig. 108.3**). The duodenum **(130)** can only be distinguished from the other intestinal loops **(140)** on the basis of its position. At this level, you should also check the kidneys **(135)** for smooth margins and possible parenchymal scarring. The presence of fat makes it easier to identify the rectus abdominis muscle **(29)** as well as the oblique muscles of the abdominal wall **(28a–c)**.

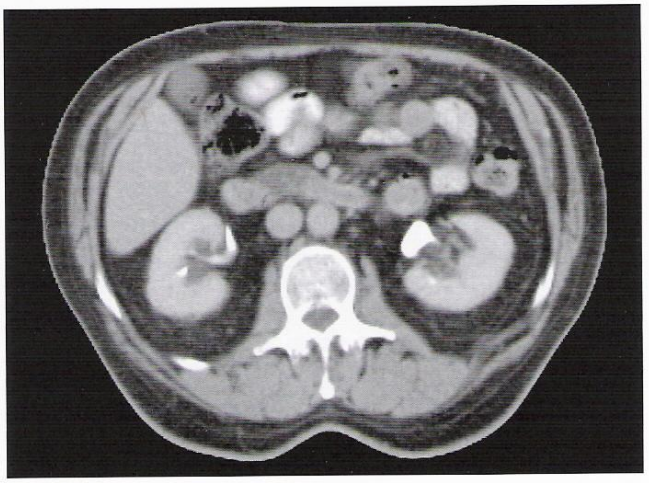

Fig. 108.1a

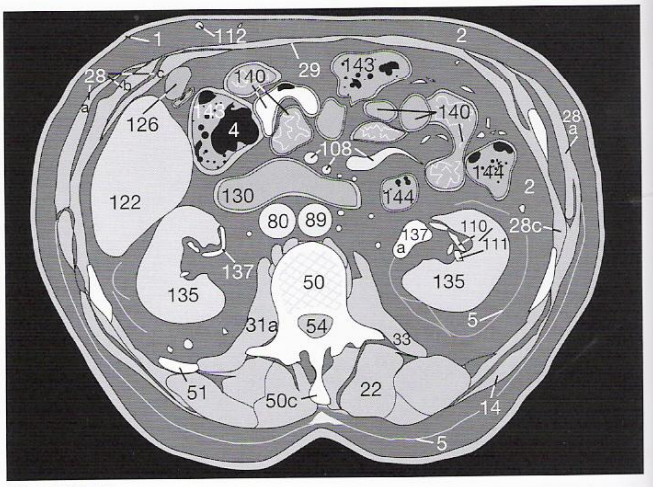

Fig. 108.1b

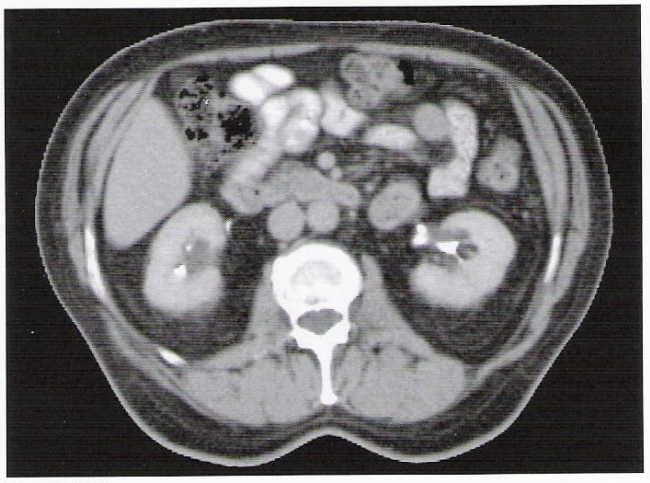

Fig. 108.2a

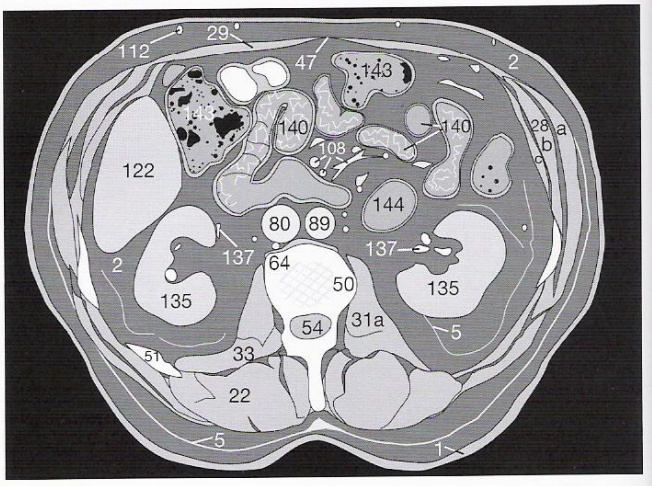

Fig. 108.2b

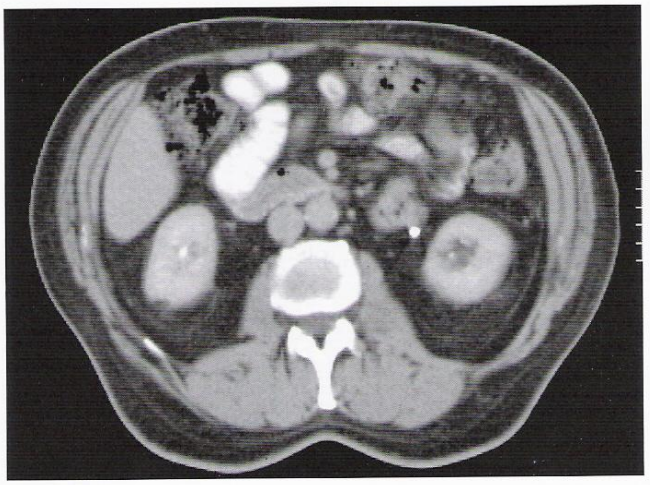

Fig. 108.3a

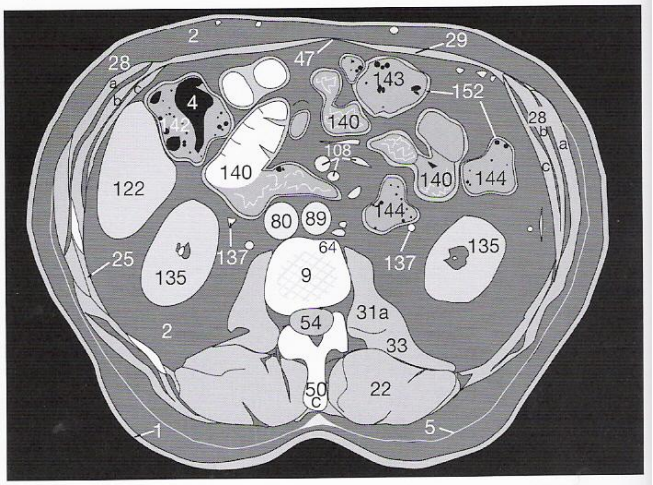

Fig. 108.3b

Note the typical position of the proximal parts of the ureters **(137)**, medial to the inferior poles of the kidneys **(135)** and anterior to the psoas muscle **(31a)**. In **Figures 109.2** and **109.3**, the lumina of both ureters appear hyperdense because CM is being excreted in the urine. Parts of the renal fascia **(5)** can be identified in **Figures 109.2** and **109.3**. Haustrations caused by the semilunar folds (haustral folds) **(149)** are typical of the colon (**142–144** in the figures below).

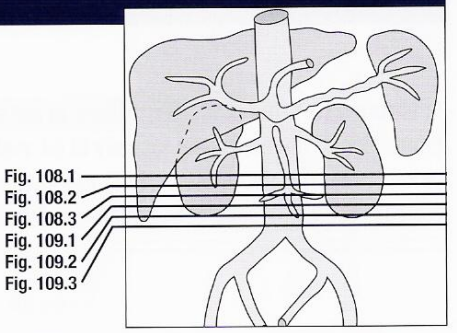

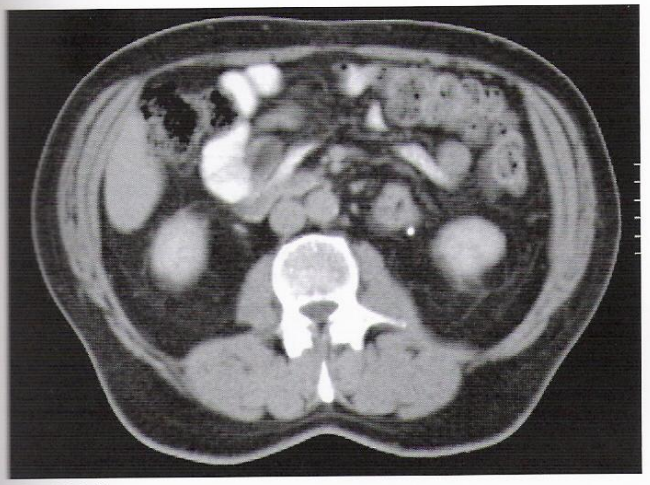

Fig. 109.1a

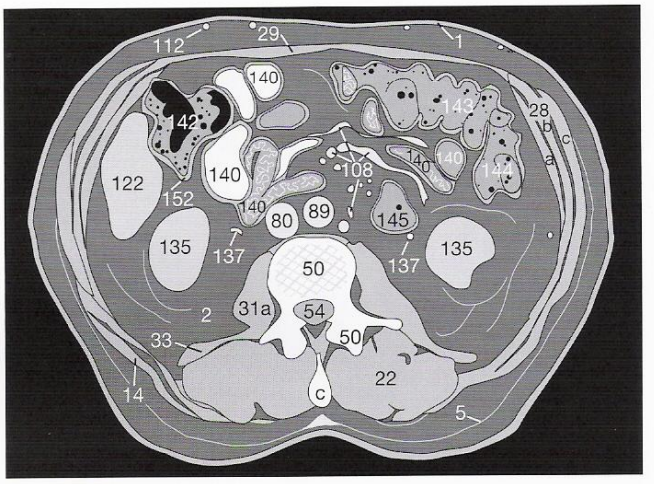

Fig. 109.1b

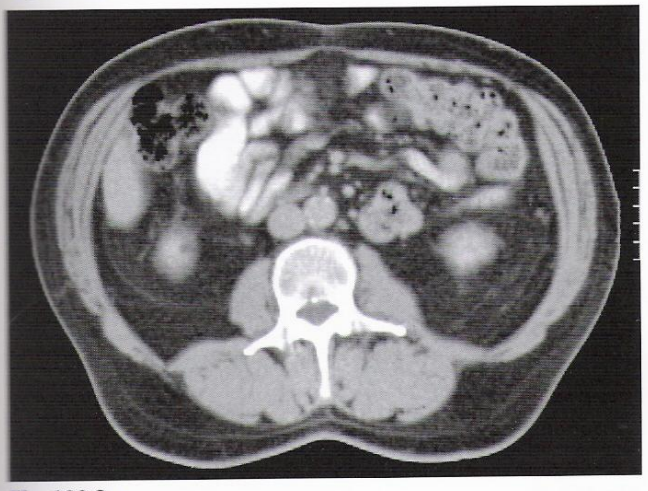

Fig. 109.2a

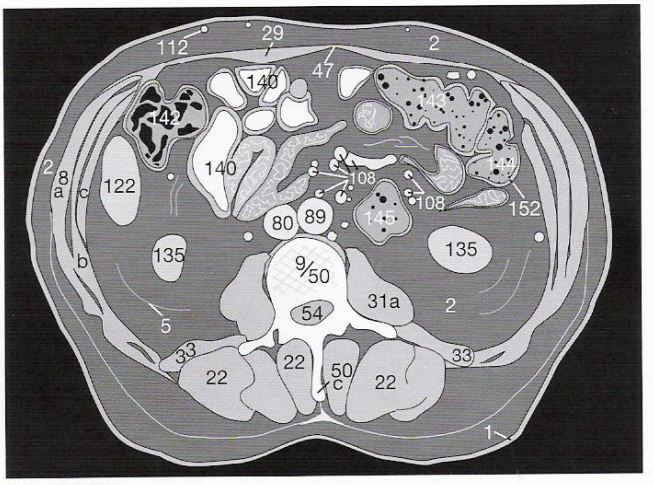

Fig. 109.2b

Fig. 109.3a

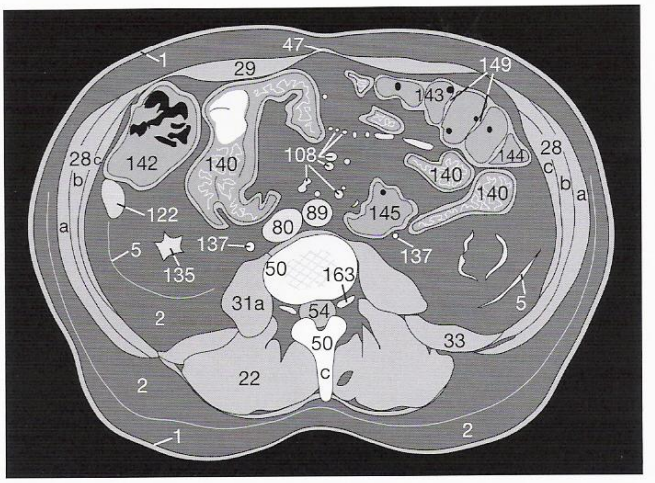

Fig. 109.3b

In **Figure 110.1**, the branching pattern of the superior mesenteric vessels **(108)** which supply the small bowel **(140)** can be seen. At the bifurcation of the aorta **(89)** (usually at L4 vertebral body, **Fig. 110.2**), the common iliac arteries **(113)** are anterior to the corresponding veins **(116)**. The two ureters **(137)** are located more laterally in front of the psoas muscles **(31a)**. Along with the iliac bones **(58)** the gluteus medius muscles **(35a)** appear and sometimes contain calcified intramuscular injections sites (cf. **Fig. 117.3**).

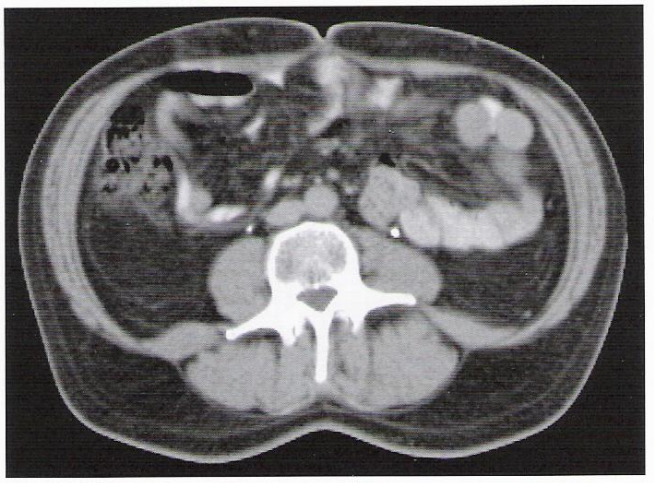

Fig. 110.1a

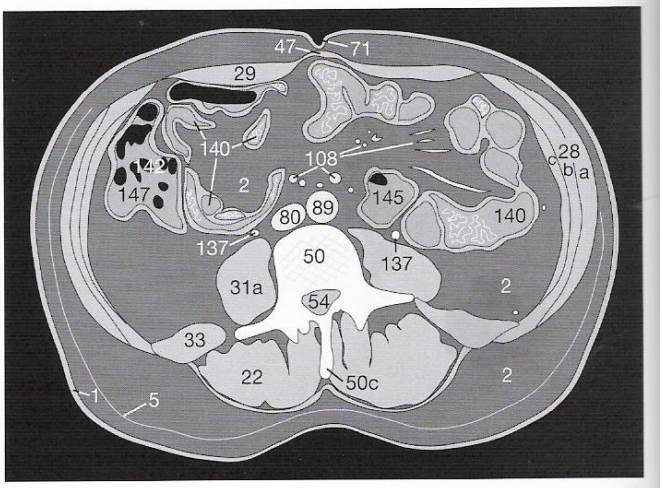

Fig. 110.1b

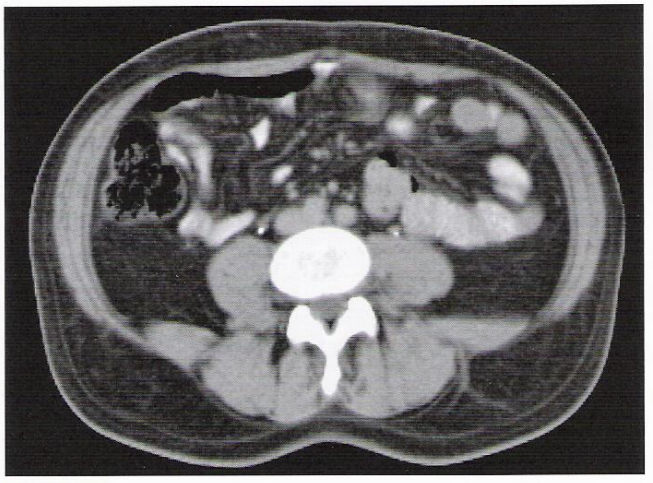

Fig. 110.2a

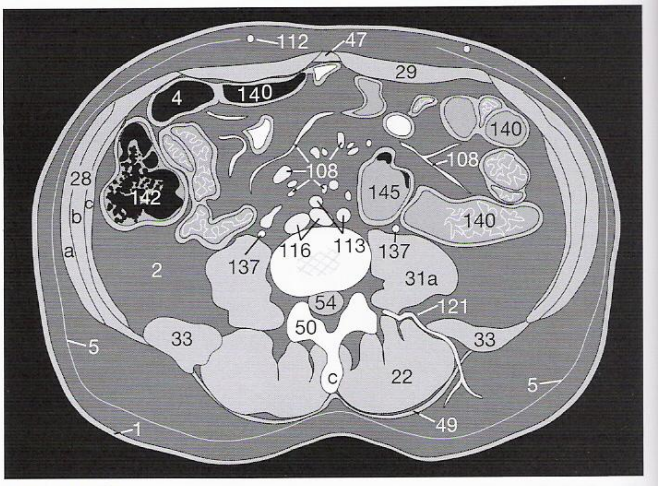

Fig. 110.2b

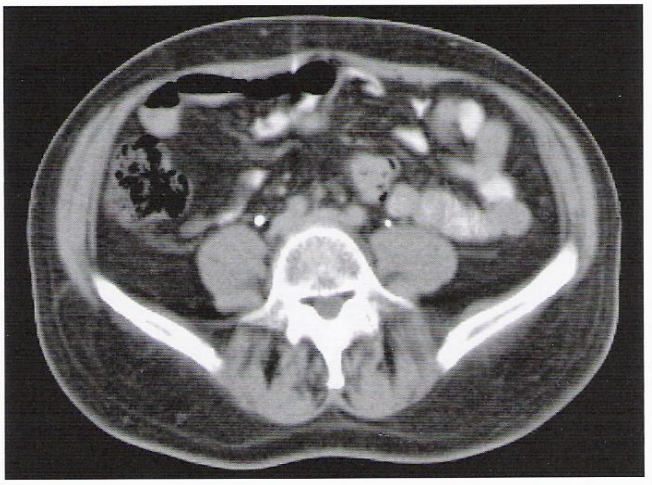

Fig. 110.3a

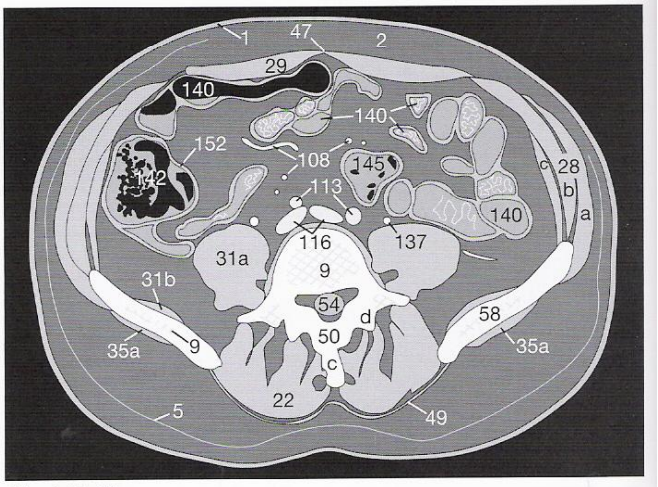

Fig. 110.3b

In order to exclude the presence of an abdominal hernia you should check for a normal width of the linea alba **(47)** between the rectus abdominis muscles **(29)**. More caudally **(Fig. 111.3)** there is a site of predilection for enlarged LNs at the division of the iliac vessels into external artery/vein **(115/118)**, which pass anteriorly, and internal artery/vein **(114/117)**, which are located more posteriorly. The transition from the lumbar spine **(50)** to the sacrum **(62)** lies at this level.

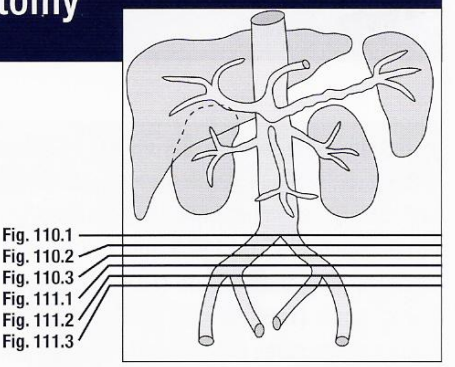

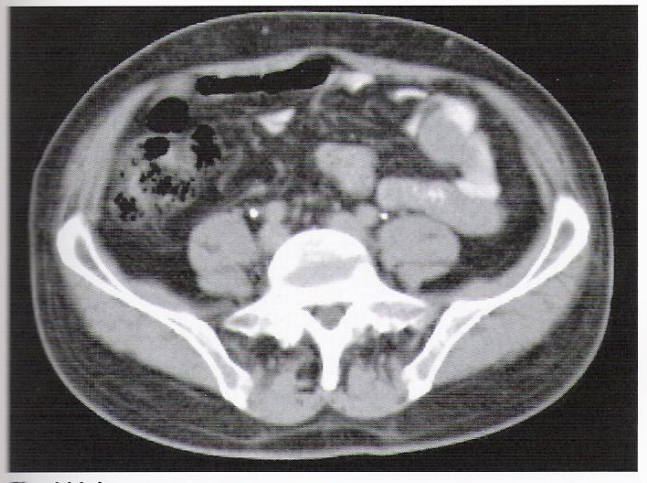

Fig. 111.1a

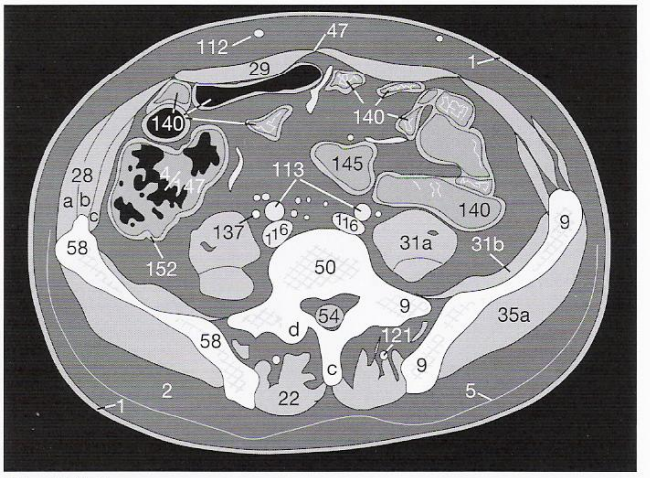

Fig. 111.1b

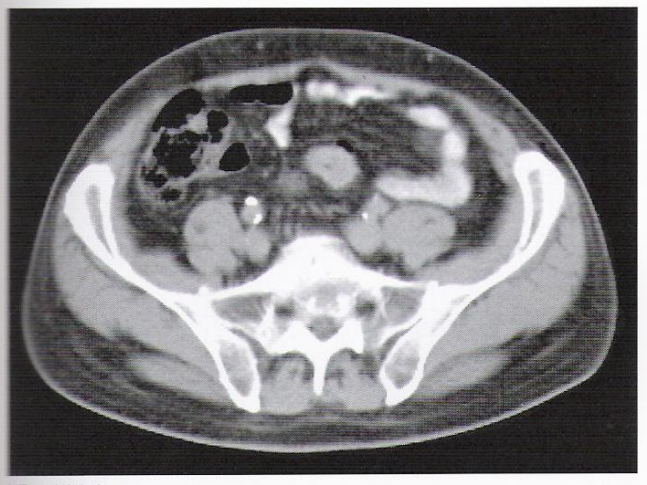

Fig. 111.2a

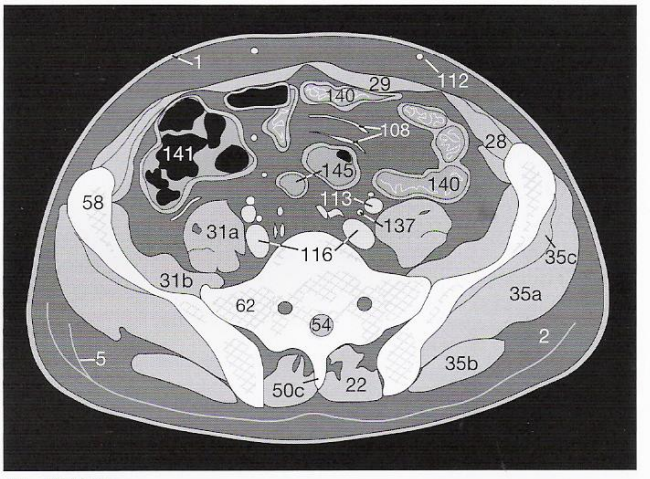

Fig. 111.2b

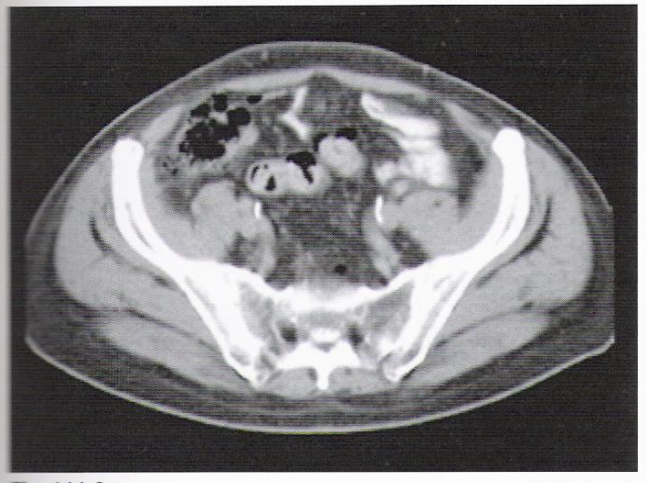

Fig. 111.3a

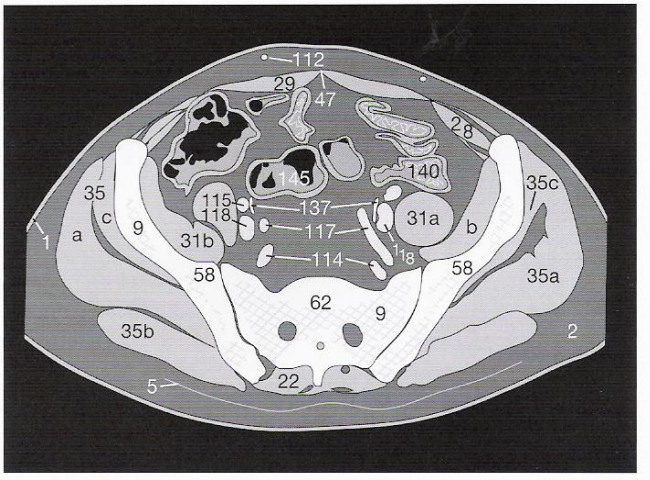

Fig. 111.3b

In the following images, the ureters **(137)** pass posteriorly to approach the lateral aspects of the base of the bladder **(138)**. Within the bladder, differences in the concentration of excreted CM in the urine can be recognized as fluid–fluid levels of different densities (**Figs. 112.3** and **113.1**). On the next page, a male pelvis is shown, demonstrating the prostate **(153)**, seminal vesicle **(154)**, spermatic cord **(155)**, and root of penis **(156)**. Note in particular the internal obturator muscles **(41a)** and the levator ani muscles **(42)** lateral to the anal canal **(146a)**; images of the female pelvis on pages 114 / 115 were not obtained as far caudally as in the male.

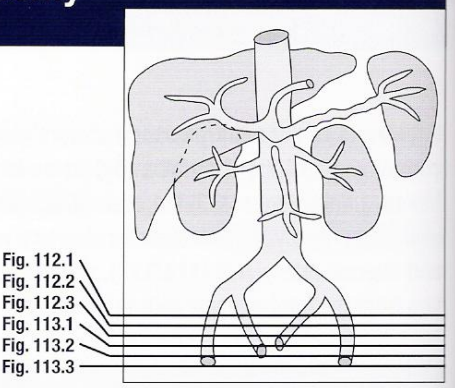

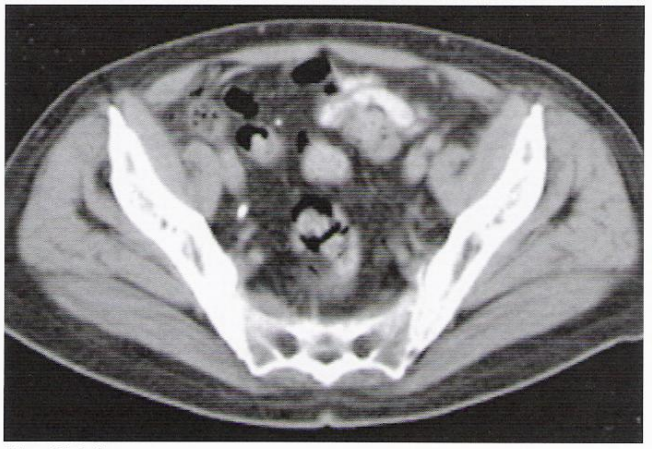

Fig. 112.1a

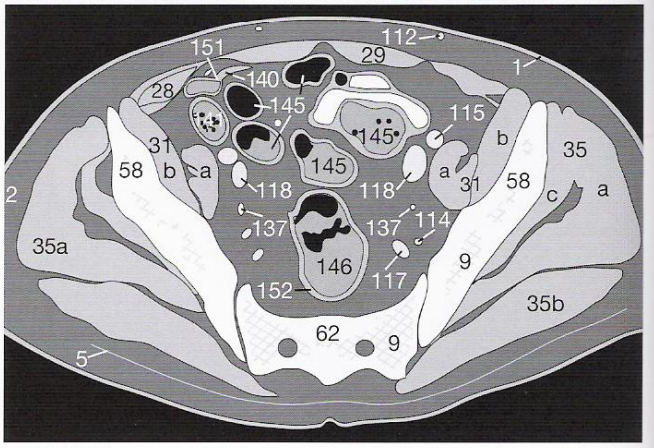

Fig. 112.1b

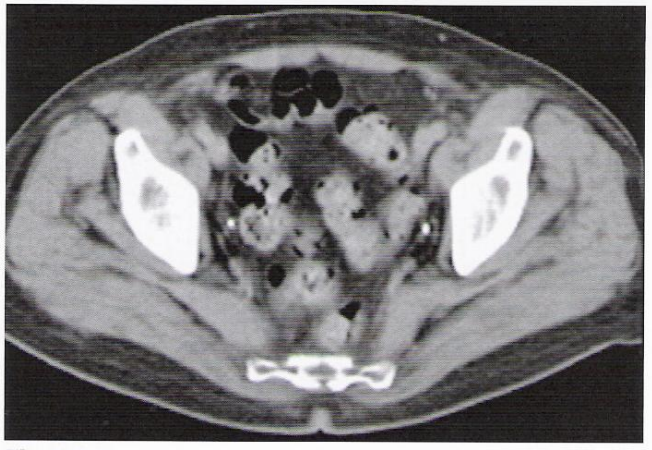

Fig. 112.2a

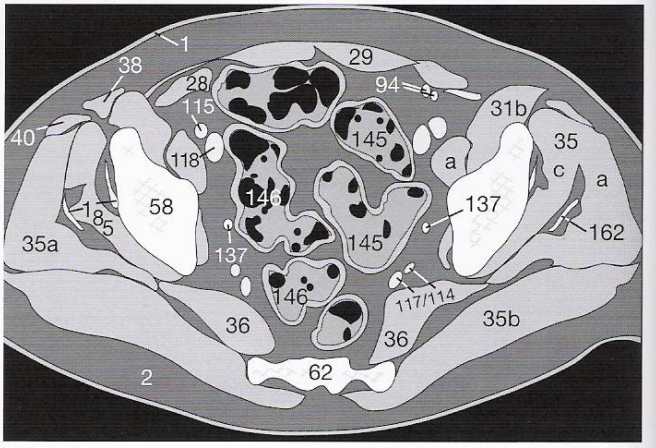

Fig. 112.2b

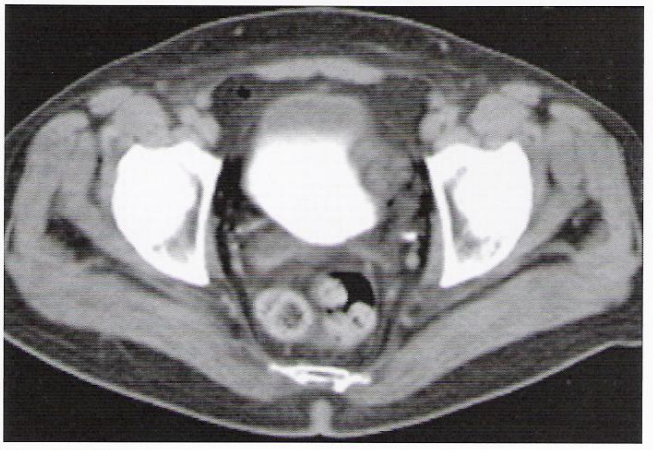

Fig. 112.3a

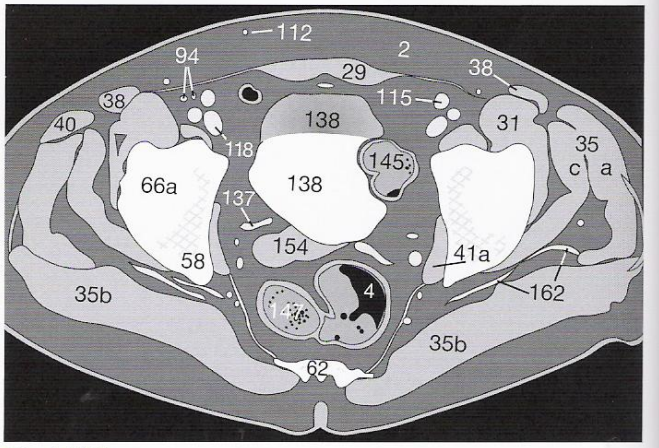

Fig. 112.3b

Fig. 113.1a

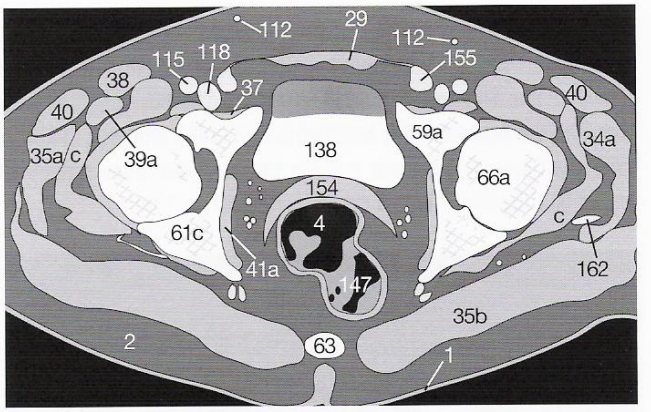

Fig. 113.1b

Fig. 113.2a

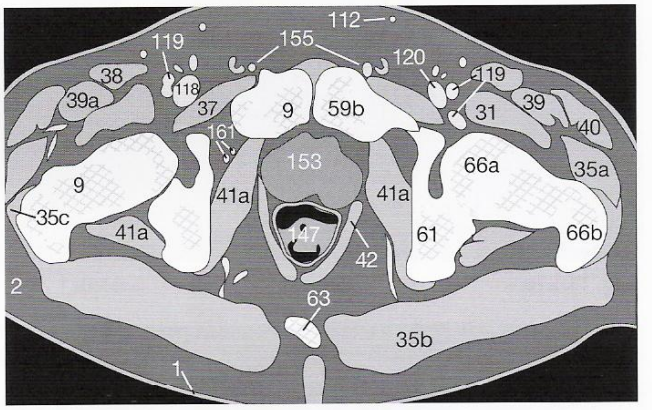

Fig. 113.2b

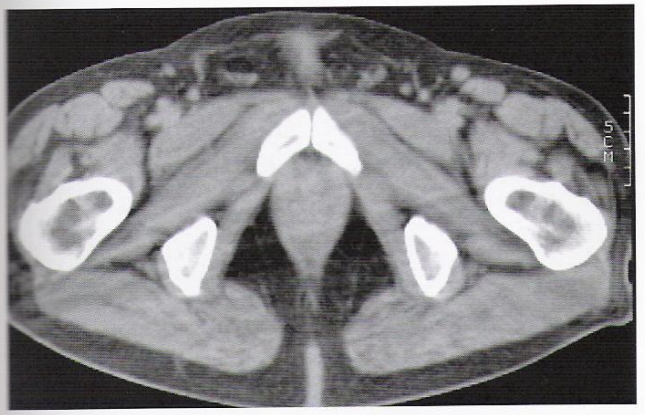

Fig. 113.3a

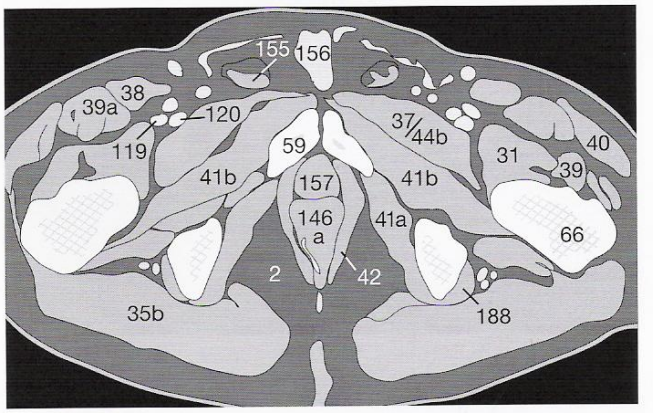

Fig. 113.3b

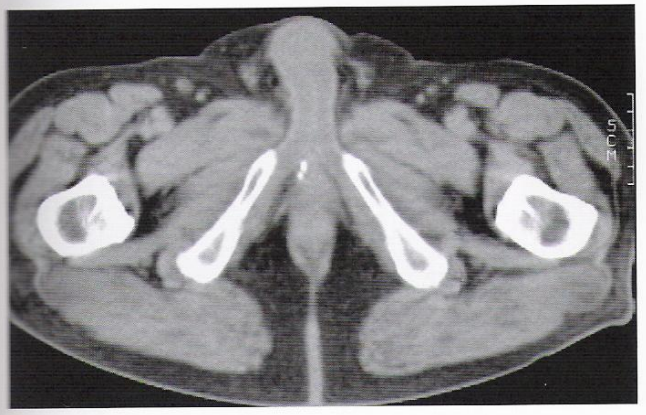

Fig. 113.4a

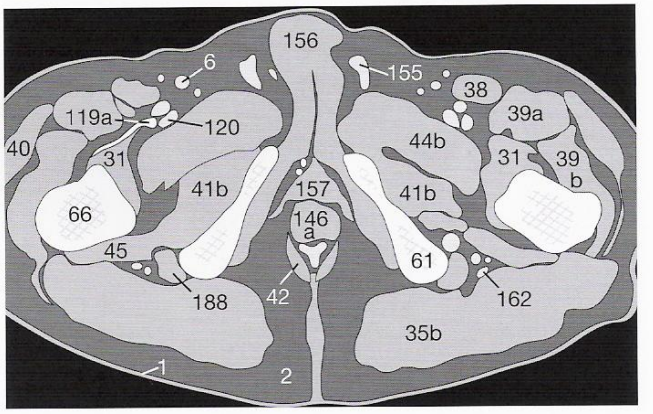

Fig. 113.4b

In the female pelvis, the size and position of the uterus **(158)** relative to the urinary bladder can vary considerably from patient to patient. The uterus may lie cranial or lateral to the bladder (**Figs. 114.1–115.1**). The cervix and the vagina are situated between the bladder **(138)** and the rectum **(146)**, whereas the ovaries **(159)** lie more laterally. Depending on age and the phase of the menstrual cycle, ovarian follicles might be misinterpreted as cystic lesions (cf. p. 133).

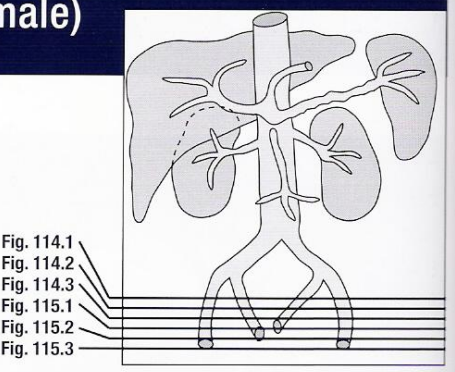

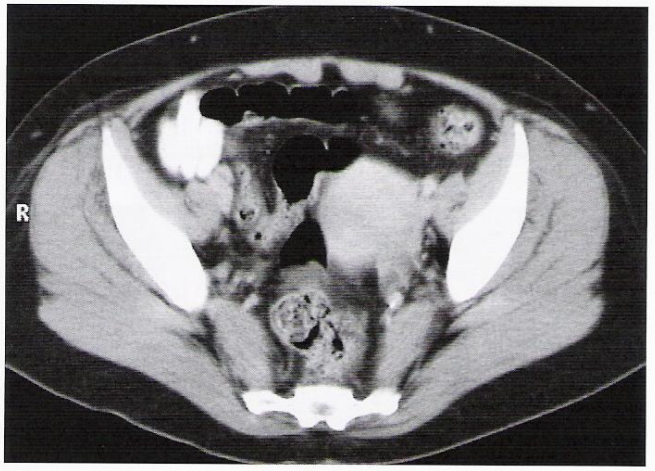

Fig. 114.1a

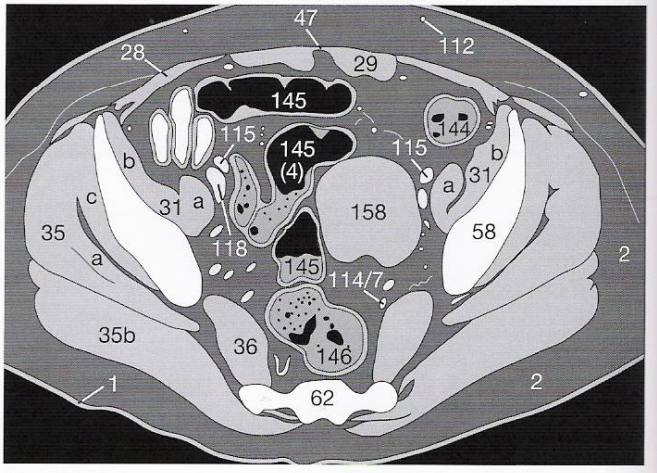

Fig. 114.1b

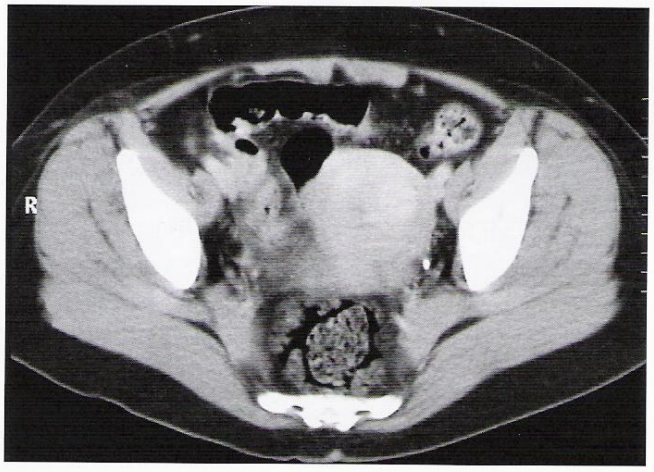

Fig. 114.2a

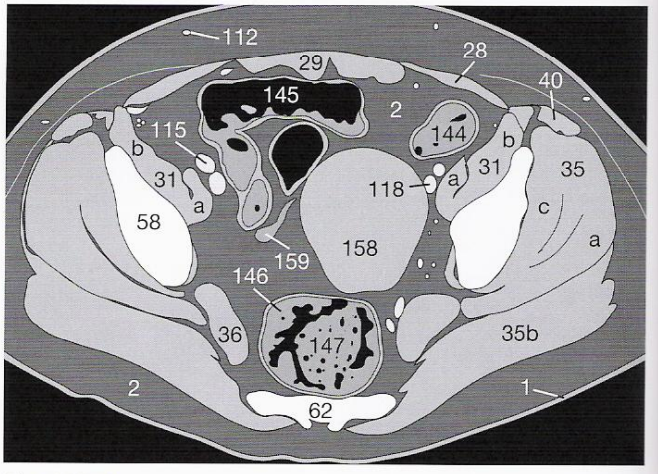

Fig. 114.2b

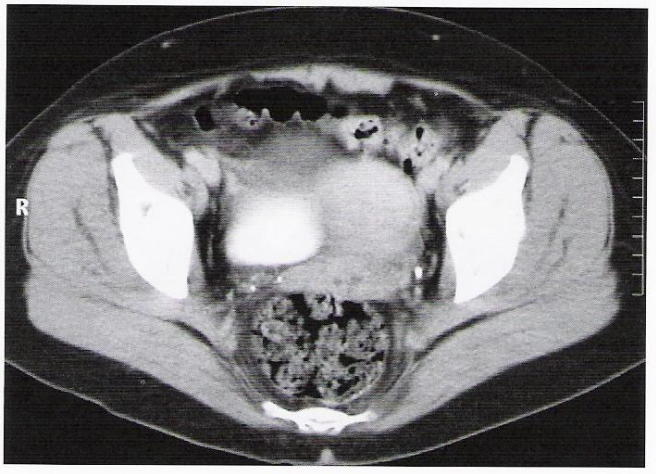

Fig. 114.3a

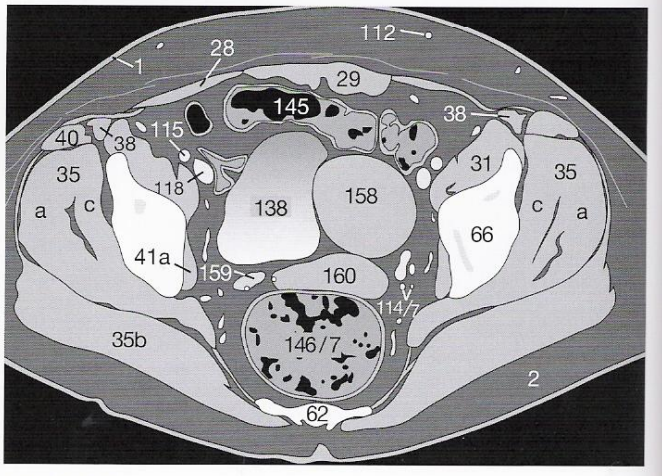

Fig. 114.3b

Free intra-abdominal fluid (ascites or hemorrhage) may occur in the rectouterine pouch between rectum and uterus, as well as in the vesicouterine space. In the inguinal region, lymph nodes **(6)** can be up to 2 cm in diameter and be normal (**Figs. 115.2** and **115.3**). The size of normal abdominal lymph nodes does not usually exceed 1 cm. It is not possible to examine the hip joints on soft-tissue windows (**Fig. 115.3**); the heads of the femurs **(66a)** in the acetabular fossae **(59/61)** can best be analyzed on bone windows (not shown here). An assessment of bone windows completes the examination of the abdominal and pelvic images.

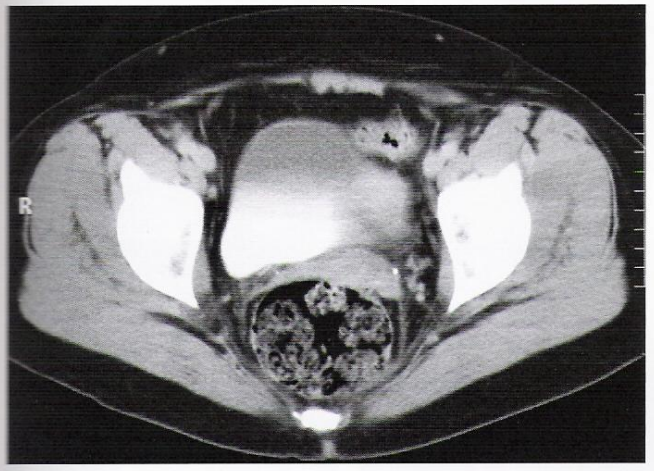

Fig. 115.1a

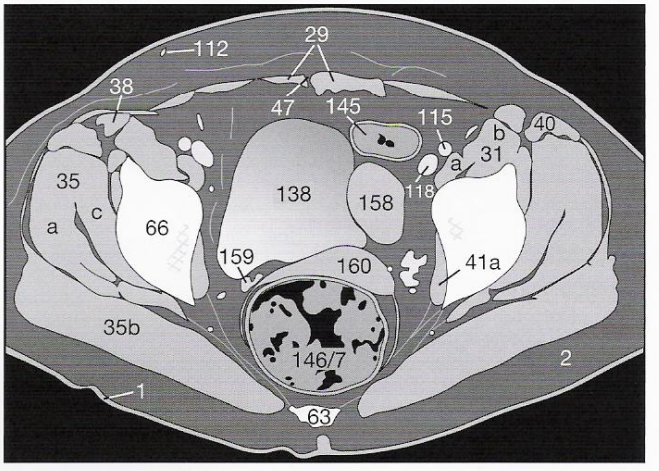

Fig. 115.1b

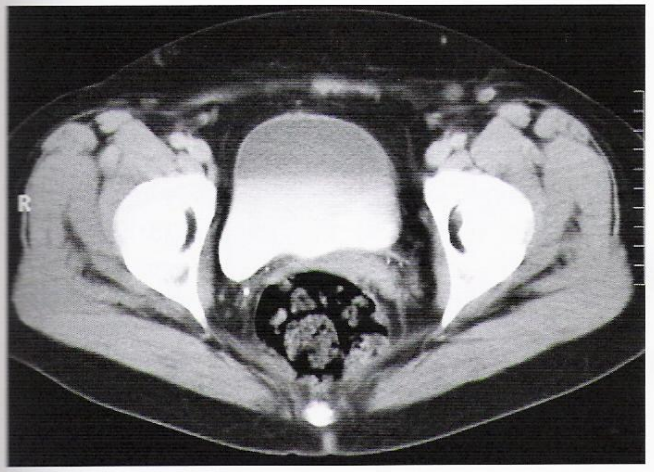

Fig. 115.2a

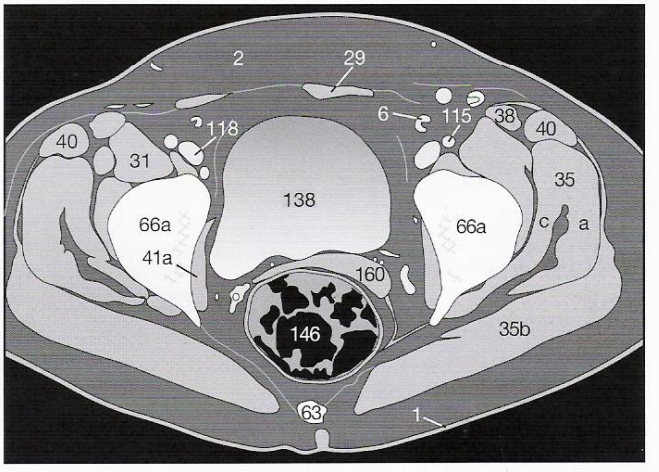

Fig. 115.2b

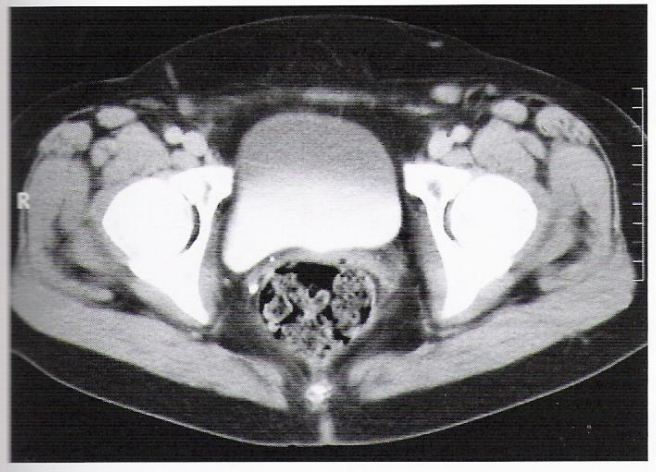

Fig. 115.3a

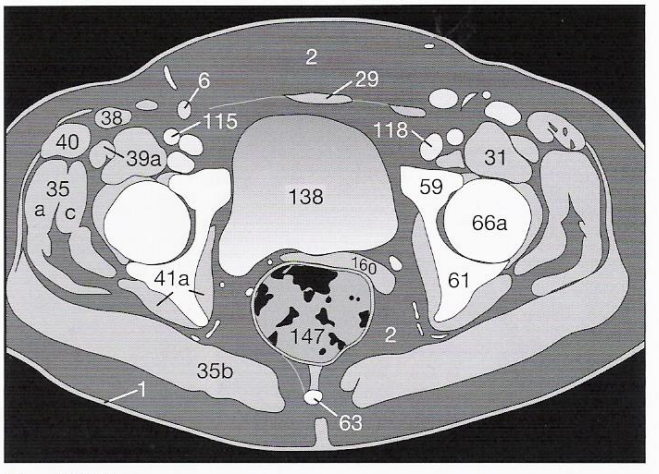

Fig. 115.3b

Anatomic Variations

For the beginner, it is important to be familiar with the most common anatomic variations which may lead to misinterpretations of CT images. In some patients, the contours of the right lobe of the liver **(122)** may appear scalloped by impressions of the diaphragm **(30)** which could be mistaken for liver lesions **(Fig. 116.1)**. The walls of an empty stomach **(129)** are thick and may suggest a malignant lesion **(129a)**.

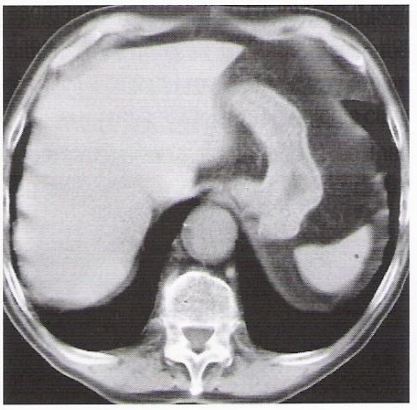

Fig. 116.1a

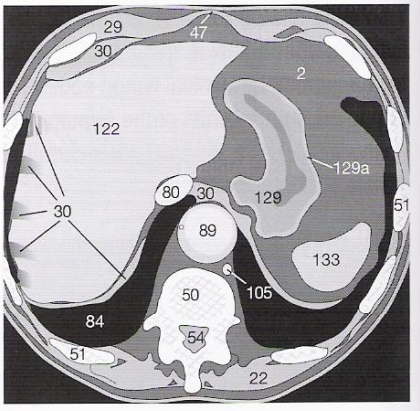

Fig. 116.1b

Ultrasound may mistake an anomalous left renal vein **(111)** for a retroaortic LN. Usually the left renal vein passes between the SMA **(106)** and the aorta **(89)**. However, the vein may be retroaortic and pass between the aorta and the spinal column **(50)** to the inferior vena cava **(80)** **(Figs. 116.2 – 116.4)**. Duplication of the left renal vein with preaortic and retroaortic components can also occur.

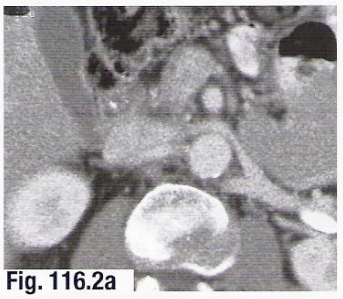

Fig. 116.2a

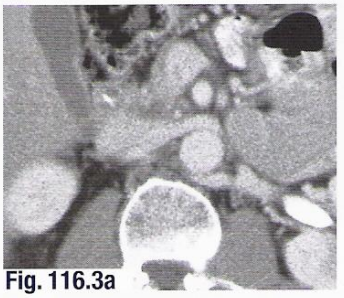

Fig. 116.3a

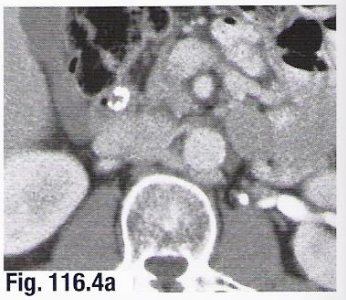

Fig. 116.4a

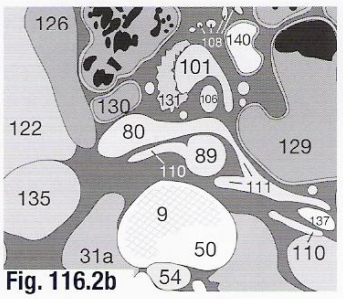

Fig. 116.2b

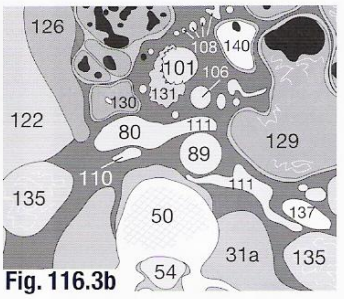

Fig. 116.3b

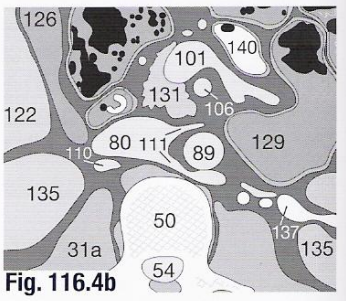

Fig. 116.4b

Characteristic Partial Volume Effects

If the wall of one organ indents that of another, cross-sectional images will make it look as if one organ were within the other. For example, the sigmoid colon **(145)** may appear "within" the urinary bladder **(138)** **(Fig. 116.5a)**. By comparing adjacent sections (**Figs. 116.5a** and **c**), it is easy to recognize that only parts of both organs have been imaged. In a similar manner, the right colic flexure **(142)** may appear to be "within" the gallbladder **(126)** **(Fig. 116.6)**.

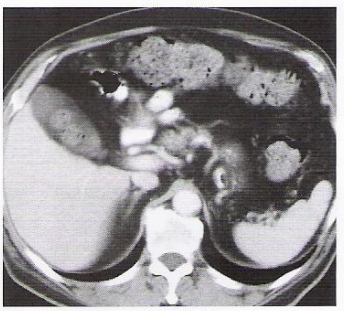

Fig. 116.6a

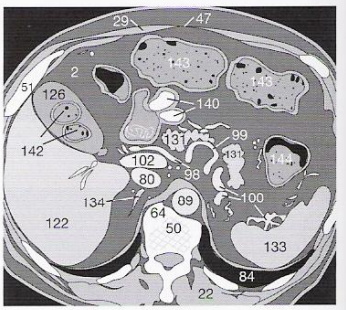

Fig. 116.6b

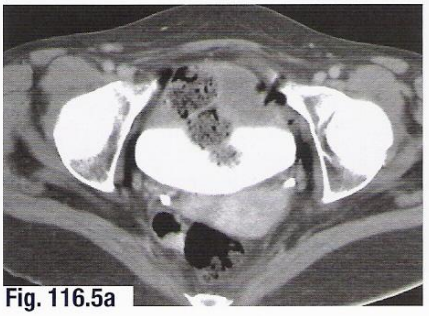

Fig. 116.5a

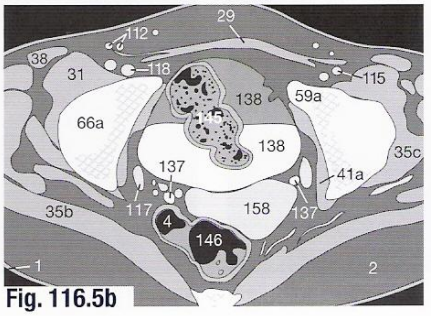

Fig. 116.5b

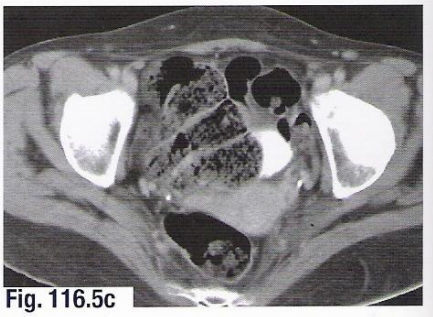

Fig. 116.5c

Lymph Node Hyperplasia

Pathologic lesions of the abdominal wall occur most frequently in the inguinal region. Lymph node hyperplasia with nodes up to 2 cm in dimension should not be considered abnormal. Large conglomerate masses of LNs (⬅) are found in non-Hodgkin's lymphoma **(Fig. 117.1)** and less frequently in Hodgkin's disease.

An inguinal hematoma **(173)** caused by hemorrhage from a femoral artery puncture site after coronary angiography should be considered **(Fig. 117.2)** in the DD.

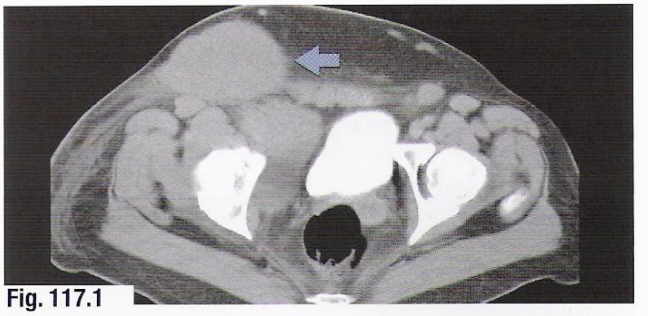

Fig. 117.1

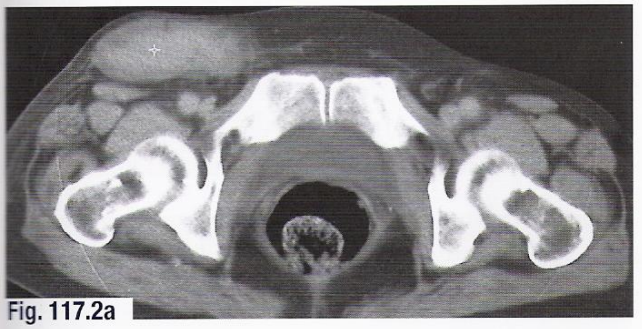

Fig. 117.2a

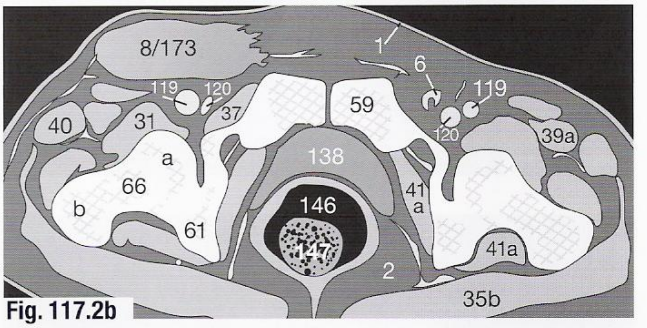

Fig. 117.2b

Abscesses

Intramuscular injection sites in the gluteal region resulting in subcutaneous fat **(2)** necrosis or postinflammatory residue (➡) typically are well-defined, hyperdense, partially calcified lesions **(Fig. 117.3)**.

An abscess may spread from the gluteal muscles to the pelvis through the ischiorectal fossa. After diffuse infiltration **(178)** of the gluteal muscles **(35)** with surrounding edema (**185** in **Fig. 117.4**), liquefaction **(181)** may occur and, depending on the localization and size, the abscess can involve the sciatic nerve **(Fig. 117.5)**.

Fig. 117.3

Fig. 117.4a

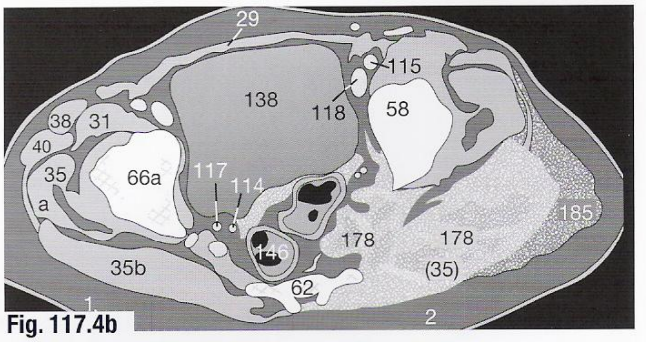

Fig. 117.4b

Fig. 117.5a

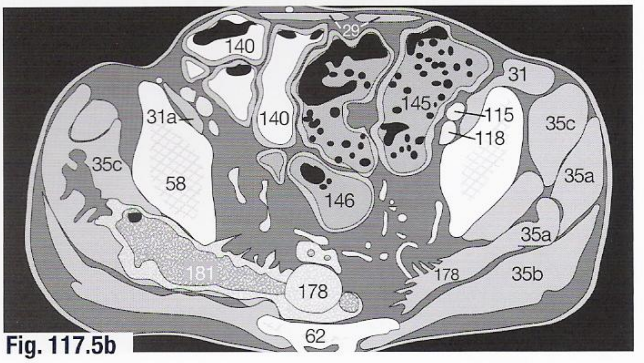

Fig. 117.5b

The CT in **Figure 118.1** shows subcutaneous lesions, resulting from heparin injections **(173)** or small hematomas that may mimic cutaneous metastases **(7)** or malignant melanomas **(Fig. 118.2)**. Larger metastases tend to invade the muscles of the abdominal wall **(29)** and often have hypodense, central necrosis **(181)**. Enhancement after intravenous CM may also point to malignancy or a florid inflammatory process. If the degree of CM enhancement is uncertain, a region of interest for densitometric analysis is placed in the lesion on a pre-CM and compared with a post-CM **(Fig. 118.2)**.

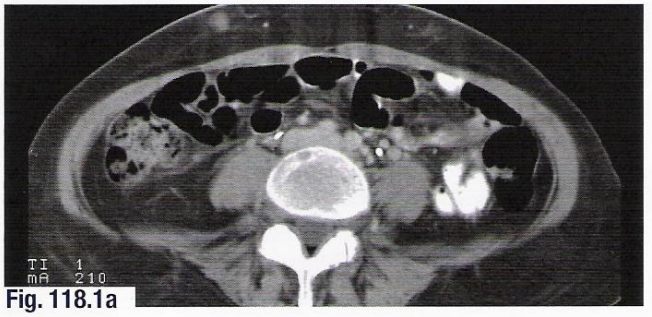

Fig. 118.1a

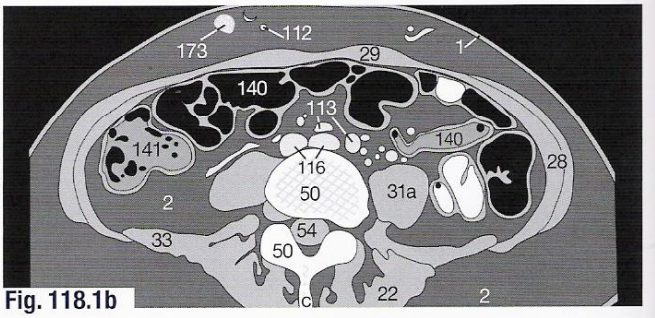

Fig. 118.1b

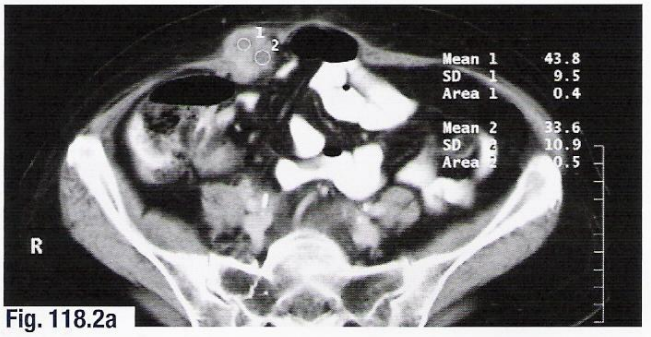

Fig. 118.2a

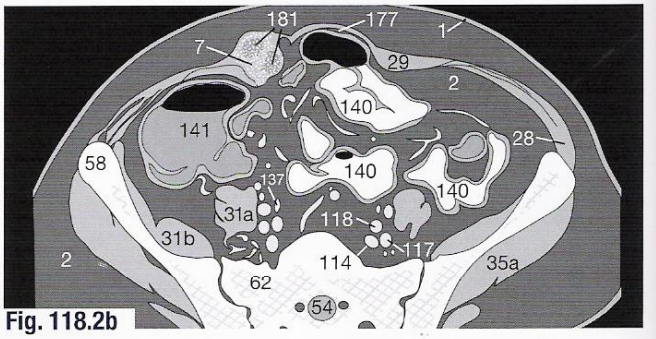

Fig. 118.2b

Metastases in the abdominal wall may not be evident until they become infected and develop into an abscess **(181)**, which was catheterized and drained in the case illustrated (**182** in **Fig. 118.3**). The second metastasis **(7)**, just beneath the right abdominal wall **(28)**, was not recognized at first because the patient's symptoms were attributed to the adjacent abscess.

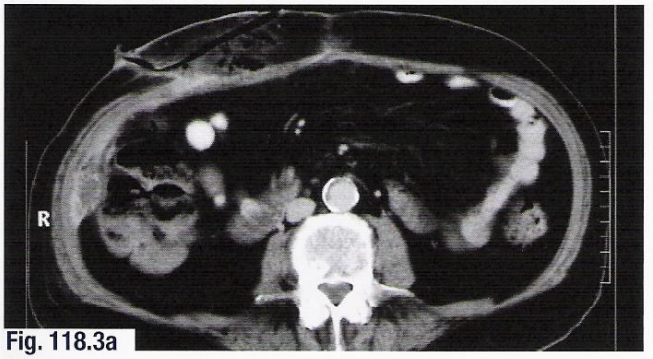

Fig. 118.3a

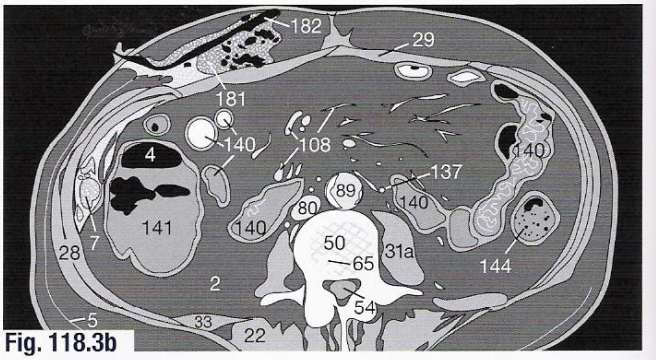

Fig. 118.3b

In elderly patients, an inguinal hernia containing small intestine, or even bilateral scrotal hernias containing loops of the small bowel **(140)** may be diagnosed. In the case in **Figure 118.4**, the processus vaginalis **(177)** was open bilaterally.

Fig. 118.4a

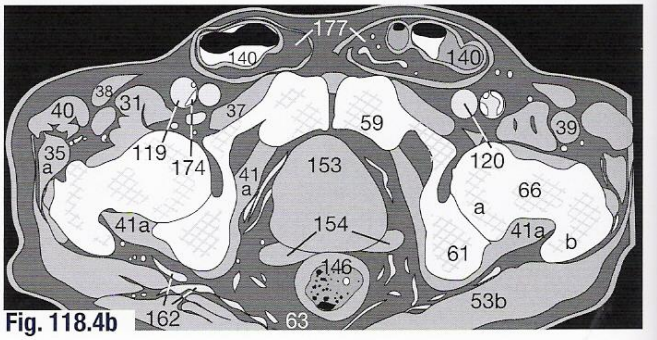

Fig. 118.4b

Segments of the Liver

If a liver biopsy or radiotherapy is planned, it is helpful to know in which segment a focal lesion is situated. The liver is horizontally subdivided (blue line in **Fig. 119.1**) by the main branches of the portal vein **(102)** into a cranial and caudal part. The main hepatic veins **(103)** mark the borders of the segments in the cranial part **(Fig. 119.2)**. The border between the left and right lobes is not marked by the falciform ligament **(124)**, but by the plane between the middle hepatic vein and gallbladder **(126)** fossa.

Left lobe	I	caudate lobe
	II	lateral segment, cranial part
	III	lateral segment, caudal part
	IV	quadrate lobe (a: cranial, b: caudal)
Right lobe	V	anterior segment, caudal part
	VI	posterior segment, caudal part
	VII	posterior segment, cranial part
	VIII	anterior segment, cranial part

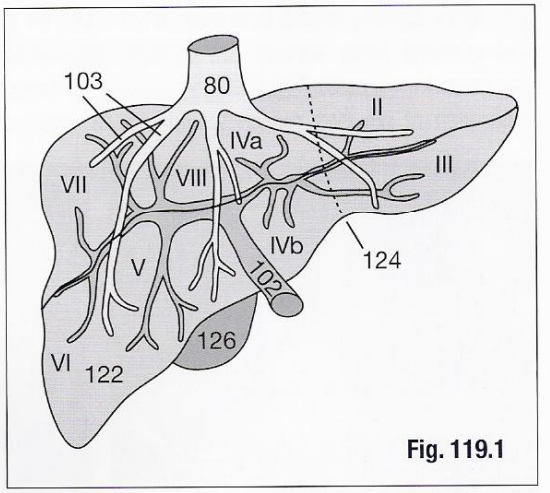

Fig. 119.1

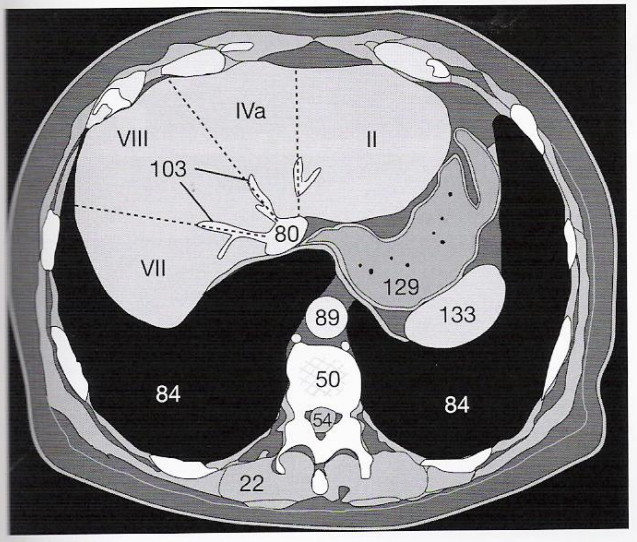

Fig. 119.2

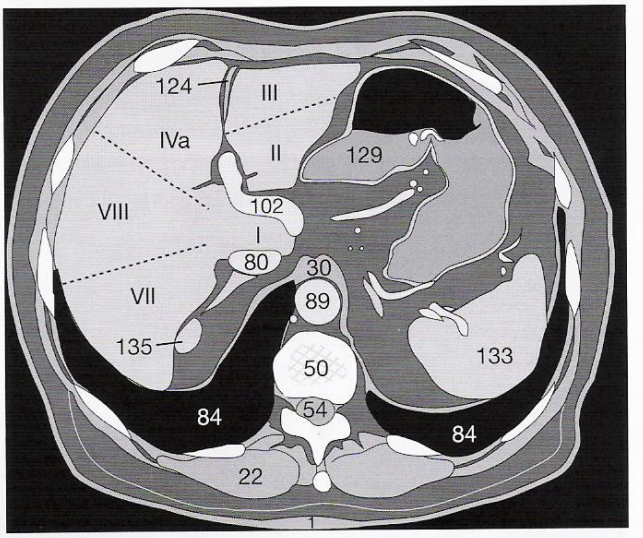

Fig. 119.3

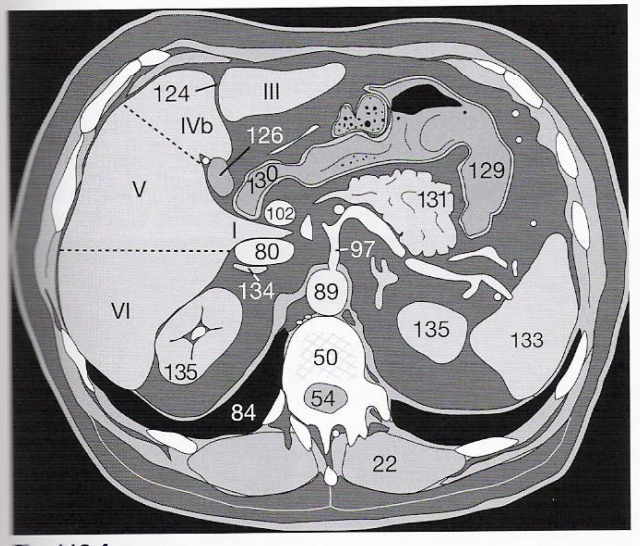

Fig. 119.4

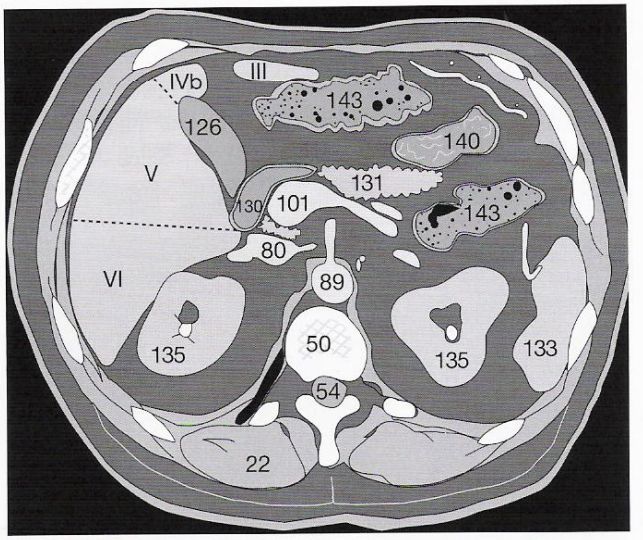

Fig. 119.5

Choice of Window

In conventional (nonhelical) CT, the unenhanced liver **(122)** is imaged on a special liver window width **(Fig. 120.1a)** set between 120 and 140 HU. Normal liver parenchyma can be more clearly distinguished from lesions on narrow-window-width images because they provide high image contrast. If there is no fatty infiltration of the liver (which would reduce attenuation), intrahepatic vessels **(103)** appear as hypodense structures. In cases of fatty infiltration, the veins may appear isodense or even hyperdense on unenhanced images. The post-contrast agents CT images are viewed using a window width of approximately 350 HU; this smoothes the gray scale contrast **(Fig. 120.1c)**.

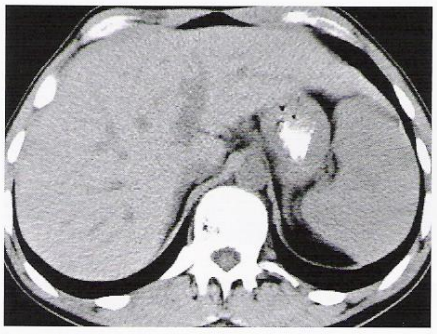

Fig. 120.1a

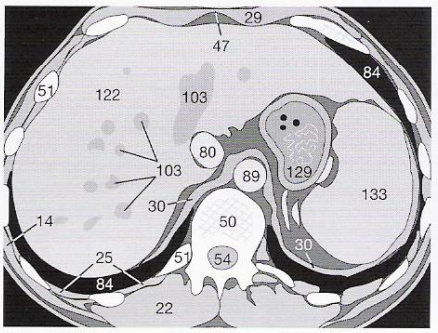

Fig. 120.1b

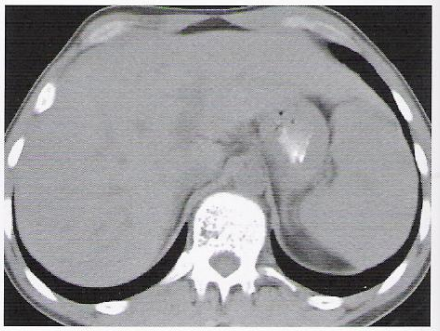

Fig. 120.1c

Passage of a Bolus of Contrast Agents

In a three-phase helical acquisition of early arterial, portal venous, and late venous phases of contrast agents enhancement, an unenhanced study is not necessary [17, 18]. Hypervascular lesions become much more clearly defined in the early arterial phase **(Fig. 120.2a)** than in the late venous phase. In the late venous (equilibrium) phase **(Fig. 120.2b)**, the density levels of the arterial, portal venous, and venous systems are practically identical.

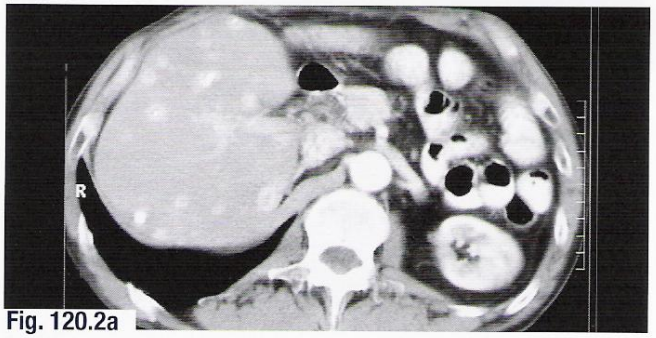

Fig. 120.2a

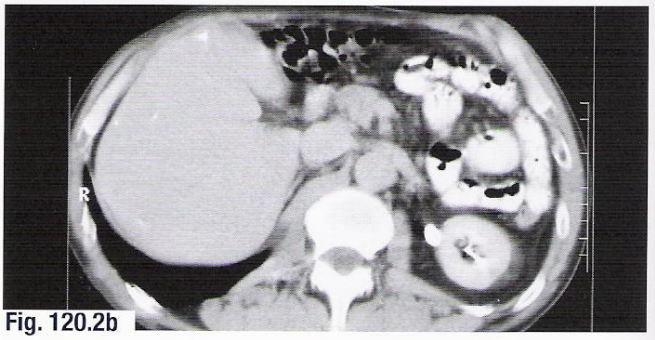

Fig. 120.2b

CT Portography

The chances of demonstrating the true extent of liver lesions (e.g. metastases) are greatly improved if contrast agents are injected directly into the SMA or the splenic artery and images are then acquired in the portal venous phase [17, 21]. Since the principal blood supply for most metastases and tumors comes from the hepatic artery, these lesions will appear hypodense within the hyperdense normal parenchyma that has enhanced with contrast agents **(Fig. 120.3a)**. In the same patient, the early arterial phase image **(Fig. 120.3b)** shows that without contrast agents portography, the extent of the metastases would have been greatly underestimated.

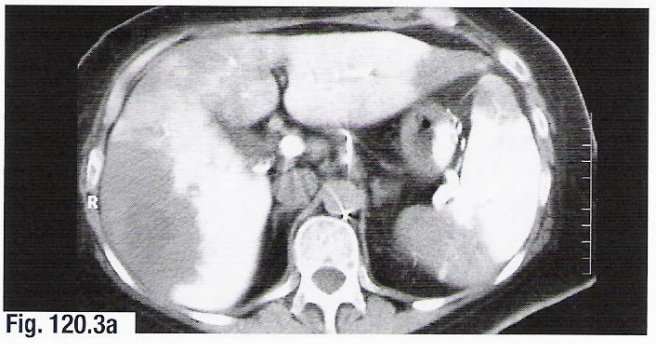

Fig. 120.3a

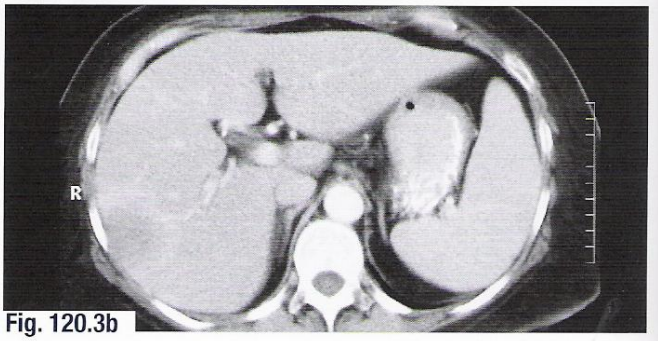

Fig. 120.3b

Hepatic Cysts

Hepatic cysts **(169)** containing serous fluid are sharply defined, thin-walled, homogeneous lesions with density values close to those of water **(Fig. 121.1)**. Partial volume effects may cause poor delineation from adjacent hepatic parenchyma **(122)** if the cysts are small. If in doubt, a ROI should be positioned within the cyst for density measurement **(Fig. 121.2a)**. It is important to ensure the ROI is correctly placed in the center of the cyst, well away from the cyst walls (cf. pp. 15 and 133). In small cysts, for example the poorly defined lesion in **Figure 121.2b**, the average density measurement was too high, because adjacent liver parenchyma was included in the calculation. Note that benign cysts do not show any significant enhancement after i.v. CM.

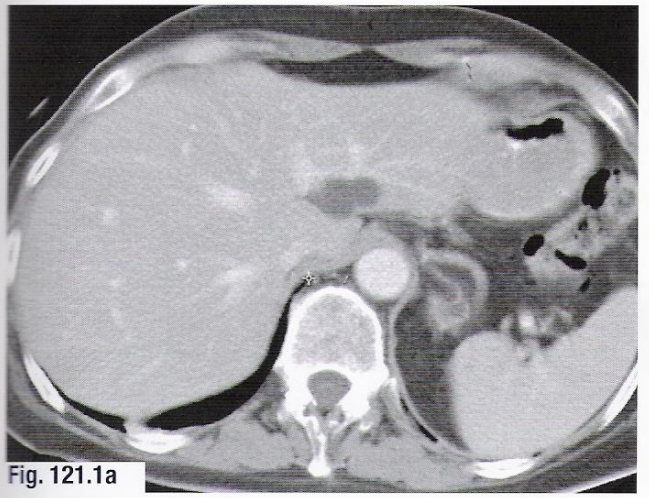
Fig. 121.1a

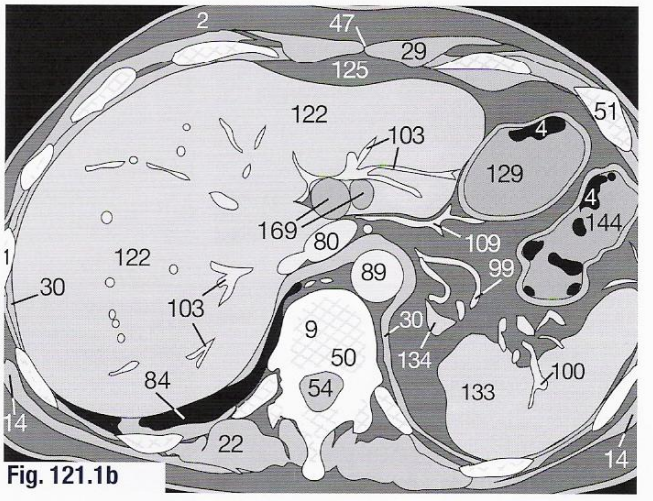

Fig. 121.1b

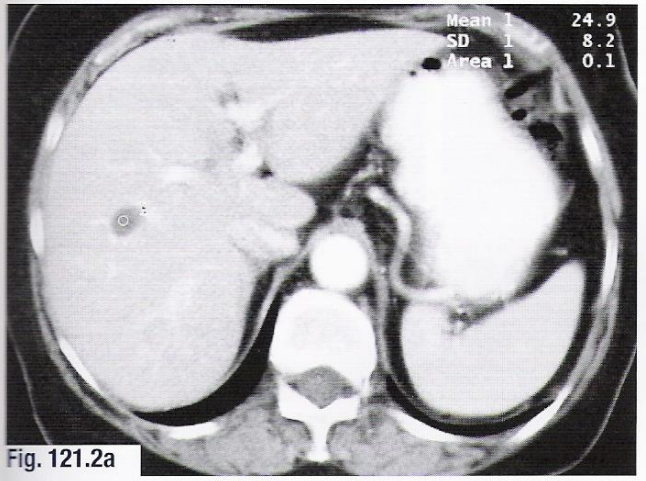

Fig. 121.2a

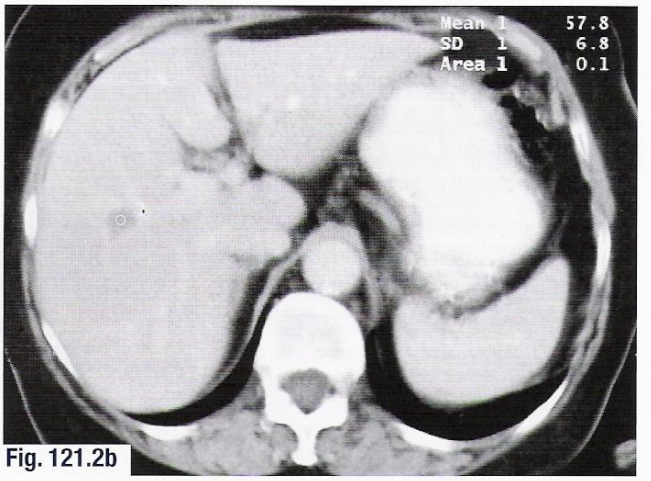

Fig. 121.2b

Hydatid *(Echinococcus granulosus)* cysts have a very characteristic multiloculated appearance, often with radially arranged septations between different cysts (**169** in **Fig. 121.3**). It may prove difficult to differentiate between collapsed, dead cysts and other intrahepatic lesions. The right lobe of the liver is most frequently affected, sometimes the left lobe or the spleen **(133)** become involved, as shown in **Figure 121.3**. The density of the cyst fluid is usually between 10 and 40 HU on an unenhanced image. Partial or complete wall calcification is frequent and the outer membrane may enhance with CM. The DD includes infections with *E. alveolaris* (not shown) and occasionally hepatocellular carcinoma that is poorly defined with irregular satellite lesions.

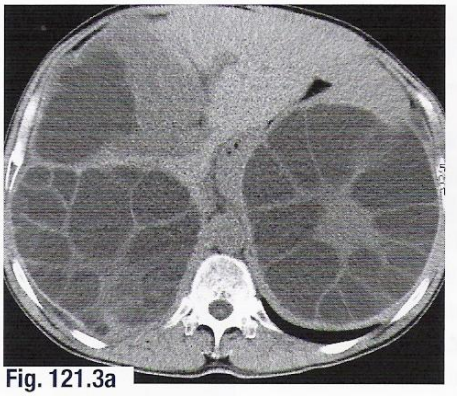
Fig. 121.3a

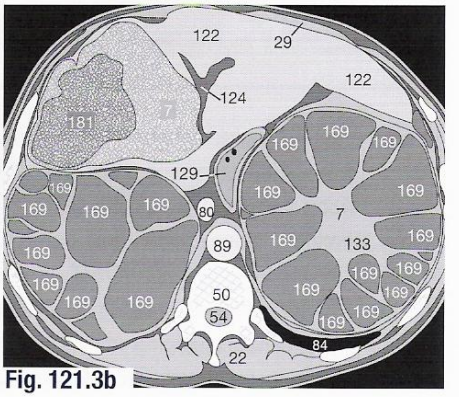

Fig. 121.3b

Liver Metastases

Multiple focal lesions within the liver suggest metastases. Common sites of origin are the colon, stomach, lung, breast, kidneys, and uterus. The morphology and vascularity differ between the types of liver metastases. An enhanced helical scan is therefore obtained in both the venous phase **(Fig. 118.1a)** and the early arterial phase **(Fig. 118.1c)**. In this manner, smaller lesions **(7)** become well defined and hepatic veins **(103)** will not be mistaken for metastases.

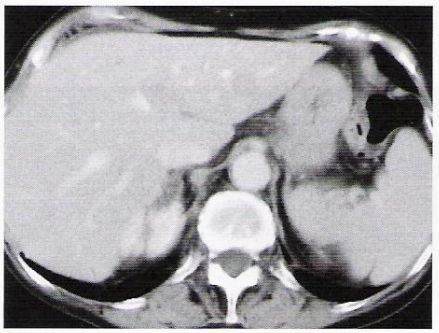

Fig. 122.1a

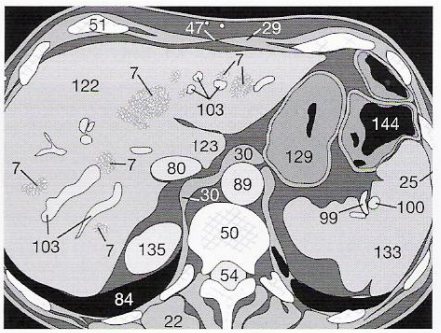

Fig. 122.1b

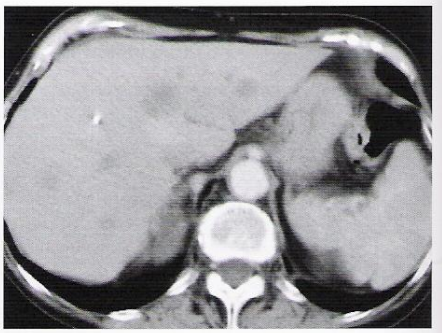

Fig. 122.1c

Hypo- and hypervascular metastases share the hypodense (dark) appearance in the venous phase because of rapid wash-out of contrast material. If spiral CT is not available, it is helpful to compare unenhanced images **(Fig. 122.2)** with enhanced images **(Fig. 122.3)**. In the example on the right, number and size of the hepatic lesions **(7)** would have been underestimated on the enhanced images. It is easily comprehensible that individual small metastases can escape detection if unenhanced images are passed over. To increase the contrast in the hepatic parenchyma **(122)**, a narrow window setting should always be used when viewing these unenhanced images (see page 117). This might even bring out small metastases **(7) (Fig. 122.2)**. These small liver metastases **(7)** differ from small cysts by exhibiting an indistinct margin and a higher density after intravenous injection of contrast medium **(Fig. 122.4)** indicative of enhancement. The average density values were 55 and 71 HU, respectively **(Fig. 122.4)**.

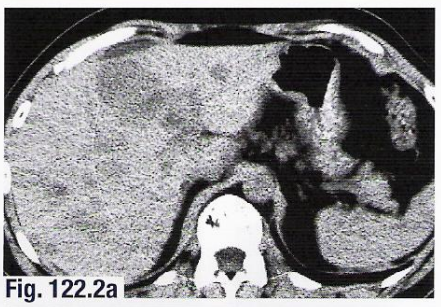

Fig. 122.2a

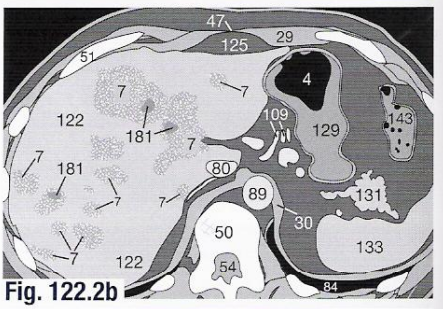

Fig. 122.2b

Fig. 122.3a

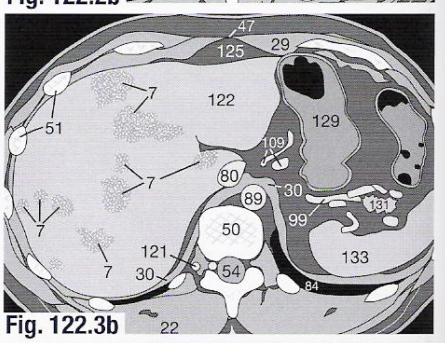

Fig. 122.3b

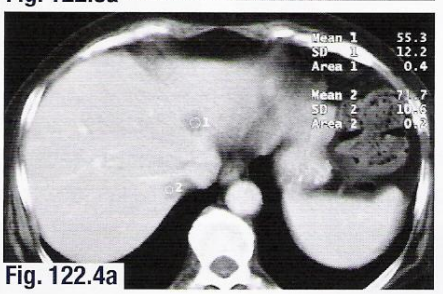

Fig. 122.4a

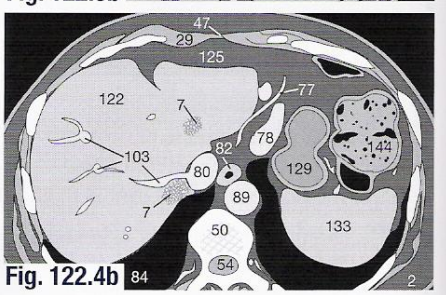

Fig. 122.4b

In case of diagnostic doubt and for reference at follow-up during therapy, it is useful to compare the CT images with ultrasound findings. Apart from the typical hypoechoic halo, metastases have varied ultrasound appearances, just as in CT images [23]. The ultrasound diagnosis may be difficult, especially when calcification in metastases leads to acoustic shadowing. Even though they are quite rare, slowly enlarging mucinous metastases (i.e. those from colon carcinomas) may become very calcified (⬋ in **Fig. 122.5**).

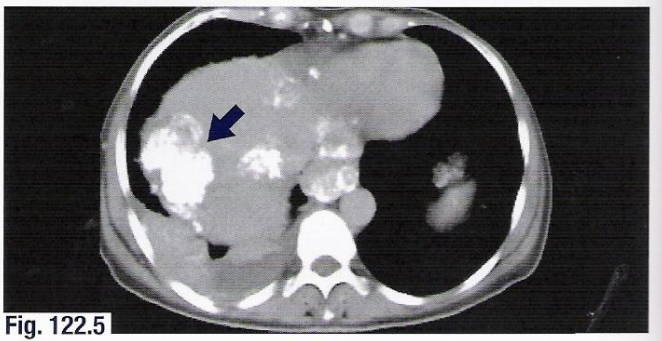

Fig. 122.5

Solid Hepatic Lesions

A hemangioma is the most common benign hepatic lesion. In unenhanced images small hemangioma are well-defined homogeneous areas of decreased attenuation. After injection of CM, enhancement typically begins in the periphery and progresses toward the center of the hemangioma **(Fig. 123.1a)**, reminiscent of the closing of an optic diaphragm. In dynamic bolus-enhanced CT sequences, enhancement progresses centripetally. Following administration of a CM bolus, a series of CT images is acquired every few seconds at the same location. Accumulation of CM within the cavities of the hemangioma (↘) leads to homogeneous enhancement in the late venous phase **(Fig. 123.1b)**. In large hemangiomas, this might take several minutes or be inhomogeneous.

Fig. 123.1a

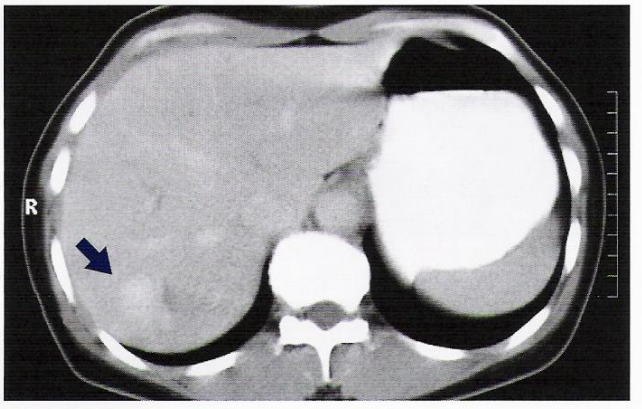

Fig. 123.1b

Hepatic adenoma (↘) occurs most frequently in women between the ages of 20 and 60 years who have a long history of taking oral contraceptives. An adenoma originates in hepatocytes and may be solitary or multiple. The adenoma is usually isodense, sometimes hypervascular **(Fig. 123.2)**, and may be accompanied by hypodense infarction, central necrosis, and/or spontaneous hyperdense hemorrhage. Surgical excision is recommended due to the possibility of acute hemorrhage and malignant degeneration. By contrast, focal nodular hyperplasia (FNH) does not show any tendency of malignant degeneration, and lesions of this kind contain biliary ducts. On unenhanced images, FNH appears as hypodense, sometimes isodense, but well-defined lesions. After i.v. CM, FNH often demonstrates an irregularly shaped, hypodense central area (*) representing its central blood supply; however this feature is seen in only 50% of all FNH **(Fig. 123.3)**.

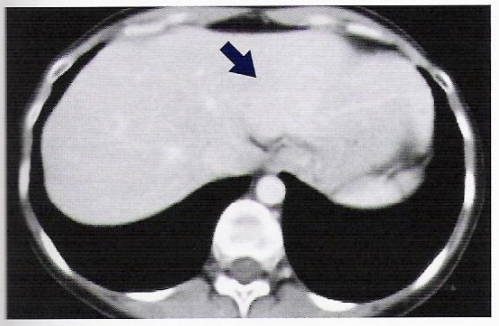

Fig. 123.2

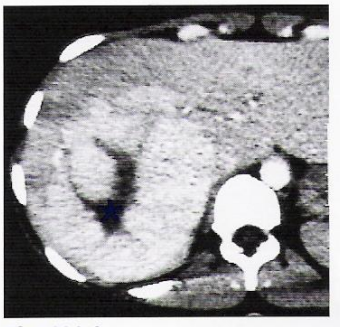

Fig. 123.3

Fig. 123.4

Hepatocellular carcinoma (HCC) often occurs in patients who have a long history of hepatic cirrhosis and is seen most often in men over the age of 40 years. In one-third of all cases, HCC is solitary although multifocal lesions are not rare. Thromboses in the branches of the portal vein caused by tumor invasion into the lumen of the vessel may be seen in one-third of cases. The CT appearance of HCC **(Fig. 123.4)** is extremely variable. On unenhanced images, HCC usually appears hypodense or isodense; CM may show diffuse or rim enhancement and central necrosis. When there is also cirrhosis, it may be difficult to define the border of an HCC.
Secondary lymphoma should be considered in the DD because it may infiltrate the liver parenchyma and may be the cause of diffuse hepatomegaly. Of course, this does not mean that every case of hepatomegaly is due to a lymphoma. Non-Hodgkin's lymphomas resemble HCC because of their similarities in vascularity and nodular growth.

Diffuse Hepatic Lesions

In fatty changes of the liver, the density of the unenhanced parenchyma, which is normally about 65 HU, may reduce so that it is either isodense or even hypodense with regard to the blood vessels (**Fig. 124.1**; cf. also p. 120). In hemochromatosis **(Fig. 124.2)**, the accumulation of iron leads to increased attenuation above 90 HU and may reach as much as 140 HU. In these cases, the natural contrast between parenchyma and vessels is even greater. Cirrhosis **(Fig. 124.3)**, resulting from chronic liver damage, has a diffuse nodular appearance and usually gives the organ an irregular, lumpy contour.

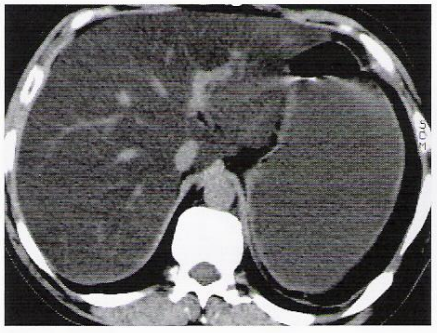

Fig. 124.1

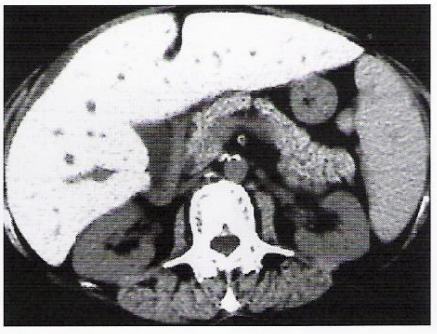

Fig. 124.2

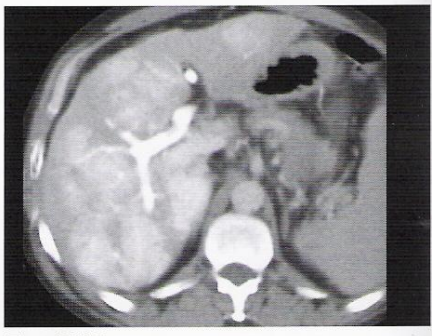

Fig. 124.3

Biliary Tract

After surgical choledochoenteric anastomosis, sphincterotomy, or endoscopic retrograde cholangiopancreatography (ERCP), hypodense gas (➡) is usually present within the intrahepatic bile ducts **(Fig. 124.4)**. These causes of biliary gas must be differentiated from gas-forming anaerobic bacteria within an abscess.

Dilatation of the intrahepatic biliary tract **(128)** is called cholestasis **(Fig. 124.5)**. It may result from gallstones, a malignant obstruction of the biliary tract, or from a pancreatic carcinoma at Vater's ampulla. In **Figure 124.5**, note the calcification **(174)** of the tortuous splenic artery **(99)** and the hepatic metastases **(7)**. These poorly defined and only slightly hypodense metastases must be differentiated from artifacts **(3)** arising from the ribs adjacent to the liver **(122)** and spleen **(133)**. These beam-hardening artifacts result from the abrupt changes in attenuation between the viscera and the rib **(51)**.

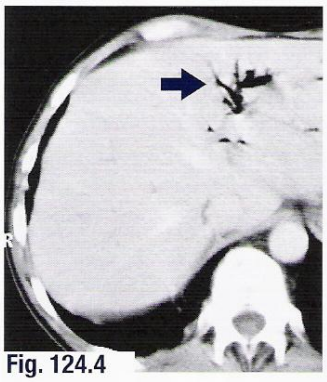

Fig. 124.4

Fig. 124.5a

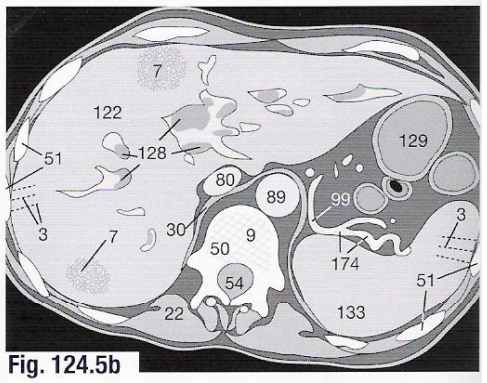

Fig. 124.5b

If it is not possible to treat the cause of cholestasis surgically, inserting a stent (**182** in **Fig. 124.6**) may decompress an obstructed biliary duct **(128)**.

Fig. 124.6a

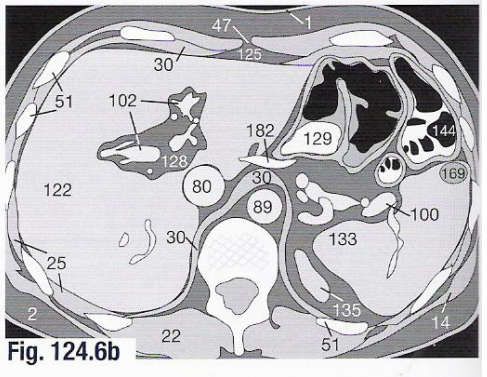

Fig. 124.6b

The size and shape of the gallbladder vary depending on when the patient last ate food. A hydrops of the gallbladder should only be diagnosed if there is very marked dilatation, that is if the diameter exceeds 5 cm in several transverse planes. The attenuation of bile is usually just greater than that of water (0 HU) but may increase to up to 25 HU if the bile is highly concentrated [4].

Cholecystolithiasis

Stones **(167)** within the gallbladder **(126)** may show different patterns of calcification **(Fig. 125.1)**. Cup-shaped and ring-like calcifications can be seen in stones containing cholesterol and bilirubin **(Fig. 125.2)**. If stones obstruct gallbladder drainage or inflammation has caused stenosis, sludge may form resulting in increased attenuation and sedimentation of bile **(Fig. 125.3)**. Common duct stones should be diagnosed using thin-section CT because smaller stones might be missed in standard thickness sections.

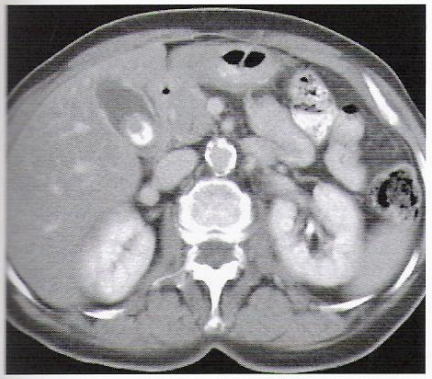

Fig. 125.1a

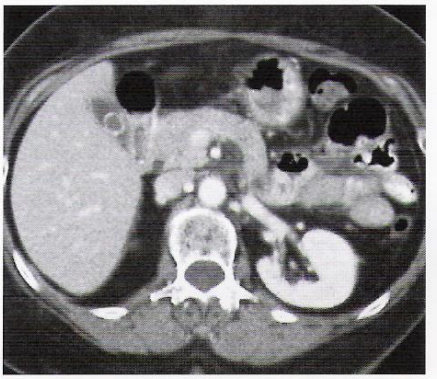

Fig. 125.2a

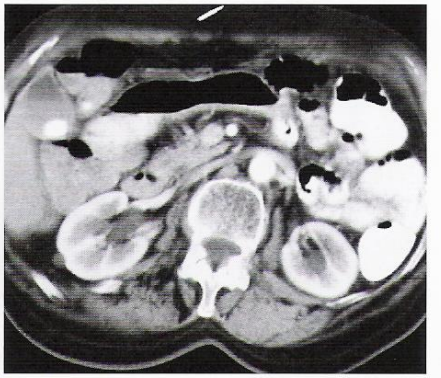

Fig. 125.3a

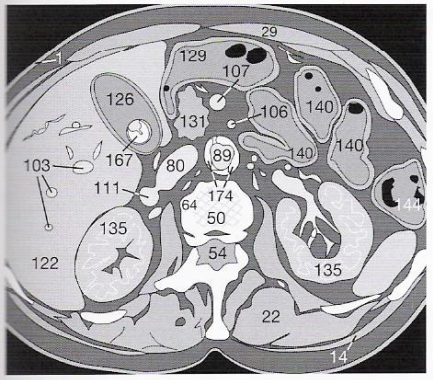

Fig. 125.1b

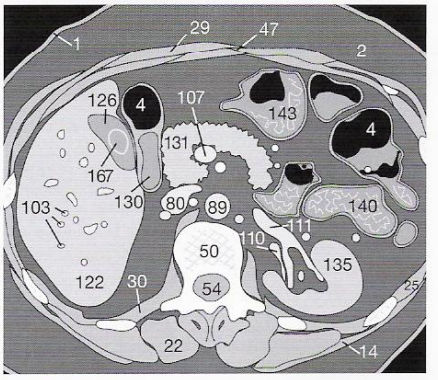

Fig. 125.2b

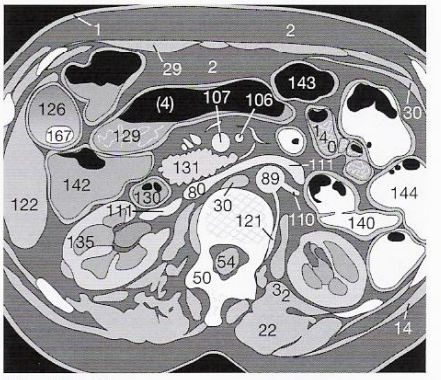

Fig. 125.3b

Chronic Inflammatory Lesions

Cholecystolithiasis can lead to chronic inflammation, resulting in a stone-filled, shrunken gallbladder, acute cholecystitis, or an empyema of the gallbladder (recognized by an irregularly thickened wall) (↖ ↗ in **Fig. 125.4**). There is an increased risk of malignant change with chronic inflammatory processes [24]. The development of a porcelain gallbladder **(Fig. 125.5)** with an egg-shell-like pattern of calcification **(174)** may be a premalignant lesion.

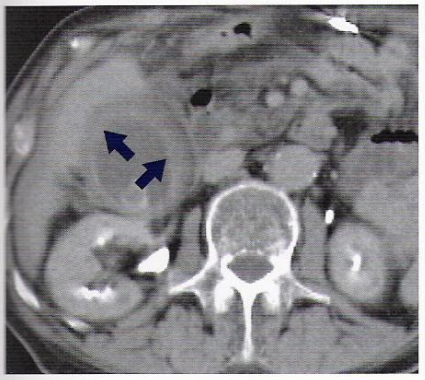

Fig. 125.4

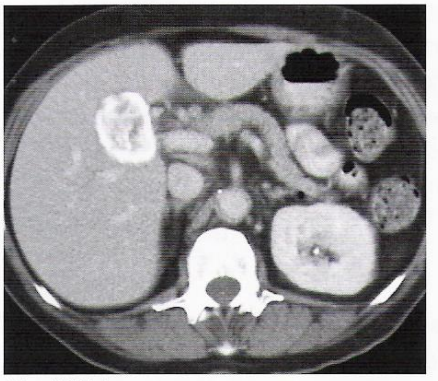

Fig. 125.5a

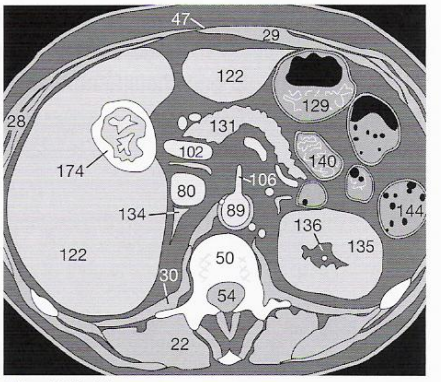

Fig. 125.5b

Contrast Enhancement

Before reading further, try to define a characteristic feature of the spleen by looking at **Figure 126.1a**. The normal splenic parenchyma **(133)** has an attenuation of approximately 45 HU on unenhanced images. The attenuation of the spleen will only appear homogeneous in an unenhanced image or in the late venous phase of an enhanced study **(Fig. 126.1c)**. In the early arterial phase **(Fig. 126.1a)**, it will enhance heterogeneously and appear patchy or marbled, a pattern representing its trabecular architecture. This pattern should not be misinterpreted as an abnormality. Note also the uneven distribution of CM within the inferior vena cava **(80)** and the two (!) hepatic metastases **(7)** in the same image **(Fig. 126.1a)**. Did you spot the areas of near-water attenuation representing perisplenic/perihepatic ascites **(8)**?

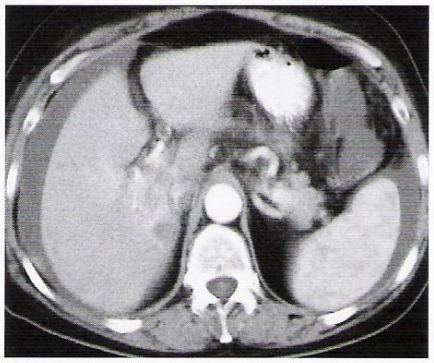

Fig. 126.1a

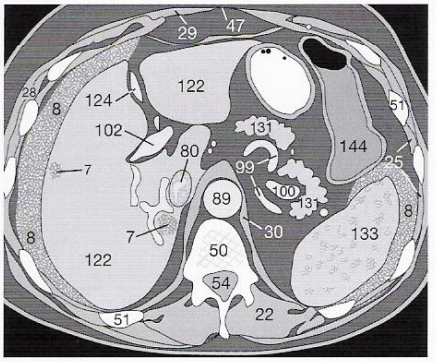

Fig. 126.1b

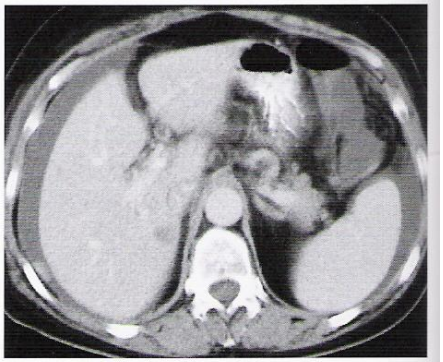

Fig. 126.1c

The splenic artery **(99)** is typically elongated and tortuous so that it may be imaged in several consecutive slices. In elderly patients, it is common to see atherosclerotic plaques (**174** in **Fig. 126.2**). Occasionally, a homogeneous splenunculus [accessory spleen ↗], well demonstrated in the surrounding fat, may be seen at the hilum or the inferior pole of the spleen **(Fig. 126.3)**. Differentiating between a splenunculus and an abnormally enlarged LN may be difficult.

Fig. 126.2a

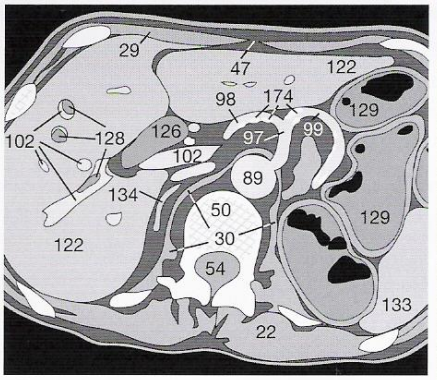

Fig. 126.2b

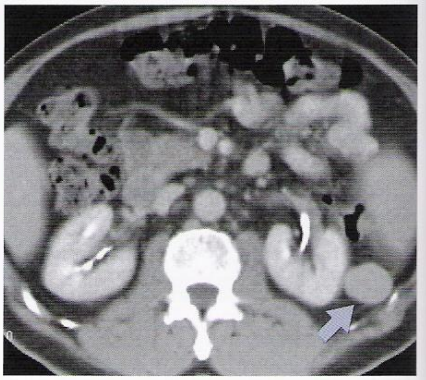

Fig. 126.3

Splenomegaly

Diffuse enlargement of the spleen **(Fig. 127.1)** may be caused by several conditions: portal hypertension, leukemia/lymphoma, myelofibrosis and hemolytic anemia, or by various storage diseases. Assessment of splenic size is made difficult by individual variations in shape. Marked splenomegaly is easily recognized, but in borderline cases of splenomegaly and for follow-up one should know the normal range of splenic size. In the transverse plane, the length of the spleen (⁞) should measure no more than 10 cm (dotted line) and its width (**d**, at right angle to the dotted line) should not exceed 5 cm **(Fig. 126.4)**.

In ultrasound, the spleen is not measured in a transverse plane but in an oblique plane parallel to the intercostal space. In this plane, the upper limit of normal is 11 cm for the long axis [28].

The craniocaudal dimension of the spleen should not exceed 15 cm, so that at a slice thickness of 1 cm it should not be visible on more than 15 sections. Splenomegaly is diagnosed if at least two of these three parameters are exceeded.

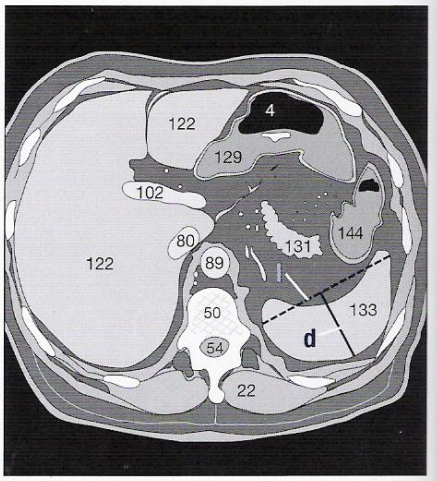

Fig. 126.4

As splenomegaly develops, the typical normal crescentic shape is lost **(Fig. 127.1)**. Gross splenomegaly, which may be caused by chronic lymphocytic leukemia, acts as a space-occupying mass and displaces adjacent organs. In **Figure 127.1**, the left kidney is compressed (⇩). If the blood supply cannot keep pace with splenic growth, infarctions (⬋) may result. These appear as hypodense areas that do not enhance with CM **(Fig. 127.2)**.

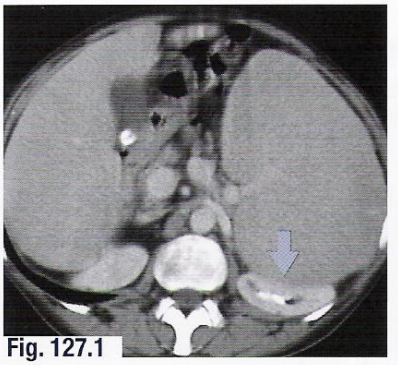
Fig. 127.1

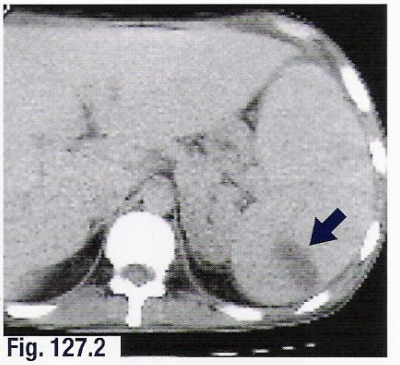
Fig. 127.2

Focal Splenic Lesions

Splenic cysts share the same characteristics of hepatic cysts (cf. p.121). Metastases in the spleen **(7)** are rare and difficult to distinguish from cysts. In the case illustrated in **Figure 127.3**, the diagnosis of splenic metastases was relatively easy because there were hepatic lesions and malignant ascites **(8)**. If there are multifocal lesions with inhomogeneous CM enhancement, a diagnosis of focal splenic lymphoma or splenic candidiasis should be considered. Ascites **(8)** may accompany candidiasis, as shown in **Figure 127.4**. Splenic lymphoma is usually characterized by diffuse infiltration and the spleen may appear normal.

The examination of the spleen **(133)** after a blunt thoracic or abdominal trauma must be meticulous. Lacerations of the parenchyma **(181)** may lead to hematomas **(8)** beneath the capsule, and delayed rupture of the capsule may cause massive hemorrhage into the abdominal cavity **(Fig. 127.5)**.

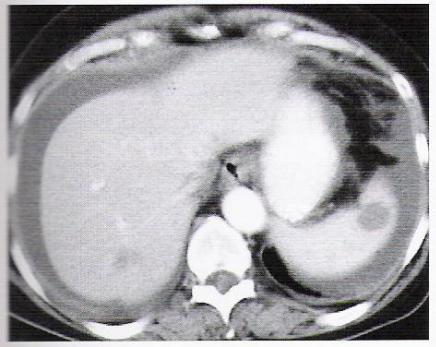
Fig. 127.3a

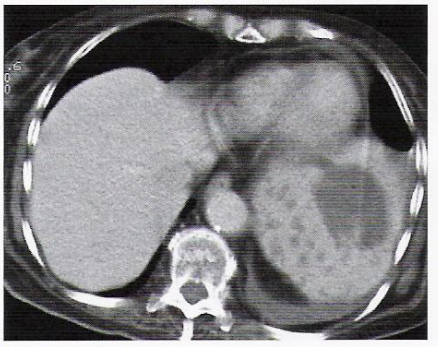
Fig. 127.4a

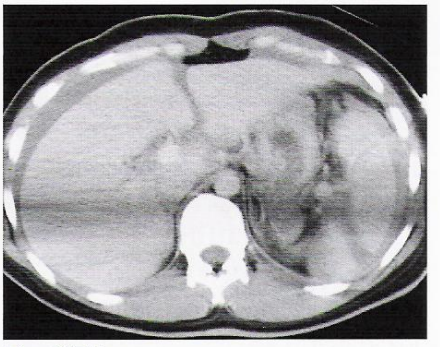
Fig. 127.5a

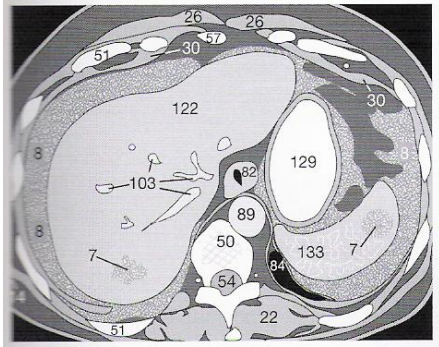

Fig. 127.3b

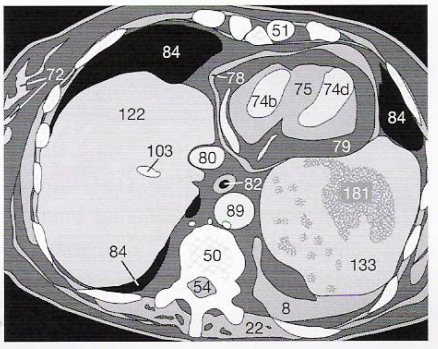

Fig. 127.4b

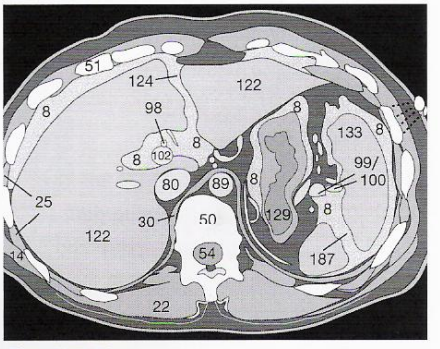

Fig. 127.5b

The remnants of smaller hematomas may present as subcapsular (⬈) or parenchymal (⬆) calcifications **(Fig. 127.6)**.

Septations within splenic cystic lesions **(Fig. 127.7)** are strongly suggestive of echinococcosis, and appear quite similar to those in the liver. In most cases the liver is also affected (cf. p.121).

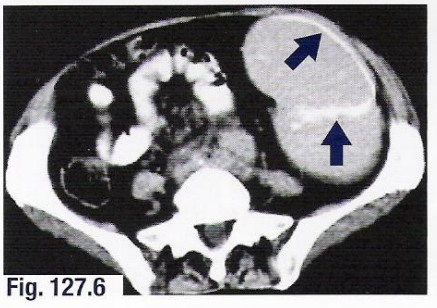
Fig. 127.6

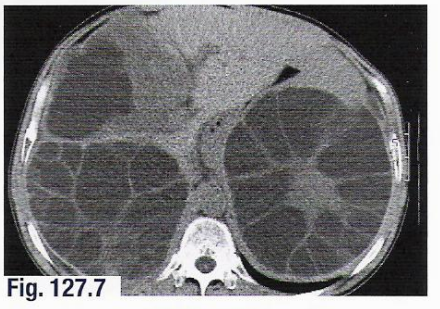
Fig. 127.7

Acute and Chronic Pancreatitis

Acute pancreatitis may present as edematous interstitial pancreatitis **(Fig. 128.1)**. Hypodense peripancreatic fluid (exudate) **(8)** and edema of the connective tissue **(185)** are frequent findings. CT shows blurring of the pancreatic contours; the normally lobular pattern of the pancreas is effaced (**Figs. 128.1** and **128.2**). In hemorrhagic necrotizing pancreatitis **(Fig. 128.2)**, the extent of necrosis is a prognostic feature.

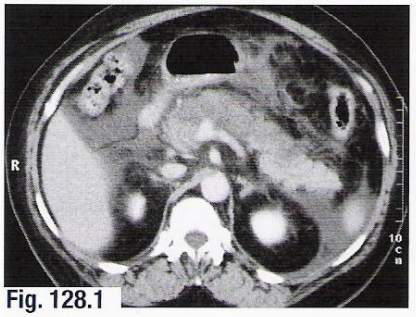

Fig. 128.1

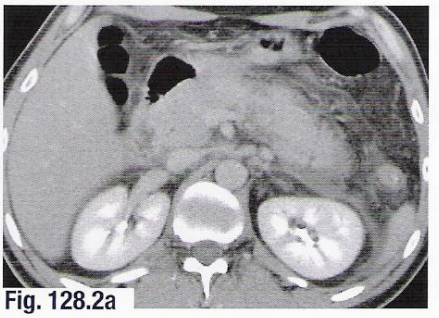
Fig. 128.2a

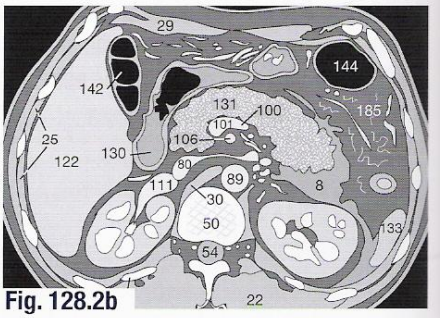

Fig. 128.2b

Chronic pancreatitis progresses either slowly and progressively or in recurrent episodes. The two most common causes of chronic pancreatitis are alcohol abuse and cholelithiasis.

Typical findings in chronic pancreatitis are fibrosis and multifocal calcifications **(174)**, irregular dilatation of the pancreatic duct **(132)**, and sometimes the formation of pseudocysts **(169)** within, or next to, the pancreas **(131)** (**Figs. 128.3** and **128.4**). The disease may lead to pancreatic atrophy as a late feature. The possibility that pancreatic carcinoma develops in association with chronic calcific pancreatitis is presently being discussed.

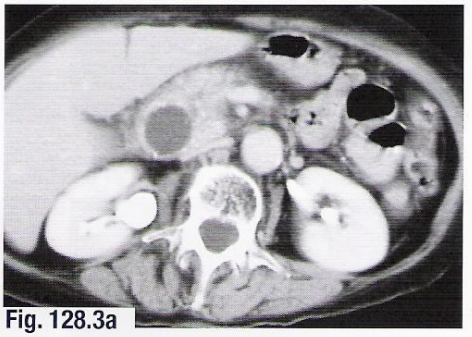
Fig. 128.3a

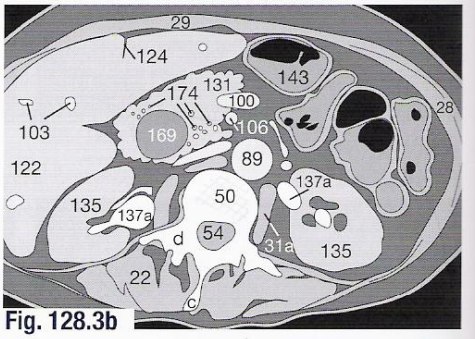

Fig. 128.3b

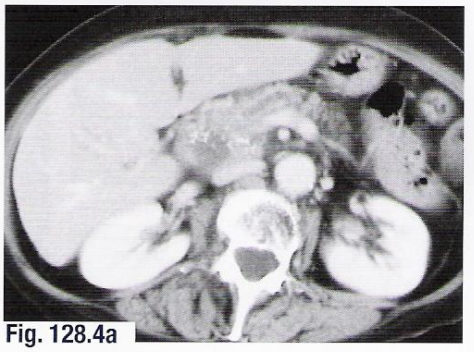
Fig. 128.4a

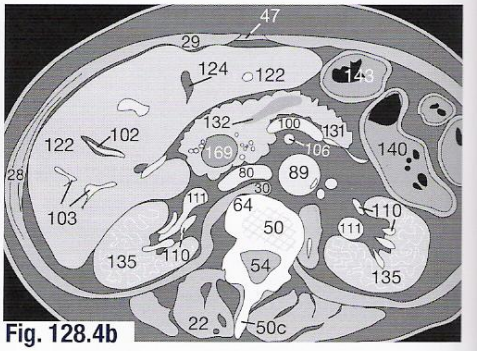

Fig. 128.4b

Pancreatic Neoplasms

Most pancreatic carcinomas **(7)** are located within the head of the pancreas **(131)**. As a result, even small tumors may cause cholestasis by obstructing the common bile duct **(127) (Fig. 128.5)**. Pancreatic carcinomas tend to metastasize very early to the liver and the regional LNs. In case of doubt, ERCP should be carried out to image the pancreatic and common bile ducts. Islet cell tumors, 75% of which are functional, are located within the body of the pancreas. The Zollinger-Ellison syndrome **(Fig. 128.6)** is caused by a gastrin-secreting tumor (⬋). Other neoplasms associated with the pancreas are insulinomas, glucagonomas, and serotonin-producing masses.

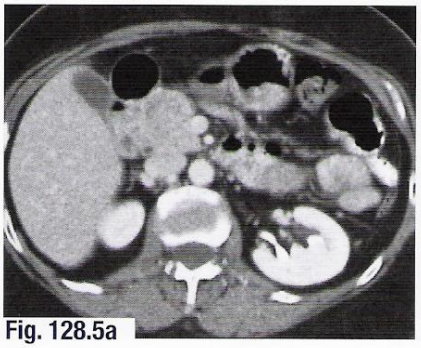
Fig. 128.5a

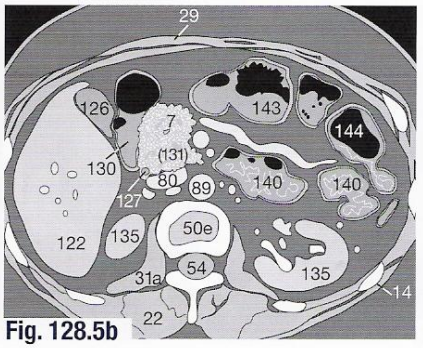

Fig. 128.5b

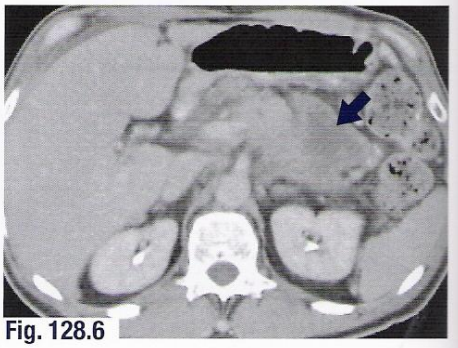
Fig. 128.6

The normal position and shape of the adrenal glands has been described on pages 105 to 106. The maximum lengths of the adrenal glands range between 2.1 and 2.7 cm, the right adrenal often being somewhat longer than the left. The thickness of the limbs should not exceed 5 to 8 mm in the transverse plane. A fusiform or nodular thickening **(7)** is likely to be abnormal in CT, and is usually indicative of hyperplasia or an adenoma of the adrenal gland (**134** in **Fig. 130.1**). Typically, the adrenals can be clearly differentiated from adjacent fat, the diaphragm **(30)**, the kidney **(135)**, the liver **(122)**, and the inferior vena cava **(80)**.

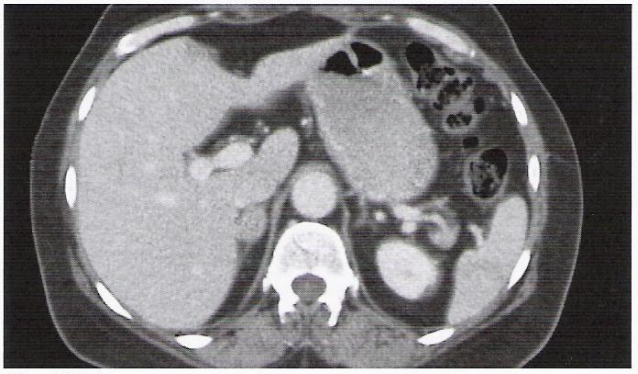

Fig. 130.1a

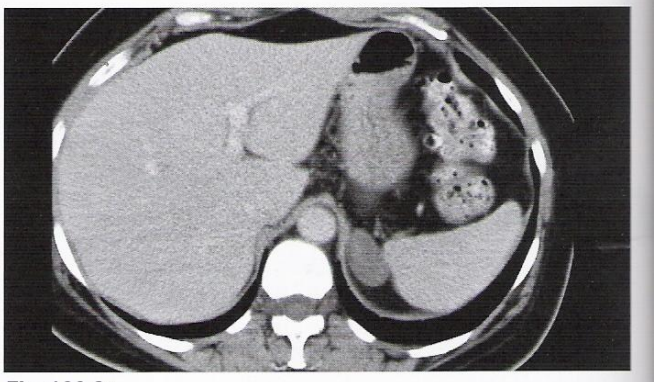

Fig. 130.2a

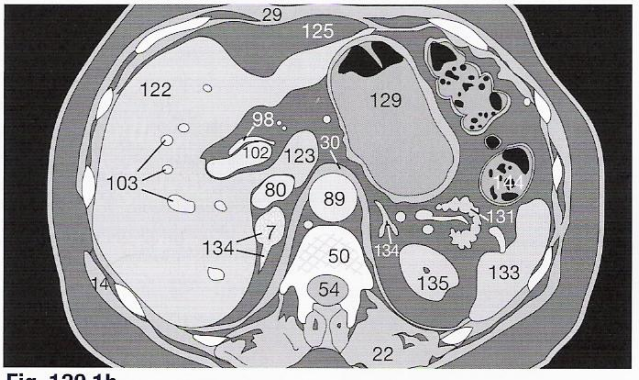

Fig. 130.1b

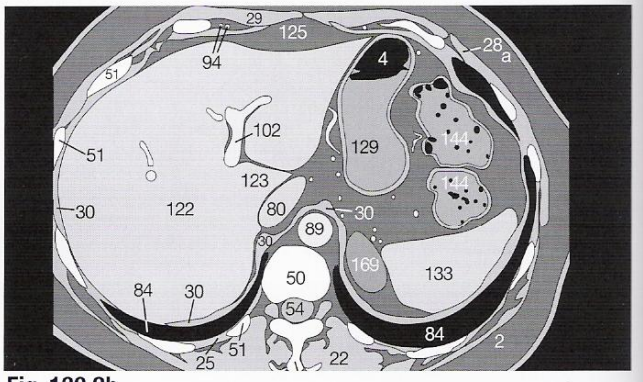

Fig. 130.2b

The following conditions may be dignosed according to the specific hormonal excess: congenital adrenal cortical hyperplasia (androgens), Conn's syndrome (aldosterone), and Cushing's syndrome (cortisone). An upper pole renal cyst **(Fig. 130.2)** or a renal angiomyolipoma (cf. **Fig. 134.4**) must be included in the DD. Attenuation values for benign cysts **(169)** should lie close to those for water (= –1 HU in the present case) **(Fig. 130.2)**. (Compare with cysts on p. 133.)

In cases of heterogeneous enlargement of the adrenal gland or infiltration of adjacent organs, a metastasis or a carcinoma **(Fig. 130.3)** must be suspected. Since bronchogenic carcinomas often metastasize to the liver and the adrenals, staging chest CT studies for lung cancer should be extended to include the caudal margin of the liver and the adrenals. Tumors of the paravertebral sympathetic trunks, which are located close to the adrenal glands, may also be detected, but they are rare. The MRI images in **Figures 130.4a** and **130.4b** show a neuroblastoma (➡) in the sagittal **(a)** and coronal **(b)** planes.

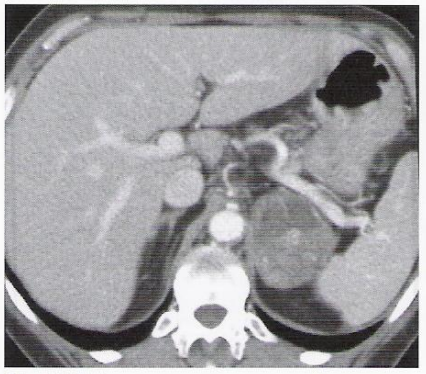

Fig. 130.3

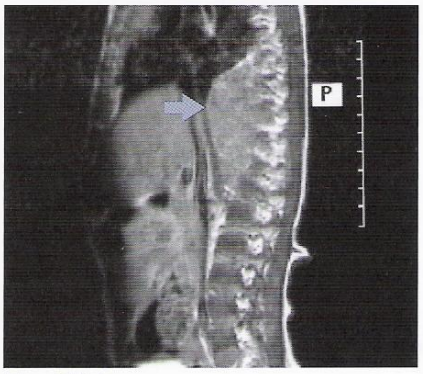

Fig. 130.4a

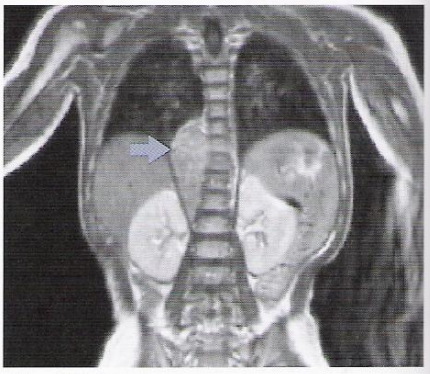

Fig. 130.4b

Whenever doubt exists whether an enlarged adrenal gland represents a benign process, densitometry (see pages 121 and 131) with determination of the enhancement pattern should be considered: benign adenomas of the adrenal gland show a tendency of a considerably more rapid wash-out of the contrast enhancement than malignant lesions, such as metastases and adrenal gland carcinomas **(Fig. 131.1)**. This method requires an additional scan at the level of the adrenal glands after 3, 10, or 30 minutes.

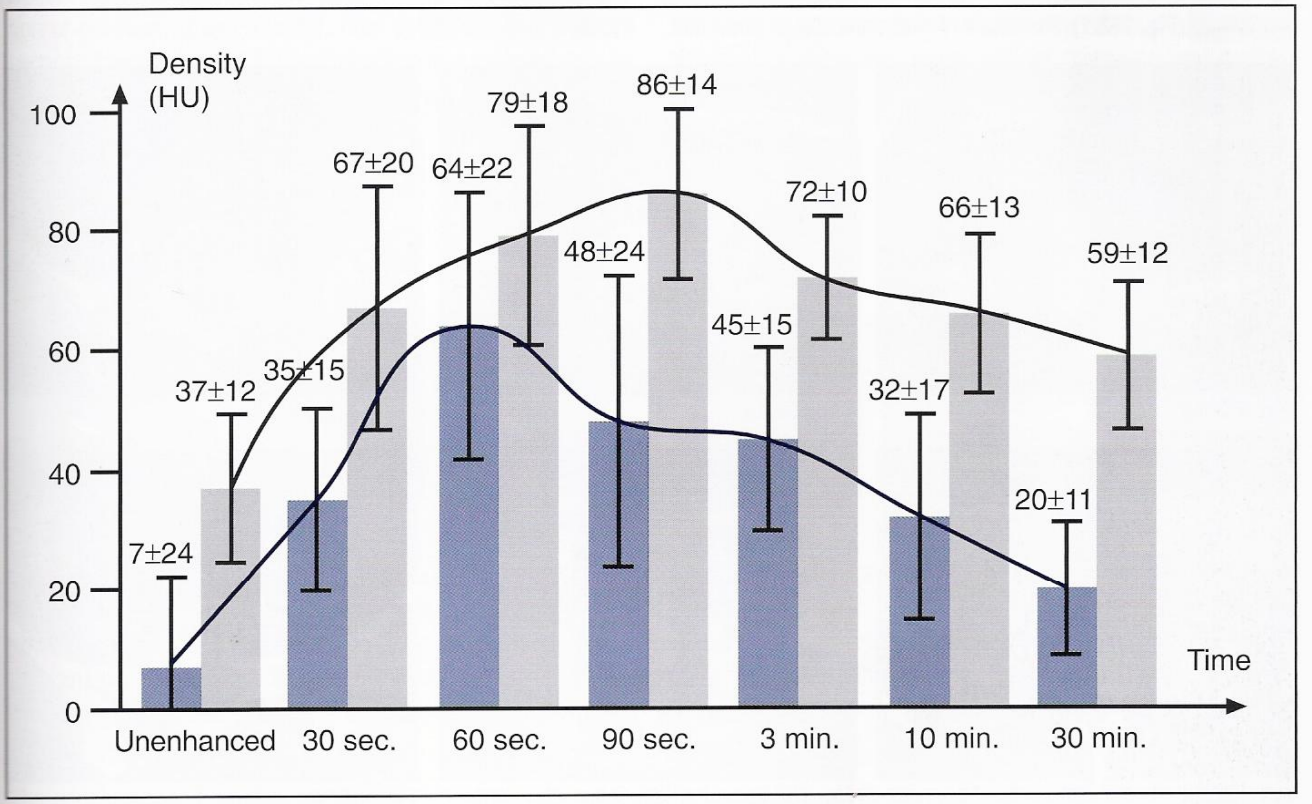

Fig. 131.1 Rapid wash-out of contrast medium in benign adrenal glands adenomas (blue) in comparison with non-adenomas (gray)

Malignant tumors of the adrenal gland tend to have a prolonged contrast enhancement. This difference can be applied to the differential diagnosis. The dynamic enhancement pattern in the adrenal glands has been extensively investigated in numerous studies, which revealed further differences in absolute and relative wash-out of the peak contrast enhancement. This wash-out pattern, however, shows a certain overlap between the tumor types, and therefore the assessment has been proven useful only when applying the following parameters [42]:

Densitometry in the DD of space-occupying lesions of the adrenal glands

Unenhanced:	< 11 HU	=>	Adenoma
10 min. after injection of contrast medium:	< 45 HU	=>	Adenoma
30 min. after injection of contrast medium:	< 35 HU	=>	Adenoma

For these three values, the range of the histograms or so-called box-whisker plots of **Fig. 131.1** does not overlap for both tumor types, and a benign tumor of the adrenal glands can be safely assumed if the measured density values fall below these values. In all other cases, a benign adenoma cannot be assumed with acceptable degree of sensitivity and specificity and further evaluation is recommended.

Congenital Variations

The attenuation of the renal parenchyma **(135)** on unenhanced images is approximately 30 HU. The kidneys occasionally develop to different sizes. If the outlines are smooth and the parenchymal thickness is not irregular, it is likely to represent unilateral renal hypoplasia **(Fig. 132.1)**. The smaller kidney need not be abnormal.

A kidney may have an atypical orientation as in **Figure 132.2**. However, if a kidney lies in the iliac fossa **(Fig. 132.3)**, this does not indicate an ectopic location, but a renal transplant **(135)**. The organ is connected to the iliac vessels **(113/116)** and the urinary bladder **(138)**.

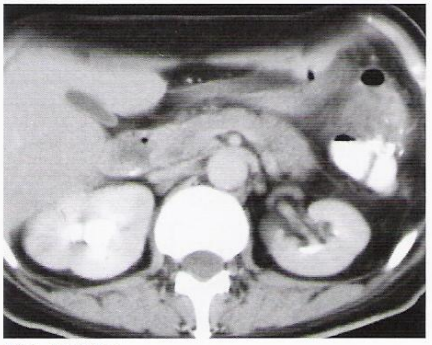

Fig. 132.1a

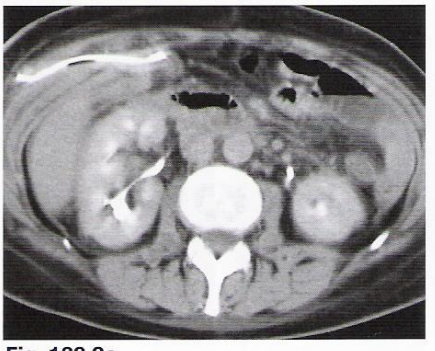

Fig. 132.2a

Fig. 132.3a

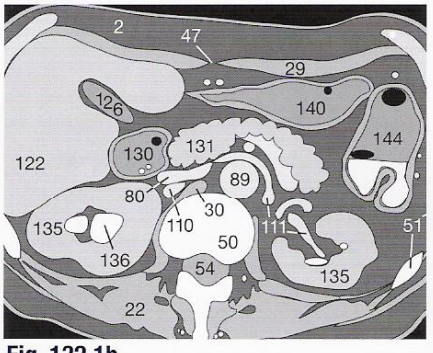

Fig. 132.1b

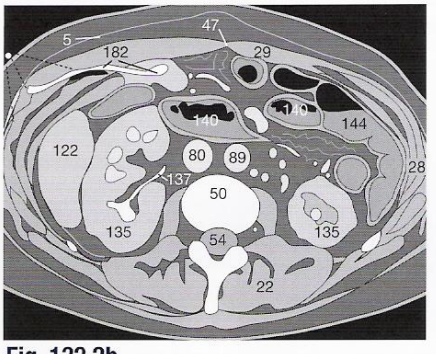

Fig. 132.2b

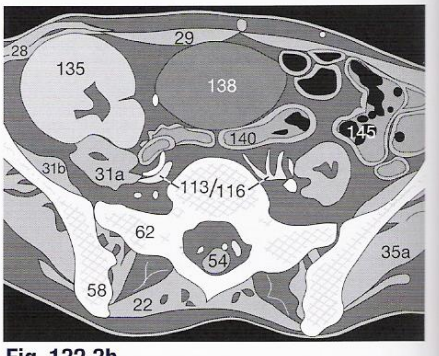

Fig. 132.3b

Marked differences in size, as in **Figure 132.2**, may indicate partial or complete renal duplication on one side. The positions and number of renal arteries may vary considerably (**110** in **Fig. 132.1b**). The renal arteries must be examined carefully for evidence of stenosis as a cause of renal hypertension. The ureter (**137** ➡) can be present as a partial or complete duplex ureter **(Fig. 132.4)**. In complete renal duplication, the renal pelvis is also duplicated.

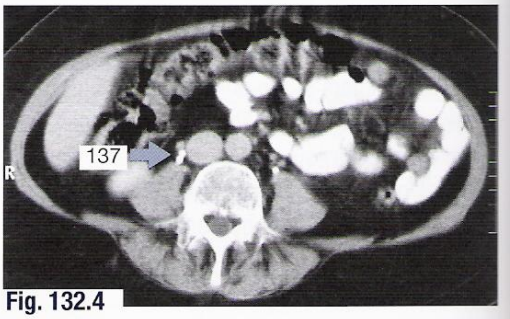

Fig. 132.4

Occasionally, the low-density fat in the hilum (✱ in **Fig. 132.5b**) is only poorly demarcated from the renal parenchyma **(135)** owing to a beam-hardening artifact or partial volume averaging **(Fig. 132.5a)**. This gives the incorrect impression of a renal tumor. Comparison with an immediately adjacent section **(Fig. 132.5c)** demonstrates that only hilar fat was present. The actual tumor in this particular example **(7)** is situated at the posterior margin of the right lobe of the liver **(122)**.

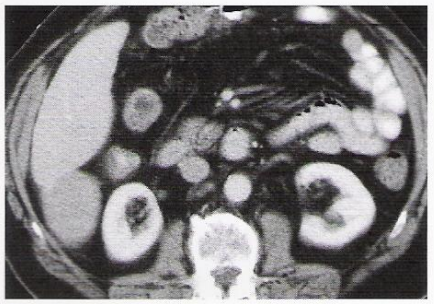

Fig. 132.5a

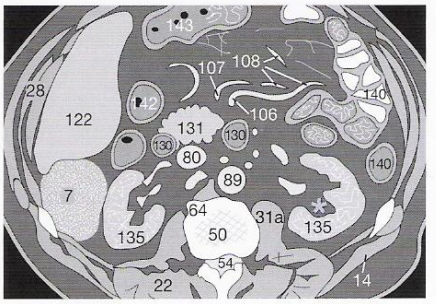

Fig. 132.5b

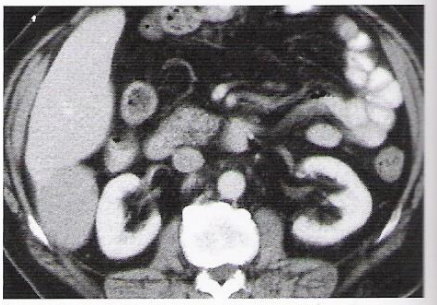

Fig. 132.5c

Cysts

Renal cysts are frequent incidental findings in adults and may be located anywhere in the parenchyma. They may be exophytic or parapelvic, in which case they can resemble a hydronephrosis. Benign cysts contain a serous, usually clear liquid with an attenuation of between –5 and +15 HU. They do not enhance with CM because they are avascular. The attenuation measurement may be inaccurate if there are partial volume averaging artifacts due to slice thickness (**Fig. 133.1**: ~ 25 HU) or to eccentric positioning of the ROI (**Fig. 133.2**: ~ 22 HU) (cf. pp. 15 and 121). Only the correct positioning of the ROI in the center of the cyst (○ in **Fig. 133.3**) will provide an accurate average of 10 HU. In rare cases, hemorrhage into benign cysts will result in hyperdense values on unenhanced images. The attenuation values will not change on post-contrast images.

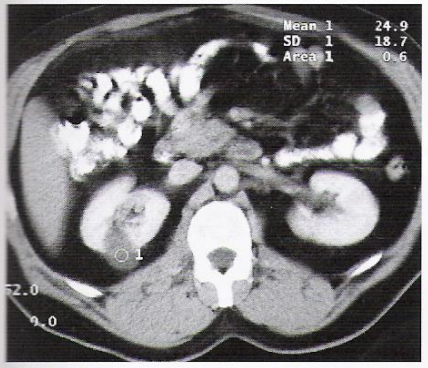

Fig. 133.1

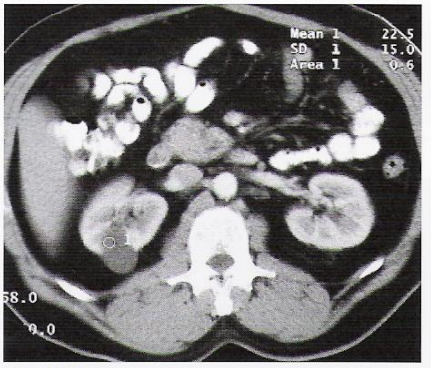

Fig. 133.2

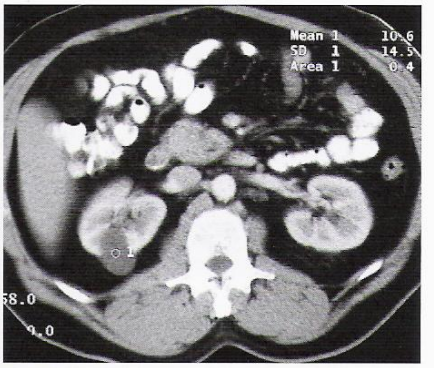

Fig. 133.3

Increased density or calcifications in a mass may indicate past renal tuberculosis, current Echinococcus infestation (hydatid disease), or a cystic renal cell carcinoma. The difference between pre- and post-contrast images also provides information on renal function: after approximately 30 seconds the well-perfused renal cortex is the first part of the kidney to accumulate the CM (cf. **Figs. 133.2** and **133.3**). After another 30 to 60 seconds the CM is excreted into the more distal tubules leading to enhancement of the medulla. The result is homogeneous enhancement of the renal parenchyma (cf. **Fig. 133.1**).

The appearances of multiple renal cysts in children with congenital autosomal recessive polycystic kidney disease are dramatically different from those of the occasional cysts found in adults, which are generally incidental findings. Polycystic kidney disease in the adult (**169** in **Fig. 133.4**) is autosomal dominant and associated with multiple cysts of the liver, the bile ducts and, more rarely, with cysts in the pancreas or with abdominal or cerebral aneurysms.

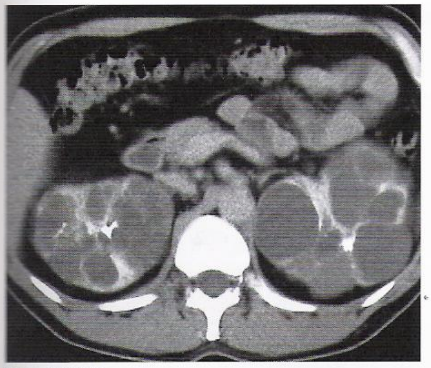
Fig. 133.4a

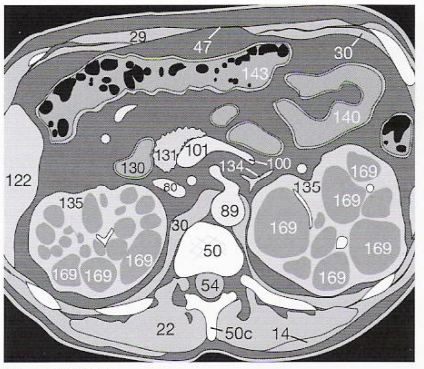

Fig. 133.4b

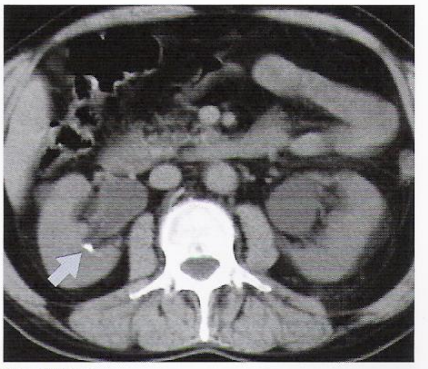
Fig. 133.5

Hydronephrosis

Parapelvic cysts may be confused with grade 1 hydronephrosis **(Fig. 133.5)**, which is characterized in the unenhanced image by a dilated renal pelvis and ureter. In grade 2 hydronephrosis, the renal calyces become poorly defined. When parenchymal atrophy ensues, the hydronephrosis is categorized as grade 3 (see p. 134). Since no CM had been given to the patient in **Figure 133.5**, the hyperdense lesion ( ) in the right kidney must be a renal calculus.

For the diagnosis of nephrolithiasis alone, CT should be avoided because of undue radiation exposure (ref. p. 174ff.). Sonography is the method of choice for nephrolithiasis as well as hydronephrosis.

Hydronephrosis, which causes dilatation of the ureter **(137)** and the renal pelvis **(136)**, impairs renal function **(Fig. 134.1)**. In this image, the left renal parenchyma **(135)** shows delayed and reduced CM enhancement as compared with the normal right kidney.

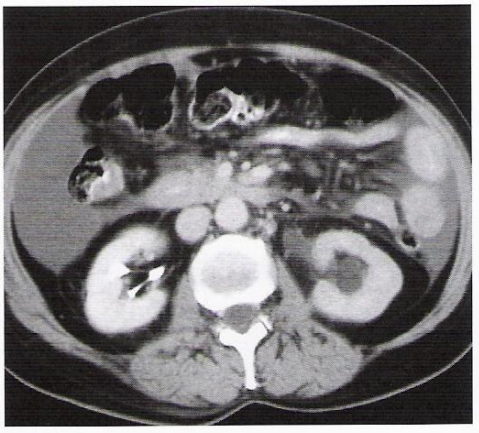

Fig. 134.1a

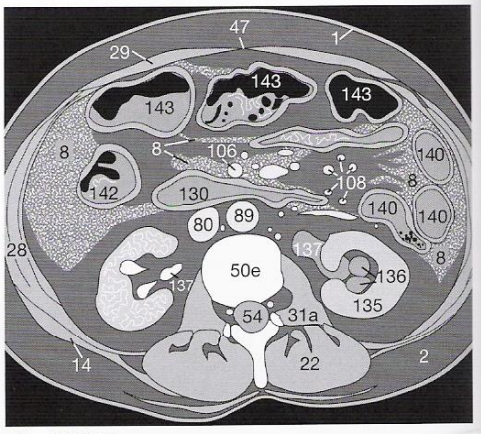

Fig. 134.1b

Chronic grade 3 hydronephrosis reduces the parenchyma to a narrow rim of tissue **(Fig. 134.2)**, resulting finally in atrophy and a non-functioning kidney. In cases of doubt, identifying the dilated ureter (↘ in **Fig. 134.2b**) can resolve the DD between a parapelvic cyst and hydronephrosis. CM accumulates in a dilated renal pelvis, but not in a cyst.

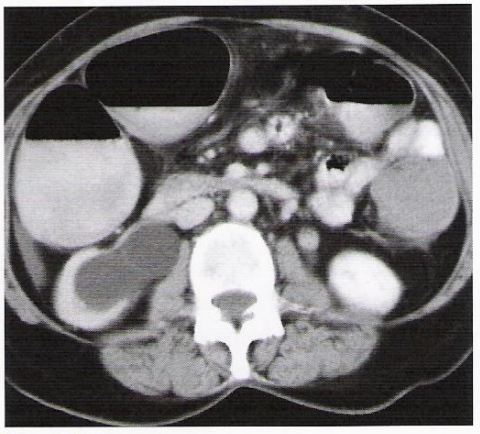

Fig. 134.2a

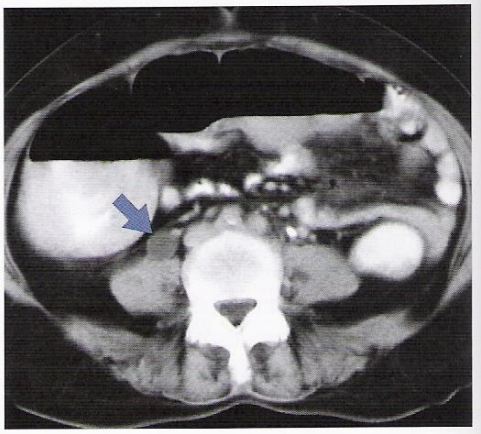

Fig. 134.2b

Solid Tumors

Enhancement with CM often helps to distinguish between partial volume averaging of benign renal cysts and hypodense renal tumors, since CT morphology alone does not provide sufficient information about the etiology of a lesion. This is especially so when a mass (✱) is poorly defined within the parenchyma **(Fig. 134.3)**. Inhomogeneous enhancement, infiltration of adjacent structures, and invasion of the pelvis or the renal vein are criteria of malignancy.

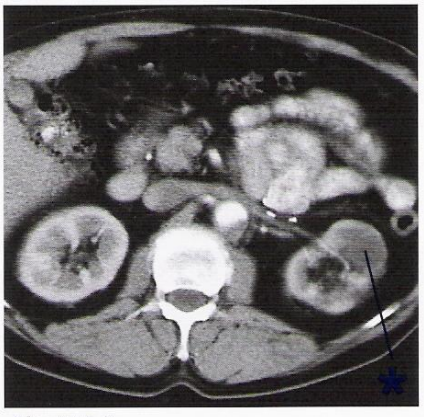

Fig. 134.3

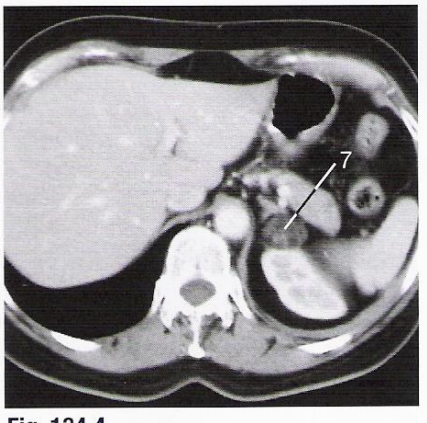

Fig. 134.4

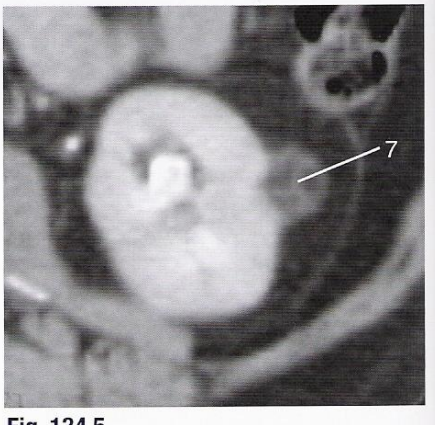

Fig. 134.5

However, when a mass consists not only of solid, inhomogeneous areas, but also contains fat, an angiomyolipoma **(7)** must be considered (**Figs. 134.4** and **134.5**). These benign hamartomas contain fat, atypical muscle fibers, and blood vessels. The vessel walls are abnormal, and the complication of intratumoral or retroperitoneal hemorrhage may occur (not depicted here).

Kidney Problems Related to Blood Vessels

If ultrasound shows fresh hemorrhage into the abdomen after penetration or blunt trauma, the source of bleeding must be located as soon as possible. The DD must include not only splenic rupture or major vessel disruption but also renal injury. On unenhanced images of a renal rupture (**Figs. 135.1a** and **135.1b**), the contours of the kidney **(135)** appear blurred, and depending on the extent of hemorrhage, hyperdense fresh hematoma **(8)** can be detected in the retroperitoneal spaces. In this case, enhanced images (**Figs. 135.1c** and **135.1b**) show that the renal parenchyma **(135)** is still well perfused and function is maintained.

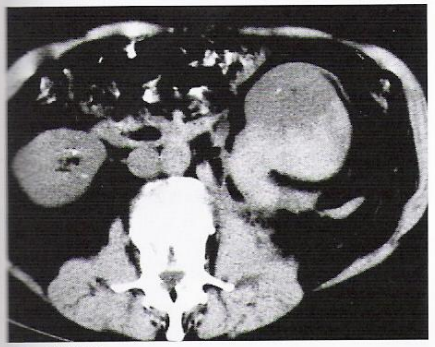

Fig. 135.1a

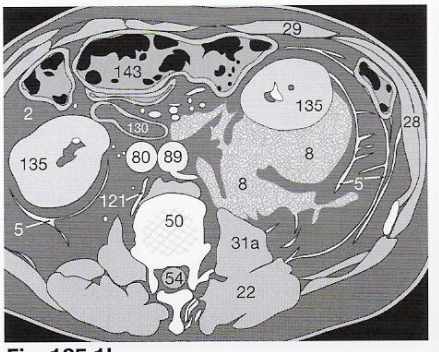

Fig. 135.1b

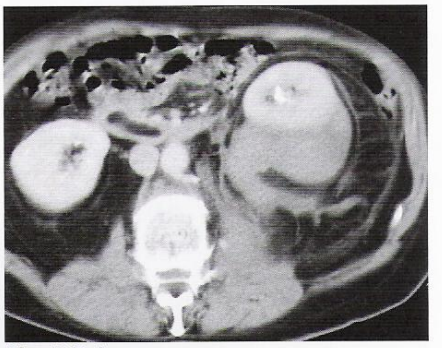

Fig. 135.1c

After **e**xtracorporeal **s**hock-**w**ave **l**ithotripsy (ESWL), renal injuries may rarely occur that lead to small hematomas or extravasation of urine from the ureter. If there is hematuria or persisting pain after ESWL, it is essential to obtain delayed images. Urine leaking into the retroperitoneal spaces (➡ in **Figs. 135.2a** through **135.2c**) would not be opacified in images obtained before the kidney has excreted CM.

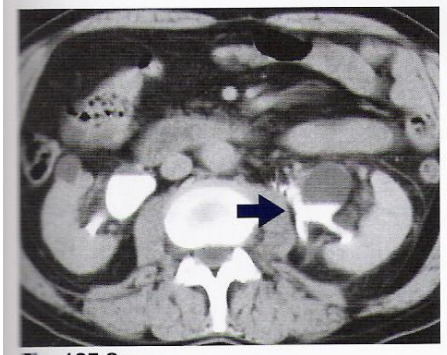

Fig. 135.2a

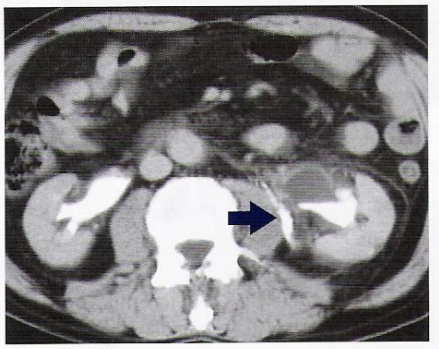

Fig. 135.2b

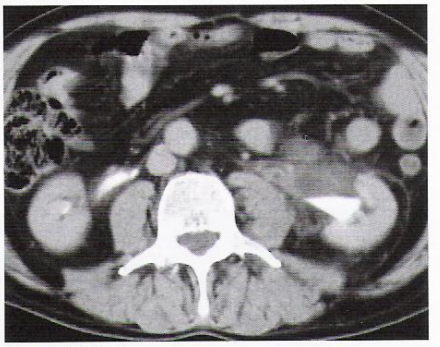

Fig. 135.2c

Renal infarctions **(180)** usually have a triangular shape on CT images corresponding to the vascular architecture of the kidney (**Fig. 135.3**). The broad base abuts the capsule and the triangle gradually tapers toward the pelvis **(136)**. A typical feature is the lack of enhancement after i.v. CM in the early perfusion phase and in the late excretion phase. Emboli usually originate in the left heart, or in the aorta in cases of atherosclerosis (**174** in **Fig. 135.3**) or aneurysms (cf. p. 142).

If there is a low attenuation filling defect **(173)** in the lumen of the renal vein **(111)** after a CM injection, the presence of bland thrombus **(Fig. 135.4)** or tumor thrombus from a renal carcinoma extending into the inferior vena cava **(80)** must be considered.

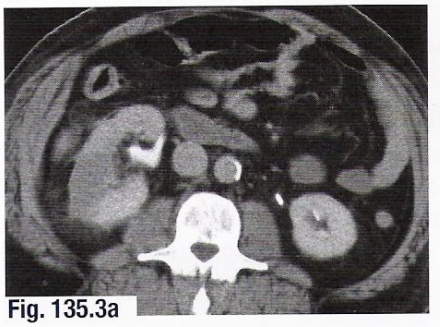

Fig. 135.3a

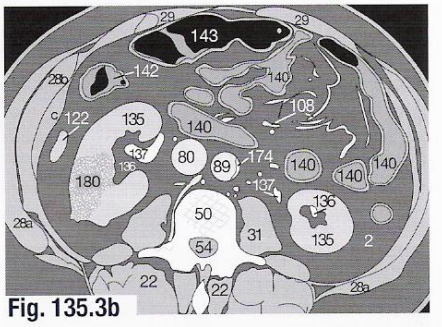

Fig. 135.3b

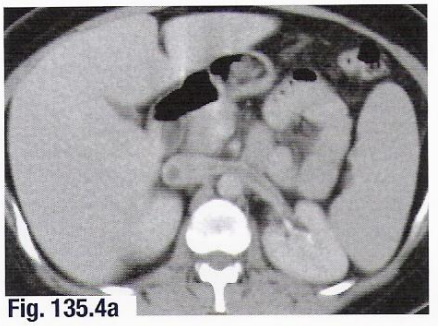

Fig. 135.4a

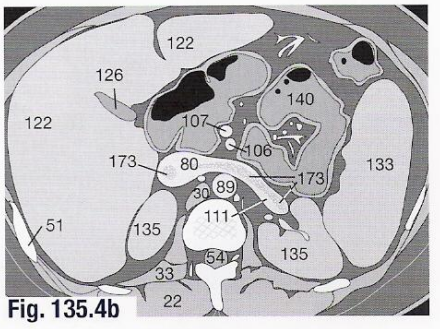

Fig. 135.4b

Catheters

The walls of the urinary bladder are best examined if the bladder is distended. If a urinary catheter **(182)** is in place at the time of CT **(Fig. 136.1)**, sterile water can be instilled as a low-density CM. Focal or diffuse wall thickening of a trabeculated bladder, associated with prostatic hyperplasia, will be demonstrated clearly. If a ureter **(137)** has been stented **(182)** for strictures or retroperitoneal tumors, the distal end of the JJ stent may be visible in the bladder lumen **(138)** (bilateral JJ stents in **Fig. 136.2**).

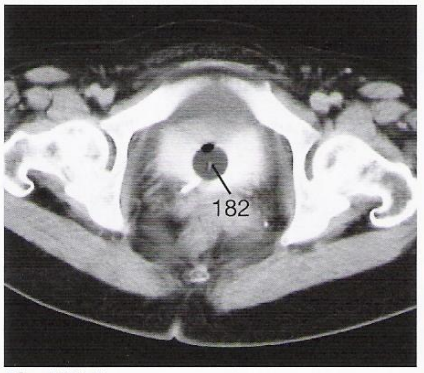

Fig. 136.1

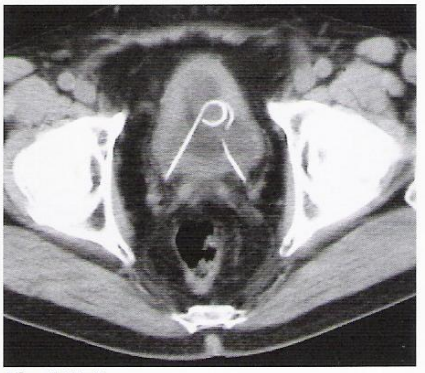

Fig. 136.2a

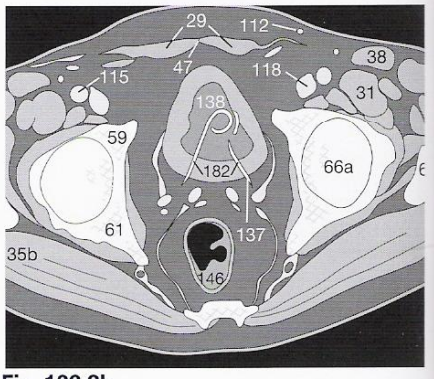

Fig. 136.2b

Diverticula

Diverticula situated at the periphery of the bladder can easily be distinguished from ovarian cysts by using CM **(Fig. 136.3)**. The "jet phenomenon" is often seen in the posterior basal recess of the bladder and is caused by peristalsis in the ureters. They inject spurts of CM-opacified urine into the bladder, which is filled with hypodense urine **(Fig. 136.4)**.

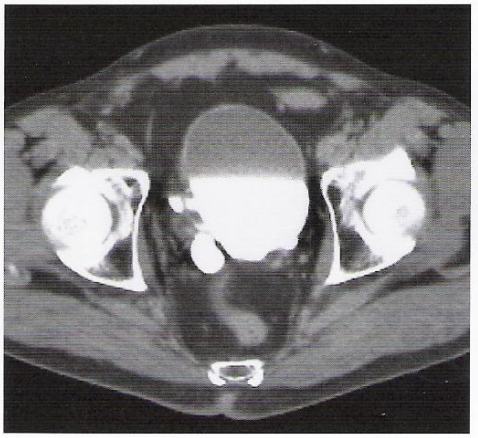

Fig. 136.3

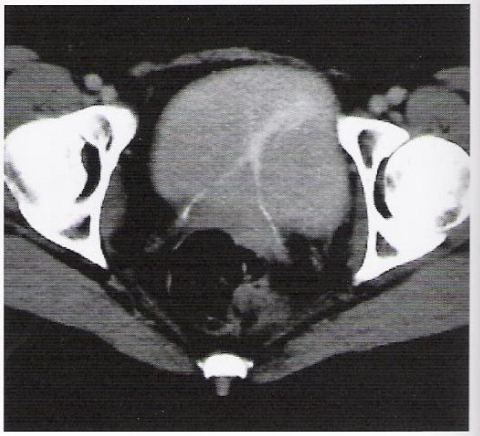

Fig. 136.4

Solid Tumors

Bladder wall tumors **(7)**, which become visible after intravenous or intravesical CM, have characteristic, irregular margins that do not enhance with CM **(Fig. 136.5)**. Tumors must not be confused with intravesicular blood clots that may occur following transurethral resection of the prostate. It is important to determine the precise size of the tumor and to what extent adjacent organs (e.g., cervix, uterus, or rectum) have been infiltrated (⇐ in **Fig. 136.6**).

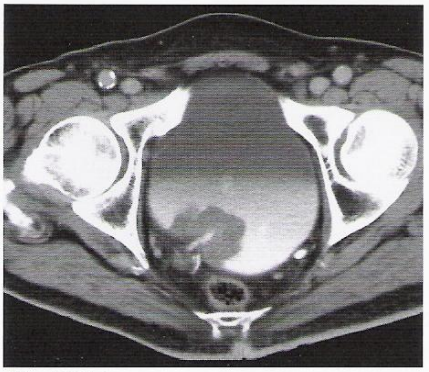

Fig. 136.5a

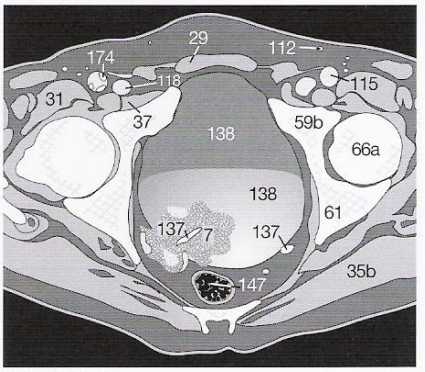

Fig. 136.5b

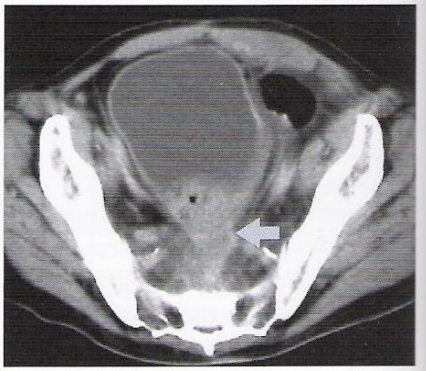

Fig. 136.6

If the bladder has been resected because of carcinoma, a urinary reservoir (*) can be constructed using a loop of small bowel (ileum conduit) which has been isolated from the GIT. Urine is excreted from the reservoir into a urostomy bag (⬅ in **Fig. 137.1b**).
In **Figure 137.2** a colostomy (⬇) is also seen (cf. p. 140).

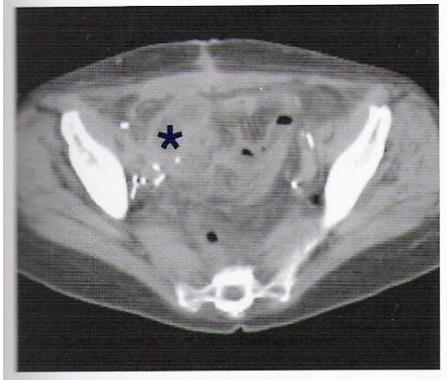

Fig. 137.1a

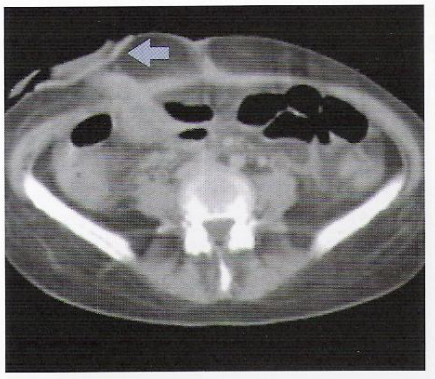

Fig. 137.1b

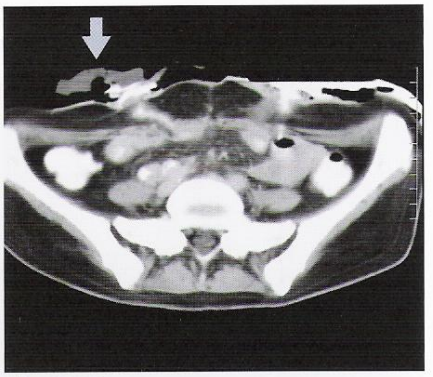

Fig. 137.2

Uterus

Foreign bodies in the uterine cavity **(158)**, e.g. an intrauterine contraceptive device **(166)**, are not always as clearly visible in a transverse image as in **Figure 137.3**. Calcifications **(174)** are a characteristic feature of benign uterine myomas. Nevertheless it can be difficult to distinguish multiple myomas from a carcinoma of the uterus (**7** in **Fig. 137.4**). If the adjacent walls of the bladder **(138)** or the rectum **(146)** are infiltrated, the tumor is most likely to be malignant **(Fig. 137.5)**. Central necrosis **(181)** occurs in both kinds of tumors and is usually indicative of a rapidly growing, malignant tumor **(Fig. 137.4)**.

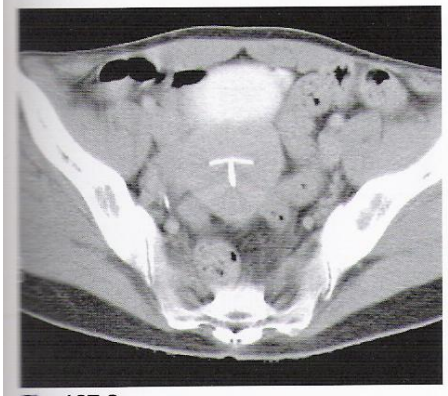

Fig. 137.3a

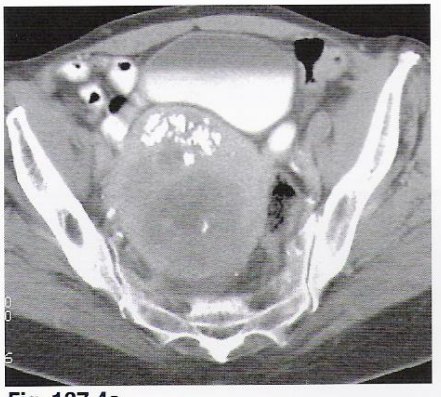

Fig. 137.4a

Fig. 137.5a

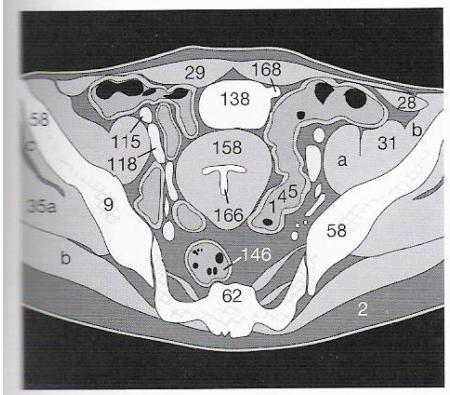

Fig. 137.3b

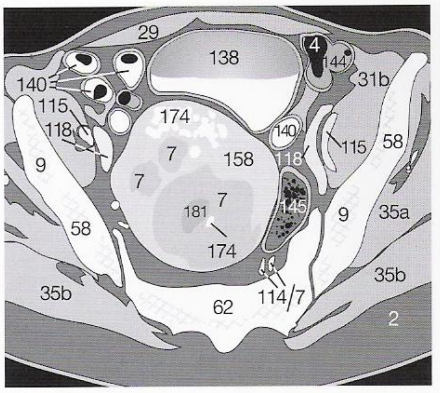

Fig. 137.4b

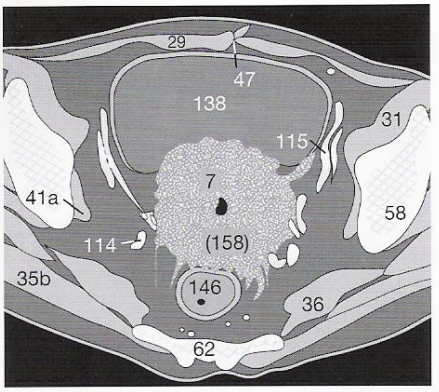

Fig. 137.5b

Ovaries

The most common ovarian lesions are thin-walled follicular cysts **(169)** that contain a clear fluid with a density equivalent to that of water, which is below 15 HU **(Fig. 138.1)**. Density measurements, however, are unreliable in small cysts (cf. p. 133). These cannot be clearly differentiated from mucinous cysts or hemorrhagic cysts. This latter type of cyst may be caused by endometriosis. Sometimes cysts reach considerable sizes **(Fig. 138.2)** with consequent mass effect.

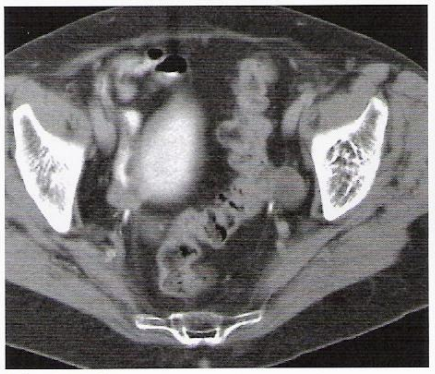

Fig. 138.1a

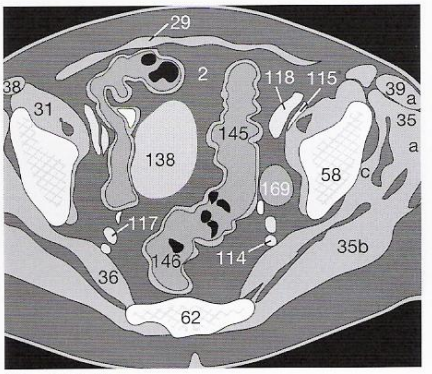

Fig. 138.1b

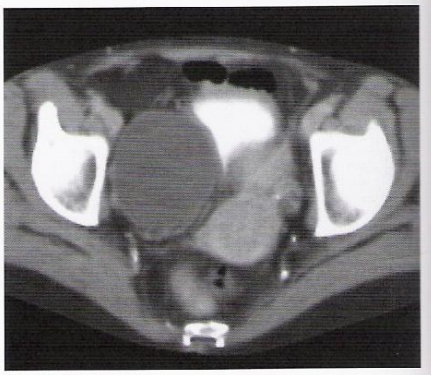

Fig. 138.2

The malignant nature of solid ovarian tumors can be suspected if there are the following general criteria used for other tumors:

1) ill-defined margins;
2) infiltration of adjacent structures;
3) enlarged regional LNs; and
4) inhomogeneous enhancement with CM.

Peritoneal carcinomatosis **(Fig. 138.3)** frequently occurs in advanced ovarian carcinoma, and is characterized by the appearance of multiple fine nodules and edema **(185)** in the greater omentum, the root of the mesenteric, and the abdominal wall, and by ascites **(8)**.

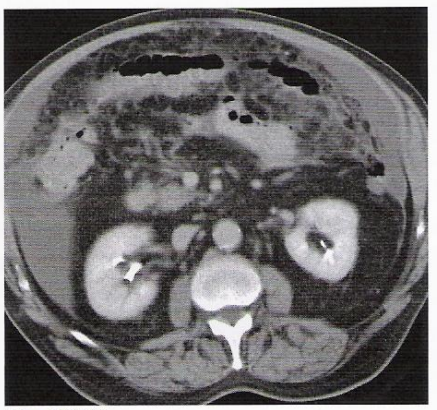

Fig. 138.3a

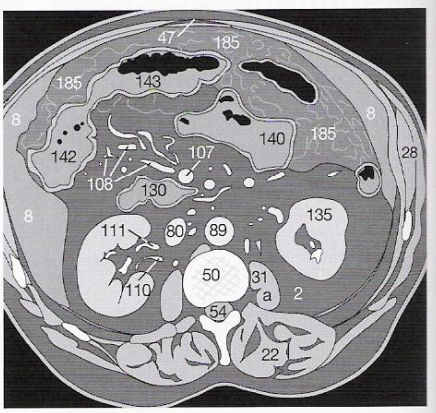

Fig. 138.3b

Prostate, Vas Deferens

High-density calcification representing postinflammatory residue is often encountered following prostatitis **(Fig. 138.4)**. Calcifications are also occasionally seen in the vas deferens **(Fig. 138.5)**. Carcinoma of the prostate is only detectable in advanced stages **(Fig. 138.6)** when the bladder wall or the adjacent ischiorectal fossa fat is infiltrated. If a prostate carcinoma is suspected, all images should be carefully viewed on bone windows for sclerotic metastases (see p. 145).

Fig. 138.4

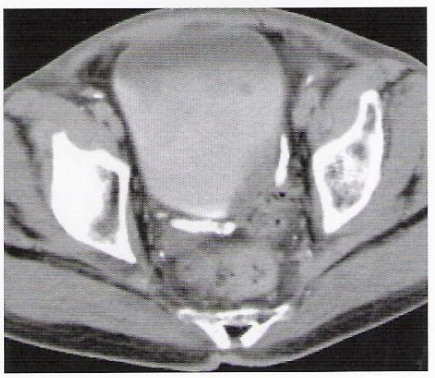

Fig. 138.5

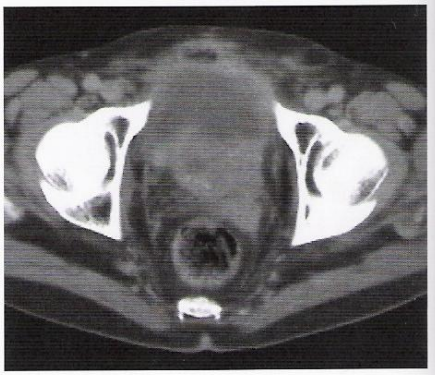

Fig. 138.6

Stomach

Despite the advantages of using water as a hypodense CM for imaging the stomach after intravenous Buscopan [15, 16], small tumors may escape detection during conventional CTs. Endoscopy and endosonography should be employed to complement CT.

Marked focal wall thickening, which occurs in carcinoma of the stomach, is usually easily recognized (⬅ in **Fig. 139.1**). In cases of diffuse wall thickening **(Fig. 134.2)**, the DD should also include lymphoma, leiomyoma, or leiomyosarkoma of the stomach. It is vital to look for bubbles of intraperitoneal gas (↙ in **Fig. 139.3**), which is evidence of a small perforation possibly occuring with ulcers or advanced ulcerating carcinomas.

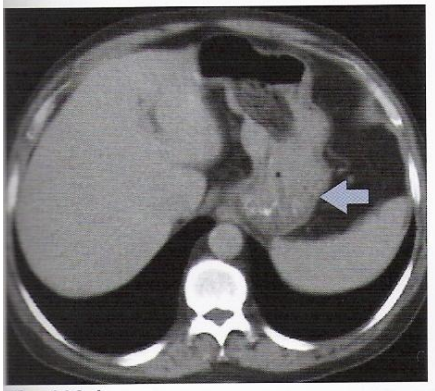

Fig. 139.1

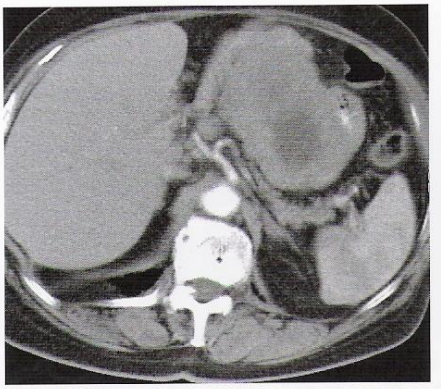

Fig. 139.2

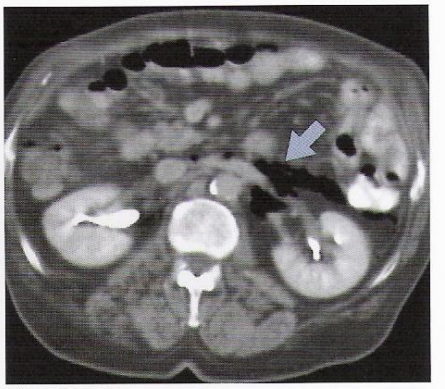

Fig. 139.3

Inflammation of the Intestines

The entire small and large bowel must be examined for wall thickening or infiltration of the surrounding fat as per the checklist on page 81. Both ulcerative colitis **(Fig. 139.4)** and Crohn's disease **(Fig. 139.5)** are characterized by thickening of the affected bowel wall (↑) so that several layers of the wall may become visible. Disseminated intravascular coagulopathy (DIC) or over-anticoagulation with warfarin may cause diffuse hemorrhage **(8)** in the bowel wall **(140)** and also lead to mural thickening **(Fig. 139.6)**. The DD should include ischemia if the abnormality is limited to segments in the territory of the mesenteric vessels, e.g., in the walls of the colon **(152)**, as a result of advanced atherosclerosis **(174)**, or an embolus **(Fig. 139.7)**. You should therefore check that the mesenteric vessels **(108)** and the walls of the intestine enhance homogeneously after i.v. CM.

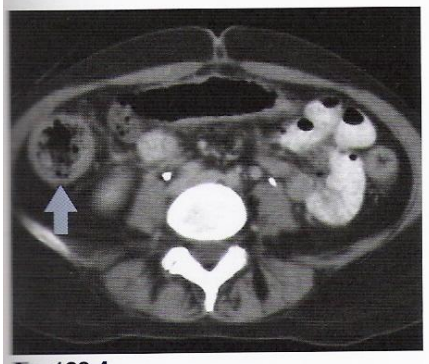

Fig. 139.4

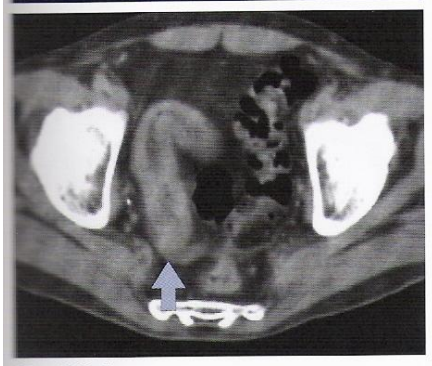

Fig. 139.5

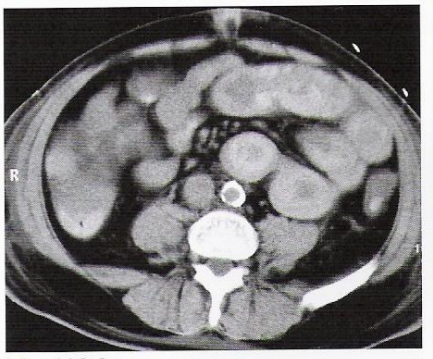

Fig. 139.6a

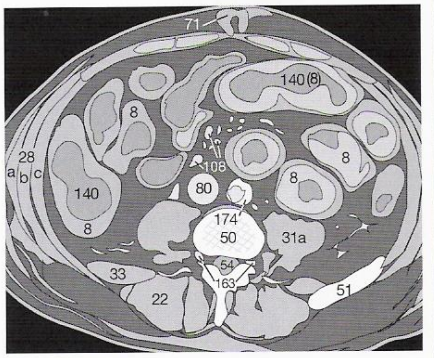

Fig. 139.6b

Fig. 139.7a

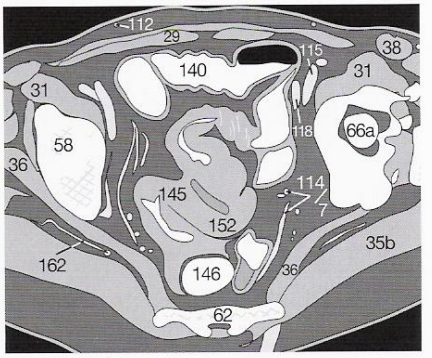

Fig. 139.7b

Colon

Elderly patients frequently have diverticular disease **(168)** of the descending colon **(144)** and sigmoid colon (**145** in **Fig. 140.1**). The condition is more significant if acute diverticulitis has developed **(Fig. 140.2)**, which is characterized by ill-defined colonic walls and edematous infiltration of the surrounding mesenteric fat (in **Fig. 140.2**).

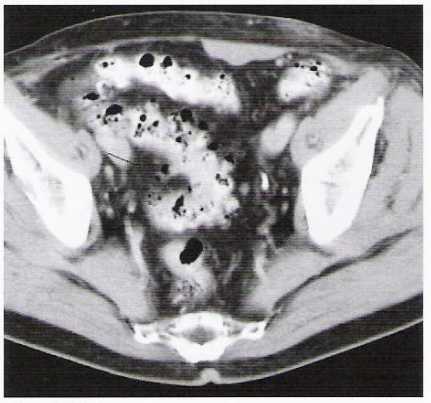

Fig. 140.1a

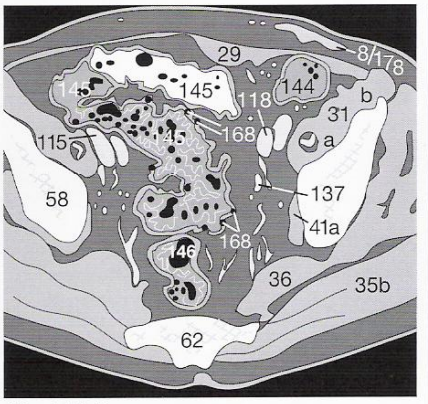

Fig. 140.1b

Fig. 140.2

Malignant thickening of the colonic wall (**152** in **Fig. 140.3**) is not always easily distinguished from that found in colitis (cf. p. 139): in both conditions there is stranding of the pericolic fat. The liver should always be checked for metastases if the cause of the colonic abnormality is uncertain.

A temporary colostomy (**170** in **Fig. 140.4**) may be necessary if a left hemicolectomy or sigmoid colectomy was performed because of perforated diverticulitis or carcinoma. The colostomy is permanent if the rectum was excised. A potential complication of a colostomy can be seen in **Figure 140.5**: there is an abscess in the abdominal wall **(181)**. A carcinoid lesion of the small bowel (in **Fig. 140.6**) may simulate a carcinoma of the colon.

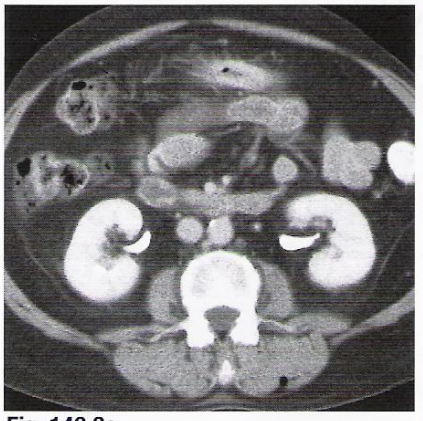

Fig. 140.3a

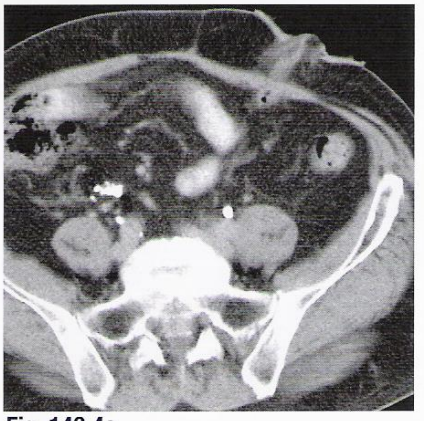

Fig. 140.4a

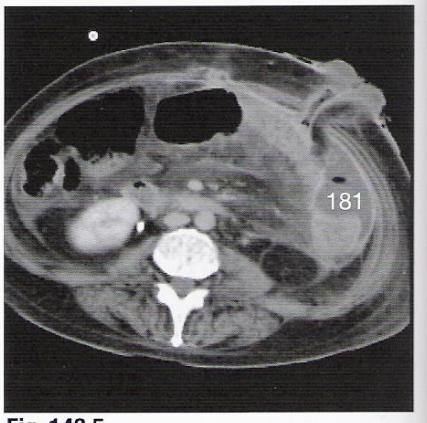

Fig. 140.5

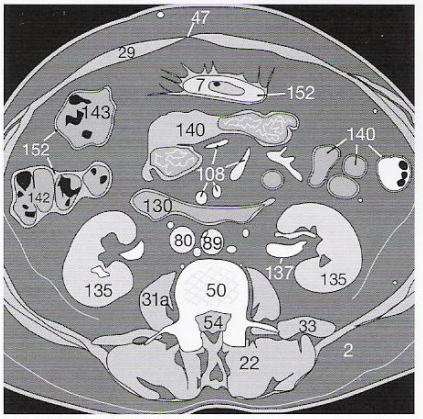

Fig. 140.3b

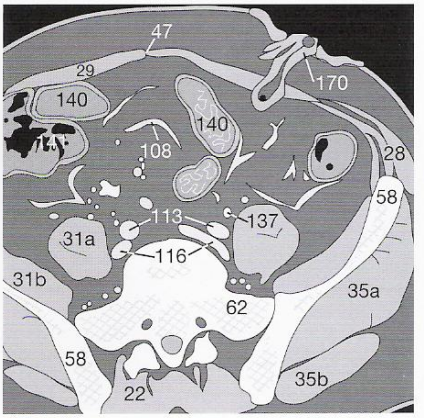

Fig. 140.4b

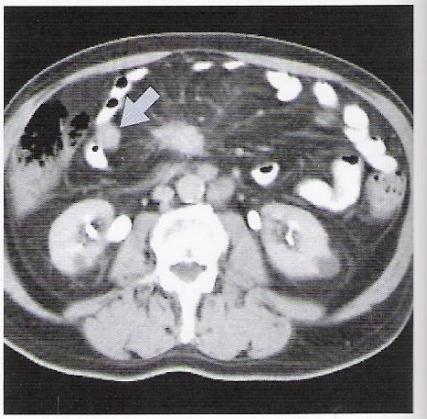

Fig. 140.6

Ileus

Horizontal air–fluid levels (↓ ↓) and atonic, dilated bowel loops (**140**) are typical features of ileus. If dilatation is recognized in the topogram **(Fig. 141.1)**, or in an overview of the abdomen, an ileus must be suspected. If only the small intestine **(Fig. 141.2)** is involved, the most likely cause is a mechanical obstruction due to adhesions. A gallstone may cause obstruction of the small bowel (gallstone ileus). This follows cholecystitis with the formation of a cholecystoenteral fistula and the passage of a gallstone into the bowel. The gallstone may obstruct the narrower caliber of the distal ileum (**167** in **Fig. 141.3**).

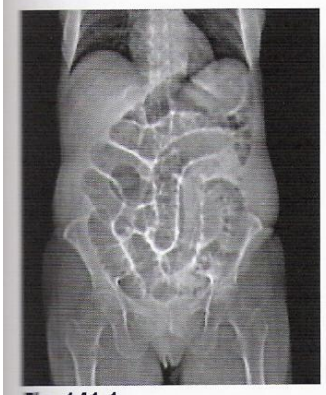

Fig. 141.1

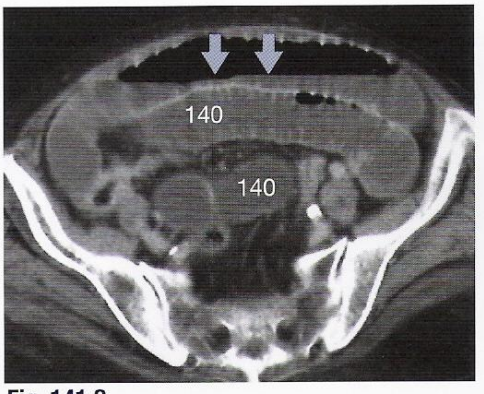

Fig. 141.2

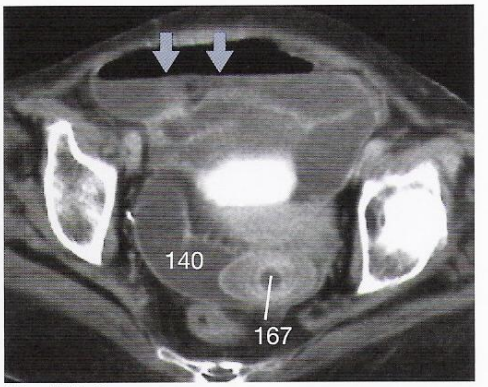

Fig. 141.3

Mechanical obstruction of the colon leads to similar air–fluid levels and dilatation (↓ ↓ in **Fig. 141.4**). When looking for the cause of an ileus, the entire colon must be examined for obstructing or constricting tumors or focal inflammation.

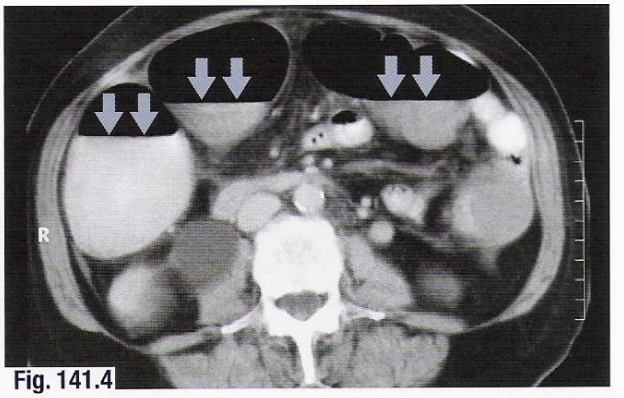

Fig. 141.4

Test Yourself! Exercise **29:**

Are there any suspicious findings other than the colic ileus in **Figure 141.4**? Does the image remind you of others in the manual? Make the most of the figures by returning to previous chapters, covering the text, and identifying as many structures as possible. You will improve your learning efficiency by reviewing the images and diagrams and using the legends to make sure you got it right.

Space for notes and completing the exercise:

Aneurysms

Ectasia or aneurysms of the abdominal aorta **(89)** are usually the result of atherosclerotic disease **(174)** which leads to mural thrombosis (**173** in **Fig. 142.1**). An aneurysm of the abdominal aorta is present if the diameter of the patent lumen has reached 3 cm or the outer diameter of the vessel measures more than 4 cm **(Fig. 142.2)**. Surgical intervention in asymptomatic patients is usually considered when the dilatation has reached a diameter of 5 cm. The general condition of the patient and the rate at which dilatation is progressing must be considered. If the patent lumen is central and is surrounded by mural thrombosis (**173** in **Fig. 142.2**), the risk of rupture and consequent hemorrhage is reduced.

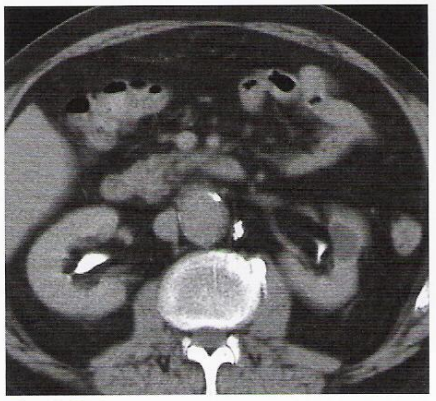

Fig. 142.1a

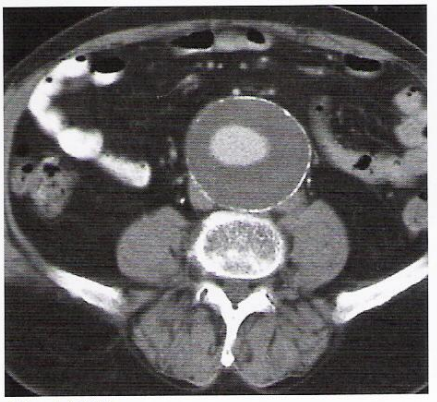

Fig. 142.2a

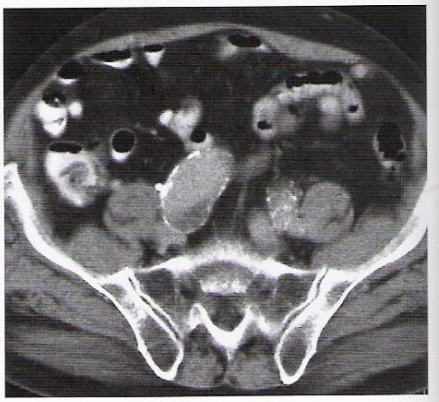

Fig. 142.3a

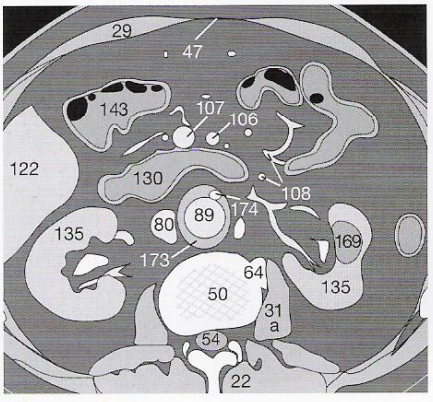

Fig. 142.1b

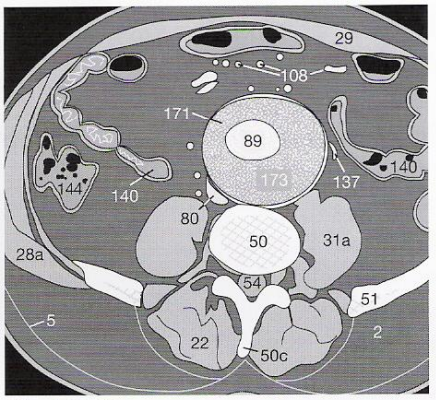

Fig. 142.2b

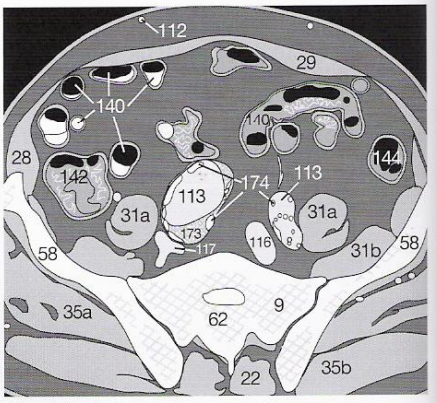

Fig. 142.3b

The risk of rupture is greater if the patent lumen is eccentric (in **Fig. 142.4**) or if the cross-sectional shape of the vessel is very irregular. Dilatation in excess of 6 cm diameter also has a high risk of rupture. Surgical planning requires the determination of whether, and to what degree, the renal, mesenteric **(97)**, and iliac **(113)** arteries are involved by the aneurysm **(Fig. 142.3)**. Sudden pain may accompany rupture or dissection, which can extend from the thoracic to the abdominal aorta (cf. p. 93). Dynamic CM-enhanced CT will show the dissection flap (**172** in **Fig. 142.5**).

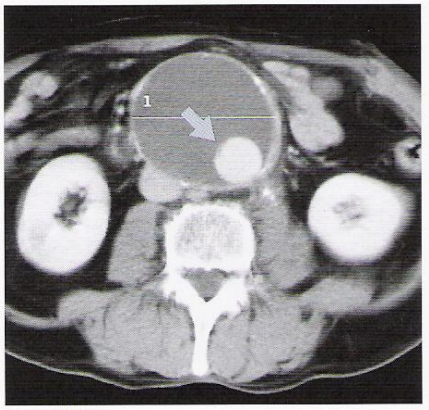

Fig. 142.4

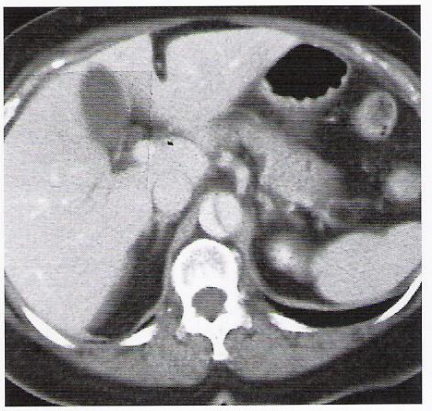

Fig. 142.5a

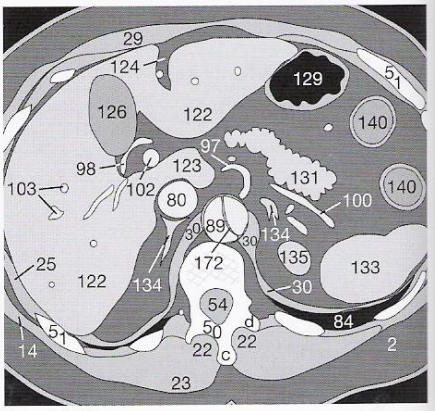

Fig. 142.5b

Venous Thromboses

In cases of thrombosis in a vein of the lower extremity ( ), venography does not always clearly show whether or not the thrombus extends into pelvic veins (**Figs. 143.1a** and **143.1b**). The CM, which is injected into a superficial vein of the foot, is often diluted to such a degree that it becomes difficult to assess the lumen of the femoral/iliac veins (in **Fig. 143.1c**). In such cases, it is necessary to perform a CT with i.v. CM.

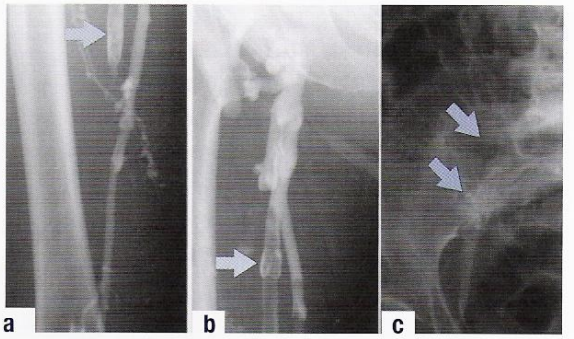

Fig. 143.1 a b c

The lumen of a vein containing a fresh thrombus ( ) is generally at least twice as large as normal **(Fig. 143.2a)**. The segment containing the thrombus is either uniformly hypodense compared with the accompanying artery, or it shows a hypodense filling defect, representing the thrombus itself. In the case illustrated on the right, the thrombus extended through the left common iliac vein ( ) to the caudal segment of the inferior vena cava **(Fig. 143.2b),** where it can be seen as a hypodense area ( ) surrounded by contrast-enhanced, flowing blood **(Fig. 143.2c)**. CT slices must be continued cranially until the inferior vena cava no longer shows any signs of thrombus (in **Fig. 143.2d**).

Fig. 143.2a

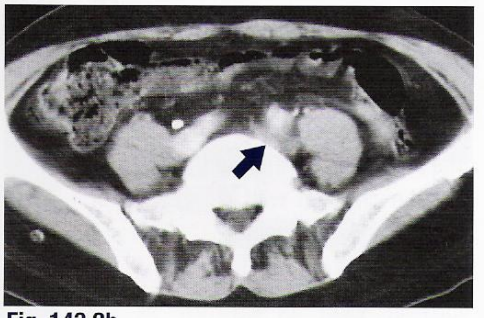

Fig. 143.2b

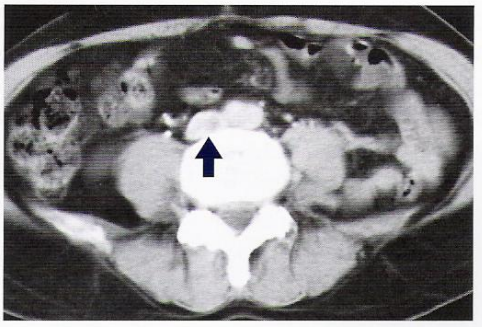

Fig. 143.2c

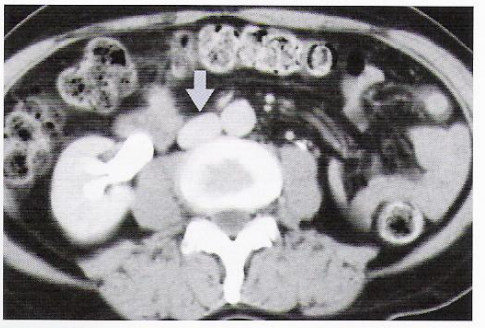

Fig. 143.2d

The injection of CM into a superficial foot vein opacifies satisfactorily only the ipsilateral leg, so it may be advisable to inject CM systemically through an arm vein in order to examine both sides of the pelvic venous system. If one side has become occluded, collaterals may develop ( ) via the prepubic network of veins **(Figs. 143.3a** and **143.3b)**. Such collaterals are known as a "Palma shunt", and these can also be surgically created if a thrombus in a deeper vein resists dissolution. You should be careful not to mistake an inguinal LN with physiologically hypodense hilar fat ("hilar fat sign" in **Fig. 143.3c**) for a partially thrombosed vein.

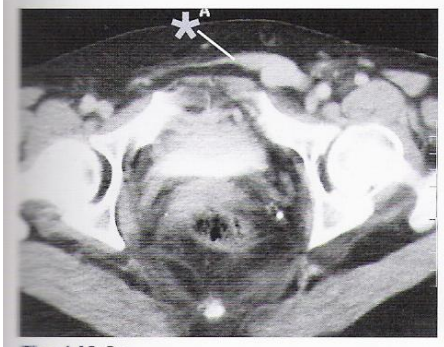

Fig. 143.3a

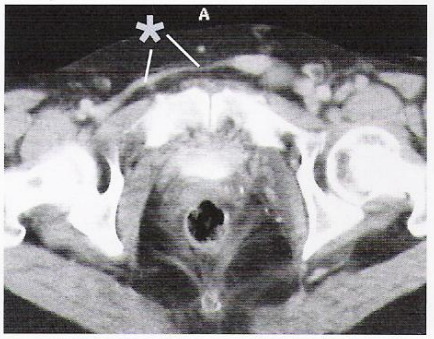

Fig. 143.3b

Fig. 143.3c

In order to avoid pulmonary embolism in cases of thrombosis **(173)** of the inferior vena cava (**80** in **Fig. 144.2**), the patient must be immobilized until the thrombus has either become endothelialized or has responded to therapy and dissolved. Occasionally, marked collateral circulation develops via the lumbar veins **(121)**.

Depending upon the individual patient and the size of the thrombus, the vessel may be surgically explored and thrombectomy performed. If thromboses are recurrent, an arterio-venous shunt may be indicated in order to avoid relapse. The success of a particular therapy may also be checked with venography or color-Doppler ultrasound.

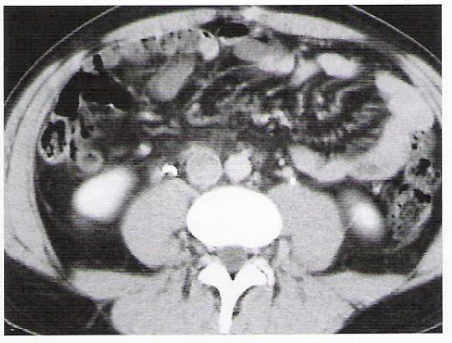

Fig. 144.1a

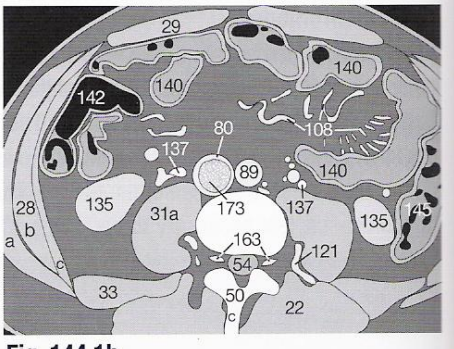

Fig. 144.1b

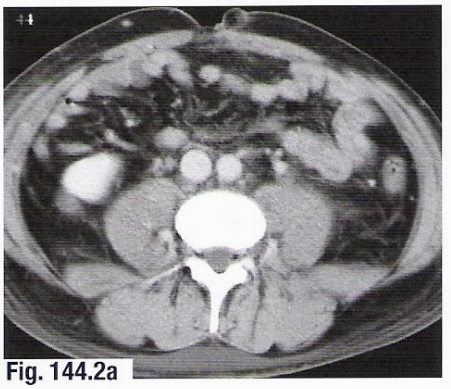

Fig. 144.2a

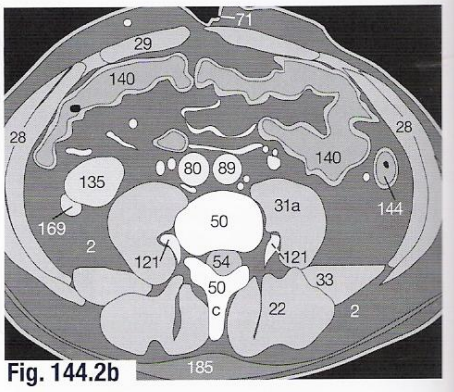

Fig. 144.2b

Enlarged Lymph Nodes

The density of LNs is approximately 50 HU, which corresponds to that of muscle. LNs with diameters below 1 cm are generally considered normal. Sizes between 1.0 and 1.5 cm are considered borderline, and those that exceed 1.5 cm are abnormally enlarged. Sites of predilection for enlarged LNs are the retrocrural, mesenteric ( ), interaortico-caval ( ), and para-aortic spaces (cf. p. 103).

Figure 144.3 illustrates the case of a patient with chronic lymphatic leukemia.

It is essential to be familiar with the major paths of lymphatic drainage. The drainage of the gonads, for example, is directly to LNs at renal hilar level. LN metastases (in **Fig. 144.4**) from a testicular tumor will be found in para-aortic nodes around the renal vessels but not in the iliac nodes, as would be expected with primary carcinomas of the urinary bladder, uterus, or prostate.

Conglomerate LN masses **(6/7)** surrounding the aorta **(89)** and its major branches such as the celiac trunk **(97)** are a typical finding in cases of non-Hodgkin lymphoma **(Fig. 144.5)**.

Fig. 144.3

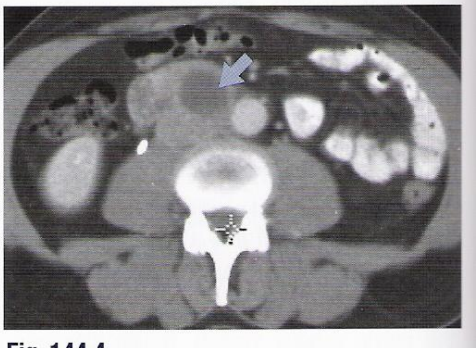

Fig. 144.4

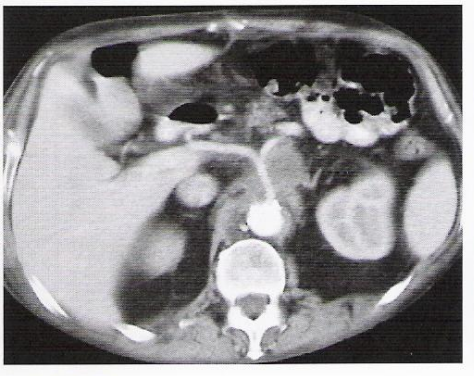

Fig. 144.5a

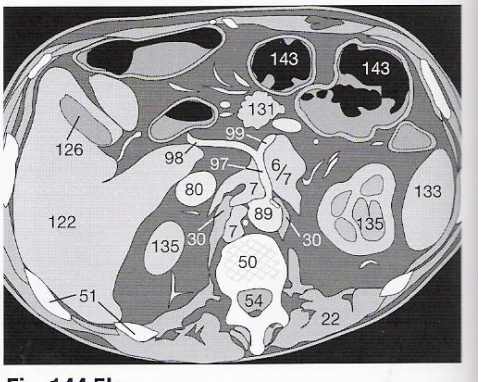

Fig. 144.5b

Normal Anatomy

The importance of examining bone windows during abdominal CTs has already been stressed on page 103. The marrow space of the iliac bones **(58)** and the sacrum **(62)** is normally homogeneous, and the surfaces of the sacroiliac joints should be smooth and regular **(Fig. 145.1)**.

Fig. 145.1a

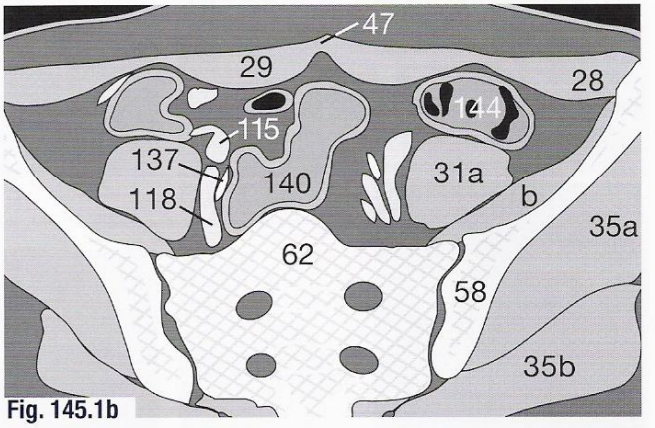

Fig. 145.1b

Metastases

Sclerotic bone metastases **(7)**, for example from a carcinoma of the prostate, are not always as evident as in **Figure 145.2a** and may vary in size and degree of calcification. Even small and poorly defined metastases should not be overlooked (* in **Fig. 145.2b**). They cannot routinely be recognized on soft-tissue windows.

Lytic metastases **(7)**, which can be seen on soft-tissue windows **(Fig. 145.3a)** only after they have reached considerable size, can be much more accurately detected on bone windows **(Fig. 145.3c)**. This case shows a metastatic disease of the right ilium **(58)** that has destroyed the trabeculae and much of the cortex. The erosion extends to the sacroiliac joint. See the following pages for further images of this patient.

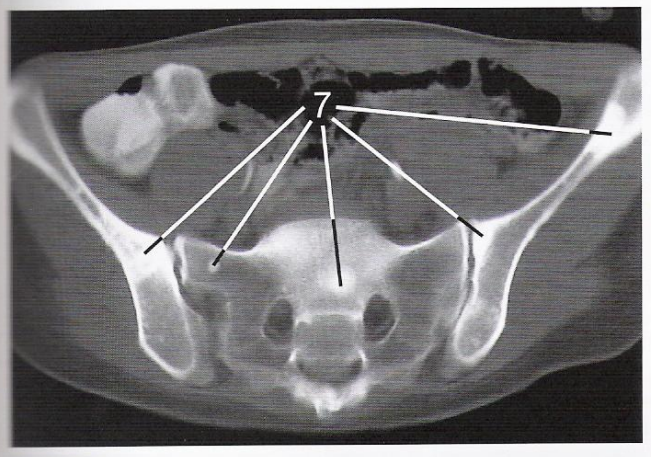

Fig. 145.2a

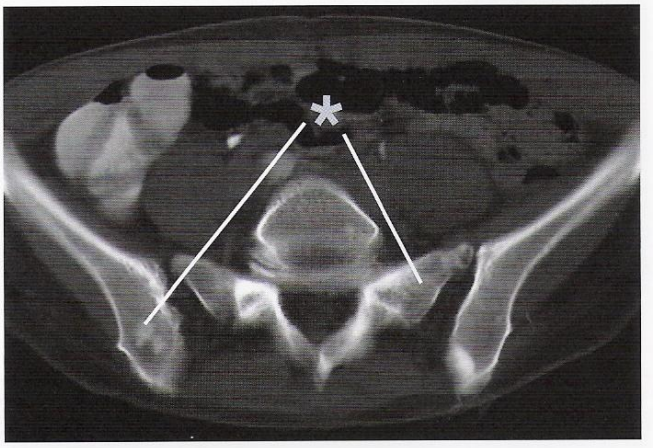

Fig. 145.2b

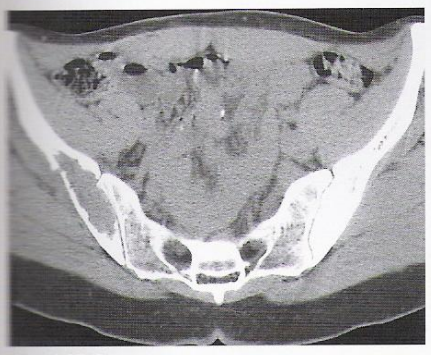

Fig. 145.3a

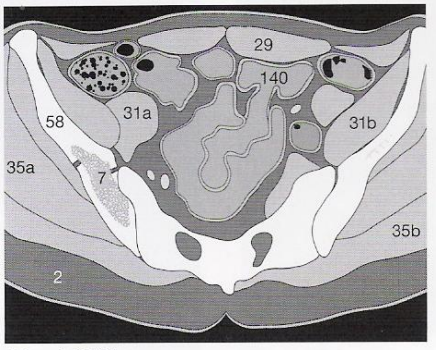

Fig. 145.3b

Fig. 145.3c

The mechanical integrity of a bone is suspect if any process involves its structure. Adjacent joint involvement must also be determined. MPRs (see p. 13) at various angles, for example sagittal or coronal, provide additional information. If necessary, 3D reconstructions can also be performed.

In the case shown on the previous page (see **Fig. 145.3**), the question of stability is easily answered: the coronal MPR **(Fig. 146.1a)** shows that the trabeculae of the right iliac bone have been completely destroyed for approximately 10 cm (➡). The lesion extends from the acetabulum to the mid-point of the sacroiliac joint and has also destroyed much of the cortex. In several areas, the cortex is disrupted (⬅). If you compare the bilateral sagittal reconstructions (**Figs. 146.1b** and **1c**), it is easy to see that there is acute risk of fracture.

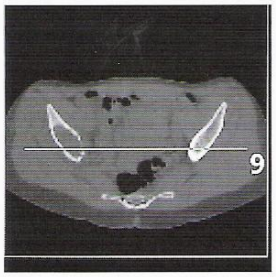

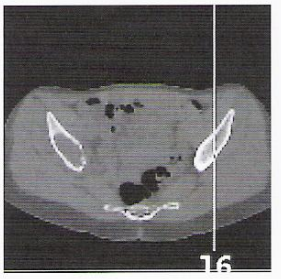

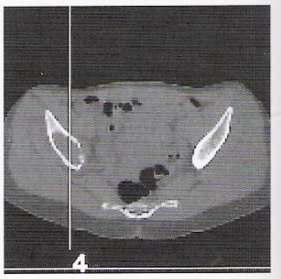

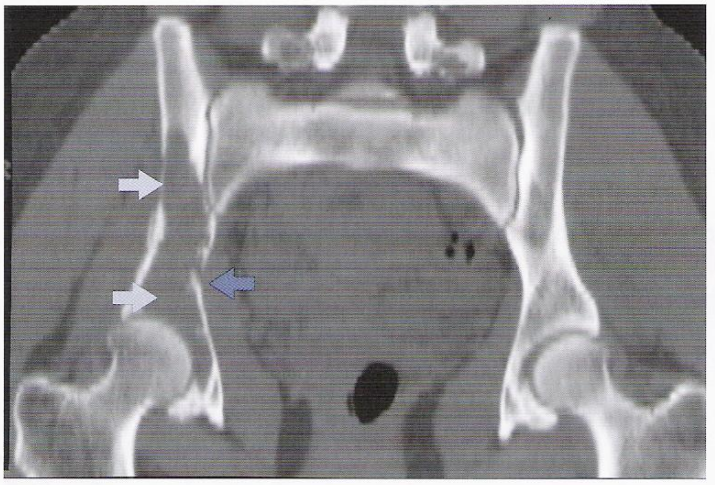

Fig. 146.1a

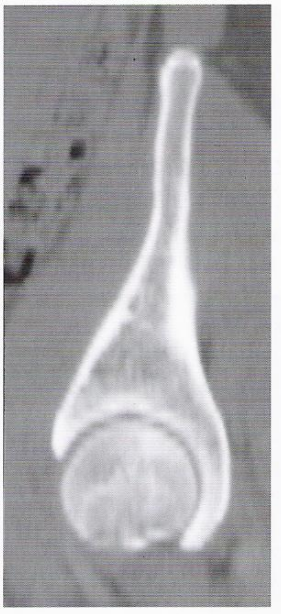

Fig. 146.1b

Fig. 146.1c

The 3D reconstruction of this pelvis **(Fig. 146.2)** does not add any more information, because it shows only the cortical disruption (↙) as seen from the lateral perspective.

The degree to which the trabeculae and marrow have been destroyed cannot be seen in this reconstruction because the attenuation level was set to detect the cortical bone, and the deeper trabeculae are therefore covered.

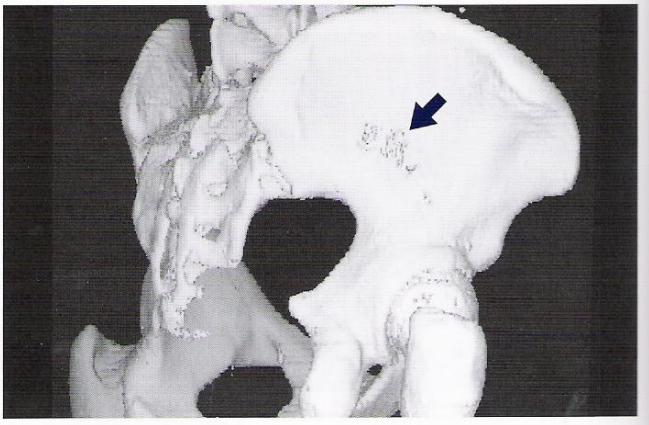

Fig. 146.2

Fractures

Bone windows should of course be used for the detection of fractures: hairline fractures and minimal dislocations cannot usually be recognized on soft-tissue windows.

It is also essential to give information on the precise fracture site and position of possible fragments for preoperative planning. In the case on the right, the fracture **(187)** of the femoral head **(66a)** is seen both in the axial plane **(Fig. 147.1)** and in the sagittal reconstruction **(Fig. 147.2)** (cf. p. 13).

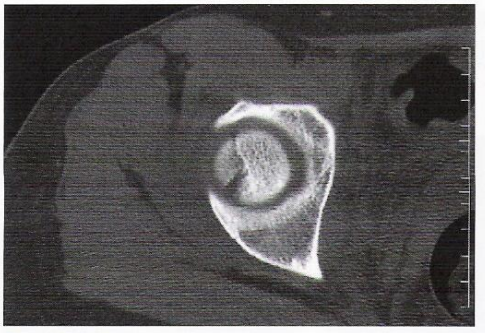

Fig. 147.1a

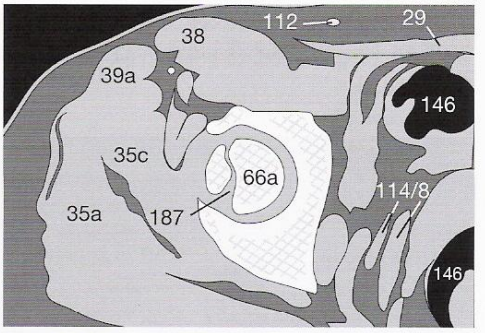

Fig. 147.1b

Fig. 147.2a

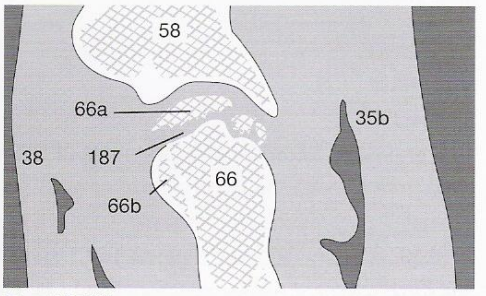

Fig. 147.2b

For joints such as the hip joint, it may be helpful to make an MPR in the oblique plane **(Figs. 147.3)**. The angle of reconstruction is shown in **Fig. 147.3a**. Be careful not to mistake the acetabular suture (⬋) with the real ischial fracture (⬈)!

Fig. 147.3a

Fig. 147.3b

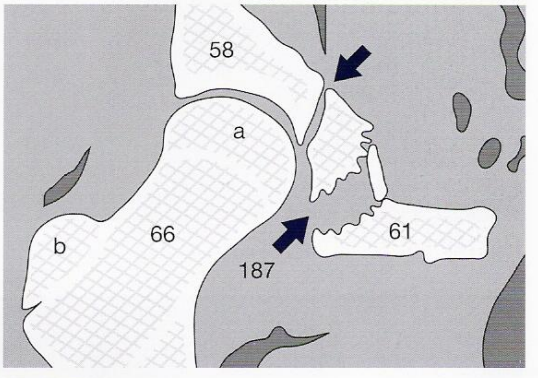

Fig. 147.3c

Another example of a fracture that may be mistaken for a suture is illustrated in **Figure 147.4**. The sutures (⬋) are bilaterally symmetric, the fractures are not.

In this case, several fragments of bone (⟷) are seen at the right iliopubic junction, but the right acetabulum is intact. Note also the asymmetry in the image which is caused by differences in the levels of the femoral heads. The patient had left acetabular dysplasia (cf. figures on p. 148).

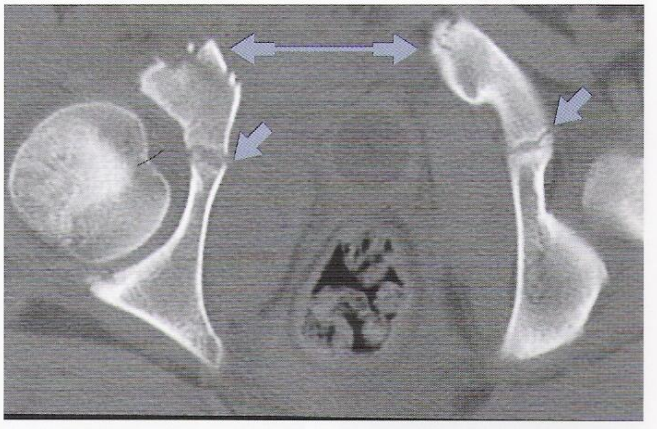

Fig. 147.4

Fragments are not always as obviously displaced nor is the fracture gap ( ) as wide as in the case illustrated in **Figure 148.1**. Look for fine breaks ( ) and discrete irregularities ( ) in the cortical outline in order not to miss a fracture or a small fragment **(Fig. 148.2)**.

Fig. 148.1

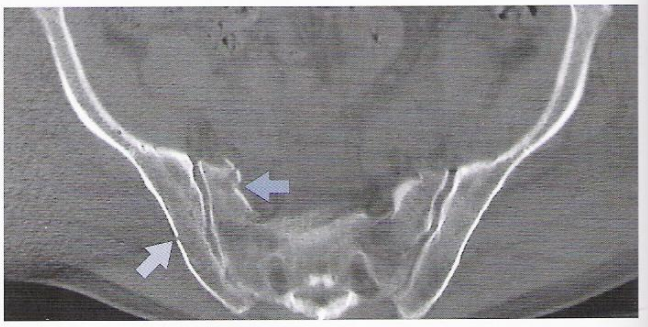

Fig. 148.2

Femoral Head Necrosis and Dysplasia of the Hip Joint

A fracture through the femoral head or even direct trauma to the hip joint may interrupt the blood supply to the head via the acetabular artery (see also **Figures 147.1** and **147.2**). Necrosis of the head makes it appear poorly defined ( ) as seen in **Figure 148.3a** and causes shortening of the leg. An image obtained 2cm more cranially shows that a pseudoarthosis has developed in association with the right acetabular dysplasia **(Fig. 148.3b)**. A 3D reconstruction gives an overview, but does not provide as much detail as a series of coronal MPRs (**Fig. 148.5b** with orientation in **Fig. 148.5a**).

Fig. 148.3a

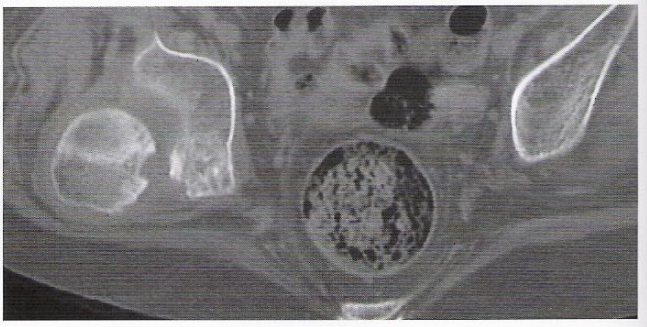

Fig. 148.3b

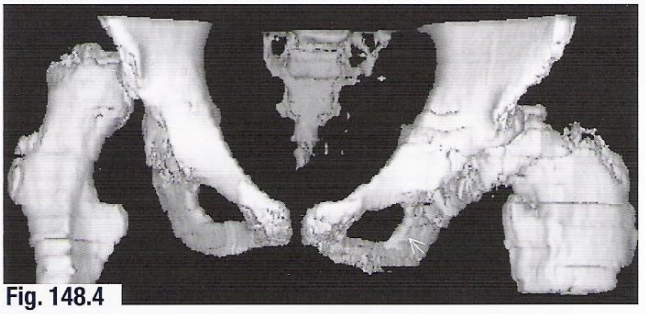

Fig. 148.4

MPRs are often used for diagnostic purposes and in planning surgery of complex fractures. They contribute valuable additional information to the conventional axial images. SCT produces particularly accurate MPR images because disruptive step artifacts can be avoided if the patient is able to cooperate by holding his or her breath.

3D reconstructions, such as the one in **Figure 142.4**, yield impressive images, but are helpful only for specific problems such as plastic surgery. The amount of time and cost necessary to acquire and reconstruct 3D images are in most cases also very high.

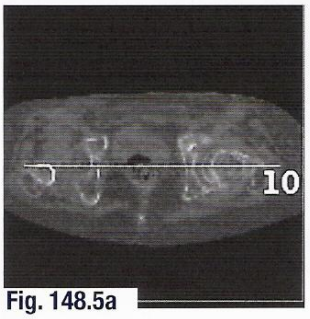

Fig. 148.5a

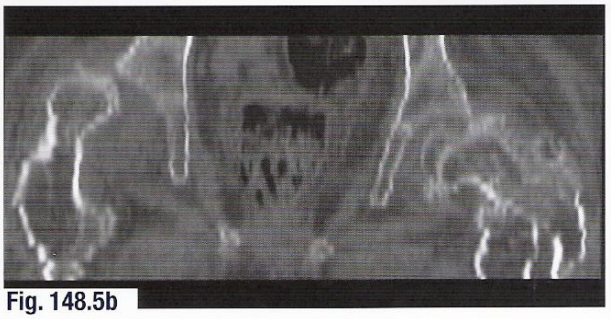

Fig. 148.5b

The images and questions on this page will again help you to check on how much you have understood; the questions become continually more difficult to answer. If you always remember the basic rules of CT reading, you will avoid jumping to the wrong conclusions. Don't look up the answers too soon!

Exercise 30:

What abnormality can you identify in **Figure 149.1**? Name as many blood vessels as you can!

Fig. 149.1

Exercise 31:

Identify as many organs and blood vessels as possible in **Figure 149.2**. Look for any abnormalities.

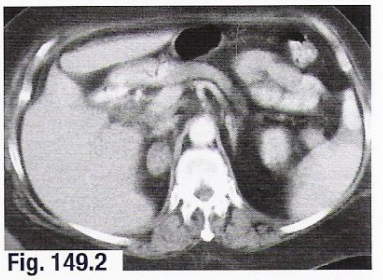

Fig. 149.2

Exercise 32:

What anatomic variation or abnormality do you recognize in **Figure 149.3**? Be sure you haven't missed anything.

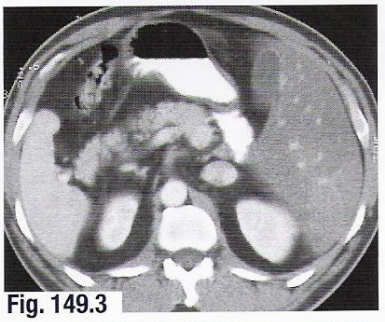

Fig. 149.3

Exercise 33:

"Do you smoke?" What abnormalities did you find in **Figure 149.4**?

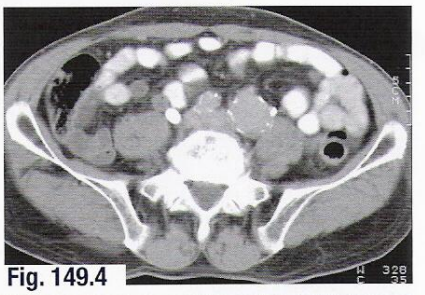

Fig. 149.4

Exercise 34:

It is easy to recognize the hepatic lesion in **Figure 149.5**. What is your DD?

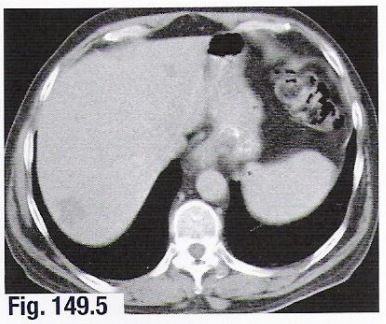

Fig. 149.5

Exercise 35:

Often abnormalities are not limited to one organ. What do your recognize in **Figure 149.6**?

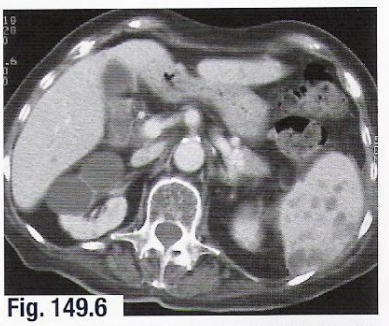

Fig. 149.6

Test Yourself!

The following questions may seem tricky, but you should be able to answer most of them if you go by the "rules of the book."

Exercise 36:

Describe the hepatic lesion in **Figure 150.1**. What steps did you take to arrive at your differential diagnosis? How would you proceed to verify it?

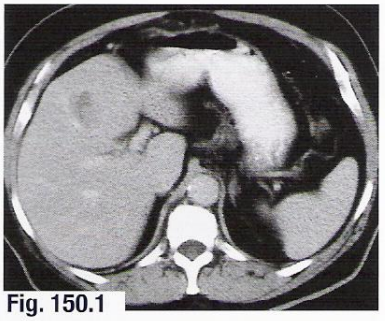

Fig. 150.1

Exercise 37:

Are the changes in **Figure 150.2** "normal," or do you suspect that they are pathologic findings?

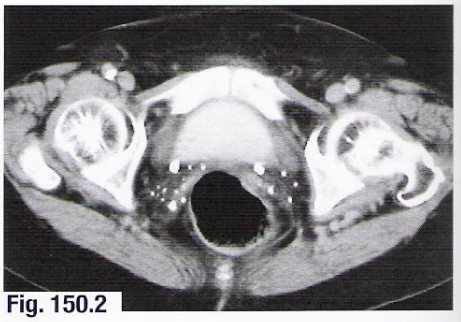

Fig. 150.2

Exercise 38:

Which of the two image levels on the right would you select for performing densitometric measurements of the kidney lesion? Why?

Fig. 150.3a

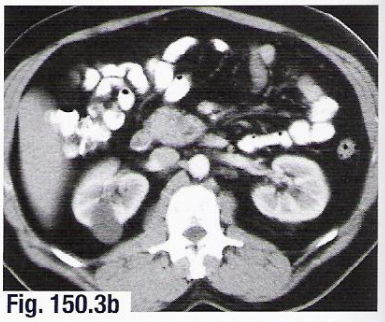

Fig. 150.3b

Exercise 39:

A patient is admitted for staging of a malignant melanoma **(Figure 150.4)**. How far advanced is the lesion? What else would you do to obtain more information?

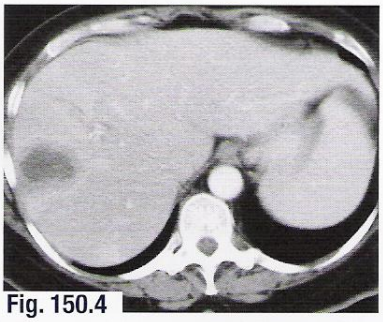

Fig. 150.4

Exercise 40:

A trauma patient could not be scanned in the prone position. What do you suspect in **Figure 150.5**, and what would you do to obtain more information?

Fig. 150.5

Exercise 41:

A problem for those who already have some routine **(Figure 151.1)**. How long did it take you to find two pathologic alterations and diagnose them accurately?

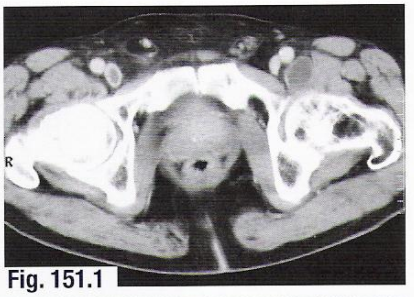

Fig. 151.1

Exercise 42:

Do you see anything abnormal in **Figure 151.2**? If so, what would you call it (the small figure indicates a structure filled with liquid)?

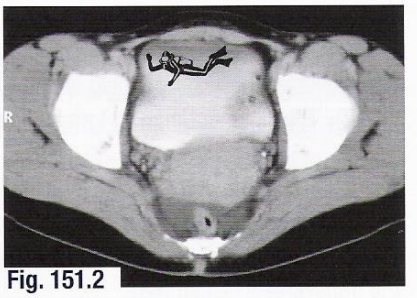

Fig. 151.2

Exercise 43:

At least three differential diagnoses should be considered for **Figure 151.3**. Which one is the most likely?

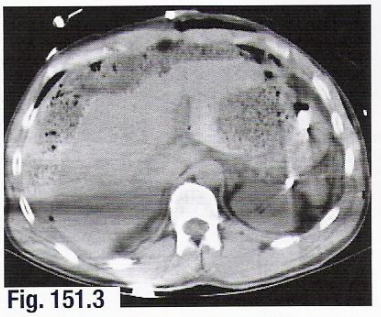

Fig. 151.3

Exercise 44:

In **Figure 151.4,** there are also several possibilities to explain the obvious alteration. Are you able to find **all** possible lesions in an image of this kind?

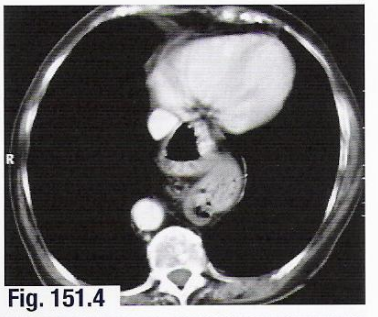

Fig. 151.4

Exercise 45:

What do you suspect is the case in **Figure 151.5**? What additional information do you need?

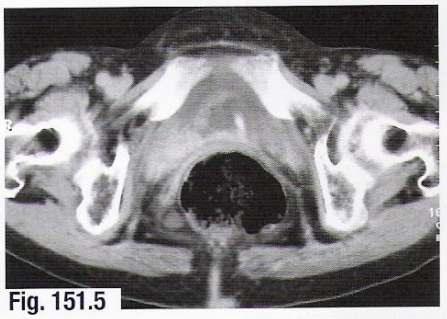

Fig. 151.5

Exercise 46:

This image **(Figure 151.6)** may contain several puzzles. Again, list the most likely diagnoses and then ask yourself what further information you need.

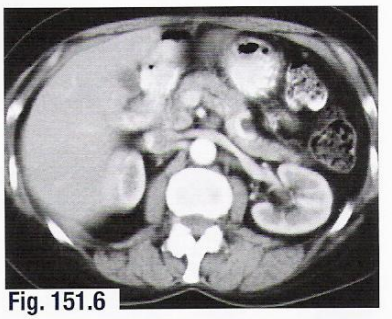

Fig. 151.6

The occipital condyles at the base of the skull articulate with the first vertebra, the atlas **(50a)**, which is the only vertebra to lack a body. The dens **(50b)** of the axis protrudes upward into the atlas and is held in place by the transverse ligament (★) **(Figs. 152.1** and **152.2)**. This ligament may be torn by a whiplash injury during road traffic accidents.

The width of the space (↔) between the anterior arch of the atlas (★★ in **Figs. 152.1** and **152.2**) and the dens is also measured, as in conventional x-ray images **(Fig. 152.3)**. In adults it should not exceed 2 mm; in children, 4 mm. The vertebral artery passes through the transverse foramen **(88)**.

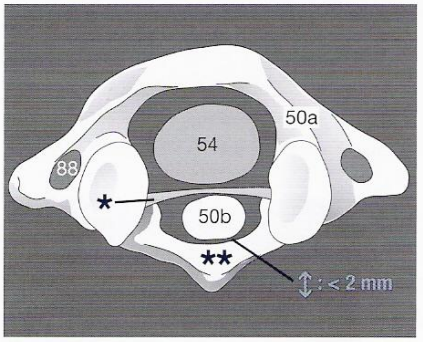

Fig. 152.1

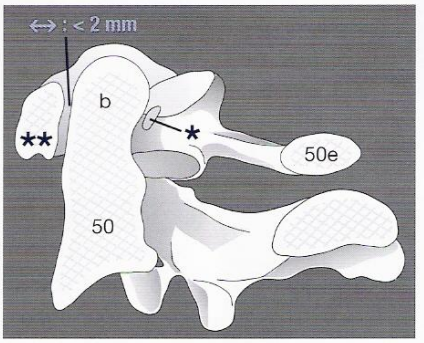

Fig. 152.2

Fig. 152.3

The images below show normal anatomy at the level of the atlas **(Fig. 152.4)** and the body of the axis **(Fig. 152.5)**. The cartilage of an intervertebral disc (**50e** in **Fig. 152.6**) will appear more homogeneous and hypodense than the typical pattern of trabeculae.

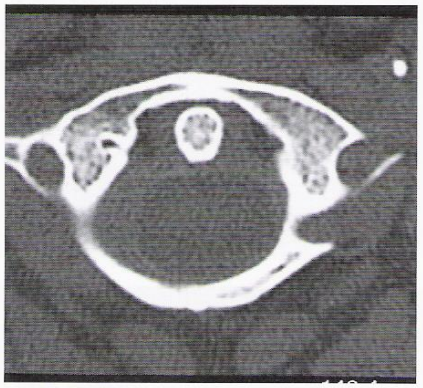
Fig. 152.4a


Fig. 152.5a

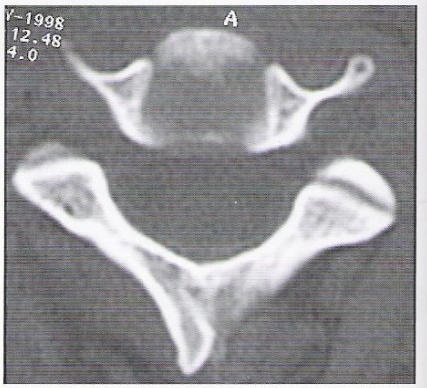

Fig. 152.6a

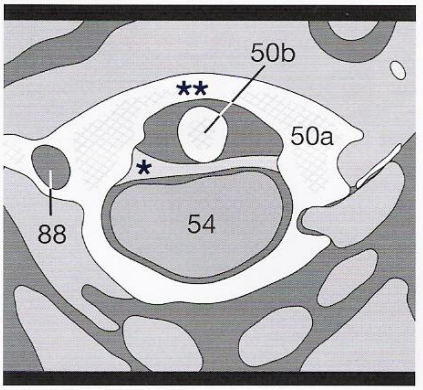

Fig. 152.4b

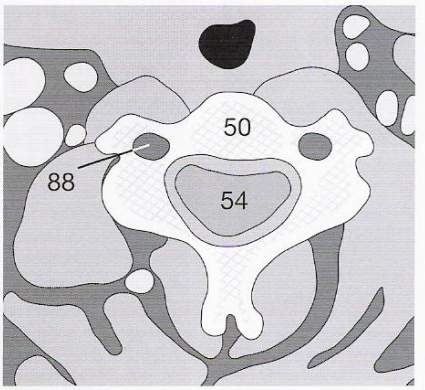

Fig. 152.5b

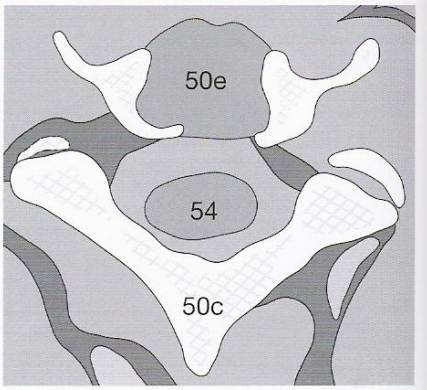

Fig. 152.6b

Cervical Disc Protrusion

A disc protrusion (prolaps of the nucleus pulposus) is demonstrated optimally in CT sections after myelography (CM in the SAS). The spinal cord is virtually isodense to CSF in unenhanced images, making it difficult to define the contours of the cord. After a myelogram, the CSF **(132)** will appear hyperdense to the cord **(54)** as well as to a disc.

Normally, the CSF uniformly surrounds the cervical cord **(Fig. 153.1)**. A disc prolapse **(7)**, protruding into the CSF space can be seen because it is hypodense to the opacified CSF. The gap between the cord **(54)** and vertebral body **(50)** is filled in. Did you recognize the pyriform fossa **(172)**, the hyoid bone **(159)**, the thyroid cartilage **(169)**, and the cricoid cartilage **(167)**?

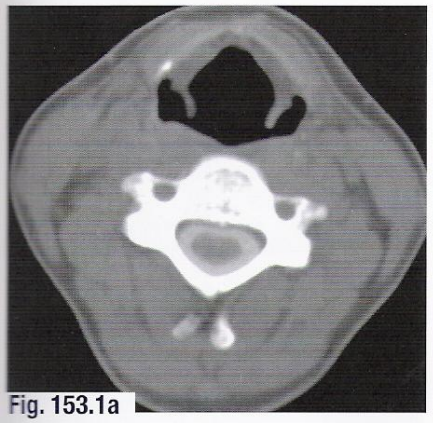

Fig. 153.1a

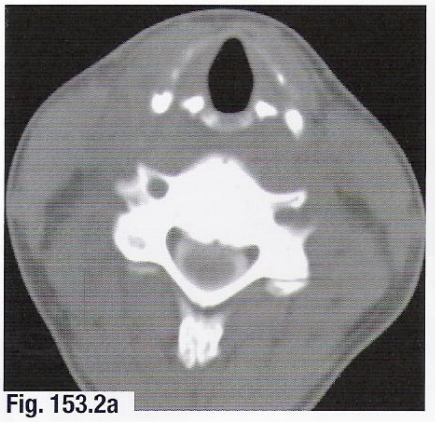

Fig. 153.2a

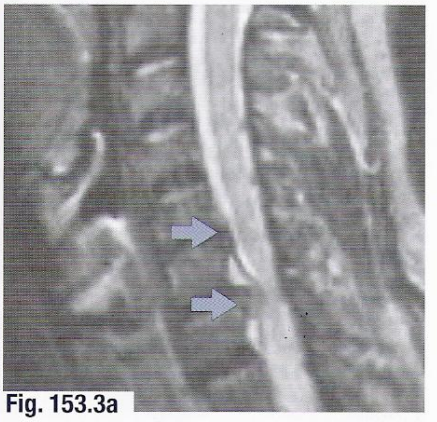

Fig. 153.3a

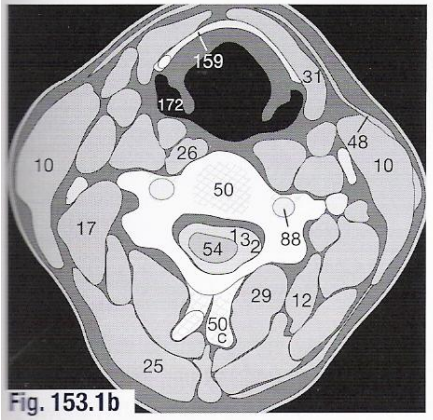

Fig. 153.1b

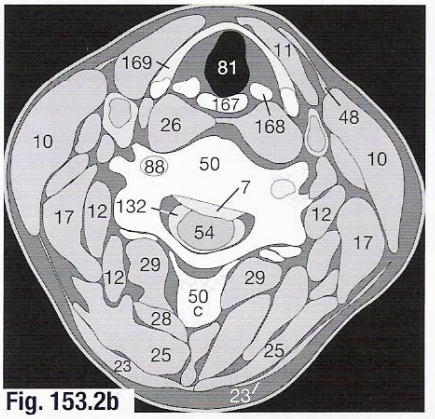

Fig. 153.2b

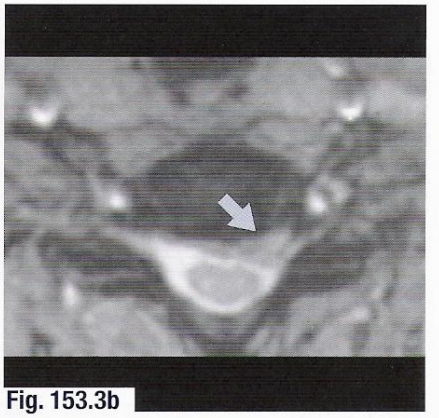

Fig. 153.3b

A disc prolapse will be seen even more clearly in an MR image. The sagittal T_2-weighted image in **Figure 153.3a** shows the extent of protrusions at two disk spaces. The disk protrudes into the hyperintense CSF space (➡) in front of the cord. The axial T_2-weighted image **(Fig. 153.3b)** shows that the prolapse extends to the left and has caused stenosis of the intervertebral foramen (↘).

Cervical Spine Fractures

It is especially important to look for fractures of the cervical spine or for torn ligaments after trauma (ref. p. 152) so that damage to the cord is avoided if the patient needs to be moved or transported. **Figures 153.4a** through **c** show a coronal MPR in which the right occipital condyle **(160)** is fractured **(188)** but the dens **(50b)** is still in normal position.

Fig. 153.4a

Fig. 153.4b

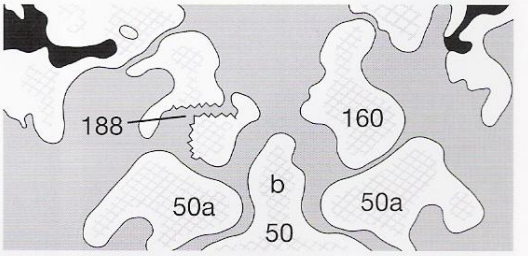

Fig. 153.4c

The thoracic vertebrae articulate with each other at their superior and inferior articular facets **(50d)** and with the ribs **(51)** at the inferior and superior costal facets and the transverse processes **(50f)**. **Figure 154.1** shows a normal thoracic image: the contours of the cortical bone are smooth and the trabeculae have a homogeneous pattern.

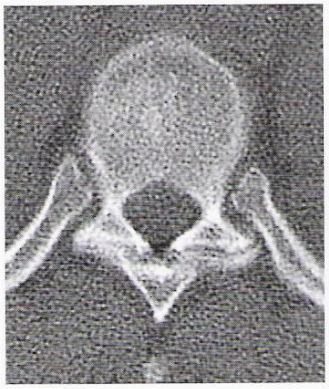

Fig. 154.1a

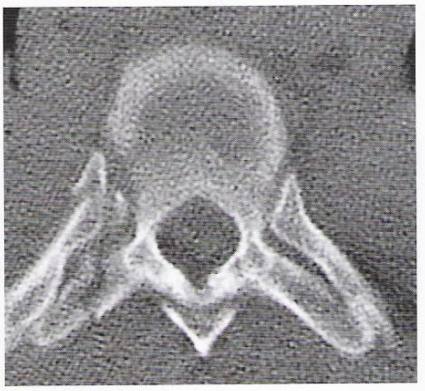

Fig. 154.2a

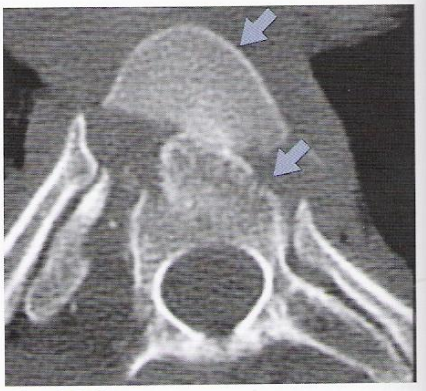

Fig. 154.3a

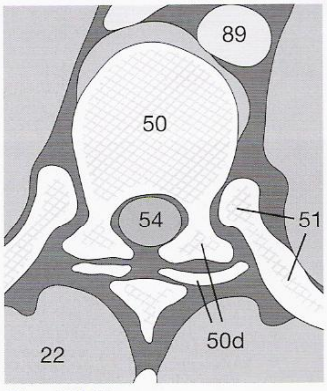

Fig. 154.1b

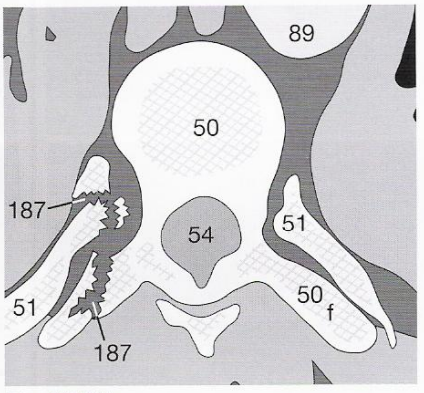

Fig. 154.2b

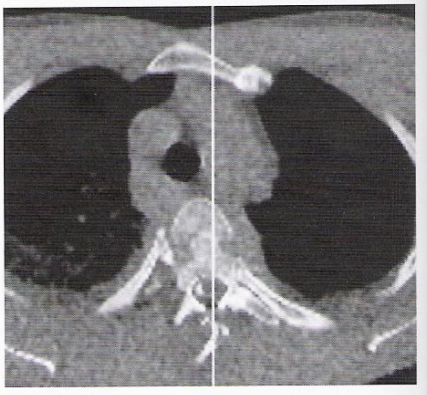

Fig. 154.3b

Fractures of the Thoracic Spine

Displaced fragments are identified by virtue of the fracture lines **(187)** and are best seen on bone windows. In **Figure 154.2**, both the transverse process **(50f)** and the corresponding rib **(51)** are fractured. In complex fracture dislocations **(Figs. 154.3)**, torsion or shearing may cause compression or complete dislocation of the spine as a whole **(Figs. 154.3a, e)**. The axial image in **Figure 154.3a** shows two vertebrae ( ) at one level; the topogram in **154.3b** indicates the position of the sagittal MPR shown in **Figure 154.3e**. The MPR gives a more precise picture of the fracture and the fragments than the oblique anterior and oblique posterior 3D views in **Figures 154.3c** and **d**.

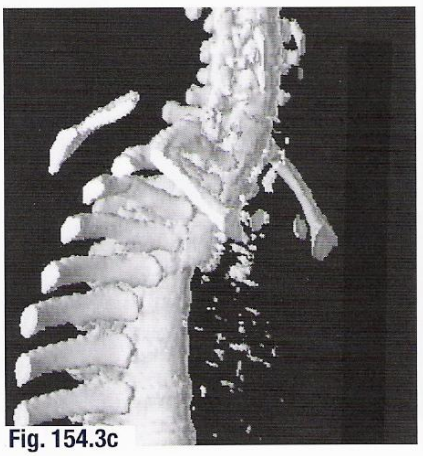

Fig. 154.3c

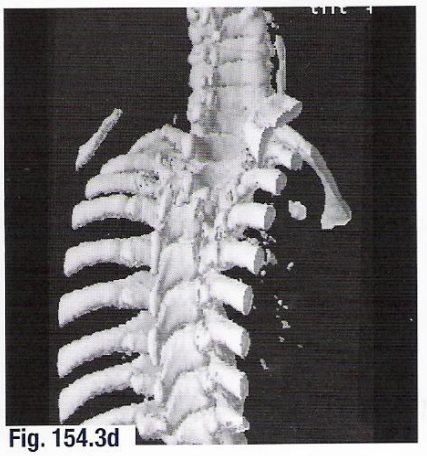

Fig. 154.3d

Fig. 154.3e

The transverse processes **(50f)** of the lumbar vertebrae are occasionally called costal processes. Lumbar vertebrae have much larger bodies **(50)** than thoracic vertebrae, and the angle of their intervertebral joints **(50d)** is smaller. Lumbar spinous processes do not extend as far caudally as the thoracic ones. Images of the normal lumbar spine usually show well-defined cortical bone and homogeneous trabeculae. At the level of a disk **(Fig. 155.2)**, the hypodense cartilage **(50e)** may seem irregularly surrounded by bone: this is an oblique partial volume effect in which parts of an adjacent body **(50)** are included with the disk. The ligamenta flava (★) extend from one lamina to the next and can sometimes be seen behind the cord **(Fig. 155.1a)**.


Fig. 155.1a

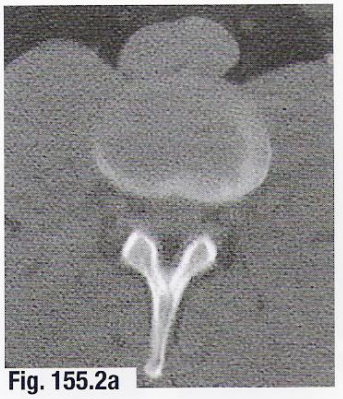
Fig. 155.2a


Fig. 155.3a

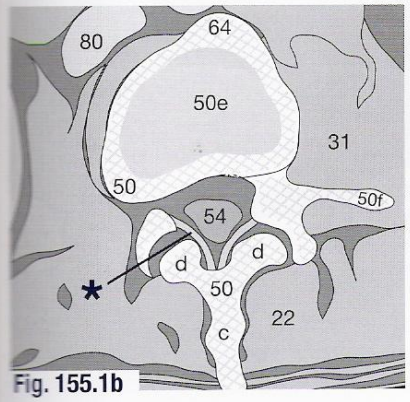

Fig. 155.1b

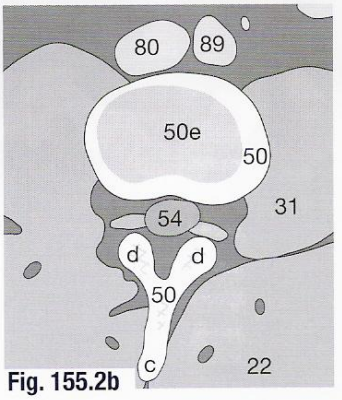

Fig. 155.2b

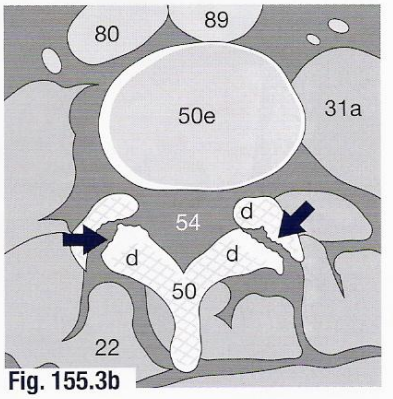

Fig. 155.3b

Degenerative change of the vertebrae can be seen in the facet joints **(50d)** **(Fig. 155.3)**. There is increased subchondral sclerosis (➡, ⬋) indicative of arthrosis of the joint.

Lumbar Disk Prolapse

As with cervical disk protrusions (see p. 153), it is important to establish whether the nucleus pulposus has protruded through the posterior longitudinal ligament. This ligament is applied to the posterior borders of the vertebral bodies and disks. Disk material that has penetrated the posterior longitudinal ligament and become detached from the disk is referred to as a sequestration (★★). This can narrow the spinal canal or a lateral recess **(Fig. 155.4)**. These structures are not well demonstrated on soft-tissue win-dows **(Fig. 155.4a)** because of their high density, but are clearly seen on bone windows **(Fig. 155.4b)**. A T_2-weighted MR image **(Fig. 155.5)** shows the extent of the prolapse: the abnormal disk (➡) is thinner, is desiccated (shows a lower signal level [darker]), and the extruded material (⬋) impinges on the theca.

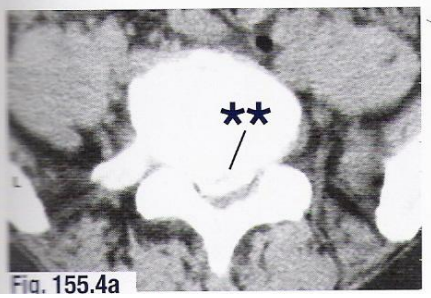

Fig. 155.4a

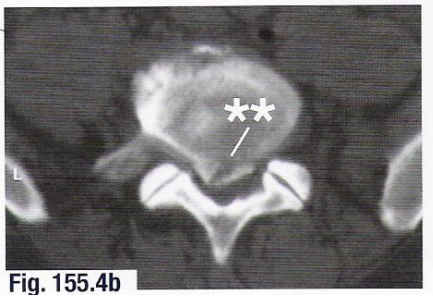

Fig. 155.4b

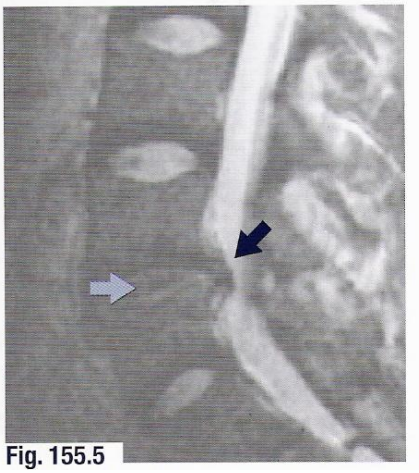
Fig. 155.5

Fractures

In conventional x-rays, it is often difficult to see the fracture of a lumbar transverse process **(50f)** if the fragment is not or only minimally dislocated **(187)**. In CT sections, however, a fracture can be clearly demonstrated **(Fig. 156.1)**. **Figure 156.2** illustrates a case in which the spinous process **(50c)** was fractured. An arthrosis may develop if a fracture has involved a joint **(Fig. 156.3)**. There are fractures of both the superior and the inferior articular processes **(50d)**.

Fig. 156.1a

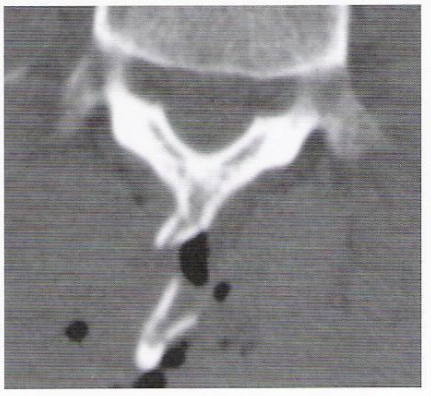

Fig. 156.2a

Fig. 156.3a

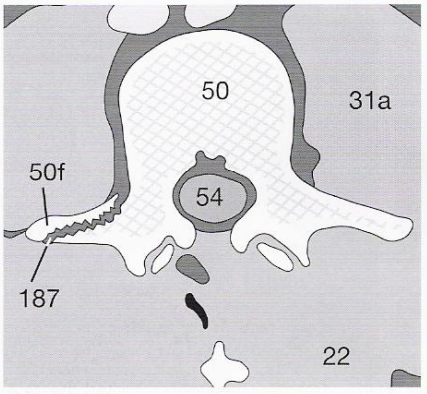

Fig. 156.1b

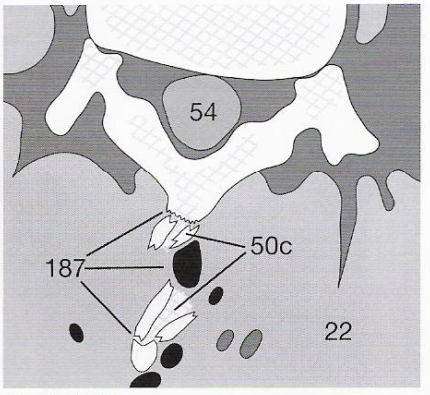

Fig. 156.2b

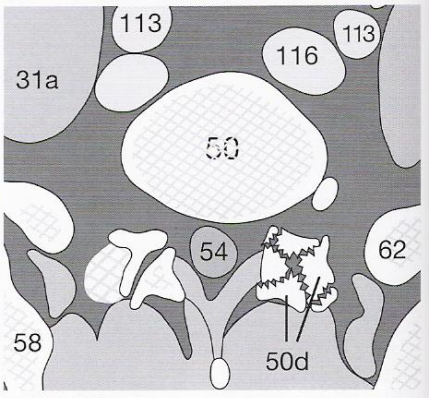

Fig. 156.3b

Older fractures do not show a well-defined fracture line **(187)**. Increased sclerosis and new bone often efface the fracture line or a pseudarthrosis may develop. In the case shown in **Figure 156.4,** the fractured pedicle has developed a pseudarthosis. In conventional x-rays, increased sclerosis following a fracture is often difficult to differentiate from that resulting from degenerative disease.

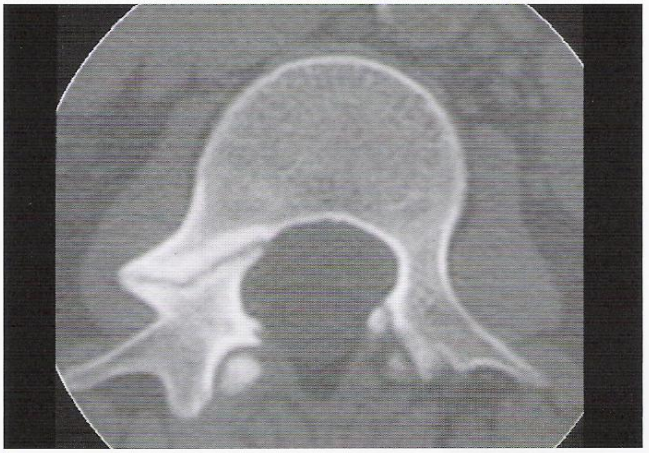

Fig. 156.4a

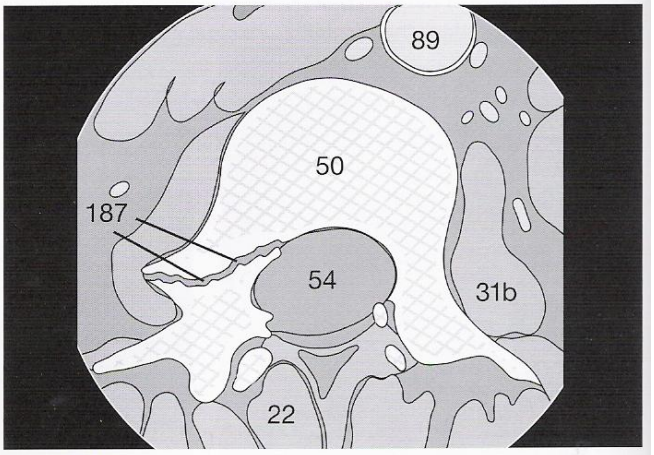

Fig. 156.4b

Tumors and Metastases

Not all bone lesions originate within the bone. Malignant tumors of paravertebral tissues can also invade the bones.

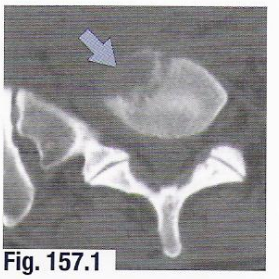
Fig. 157.1

Figure 157.1 shows an osteolytic lesion (↘) in the body of a lumbar vertebra in a patient with carcinoma of the cervix. On soft-tissue windows **(Fig. 157.2)**, there is a paravertebral metastasis **(7)** which has surrounded the bifurcation of the common iliac artery **(114/5)** and has infiltrated the right anterolateral aspect of the vertebral body.


Fig. 157.2a

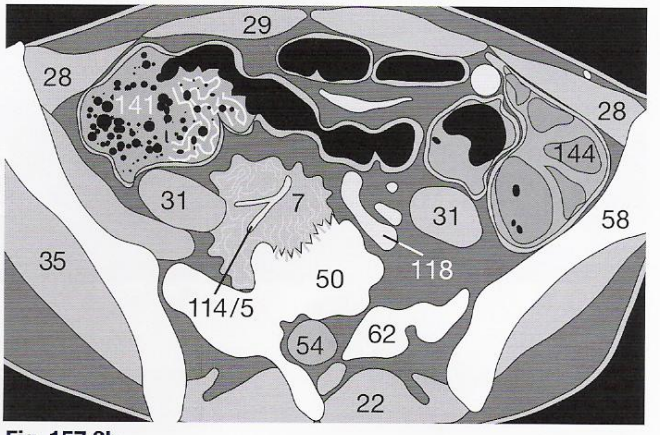

Fig. 157.2b

MPRs in the coronal (**Figs. 157.3a** and **b**) and sagittal (**Figs. 157.4a** and **b**) planes show the extent to which the bone has been eroded and that there is risk of fracture. As in **Figure 146.2**, the 3D reconstructions (**Figs. 157.5a** and **b**) clearly show the lesion from anterior and lateral perspectives, but not the degree to which the interior trabeculae have been destroyed.


Fig. 157.3a

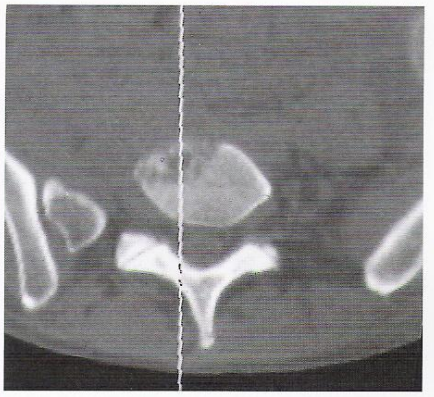
Fig. 157.4a

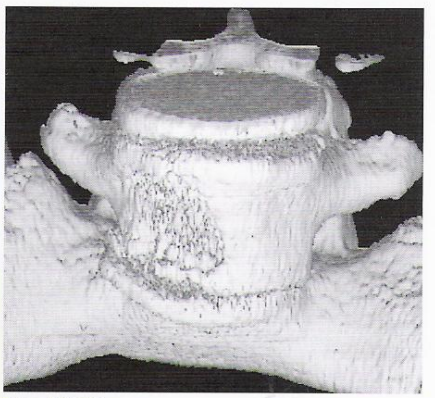
Fig. 157.5a

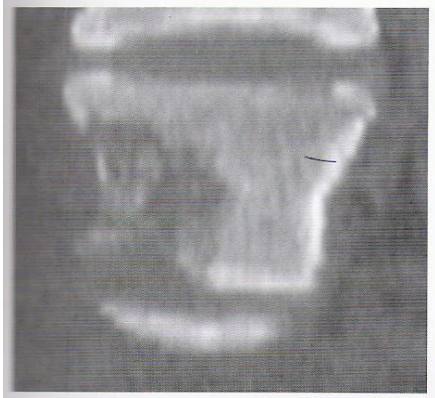
Fig. 157.3b


Fig. 157.4b


Fig. 157.5b

Infection

Abscesses in the paravertebral soft tissues or infective or inflammatory arthritides **(181)** in the small joints of the spine may lead to diskitis which ultimately destroys the intervertebral disk **(Fig. 158.1)**. An advanced abscess can be detected on soft-tissue windows **(Fig. 158.1a)** as an area of heterogeneous density surrounded by a hyperdense enhancing rim representing reactive hyperperfusion. On bone windows **(Fig. 158.1c)**, only small remnants of bone belonging to the vertebral body are present and some are displaced.

Fig. 158.1a

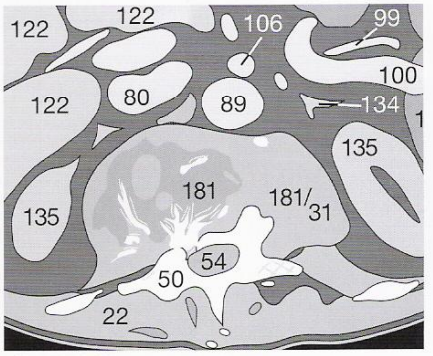

Fig. 158.1b

Fig. 158.1c

Methods of Stabilization

If therapeutic measures such as chemotherapy, antibiotics, and/or surgery have been effective in the treatment of a metastasis or infection, it is possible to stabilize the spine by inserting bone prosthetic material **(Fig. 158.2a, b)**.

The choice of material depends upon the size of the defect and upon other individual factors. In follow-up examinations, these materials may cause considerable image artifacts because of their high relative density.

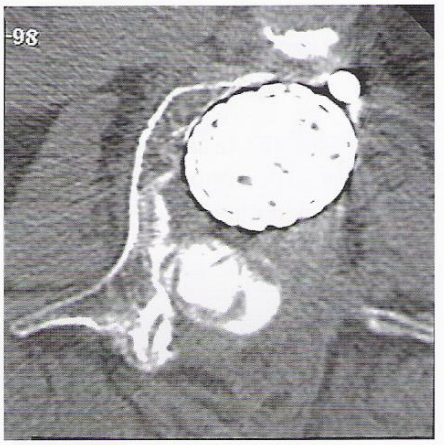

Fig. 158.2a

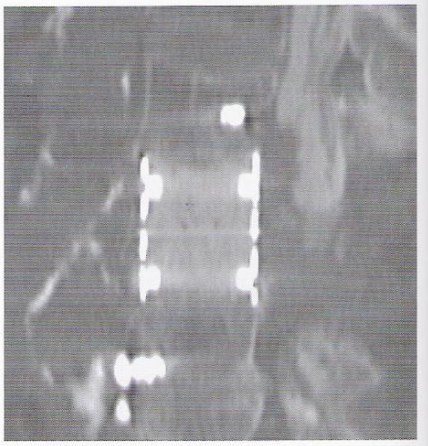

Fig. 158.2b

Space for additional notes:

The anterior muscles of the thigh include the sartorius muscle **(38)**, and the four components of the quadriceps muscle **(39)**. The most anterior is the rectus femoris **(39a)**, and lateral to this is the vastus lateralis **(39b)**. The vastus intermedius **(39c)** and vastus medialis **(39d)** form the anterolateral borders of the adductor canal. This contains the superficial femoral artery and vein **(119/120)**. The adductor muscles comprise the superficially located gracilis muscle **(38a)** and the adductor longus **(44a)**, brevis **(44b)**, and magnus **(44c)** muscles. The pectineus muscle **(37)** is only seen in the most caudal images of the pelvis.

The posterior muscles of the thigh extend the hip joint and flex the knee joint. The group consists of the long and short heads of the biceps femoris muscle **(188)** and the semitendinosus **(38b)** and semimembranosus muscles **(38c)**. In the proximal third of the thigh **(Fig. 159.1)**, the hypointense tendon of the biceps muscle is adjacent to the sciatic nerve **(162)**. In the distal third of the thigh **(Fig. 159.3)**, the medial popliteal nerve **(162a)**, which supplies the dorsal muscles, can be seen separate from the lateral popliteal nerve **(162b)**. Note the close relationship of the profunda femoris artery and vein **(119a/120a)** to the femur **(66)** and the superficial posi-tion of the long saphenous vein **(211a)**.

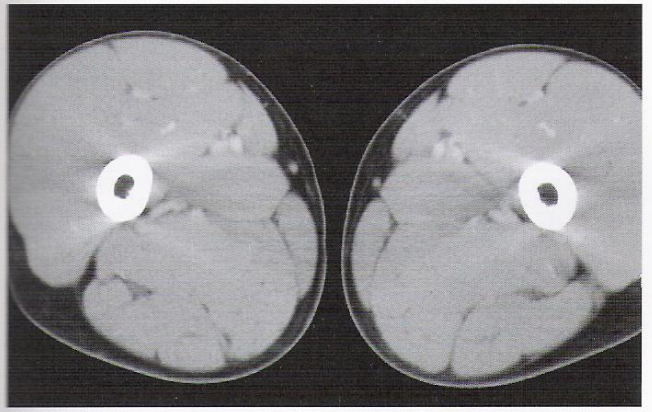

Fig. 159.1a

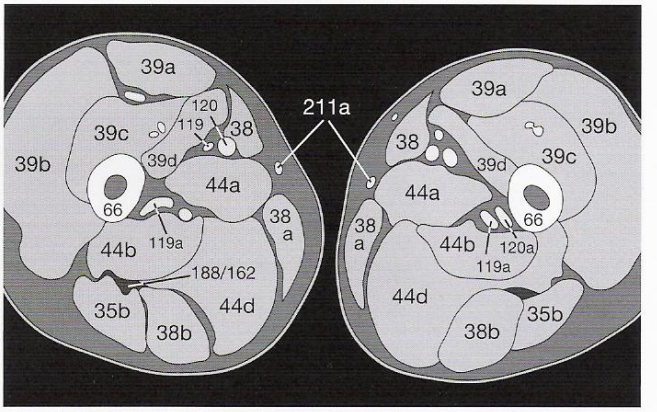

Fig. 159.1b

Fig. 159.2a

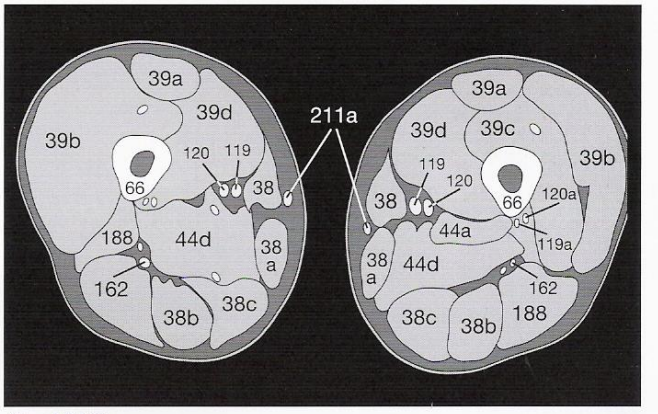

Fig. 159.2b

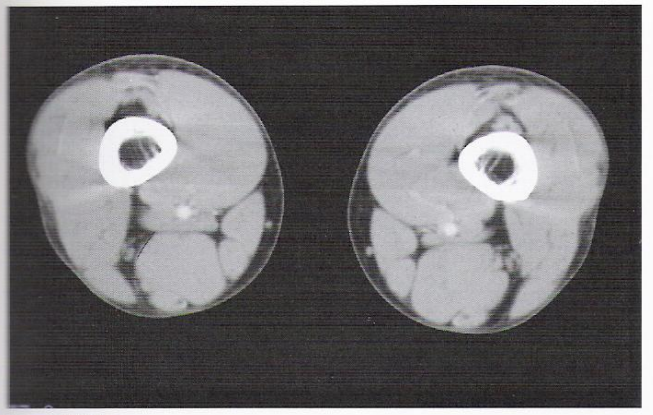

Fig. 159.3a

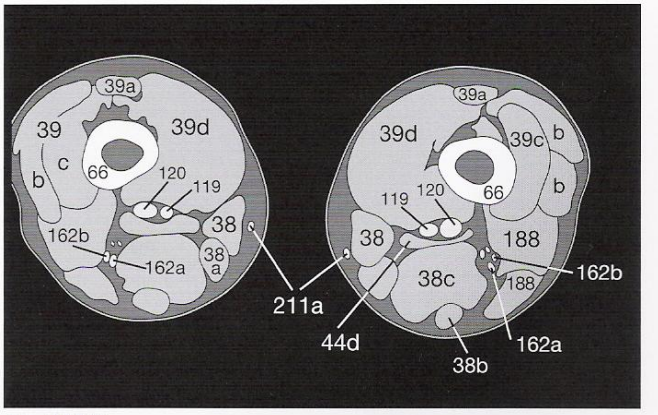

Fig. 159.3b

The popliteal artery **(209)** and vein **(210)**, formed cranial to the joint line, are demonstrated at the level of the patella **(191)** in the fossa between the femoral condyles **(66d)** **(Fig. 160.1)**. The tibial nerve **(162a)** lies directly posterior to the vein, whereas the fibular (peroneal) nerve **(162b)** lies more laterally. The medial **(202a)** and lateral **(202b)** heads of the gastrocnemius muscle and the plantaris muscle **(203a)** can be seen posterior to the femoral condyles. The long saphenous vein **(211a)** lies medially in the subcutaneous fat covering the sartorius muscle **(38)**, and the biceps femoris muscle **(188)** lies laterally.

On the section just caudal to the patella **(Fig. 160.2)**, the patellar tendon **(191c)** can be identified, posterior to which is the infrapatellar fat pad **(2)**. Between the femoral condyles lie the cruciate ligaments **(191b)**.Transverse sections such as these are frequently combined with coronal and sagittal MPRs (see also the images of a fracture on p. 167).

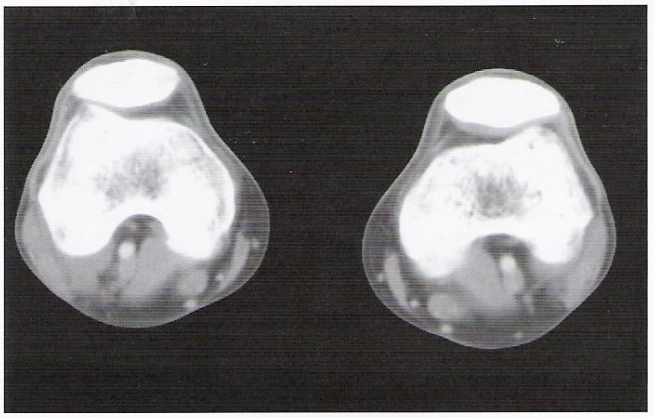

Fig. 160.1a

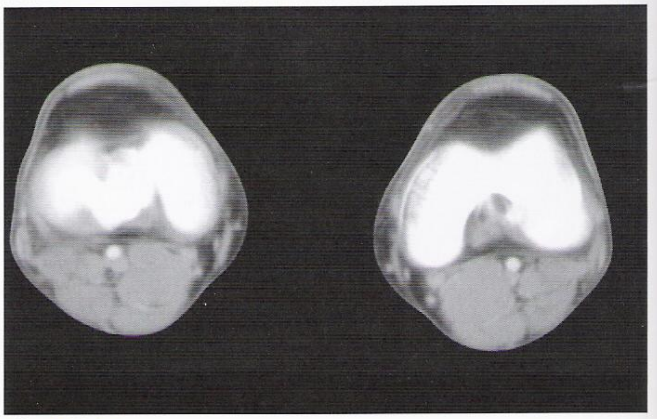

Fig. 160.2a

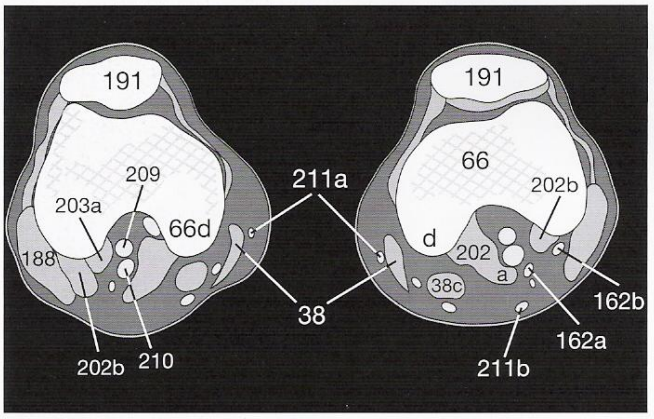

Fig. 160.1b

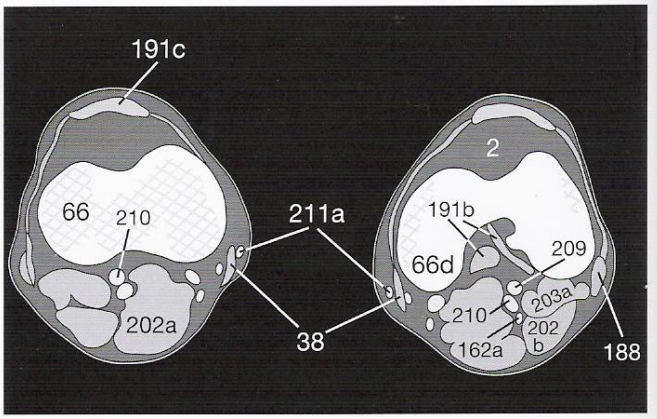

Fig. 160.2b

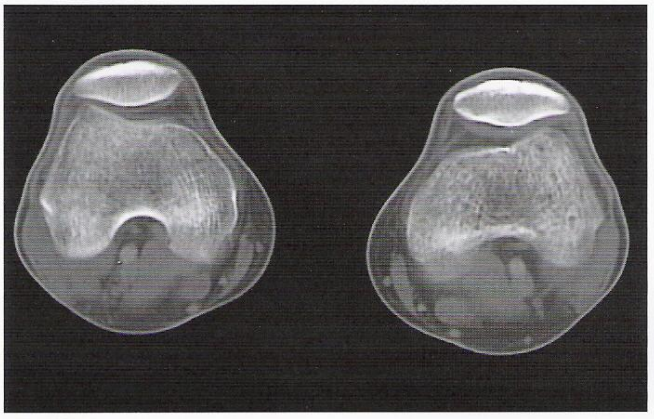

Fig. 160.1c

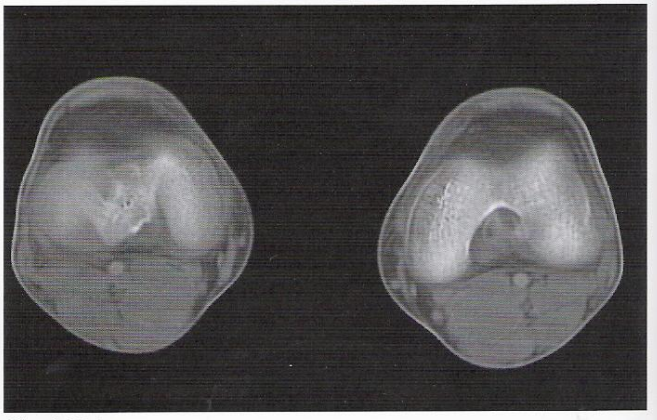

Fig. 160.2c

The muscles of the lower leg are separated into four compartments by the interosseus membrane between the tibia **(189)** and the fibula **(190)** and by the lateral and posterior intermuscular septa (**Figs. 161.1** to **161.3**). The anterior compartment contains the tibialis anterior muscle **(199)**, the extensor hallucis longus muscle **(200a)** and the digitorum longus muscle **(200b)** next to the anterior tibial vessels **(212)**.

The lateral compartment contains the peroneus longus **(201a)** and brevis **(201b)** muscles next to the peroneal vessels **(214)**. In slender individuals who have no fat between the muscles, these vessels and the peroneal nerve are only poorly defined **(Fig. 161.2)**.

The flexor muscles can be separated into a superficial and a deep group. The superficial group encompasses the gastrocnemius muscle with medial **(202a)** and lateral **(202b)** heads, the soleus muscle **(203)**, and the plantaris muscle **(203a)**. The deep group includes the tibialis posterior **(205)**, the flexor hallucis longus **(206a)**, and the flexor digitorum longus muscles **(206b)**. These muscles are particularly well defined in the distal third of the lower leg **(Fig. 161.3)**. The tibil alis posterior vessels **(213)** and the tibial nerve **(162a)** pass between the two flexor groups.

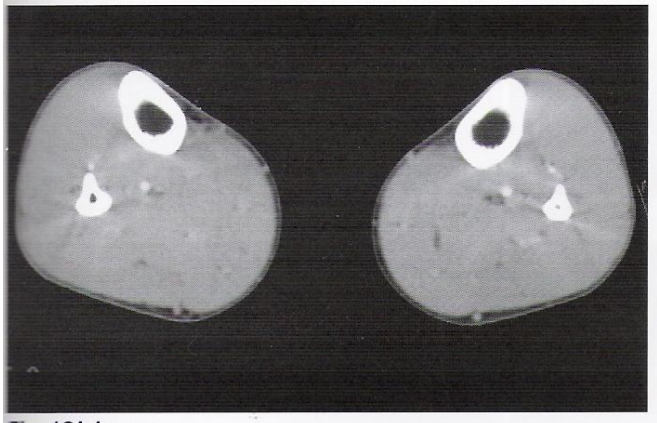

Fig. 161.1a

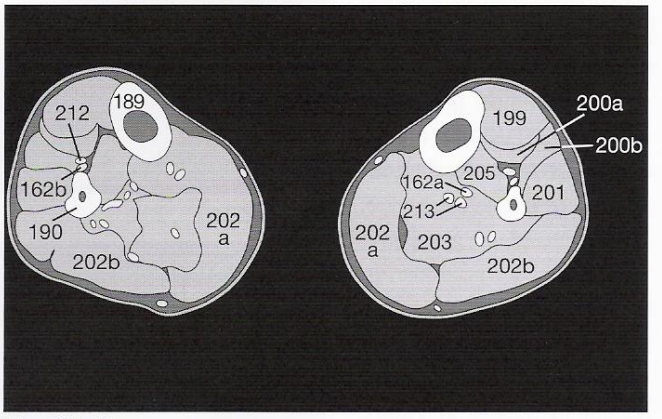

Fig. 161.1b

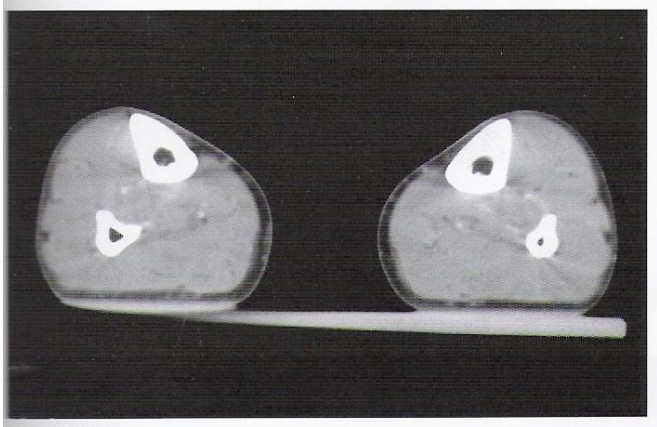

Fig. 161.2a

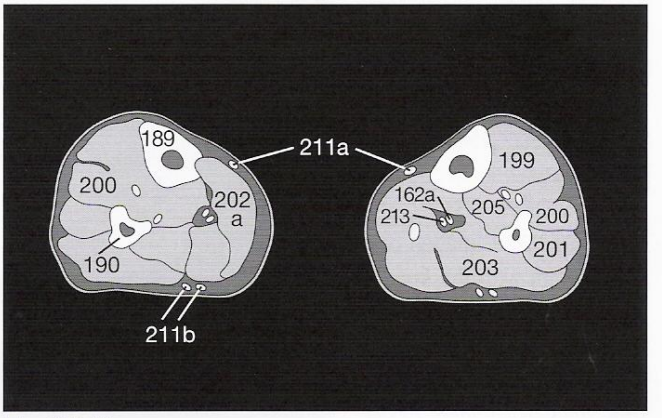

Fig. 161.2b

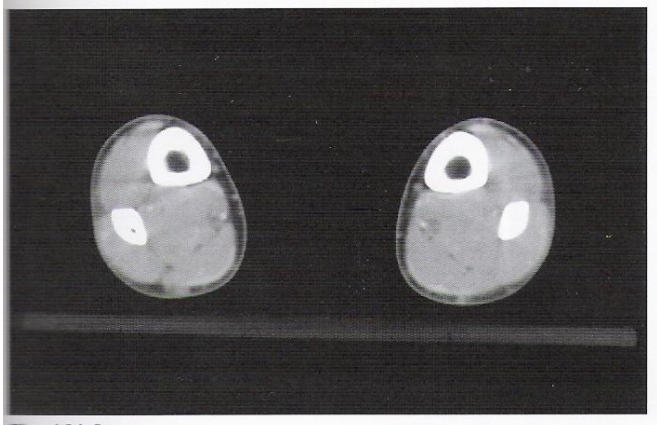

Fig. 161.3a

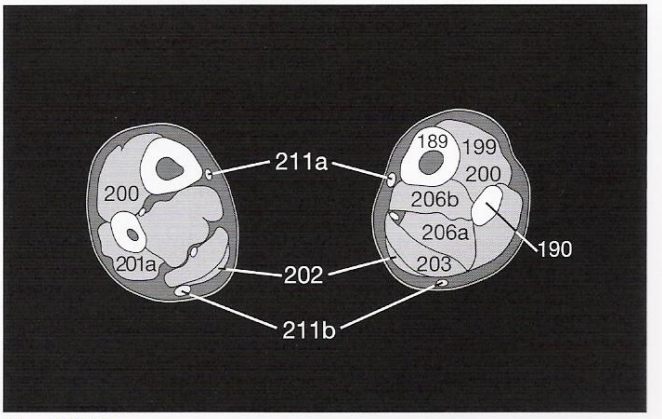

Fig. 161.3b

The following three pages show the normal anatomy of the foot on the bone window. You will find the numbers to the legends in the back fold-out.

The image series begins in a plane through the talus **(192)** just distal to the talocrural joint. **Figure 162.1** shows the distal end of the fibula or lateral malleolus **(190a)** as well as the upper part of the calcaneous **(193)**. In **Figure 162.2**, the sustentaculum tali **(193a)** of the calcaneous is seen.

More distally, additional metatarsal bones are seen: the navicular bone **(194)** has begun to appear in **Figure 162.2**, but its joint with the talus is better assessed in **Figure 162.3**. The articular surfaces are normally smooth and the synovial space between the bones is of uniform width.

Compare these images of a normal foot with the images of fractures on pages 164 and 165.

The Achilles tendon **(215)**, which arises from both the soleus **(203)** and the gastrocnemius **(202)** muscles, is seen posteriorly on these images.

Fig. 162.1a

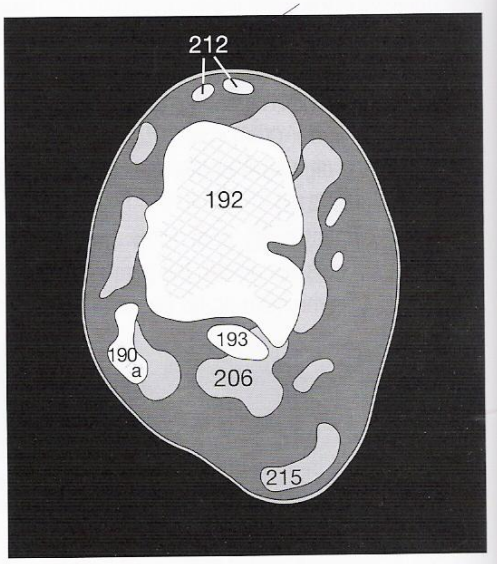

Fig. 162.1b

Fig. 162.2a

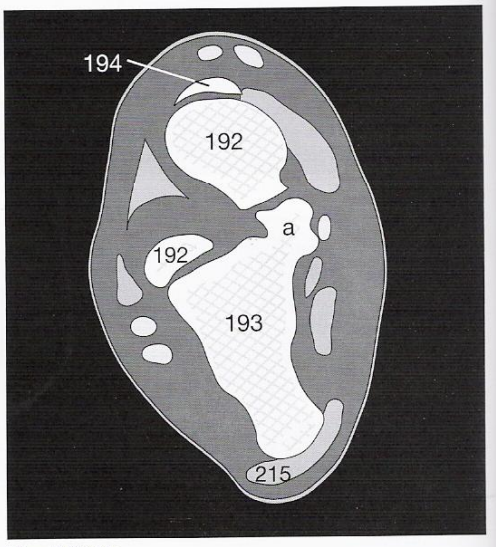

Fig. 162.2b

Fig. 162.3a

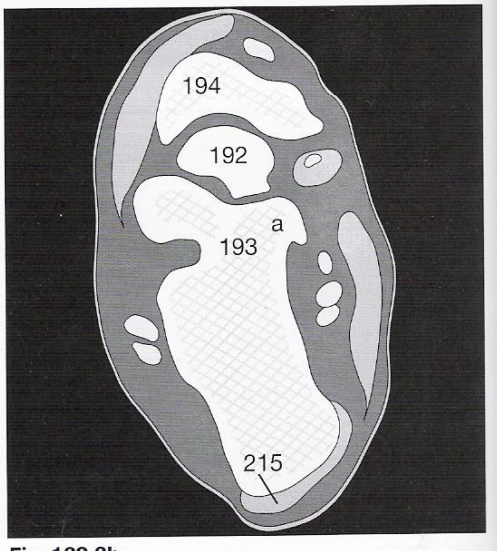

Fig. 162.3b

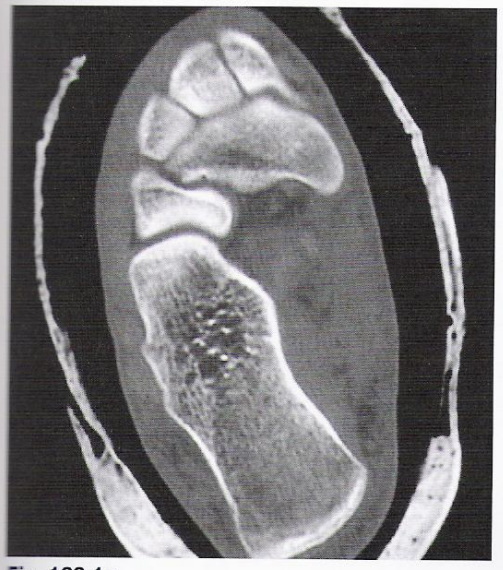

Fig. 163.1a

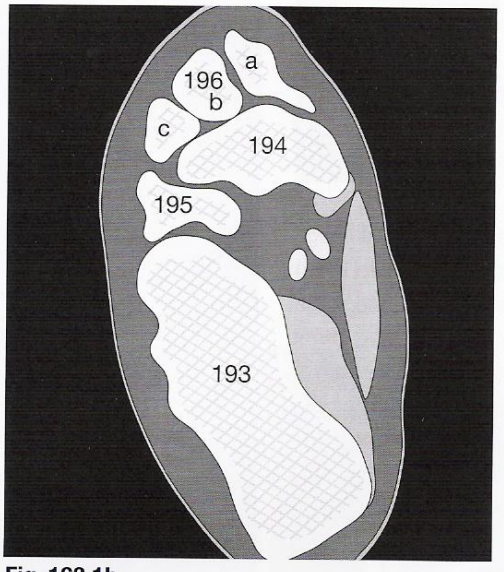

Fig. 163.1b

The cuboid bone **(195)** is seen on the lateral margin of the foot, between the calcaneus **(193)** and the navicular **(194)**. The lateral **(196c)**, intermediate **(196b)**, and medial **(196a)** cuneiform bones lie anterior to the navicular **(Fig. 163.1)**.

The transition to the metatarsal bones **(197)** is not always well defined, because the plane of the tarsometatarsal joints is at an oblique angle to the sections (partial volume effects **(Fig. 163.2)**. The joints can be more clearly assessed in multiplanar reconstructions that take this obliquity into account (cf. **Fig. 164.1**).

The lumbrical and quadratus plantae muscles and the short flexor muscles of the foot **(208)** are seen just below the arch of the metatarsal bones. These muscles are only poorly defined in CT images **(Fig. 163.3)**.

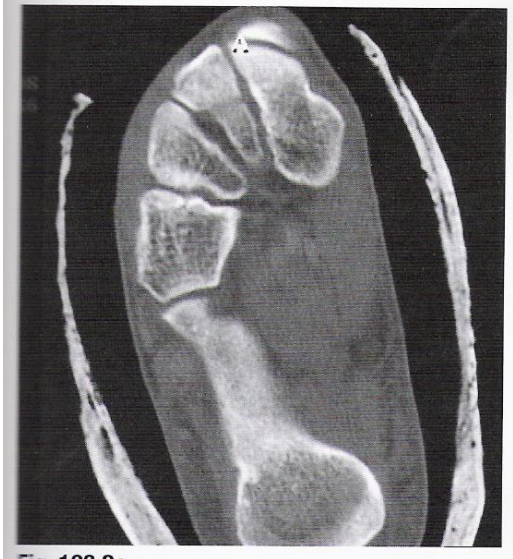

Fig. 163.2a

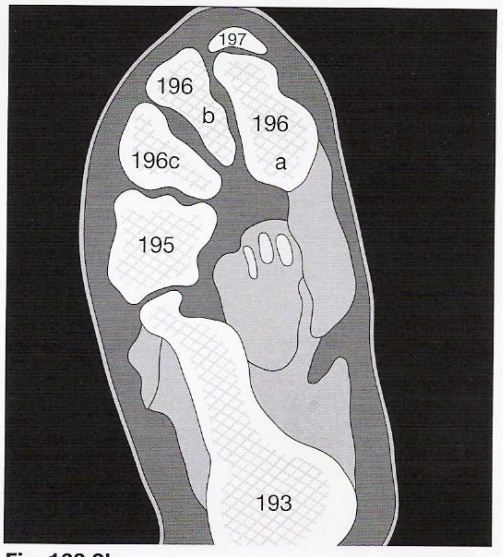

Fig. 163.2b

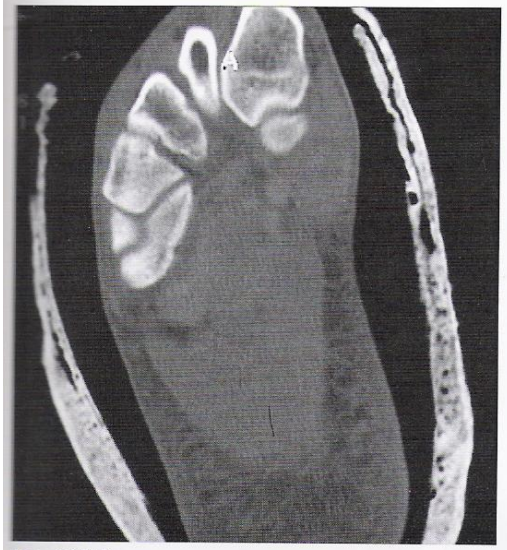

Fig. 163.3a

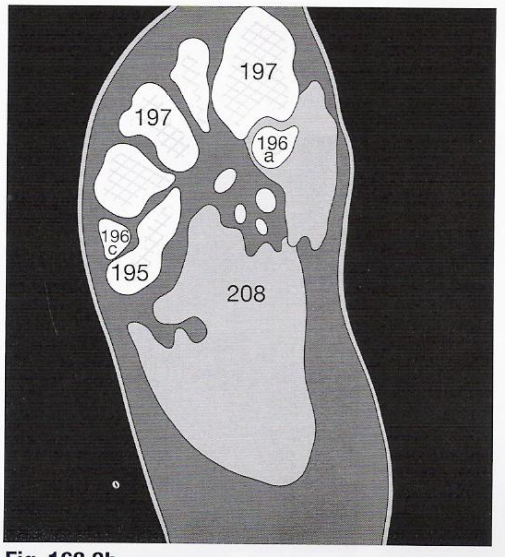

Fig. 163.3b

Multiplanar reconstructions are very valuable for visualizing fractures of the foot. The lateral digital radiograph in **Figure 164.1a** indicates the angle of the image plane, parallel to the long axis of the foot, seen in **Figure 164.1b**. This reconstructed image extends from the lateral **(190a)** and medial **(189a)** malleoli (at the lower edge of the image) through the talus **(192)** and the navicular **(194)** to the three cuneiform bones **(196a–c)**. Two of the metatarsal bones **(197)** are included in the section. Note that the surfaces of the joints are smooth and evenly spaced. The sagittal image in **Figure 164.2b** was reconstructed slightly more laterally (see position in **164.2a**) so that the cuboid bone **(195)** is included. The short flexor muscles **(208)** and the plantar ligaments are seen below the arch of the foot. The Achilles tendon **(215)** is seen posteriorly.

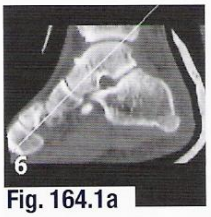

Fig. 164.1a


Fig. 164.1b

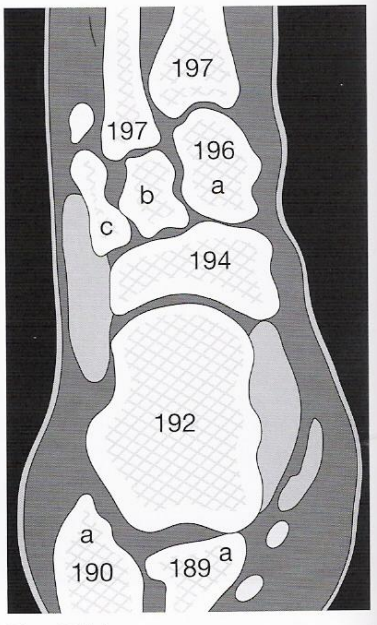

Fig. 164.1c

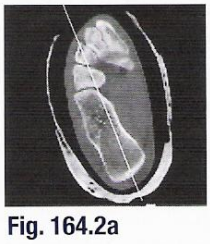
Fig. 164.2a


Fig. 164.2b

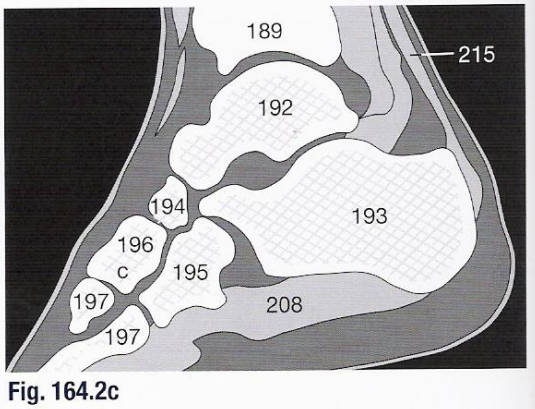

Fig. 164.2c

Diagnosis of Fractures

Typical signs of a fracture can be seen in the original axial plane **(Fig. 164.3a)**: irregularities in the cortical outline (↓), displaced fragments (↙) and a fracture line (←) in the calcaneous. The MPR in the coronal plane (indicated in **Fig. 164.3b**) shows that not only is the calcaneous (↖) fractured, but there is a hairline fracture of the talus (→) involving the ankle joint **(Fig. 164.3c)**.

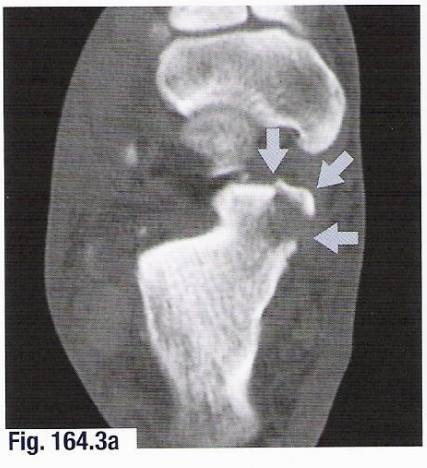
Fig. 164.3a


Fig. 164.3b


Fig. 164.3c

Fractures of the foot may initially escape detection in conventional x-rays if there is no major displacement of bone fragments. If the foot remains painful, a follow-up x-ray may show the fracture because fine hairline fractures can be seen when filled with hemorrhage. As an alternative, CT would show discrete fracture lines **(187)**, as for example of the talus **(192)** in **Figure 165.1**.

In chronic fractures, the displaced fragment (✱) has usually become rounded off **(Fig. 165.2)**. In this example, it is obvious that there were actually two fragments because a second fracture line (⬇) is seen next to the main one **(187)**.

It is often difficult to treat comminuted fractures of the calcaneus **(193)**, incurred for example during a fall **(Fig. 165.3)**, because there are many small displaced fragments. A stabile reconstruction of the arch of the foot may not be possible, resulting in a long period of sick leave.

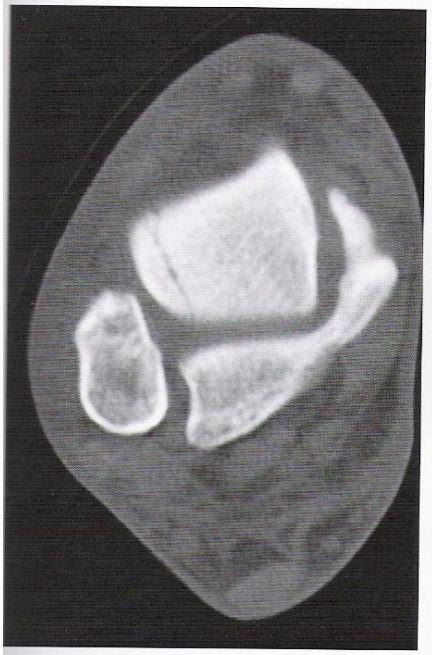

Fig. 165.1a

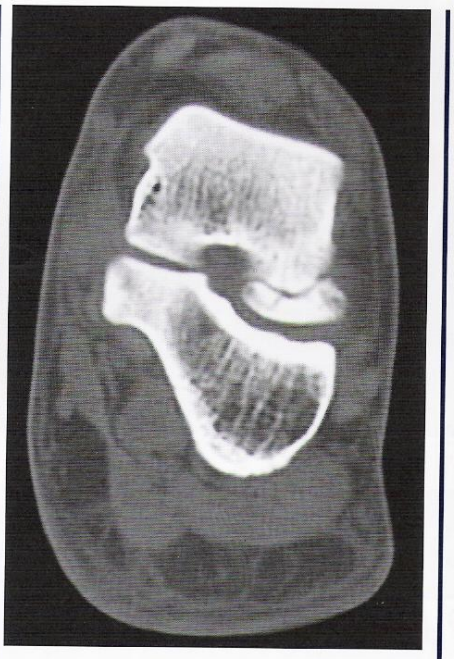

Fig. 165.2a

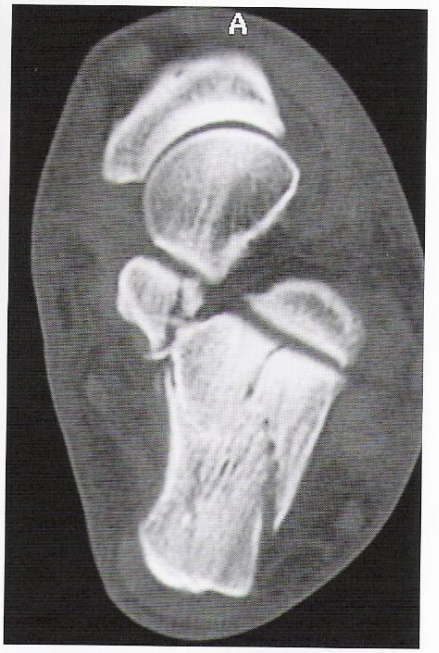

Fig. 165.3a

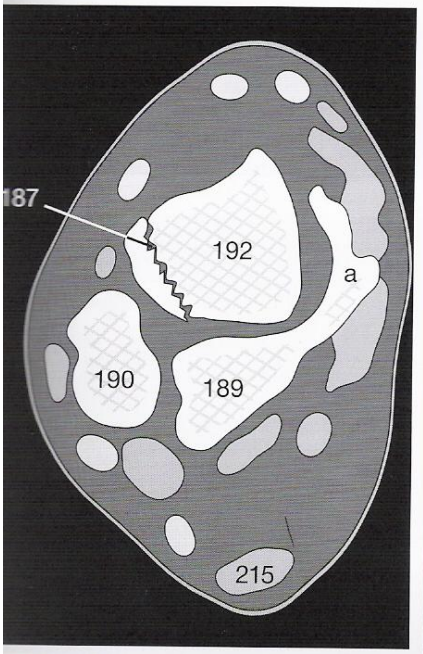

Fig. 165.1b

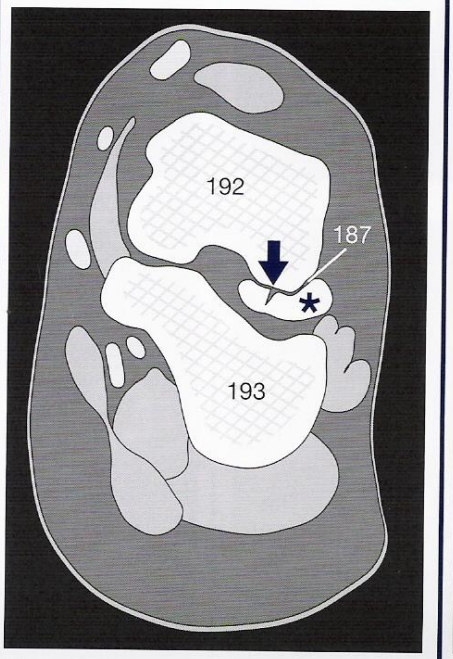

Fig. 165.2b

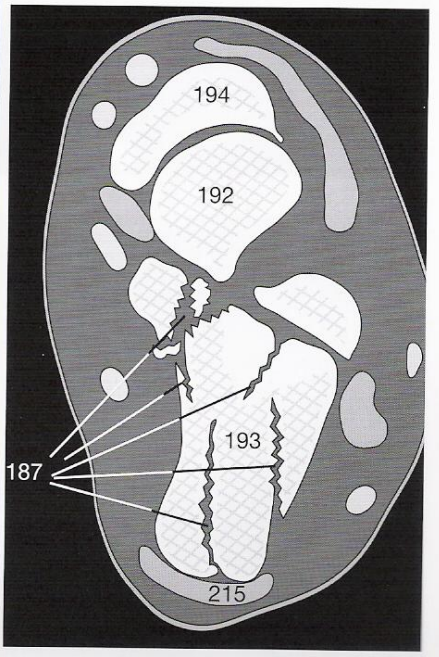

Fig. 165.3b

Infections

The assessment of fractures of long bones is generally the domain of conventional radiology. But CT examinations are helpful for locating displaced fragments and in the preoperative planning of comminuted fractures. Infections, however, are more accurately imaged by CT than by conventional radiographs because bone destruction is more readily seen on bone windows **(Fig. 166. 1c)** and soft-tissue involvement **(178)** is documented on soft-tissue windows **(Fig. 166.1a)**. This patient had septic arthritis of the left hip joint with involvement of the acetabulum **(60)** and femoral head **(66a)**.

The abscess appears more clearly after contrast enhancement (cf. **Figs. 166.2a** and **166.2c**). The increased vascularity of the wall and the fluid within the abscess **(181)** are well demarcated from surrounding fat **(2)**. Adjacent muscles **(38, 39, 44)** are no longer individually defined because of edema (compare with the right leg). Gas **(4)** has been produced and is loculated in the adjacent tissues.

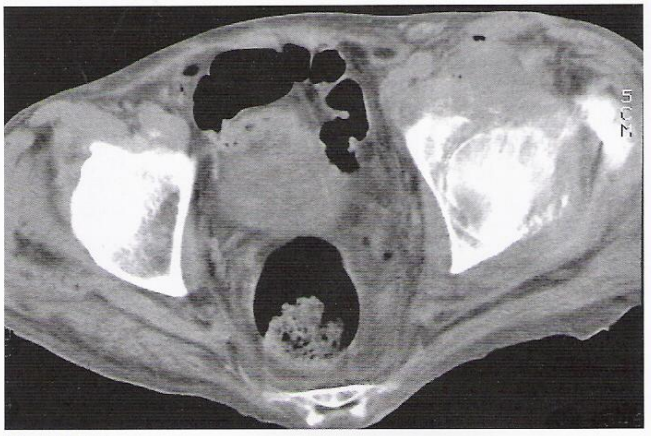

Fig. 166.1a

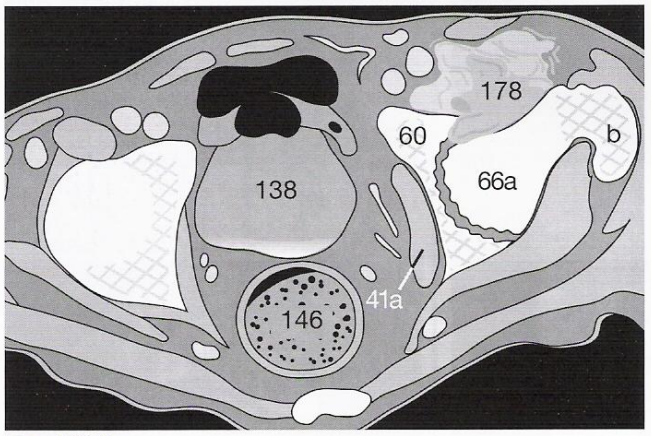

Fig. 166.1b

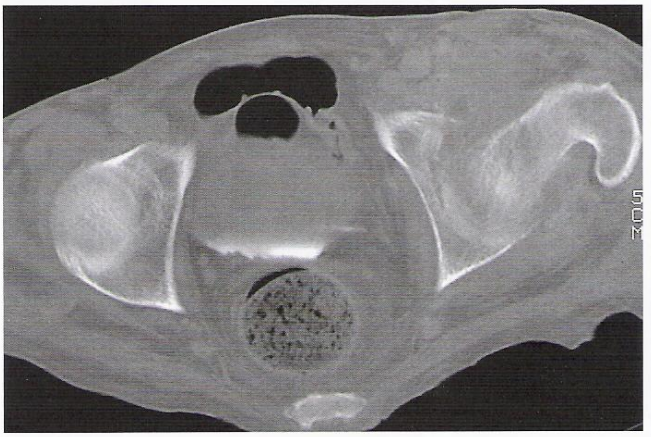

Fig. 166.1c

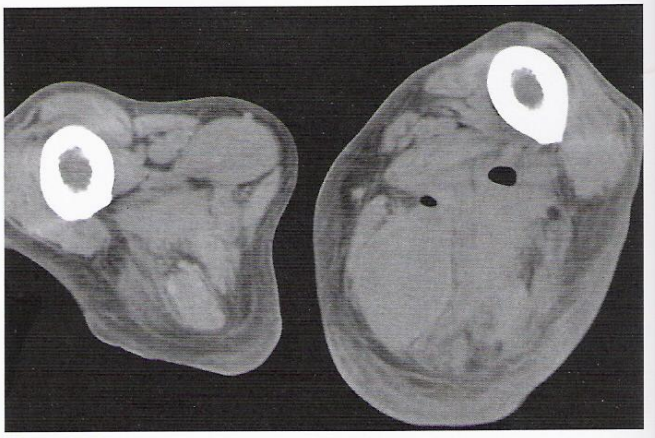

Fig. 166.2a

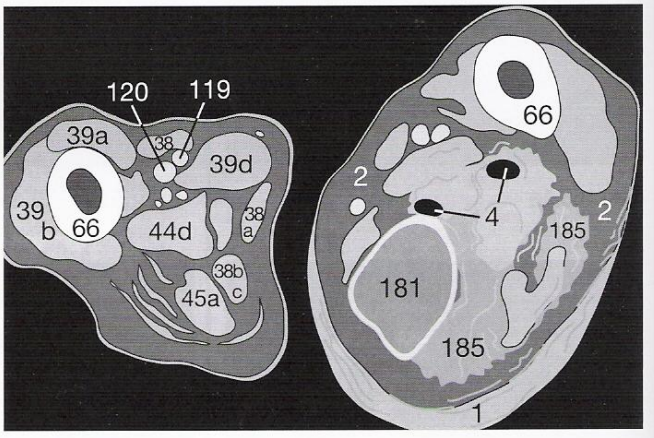

Fig. 166.2b

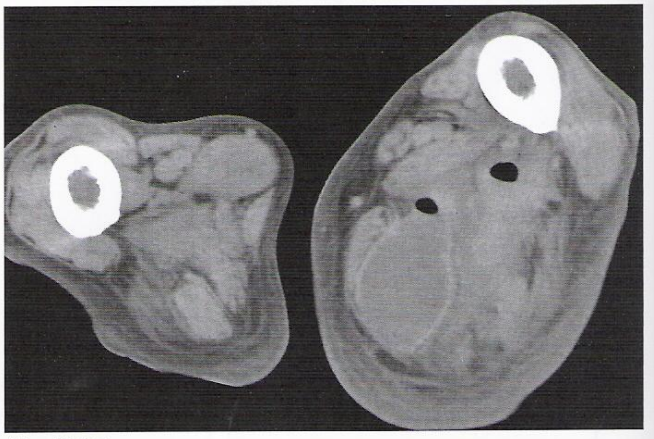

Fig. 166.2c

Fractures

If a fracture involves the knee joint, it is particularly important to reduce the fragments accurately to avoid joint surface incongruities that might lead to arthosis. In the case below, axial sections clearly show the lateral displacement of a large fragment ( ) of the tibia (**Figs. 167.1a** and **167.1b**). The coronal MPR (**Fig. 167.2b**, with level shown in **167.2a**) illustrates how much of the tibial plateau is affected.

Fig. 167.1a

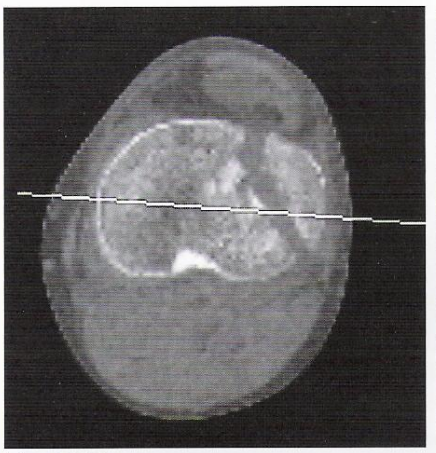

Fig. 167.2a

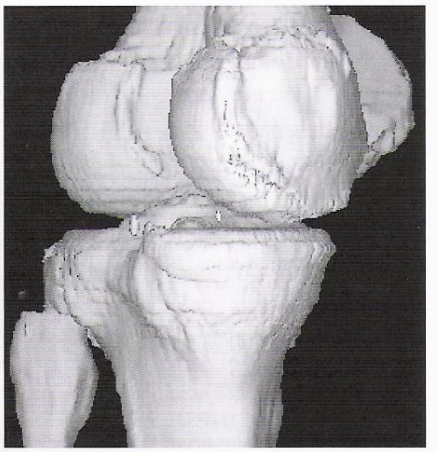

Fig. 167.3a

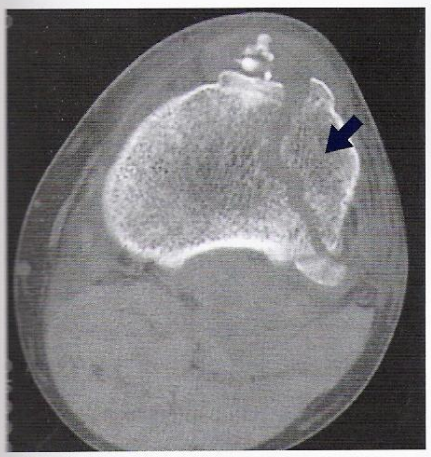

Fig. 167.1b

Fig. 167.2b

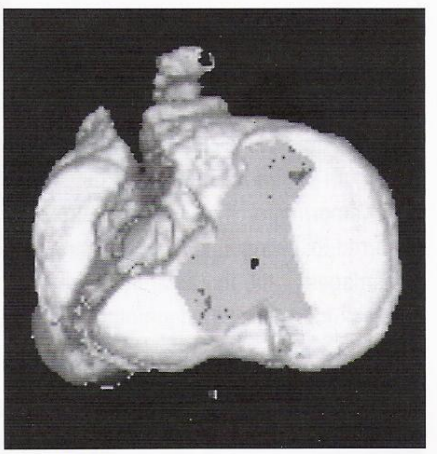

Fig. 167.3b

The 3D reconstruction seen from a posterolateral projection **(Fig. 167.3a)** is not very helpful, but the view from cranial **(Fig. 167.3b)** gives a good impression of the tibial plateau and fracture line because the femoral condyles have been excluded.

Checklist Skeletal System: Fracture Diagnosis

- → Step-off or discontinuity of the cortex (evidence of fracture)?
- → Articular involvement of a fracture (risk of secondary degenerative changes)?
- → Stability on weight-bearing?

  Spine: e.g., 3-column model according to Denis (C-spine); A-B-C classification according to Magerl (T-spine)
- → Simple fracture or comminuted fracture, extent of displacement of the fracture fragments (surgical planning)?
- → Age of the fracture?
  - Acute => ragged and sharply demarcated fracture clefts
  - Old => sclerotic rim, callus formation

    Risk of pseudoarthrosis with persistent fracture cleft?
- → Traumatic or pathologic fracture (underlying bone tumor)?

It is not always possible to determine the nature of a lesion from CT appearance and densitometry alone. In these cases, needle biopsies may be carried out under ultrasound or CT guidance. The patient's platelet count and coagulation status must be checked and informed consent obtained.

In **Figure 161.1**, a mass in the caudate lobe (*) of the liver **(122)** is being biopsied. The close proximity of the hepatic artery and portal vein **(98/102)** and inferior vena cava **(80)** leave only a narrow path for the needle to approach from the right side **(Fig. 168.1a)**. Firstly the section on which the lesion appears largest is determined. The skin is cleaned and anesthetized with local anaestheic.

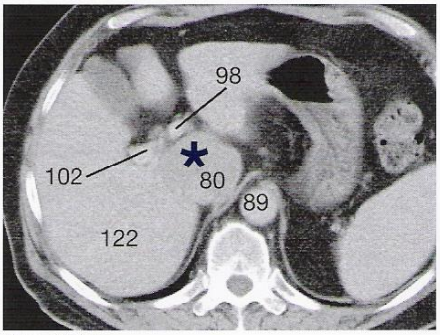

Fig. 168.1a

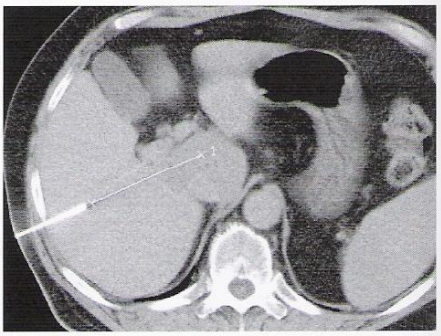
Fig. 168.1b

The needle is then inserted through the liver parenchyma toward the lesion. Slight changes in angle may be necessary (**Figs. 168.1b, 168.1c,** and **168.1d**). Distances can also be calculated during the procedure, as seen in **Figure 168.1b**. After biopsy has been completed, an image is acquired to detect any hemorrhage. If a pneumothorax occurred following lung biopsy, expiratory images of the thorax are acquired to check for a tension pneumothorax.

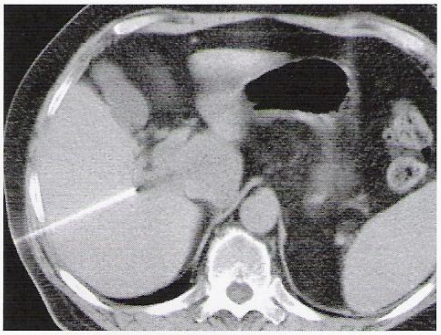
Fig. 168.1c

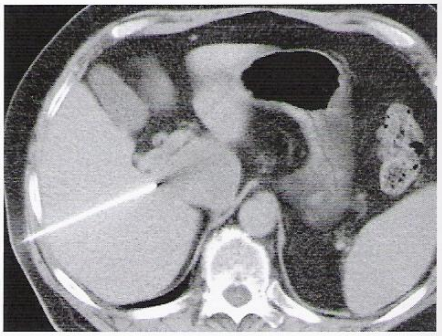
Fig. 168.1d

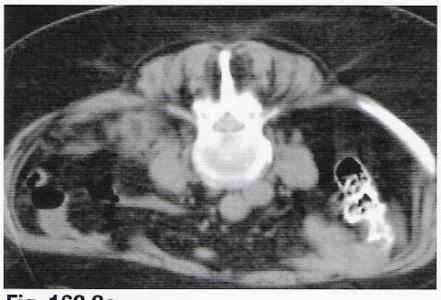
Fig. 168.2a

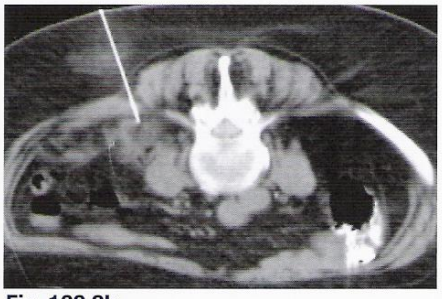
Fig. 168.2b

If there is a retroperitoneal lesion close to the spinal column, a biopsy may be carried out in the prone position. The orientation in **Figure 168.2** is therefore unusual and one must be careful not to confuse left with right, but the procedure is identical.

After selection of the optimal level (largest diameter of the lesion), and after skin cleaning and local anesthesia, the needle is inserted **(Fig. 168.2b)** and the biopsy taken. The material should be promptly prepared for cytology and histology.

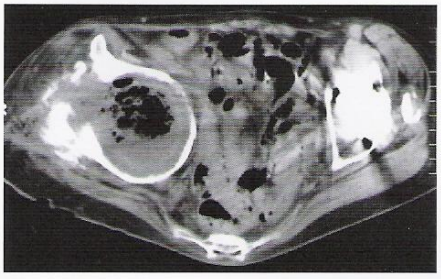
Fig. 168.3a

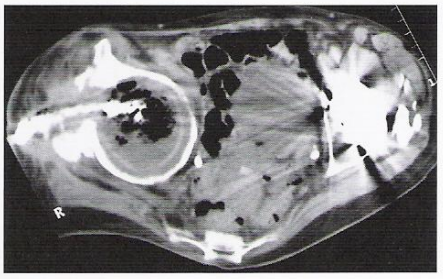
Fig. 168.3b

The size and extent of a cutaneous fistula can often be more clearly assessed if CM is instilled through a tube **(Fig. 168.3)**. In this example, the hip had become infected and an abscess filled the joint after prosthetic surgery.

Of course, definitive protocols do not exist for all indications. Nevertheless, protocols based on experience can be recommended, to be adapted to the specific CT unit and clinical question by the examiner. Typically, a slow gantry rotation is used to diagnose fractures (rotation = 1.5 seconds) and fast gantry rotation to evaluate the soft tissues (rotation = 0.8 - 1.0 seconds). If no reconstruction interval (RI) is provided, a conventional acquisition without spiral technique is favored. The stated parameters apply to the Siemens Emotion Single CT. The abbreviations of the parameters are found on page 170.

Indications	ST/ Table Feed/ RI all in [mm]	Pitch	Rot. [sec.]	Voltage [kV]	Current [mAs]	Kern	Scan direction	With CM [HU]	CM: Amount/flow [ml / ml/sec.]	Delay [sec.]
Skull:	Infratentorial: 3 / 3 / –		1,5	130	260	H 30		250 / 40	60 / 1,5	–
Bleeding ?										
Metastases ?	Supratentorial: 8 / 8 / –		1,5	130	260	H 30	caudocranial	90 / 35		60
Fracture ?				130	260	H 30	caudocranial	1500 / 450		–
Mid-facial bones:										
Coronal, fracture ?	2 / 3 / 1	1,5	1	130	80	H 70	craniocaudal	1500 / 450		–
Axial	2 / 3 / 2	1,5	1	130	80	H 70	craniocaudal	1500 / 450		
Axial to coronal reconstruction	2 / 3 / 1	1,5	1	130	80			and 350 / 40		
Petrous bone:	1 / 1,5 / 0,5	1,5	1,5	130	135	H 80	craniocaudal	1500 / 450		
C1 and C2 multiple trauma:	2 / 2 / 2	1	1	130	170	B 50	craniocaudal	350 / 40	–	–
								1500 / 450		
Extremities (fracture?):	2 / 2 / 1,5	1	1	130	70	B 80	craniocaudal	350 / 450		
								1500 / 450		
Neck:										
Thyroid carcinoma ?	5 / 5 / 5	1	0,8	130	100	B 50	craniocaudal	350 / 40	70 / 2,0	25 – 40
Staging of the pulmonary apex								2000 / - 300		
Thorax/abdomen: Staging ?										
Liver arterial + thorax	5 / 7,5 / 4	1,5	0,8	130	140	B 40	craniocaudal	350 / 40	120 / 3,0 – 5,0	BT
Liver portovenous + pelvis	8 / 12 / 8	1,5	0,8	110	140	B 40	craniocaudal	350 / 40		post 90
Gynecologic + other tumors of the lesser pelvis	5 / 8 / 5	1,6	0,8	130	140	B 40	craniocaudal	350 / 40	100 / 2,5	60
Vena cava: Thrombosis	8 / 12 / 8	1,5	0,8	130	140	B 40	craniocaudal	350 / 40	120 / 2,5 2x 50ml bipedal	90 – 100
Pulmonary embolism:	2 / 4 / 2	2	0,8	130	100	B 40	craniocaudal	350 / 40	120 / 3,0 – 4,0	BT
								2000 / -300	–	A.asc.
Lung: Soft tissue window	5 / 8 / 5	1,5	0,8	130	110	B 40	caudocranial	350 / 40	100 / 2,0	BT
Pulmonary window								2000 / -300		
Liver series: hemangioma ? (dynamic at the same level)	8 / 0 / –		1,0	130	140	B 40	craniocaudal	350 / 40	130 / 2,0	–
Adrenal glands: Tumor ?										
Unenhanced	5 / 7,5 / 4	1,5	0,8	130	120	B 40	caudocranial	350 / 40	80-100 / 2,0	arterial:
Arterial	5 / 7,5 / 4	1,5	0,8	130	140	B 40				BT
Portovenous	5 / 7,5 / 4	1,5	0,8	130	140	B 40				Venous:
Late venous	5 / 7,5 / 4	1,5	0,8	130	140	B 40				about 90
Perfusion: Head - unenhanced	Basis 3 / 3 / - Neurocran. 8 / 8 / -		1,5	130	260	H 30	caudocranial	250 / 40 + 90 / 35		
IV CM-concentration 300-370	10 / 0 / –		1	110	106	H 30		350 / 40	40 / 8	
Bone: Densitometry L-spine	10 / 0 / –		1	80	81	S 80	craniocaudal	350 / 40		
Dental:	1 / 1,5 / 0,5	1,5	0,8	130	90	H 70	craniocaudal	1500 / 450		

Examination Protocols for 4-slice Spiral CT

These are the examination protocols for a 4-slice spiral CT, established for the Siemens Sensation 4. For clinical questions not suitable for spiral technique in our experience, the expression "**seq.**" is listed instead of the table feed per rotation ("**feed/rot.**"). The collimation ("**coll.**") must be selected by the examiner in advance, while in multislice scanners the reconstructed effective section thickness ("**ST**") can be selected later. The reconstruction interval ("**RI**") states the distance between the sections for the subsequent reconstruction from the three-dimensional data set. The term **kernel** refers to the edge algorithm of the manufacturer: **H** = Head, **U** = Ultrahigh, **B** = body.

For the application of the contrast medium ("**CM**"), the amount in ml of a concentration of 300-350 g iodine/ml and the flow rate of the injector ("**flow**") in ml/second is stated. In addition, the term "**delay**" states in seconds when the gantry begins its data acquisition after the beginning of the injection of contrast medium. The term "**BT**" refers to bolus tracking, an automated software program. For instance, an ROI is placed over the descending aorta, and when the intravascular density exceeds a preselected level (e.g., the bolus of contrast medium is arriving), data acquisition begins automatically (see page 176). In modern units, the examiner selects the craniocaudal span of the body region to be examined, the desired examination time, the rotation speed, and the section collimation. The scanner then optimizes table feed and pitch on its own.

Seq. = Sequential data acquisition
Feed/rot. = Table feed per rotation
Coll. = Section collimation
ST = Section thickness
RI = Reconstruction interval
CM = Contrast medium
Flow = CM volume/ time
Delay = Delay after the beginning of the CM injection
BT = Automatic bolus tracking
Pitch = Pitch
kV = Tube voltage
mAs = Tube current
Kern = Kernel, edge algorithm
ST = Sinus thrombosis
MPR = Multiplanar reconstruction
MIP = Maximum intensity projection
RTP = Renal transplant
HCC = Hepatocellular carcinoma

Organ	Indications		Coll [mm]	ST [mm]	Feed / rotation	Pitch	RI [mm]	Sec / rotation	Voltage (kV)	Current (mAs)	Kern	Window with CM	MPR	Delay [sec]	CM / flow [ml/ml/sec]
Skull	Bleeding	Basis	4 x 1	4	Seq.		4	0,75	120	300	H 40	110 / 35			–
		Cereb	2 x 8	8	Seq.		8	0,75	120	260	H 40	80 / 35			–
	Tumor, Metastases	Basis	4 x 1	4	Seq.		4	0,75	120	300	H 40	110 / 35		60	50 / 2,5
		Cereb	2 x 8	8	Seq.		8	0,75	120	250	H 30	80 / 35			
	Venous vessels (ST)													35	
Orbit	Tumor		4 x 1	4	3,5	0,88	4	0,75	120	100	H 20	250 / 50		45	75 / 2,0
				1,25			1				H 20	250 / 50	Coronal		
	Fracture		4 x 1	2	3,5	0,88	2	0,75	120	100	H 60	3000 / 600		–	–
				1,25			1				H 60	3000 / 600	Coronal		
Paranasal sinuses	Sinusitis, nasal polyposis		4 x 1	4	3,5	0,88	4	0,75	120	80	H 50	1500 / 50		–	–
	Only for coronal MPR			1,25			1				H 50	1500 / 50	Coronal		
Facial bones	Tumor		4 x 1	3	3,5	0,88	3	0,75	120	100	H 50	350 / 50		45	75 / 2,0
											H 40	350 / 50	Coronal		
Petrous bone	Fracture		2 x 0,5	0,5	1	1	0,4	1	120	100	U 90	3000 / 600	Coronal	–	–
	Only for film documentation			1			1				U 90	3000 / 600			
Neck	Lymphoma, Tumor		4 x 2,5	5	13,8	1,38	5	0,75	120	200	B 40	250 / 50		45	100 / 3,0
Chest	Fibrosis, fungi	Unenhanced	4 x 1	5	7	1,75	5	0,5	120	90	B 60	2000 / -500		–	–
		HR	4 x 1	1,25	6	1,5	1	0,75	120	90	B 70	2000 / -500	Coronal	–	–
				7			7				B 40	350 / 50			
	NPL, lymphoma	Arterial	4 x 2,5	7	30	3	7	0,5	120	90	B 40	350 / 50		25-30 (BT)	50-80 / 2,0
	Pulmonary emboli	Arterial	4 x 2,5	3	30	3	3	0,5	120	90	B 40	350 / 50		20-25 (BT)	80 / 3,0
				7			7								

The pitch was calculated according to the formula:

$$\text{Pitch} = \frac{\text{Feed / rotation}}{\text{Collimation (e.g. 4 x 2,5 =10)}}$$

Organ	Indications		Coll [mm]	ST [mm]	Feed / rotation	Pitch	RI [mm]	Sec / rotation	Voltage (kV)	Current (mAs)	Kern	Window with CM	Reconstruct.	Delay [sec]	CM / flow [ml/ml/sec]
Chest - Liver	Bronchial carcinoma (BC)	Arterial	4 x 5	7 7	30	1,5	7 7	0,5	120	90	B 30 B 60	350 / 50 2000 / -300			80-100 / 3,0
Abdomen	NPL, lymphoma	Arterial	4 x 2,5	5	12,5	1,25	5	0,5	120	155	B 30	200 / 40		25-30	100-120 / 3,0
		Venous	4 x 2,5	5	12,5	1,25	5	0,5	120	155	B 30	350 / 50		50-75	
	Stomach: Hydro CT	Arterial	4 x 2,5	5	12,5	1,25	5	0,5	120	155	B 30	350 / 50		25-30	100-120 / 3,0
	(stomach filled with H_2O)	Venous	4 x 2,5	5	12,5	1,25	5	0,5	120	155	B 30	350 / 50		50-75	
Pancreas/kidneys	NPL	Unenhanced	4 x 5	7	25	1,25	7	0,5	120	155	B 30	350 / 50			
		Arterial	4 x 1	3	4	1	3	0,5	120	165	B 30	350 / 50		30-40	100-120 / 3,0
		Venous	4 x 2,5	5	12,5	1,25	5	0,5	120	155	B 30	350 / 50		(BT)	
Adrenal glands	Adenoma	Unenhanced	4 x 2,5	5	12,5	1,25	5	0,5	120	155	B 30	350 / 50		–	
		Arterial	4 x 1	3	4	1	3	0,5	120	165	B 30	350 / 50		30-40	100-120 / 3,0
		After 3 min	4 x 2,5	5	12,5	1,25	5	0,5	120	155	B 30	350 / 50		(BT)	
	Optional	After 10 min	4 x 2,5	5	12,5	1,25	5	0,5	120	155	B 30	350 / 50			
3-phase liver	Hemangioma, HCC	Unenhanced	4 x 2,5	5	12,5	1,25	5	0,5	120	155	B 30	350 / 50			
		Arterial	4 x 1	3	4	1	3	0,5	120	165	B 30	250 / 40		25-30	100-120 / 3,0
		Venous + optional pelvis	4 x 2,5	5	12,5	1,25	5	0,5	120	155	B 30	350 / 50		(BT)	
Chest-abdomen	NPL, lymphoma	Arterial	4 x 5	7	25	1,25	7	0,5	120	155	B 30	350 / 50		25-30	120 / 3,0
		Venous	4 x 5	7	25	1,25	7	0,5	120	155	B 30	350 / 50		(BT)	
		Lung		7			7				B 70	2000 / -500			
Pelvis	Vascular state (RTP)	Unenhanced	4 x 2,5	5	12,5	1,25	5	0,5	120	155	B 30				
	DVT	Venous	4 x 2,5	5	12,5	1,25	5	0,5	120	155	B 30			100 (BT)	140 / 3,0
Heart		Trigger	4 x 1	1,25	1,5	0,38	0,8	0,5	120	400	B 30	350 / 50	MPR/MIP		120 / 3,0
CT Angio	Cranial vessels	Arterial	4 x 1	1,25	5	1,25	1	0,5	140	90	H 10	110 / 35	MIP/VRT	18 (BT)	75 / 3,0
	Cervical vessels	Arterial	4 x 1	1,5	5,5	1,38	1	0,5	120	100	B 20	350 / 50	MIP/VRT	15 (BT)	110 / 3,5
	Abdominal. vessels	Arterial	4 x 1	1,25	6	1,5	1	0,5	120	130	B 20	350 / 50	MIP/VRT	20-25	100-120 / 3,0
	Iliofemoral vessels	Arterial	4 x 2,5	3	15	1,5	1,5	0,5	120	130	B 20	350 / 50	MIP/VRT	25-30	150 / 2,5-3,0
C spine	Fracture	Unenhanced	4 x 1	2	5,5	1,38	2	0,75	120	150	B 70	3000 / 600	MPR		
L spine	Fracture	Unenhanced	4 x 1	2	2,5	0,6	2	0,75	120	330	B 20	3000 / 600	MPR		
	Myelo-CT	Unenhanced	4 x 1	2	2,5	0,6	2	0,75	120	330	B 20	3000 / 600			
	Only for MPR			1,25			1				B 20	3000 / 600	Sagittal		
Aorta	Dissection Aneurysm	Arterial	4 x 2,5	3	15	1,5	1,5	0,5	120	130	B 30	350 / 50	Coronal	20 (BT)	120-140 / 3,0
Hand/Feet	Fracture – Detail diagnosis	Unenhanced	2 x 0,5	0,5	1	1	0,3	0,75	120	100	U 90	3000 / 600	Coronal/ sagittal		
Knee	Bone	Unenhanced	4 x 1	1,25	4	1	1	0,75	120	90	B 60	3000 / 600			
	Soft tissues			5			5				B 30	350 / 50			
Dental	Before implantation	Unenhanced	4 x 1	1	2,7	0,68	0,8	0,75	120	70	H 60	3000 / 600	Dental evaluation		
Bone			4 x 2,5	10	Seq.			0,5	80	125	S 80	1800 / 500	Bone density		
Perfusion	Bleeding	Infratentorial	4 x 1	4	Seq.		4	0,75	120	300	H 40	110 / 35			
		Supratentorial	2 x 8	8	Seq.		8	0,75	120	260	H 40	80 / 35			
	Stroke	Arterial	2 x 5	10	Multiscan		10	1	80	250	H 30	120 / 35	Perfusion state	4	80 / 5,0

Examination Protocols for 16-slice Spiral CT

The parameters listed here apply to the 16-slice spiral CT, also as established for a Siemens scanner:

Seq. = Sequential data acquisition
Feed/rot. = Table feed per rotation
Coll. = Section collimation
ST = Section thickness
RI = Reconstruction interval
CM = Contrast medium
Flow = CM volume/ time
Delay = Delay after the beginning of the CM injection
BT = Automatic bolus tracking
Pitch = Pitch
kV = Tube voltage
mAs = Tube current
Kern = Kernel, edge algorithm
ST = Sinus thrombosis
MPR = Multiplanar reconstruction
MIP = Maximum intensity projection
RTP = Renal transplant
HCC = Hepatocellular carcinoma

The pitch was calculated according to the formula:

$$\text{Pitch} = \frac{\text{Feed / rotation}}{\text{Collimation (e.g. 16 x 1 =16)}}$$

Organ	Indications		Coll [mm]	ST [mm]	Feed / rotation	Pitch	RI [mm]	Sec / rotation	Voltage (kV)	Current (mAs)	Kern	Window with CM	MPR	Delay [sec]	CM / flow [ml/ml/sec]
Skull	Bleeding	Infratentorial	16 x 0,75	4	5	0,42	4	0,75	120	260	H 40	110 / 35			–
		Supratentorial	16 x 1,5	8	10	0,42	8	0,75	120	260	H 40	80 / 35			–
	Tumor. Metastases	Infratentorial	16 x 0,75	4	5	0,42	4	0,75	120	260	H 40	110 / 35		60	50 / 2,0
		Supratentorial	16 x 1,5	8	10	0,42	8	0,75	120	260	H 40	80 / 35			
Skull: ST	Venous vessels (SVT)													35	
Orbita	Tumor		16 x 0,75	4	5	0,42	4	0,75	120	100	H 30	250 / 50		45	75 / 2,0
				1			0,7				H 30	250 / 50	Coronal		
	Fracture		16 x 0,75	2	5	0,42	2	0,75	120	100	H 60	3000 / 600	–	–	–
				1			0,7				H 60	3000 / 600	Coronal		
Paranasal sinuses	Sinusitis, nasal polyposis		16 x 0,75	4	5	0,42	4	0,75	120	80	H 40	1500 / 50		–	–
	Only for coronal MPR			1			0,7				H 60	1500 / 50	Coronal		
Facial bones	Tumor		16 x 0,75	3	5	0,42	3	0,75	120	100	H 30	350 / 50		45	75 / 2,0
	Fracture			1			0,7				H 60	3000 / 600	Coronal		
Petrous bone	Fracture		16 x 0,75	0,75	5	0,42	0,5	1	120	120	U 90	3000 / 600	Coronal	–	–
	Only for film documentation			1			1				U 90	3000 / 600			
Neck	Lymphoma, tumor		16 x 1,5	5	24	1	5	0,75	120	150	B 30	250 / 50		45	100 / 3,0
Chest	Fibrosis, fungi	Unenhanced	16 x 1,5	5	30	1,25	5	0,5	120	100	B 40	350 / 50		–	–
		HR	16 x 0,75	1	13,5	1,13	0,7	0,75	120	90	B 80	2000 / -500	Coronal	–	–
				5			5				B 30	350 / 50			
	NPL, lymphoma	Arterial	16 x 1,5	6	30	1,25	6	0,5	120	100	B 40	350 / 50		25-30 (BT)	80 / 2,0
	Pulmonary emboli	Arterial	16 x 0,75	5	15	1,25	5	0,5	120	100	B 30	350 / 50	Coronal	20-25 (BT)	100-120 / 3,5
				1			0,7						Sagittal		

Organ	Indications		Coll [mm]	ST [mm]	Feed / rotation	Pitch	RI [mm]	Sec / rotation	Voltage (kV)	Current (mAs)	Kern	Window with CM	Recon-struct.	Delay [sec]	CM / flow [ml/ml/sec]
Chest - Liver	Bronchial carcinoma (BC): Lung window	Arterial	16 x 1,5	6 6	30	1,25	6 6	0,5	120	100	B 40 B 70	350 / 50 2000 / -500		25-30	80 / 2,5
Abdomen	NPL, lymphoma	Arterial	16 x 0,75	5	12	1	5	0,5	120	140	B 30	200 / 40		20-25	100-120 / 3,5
		Venous	16 x 1,5	5	24	1	5	0,5	120	120	B 30	350 / 50	Coronal	50-75	
	Stomach: Hydro CT (stomach filled with H_2O)	Arterial	16 x 0,75	5	12	1	3	0,5	120	140	B 30	350 / 50		25-30	100-120 / 3,5
		Venous	16 x 0,75	3	12	1	3	0,5	120	140	B 30	350 / 50		50-75	
Pancreas/ kidneys	NPL	Unenhanced	16 x 1,5	5	24	1	5	0,5	120	120	B 30	350 / 50			
		Arterial	16 x 0,75	5	12	1	5	0,5	120	140	B 30	350 / 50	Coronal	20-25	100-120 / 3,5
		Venous	16 x 1,5	5	24	1	5	0,5	120	120	B 30	350 / 50		50-75	
Adrenal glands	Adenoma	Unenhanced	16 x 1,5	5	24	1	5	0,5	120	120	B 30	350 / 50		–	
		Arterial	16 x 0,75	1	12	1	0,7	0,5	120	140	B 30	350 / 50	Coronal	30-40	100-120 / 3,0
		After 3 min	16 x 1,5	3	24	1	3	0,5	120	120	B 30	350 / 50		(BT)	
	Optional	After 10 min	16 x 1,5	5	24	1	5	0,5	120	120	B 30	350 / 50			
3-phase liver	Hemangioma, HCC	Unenhanced	16 x 1,5	5	24	1	5	0,5	120	120	B 30	350 / 50			
		Arterial	16 x 0,75	5	12	1	5	0,5	120	140	B 30	250 / 40	Coronal	20+25	100-120 / 3,5
		Venous + optional pelvis	16 x 1,5	5	24	1	5	0,5	120	120	B 30	350 / 50		50-75	
Chest-Abdomen	NPL, lymphoma	Arterial	16 x 1,5	5	24	1	5	0,5	120	140	B 30	350 / 50		25-30	120 / 3,0
		Venous	16 x 1,5	5	24	1	5	0,5	120	140	B 30	350 / 50		(BT)	
		Lung		7			7				B 70	2000 / -500			
Pelvis	Vascular state (RTP)	Unenhanced	16 x 0,75	5	24	1	5	0,5	120	140	B 30	350 / 50			
	DVT	Venous	16 x 1,5	3	12	1	3	0,5	120	140	B 30	350 / 50		100 (BT)	120 / 3,0
Heart		Trigger	16 x 0,75	1	3,4	0,29	0,7	0,42	120	550	B 30	350 / 50	MPR/MIP		100 / 3,0
CT Angio	Cranial vessels	Arterial	16 x 0,75	1	15	1,25	0,7	0,5	140	100	H 20	110 / 35	MIP/VRT	18 (BT)	75 / 3,5
	Cervical vessels	Arterial	16 x 0,75	1	12	1	0,7	0,5	120	120	B 30	350 / 50	MIP/VRT	15 (BT)	100 / 4,0
	Abdominal vessels	Arterial	16 x 0,75	1	15	1,25	0,7	0,5	120	130	B 30	350 / 50	MIP/VRT	20-25	100-120/3,0-3,5
	Pelvic-leg vessels	Arterial	16 x 1,5	2	24	1	1,5	0,5	120	130	B 30	350 / 50	MIP/VRT	25-30	150 / 3,0-3,5
C spine	Fracture	Arterial	16 x 0,75	1	12	1	0,7	0,75	120	150	B 70	3000 / 600	MPR		
L spine	Fracture	Unenhanced	16 x 0,75	1	6	0,5	0,7	0,75	120	330	B 60	3000 / 600	MPR		
	Myelo-CT	Unenhanced	16 x 0,75	3	6	0,5	3	0,75	120	330	B 60	3000 / 600			
	Only for MPR	Unenhanced		1			0,7				B 60	3000 / 600	MPR		
Aorta	Dissection Aneurysm	Arterial	16 x 1,5	2	21	0,88	1	0,5	120	130	B 30	350 / 50	MPR/MIP VRT	20 (BT)	120 / 3,0
Hand/Feet	Fracture – Detail diagnosis	Unenhanced	16 x 0,75	0,75	6,8	0,57	0,5	0,75	120	120	U 90	3000 / 600	MPR		
Knee	Bone	Unenhanced	16 x 0,75	1	13,5	1,13	0,7	0,75	120	120	B 60	3000 / 600	MPR		
	Soft tissues			5			5				B 30	350 / 50			
Dental	Before implantation	Unenhanced	16 x 0,75	0,75	6	0,5	0,5	0,75	120	80	H 60	3000 / 600	Dental evaluation		
Bone			2 x 5,0	10	Seq.			0,5	80	125	S 80	1800 / 500	Bore density		
Perfusion	Bleeding	Infratentorial	16 x 0,75	4	5,1	0,43	4	1	120	260	H 40	110 / 35			
		Supratentorial	16 x 1,5	8	10,2	0,42	8	1	120	260	H 40	80 / 35			
	Stroke	Arterial	16 x 1,5	12	Multiscan		1	1	80	209	H 30	120 / 35	Perfusion state	4	40 / 8,0

Radiation Dose/Cancer Risk

The **physical radiation dose D** (energy absorbed per unit mass) is expressed in Gray (Gy), used for any type of radiation and also in the radiation therapy of malignant tumors. It has to be distinguished from the **equivalence dose H** expressed in Sievert (Sv), which represents the physical radiation dose multiplied by a proportionality factor that considers the unique radiation sensitivity of a particular tissue: Epithelium, mucosa of the respiratory and gastrointestinal tract and other tissues with a high rate of cell division (e.g., blood forming cells of the bone marrow) are more sensitive to ionizing radiation than tissue with dormant cell division.

An even better comparison of the biologic effect can be achieved with the **effective dose E**, which is the sum of the doses delivered to the individual organ. This effective dose, which weighs the relative inherent sensitivities, is also expressed in Sievert (Sv) or **Millisievert (mSv)**.

Furthermore, the patient's age at the time of radiation exposure must be included in a rational assessment of the radiation risk since the latency period of a radiation-induced tumor can be rather long (decades). **Table 174.1** lists the risk coefficients of different organs following a low-dose exposure to the entire body.

Tab. 174.1 **Age-dependency of cancer mortality caused by ionizing radiation**
Estimated risk factors in (% / Sv) for men / *women (italics)*

Age at exposure	Total	Leukemia	Lung/Respiratory	MDT	Chest	Others
5 years	12,8 / *15,3*	1,1 / *0,8*	0.2 / *0,5*	3,6 / *6,6*	*1,3*	7,8 / *6,3*
15 years	11,4 / *15,7*	1,1 / *0,7*	0,5 / *0,7*	3,7 / *6,5*	*3,0*	6,1 / *4,8*
25 years	9,2 / *11,8*	0,4 / *0,3*	1,2 / *1,3*	3,9 / *6,8*	*0,5*	3,7 / *2,9*
45 years	6,0 / *5,4*	1,1 / *0,7*	3,5 / *2,8*	0,2 / *0,7*	*0,2*	1,2 / *1,0*
65 years	4,8 / *3,9*	1,9 / *1,5*	2,7 / *1,7*	0,1 / *0,5*	-	0,1 / *0,2*
85 years	1,1 / *0,9*	1,0 / *0,7*	0,2 / *0,1*	- / *0,04*	-	- / -
Mean	7,7 / *8,1*	1,1 / *0,8*	1,9 / *1,5*	1,7 / *2,9*	*0,7*	3,0 / *2,2*

This implies that the risk of radiation-induced malignancies markedly decreases with increasing age at the time of exposure. But not only the patient's age, but also the amount of the individual dose and the length of the time intervals play a decisive role. As a rule of thumb, the lower the individual dose and the longer the intervals between several radiation exposures, the lower the risk of a subsequently induced neoplasm. Among other factors, this depends on the capability of the cellular nuclei to repair DNA breaks with the help of repair enzymes as long as the reparative capacity is not exceeded by high individual doses. Evidence even exists that protective effects predominate in the low-dose range through activation of protective cell factors (DNA reparase and others). For a better assessment of the risk associated with the medical application of ionizing radiation, it is revealing to consider the daily exposure from natural background radiation: The major component of the natural radiation exposure comes from radon, a noble gas, which gets into the air through the building materials of houses and apartments. Using a strictly theoretical calculation, radon and its decay products may induce 5 to 10% of all bronchial carcinomas. In contrast, medical application of ionizing radiation "only" induces less than 1.5% of all malignancies.

The average annual radiation exposure of about 2.4 mSv has to be put in perspective with the man-made radiation exposure of 1.8 mSv **(Table 174.2)**.

Radiation Source	effektive annual dose	% of annual exposure
Inhalation of radon in apartments	~ 1,4	33,3 %
Terrestric radiation	~ 0,4	9,5 %
Cosmic radiation	~ 0,3	7,1 %
Incorporation of radioactive isotopes	~ 0,3	7,1 %
Subtotal of natural radiation exposure	**~ 2,4 mSv**	**57,0 %**
Application of ionizing radiation in medicine	~ 1,5	35,7 %
Accident of the Chernobyl nuclear reactor (Europe)	~ 0,02	0,5 %
Fall-out from nuclear weapon tests	~ 0,01	0,2 %
Operation of nuclear reactors	~ 0,01	0,2 %
Occupational radiation exposure	~ 0,01	0,2 %
Subtotal of man-made radiation exposure	**~ 1,8 mSv**	**43,0 %**
Total annual radiation exposure in the Federal Republic of Germany	**~ 4,2 mSv**	**100,0 %**

Tab. 174.2 Relative contribution of several radiation sources to the total annual exposure (Europe).

In general, "hard" x-rays used for conventional radiography of the chest are scattered and absorbed less in human tissue than "soft" x-rays used for mammography. The scatter radiation also contributes to the absorption and consequently to the risk associated with a particular examination. Because of the tissue-dependent variability of the risk factors and the different characteristics of the various modalities used in diagnostic radiology, the organ doses are quite diverse **(Table 175.1)**.

Examination	Organ / tissue	Organ dose	Effective dose E
Conventional radiology, chest	Lung, breast	0,3 mSv	0,2 mSv
Conventional radiology, skull	Red bone marrow	4,0 mSv	0,2 mSv
Radiology, C-spine	Thyroid gland	4,5 mSv	2,0 mSv
Radiology, T-spine	Breast, lung	14,0 mSv	5,0 mSv
Radiology, L-spine	Red bone marrow	1,0 mSv	0,4 mSv
DSA of the heart	Lung	20,0 mSv	10,0 mSv
DSA of the kidneys	Red bone marrow	30,0 mSv	10,0 mSv
Fluoroscopy, UGI series	Red bone marrow	17,0 mSv	6,0 mSv
Fluoroscopy, BE	Red bone marrow	3,0 mSv	3,0 mSv
Cranial CT	Red bone marrow	5,0 mSv	2,0 mSv
Chest CT	Lung, chest	20,0 mSv	10,0 mSv
Abdomen CT	Red bone marrow	10,0 mSv	7,0 mSv

Tab. 175.1 Radiation dose of different radiographic examinations.

Together with arteriography and fluoroscopy, CT is responsible for a rather high radiation exposure in diagnostic radiology. Multiplying the individual values with the number of the different examinations performed annually reveals that CT is responsible for about a third of the collective total dose. The different CT examinations deliver the following average radiation doses **(Table 175.2)**.

Type of spiral CT	Emotion 1 row	Emotion 2 rows	Emotion 6 rows	Sensation 10 rows	Sensation 16 rows
Head	4,2 / *4,5* mSv	4,2 / *4,5* mSv	4,4 / *4,7* mSv	4,6 / *4,8* mSv	4,5 / *4,8 mSv*
Chest	3,9 / *5,0* mSv	2,6 / *3,3* mSv	3,2 / *4,1* mSv	3,0 / *3,8* mSv	2,8 / *3,6 mSv*
Abdomen/ pelvis	3,7 / *8,8* mSv	3,7 / *5,6* mSv	6,3 / *9,6* mSv	6,0 / *9,0* mSv	6,5 / *10,0 mSv*

Tab. 175.2 Comparison of doses in millisievert (mSv) for different CT units of Siemens Medical Systems.Values for men / *women (italics)*.

This does not consider the effects of the section thickness (see page 9-11): As a rule of thumb, the thinner the section thickness the higher the radiation dose **(Table 175.3)**.

The radiation exposure is slightly higher in units with compact geometry and shorter focus distance (Emotion 6).

Preselected collimation	Somatom plus 4 1 row	Somatom Volume Zoom 4 row	Emotion 6 row	Sensation 16 row
4 x 5,0 mm	4,5	4,6	6,8	-
4 x 2,5 mm	4,3 (3 mm)	5,1	7,2	4,2 (1,5 mm)
4 x 1,0 mm	4,9	6,1	8,4	4,7 (0,75 mm)

Tab. 175.3 Dosis increase per 100 mAs for thin section collimation.

Comparison with air traveling is often used in public health discussions: On a long, high altitude transatlantic flight, cosmic rays cause a not irrelevant additional exposure. On a flight from Europe to the West Coast of the U.S.A., this can easily be in the range of certain CT examinations. Other calculations of the cancer risk compare conventional chest radiography with cigarette smoking: A single chest radiograph is believed to have the same cancer risk as smoking seven cigarettes. It should be kept in mind, however, that all mathematically models include several aspects and cofactors that are elusive to exact statistically calculations.
While these comparisons put into perspective an excessive concern of the potential risk of medical radiographic examinations, they should not be misused to belittle the radiation risk. To avoid unnecessary risks to the general population, it has become established policy to avoid dispensable radiation exposure in conventional radiology and CT, and to take advantage of any possible reduction of radiation exposure to patients.

It is for the same reason that pulsed fluoroscopy has replaced continuous fluoroscopy for upper GI series, enteroclysis and barium enema: The examiner selects between several pulse sequences with 1, 2, 4, and 8 images per second. The resultant dose reduction is considerable. The next pages describe solutions suitable for dose reduction that are especially applicable for CT.

Automatic Bolus Tracking (BT)

For CT, several techniques are available for reducing the radiation dose to the patient. Especially CT requiring optimal contrast enhancement in the vessels, e.g., above all CT angiography, should be performed with automatic bolus tracking to avoid unnecessary duplications because of inadequate intravascular contrast enhancement. This software solution offers the examiner the possibility to place a region of interest (ROI) (⬀) just before or at the beginning of the target region, e.g., the lumen of the descending aorta **(Fig. 176.1a)**. After selecting a certain threshold value for the density of the aorta, e.g., 100 HU, the unit measures the density automatically at the preselected site every second after the beginning of the intravenous injection of contrast medium, usually through the cubital vein.
Data acquisition (the actual scanning process) begins as soon as the density in the aortic lumen exceeds the threshold value, i.e., exactly when the bolus of the contrast medium has reached the selected target region after passage through the pulmonary circulation **(Fig. 176.1b)**.

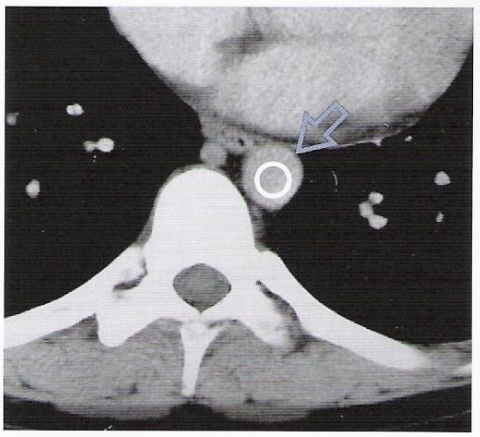

Fig. 176.1a Position of ROI, e.g., over the descending aorta.

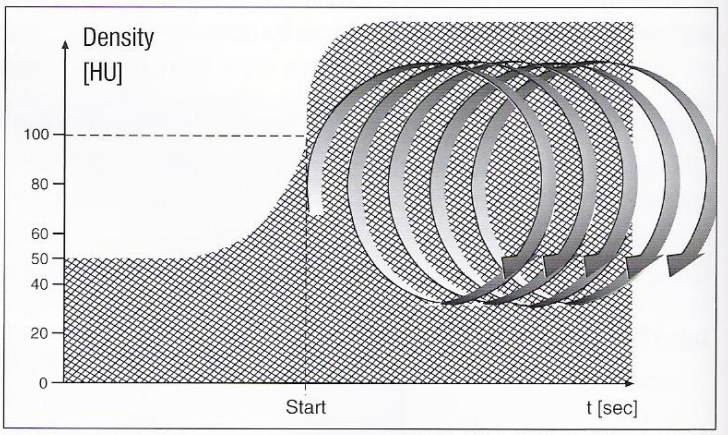

Fig. 176.1b Automatic delay of data acquisition until arrival of the CM bolus at the target region.

In addition, the amount of contrast medium needed to achieve the same contrast enhancement can be reduced: sterile physiologic NaCl solution is injected from a second syringe of the injection pump (see front cover flap) at the same flow rate immediately following the injection of contrast medium in order to push the contrast medium faster and at a higher concentration through the brachial veins toward the heart and through the pulmonary circulation.

Taking Advantage of the Pitch

By using a faster table feed to increase the pitch, a few single-slice CT units can reduce the effective patient dose by spreading the spiral of data acquisition (see **Fig. 8.4**).
The software of the multislice technology uses a compensatory mechanism that automatically increases the tube current whenever the examiner increases the pitch – effectively delivering the same total dose for the examination. For a 16-slice CT, the examiner can select the craniocaudal span of the z-axis, the collimation and scan time for the desired volume – and the software determines the optimal table feed or, respectively, pitch, and the tube current.

Reduced Tube Current for Thin Patients and Children

As a rule of thumb, the noise doubles for each 8-cm increase in the patient's diameter. Dose and noise are exponentially related: Doubling the dose reduces the noise only by a factor of 1.4. To penetrate thin patients and children for a satisfactory image, a markedly lower radiation dose is adequate. In older units lacking instant radiation measurements at the level of the detectors and modulation of the tube current (see below), the dose can be reduced by lowering the preselected tube current (mAs).

Automatic Tube Current Modulation

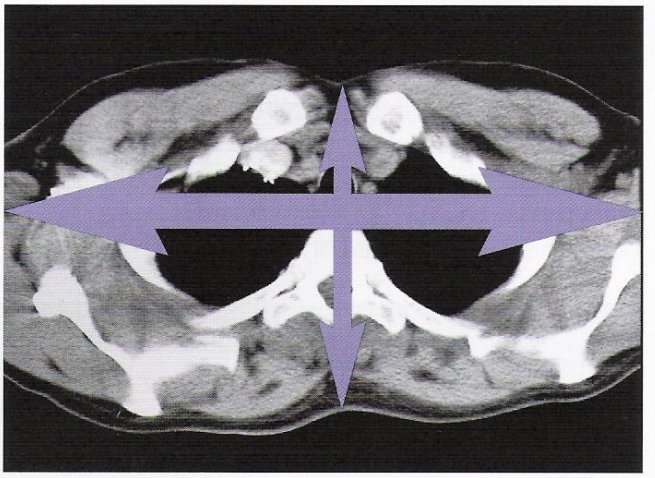

Fig. 177.1

The idea underlying this feature of the combined applications to reduce exposure (CARE) is as simple as it is effective: it is based on the assumption that the cross-sections of most body regions are oval rather than circular. With the patient supine, the AP diameter (↕) of the chest, abdomen, and pelvis is definitely shorter than the transverse diameter (↔). Consequently, the tube current is higher in lateral angulation than in anterior or posterior angulation **(Fig. 177.1)**. After each semi-circulation, e.g., every 180 degrees, the same dosis is needed since the additive attenuation of the x-rays is directionally neutral **(Fig. 177.2)**. It is the essence of the automated modulation that the tube current measures the attenuation profile for each tube angulation and calculates the corresponding minimal dose still adequate to achieve an optimal image after an additional 180-degree angulation. As a result, the tube current is modulated with a 180-degree delay. Plotting the tube current along the time axis displays a curve reminiscent of a sinus curve with the amplitudes tending to decrease from the shoulder to the legs **(Fig. 177.3)** and with maxima at the level of the shoulder and pelvis.

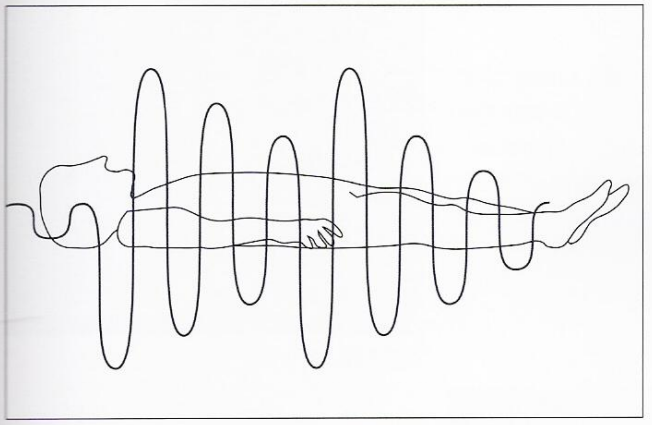

Fig. 177.2

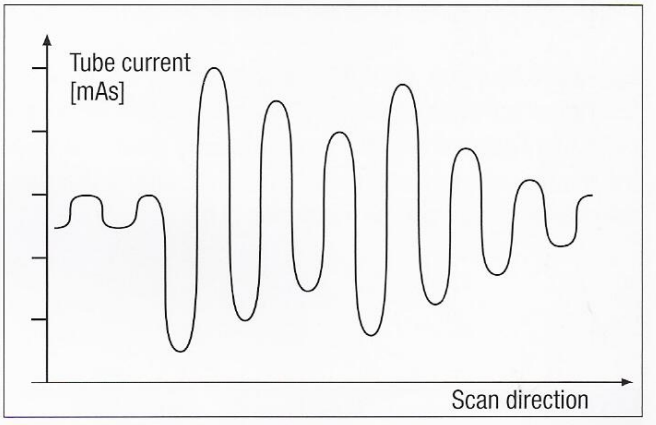

Fig. 177.3

Compared with units delivering the same image quality without tube current modulation, the dose-reducing potential of this technique is impressive, with the highest reduction coinciding with areas of considerable radiation absorption, e.g., at the shoulder and pelvis **(Table 177.1)**.

In addition, the life expectancy of the x-ray tube is extended and image artifacts induced by the arms placed along the patient's body, as frequently found in trauma and ICU patients, are reduced.

Effects of automatic tube current modulation

Body region	Dose reduction
Skull	14 – 26 %
Shoulder region	22 – 56 %
Chest	19 – 27 %
Abdomen	11 – 24 %
Pelvis	21 – 30 %
Extremities	33 – 41 %

Tab. 177.1

Bringing out the information contained in images of CT angiography requires a review using different perspectives (MIP = maximum intensity projection), different reconstruction planes (MPR = multiplanar reconstruction) or a three-dimensional visualization (VRT = volume rendering technique). All these reconstruction images used to be degraded by the resolution of 0.5 mm per pixel length in the transverse plane (xy-plane) and a markedly higher resolution along the body axis (z-axis), resulting in an anisotropic voxel (see page 8) with different lengths. The advances of the multidetector CT (MDCT) with the introduction of the 16-slice technology in the year 2001 permit the inclusion of an adequately large body volume with almost isotropic voxels in the sub-millimeter range with justifiable scan times. The following pages present recommended examination protocols for different vascular regions including several representative images.

Intracranial Arteries

The individual axial sections are usually supplemented with displays using MIP and, e.g., sagittal MPR as well as VRT (see above). A good diagnostic evaluation of the cerebral arteries can be achieved with thin overlapping section reconstructions using a section thickness of 1.0 to 1.25 mm and a reconstruction interval (RI) of 0.6 to 0.8 mm.

To achieve a high vascular contrast, the data acquisition has to be exactly timed to encompass the first passage of contrast medium through the circle of Willis with a start delay of 20 seconds, if possible before contrast medium has reached the venous sinus. If bolus tracking (BT) is not available, a test bolus should be injected to determine the individual circulation time. The following examination protocols can serve as guides for the visualization of the circle of Willis:

CT system	Coll. [mm]	ST [mm]	Feed / Rot.	Pitch	RI [mm]	Sec./ Rot.	Volt. [KV]	Current [mAs]	Kernel	Window [W/C]	Delay [sec]	CM [ml / ml/sec]
1 row	1	1,0	2	2,0	0,5	0,8	110	120	H 30	250 / 40	18 - 22	120 / 3,0
4 rows	4 x 1	1,25	5	1,25	1,0	0,5	120	90	H 10	110 / 35	18 / BT	75 / 3,0
16 rows	16 x 0,75	1,0	15	1,25	0,7	0,5	120	100	H 20	110 / 35	18 / BT	75 / 3,5

The subsequently reconstructed individual sections can display the vessels as seen from below with transverse MIP **(Fig. 178.1b)**, from the front with coronal MIP **(Fig. 178.1c)** or from the side with sagittal MIP **(Fig. 179.1a)**. The first two planes clearly show the major branches of the anterior **(91a)** and middle **(91b)** cerebral arteries.

Figure 178.1d shows a 3D VRT of another patient with an aneurysm (⬋) arising from the anterior communicating artery. The junction of both vertebral arteries **(88)** to form the basal artery **(90)** and posterior cerebral arteries **(91c)** is clearly identified. Furthermore, the branches of the anterior circulation are identifiable: branches of the medial cerebral artery **(91b)** and the pericallosal arteries **(93)**.

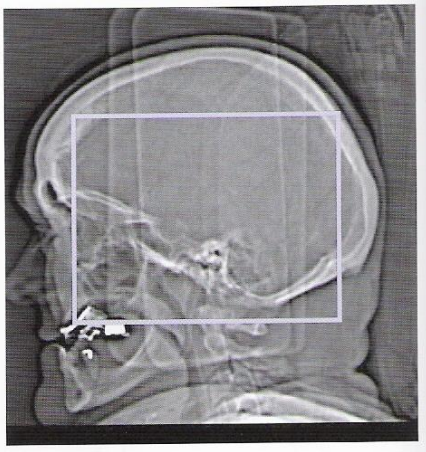

Fig. 178.1a

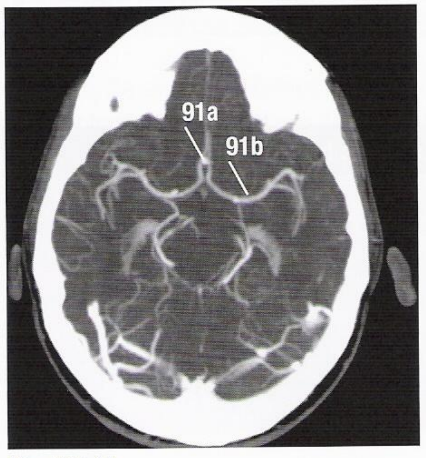

Fig. 178.1b

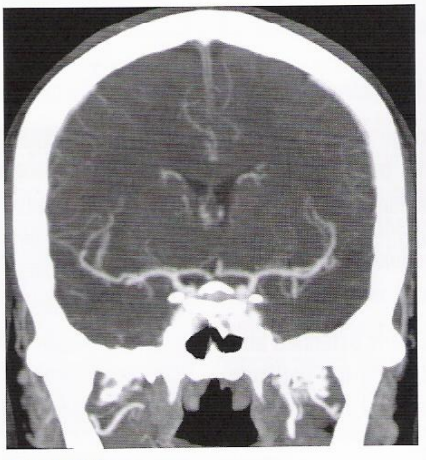

Fig. 178.1c

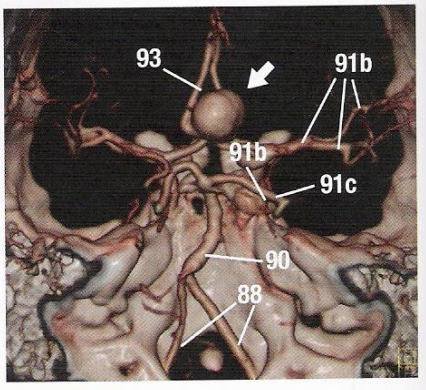

Fig. 178.1d

Venous Sinus

To visualize the venous channels, the FOV has to be extended to the sagittal cranial vault **(Fig. 179.1a)** and the start delay increased to about 100 seconds. Craniocaudal sections are recommended for both types of CTA (arterial and venous cerebral vessels). The sagittal plane **(Fig. 179.1b)** preferably shows contrast in the vein of Galen **(100)** and venous channels **(101a, 102a)**.

CT system	Coll. [mm]	ST [mm]	Feed / Rot.	Pitch	RI [mm]	Sec./ Rot.	Volt. [KV]	Current [mAs]	Kernel	Window [W/C]	Delay [sec]	CM [ml / ml/sec]
4 rows	4 x 1	1,25	5	1,0 - 1,5	0,8	0,5	120	90	soft	110 / 35	100	120 / 3,0

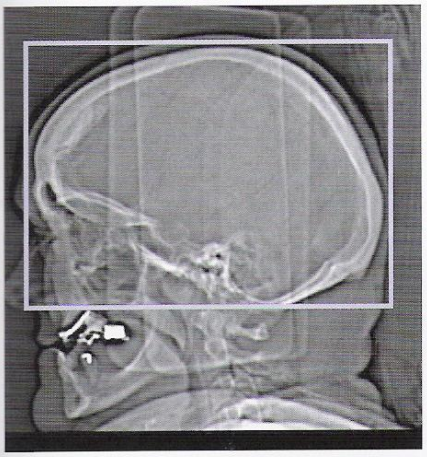

Fig. 179.1a

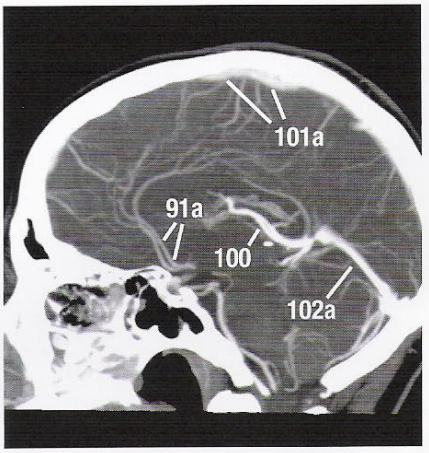

Fig. 179.1b

Carotid Arteries

Important criteria for stenotic processes of the carotid arteries are the exact determination of the severity of the stenosis. It is for this reason that the examination is carried out with thin sections, for instance, 4 x 1 mm or 16 x 0.75 mm, allowing direct planimetric quantification of the stenosis with adequate accuracy on individual axial sections. Furthermore, the sagittal and coronal MIP (0.7 – 1.0 mm RI with 50% sectional overlapping) shows no major step deformity (see page 8).

The best reconstruction with maximal contrast of the carotid artery is achieved with minimal contrast in the jugular vein. Therefore, the use of a bolus tracking program is strongly advised. If a preceding Doppler examination suggests a vascular process at the bifurcation, transverse images in caudocranial direction are recommended. For processes near the cranial base, a craniocaudal direction can be superior. VRT often proves helpful to get oriented **(Figs. 180.1d, e)**.

CT system	Coll. [mm]	ST [mm]	Feed / Rot.	Pitch	RI [mm]	Sec./ Rot.	Volt. [KV]	Current [mAs]	Kernel	W / C [HU]	Delay [sec]	CM [ml / ml/sec]
1 row		2,0	4,0	2	1,0	0,8	110	120	B 30	350 / 50	12 - 15	100 / 3,0
4 rows	4 x 1	1,5	5,5	1,38	1,0	0,5	120	100	B 20	350 / 50	15 / BT	110 / 3,5
16 rows	16 x 0,75	1,0	12,0	1	0,7	0,5	120	120	B 30	350 / 50	15 / BT	100 / 4,0

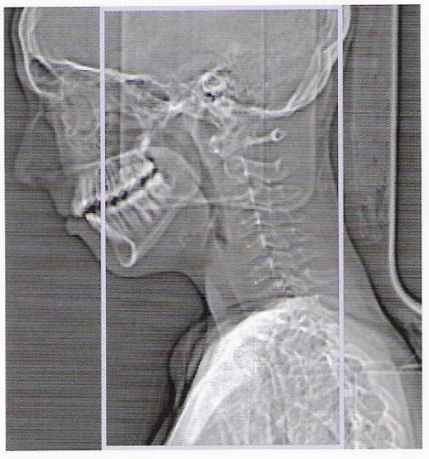

Fig. 180.1a

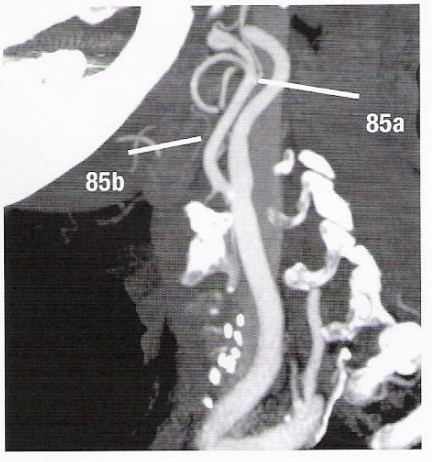

Fig. 180.1b

Fig. 180.1c

Figure 180.1 shows the lateral topogram **(a)** for positioning of the FOV as well as lateral **(b)** and anterior **(c)** images of an MIP and an image in VRT **(d)**, showing normal findings. In contrast, **Figure 180.2** shows images of sagittal MIP and VTR that reveal two indentations of the vascular contrast column at the typical site for a carotid stenosis: The left ACI **(85a)** shows a short segment of a severe luminal narrowing just distal to the bifurcation ( ) after a preceding bulbar stenosis ( ) of the ACC **(85)** at the origin of the ACE **(85b)**.

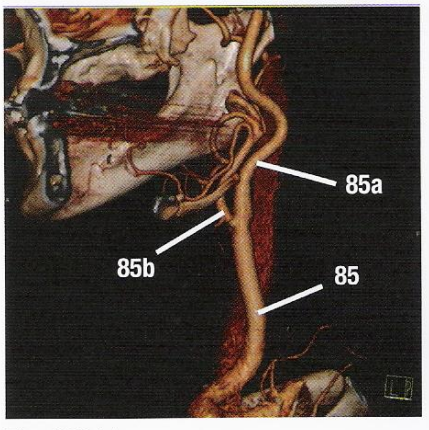

Fig. 180.1d

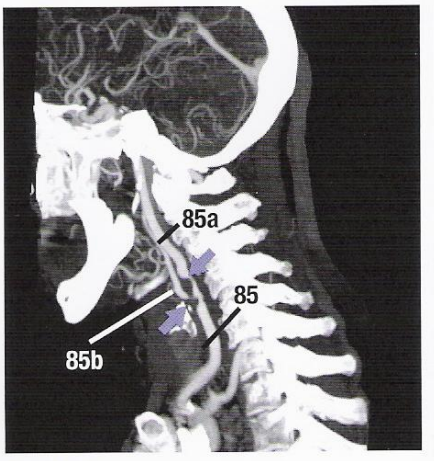

Fig. 180.2a

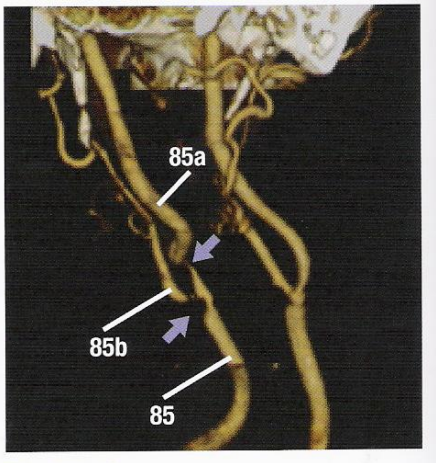

Fig. 180.2b

Aorta

The CT angiography of the aorta must above all exclude aneurysms, isthmus stenoses and possible dissection, and if present, visualize their extent. Automatic bolus tracking (BT: ROI placed over the aorta) is advisable, especially in patients with cardiac diseases who have variable pulmonary circulation times of contrast medium. Imaging in caudocranial direction can minimize the respiration-induced motion artifacts that primarily affect the regions close to the diaphragm since involuntary respiratory excursions are more likely at the end of the examination. Furthermore, caudocranial imaging avoids the initial venous inflow of contrast medium through the subclavian and brachiocephalic veins and any superimposition on the supra-aortic arteries.

CT system	Coll. [mm]	ST [mm]	Feed / Rot.	Pitch	RI [mm]	Sec./ Rot.	Volt. [KV]	Current [mAs]	Kernel	W / C [HU]	Delay [sec.]	CM [ml / ml/sec]
1 row	unenhanced	8,0	12,0	1,5	8,0	0,8	110	80	B 30	350 / 40		
1 row	CM	3,0	6,0	2,0	1,0	0,8	110	100	B 30	350 / 50	BT	120 / 3,0
4 rows	4 x 2,5	3,0	15,5	1,5	1,5	0,5	120	130	B 20	350 / 50	BT	130 / 3,0
16 rows	16 x 1,5	2,0	21,0	0,9	1,0	0,5	120	130	B 30	350 / 50	20 / BT	120 / 3,0

As reconstruction images, MIP and MPR **(Figs. 182.2, 182.3)** often allow an exact quantification of the vascular pathology as survey images in VRT **(Fig 182.4)**, as seen here as an example of an infrarenal aneurysm of the abdominal aorta: The aneurysmal dilatation **(171)** begins immediately distal to the renal arteries **(110)** and spares both the superior mesenteric artery **(106)** and iliac arteries **(113)**.

For planning any vascular surgery, it is crucial to know any involvement of visceral and peripheral arteries and any possible associated dissection. Furthermore, the level of the aortic origin of the artery of Adamkiewicz, which supplies the thoracospinal transition of the spinal cord, must be considered for aneurysms of the descending thoracic aorta.

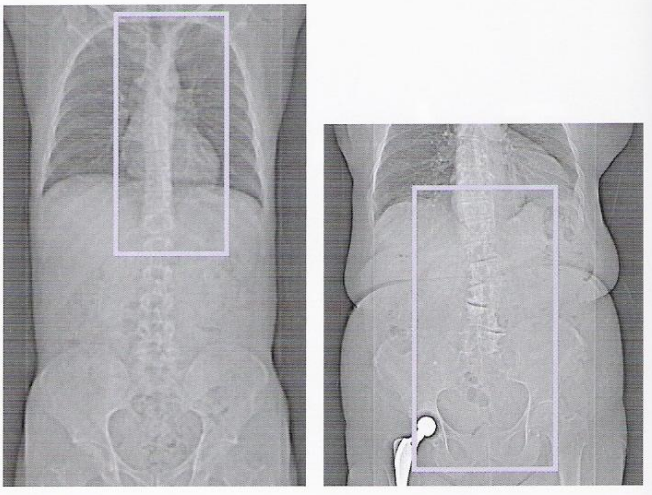

Fig. 182.1 a b

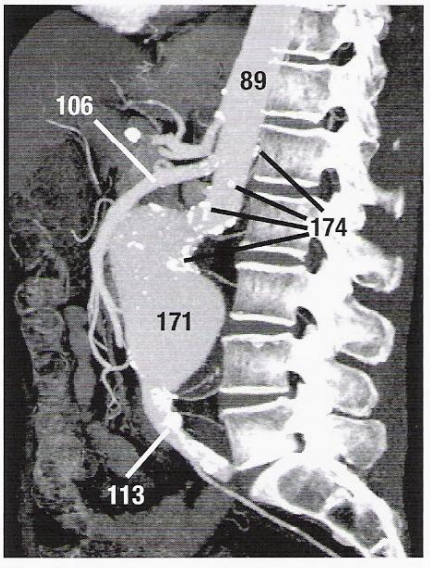

Fig. 182.2

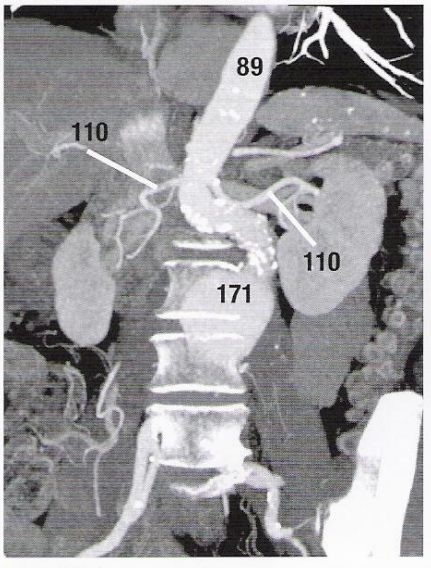

Fig. 182.3

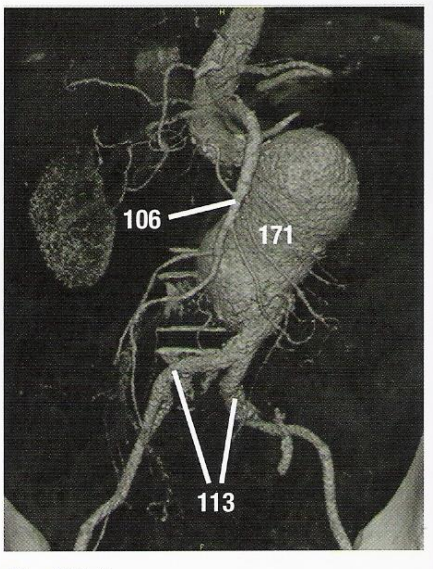

Fig. 182.4

Frequently, a cine mode review of the coronal or sagittal MPR images on a second monitor can be helpful for a quick and convincing determination of the extent of a pathologic finding, as shown here in a case of thrombosis within an abdominal aortic aneurysm. The cine mode of the coronal MPR images reveals not only an infrarenal thrombus **(173)** along the left lateral wall **(Fig. 183.1)** but also a second thrombus further cranial along the right lateral wall at the level of the origin of the right renal artery **(110)** **(Fig. 183.1)**, which is still perfused **(Fig. 183.3)**. The individual axial sections **(Figs. 183.4, 5)** allow a planimetric quantification of the stenosis, and the sagittal MPR **(Fig. 183.6)** a clear separation from the origin of the anterior mesenteric artery **(106)**.

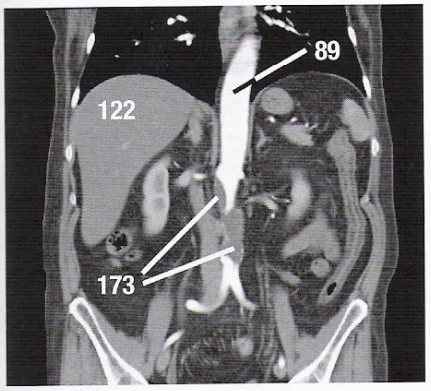

Fig. 183.1

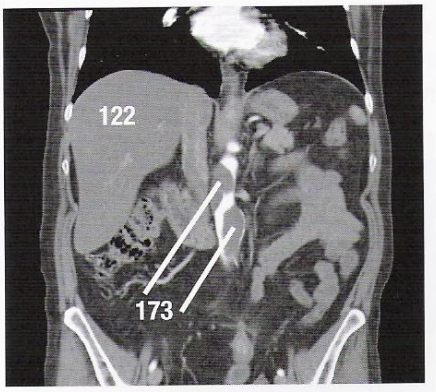

Fig. 183.2

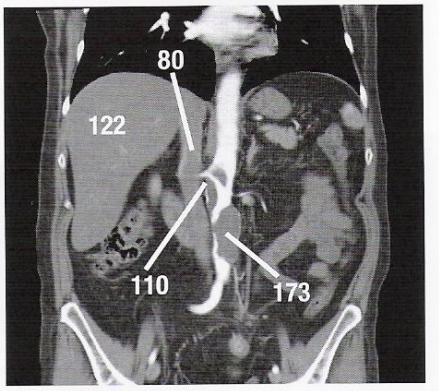

Fig. 183.3

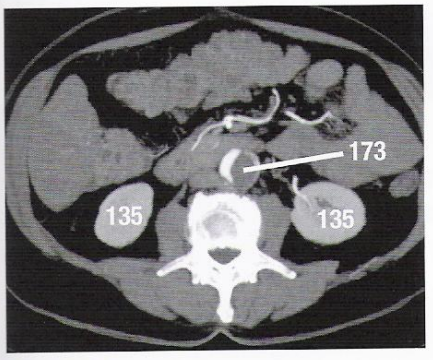

Fig. 183.4

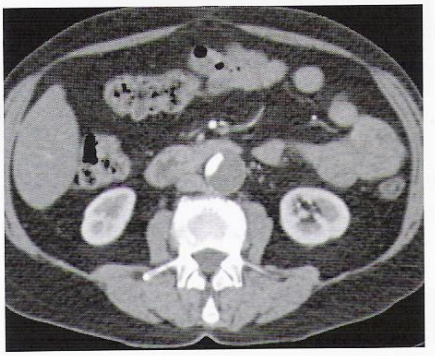

Fig. 183.5

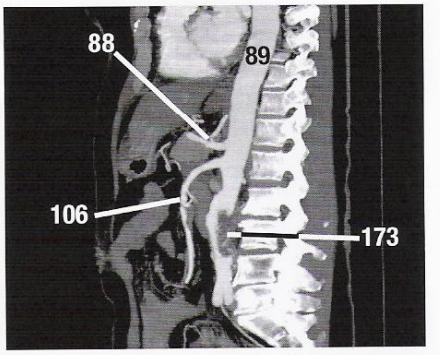

Fig. 183.6

Of course, the benefit of the three-dimensional visualization by means of VRT also depends on the viewing angle. While viewing from an angle **(Fig 183.7)** can underestimate the extent of the thrombus and easily mistake it for a soft plaque, the extent is much better appreciated if seen from different viewing angles **(Figs. 183.8 and 183.9)**. The final images illustrate the effect of a careful elimination of interfering superimposed osseous structures. Because of its high density, the lumbar spine dominates the initial image **(Fig. 183.8)**, and the vascular findings are only fully appreciated after subtraction of the lumbar spine **(Fig. 183.9)**.

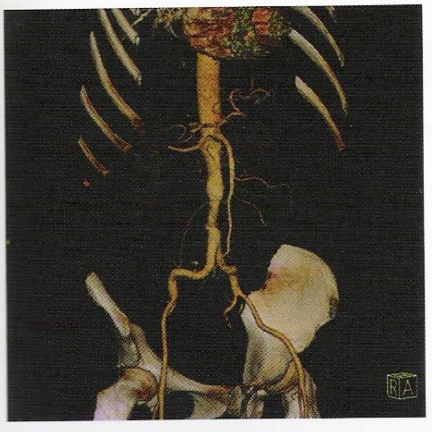

Fig. 183.7

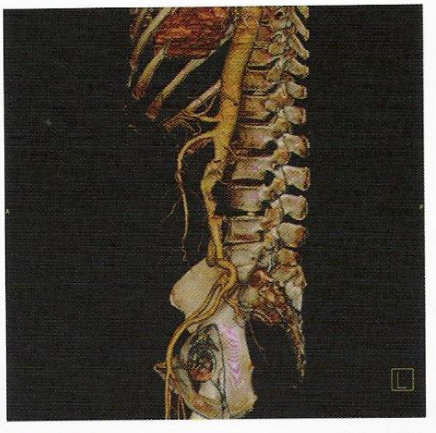

Fig. 183.8

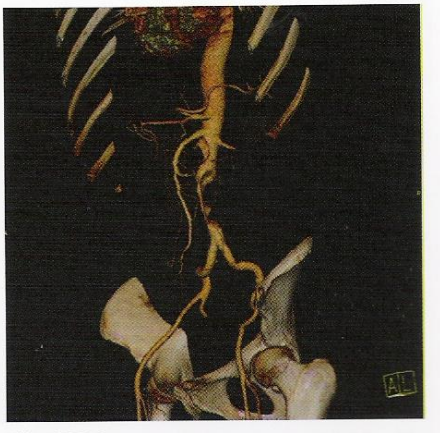

Fig. 183.9

Coronary Arteries

Visualizing the coronary arteries represents a special challenge since the cardiac contractions require short scan times and exact timing. For a cardiac rate exceeding 70 beats per minute, a premedication with a beta blocker should be considered unless contraindicated in view of other clinical findings. Even the shortest rotation times available (0.42 seconds for a 16-slice CT at the time of the publication of this book) require additional EKG triggering. To achieve a diagnostic image quality, the width of the FOV should be reduced to the cardiac size and the craniocaudal acquisition should begin just above the tracheal bifurcation and extent to the diaphragm **(Fig. 184.1)**. Oblique MIPs parallel to the main branch of the left coronary artery as well as special projections of the RIVA and RCA (right coronary artery) and 3D views are obtained. The application of contrast medium should be biphasic with an initial bolus of 40 ml at a flow rate of 4 ml/s and, after a pause of 10 seconds, a second bolus of 80 ml at a flow rate of 2 ml/s. Bolus tracking should be used with the ROI over the ascending aorta.

CT system	Coll. [mm]	ST [mm]	Feed / Rot.	Pitch	RI [mm]	Sec./ Rot.	Volt. [KV]	Current [mAs]	Kernel	W / C [HU]	Delay [sec.]	CM [ml / ml/sec]
4 rows	4 x 1,0	1	1,5	0,37	0,5	0,5	120	250 - 400	B 20	500 / 80	BT	120 / 2-4
16 rows	16 x 0,75	1	3,6	0,3	0,5	0,42	120	400	heart	450 / 60	BT	120 / 2-4

The following images compare a CT **(Fig. 184.2a)** of the left coronary artery **(77a),** including circumflex branch **(77c)** and RIVA **(77b)**, with coronary angiography taken as gold standard **(Fig. 184.2b)**. **Figures 184.3a** and **184.3b** show the same comparison for the right coronary artery **(77d)**.

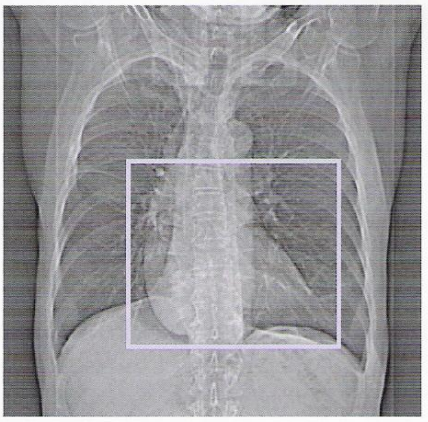

Fig. 184.1

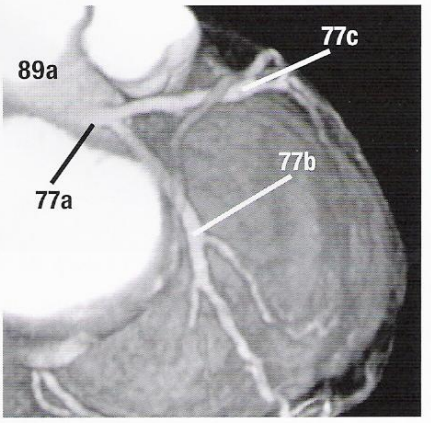

Fig. 184.2a

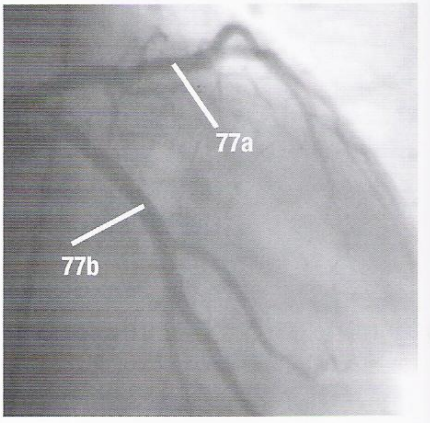

Fig. 184.2b

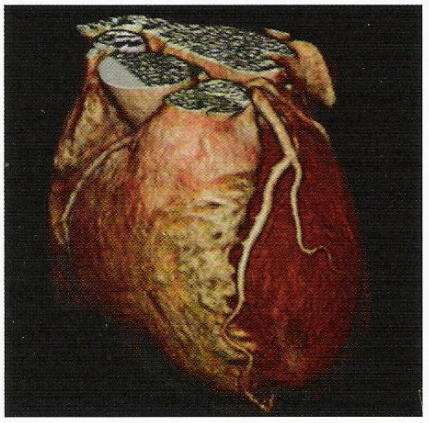

Fig. 184.4

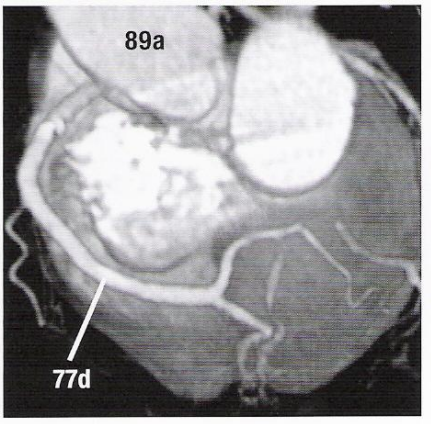

Fig. 184.3a

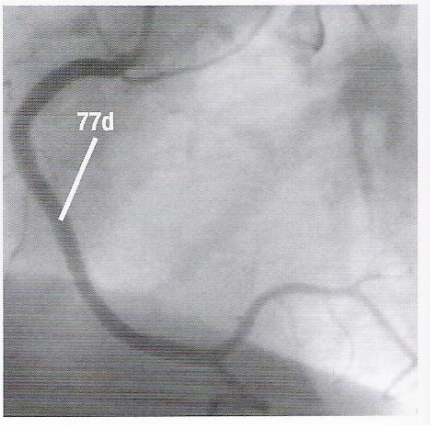

Fig. 184.3b

Screening for Coronary Artery Calcifications

Compared with angiographic imaging of the coronary arteries illustrated on the preceding pages, a slightly thicker section can be selected when screening the coronary arteries for calcifications. Administration of contrast medium is not necessary, and the unenhanced images are obtained in craniocaudal direction.

CT system	Coll. [mm]	ST [mm]	Feed / Rot.	Pitch	RI [mm]	Sec./ Rot.	Volt. [KV]	Current [mAs]	Kernel	W / C [HU]
4 rows	4 x 2,5	3	1,5	0,37	0,5	0,5	120	133	heart medium	370 / 50
16 rows	16 x 1,5	3	3,6	0,3	0,5	0,42	120	130	heart	450 / 60

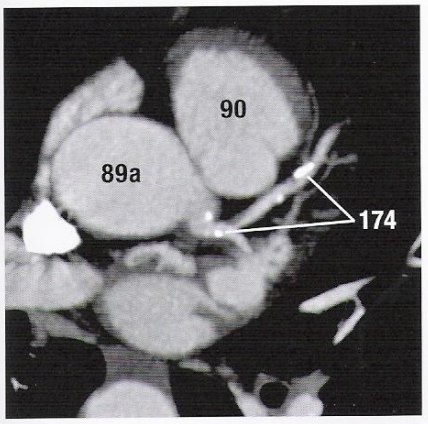

Fig. 185.1

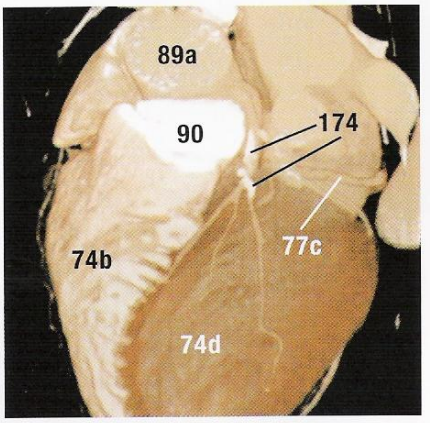

Fig. 185.2

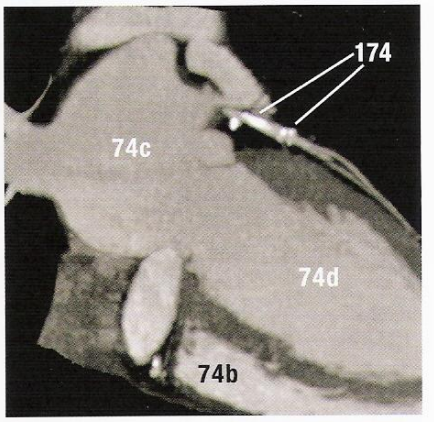

Fig. 185.3

Quantification of coronary calcifications **(174)** is best carried out on a dedicated separate work station but can also be done on a normal work station after postprocessing **(Fig. 185.1-3)**. In this case, however, the unenhanced images are used to obtain, for instance, the Agatston score [43, 44], which correlates with the risk of coronary artery disease.

Agatston Score		Clinical Relevance	Recommended Therapy
0	(negative, no identifiable calcific plaques)	Negative predictive value for coronary artery disease 90 - 95%	None
1 - 10	(minimal identifiable calcific plaque burden)	Stenosis unlikely	General guidelines for prevention
11 - 100	(definite, at least mild calcific plaque burden)	Coronary artery disease possible	Further evaluation indicated
101 - 400	(definite, at least moderate calcific plaque burden)	Coronary artery disease with stenosis possible	Institute risk factor modification and specific cardiac therapy
> 400	(extensive calcific plaque burden)	High probability for coronary artery disease with stenosis possible	Stress EKG is indicated – depending on outcome followed by coronary angiogram

Useful suggestions and recommendations for conducting screening for coronary artery calcifications can be found in the following original articles:

[43] Kopp AF, Ohnesorge B, Becker C et al: Reproducibility and accuracy of coronary calcium measurements with multi-detector row versus electron-beam-CT. Radiology (2002) 225: 113-119

[44] Rumberer JA, Brundage BH, Rader DJ et al: Electron beam CT coronary calcium scanning. Review and guidelines for use in asymptomatic persons. Mayo Clin Proceed (1999) 74: 243-252

[45] Janowitz WR, Agatston AS, Viamonte M: Comparison of serial quantitative evaluation of calcified coronary artery plaque by ultrafast computed tomography in persons with and without obstructive coronary artery disease. Am J Cardiol (1991) 68: 1-6

[46] Haberl R, Becker A, Leber A et al: Correlation of coronary calcification and angiographically documented stenoses in patients with suspected CAD: results of 1764 patients. J Am Coll Cardiol (2001) 37: 451-457

Pulmonary Vasculature (Pulmonary Emboli)

FOV and volume to be scanned are marked on the topogram **(Fig. 186.1)**, beginning from just above the aortic arch, to visualize primarily the central hilar vessels and the heart with the right atrium (a possible source of emboli). Lateral and apical regions of the lung are dispensable. The total acquisition time should not exceed 15 seconds in order to complete the examination during a single breath hold without artifacts. The images are best obtained from caudal to cranial, to have the motion-sensitive areas close to the diaphragm already completed during the end phase and to minimize the artifacts caused by the venous inflow of contrast medium through brachiocephalic veins and superior vena cava. Exact timing with bolus tracking (BT, ROI over the pulmonary outflow tract) is strongly advised. The reconstructed sections should not be less than 3 mm in width. The sections for the MIP should be close to 1.0 mm to avoid overlooking small subtle pulmonary emboli.

CT system	Coll. [mm]	ST [mm]	Feed / Rot.	Pitch	RI [mm]	Sec./ Rot.	Volt. [KV]	Current [mAs]	Kernel	W / C [HU]	Delay [sec.]	CM [ml / ml/sec]
4 rows	4 x 1,0	1-3	6,0	1,5	0,5	0,5	120	140	B 20	420 / 60	16 / BT	120 / 4,0
16 rows	16 x 0,75	1-3	15,0	1,25	0,5	0,5	120	130	B 30	450 / 60	16 / BT	120 / 4,0

The vascular lumina contrast well with the pulmonary tissue **(Figs. 186.2 - 186.5)** and extend all the way to the periphery. Acute pulmonary emboli **(Figs. 186.6** and **186.7)** cause intravascular defects representing thrombi **(173)**, located in this case in the right pulmonary artery **(90a)**.

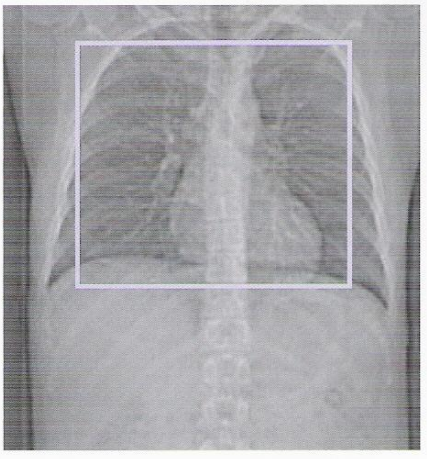

Fig. 186.1

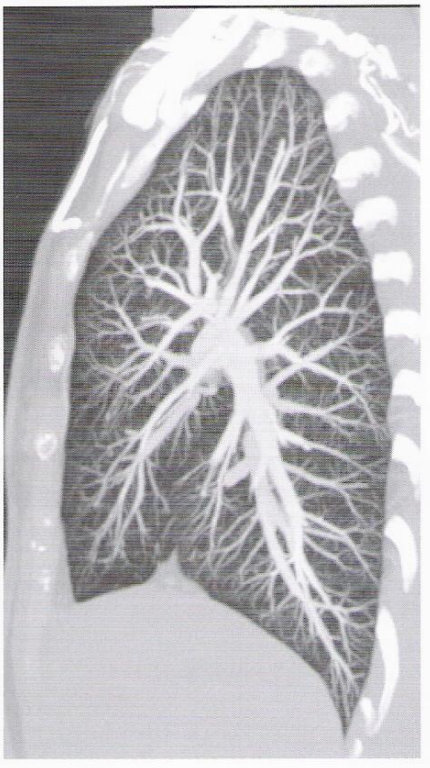

Fig. 186.2

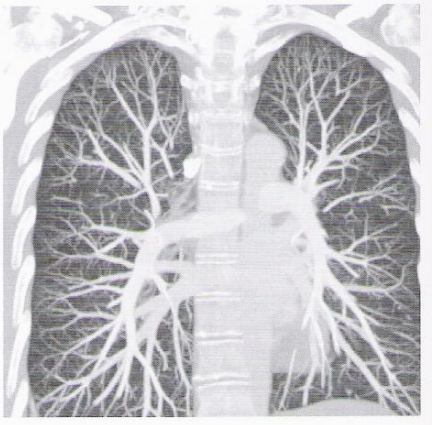

Fig. 186.3

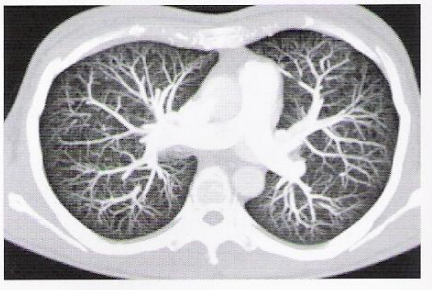

Fig. 186.4

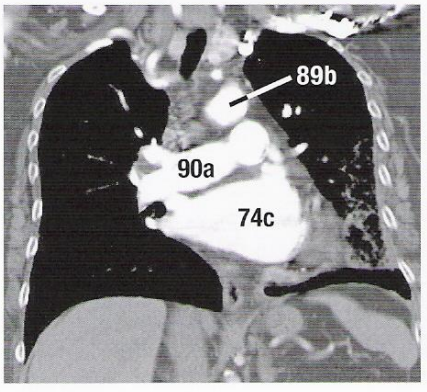

Fig. 186.5

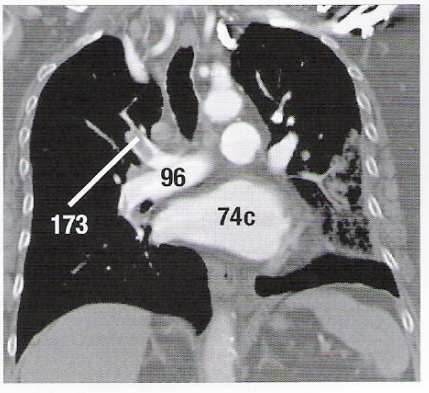

Fig. 186.6

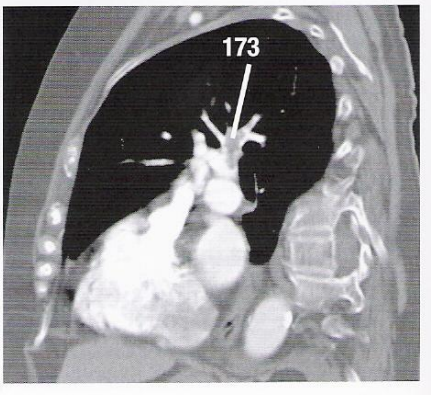

Fig. 186.7

Abdominal Vessels

Most pathologic vascular processes are located close to the center at the origin of major vascular branches, allowing the FOV to be confined to the central two thirds of the abdominal space on the topogram **(Fig. 187.1)**. The origins of the vessels arising from the abdominal aorta are visualized on axial sections and on MIP and MPR images. If a larger volume needs to be acquired on the z-axis, a four-slice CT needs a collimation of 4 x 2.5 mm to achieve an acceptable acquisition time during one breath hold. In contrast, a suspected renal artery stenosis requires a reduction of the acquisition volume to the renal region. To achieve an adequate visualization of possible stenoses in thin renal arteries, the examination should be performed with thin sections of, for instance, 4 x 1 mm and with an RI of only 0.5 mm.

Since the individual circulation times often vary, a fixed delay of the injection of contrast medium is not recommended, and the use of a test bolus or bolus tracking is suggested instead. The ROI to register the increase in density (arrival of the contrast medium = commencement of the measurement) is best placed over the lumen of the descending aorta (see page 176).

CT system	Coll. [mm]	ST [mm]	Feed / Rot.	Pitch	RI [mm]	Sec./ Rot.	Volt. [KV]	Current [mAs]	Kernel	W / C [HU]	Delay [sec.]	CM [ml / ml/sec]
1 row		3,0	6,0	2,0	1,5	0,8	110	100	B 30	350 / 50	20 / BT	120 / 3,0
4 rows	4 x 1,0	1,25	6,0	1,5	1,0	0,5	120	130	B 20	350 / 50	20 / BT	110 / 3,0
16 rows	16 x 0,75	1,0	15,0	1,25	0,7	0,5	120	130	B 30	350 / 50	20 / BT	110 / 3,5

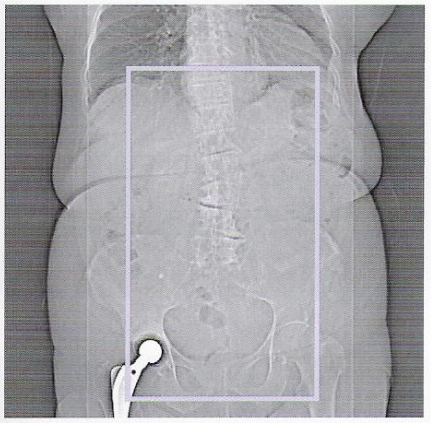

Fig. 187.1

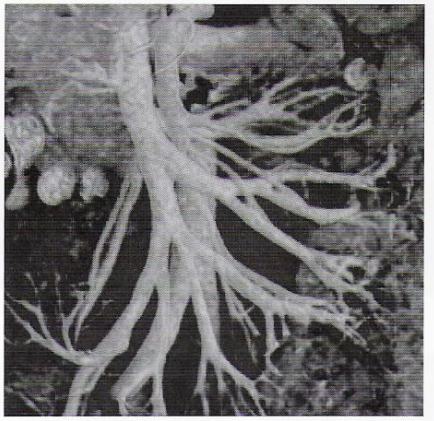

Fig. 187.2

Fig. 187.3

The FOV is placed over the central abdominal space (**Fig. 187.1**). Normally, the visceral branches of the abdominal aorta show a good luminal contrast without filling defects, including the branches of the mesenterial vessels as shown in **Figures 187.2** and **187.3**. In case of an occlusion of the superior mesenteric artery **(106)**, the interrupted vascular lumen (⬅) and the collateral vessels (↗) are easily recognized on VRT and MIP images **(Figs. 187.4-6)**.

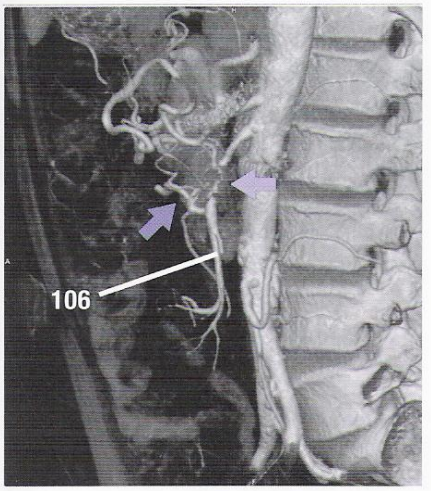

Fig. 187.4

Fig. 187.5

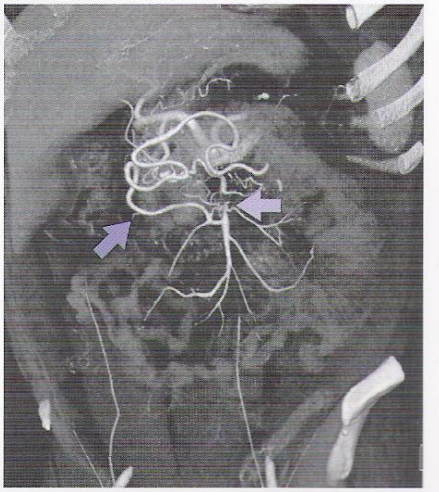

Fig. 187.6

Iliofemoral Vessels

For CT angiography of the iliofemoral vessels, the patient is placed feet first on the table. The length of the relevant body region along the z-axis is critical **(Fig. 188.2)**, and therefore it is generally preferred to use a wide collimation of 4 x 2.5 mm or 16 x 1.5 mm (instead of 4 x 1 mm or 16 x 0.75 mm), which allows a faster table feed. Narrow overlapping reconstructions should guarantee the quality of the final images.

Problems can arise with the timing of the injection of contrast medium, especially with unilateral high-degree stenoses because of the slow flow (see below) in the peripheral vessels of the affected side. If bolus tracking (BT) is used, the ROI is placed over the descending thoracic aorta or abdominal aorta to register the increase in the contrast medium-induced density (see page 176). Already VRT images allow a good overview from the aortic bifurcation to the ankle in most cases **(Fig. 188.1)**.

CT system	Coll. [mm]	ST [mm]	Feed / Rot.	Pitch	RI [mm]	Sec./ Rot.	Volt. [KV]	Current [mAs]	Kernel	W / C [HU]	Delay [sec.]	CM [ml / ml/sec]
4 rows	4 x 2,5	3,0	15,0	1,5	1,5	0,5	120	130	B 20	350 / 50	25 / BT	150 / 3,0
16 rows	16 x 1,5	2,0	24,0	1,0	1,5	0,5	120	130	B 30	350 / 50	25 / BT	150 / 3,5

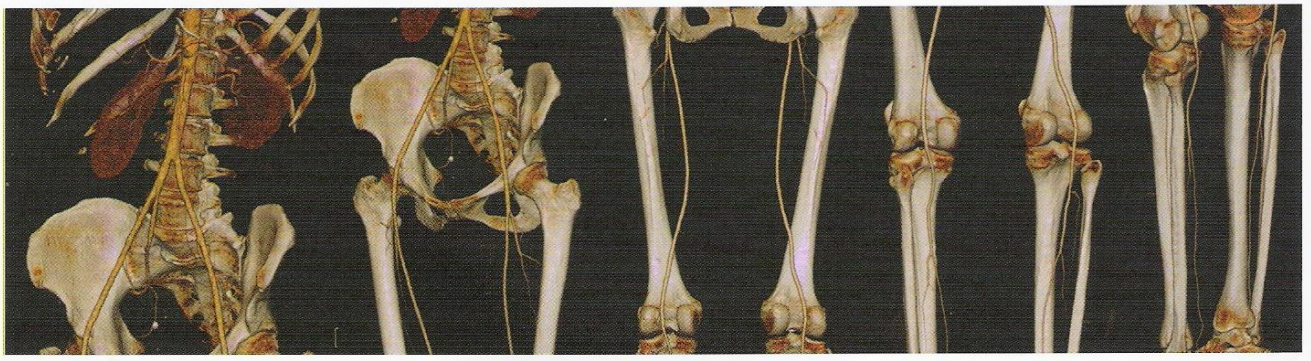

Fig. 188.1

Fig. 188.2

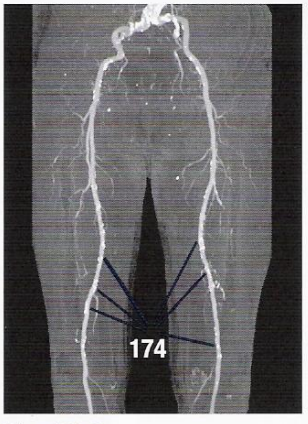

Fig. 188.3

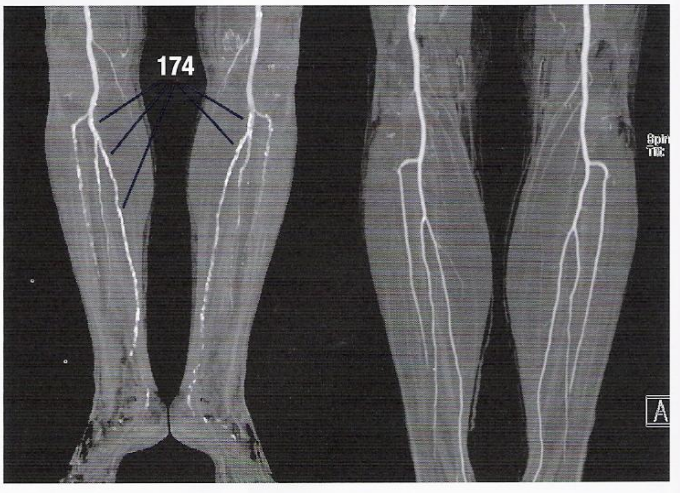

Fig. 188.4 a 4 b

In cases of peripheral arterial occlusive disease, both arteriosclerotic plaques **(174)** and luminal narrowing with impaired flow distally **(Fig. 188.4a)** are clearly recognized in comparison with a normal post-stenotic flow in the tibioperoneal vessels **(Fig. 188.4b)**. In high-degree peripheral arterial occlusive disease examined with a table feed of > 3 cm/sec, the flow can be so much delayed that the craniocaudal acquisition leaves the bolus behind.

Vascular Prothesis

CT angiography is also suitable to follow implanted stents or vascular prostheses **(182)** that interfere with the assessment of mural calcifications because of acoustic shadowing **(Fig. 189.1-3)** in color duplex sonography images.

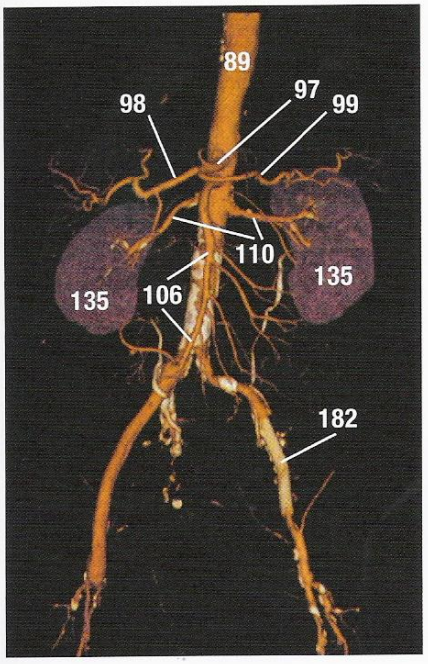

Fig. 189.1

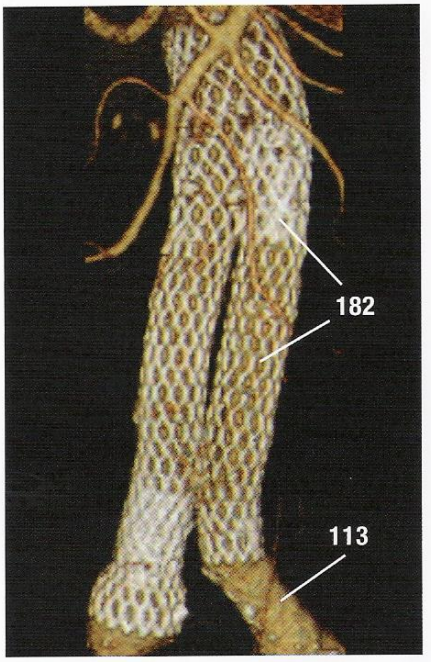

Fig. 189.2

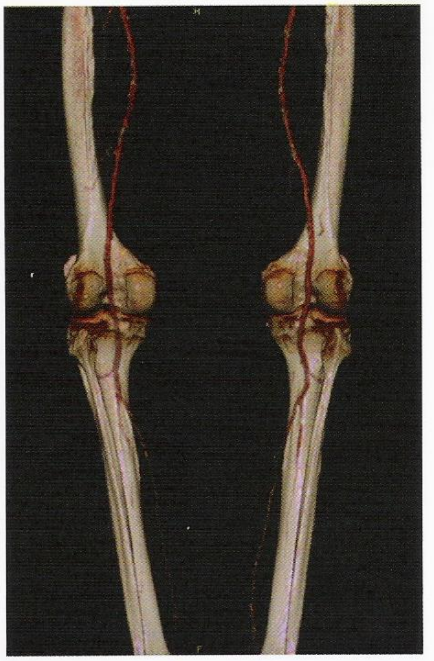

Fig. 189.3

Outlook

CT angiography undergoes rapid technical changes and its advancement can be expected to escalate due to more chip capacity and increasing computer power. It is foreseeable that separate work station with user-friendly software and partially automated programs will shorten reconstructions using VRT further. Generating images of the descending aorta **(Fig. 189.4)** or major thoracic vessels **(Fig. 189.5)** with VRT and MIP as illustrated here will become ever more effortless. This represents a challenge for the user to stay abreast with the technical developments and to keep the departmental protocols of the various CTA applications up to date.

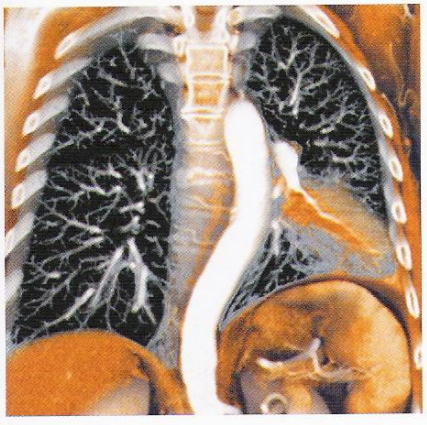

Fig. 189.4

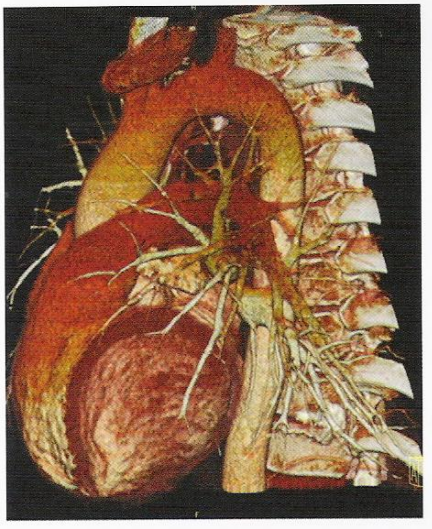

Fig. 189.5a

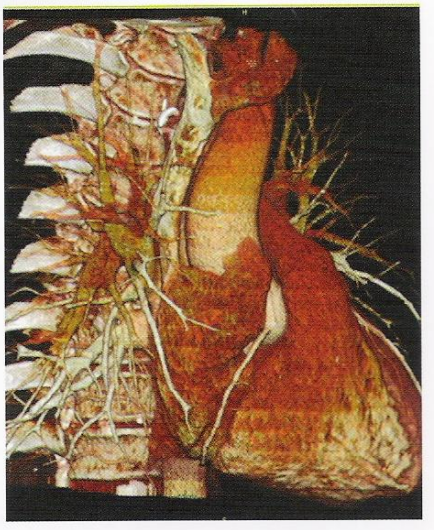

Fig. 189.5b

Test Youself !

Tests 47 to 49:

The following three images contain several pathologic findings, some obvious and others rather subtle. Good luck when tackling the tests! The answers can be found on page 202 below.

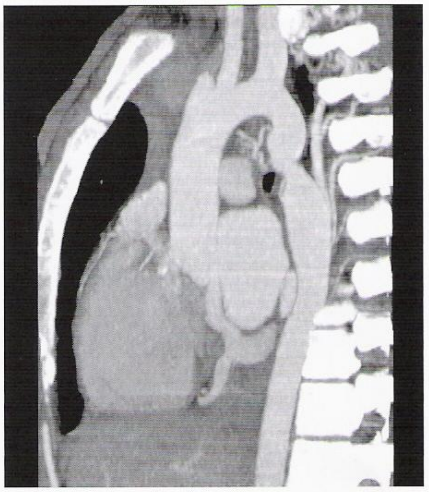

Fig. 190.1

Fig. 190.2

Fig. 190.3

A Primer of CT Evaluation

Occasionally, the beginner faces the question to decide whether a finding represents a true lesion or just an artifact. A contralateral comparison or a comparison with adjacent cranial or caudal sections can often be helpful. Furthermore, uncertainty arises when describing a lesion without familiarity with the appropriate vocabulary. This primer aims to remedy these problems.

A General Approach to an Abnormality of the CT Morphology:

Where ?	Location, lateralization, relative position to other organs/vessels
Size ?	Size (diameter in [mm, cm]; important, e.g., monitoring of therapy)
Density ?	Relative to its surrounding: isodense (equal density); hyperdense (denser); or hypodense (less dense)
Structure ?	Homogenous (e.g., fluids) or heterogenous / septate / geographic
Shape ?	Tubular (vessels, muscles, …) or nodular (tumor, lymph nodes)? Reticular (resembling a net), striate of diffuse?
Demarcation ?	Sharply marginated (more likely benign) or indistinctly marginated (infiltration into the surrounding, e.g., inflammation, malignancy) Caution: Partial volume effect can mimic an indistinct margin!
Perfusion ?	No, peripheral, homogenous or heterogenous contrast enhancement
Expansion ?	Space-occupying effect not invariably to be equalled with malignancy: e.g., large benign cysts can displace adjacent vessels

B Useful Terms, *in Alphabetic Order*

(⇨ Application, Possible Significance)

Air inclusions ⇨ Infection with gas-forming bacteria ⇨ compound fracture

Ampullary Dilatation of the renal pelvis (⇨ physiologic variant or obstructive uropathy)

Articular involvement Evaluation of fractures (⇨ risk of degenerative osteoarthritis)

Bolus CT Dynamic examination, often without table movement to assess the contrast enhancement pattern

Bullae Lung (⇨ pulmonary emphysema)

Capping Periventricular abnormality in the white matter (⇨ transependymal diffusion of CNS; sign of SAE)

Cavity Intrapulmonary hollow space (⇨ tuberculosis)

Central In the center of a lesion or close to the hilum of parenchymatous organs

Clubbing e.g., of a limb of the adrenal gland (⇨ adenoma, metastases)

CM Contrast medium, given orally, rectally or intravenously

Concentric Location of intravascular thrombi (⇨ aortic aneurysm)

Course of fracture lines Evaluation with additional MPR (⇨ surgical planning)

Crescentic Typical configuration, e.g., subdural hematoma or perihepatic effusion / ascites

Defect Pathologic phenomenon in opacified vessels / urinary collecting system

Defect In opacified vessels (⇨ thrombus), in urinary bladder (⇨ tumor, blood clot)

Demarcation Depending on the vascularization, lesions become visible only after administration of contrast medium

Dense band Band-like density (⇨ lung, connective tissue: post-inflammatory, scar)

Densitometry Measuring of density (⇨ differential diagnosis)

Diffuse Uniform, neither focal nor nodular; e.g., liver: hypodense ⇨ hepatic steatosis (fatty liver) hyperdense ⇨ hemochromatosis

Dumbbell-like Typical calcification pattern of benign hamartomas (⇨ lung)

Eggshell-shaped Calcification pattern of perihilar lymph nodes (lung ⇨ silicosis; porcelain gallbladder)

Enhancement Increased density due to accumulation of contrast medium

Enhancement pattern Perfusion pattern (homogenous, timely or delayed)

Excentric Intravascular location of thrombi (⇨ aortic aneurysm)

Fluid Levels Phenomenon (⇨ sedimented hematoma) or air-fluid levels (⇨ paralytic ileus or intestinal obstruction)

Fractures Cortical step deformity, displacement, number of fragments, stability, articular surface?

Ground glass density Diffuse, slight increase density seen in perifocal edema (⇨ fat, lung)

Halo Confined perifocal edema (⇨ around inflammatory foci and metastases)

Hemorrhagic Blood-containing (⇨ large infarcts, e.g., cerebral)

Hilar fat Benign criterion for lymph nodes (⇨ nodal index)

Honeycombing Typical for vascular rarefaction in the lung (⇨ emphysema)

HRCT High resolution computed tomography (thin sections) (⇨ lung; also for MPR and 3D)

Hyperdense Denser than the surrounding tissue (bright ⇨fresh cerebral bleeding or calcification)

Hyperperfusion Enhancement (⇨ inflammation, hypervascular tumor)

Hypodense Less dense than the surrounding (dark ⇨ fluid, fat, air)

Imbibition Striate to diffuse enhancement (⇨ fatty tissue: scar, inflammation)

Indentation Blunt convex bulging / displacement of adjacent structures (⇨ tumors)

Indistinct Outline of a lesion (see marginal indistinctness)

Indistinct margin Caused by inflammatory and tumorous infiltration of the surrounding tissue (caution: DD partial volume effect)

Induration Thickened fibrous tissue (⇨scar, pulmonary fibrosis)

Infiltration Perifocal extension of an inflammatory or malignant process

Inflow effect Incomplete mixing of contrast medium, can mimic intravascular thrombi

Intramural Located in the wall of a hollow viscus (⇨ gas, tumor)

Iris effect Centripetal enhancement (⇨ hepatic hemangiomas)

Isodense As dense as … (= isointense)

Jet effect Inflow of opacified urine from the ureter into the urinary bladder

Lacuna Lacunar defect (⇨ late stage after cerebral infarct, isointense with CSF)

LN Lymph node (for size see checklists, ⇨ hilar fat)

Lymphangiomatosis Ground glass-density (⇨ pulmonary parenchyma, breast carcinoma)

MPR Multiplanar reconstruction of various image planes (sagittal, coronal ⇨ diagnostic evaluation of e.g. fractures)

Multiphase technique Data acquisition during early arterial, portovenous or late venous passage of the contrast medium bolus (⇨ spiral CT of the liver)

Multislice New multislice technique consisting of simultaneous acquisitions of several sections in spiral mode

Mural thickness Single or multiple layers (wall of a hollow viscus: ⇨ ischemia, inflammation)

Narrowed parenchymal rim ⇨ Renal atrophy (degenerative, hydronephrosis)

Necrosis Central, hypodense or homogenous liquefaction

Nodal index Longitudinal-transverse diameter ratio (characterization of lymph nodes)

Nodular Nodular configuration (⇨ lymph nodes, tumors, adenomas), miliary < granular < fine-nodular < large-nodular < confluent (⇨ pulmonary interstitium)

Obliterated Surface of cerebral gyri (⇨ cerebral edema, DD: child) or pancreas outline (⇨ acute pancreatitis)

Osteolytic Destruction of bony matrix (⇨ metastases, multiple myeloma)

Osteoproliferative Osseous apposition (⇨ degenerative), less frequent due to sclerotic metastases

Partial volume effect Effect of partial volume (causes apparent indistinctness)

Patchy Parenchymal perfusion pattern in the spleen during the early arterial phase

Perifocal Circular around a lesion (edematous zone)

Perihilar Topographic description of an intrapulmonary lesion

Peripheral Along the periphery, in contrast to central

Pitch Ratio of table feed per rotation and section thickness (⇨ spiral technique, see p. 8 / 9)

Pixel Picture element (image formation, see p. 14)

Plaque Intravascular (⇨ arteriosclerosis), pleura-based (⇨ asbestosis)

Polycyclic = scalloped, cauliflower-like (⇨ hilar lymph nodes of the lung, e.g., Boeck's disease)

Popcorn Typical pattern of benign calcifications (⇨ lung)

Process Favored term for "I don't know what is means"

Pseudocysts ⇨ chronic pancreatitis

Pulsation Can induce artifacts along vessels (⇨ aortic aneurysm)

Rarefaction Less vessels per pulmonary volume (⇨ emphysema, S/P lobectomy)

Respecting soft-tissue planes Lacking in malignant tumors or advanced inflammations (no longer respecting natural borders => infiltration)

Retention cyst Convex projection into the paranasal sinus, homogenous

Reticular Net-like pattern (⇨ fibrosis of the pulmonary interstitium)

Retrocrural Preferred posterior paravertebral lymph node station

Risk of herniation Internal herniation of brain stem due to increased intracranial pressure (⇨ quadrigeminal and ambient cisterns)

ROI Region of interest (⇨ densitometry)

Round lesion Focal space-occupying lesion (only intrapulmonic)

Scalloped enhancement Peripheral contrast enhancement (⇨ glioblastoma)

Site of predilection Preferred site for certain changes (⇨ lymph nodes, metastases)

Sludge Thickened bile (⇨ cholestasis, cholecystitis)

Space-occupying process Tumor of unknown nature (ubiquitously applicable)

Spindle-shaped Biconvex configuration (⇨ aortic aneurysm; epidural hematoma)

Spiral CT Acquisition of a 3D data set with continuous table feed and any section reconstruction, see p. 7

Stellar Hypodense star-like figure (⇨ FNH of the liver)

Stellate Septation (⇨ echinococcal cyst)

Stent Short tube of various materials to stent vessels, ureter or common bile duct

Step deformity bony Cortex (⇨ fracture diagnosis)

Structure Non-descriptive term of a lesion, try to use more precise term

Subcarinal Preferred lymph node station

Timely Symmetric and timely renal enhancement and excretion of contrast medium = normal

Triangular Wedge-shaped (⇨ typical infarct pattern, scar residue)

Tumor extension Renal vein or vena cava (⇨ renal tumor)

Vascular configuration Normal configuration of the pulmonary hila

Voxel Volume element (image formation, see page 14)

Wedge-shaped Triangular configuration (⇨ typical infarct pattern, scar residue)

B Practical Terms, *Organ-related*

The following list contains helpful terms, which are used for interpreting CT examinations of a particular organ. Terms locating the findings are followed by terms describing typical morphologic changes, which are incorporated with possible conclusions and subsequent organ-related peculiarities.

The list does not claim to be complete (this would make it far too convoluted), but should help the reader to look up some of the most frequent organ-related terms quickly.

Skull, intracranial

Locational descriptions

- Supra- / infratentorial
- Frontal / temporal / parietal / occipital
- Singular / multiple
- White matter / cortical

Typical morphology ⇨ possible diagnoses

- Midline displacement, obliterated cisterns, effaced sulci, narrow subarachnoid space or small ventricles;
  Obliterated white matter / cortex interface
  ⇨ increased intracranial pressure; possible herniation
- Capping
  ⇨ Transependymal diffusion of advanced increased ventricular CSF pressure
- Intracranial air inclusions
  ⇨ Compound fracture of the cranial vault or cranial base
- Cystic homogeneous hypodense
  ⇨ Hygroma / arachnoidal cyst
- Hyperdense, biconvex / crescentic space-occupying process along the internal table of cranial vault
  ⇨ epidural / subdural hematoma
- Hyperdense extracerebral CSF space
  ⇨ Subarachnoidal hemorrhage
- Hypodense white matter lesions
  ⇨ Infarcts, embolic residues
- CSF-isodense lacunar defect
  ⇨ Infarct residue
- Peripheral scalloped enhancement
  ⇨ Typical for glioblastoma
- Subtle rounding of the temporal horn
  Early increase in CSF pressure
- Ventricular enlargement
  ⇨ Internal hydrocephalus
  ⇨ increased CSF pressure !

Notable findings

- Immediate therapeutic intervention with pending herniation !

Paranasal sinuses

Locational descriptions

- Frontal sinus, ethmoid sinus, sphenoid sinus, maxillary sinus
- Semilunar canal (important drainage duct)

Typical morphology ⇨ possible diagnoses

- Round, broad-based, convex homogeneous space-occupying lesion ⇨ retention cyst

Notable findings

- Normal variants: Haller's cells, pneumatic nasal conchae or uncinate process
- Risk of visual loss with orbital fracture
- Fracture classification of facial bones according to Le Fort (see page 63)

Orbit

Locational descriptions

- Orbital floor, orbital roof, medial and lateral orbital wall, retrobulbar

Typical morphology ⇨ possible diagnoses

- Thickened extraocular muscles
  ⇨ Endocrine ophthalmopathy, Myositis

Notable findings

- Risk of vision loss with fractures of the orbital floor solely through cicatricial pull on the orbital fatty tissue

Neck

Locational descriptions

- Nuchal, submandibular, prevertebral, paratracheal, parapharyngeal, epiglottic, subglottic, neurovascular bundle, intra- / suprahyoidal

Typical morphology ⇨ possible diagnoses

- Heterogenous internal structure, possibly with intrathyroidal calcifications ⇨ nodular struma
- Multiple ovoid lesions along the neurovascular bundle ⇨ lymph nodes

Chest

Locational descriptions

- Peripheral = subpleural / central = perihilar;
- Basal / apical, segmental / lobular;
  Name segment !

Typical morphology ⇨ possible diagnoses

- Polycyclic bulky hila
  ⇨ Boeck's disease; hilar nodal metastases
- Multiple, only indistinctly outlined nodules
  ⇨ pulmonary metastases / granulomas
- Sharply outlined, striate density without perifocal edema ⇨ fibrotic edema
- Perifocal ground glass-like density in HRCT
  ⇨ Acute inflammatory process
- Irregular nodular thickened interlobar septae with fine-reticular thickening
  ⇨ Lymphangiomatosis
- Bullae with vascular rarefaction, honey combing
  ⇨ emphysema
- Cavity with layered ground glass density below air pocket ⇨ aspergilloma
- Fusiform thickening along interlobar space
  ⇨ encapsulated pleural effusion
- Apical pleural thickening, cavities, hilar lymph nodes ⇨ tuberculosis
- Popcorn-like or club-like calcifications
  ⇨ benign hamartomas, post-inflammatory residues

Notable findings

- Normal variant of the azygous lobe
- HRCT with thinner sections (do you remember the rational? Refer to p. 86-87)
- Don't forget the pulmonary window

Liver

Locational descriptions

- Subdiaphragmatic, subcapsular, perihilar, name the segment (not only the lobe), periportal, diffuse / focal / multifocal, parahepatic

Typical morphology ⇨ possible diagnoses

- Diffuse hypodensity with resultant hyperdense vessels (unenhanced)
  ⇨ fatty liver (hepatic steatosis)
- Diffuse hyperintensity ⇨ hemochromatosis
- Homogeneous-hypodense, round sharply marginated round lesion without enhancement
  ⇨ benign cysts
- Focal round lesion with enhancement
  ⇨ metastases; abscess
- Round lesion with central hypodense stellar figure ⇨ FNH
- Cameral cysts with stellate septations
  ⇨ echinococcus (splenic involvement?)
- Hypodense cannulated, but irregularly branching ⇨ cholestasis
- "intraparenchymal" hypodense air pockets
  ⇨ pneumobilia; S/P biliointestinal anastomosis

Notable findings

- Multiphase spiral CT: early arterial, portal and late venous for improved detection of focal lesions
- Dynamic bolus CT without table feed
  ⇨ iris effect in hemangiomas
- Portography CT after preceding catheter-placement into splenic or mesenteric artery

Gallbladder

Typical morphology ⇨ possible diagnoses

- Multi-layered edematous wall thickening with perifocal "ascites" ⇨ acute cholecystitis
- Intraluminal wall-based thickening with calcification ⇨ polyp
- Intraluminal sedimentation phenomenon ⇨ sludge
- Eggshell-like peripheral calcification ⇨ Porcelain gallbladder, precancerosis

Spleen

Locational descriptions

- Subdiaphragmatic, subcapsular, perihilar, perisplenic

Typical morphology ⇨ possible diagnoses

- Leopard-like marble pattern during the early arterial phase of enhancement ⇨ physiologic
- Wedge-shaped perfusion defect ⇨ infarct
- Perisplenic round lesion, isodense with splenic parenchyma ⇨ accessory spleen; LN

Pancreas

Locational descriptions

- Head, body, tail, peripancreatic fatty tissue, uncinate process

Typical morphology ⇨ possible diagnoses

- Diffuse enlargement with obliterated outline and exudate pathways ⇨ acute pancreatitis
- Atrophic organ, dilated ducts, calcifications and pseudocysts ⇨ chronic pancreatitis

Kidneys

Locational descriptions

- Parapelvic, medullary, parenchymal, cortical, subcapsular, arising, polar, perirenal, uni- / bilateral, lateralization

Typical morphology ⇨ possible diagnoses

- Homogenous-hypodense, round, sharply demarcated space-occupying lesion without contrast enhancement ⇨ benign cyst
- Hypodense clubbing of the collecting system ⇨ obstruction; ampullary renal pelvis, parapelvic cyst
- Irregular wall thickening of the cyst with contrast enhancement ⇨ suspicious for malignancy
- Thinning of the parenchymal rim, generalized decrease in size ⇨ renal atrophy
- Heterogenous space-occupying lesion extending beyond the organ outline ⇨ renal cell carcinoma
- Hypodense wedge-shaped perfusion defect ⇨renal infarct

Notable findings

- Densitometry of cystic changes for comparison with unenhanced sections
- Evaluation of excretion: symmetric, timely? Dilated ureteral lumen?

Urinary Bladder

Locational descriptions

- Intra-, extra-, paravesical, bladder floor, bladder roof, trigonum

Typical morphology ⇨ possible diagnoses

- Diffuse wall thickening ⇨ cystitis, trabeculated bladder; edema following radiation
- Focal wall thickening, polypoid projecting into the lumen ⇨ suspicious for malignancy

Notable findings

- Jet effect, diverticulum, catheter balloon; indwelling catheter to be clamped before examination!

Genital Organs

Locational descriptions

- Parametrial, intramural, submucosal, endometrial, ischial fossa, pelvic wall, periprostatic

Typical morphology ⇨ possible diagnoses

- Hypodense, water-isodense space-occupying lesion in the scrotum ⇨ hydrocele, varicocele
- Nodular thickening of the myometrium ⇨ benign myomas, but also small uterine cancers
- Growth beyond organ outline, infiltration of rectal and bladder wall ⇨ suspicious for malignancy

Notable findings

- Thin sections through the lesser pelvis, rectal administration of contrast medium

Gastrointestinal Tract

Typical morphology ⇨ possible diagnoses

- Generalized diffuse wall thickening ⇨ lymphoma; ischemia; ulcerative colitis
- Segmental wall thickening ⇨ Crohn's disease
- Air-fluid levels within lumen and dilatation ⇨ intestinal atony to ileus
- Free air in the abdomen ⇨ perforation
- Intramural air ⇨ suspicious for necrotic intestinal wall (ischemic or inflammatory); caution: DD diverticulum!

Notable findings

- Selection of suitable oral contrast medium (refer to p. 19)

Vessels / retroperitoneum

Locational descriptions

- Para-aortal, paracaval, interaortocaval, prevertebral, retrocrural, mesenteric, para-iliac, inguinal, cervical

Typical morphology ⇨ possible diagnoses

- Dilated aortic lumen with different times of opacification and detection of a septum ⇨ dissected aneurysm
- Reticulonodular thickening of the peritoneum with nodular projections and ascites ⇨ peritoneal carcinomatosis
- Endoluminal hypodense defects ⇨ thrombi; caution: DD inflow effect (refer to pp. 21 – 23, 73)

Bone / Skeleton

Locational descriptions

- Cortical, subchondral, juxta-articular, metaphyseal, diaphyseal, epiphyseal, intra- and extraspinal

Typical morphology ⇨ possible diagnoses

- Step-deformity of the cortex, cortical break, fracture line ⇨ fracture
- Articular involvement ⇨ risk of secondary degenerative osteoarthritis
- Focal hypodensity of the spongiosa with absent trabeculae ⇨ pathologic bone marrow infiltration

Notable findings

- Evaluation of stability, MPR, 3D reconstruction, myelo-CT of the spine

C Checklists

The checklists represent the third part of this primer. They are not repeated here. They can be found as inserts or on the following pages:

Solutions to Test Yourself!

The exercises and solutions have been numbered consecutively. Some of the exercises have several different correct solutions. If the exercises can be solved simply by referring to the chapters in the book, I have indicated where you will find the necessary information.

After you have completed the exercises, compare your score and results with those of your colleagues. The score on the right gives you an impression of the degree of difficulty. Enjoy the challenge!

Solution to exercise 1 (p. 32): — 9 Points

You will find the sequence for interpreting CCTs on page 26. Each step gives you ½ point with 3 extra points for the correct sequence, which adds up to 9.

Solution to exercise 2 (p. 45): — 9 Points

	Level	Width	Gray scale	
Lung/pleural window	- 200 HU	2000 HU	-1200 to + 800 HU	3
Bone window	+300 HU	1500 HU	- 450 to +1050 HU	3
Soft-tissue window	+ 50 HU	350 HU	- 125 to + 225 HU	3

Solution to exercise 3 (p. 45): — 10 Points

a)	Barium sulfate	Routine for abdominal/pelvic CT if there are no contraindications	30 min before CT of upper abdomen 60 min before full abdominal CT	4
b)	Gastrografin	Water soluble, but expensive; if perforation ileus or fistulas are suspected; prior to surgery	20 min before CT of upper abdomen 45 min before full abdominal CT	4
				1
No oral CM shortly after surgery for an ileal conduit!				1

Solution to exercise 4 (p. 45): — 6 Points

a)	Renal failure (creatinine, possibly creatinine clearance, function following kidney transplant or nephrectomy)	2
b)	Hyperthyroidism (clinical signs? if yes, hormone status, possibly thyroid ultrasound and scintigraphy)	2
c)	Allergy to CM (has CM-containing iodine already been injected? Are there any known previous allergic reactions?)	2

Solution to exercise 5 (p. 45): — 2 Points

Tubular and nodular structures can be differentiated by comparing a series of images.

Solution to exercise 6 (p. 45): — 3 Points

Vessels in which beam-hardening artifacts occur because of CM inflow are the superior vena cava, inferior vena cava, and the subclavian vein.

Solution to exercise 7 (p. 48): — 3 Points

Fractures, inflammatory processes, and tumors or metastases can cause swelling of mucous membranes and retention of fluids in the mastoid sinuses and middle ear; these are normally filled with air.

Solution to exercise 8 (p. 57): — 18 Points

This image requires careful study. You will discover several types of intracranial hemorrhage and the complications resulting from them.

• Bruising of the left frontoparietal soft tissues (extracranial, indicative of trauma to the head)	1
• Subdural hematoma over the right hemisphere extending to occipital levels (hyperdense)	2
• Edema in the right frontoparietal areas, possibly accompanied by an epidural hematoma	2
• Signs of subarachnoid bleeding in several sulci in parietal areas on the right, adjacent to the falx	2
• The hematoma has penetrated into the right lateral ventricle, which is practically obliterated	4
• Choroid plexus in the left lateral ventricle appears normal	1
• There is a midline shift toward the left, and edema surrounds the periventricular white matter on the right	2
• Raised intracranial pressure (obstructed ventricle) and herniation of the brain (edema) can be expected	4

Solution to exercise 9 (p. 72):

9 Points

Gray and white matter appear well defined on narrow brain windows.

Level	Width	Gray scale	
+ 35 HU	80 HU	- 5 HU to + 75 HU	3

CCT sections are normally oriented parallel to the orbitomeatal line, so that initial and follow-up studies can be precisely compared. **2**

2-mm sections at 4-mm increments are acquired through the petrosal bone, then thickness and table movement are set at 8 mm. **2**

2

Solution to exercise 10 (p. 72):

16 Points

Intracerebral hemorrhage	in early phases hyperdense, often with hypodense peripheral edema	2
Subarachnoid hemorrhage	hyperdense blood instead of hypodense CSF in the sulci and cisterns	2
Subdural hemorrhage	hyperdense crescentic area close to the calvaria, concave toward the cortex, not limited by cranial sutures	4
Epidural hemorrhage	hyperdense, biconvex area close to the calvaria, smooth toward the cortex, always limited by cranial sutures	4
Complications	hemorrhage into a ventricle, CSF flow is obstructed, edema, danger of herniation	4

Solution to exercise 11 (p. 72):

2 Points

Subarachnoid hemorrhage in children may be visible only next to the falx or in the lateral (Sylvian) fissure.

Solution to exercise 12 (p. 72):

10 Points

Practice makes perfect!

Solution to exercise 13 (p. 72):

4 Points

Fracture of the right frontal bone and absent right frontal sinus (the latter is a congenital variation, not a hemorrhage, as indicated by the osseous trabeculae)

Solution to exercise 14 (p. 72):

8 Points

This was a difficult question. In the left internal jugular vein there is unusual sedimentation of the CM due to slow blood flow. The asymmetry of the jugular veins is not a sign of thrombosis. A left cervical abscess makes the neck muscles appear poorly defined.

Solution to exercise 15 (p. 73):

4 Points

In this patient the surface subarachnoid spaces are clearly too narrow and the ventricles distended. These signs indicate that CSF drainage is reduced or blocked and there is imminent danger of brain herniation. There is generalized brain edema. A neurosurgeon should be consulted about inserting an intraventricular shunt.

Solution to exercise 16 (p. 73):

3 Points

It is possible to mistake the subarachnoid hemorrhage around the left frontal lobe as an artifact. The left frontal cortex is outlined by blood. If you did not see any abnormality, return to the chapter about the head.

Solution to exercise 17 (p. 73):

6 Points

You have of course taken the hint about not giving up too soon; the right medial rectus muscle **(47c)** is thickened. It is the second muscle to become involved in endocrine ophthalmopathy.

If you cannot remember which muscle is affected first, return to page 61.

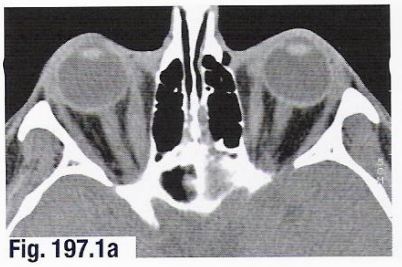

Fig. 197.1a

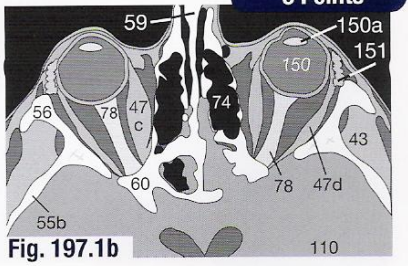

Fig. 197.1b

Solution to exercise 18 (p. 73):

12 Points

Part of the question was misleading, but this was intentional, and I hope you take it in the right spirit. No fresh intracranial bleeding can be seen in this image **(Fig. 73.4** is the same as **Fig. 198.1)**. The abnormality in the left frontal lobe is an area of reduced attenuation representing an earlier hemorrhage **(180)** which has now reached the resorption phase (4 points). The extracranial swelling and bruising in the left frontoparietal area (1 point) is also 2 weeks old. In order to determine the nature of the hyperdense foci, particularly on the right side, you should of course ask to see adjacent images (4 points).

The next caudal section **(Fig. 198.2)** shows that these foci are formed by the orbital roofs **(*)**, the sphenoid bone **(60)**, and the petrosal bone **(**)** (1 point for each). These partial volume effects were discussed on page 53. If you misinterpreted them in the question, take it as a warning and you will be less likely to make this mistake again.

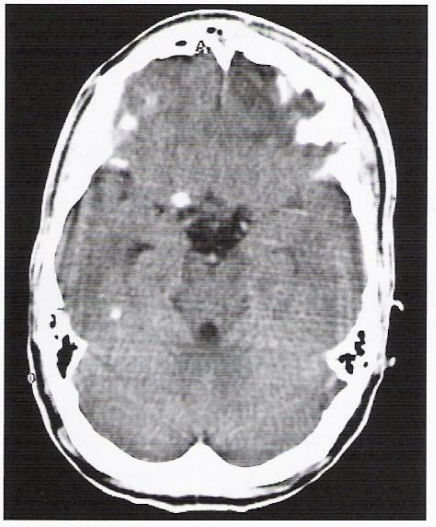

Fig. 198.1a

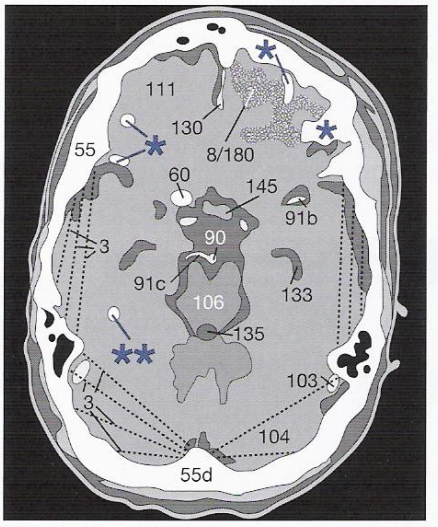

Fig. 198.1b

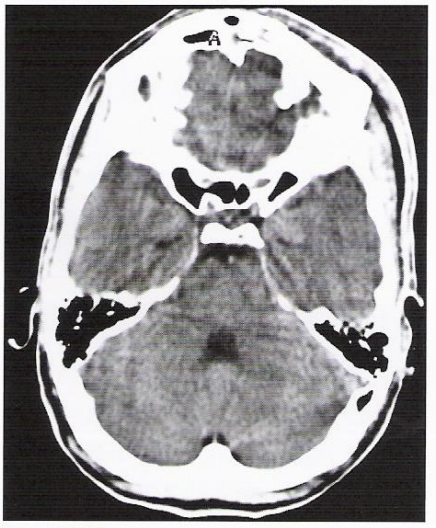

Fig. 198.2a

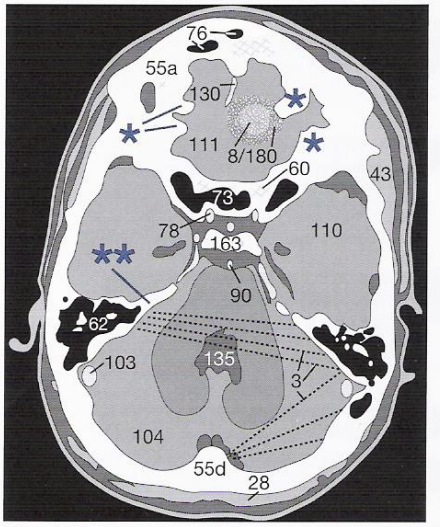

Fig. 198.2b

Solution to exercise 19 (p. 82):

13 Points

Compare your checklist for CCT with the one on page 74.
As in exercise 1, each item is worth ½ point and the correct sequence is worth 3 points.

Solution to exercise 20 (p. 100):

4 Points

There is an area of low attenuation due to incomplete CM filling in the azygos vein, most likely because of a thrombosis (2 points). The esophagus is not well defined. There are hypodense lines crossing the pulmonary trunk and right pulmonary artery which are artifacts because they extend beyond the lumen of the vessels (2 points).

Solution to exercise 21 (p. 100):

4 Points

Did you suggest doing bronchioscopy or biopsy in order to know more about the "lesion"? Then you must revisit the basic rules of CT interpretation. But if you remembered to look first of all at the other images in the series, as for example the one on the right, you will have seen that the "lesion" belongs to the sternoclavicular joint ( ).
This is another example of a partial volume effect. There is degenerative change in this joint, but no pulmonary lesion or inflammation.

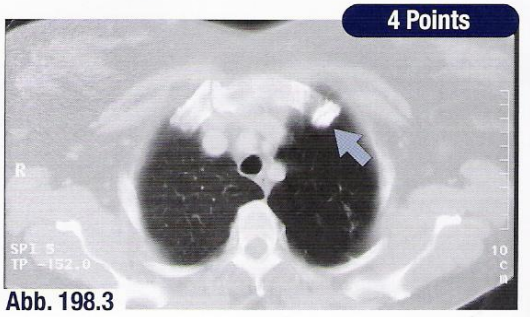

Abb. 198.3

Solution to exercise 22 (p. 100):

The cause of sudden back pain in this patient was the dissection **(172)** of the aortic aneurysm (1 point). At this level, both the ascending **(89a)** and the descending **(89c)** aorta (1 point each) show a dissection flap. It is a de Bakey type I dissection (1 point).

4 Points

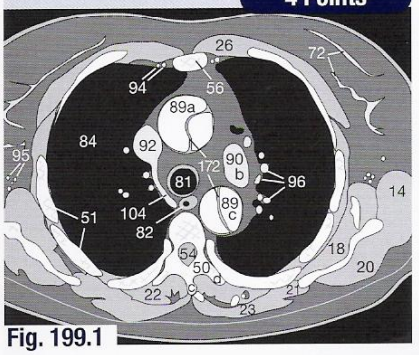

Fig. 199.1

Solution to exercise 23 (p. 100):

This is a case of bronchial carcinoma (the bronchial obstruction is not seen at this level). There is atelectasis of the entire left lung **(84)** (2 points) and an effusion **(8)** fills the pleural spaces (2 points). Did you detect the metastatic mediastinal LN **(6)**? (2 points)

6 Points

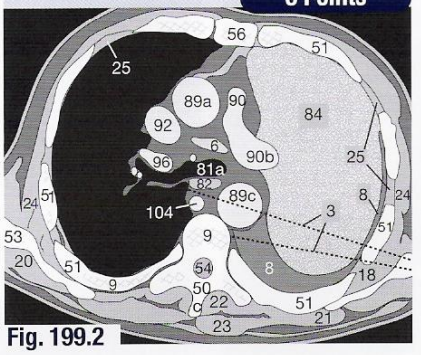

Fig. 199.2

Solution to exercise 24 (p. 101):

The most obvious abnormality is the bronchial carcinoma **(7)** in the left lung. The right lung shows emphysematous bullae **(176)**. CT-guided biopsy of the tumor should be possible without causing a pneumothorax because it has a broad pleural base (2 points).

6 Points

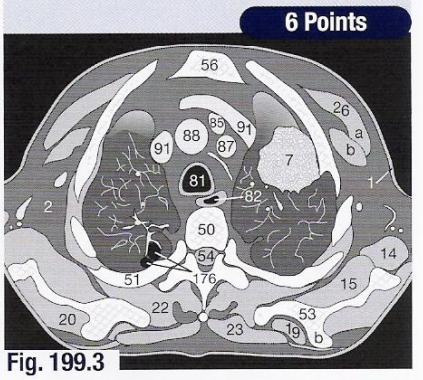

Fig. 199.3

Solution to exercise 25 (p. 101):

The small metal clip **(183)** is a hint that the stomach has been surgically transposed into the mediastinum. The thick-walled structure with the irregular lumen is a part of the stomach **(129)**, not an esophageal tumor. At the moment of data acquisition the stomach was contracting and is therefore not as easily identified as in **Figure 91.2**.

4 Points

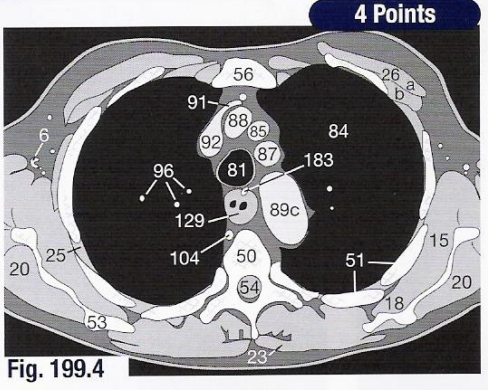

Fig. 199.4

Solution to exercise 26 (p. 101):

You are already familiar with this tragic case of bronchial carcinoma in a young pregnant woman (thus no CM enhancement, see **Fig. 98.2**). The anterior locule of the malignant effusion (3 points) had caused the right lung to collapse (2 points) and was therefore drained. After the fibrin clot had been removed from the catheter the lung was reinflated and the mother's life was prolonged until the birth of her healthy child. Did you notice the metastatic LN in the right axilla? (1 point)

6 Points

Solution to exercise 27 (p. 101):

Perhaps the first thing you noticed was the irregular contour of the diaphragm **(30)** (1 point), but this is a normal finding. The patient was a smoker and had complained of weight loss.

You should first ask for lung windows in order to check for metastases **(7)** or primary bronchial carcinoma (5 points). When a chest is examined, it should become your standard procedure to use both soft-tissue and lung windows **(Fig. 199.5a)**.

6 Points

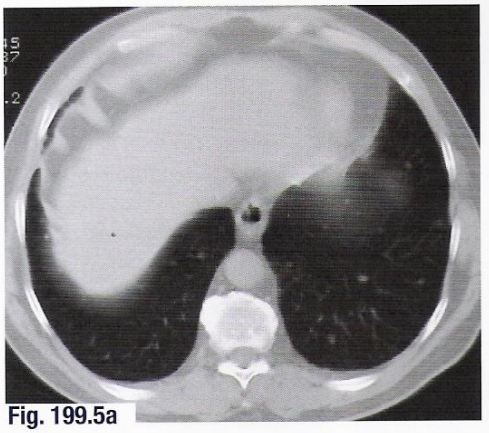

Fig. 199.5a

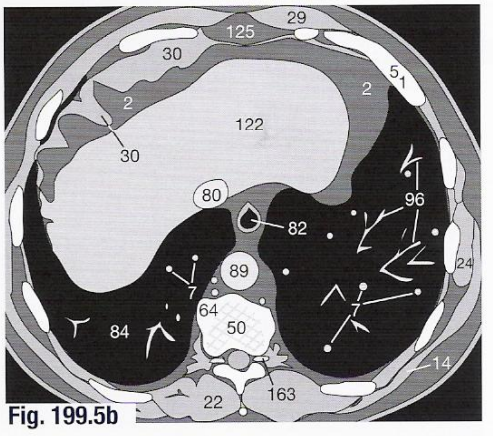

Fig. 199.5b

Solution to exercise 28 (p. 101):

These two images show an aberrant branch of the aortic arch: The subclavian artery passes posterior to the trachea and the esophagus toward the right side of the body. You may remember that this anatomic variation was mentioned, but not shown, on page 120.

4 Points

Solution to exercise 29 (p. 141): **4 Points**

In addition to the air–fluid levels in the dilated bowel (2 points) associated with an ileus, you should have seen the dilated right ureter anterior to the psoas muscle (2 points). The correct diagnosis is therefore ileus and hydronephrosis. You may recognize this particular case as the same one shown in **Figure 134.2a**, at a slightly more cranial level.

Solution to exercise 30 (p. 149): **7 Points**

This is a case of left inguinal hernia **(177)** (1 point). There are normal LN bilaterally **(6)** (1 point). Did you identify the femoral artery **(119)**, the profunda femoris artery **(199a)**, the femoral vein **(120)**, the deep femoral vein, and the gluteal vessels **(162)** (1 point each)?

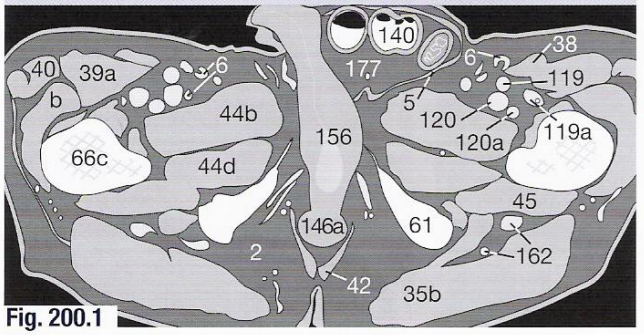

Fig. 200.1

Solution to exercise 31 (p. 149): **7 Points**

You should have seen the adenoma **(134)** in the right adrenal gland (2 points). For ½ point each you should be able to name ten other organs. Consult the number legends if you are uncertain.

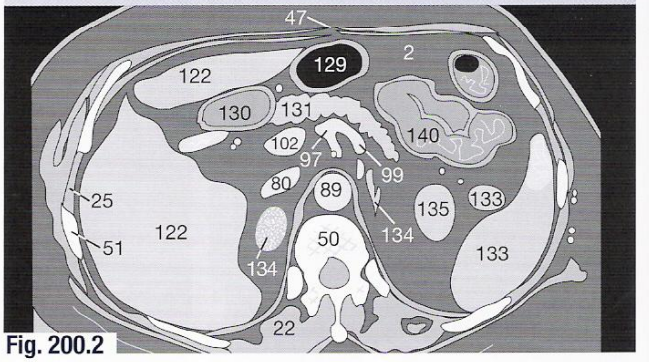

Fig. 200.2

Solution to exercise 32 (p. 149): **4 Points**

This is indeed a case of situs inversus (2 points). You will also have noticed that the attenuation of the liver **(122)** is abnormally low: fatty liver (2 points).

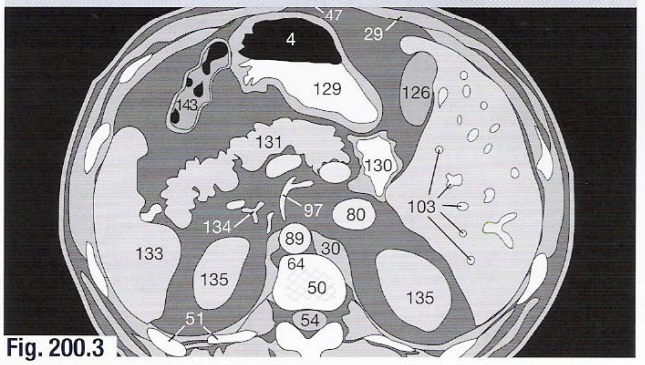

Fig. 200.3

Solution to exercise 33 (p. 149): **3 Points**

The question itself will have drawn your attention to the atherosclerotic plaques **(174)** in the common iliac arteries **(113)** (1 point). The left one is part of an aortic aneurysm (2 points).

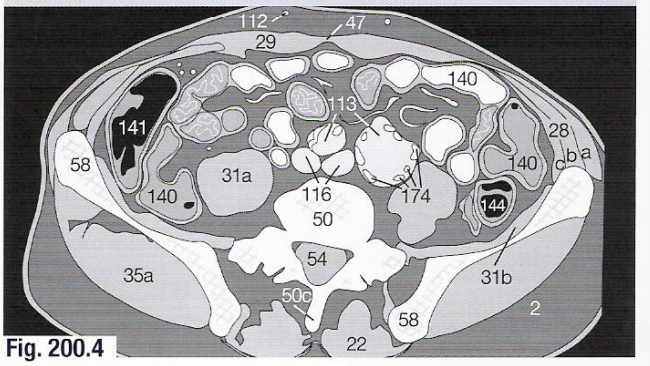

Fig. 200.4

Solution to exercise 34 (p. 149): **6 Points**

Hopefully you saw the fairly large, irregular metastasis **(7)** in the posterior segment of the liver **(122)** (1 point). Did you also see the smaller, more anterior metastasis? (3 points). The DD may have included an atypical hepatic cyst (1 point) or, for the anterior lesion, partial volume averaging of the falciform ligament (1 point).

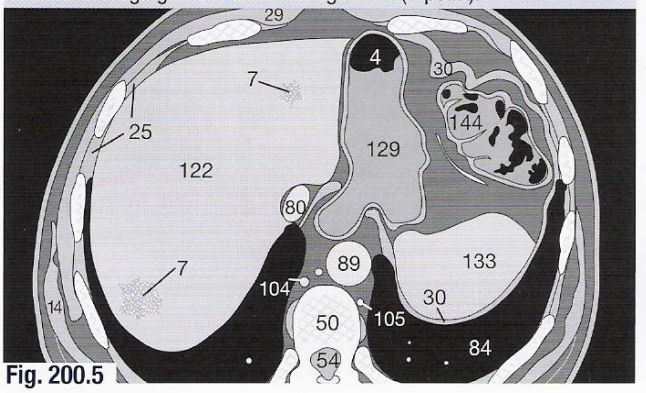

Fig. 200.5

Solution to exercise 35 (p. 149): **5 Points**

The two cysts **(169)** in the right kidney **(135)** are impossible to miss (1 point). But there are also multiple, hypodense lesions in the spleen **(133)**, due to splenic candidiasis (3 points). You may also have considered a rare case of nodular lymphoma or melanoma metastases in the spleen (½ point each).

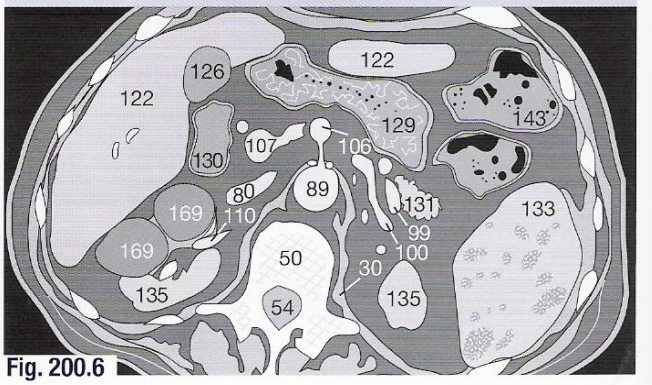

Fig. 200.6

Solution to exercise 36 (p. 150): **6 Points**

Figure 201.1 is the section next to the one in **Figure 150.1** and shows that the hypodense area in the liver is the gallbladder. If you suggested doing anything else, for example aspiration or biopsy, before seeing adjacent sections, take 3 points away.

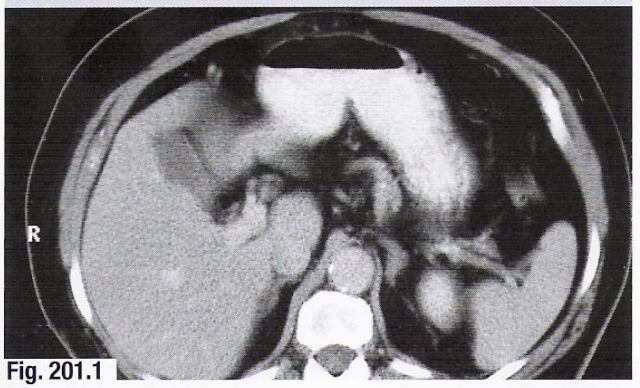

Fig. 201.1

Solution to exercise 37 (p. 150): **5 Points**

You may have thought that the hyperdense foci next to the rectum **(146)** represent calcified LN **(6)** (1 point). However, the lymphatics are so well demarcated because they are still opacified after lymphography (3 points). Did you also notice the atherosclerotic plaques **(174)** in the femoral arteries **(119)** (1 point)?

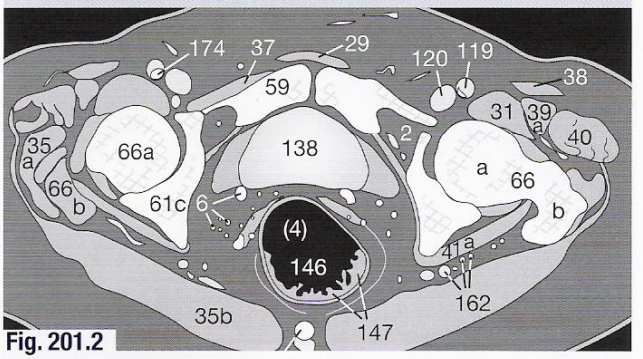

Fig. 201.2

Solution to exercise 38 (p. 150): **3 Points**

You will achieve the most accurate densitometry of a cyst if you select a section without any partial volume effects from renal parenchyma as in **Figure 150.3b** (1 point). Results of measurements in **Figure 150.3a** would be too high (2 points). Since this very case was discussed on page 133, take away 2 points for the incorrect answer.

Solution to exercise 39 (p. 150): **7 Points**

The illustration showed only one metastasis in the right lobe of the liver (1 point) in a case of hepatomegaly (1 point). By using triphasic SCT, additional metastases become visible (2 points). CT arterial portography (3 points) is more invasive than SCT alone, but it demonstrated that the spleen also has metastases.

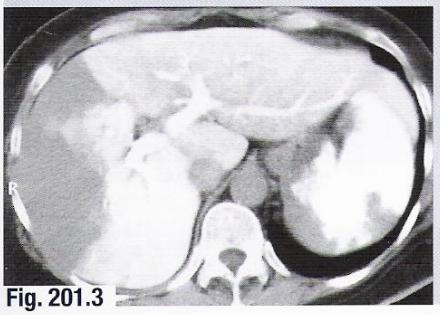

Fig. 201.3

Solution to exercise 40 (p. 150): **6 Points**

For further documentation you should ask to see bone windows (2 points) and of course the adjacent sections (2 points) in order to assess the pelvic fracture. It is also important to determine whether the acetabular fossa was involved (2 points). The fractures of the pubic bones were already visible on soft-tissue windows **(Fig. 150.5)** because the fragments were slightly displaced.

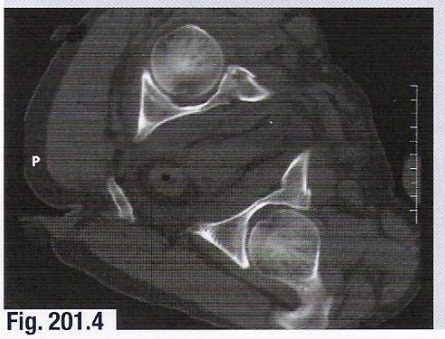

Fig. 201.4

Solution to exercise 41 (p. 151): **10 Points**

If you detected the fresh thrombosis **(173)** in the right femoral vein **(118)**, you get 3 points. Did you also see the synovial cyst **(175)** on the left (3 points)? Your DD may have included a lymphoma, a femoral or inguinal hernia, or a metastasis (1 point each). If you mistook the cyst for thrombosis of the left femoral vein as well, take away 3 points! The vein **(118)** lies next to the cyst.

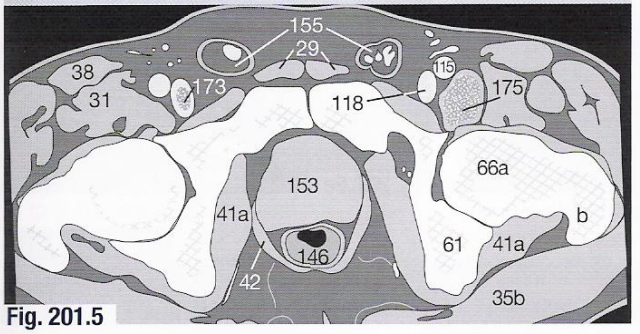

Fig. 201.5

Solution to exercise 42 (p. 151): **7 Points**

Another example of a partial volume effect: the sigmoid colon was only apparently "within" the urinary bladder (4 points). The first thing you should have asked to see was adjacent sections

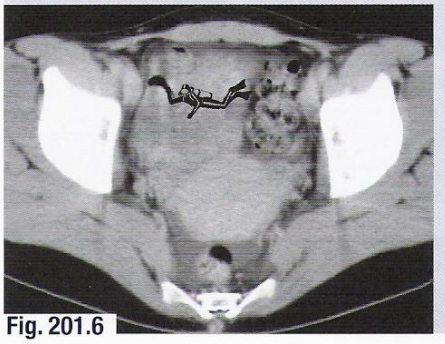

Fig. 201.6

You may remember that this case was discussed on page 116 (see **Fig. 116.5a**). There's also pararectal ascites (1 point).

Solutions to Test Yourself!

Solution to exercise 43 (p. 151): 11 Points

The beam-hardening artifacts **(3)** due to drainage tubes **(182)** were a hint that this image was taken shortly after surgery (2 points). The abnormal structures containing gases **(4)** are surgical packs (5 points) placed to control bleeding after multiple trauma. When the patient's condition had stabilized they would be removed in a second operation. Your DD may have included fecal impaction in Chilaiditi's syndrome (2 points) or an abscess with gas-forming bacteria (2 points).

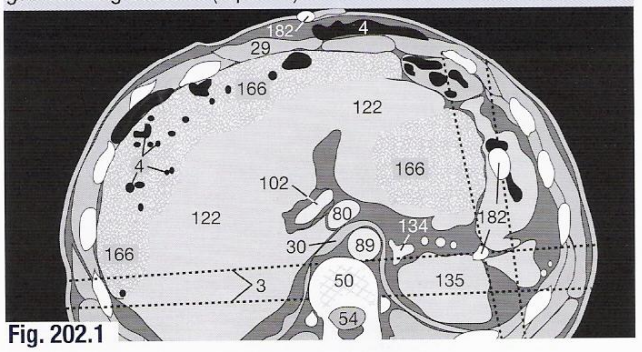

Fig. 202.1

Solution to exercise 44 (p. 151): 8 Points

You may have thought that **Figure 151.4** shows a gastric pullthrough for esophageal carcinoma (1 point) or that the esophageal walls are thickened due to metastases (2 points). However, this was a case of a paraesophageal sliding hiatus hernia (3 points). If you forgot to ask for lung windows, you will not have seen the large right paramediastinal emphysematous bulla (➡) (2 points).

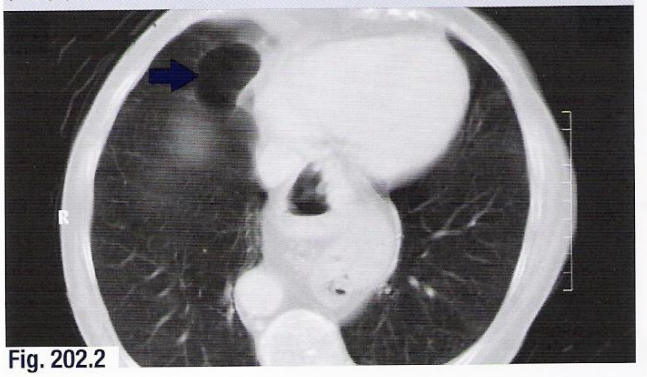

Fig. 202.2

Solution to exercise 45 (p. 151): 11 Points

In **Figure 151.5** a poorly defined tangential section of a diverticulum of the urinary bladder can be seen next to the rectum on the right side (✱) (5 points). Your DD may have included a pararectal LN (2 points). The irregularities in the attenuation values of the urine are due to CM and the 'jet phenomenon' (2 points each). **Figures 202.3** and **202.4** are adjacent to **Figure 151.5**.

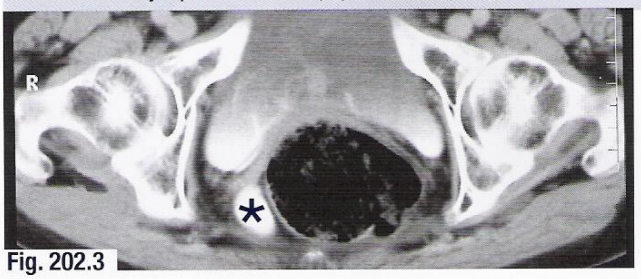

Fig. 202.3

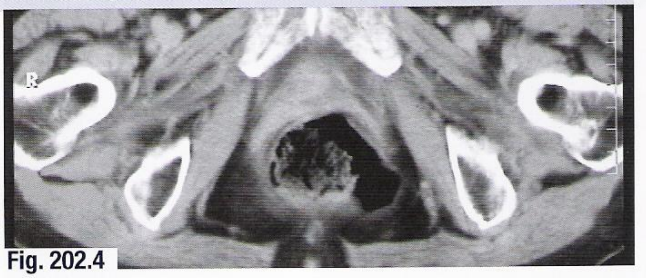

Fig. 202.4

Solution to exercise 46 (p. 151):

The same old problem! The hyperdense (enhanced) C-shaped structure in the pancreas **(131)** in **Figures 151.6** or **202.5** is a loop of the splenic artery **(99)** (4 points). The adjacent sections (c, d, and e) show that the splenic artery can be very tortuous.

4 Points

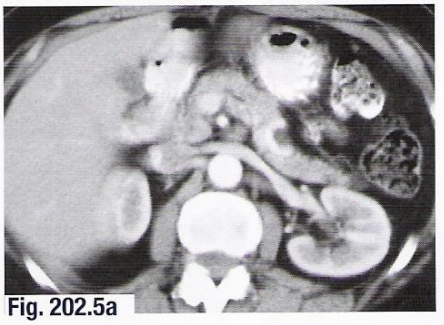

Fig. 202.5a

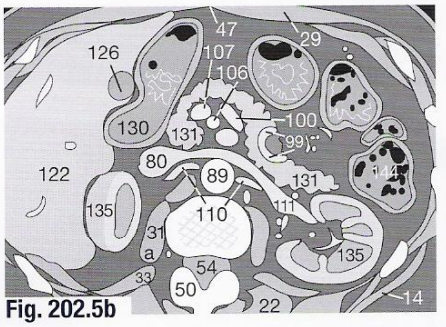

Fig. 202.5b

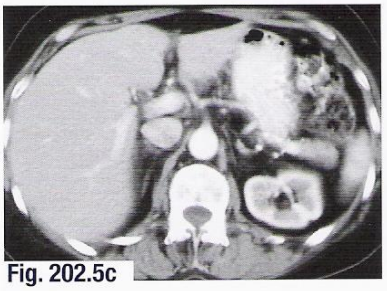

Fig. 202.5c

Fig. 202.5d

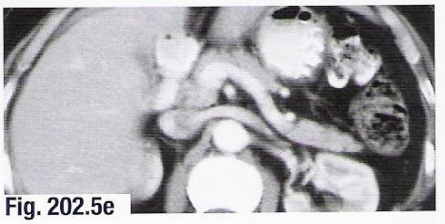

Fig. 202.5e

Solution to exercise 47-49 (p. 190): 6 Points

A stenosis of the thoracic aorta is clearly identified **(Fig. 190.1)**, as well as a thrombus in the right pulmonary vessels **(Fig. 190.2)** and an inflow effect of contrast medim into the superior vena cava as differential diagnosis of a genuine cava thrombosis **(Fig. 190.3)**.

Thieme

Excerpt from:
Hofer, Matthias
CT Teaching Manual
ISBN 3-13-124352-X
ISBN 1-58890-277-3

Checklist for Abdominal Readings

Abdominal wall:	(especially periumbilical and inguinal regions) hernias, enlarged lymph nodes?
Liver and spleen:	homogeneous parenchyma without focal lesions? well-defined outline?
Gallbladder:	well-defined, thin wall? calculi?
Pancreas, adrenals:	well-defined, size normal?
Kidneys, ureter and bladder:	symmetric excretion of CM? obstruction, atrophy, bladder wall smooth and thin?
Reproductive organs:	homogeneous prostate of normal size? spermatic cord, uterus, and ovaries?
GIT:	well defined? normal thickness of walls? stenoses or dilations?
Retroperitoneum:	vessels: aneurysms? thromboses? enlarged lymph nodes? mesenteric (normal < 10 mm) retrocrural (normal < 7 mm) para-aortic (normal < 7 mm) pariliacal (normal < 12 mm) parainguinal (normal < 18 mm)
Bone window:	lumbar spine and pelvis: degenerative lesions? fractures? focal sclerotic or lytic lesions? spinal stenoses?

Thieme

Excerpt from:
Hofer, Matthias
CT Teaching Manual
ISBN 3-13-124352-X
ISBN 1-58890-277-3

Checklist for Thorax Readings

1. On the soft-tissue window:

- soft tissues, especially:
  - axillary LNs
  - breast (malignant lesions?)
- mediastinum in four regions:
  - from the aortic arch cranially (LNs?, thymoma/goiter?)
  - hilar region (configuration and size of vessels, lobulated and enlarged?
  - heart and coronary arteries (sclerosis?)
  - four typical sites of predilection for LNs:
    - anterior to aortic arch (normal: almost none or < 6 mm)
    - in the aortopulmonary window (normal: < 4 LNs < 15 mm)
    - subcarinal (normal: < 10 mm; DD: esophagus)
    - next to descending aorta (normal: < 10 mm; DD: azygos)

2. On the lung window:

- Parenchyma of the lung:
  - normal branching pattern and caliber of vessels?
  - vascular oligemia only at interlobar fissures? bullae?
  - any suspicious lung foci? inflammatory infiltrates?
- Pleura
  - plaques, calcification, pleural fluid, pneumothorax?
- Bones (vertebrae, scapula, ribs):
  - normal structure of marrow?
  - degenerative osteophytes?
  - focal lytic or sclerotic processes?
  - stenoses of the spinal canal?

Management of Acute Reactions in Adults I

Urticaria

1. Discontinue injection if not completed
2. No treatment needed in most cases
3. Give H_1-receptor blocker: Diphenhydramine (Benadryl®) PO / IM / IV 25-50 mg
   If severe or widely disseminated:
   Alpha agonist (arteriolar and venous constriction)
   Epinephrine SC (1:1,000) 0.1-0.3 ml = 0.1-0.3 mg
   (if no cardiac contraindications)

Bronchospasm

1. Give O_2 6-10 liters / min (via mask)
   Monitor: electrocardiogram, O_2 saturation (pulse oximeter), and blood pressure.
2. Give beta-agonist inhalers: bronchiolar dilators, such as metaproterenol (Alupent®), terbutaline (Brethaire®), or albuterol (Proventil®, Ventolin®) 2-3 puffs; repeat prn.
   If unresponsive to inhalers, us SC, IM or IV epinephrine
3. Give epinephrine SC or IM (1:1,000) 0.1-0.3 ml (= 0.1-0.3 mg) or, if hypotension evident,
   Epinephrine (1:10,000) slowly IV 1 ml (= 0.1 mg)
   Repeat as needed up to a maximum of 1 mg

Alternetively:
Give aminophylline: 6 mg / kg IV in D5W over 10-20 minutes (loading dose), then 0.4-1 mg / kg / hr, as needed (caution: hypotension)

Call for assistance (e.g., cardiopulmonary arrest response team) for severe bronchospasm or if O_2 saturation < 88% persists.

Facial or Laryngeal Edema

1. Give alpha agonist (arteriolar and venous constriction): Ephinephrine SC or IM (1:1,000) 0.1-0.3 ml (= 0.1-0.3 mg) or, if hypotension evident,
   Epinephrine (1:10,000) slowly IV 1 ml (= 0.1 mg)
   Repeat as needed up to a maximum of 1mg
2. Give O_2 6-10 liters / min (via mask)
   If not responsive to therapy or if there is obvious acute laryngeal edema, seek appropriate assistance (e.g., cardiopulmonary arrest response team)

Hypotension with Tachycardia

1. Legs elevated 60° or more (preferred) or Trendelenburg position
2. Monitor: electrocardiogram, pulse oximeter, blood pressure
3. Give O_2 6-10 liters / min (via mask)
4. Rapid intravenous administration of large volumes of isotonic Ringer's lactate or normal saline.

If poorly responsive:
Epinephrine (1:10,000) slowly IV 1 ml (= 0.1 mg) (if no cardiac contraindications)
Repeat as needed up to a maximum of 1 mg
If still poorly responsive seek appropriate assistance (e.g., cardiopulmonary arrest response team)

(For more recommendations see back side of this card)

Premedication

➡ In case of mild idiosyncratic reaction to CM:

The following question need to be answered first:

1.) Has it been established that a past incident was due to idiosyncracy?
- In 90% of cases symptoms appear within 30 minutes of CM injection
- CM-containing iodine may have been administered for CT, angiography, venography and IVP, but not for MRI

2.) How serious was the idiosyncratic reaction ?
- dysponoea / laryngeal edema / asthma attack
- hypotension / shock

→ CM should not be applied unless absolutely necessary

- sudden sneezing
- nausea / vomiting
- rash / edema / pruritis

→ CM may be applied following premedicarion

a) Timing of premedication
- approximately 30 to 60 min before CM injection; to be remembered when scheduling CT

b) Gastrointestinal complications
- H1-receptor antagonist with good anti-emetic action (e.g., prochlorperazine [Compazine®], 5-10 mg, i.v.)
- H1-receptor antagonist with potent anti-allergic effect (e.g., diphenhydramine [Benandryl®], 25-50 mg) slowly i.v. **not to be mixed with:**
- H2-receptor antagonist (e.g., cimetidine [Tagamet®], 300 mg)
- Glucocorticoids i.v. (100-250 mg Solu-Decortin-H)

c) The patient must be informed about possible side effects of premedication:
- Slowed reactions, disturbances of speed and vision.
  → Driving a motor vehicle must be avoided for about 8 hours.
- Increased intraocular pressure.
  → Medication not to be used in glaucoma!
- Urinary retention.
  → Special monitoring of patients with hypertrophic prostate.

➡ In Patients with Graves' Disease or Autonomous Nodule(s)

Suppressed TSH, but normal serum T_3/T_4 values:
- Potassium perchlorate solution, 50 drops (about 1.0 g), on the eve of the examination, and 20 drops, t.i.d. after the examination for 10 to 14 days (after an angiogram and enhanced CT, the serum iodide level remains markedly elevated: 10^4-fold!
  → No potassium perchlorate during pregnancy, use methimazole instead (see below)!

Suppressed TSH and elevated serum T_3/T_4 values:
- Add methimazole, 10 mg t.i.d. over the same period.
  → Caution in overt thyrotoxicosis due to Graves' disease, toxic adenoma or toxic nodular goiter (Plummer's desease)!

Checklist for Reading Cervical CT Images

- Symmetry of neck musculature?
- Fat planes preserved and sharply demarcated?
- Normal perfusion of vessels?
- Thromboses or atherosclerotic stenoses?
- Symmetry and definition of salivary glands?
- Thyroid parenchyma homogeneous without nodules?
- Any focal pathologic enhancement with CM?
- Narrowing of the tracheal lumen?
- Assessment of lymph nodes? Number and size?
- Cervical vertebrae examined in bone window?
- Vertebral canal patent or narrowed?

Lymph Nodes	Normal Diameters
Anterior mediastinum	< 6 mm (DD: thymus!)
Aortopulmonary window	< 15 mm (normal fewer than 4 nodes)
Perihilar	< 10 mm
Subcarinal	< 10 mm (DD: esophagus!)
Paraaortic	< 7 mm (DD: azygos vein!)
Mesenteric	< 10 mm
Parailiac	< 12 mm (DD: ovaries!)
Parainguinal	< 18 mm

These values are intended as guidelines, larger lymph nodes are not necessarily pathological.

Thieme
Excerpt from:
Hofer, Matthias
CT Teaching Manual
ISBN 3-13-124352-X
ISBN 1-58890-277-3

Management of Acute Reactions in Adults II

Hypotension with Bradycardia
(Vagal Reaction)

1. Monitor vital signs
2. Legs elevated 60° or more (preferred) or Trendelenburg position
3. Secure airway: give O_2 6-10 liters / min (via mask)
4. Secure IV access: rapid fluid replacement with Ringer's lactate or normal saline
5. Give atropine 0.6 mg IV slowly if patient does not respond quickly to steps 2-4
6. Repeat atropine up to a total dose of 0.04 mg / kg (2-3 mg) in adult
7. Ensure complete resolution of hypotension and bradycardia prior to discharge

Hypertension, Severe

1. Give O_2 6-10 liters / min (via mask)
2. Monitor electrocardiogram, pulse oximeter, blood pressure
3. Give nitroglycerine 0.4-mg tablet, sublingual (may repeat x3) *or* topical 2% ointment, apply 1 in. strip
4. Transfer to intensive care unit or emergency department
5. For pheochromocytoma – phentolamine 5 mg IV

Seizures or Convulsions

1. Give O_2 6-10 liters / min (via mask)
2. Consider diazepam (Valium®) 5 mg (or more, as appropriate) or midazolam (Versed®) 0.5-1 mg IV
3. If longer effect needed, obtain consultation; consider phenytoin (Diantin®) infusion – 15-18 mg / kg at 50 mg / min
4. Careful monitoring of vital signs required, particularly of pO_2 because of risk to respiratory depression with benzodiazepine administration
5. Consider using cardiopulmonary arrest response team for intubation if needed

Pulmonary Edema

1. Elevate torso; rotating tourniquets (venous compression)
2. Give O_2 6-10 liters / min (via mask)
3. Give diuretics – furosemide (Lasix®) 20-40 mg IV, slow push
4. Consider giving morphine (1-3 mg IV)
5. Transfer to intensive care unit or emergency department
6. Corticosteroids optional

Thieme
Excerpt from:
Hofer, Matthias
CT Teaching Manual
ISBN 3-13-124352-X
ISBN 1-58890-277-3

Checklist: Preparing the Patient

Four aspects should be considered:

Renal function? (elimination of CM)
- Creatinine: normal 0.7 - 1.3 mg/dl = 60-130 µmol/l
- Creatinine clearance: normal 100-160 ml / min, if there is creatinine retention, 2 liters of liquid orally after i.v. CM will increase diuresis (special monitoring if cardiac failure)

Idiosyncratic reaction to CM? (premedication necessary, be informed about glaucoma, prostate hypertrophy)
- Patient should receive premedication and CM on an empty stomach (reduces the chances of aspiration in severe incidents with loss of consciousness)
- If premedication is necessary befor oral CM, the patient must be at the unit at least one hour before CT begins

Abdominal or pelvic CT? Scheduling OK?
- To apply oral CM patient must be at unit 30 minutes prior to CT
- previous GIT imaging procedures with oral CM? (this may cause artifacts up to 3 days later due to residual CM)

Hyperthyroidism? If problems with iodine-containing CM are suspected, fT_3, fT_4 and TSH should be determined; possibly also ultrasound or scintigraphy

Checklist for Referral Sheet

Necessary information:
- What region or regions of the body will be scanned?
- What disease? since when?
- Clinical observations
- Previous operations or radiotherapy? When?
- Previous CT? Include printouts if possible.
- Renal parameters: at least current creatinine levels
- Thyroid parameters or statement that hyperthyroidism is not suspected
- Any known incident of hypersensitivity to CM?

For abdominal and pelvic CTs: (because CM is administered orally)
- Is abdominal surgery planned? (water-soluble CM)
- Is there an ileal conduit or urostomy bag? (inition scan unenhanced, then enhanced scan)
- Is a lesion suspected in the lesser pelvis? (rectal CM)

Checklist for Reading Cranial CTs

- Age of the patient? Medical history?
- Posttraumatic changes in the soft-tissue structures: bruises / tumors?
- Normal contours of quadrigeminal and basal cisterns? (Risk of brainstem herniation)
- Size and contours of ventricles and CSF spaces appropriate to patient's age?
- Any blockage to flow of CSF (obstructive hydrocephalus) or signs of brain edema (=effaced sulci)?
- Asymmetries: due to head position or true asymmetry?
- Plain or contrast-enhanced CT: cerebral arteries regular? (Especially after injection of CM)
- Calcifications in the choroid plexus and pineal body only? (Common findings) Any additional hyperdense foci?
- Paraventricular white matter and cortex inconspicuous and well defined? Any focal lesions or local edema?
- Basal ganglia and internal capsule intact? (Most common locations of cerebral infarctions)
- Brainstem, pons and cerebellum normal?
- Skull checked for fractures and metastases in the bone window?

Type of bleeding	Characteristics
Subarachnoid bleeding	Hyperdense blood in the subarachnoid space or the basal cisterna instead of hypodens CSF
Subdural bleeding	Fresh hematoma: crescent, hyperdense bleeding close to the calvaria with ipsilateral edema; hematoma is concave toward hemisphere; may extend beyond cranial sutures
Epidural bleeding	Biconvex, smooth ellipsoidal in shape; close to calvaria; does not exceed cranial sutures; usually hyperdense, rarely sedimented

Who needs this book?

You are an undergraduate interested in computed tomography:

This manual introduces you in an easily understandable way to the technology of, and the fascinating images produced by modern CT scanners.

You will begin by studying the atlas sections, learning step-by-step to interpret normal anatomic findings in the cross-sectional images.

Even as a beginner you can systematically examine images of abnormalities and practice differential diagnoses.

You are a radiology technician and would like to know more about computed tomography, for example:

- how to carry out measurements of density,
- which contrast media are appropriate for a specific case,
- when the use of high-resolution CT is indicated,
- what the best injection protocol is when using a pump injector for spiral CT.
- how to perform your CT-scans using detailed protocols for the most common exams.

You are referring a patient for CT examination:

The book explains how you can best prepare your patient for CT procedures and what your colleagues in the radiology unit need to know about your patient.

If you are not versed in reading CT studies, the book will help you acquire the basics necessary for understanding your patient's images.

You have just begun an internship/residency in diagnostic radiology:

The Manual contains an atlas with detailed coded drawings for each CT image. You can quickly refresh your memory of cross-sectional anatomy and correlate 3D structures with features in the images.

You can learn the basics of differential diagnosis of CT morphology, both normal and abnormal. Numerous examples, arranged according to regions or systems, illustrate normal variations and abnormalities.

The book provides detailed information about contrast media, for example, when to use which medium to achieve optimal enhancement. Pharmacologic problems are dealt with, such as side effects or adverse reactions.

Practical hints and suggestions help you avoid the typical beginner's mistakes.

Recent technical developments such as Multidetector-Spiral-CT and CT-Angiography are presented as well.

Praise for the 1st German edition

"...more than 1000 illustrations add up to an impressive atlas ... convinces through its well-structured, didactic style..."
(Hand-Med, University of Jena, 1:1998)

"...its didactic style makes this an ideal book for the beginner at CT; learning becomes both practical and enjoyable...;
...it is much easier to remember information you have actively worked to acquire..."
(Klimax, University of Mannheim, 5/1998)

"...amazing value for your money!"
(Deutsches Ärzteblatt, Nr. 48: 1997)

"...the text is never dull, even in the more theoretical chapters...; ...at low cost, this is a good coursebook for additional studies..."
(Curare, ASTA Hannover, 11:1997)

"...ideally tailored to the needs of the beginner...;
...more than 500 CT images open up the world of the 'gray pictures'...;
...especially enjoyable if you learn by seeing ...;
...you will want to refer to it later on in the clinic..."
(Äskulap, University of Göttingen, 1998)

ISBN 3-13-124352-X
9 783131 243522

ISBN 1-58890-277-3
9 781588 902771